Fossil

Record

25 (1) 2022

MUSEUM FÜR
NATURKUNDE
BERLIN

PENSOFT®

Fossil Record
An International Journal of Palaeontology

Editor-in-Chief

Editorial Secretary

Editorial Board

Fossil Record

2022. Volume 25. Issue 1

ISSN: 2193-0066 (print), 2193-0074 (online)

In Focus

The cover picture shows *Radula patrickmuelleri* sp. nov., holotype

See paper of **Feldberg K, Schäfer-Verwimp A, Li Y, Renner MAM** Extending the diversity of the bryoflora in Kachin amber (Myanmar), with the description of *Radula patrickmuelleri*, sp. nov. and *R. tanaiensis*, sp. nov. (Jungermanniopsida, Porellales, Radulaceae).

Cover design

PENSOFT®

Fossil Record
An International Journal of Palaeontology

Content of volume **25** (**1**) 2022

Abstract & Indexing Information

Biological Abstracts® (Thompson ISI)
BIOSIS Previews® (Thompson ISI)
Camgridge Scientific Abstracts (CSA/CIG)
Web of Science® (Thompson ISI)
Zoological Record™ (Thompson ISI)

Fossil Record 25 (1) 2022, 1–10 | DOI 10.3897/fr.25.79595

A neomorphic ossification connecting the braincase, squamosal, and quadrate in choristoderan reptiles: insights from µCT data

Wanying Qin[1], Hongyu Yi[2,3], Keqin Gao[1]

1 *School of Earth and Space Sciences, Peking University, Beijing, 100871, China*
2 *Key Laboratory of Vertebrate Evolution and Human Origins of Chinese Academy of Sciences, Institute of Vertebrate Paleontology and Paleoanthropology, Chinese Academy of Sciences, Beijing, 100049, China*
3 *CAS Center for Excellence in Life and Paleoenvironment, Beijing, 100044, China*

http://zoobank.org/4FA98D61-B918-4986-9D51-A15B0DBA5D6E

Corresponding author: Hongyu Yi (yihongyu@ivpp.ac.cn)

Academic editor: Florian Witzmann ♦ **Received** 3 September 2021 ♦ **Accepted** 20 December 2021 ♦ **Published** 7 February 2022

Abstract

Choristoderes are extinct semi-aquatic to aquatic diapsid reptiles, occupying a similar niche as modern crocodilians from the Jurassic to the Miocene. Distinct from other diapsids, choristoderes have a neomorphic ossification between the braincase, squamosal, and quadrate. This neomorphic bone is described as thin and plate-like in long-snouted choristoderes (Neochoristodera), yet little is known about its presence and morphology in short-snouted non-neochoristoderes that are sister groups to Neochoristodera. Using X-ray micro-CT scanning, this study describes in detail the neomorph of two non-neochoristoderes, *Coeruleodraco jurassicus* and *Philydrosaurus proseilus*. The neomorph of both species is found between the parietal, quadrate, and squamosal. The shape of the neomorph resembles a pyramid in three-dimensions, with a triangular dorsal surface and a prominent ventral process. This confirms the neomorph is shared among early and late branching choristoderes; therefore, presence of the neomorph is a potential synapomorphy of Choristodera. In addition, the pterygoquadrate foramen is identified in non-neochoristoderes for the first time, located between the neomorph and quadrate in *C. jurassicus*. In the holotype of *P. proseilus*, the neomorph and quadrate were dislocated, but a possible pterygoquadrate foramen is identified between the two bones. Although the neomorph and pterygoquadrate foramen have been suggested to be homologous with the stapes and stapedial foramen in *Champsosaurus*, more evidences are required to confirm this homology in non-neochoristoderes, because 1) the neomorph is long and plate-like in neochoristoderes, but pyramid-shaped in non-neochoristoderes; 2) in *Champsosaurus*, the neomorph is situated lateral to the prootic and opisthotic; in *C. jurassicus* and *P. proseilus*, articulation between the neomorph and prootic (or opisthotic) cannot be confirmed due to damage to the braincase during preservation. To understand the origin of the neomorph, more intact specimens are needed to assess contact relationships between the neomorph and otic region in non-neochoristoderes.

Key Words

Choristodera, *Coeruleodraco*, micro-CT scan, neomorph, *Philydrosaurus*

1. Introduction

Choristoderes are a group of extinct aquatic-to-semi-aquatic diapsid reptiles, with a fossil record from the Middle Jurassic (Evans 1990) to Early Miocene (Evans and Klembara 2005). They were found across the Laurasia, including North America, Europe, and East Asia (Evans and Hecht 1993, Matsumoto and Evans 2010). Possible choristoderan dentary fragments and vertebral centra were found from the Middle Jurassic of Africa (Haddoumi et al. 2016). In the Cretaceous and Paleogene, several species of choristoderes were large predators, with a long snout and stout body resembling modern crocodilians (Gao 2007, Matsumoto and Evans 2010). These long snouted species form a monophyletic clade, Neochoristodera (Evans and Hecht 1993), including *Champsosaurus* (Cope

1876, Brown 1905, Russell 1956, Erickson 1972, Gao and Fox 1998) and *Simoedosaurus* (Russell-Sigogneau and Russell 1978, Erickson 1987) from North America and Europe. In Asia, neochoristoderes are found from the Lower Cretaceous, including *Ikechosaurus* (Brinkman and Dong 1993), *Tchoiria* (Efimov 1975, Efimov and Storrs 2000, Ksepka et al. 2005), and *Mengshanosaurus* (Yuan et al. 2021). Sister to neochoristoderes are short snouted species collectively called non-neochoristoderes (*sensu* Matsumoto and Evans 2010), including *Cteniogenys* from North America and Europe (Evans 1990, Gao and Fox 1998) and *Lazarussuchus* from Europe (Hecht 1992, Evans and Klembara 2005). In addition, seven genera have been reported from the Lower Cretaceous of East Asia and Siberian Russia, including *Coeruleodraco* (Matsumoto et al. 2019), *Monjurosuchus* (Endo 1940, Gao et al. 1999, 2000), *Philydrosaurus* (Gao and Fox 2005), *Shokawa* (Evans and Manabe 1999), *Hyphalosaurus* (Gao and Ksepka 2008), *Heishanosaurus* (Dong et al. 2020), and *Khurendukhosaurus* (Skutschas 2008, Matsumoto et al. 2009).

Distinct from other diapsids, choristoderes have a neomorphic ossification between the braincase and pterygoquadrate (Fox 1968). In neochoristoderes, descriptions vary about the shape of the neomorph (*sensu* Fox 1968) and its relationship with the pterygoquadrate foramen. Fox (1968) first identified the neomorph in *Champsosaurus lindoei* (UALVP 931) and *C. natator* (NMC 8922) as a triangular bone between the quadrate, squamosal, parietal, prootic, and pterygoid. The pterygoquadrate foramen is surrounded by the neomorph, quadrate, and squamosal. Based on another *C. lindoei* specimen (RTMP 87.36.41), Gao and Fox (1998) identified a large and elongated neomorph forming the pterygoquadrate foramen with the quadrate. Contrary to Gao and Fox (1998), a recent study of *C. lindoei* (CMN 8920) showed the pterygoquadrate foramen was enclosed within the neomorph (Dudgeon et al. 2020). In *C. gigas*, the neomorph was suggested as a part of the parietal (Erickson 1972). In *Simoedosaurus* (Russell-Sigogneau and Russell 1978, Erickson 1987) and *Ikechosaurus sunailinae* (Brinkman and Dong 1993), the neomorph is large and elongate, and the pterygoquadrate foramen is found between the neomorph and quadrate. In *Tchoiria* (Ksepka et al. 2005), the neomorph is present, but the pterygoquadrate foramen has not been identified. In *Mengshanosaurus* (Yuan et al. 2021), the neomorph and pterygoquadrate foramen remain unknown.

In non-neochoristoderes, the neomorph is poorly known, and the pterygoquadrate foramen has not been recognized in published materials. In *Cteniogenys*, the neomorph was inferred to be present according to articulation facets on an isolated quadrate (Evans 1990). Similarly, a facet for the neomorph is recognized on the quadrate of *Monjurosuchus* (Matsumoto et al. 2007) and *Heishanosaurus* (Dong et al. 2020). In *Shokawa* and *Khurendukhosaurus*, their skull elements are poorly known, and presence or absence of their neomorph have not been confirmed (Russell-Sigogneau and Efimov 1984, Evans and Manabe 1999, Skutschas 2008, Matsumoto et al. 2009). Using µCT scanning, the neomorph of *Coeruleodraco* was described as a small plate-like bone, but the pterygoquadrate foramen remains unknown (Matsumoto et al. 2019). In *Hyphalosaurus* (Gao and Ksepka 2008) and *Philydrosaurus* (Gao and Fox 2005), well preserved skulls have been known. It is possible to observe their neomorph and pterygoquadrate foramen by µCT scanning.

In this study, we describe the neomorph in two non-neochoristoderes: *Coeruleodraco jurassicus* and *Philydrosaurus proseilus* (Gao and Fox 2005, Gao et al. 2007, Matsumoto et al. 2019). Skulls of the two species are available to us for high-resolution CT scanning, which required separating the skull from the postcranial skeleton and preparing the skull out of the matrix. The neomorph in the holotype of *C. jurassicus* is crushed (Matsumoto et al. 2019); here we describe this bone in a new specimen with a more intact temporal region (PKUP V2003). The neomorph in the holotype of *P. proseilus* is largely blocked from external view by surrounding bones (Gao and Fox 2005); in this study, we CT-scanned the skull of the holotype (PKUP V2001) to reconstruct the neomorph in three dimensions.

Institutional abbreviations: CMN, Canadian Museum of Nature, Ottawa, Canada; IGM, Geological Institute of the Mongolian Academy of Sciences, Mongolia; IVPP, Institute of Vertebrate Paleontology and Paleoanthropology, Chinese Academy of Sciences, Beijing, China; LPMC, Paleontological Museum of Liaoning, Shenyang, China; PKUP, Peking University Paleontological Collections, Beijing, China; RTMP, Royal Tyrrell Museum of Palaeontology, Drumheller, Alberta, Canada. UALVP, Laboratory for Vertebrate Paleontology, Department of Biological Sciences, University of Alberta, Edmonton, Canada.

2. Materials and methods

A new specimen of *Coeruleodraco jurassicus* (PKUP V2003, Fig. 1a, b) and the holotype of *Philydrosaurus proseilus* (PKUP V2001, Fig. 1c) were first prepared out the matrix for µCT scanning. The new specimen of *C. jurassicus* (PKUP V2003) was found from the type locality of the species, Nanshimenzi of Qinglong County, Hebei Province, China. It consists of a nearly complete adult skeleton with a well-preserved skull exposed in ventral view (Fig. 1a). The new specimen is referred to *C. jurassicus* based on a combination of the following characters: short snout, the preorbital region of the skull (17.8 mm) being shorter than the postorbital region (25.3 mm), small lower temporal fenestra, 39 marginal teeth, tubercular posterior projections of the squamosal, and ischiadic plate with a posterodorsal process.

Specimens were scanned using a Nikon XT H 320 LC Industrial CT scanner at China University of Geosciences (Beijing). The skull of *Coeruleodraco jurassicus* (PKUP V2003) is preserved in two blocks divided by a natural crack; therefore, the two blocks were scanned

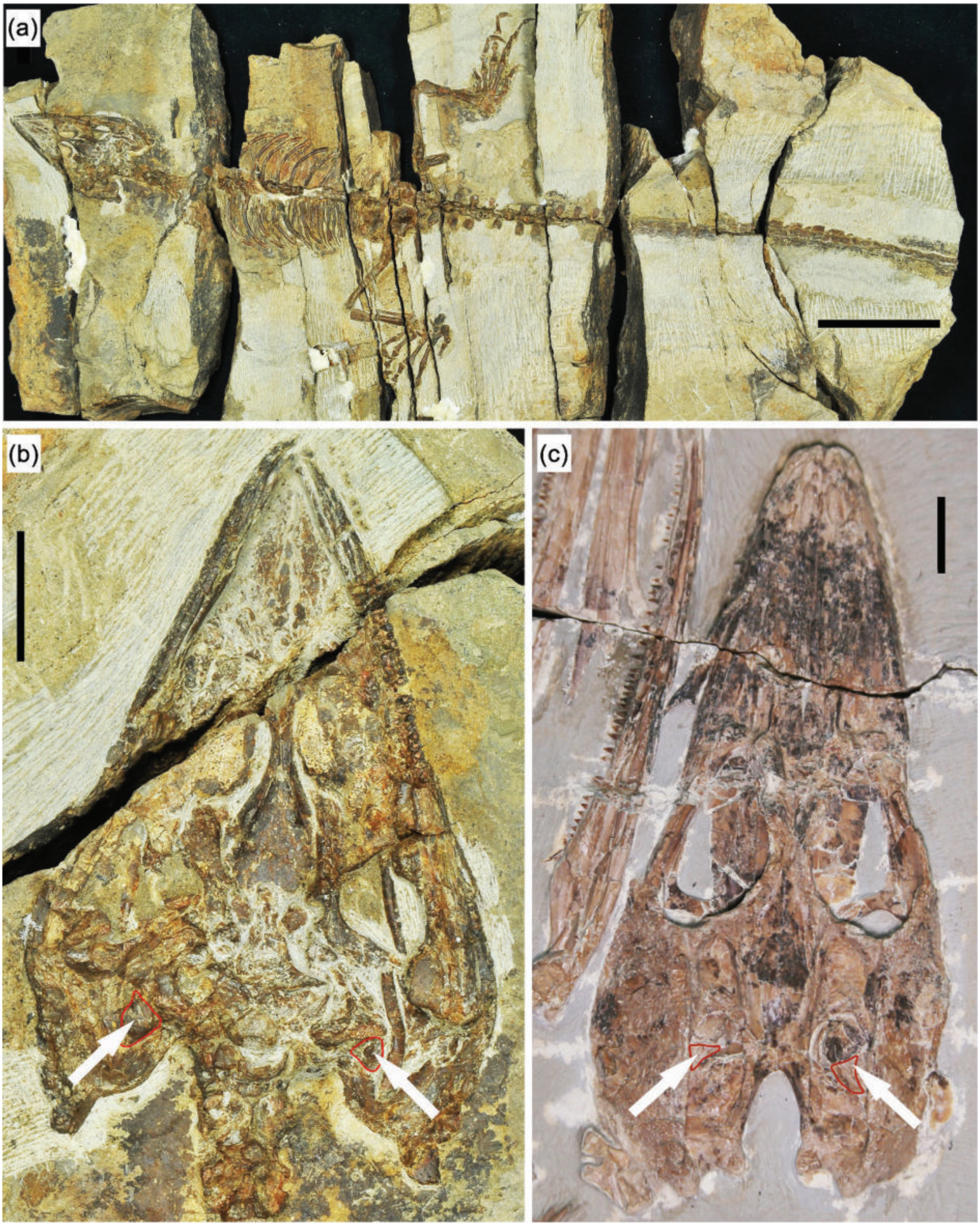

Figure 1. Photographs of the two specimens CT scanned in this study. Arrows and red lines denote the neomorphs. **a.** A new specimen of *Coeruleodraco jurassicus* (PKUP V2003); **b.** The skull of PKUP V2003 in ventral view; **c.** The skull of *Philydrosaurus proseilus* (PKUP V2001) in dorsal view. Scale bars: 50 mm (**a**); 10 mm (**b, c**).

separately using the same spatial resolution and virtually stitched together using VGSTUDIO MAX (Volume Graphics, Heidelberg, Germany). The same procedure applies to *Philydrosaurus proseilus*, as the skull (PKUP V2001) is also preserved in two blocks. Spatial resolution is 44.3220 μm for the *C. jurassicus* skull (PKUP V2003) and 39.5442 μm for the *P. proseilus* skull (PKUP V2001). The CT data were processed using VGSTUDIO MAX,

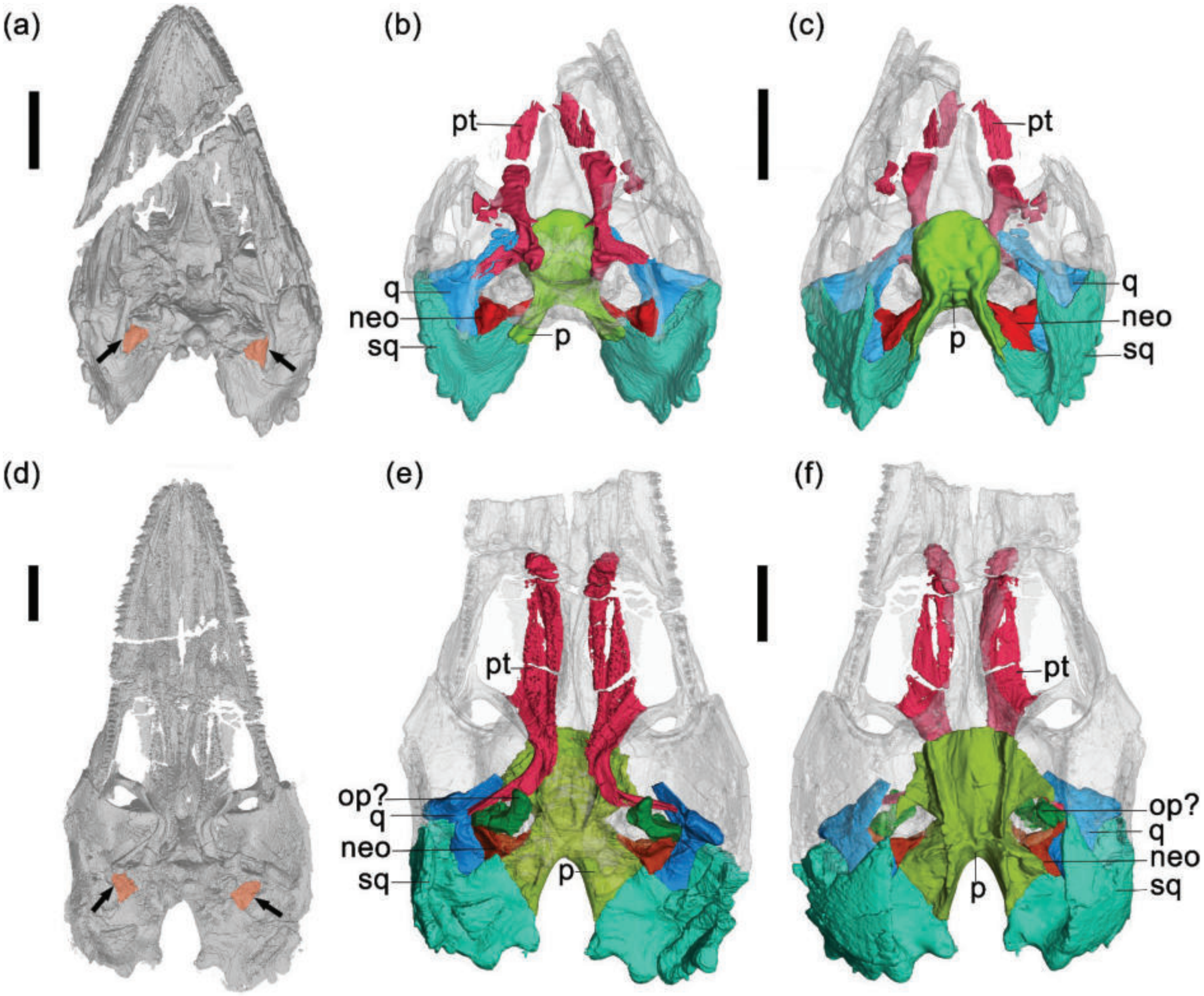

Figure 2. Virtual CT models of the *Coeruleodraco jurassicus* (PKUP V2003) and *Philydrosaurus proseilus* (PKUP V2001) skulls showing the neomorph: **a.** *C. jurassicus* skull in ventral view, arrows denoting the neomorphs (red marked); **b.** *C. jurassicus* skull showing the neomorph and surrounding bones in ventral view; **c.** *C. jurassicus* skull showing the neomorph and surrounding bones in dorsal view; **d.** *P. proseilus* skull in ventral view, arrows denoting the neomorphs (red marked); **e.** *P. proseilus* skull showing the neomorph and surrounding bones in ventral view; **f.** *P. proseilus* skull shows the neomorph and surrounding bones in dorsal view. Abbreviations: neo, neomorph; op, opisthotic; p, parietal; pt, pterygoid; q, quadrate; sq, squamosal. Scale bars: 10 mm.

including three-dimensional reconstruction of the skulls and segmentation of individual bones (parietal, squamosal, pterygoid, quadrate, and neomorph) (Fig. 2).

3. Description

3.1. The neomorph of *Coeruleodraco jurassicus*

The new specimen of *Coeruleodraco jurassicus* (PKUP V2003) consists of a nearly complete skeleton with the skull exposed in ventral view (Fig. 1a). The neomorph is partially exposed; a small ventral process of the neomorph can be observed anterior to the squamosal on both sides of the skull (Figs 1b, 2a). Using CT scanning, the dorsal portion of the neomorph has been virtually reconstructed, following sutures between the neomorph and other bones in the medial wall of the supratemporal fenestra (Fig. 2b, c).

The neomorph has an anteroposteriorly broad lateral process, an elongated medial process extending anteromedially, and a tuber-like ventral process (Fig. 3). The lateral process of the neomorph shares a long suture with the quadrate, and the long medial process articulates with the squamosal and parietal (Fig. 3d). The medial process of the neomorph extends anteriorly along the supratemporal process of the parietal, but it does not contact the pterygoid (Fig. 2b). Unlike in *Champsosaurus lindoei* (Dudgeon et al. 2020: fig. 1), the pterygoid of *Coeruleodraco jurassicus* has a short posterior process that does not extend beyond the parietal table. Ventrally, the neomorph has a distinct projection, but it is unclear whether this ventral process (or the ventral margin) contacts the opisthotic as in *C. lindoei* (Dudgeon et al. 2020: fig. 1). Although fragmentary bones are present surrounding the ventral process of the neomorph, none of the fragments can be identified as the prootic or

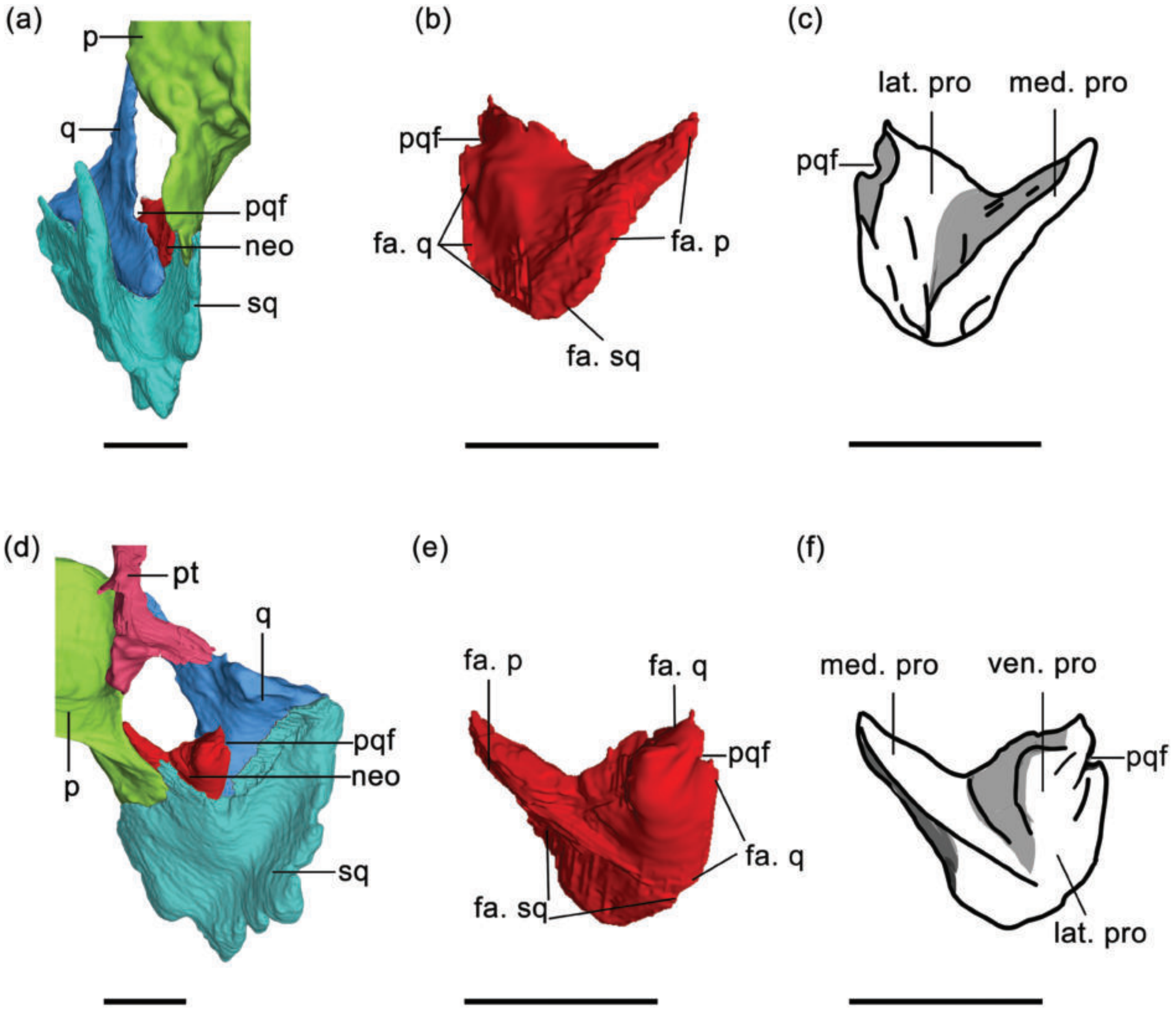

Figure 3. Morphology of the neomorph of *Coeruleodraco jurassicus* (PKUP V2003): **a.** The neomorph in the medial wall of the left supratemporal fenestra in dorsal view, with the pterygoquadrate foramen between the neomorph and quadrate; **b.** The left neomorph in dorsal view; **c.** Line drawing of the left neomorph in dorsal view; **d.** The left neomorph and surrounding bones in ventral view; **e.** The left neomorph in ventral view; **f.** Line drawing of the left neomorph in ventral view. Abbreviations: fa. p, articulation facet with the parietal; fa. q, articulation facet with the quadrate; fa. sq, articulation facet with the squamosal; lat. pro, lateral process of the neomorph; med. pro, medial process of the neomorph; neo, neomorph; p, parietal; pqf, pterygoquadrate foramen; pt, pterygoid; q, quadrate; sq, squamosal; ven. pro, ventral process of the neomorph. Scale bars: 5 mm.

opisthotic due to strong distortions of the braincase on both sides of the skull.

Between the neomorph and quadrate, there is a small foramen that we identify as the pterygoquadrate foramen (Fig. 3a). The neomorph is slightly dislocated due to lateral compression of the skull, but it clearly has a small recess forming the medial and posterior margins of the pterygoquadrate foramen. Unlike the condition in *Champsosaurus* (Fox 1968, Dudgeon et al. 2020), no groove develops near the pterygoquadrate foramen on the neomorph. In *Champsosaurus*, the margin of the pterygoquadrate foramen is either fully enclosed within the neomorph (Dudgeon et al. 2020), or bordered by the neomorph and quadrate as in *Ikechosaurus* (Brinkman and Dong 1993, Gao and Fox 1998). In the new specimen (PKUP V 2003), the anterior margin of the pterygoquadrate foramen shows a small gap between the neomorph and quadrate (Fig. 3a). With the current resolution of the CT data, it could not be determined whether the gap was caused by dislocation of the neomorph and quadrate, or the gap was originally bordered by the prootic or opisthotic. The braincase is damaged, and bones in the otic region cannot be identified (Fig. 2). Future specimens with a better-preserved braincase are required to resolve this question.

3.2. The neomorph of *Philydrosaurus proseilus*

The skull of *Philydrosaurus proseilus* holotype (PKUP V2001) is exposed dorsally. Anterior to the squamosal, the neomorph is visible in the medial wall of both supratemporal fenestrae. Dorsal exposure of the neomorph is limited

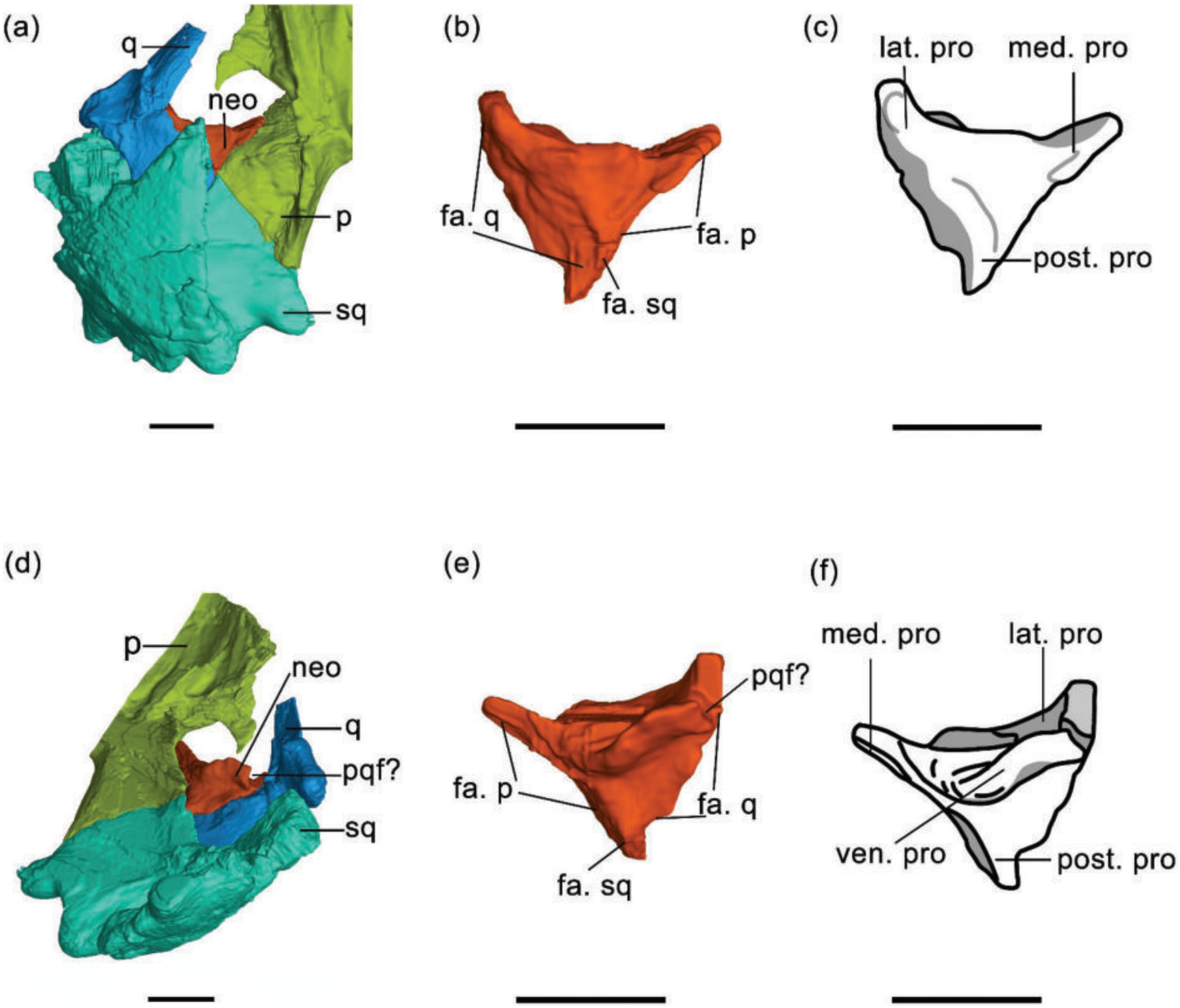

Figure 4. Morphology of the neomorph of *Philydrosaurus proseilus* (PKUP V2001): **a.** The neomorph in the medial wall of the left supratemporal fenestra in dorsal view; **b.** The left neomorph in dorsal view; **c.** Line drawing of the left neomorph in dorsal view; **d.** The left neomorph and surrounding bones in ventrolateral view, with the possible pterygoquadrate foramen between the neomorph and quadrate; **e.** The left neomorph in ventral view; **f.** Line drawing of the left neomorph in ventral view. Abbreviations: fa. p, articulation facet with the parietal; fa. q, articulation facet with the quadrate; fa. sq, articulation facet with the squamosal; lat. pro, lateral process of the neomorph; med. pro, medial process of the neomorph; neo, neomorph; p, parietal; post. pro, posterior process of the neomorph; pqf, pterygoquadrate foramen; q, quadrate; sq, squamosal; ven. pro, ventral process of the neomorph. Scale bars: 5 mm.

(Fig. 1c): on both sides of the skull, the anterior part of the neomorph is covered by several fractured bones, and the lateral part is overhung by the postorbital and squamosal. The fractured bones may be from the otic region, but they are too damaged to be identifiable. With μCT data, the morphology of the whole neomorph is revealed, including its ventral articulation with the quadrate (Fig. 2d–f).

In dorsal view, the neomorph of *Philydrosaurus proseilus* has three processes oriented medially, posteriorly, and laterally (Fig. 4). As in *Coeruleodraco jurassicus*, the medial process extends along the supratemporal process of the parietal. Anterior to the neomorph are a cluster of bone fragments possibly from the lateral wall of the braincase, but they are too crushed to be identified. In ventral view, the neomorph has a large ventral process from which extends a prominent bony ridge to the anteromedial tip of the bone (Fig. 4e, f). Differing from the condition in *Champsosaurus lindoei* (Dudgeon et al. 2020), the neomorph does not contact the pterygoid, and the pterygoid of *P. proseilus* lacks a long posterior process extending to the posterior margin of the parietal table. Anterior to the neomorphs on both sides of the skull, a pair of wing-shaped bones can be segmented in the CT data (Fig. 2e, f). With an expanded medial process and a long lateral process, this bone is identified as the opisthotic. However, the opisthotic has been shifted forward during preservation, making it uncertain with regard to the contact relationship between the opisthotic and neomorph.

The neomorph does not fully enclose a pterygoquadrate foramen. At the anterior tip of its lateral process, the neomorph has a small medially-concaving notch that seems to match a laterally-concaving notch in the quadrate (Fig. 4d). This indicates the pterygoquadrate foramen is probably between the neomorph and quadrate,

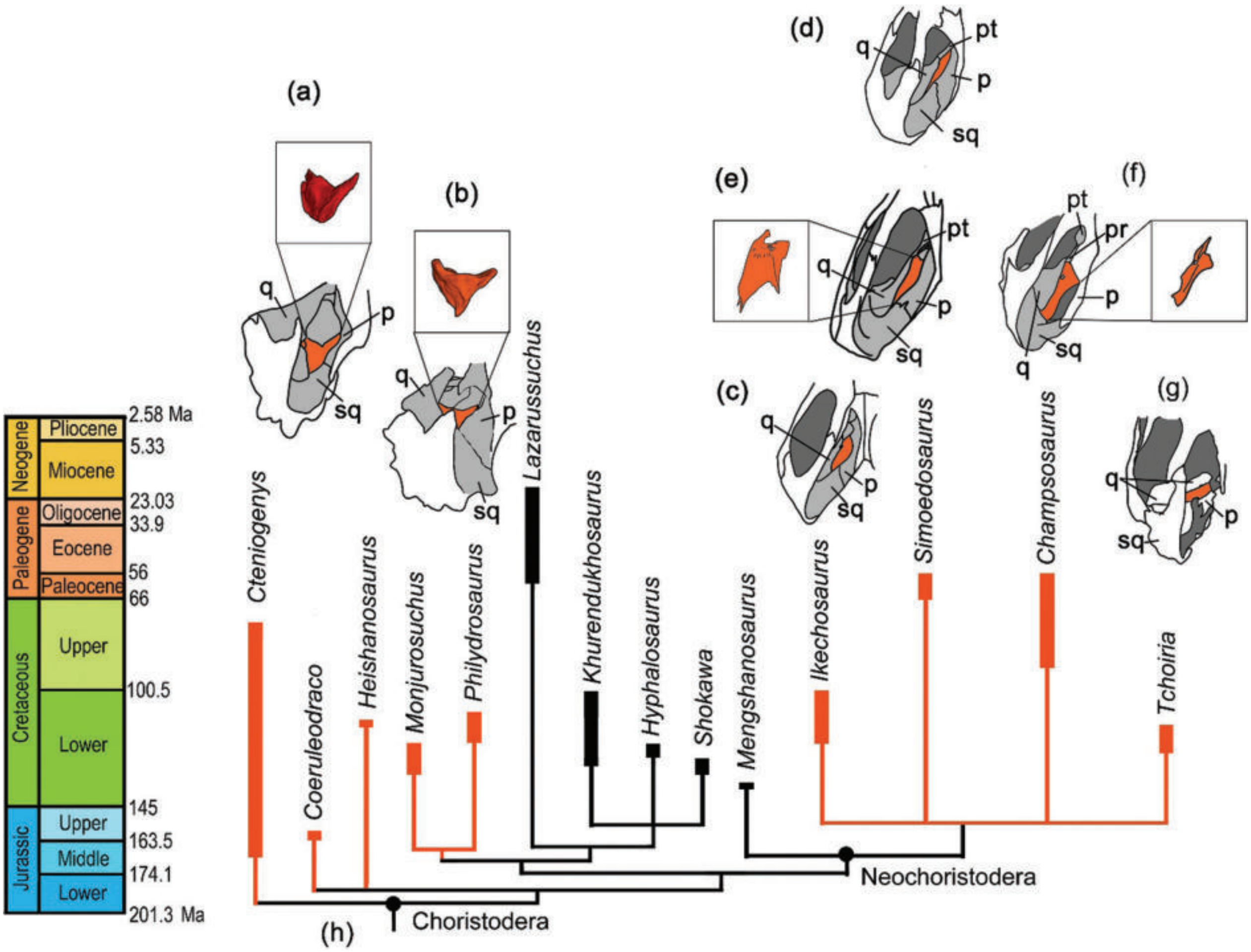

Figure 5. Morphological evolution of the neomorph in Choristodera. Red branches are taxa in which the neomorph is identified. Line drawings are the left supratemporal fenestra of choristoderes in dorsal view, the neomorph highlighted in red: **a.** *Coeruleodraco jurassicus* (PKUP V2003); **b.** *Philydrosaurus proseilus* (PKUP V2001); **c.** *Ikechosaurus sunailinae* (IVPP V9611-3), adapted from Brinkman and Dong (1993); **d.** *Simoedosaurus dakotensis*, adapted from Erickson (1987); **e.** *Simoedosaurus lemoinei*, adapted from Russell-Sigogneau and Russell (1978), the neomorph is in medial view; **f.** *Champsosaurus lindoei* (CMN 8920), adapted from Dudgeon et al. (2020); **g.** *Tchoiria klauseni* (IGM 1/8), adapted from Ksepka et al. (2005); the line drawing is mirrored from the right supratemporal fenestra for comparisons with other species; **h.** Cladogram of Choristodera, composited from Dong et al. (2020) and Yuan et al. (2021). Line drawings not to scale. Abbreviations: p, parietal; pr, prootic; pt, pterygoid; q, quadrate; sq, squamosal.

similar to the condition in *Coeruleodraco jurassicus* (Fig. 3a). However, the neomorph and quadrate are slightly dislocated on both sides of the skull, and it cannot be determined how the notches on the bones contact each other in life. This possible pterygoquadrate foramen needs to be confirmed with more specimens.

4. Discussion

The neomorph was first identified in *Champsosaurus* as a unique ossification connecting the braincase and pterygoquadrate (Fox 1968). This bone was later discovered in other neochoristoderes, including *Simoedosaurus*, *Ikechosaurus*, and *Tchoiria* (Russell-Sigogneau and Russell 1978, Brinkman and Dong 1993, Gao and Fox 1998, Ksepka et al. 2005). Although its presence remains unconfirmed in *Mengshanosaurus* (Yuan et al. 2021), the neomorph possibly represents a synapomorphy of all neochoristoderes. Among non-neochoristoderes (Fig. 5), the neomorph has been reported in *Cteniogenys*, *Coeruleodraco*, *Monjurosuchus*, and *Heishanosaurus* (Evans 1990, Matsumoto et al. 2007, Matsumoto et al. 2019, Dong et al. 2020), and it was discovered in *Philydrosaurus* in this study. Finding the neomorph in multiple species close to the root of the choristoderan tree implies this unique ossification might be shared among all choristoderes (Fig. 5).

The neomorph of *Coeruleodraco jurassicus* was previously described as a small bone in the temporal region (Matsumoto et al. 2019). This may be a result of distortion of the holotype. In the new specimen, the neomorph forms the medial wall of the supratemporal fenestra and shares extensive sutures with the quadrate and parietal. In addition, the shape of the neomorph differs between short-snouted and long-snouted taxa. The neomorph of the short-snouted *C. jurassicus* and *Philydrosaurus proseilus* resembles a pyramid in three dimensions, with a triangular dorsal surface and a large ventral process. In the long-snouted neochoristoderes, such as *Champsosaurus* and *Simoedosaurus* (Fig. 5), the neomorph is elongate and plate-like, lacking a ventral process (Russell-Sigogneau and Russell 1978, Brinkman and Dong 1993, Ksepka et al. 2005, Dudgeon et al. 2020) (Fig. 5). This shape disparity suggests varying structural roles of the neomorph among choristoderes, as the supratemporal fenestra is much more expanded anteroposteriorly in the long-snouted species than that in short-snouted species.

As in several neochoristoderes (*Champsosaurus* Dudgeon et al., 2020; *Simoedosaurus* Russell-Sigogneau & Russell, 1978; *Ikechosaurus* Brinkman & Dong, 1993), the neomorph cooccurs with the pterygoquadrate foramen in *Coeruleodraco jurassicus* (Fig. 3) and possibly in *Philydrosaurus proseilus* (Fig. 4). In *C. jurassicus*, the pterygoquadrate foramen is between the neomorph and quadrate (Fig. 3). In neochoristoderes, this foramen is either fully enclosed by the neomorph (Dudgeon et al. 2020) or situated between the neomorph and quadrate (Brinkman and Dong 1993, Gao and Fox 1998). Although the pterygoquadrate foramen has been suggested to be homologous with stapedial foramen in *Champsosaurus* (Dudgeon et al. 2020)—and the neomorph being homologous with the stapes—this hypothesis remains to be proven in non-neochoristoderes. The neomorph is long and plate-like in neochoristoderes (Russell-Sigogneau and Russell 1978, Brinkman and Dong 1993, Ksepka et al. 2005, Dudgeon et al. 2020) but pyramid-shaped in non-neochoristoderes (Figs 2–5). The neomorph is situated lateral to the otic region in *Champsosaurus lindoei* (Dudgeon et al. 2020). This condition cannot be confirmed in *Coeruleodraco jurassicus* and *Philydrosaurus proseilus*, as CT scans of available specimens show the braincase is badly crushed by dorsoventral compressions. Previous studies on the *C. jurassicus* holotype noted a possible stapes preserved with the neomorph, although the authors suggested higher-resolution CT scanning to confirm the presence of the stapes (Matsumoto et al. 2019). Little is known about the braincase wall in other non-neochoristoderes. *Monjurosuchus* and *Hyphalosaurus* from the Early Cretaceous Jehol Biota are preserved in articulation and in three dimensions, but their specimens are generally dorsoventrally compressed, hindering the understanding of their lateral braincase wall (Gao and Li 2007, Gao and Ksepka 2008). More intact specimens are needed to assess the contact between the neomorph and the otic region in non-neochoristoderes.

5. Conclusions

This study provides detailed morphological descriptions about the neomorph of two short-snouted choristoderes, *Coeruleodraco jurassicus* and *Philydrosaurus proseilus*. The neomorph connects the braincase (parietal), quadrate, and squamosal. The shape of the neomorph varies in the evolution of Choristodera and shows a greater elongation in neochoristoderes than in non-neochoristoderes. In the two species examined here, the neomorph has a triangular dorsal surface and a prominent ventral process, differing from the plate-like shape in neochoristoderes. The pterygoquadrate foramen is identified in *C. jurassicus*, and it is likely present in *P. proseilus*. More intact specimens are needed to assess the contact between the neomorph and the otic region in non-neochoristoderes.

Data availability

All specimens discussed in this paper are deposited in public museums. The original CT data is available upon request to the authors.

Author contributions

GK and WQ collected and described the fossil material. WQ, HY and GK prepared the figures and wrote the manuscript.

Financial support

This project is funded by the Strategic Priority Research Program of the Chinese Academy of Sciences (XDA19050102, XDB18030504, XDB26000000), the Chinese Academy of Sciences Pioneer grants, the International Partnership Program of Chinese Academy of Sciences (Grant No. 132311KYSB20190010), and the National Natural Science Foundation of China (Grant No. 41702020 and 41688103).

Acknowledgements

The CT scanning was performed at the Micro-focus Industrial Computerized Tomography (ICT) Laboratory of China University of Geosciences (Beijing). We thank Jia Jia at the University of Calgary for his help in using VGSTUDIO MAX for three-dimensional reconstructions of the skulls. Yingjie Li prepared the fossil specimens for CT scanning. Liping Dong at the Institute of Vertebrate Paleontology and Paleoanthropology (CAS) provided specimen access of the *Coeruleodraco jurassicus* holotype. Yalei Yin at Peking University provided useful comments on an early version of the article.

Reference

Brinkman DB, Dong ZM (1993) New material of *Ikechosaurus sunailinae* (Reptilia: Choristodera) from the Early Cretaceous Laohongdong Formation, Ordos Basin, Inner Mongolia, and the interrelationships of the genus. Canadian Journal of Earth Sciences 30: 2153–2162. https://doi.org/10.1139/e93-186

Brown B (1905) The osteology of *Champsosaurus* Cope. American Museum of Natural History, Memoirs 9: 1–26.

Carroll RL (1981) Plesiosaur ancestors from the Upper Permian of Madagascar, Philosophical Transactions of the Royal Society of London, Series B 293: 315–383. https://doi.org/10.1098/rstb.1981.0079

Cope ED (1876) On some extinct reptiles and Batrachia from the Judith River and Fox Hills beds of Montana. Proceedings of the Academy Natural Sciences of Philadelphia 28: 340–359.

Dong L, Matsumoto R, Kusuhashi N, Wang Y, Wang Y, Evans SE (2020) A new choristodere (Reptilia: Choristodera) from an Aptian–Albian coal deposit in China. Journal of Systematic Palaeontology: 1–20. https://doi.org/10.1080/14772019.2020.1749147

Dudgeon WT, Maddin HC, Evans DC, Mallon JC (2020) Computed tomography analysis of the cranium of *Champsosaurus lindoei* and implications for choristoderan neomorphic ossification. Journal of Anatomy 236(4): 630–659. https://doi.org/10.1111/joa.13134

Efimov MB (1975) *Champsosaurus* from the Lower Cretaceous of Mongolia. Trudy Sovmestnoi Sovetsko-Mongol'skoi Paleontologicheskoi Ekspeditsii 2: 84–93.

Efimov MB, Storrs GW (2000) Choristodera from the Lower Cretaceous of northern Asia. In: Benton MJ, Shishkin MA, Unwin DM, Kurochkin EN (Eds) The age of dinosaurs in Russia and Mongolia. Cambridge University Press, Cambridge, 390–401.

Endo R (1940) A new genus of Thecodontia from the *Lycoptera* beds in Manchoukuo. Bulletin of Central National Museum of Manchoukuo 2: 1–14.

Erickson BR (1972) The lepidosaurian reptile *Champsosaurus* in North America. Science Museum of Minnesota, Monograph (Paleontology) 1: 1–9.

Erickson BR (1987) *Simoedosaurus dakotensis*, new species, a diapsid reptile (Archosauromorpha: Choristodera) from the Paleocene of North America. Journal of Vertebrate Paleontology 7: 237–251. https://doi.org/10.1080/02724634.1987.10011658

Evans SE (1990) The skull of *Cteniogenys*, a choristodere (Reptilia: Archosauromorpha) from the Middle Jurassic of Oxfordshire. Zoological Journal of the Linnean Society 99: 205–237. https://doi.org/10.1111/j.1096-3642.1990.tb00561.x

Evans SE, Hecht MK (1993) A history of an extinct reptilian clade, Choristodera: longevity, Lazarus-taxa, and the fossil record. Evolutionary Biology 27: 323–338. https://doi.org/10.1007/978-1-4615-2878-4_8

Evans SE, Manabe MA (1999) Choristoderan reptile from the Lower Cretaceous of Japan. Special Papers in Palaeontology 60: 101–119.

Evans SE, Klembara J (2005) A choristoderan reptile (Reptilia; Diapsida) from the lower Miocene of northwest Bohemia (Czech Republic). Journal of Vertebrate Paleontology 25: 168–181. https://doi.org/10.1671/0272-4634(2005)025[0171:ACRRDF]2.0.CO;2

Fox RC (1968) Studies of Late Cretaceous vertebrates, 1. The braincase of *Champsosaurus* Cope (Reptilia: Eosuchia), Copeia 1968(1): 100–109. https://doi.org/10.2307/1441556

Gao K (2007) Phylogenetic and ecomorphic diversity and biogeographic evolution of Choristodera as a distinct diapsida clade. Journal of Palaeogeography 9: 541–550.

Gao K, Fox RC (1998) New choristoderes (Reptilia: Diapsida) from the Upper Cretaceous and Paleocene, Alberta and Saskatchewan, Canada, and phylogenetic relationships of Choristodera. Zoological Journal of the Linnean Society 124: 303–353. https://doi.org/10.1111/j.1096-3642.1998.tb00580.x

Gao K, Fox RC (2005) A new choristodere (Reptilia: Diapsida) from the Lower Cretaceous of western Liaoning Province, China, and phylogenetic relationships of Monjurosuchidae. Zoological Journal of the Linnean Society 145: 427–444. https://doi.org/10.1111/j.1096-3642.2005.00191.x

Gao K, Li Q (2007) Osteology of *Monjurosuchus splendens* (Diapsida, Choristodera) based on a new specimen from the Lower Cretaceous of western Liaoning, China. Cretaceous Research 28: 261–271. https://doi.org/10.1016/j.cretres.2006.07.001

Gao K, Ksepka D (2008) Osteology and taxonomic revision of *Hyphalosaurus* (Diapsida: Choristodera) from the Lower Cretaceous of Liaoning, China. Journal of Anatomy 212: 747–768. https://doi.org/10.1111/j.1469-7580.2008.00907.x

Gao K, Tang Z, Wang X (1999) A long-necked diapsid reptile from the Upper Jurassic/Lower Cretaceous of Liaoning Province, northeastern China. Vertebrate PalAsiatica 37: 1–8.

Gao K, Evans SE, Ji Q, Norell MA, Ji S (2000) Exceptional fossil material of a semi-aquatic reptile from China: the resolution of an enigma, Journal of Vertebrate Paleontology 20: 417–421. https://doi.org/10.1671/0272-4634(2000)020[0417:EFMOAS]2.0.CO;2

Gao K, Ksepka D, Hou L, Duan Y, Hu D (2007) Cranial morphology of an Early Cretaceous monjurosuchid (Reptilia: Diapsida) from Liaoning Province of China and evolution of choristoderan palate. Historical Biology 19: 215–224. https://doi.org/10.1080/08912960601106391

Haddoumi H, Allain R, Meslouh S, Metais G, Monbaron M, Pons D, Rage JC, Vullo R, Zouhri S, Gheerbrant E (2016) Guelb el Ahmar (Bathonian, Anoual Syncline, eastern Morocco): First continental flora and fauna including mammals from the Middle Jurassic of Africa. Gondwana Research 29: 290–319. https://doi.org/10.1016/j.gr.2014.12.004

Hecht MK (1992) A new choristodere (Reptilia, Diapsida) from the Oligocene of France: an example of the Lazarus effect, Geobios 25: 115–131. https://doi.org/10.1016/S0016-6995(09)90041-9

Ksepka DT, Gao K, Norell MA (2005) A new choristodere from the Cretaceous of Mongolia, American Museum Novitates 3468: 1–22. https://doi.org/10.1206/0003-0082(2005)468%3C0001:ANCFTC%3E2.0.CO;2

Matsumoto R, Evans SE (2010) Choristoderes and the freshwater assemblages of Laurasia, Journal of Iberian Geology 36(2): 253–274. https://doi.org/10.5209/rev_JIGE.2010.v36.n2.11

Matsumoto R, Evans SE, Manabe M (2007) The choristoderan reptile *Monjurosuchus* from the Early Cretaceous of Japan. Acta Palaeontologica Polonica 52: 329–350.

Matsumoto R, Suzuki S, Tsogtbaatar K, Evans SE (2009) New material of the enigmatic reptile *Khurendukhosaurus* (Diapsida: Choristodera) from Mongolia. Naturwissenschaften 96: 233–242. https://doi.org/10.1007/s00114-008-0469-6

Matsumoto R, Dong L, Wang Y, Evans SE (2019) The first record of a nearly complete choristodere (Reptilia: Diapsida) from the Upper Jurassic of Hebei Province, People's Republic of China. Journal of Systematic Palaeontology 17(1): 1–18. https://doi.org/10.1080/14772019.2018.1494220

Matsumoto R, Buffetaut E, Escuillie F, Hervet S, Evans SE (2013) New material of the choristodere *Lazarussuchus* (Diapsida, Choristodera) from the Paleocene of France. Journal of Vertebrate Paleontology 33: 319–339. https://doi.org/10.1080/02724634.2012.716274

Moon BC, Kirton AM (2016) Ichthyosaurs of the British Middle and Upper Jurassic, PART 1. *Ophthalmosaurus*. Monograph of the Palaeontographical Society 170(647): 1–84. [pls 1–30] https://doi.org/10.1080/02693445.2016.11963958

Reisz R (1981) A diapsid reptile from the Pennsylvanian of Kansas, Special Publications of the Museum of Natural History. University of Kansas 7: 1–74. https://doi.org/10.5962/bhl.title.8440

Russell LS (1956) The Cretaceous reptile *Champsosaurus natator* Parks. National Museum of Canada, Bulletin 145: 1–51.

Russell-Sigogneau D, Russell DE (1978) Étude ostéologique du Reptile *Simoedosaurus* (Choristodera). Annales de Paléontologie (Vertébrés) 64: 1–84.

Skutschas PP (2008) A choristoderan reptile from the Lower Cretaceous of Transbaikalia, Russia. Neues Jahrbuch für Geologie und Paläontologie–Abhandlungen 247(1): 63–78. https://doi.org/10.1127/0077-7749/2008/0247-0063

Yuan M, Li D, Ksepka TD, Yi H (2021) A juvenile skull of the longirostrine choristodere (Diapsida, Choristodera), *Mengshanosaurus minimus* gen. et sp. nov., with comments on neochoristodere ontogeny. Vertebrata PalAsiatica 59(3): 213–228.

Fossil Record 25 (1) 2022, 11–24 | DOI 10.3897/fr.25.80134

The first adult mantis lacewing from Baltic amber, with an evaluation of the post-Cretaceous loss of morphological diversity of raptorial appendages in Mantispidae

Viktor Baranov[1], Ricardo Pérez-de la Fuente[2], Michael S. Engel[3], Jörg U. Hammel[4], Christine Kiesmüller[5], Marie K. Hörnig[5], Paula G. Pazinato[1], Corleone Stahlecker[1], Carolin Haug[1,6], Joachim T. Haug[1,6]

1 *Biocenter, Ludwig-Maximilians-Universität München (LMU Munich), Großhaderner Str. 2, 82152, Planegg-Martinsried, Germany*
2 *Oxford University Museum of Natural History, Parks Road, Oxford, OX1 3PW, UK*
3 *Division of Entomology, Natural History Museum, and Department of Ecology & Evolutionary Biology, 1501 Crestline Drive - Suite 140, University of Kansas, Lawrence, Kansas 66045, USA*
4 *Institute of Materials Research, Helmholtz-Zentrum Geesthacht, Max-Planck-Straße 1, 21502, Geesthacht, Germany*
5 *Zoological Institute and Museum, Cytology and Evolutionary Biology, University of Greifswald, Soldmannstr. 23, 17489, Greifswald, Germany*
6 *GeoBio-Center at LMU, Richard-Wagner-Str. 10, 80333, Munich, Germany*

http://zoobank.org/2EE2A776-4953-4FB1-906E-38447A905766

Corresponding author: Viktor Baranov (baranow@biologie.uni-muenchen.de)

Academic editor: Alexander Schmidt ♦ **Received** 8 September 2021 ♦ **Accepted** 3 January 2022 ♦ **Published** 7 February 2022

Abstract

Mantis lacewings (Neuroptera: Mantispidae) are prominent and charismatic predatory representatives of Insecta. Nevertheless, representatives of the group are surprisingly scarce in Paleogene deposits after a relative abundance of specimens known from Cretaceous. Here we present *Mantispa? damzenogedanica* sp. nov., representing the first adult of Mantispidae described from Baltic amber and the only Eocene adult mantispid hitherto preserved in amber. The new fossil species is also among the earliest representatives of Mantispinae, certainly the oldest adult of this group described from amber. Additionally, we discuss the changes through time in the ecological morphospace within Mantispidae based on the morphological diversity (≈disparity) of the raptorial legs. Possible explanations for the post-Cretaceous decline in the morphological diversity of mantis lacewings are posited.

Key Words

amber, fossil, lacewings, mantid flies, morphology, Neuroptera, shape

1. Introduction

Many of the numerous representatives of Insecta unfortunately invoke revulsion in most people. Nonetheless, some groups can inspire greater collective fascination and even appreciation and affection, such as butterflies and bees. Alongside these are the praying mantises (Mantodea), which are often kept and bred as pets as well as featured in zoological displays and educational programs (McMongile 2013, Green 2014). For non-entomologists, it is generally unknown that several other insect lineages bear a resemblance to praying mantises and show similar specializations. Adults of Mantispidae resemble many highly-specialized praying mantises not only in the morphology of the raptorial (i.e., grasping) forelegs, but also in the elongation of the prothorax, the often considerably anterior insertion of the forelegs, practically below the head, or the exophthalmic compound eyes on the highly mobile head, aiding in the detection of prey.

Mantis lacewings are representatives of Neuroptera (i.e., lacewings and their relatives). Neuroptera today comprise about 6,000 species worldwide (Engel et al.

2018, Winterton et al. 2018, Snyman et al. 2020, Ardila-Camacho et al. 2021). Mantispidae are classified within the larger group Mantispoidea, which aside from mantis lacewings also includes the groups Rhachiberothidae (thorny lacewings) and Berothidae (beaded lacewings), as well as extinct groups such as Mesoberothidae and Dipteromantispidae (Ardila-Camacho et al. 2021). Relationships of Mantispidae within Neuroptera, as well as its interrelationships within the group, have been recently revised by Ardila-Camacho et al. (2021) based on morphological characters. These authors recovered a single origin of the raptorial appendages within Mantispoidea, with Berothidae as sister group to Rhachiberothidae + Mantispidae (Ardila-Camacho et al. 2021). These authors, however, did not recover a monophyletic Mantispidae, as they recovered Symphrasinae as sister group to Rhachiberothidae, a result congruent with that of Winterton et al. (2018) based on anchored phylogenomics. As a result, Ardila-Camacho et al. (2021) classified Symphrasinae within Rhachiberothidae.

Although diverse by neuropteran standards, mantis lacewings lack the remarkable diversity of other holometabolans, such as beetles, wasps, and flies. The group Neuroptera, and in fact the more inclusive group Neuropterida, which includes the species-poor lineages Megaloptera and Raphidioptera, is likely to have been significantly more diversified and disparate in the Cretaceous (e.g., Aspöck and Aspöck 2007, Liu et al. 2016, 2018, Wang et al. 2016, Badano et al. 2018, Haug et al. 2019a, b, 2020a, b, c, in press, Lu et al. 2020, Zippel et al. 2021). Such a pattern has been observed for several constituent lineages of Neuropterida, for which it seems that the loss of morphological diversity (≈ disparity) was not a one-step event as is often assumed in relation to the end-Cretaceous or other mass extinction events. Instead, the Eocene fauna, at least, has been found to have a kind of transitional diversity between the Cretaceous and modern ones – less diverse than the Cretaceous, but still noticeably differing from the extant fauna (e.g., Haug et al. 2020a), the latter in line with its paratropical climate versus temperate environments today in the same region.

Mantis lacewings seem to have been more dominant, or at least common, in the Cretaceous, as demonstrated by numerous adult mantis lacewings in Cretaceous deposits, especially in amber (Poinar and Buckley 2011, Pérez-de la Fuente and Peñalver 2019, Lu et al. 2020, Shi et al. 2020a, b), although they have also been discovered in sedimentary rocks (Jepson et al. 2013). Some of these mantis lacewings also exhibit a more disparate range of morphologies relative to their modern counterparts, especially in their raptorial forelegs (Lu et al. 2020, Shi et al. 2020b), reinforcing the notion of a loss of morphological diversity in Mantispidae.

The Eocene record of Mantispidae is rather sparse and hampers a further understanding of the evolution of the group. A single adult specimen from British amber, *Whalfera venatrix* Whalley 1983, has hitherto been reported as a putative mantis lacewing (Whalley 1983, Willmann 1994). This species, however, was later reassessed as a representative of Rhachiberothidae (Engel 2004, Makarkin and Kupryjanowicz 2010, Ardila-Camacho et al. 2021). From the otherwise profusely rich Baltic amber only larval stages of mantis lacewings have been reported (Ohl 2011, Wunderlich 2012), and even these have been few in number (namely four larvae in two pieces of amber). This fact is noteworthy given that, although more than a dozen adults are known from Cretaceous ambers (Poinar and Buckley 2011, Pérez-de la Fuente and Peñalver 2019, Lu et al. 2020, Shi et al. 2020a, b), only a few larvae have yet been discovered (Haug et al. 2018, 2021a; Pérez-de la Fuente and Peñalver 2019).

Here we report the first adult of Mantispidae from Baltic amber and place it into a larger framework regarding the quantitative morphology of raptorial forelegs across the lineage in terms of extant and extinct diversity. These morphometric comparisons serve as a proxy for the breadth of ecologies and predatory behaviors within Mantispidae during different episodes of their evolutionary history.

2. Material and methods

2.1. Material

The specimen studied herein corresponds to an adult mantis lacewing preserved in Eocene Baltic amber. The specimen was found at the Yantarny mine, Kaliningrad (Russia), and originally belonged to the personal collection of Jonas Damzen, who acquired it from a commercial source in Yantarny, Kaliningrad District. The specimen is now deposited in the Museum of Gdańsk (Gdańsk, Poland), under the accession number MG/B/1172. The sediments bearing the Baltic amber have sometimes been stratigraphically placed as late Bartonian to earliest Priabonian, with the richer concentrations of amber lower among these, based on lithological and palynological data (Kasiński et al. 2020). However, determining the age of Baltic amber is a complex issue and a matter of ongoing debates (Sadowski et al. 2017, Baranov et al. 2019, Kasiński et al. 2020). The minimal age of Baltic amber appears to be 34 Ma, with recent studies pointing to a late Eocene age (Sadowski et al. 2017, Baranov et al. 2019).

2.2. Documentation methods

The specimen was documented using microscopy and synchrotron radiation-based X-ray computed microtomography (SR-µCT). First, the specimen was examined under a Keyence VHX-6000 digital microscope under different light settings (Haug et al. 2013a, Hörnig et al. 2016). Stacks of photographs were recorded from the specimen in different views, which were fused into single sharp images. Thus, all photographs presented are composite images. Adjacent image details were merged into large panorama images. Additionally, the HDR function was used to prevent areas that were excessively dark and too bright to appear on the photographs (cf. Haug et al. 2013a). All processing was done automatically by the built-in software.

The amber specimen was scanned with Imaging Beamline P05 (IBL; Greving et al. 2014, Wilde et al. 2016) operated by the Helmholtz-Zentrum Hereon at the PETRA III storage ring (Deutsches Elektronen Synchrotron – DESY, Hamburg, Germany), using a photon energy of 18 keV and a sample-to-detector distance of 100 mm. Projections were recorded with a custom developed 20 MP CMOS camera system with an effective pixel size of 1.28 µm (Lytaev et al. 2014). For each tomographic scan 3601 projections at equal intervals between 0 and π were recorded. Tomographic reconstruction was conducted by applying a transport of intensity phase retrieval approach and using the filtered back projection algorithm (FBP) carried out in a custom reconstruction pipeline using Matlab (Math-Works) and the Astra Toolbox (Moosmann et al. 2014, van Aarle et al. 2015, 2016). Raw projections were binned twice for further processing, resulting in an effective pixel size of the reconstructed volume (voxel) of 2.56 µm. We have reconstructed the scanned volumes using Drishti ver. 2.6.6 (Limaye 2012). To decrease the demands of RAM and video card of the computer used, we have downscaled all the tiff images by 50% and subsequently cropped the empty space around the amber piece using Fiji 'scale' and 'crop' functions (Schindelin et al. 2012). After that we rendered the 3D volume of the animal in Drishti ver. 2.6.6 (Limaye 2012).

2.3. Morphometric analysis

In order to provide a comparative framework, we considered all fossil representatives of the group Mantispidae from the literature in which the profemur and its inner integumentary processes bearing terminal modified setae (i.e., the often so-called 'spines'), including the largest of such processes if present (the so-called major 'spine'), were accessible. Therefore, a total 22 fossil specimens, plus the new species, were included (see Suppl. material 2: Table S1 for sources of the images; table is supplied as online supplement here: https://github.com/chironomus/Mantispidae-shape-analysis/blob/main/_CLEANED_FOR_EOCENE_Raptorial_Neuropterans.xls from here on referred as "Supplement table 1"). We redrew the profemoral functional lateral outline (≈ evolutionary anterior side of appendage) of these fossil species in Adobe Illustrator CS2 or Inkscape. Final outlines were transformed into 24-bit bmp-files (available here https://github.com/chironomus/Mantispidae-shape-analysis). The data set was supplemented by 38 extant specimens encompassing all the mantis lacewings ingroups ('subfamilies') also redrawn from the literature (see Suppl. material 1 https://github.com/chironomus/Mantispidae-shape-analysis/blob/main/_CLEANED_FOR_EOCENE_Raptorial_Neuropterans.xls), for which images of the femora of the raptorial legs were available in lateral view. Due to preservational limitations, many fossil specimens were omitted from the analysis. See Suppl. material 2: Table S1 (https://github.com/chironomus/Mantispidae-shape-analysis/blob/main/_CLEANED_FOR_EOCENE_Raptorial_Neuropterans.xls) for the complete list of the specimens analysed.

The program package Shape was used for further analysis (Iwata and Ukai 2002). At first, shapes (outlines of the profemora) were translated into numerical enumerators (chain code) via Elliptic Fourier Transformation, while in a second step the outlines were aligned. Finally, the data set was subjected to a Principal Component Analysis (PCA). Ten harmonics were used as a base setting. Scatterplots of the main dimensions (PCs) were plotted in OpenOffice Calc. Final representations were re-drawn in Adobe Illustrator CS2.

2.4. Morphological terminology

Wing venation interpretation and nomenclature follows that of Breitkreuz et al. (2017), and other terminology follows that used elsewhere for Mantispidae (e.g., Pérez-de la Fuente and Peñalver 2019, Lu et al. 2020).

3. Results

3.1. Systematic palaeontology

Neuroptera Linnaeus, 1758
Mantispidae Leach, 1815
Mantispinae Leach, 1815
***Mantispa* Illiger in Kugelann, 1798**

***Mantispa? damzenogedanica* sp. nov.**
http://zoobank.org/8C79CEEC-9800-4EB3-9665-B6FE756F83FF
Figs 1–4

Derivatio nominis. The specific epithet is a combination of 'Damzen', honouring Mr. Jonas Damzen (Vilnius), who found, prepared, and made the specimen available, and 'gedanicum', relative to Gedania, one of the Latin names for Gdańsk (Poland), where the specimen will be housed permanently.

Holotype. MG/B/1172, Museum of Gdańsk (Gdańsk, Poland). The specimen is well preserved, albeit missing distal parts of some appendages and heavily covered by white foam (= 'Verlumung'), particularly thick on the posterior part of the body, namely the abdomen. A single spider and six non-biting midges (Diptera: Chironomidae: Chironominae: Tanytarsini) are present as syninclusions.

Type locality and age. Baltic amber from Yantarny mine in Yantarny, Kaliningrad (formerly Palmnicken, Königsberg), Russia; Eocene (late Bartonian–earliest Priabonian). The precise extraction location within the Yantarny mine remains unknown.

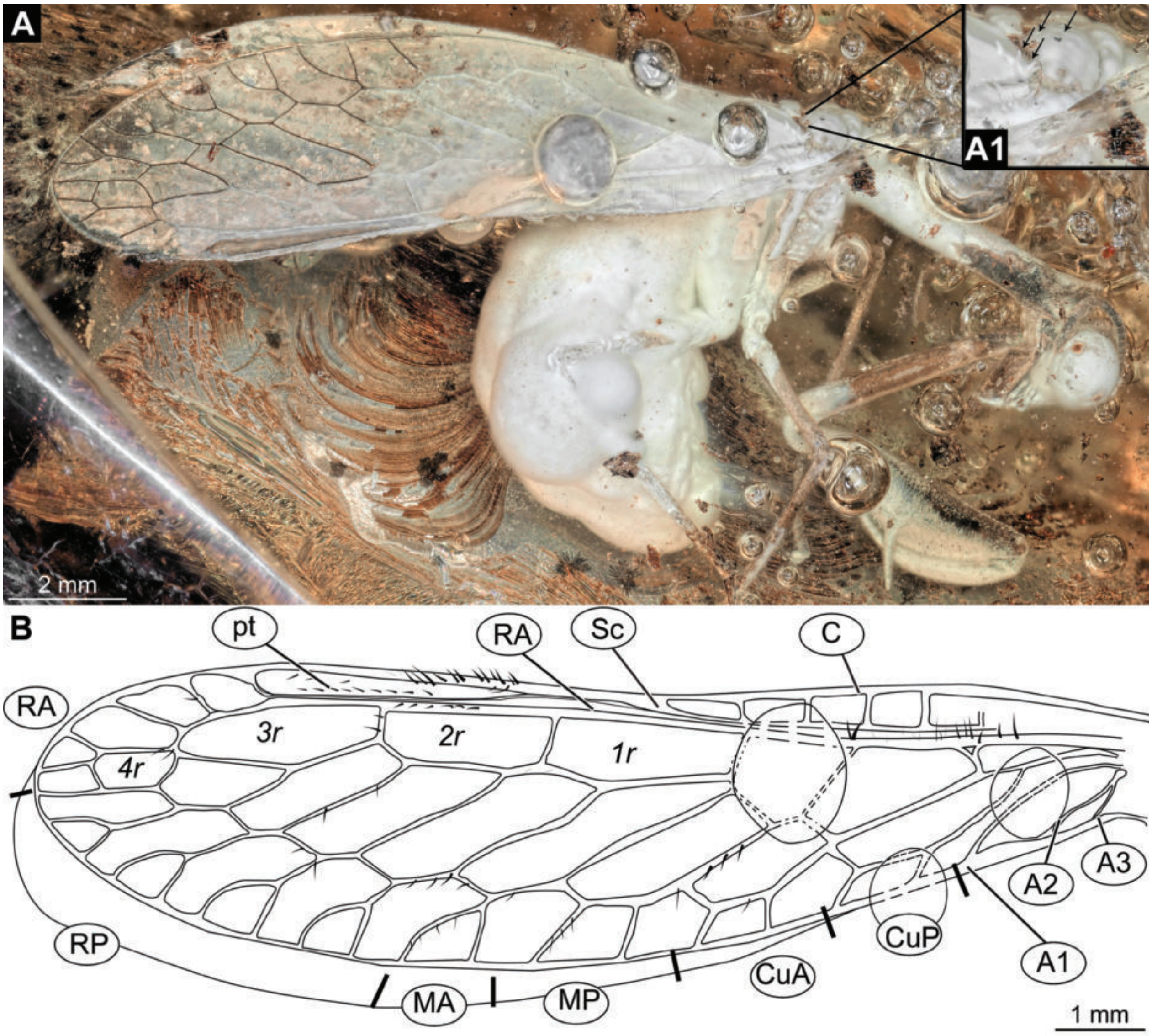

Figure 1. *Mantispa? damzenogedanica* sp. nov., holotype MG/B/1172. **A.** Photograph of the habitus in lateral view; **A1.** Mesothorax with stout setae visible through the Verlumung, enlarged (arrows); **B.** Drawing of the right forewing. Abbreviations (mostly veins): 1–4r = radial cells; A = anal; CuA = cubitus anterior; CuP = cubitus posterior; C = costa; MA, media anterior; MP, media posterior; pt = pterostigma; RA = radius anterior; RP = radius posterior; Sc = subcosta.

ZooBank. In accordance with the ICZN, the specific epithet is registered in ZooBank (www.zoobank.org) under the following LSID: 8C79CEEC-9800-4EB3-9665-B6FE756F83FF.

Diagnosis. The new specimen can be distinguished from all extant and fossil mantis lacewing representatives based on the following combination of characters: Head moderately wider than long; antennae relatively short, with flagellomeres compact and slightly wider than long in profile, last flagellomere gradually tapering distally; distal third of antennae seemingly with a pale band; occiput, pronotum and mesothorax bearing short, stout, erect setae, at least those from the occiput and pronotum not confined to raised bases; pronotum about 4.6× times longer than wide posteriorly, lacking abrupt constrictions throughout, apparently smooth; forewing with pterostigma well sclerotized, elongate, bearing sparse macrosetae along its entire length, distally ending at the midlength of cell 3r, proximal end tapered; forewing lacking supernumerary radial crossveins, with cell 4r small, proximally closed by a brief 3ra-rp crossvein; profemur with major integumentary process ('spine') smooth, length 0.52× the profemoral length, with ten smaller processes.

Description. Sex unknown. Winged lacewing, total length 13.7 mm as preserved. Head. Broad, short, moderately wider than long, 1.5 mm wide, 0.9 mm long, roughly triangular in anterior view. Ocular segment recognizable by large, ovoid compound eyes, 0.97 mm in diameter, prominent yet not particularly abutting, and trapezoid labrum, about 0.30 mm long. Posterior region of head capsule (occiput) with short, stout, erect setae visible through Verlumung, apparently not confined to raised bases. Antenna long (about 1.9 mm), with at least

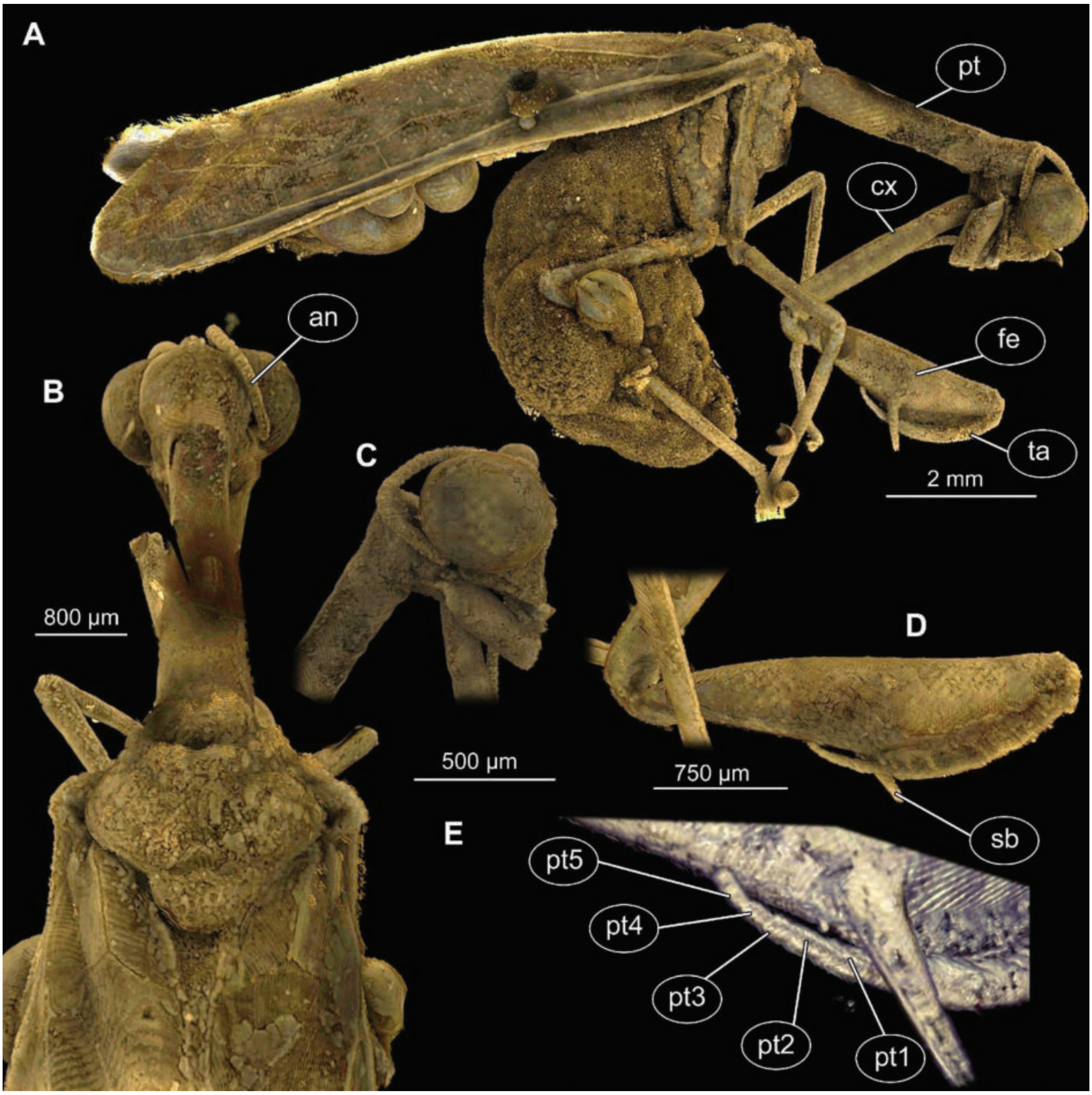

Figure 2. *Mantispa? damzenogedanica* sp. nov., holotype MG/B/1172, all volume renderings based on SRµCT. **A.** Habitus in lateral view; **B.** Head and thorax in dorsal view; **C.** Head and anterior pronotum in lateral view; **D.** Left raptorial foreleg in lateral view; **E.** Detail of the former. Abbreviations: an = antenna; cx = coxa; fe = femur; pt = prothorax; pt1–5 = tarsomeres 1–5; ta = protarsus; sb = submedial 'spine'.

22 articles (scapus, pedicellus, flagellomeres); distal third of antennae seemingly with a pale band. Flagellomeres rectangular in profile, slightly wider than long, compact, not significantly expanding in width distally. Mandibles 0.32 mm long. No further details accessible. Maxillae elongate, with proximal part, stipes (with two endites, galea and stipes), and distal part, palp, visible. Lacinia elongate, with eight strong distal teeth, 0.40 mm long. Galea about 0.14 mm long. Maxillary palp arising latero-distally from stipes, cylindrical, with three visible palpomeres. Total length of the palpomeres 0.50 mm long.

Labium oval in general shape. Details challenging to discern due to partial concealing by structures of thorax.

Thorax. Prothorax elongate, with pronotum tubular (fully fused ventrally), cylindrical, slightly decreasing in diameter distally, then expanding from its distal 2/3 onwards, 3× longer than wide (maximum width), 3.2 mm long, 1.1 mm wide basally, 0.6 mm wide medially, 0.8 mm wide distally. Prothorax densely covered with microtrochia, with smooth dorsal surface. Maculae (i.e., paired anteriodorsal areas of the pronotum distinctive in colour and/or shape, if apparent) with inconspicuous acute cusps. Pronotum very elongate, about 4.6× longer than wide posteriorly, lacking transversal ridges or corrugations (exact texture unknown due to Verlumung covering); pronotal prozone gently raised in lateral view,

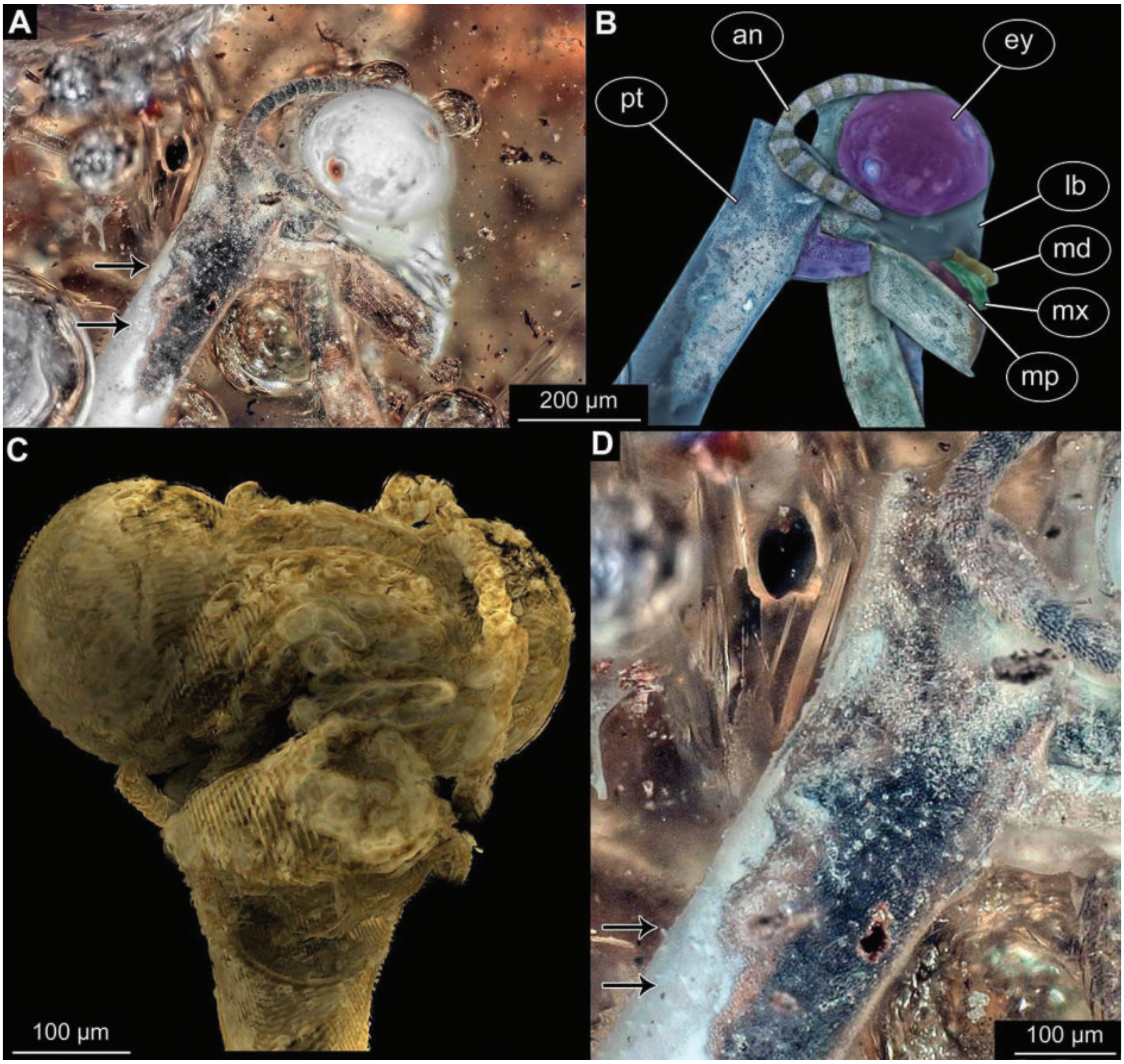

Figure 3. *Mantispa? damzenogedanica* sp. nov., holotype MG/B/1172. **A.** Photograph of the head and anterior pronotum in lateral view; **B.** Same, tagged and colour-marked; **C.** Head in ventral view, volume rendering based on SRµCT, showing visible mouthparts; **D.** Detail of the anterior pronotum in lateral view; note the stout setae (arrows). Abbreviations: an = antenna; ey = eyes; lb = labrum; md = mandible; mp = maxillary palp; mx = maxilla, proximal part; pt = prothorax.

anterior edge with two lateral rounded invaginations and a median, rather acute protrusion in dorsal view. Pronotum with short, stout, erect setae visible through Verlumung, not confined to raised bases. Prothorax bearing a pair of prominent appendages in far anterior position, i.e., the raptorial forelegs (only one preserved more completely). Coxa 3.40 mm long; trochanter, ca. 0.60 mm long; femur prominent, 3.30 mm long; tibia 2.48 mm long; tarsus 0.25 mm long; pretarsus not visible. Femur compressed, with prominent integumentary processes (‘spines’) originating medially; most prominent ‘spine’ submedial in position, located at 0.85 mm from proximal edge; at least ten additional, less-developed ‘spines’ present; exact armature hard to discern due to Verlumung. Stitz organs (terminal, sensory chitinous cones on integumentary processes) not discernible. Combined length of tibia and tarsus much shorter than that of femur. Tarsus composed of five tarsomeres. Tarsomere 1 not distally extended, longer than remaining tarsomeres. Pretarsal claw not visible; possible arolium not discernible.

Mesothorax trapezoid in dorsal view, 0.80 mm long. Dorsal surface with several setae visible through Verlumung. Femur 2.20 mm long; tibia 1.70 mm long; basitarsus 2.20 mm long; pretarsal claws simple.

Forewing 9.9 mm long, 2.7 mm wide, relatively narrow in shape; membrane apparently hyaline, with no visible infuscations (i.e., darkened areas) other than that of the pterostigma. Venation dark in colour; trichosors (i.e., veinlet-like structures between proper wing veins present

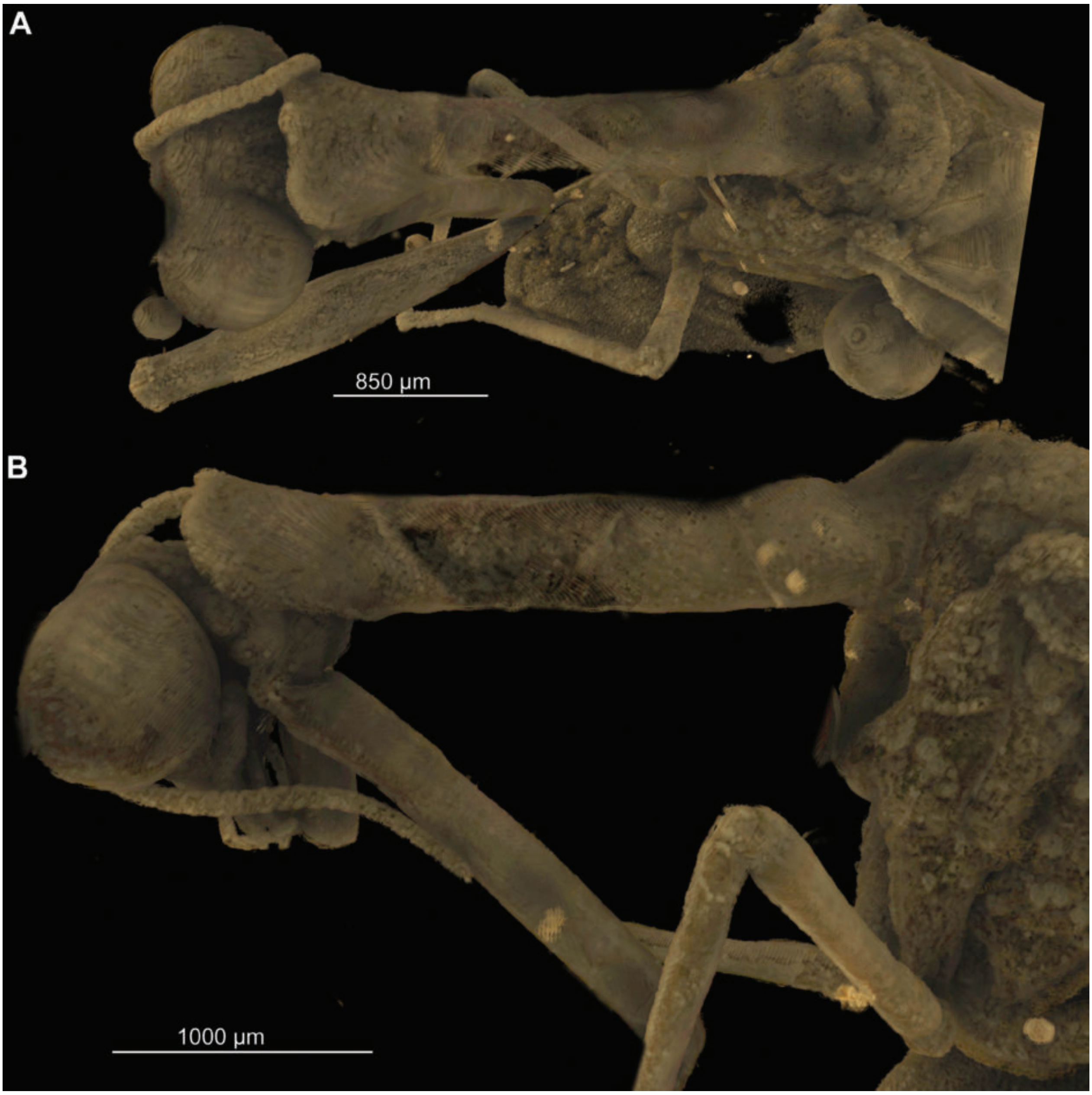

Figure 4. *Mantispa? damzenogedanica* sp. nov., holotype MG/B/1172, volume renderings based on SRµCT. **A.** Pronotum, dorso-oblique view; **B.** Pronotum, lateral view.

at the wing margin, often highly setose) absent along all costal margin; all veins sparsely setose, with R bearing particularly long setae; humeral vein not visible; five costal veinlets present; Sc apparently meeting C half the length of 1rp cell; no sc-r or sc-ra crossveins visible, if present; pterostigma well-sclerotised, apparently tapered basally, gently expanding distally, bearing sparse setae, beginning distally of 1ra-rp crossvein, ending midway of cell 3r; distal edge of pterostigma sub-perpendicular to costal margin (not markedly oblique/subparallel); space between C and RA relatively broad throughout; radial triangle distinct, relatively small; four radial cells (1r–4r) between RA and main branch of RP, the distalmost (4r) distinctly small, subtrapezoid, closed proximally by a very brief 3ra-rp crossvein; RP with five posterior branches; media simple, reaching wing margin right below cell 1r; CuA and CuP simple, forking not visible (blocked by a bubble), but likely proximal to radial triangle; cup-a1 crossvein not visible (blocked by a bubble); all anal veins simple, A1 concave; A2 sinuous, A3 slightly convex, these two fused proximally with a thick common stem; a1-a2 crossvein not visible.

Metathorax difficult to observe both on optical and 3d images. Femur 1.80 mm long; tibia 2.30 mm long; basitarsus 3.50 mm long, further distal tarsomeres not preserved. Hind wings almost entirely covered by the forewings and hence venation not discernible.

Abdomen. Abdomen largely concealed by Verlumung. Individual segments not discernible. Tergites appear simple, not keeled. Genitalia not visible.

3.2. Morphometric analysis

The final data set included three species of Mantispidae from the Jurassic, 14 from the Cretaceous, two from the Eocene, three from the Miocene, and 38 extant specimens. These encompass a wide diversity of the group, including representatives from all major ingroups ('subfamilies'), both extinct and extant. The shape analysis resulted in five effective principal components (PCs). For the graphical representation of the PC's correspondence to morphology, see Suppl. material 1: Fig. S1.

PC1 explains 43.08% of the overall variation. It is dominated by overall stoutness of the profemur and the size of the major, sub-medial integumentary process (='spine'), if present. A low value indicates an overall stout shape and a poorly developed major 'spine'. A high value indicates a more elongate shape and a well-differentiated major 'spine'.

PC2 explains 27.84% of the overall variation. It is dominated by overall stoutness of the profemur and the size of the major 'spine', if present. A low value indicates that this structure is more differentiated and elongate in shape, whereas a high value indicates that it is less developed, has a stouter shape, and the major 'spine' is less well set off.

PC3 explains 11.15% of the overall variation. It is dominated by the position of the major 'spine' (if present) along the proximal distal axis. A low value indicates a more distal position, whereas a high value indicates a more proximal position.

PC4 explains 5.22% of the overall variation. It is dominated by the shape of the proximal part of the profemur. A low value indicates a more pointed shape, while a high value indicates a more rounded shape.

PC5 explains 3.78% of the overall variation. It is dominated by the differentiation of the 'spines'. A low value indicates fewer, well set off 'spines', while a high value indicates a greater proportion of not-so-well set off 'spines'.

4. Discussion

4.1. Remarks on the new species

Inclusion in amber is an exceptional form of preservation. Nonetheless, while some specimens appear almost life-like and provide access to the finest of details, certain phylogenetically informative structures can be obscured. Different kinds of x-ray microtomography have significantly improved this circumstance, revealing structures of interest, which are often concealed by different elements such as other body structures, air bubbles, debris, or even Verlumung. Still, this method also has its limitations, and it can only resolve structures that are sufficiently well preserved and/or have enough contrast relative to other materials, particularly the surrounding matrix. This is also the case in the new specimen.

The specimen clearly is a representative of the group Mantispinae owing to, among other characters, the concave head vertex in frontal view (not domed); the forewing lacking trichosors, with 2A and 3A veins fused proximally with a thick common stem and a reduced jugal lobe; the mesonotal lobes angled anteriorly (rather than gently and broadly rounded); the procoxae lacking a transverse sulcus; the probasitarsus elongate, longer than remaining protarsomeres; the combined length of protibia and protarsus much shorter than that of the profemur; and the presence of simple, unbranched mesopretarsal claws (Lambkin 1986, Snyman et al. 2018). Assignment of the new species to the genus *Mantispa* is based on the head shape; the antennal flagellum being much shorter than the prothorax; all the flagellomeres being of similar shape, about as long as broad in profile; the presence of thick, erect setae on the occiput, prothorax, and mesothorax (diagnostic for *Mantispa* sensu Snyman et al. 2018); the prothorax generally cylindrical in shape and smooth, i.e., lacking corrugations or wrinkles; the forewing having Sc contacting C for a short distance prior to running along pterostigma; the elongate pterostigma; and the presence of a mesoscutal furrow, albeit weakly so (Snyman et al. 2018). Snyman et al. (2012, 2015) considered a pale band on the distal third of the antenna and a granulated prothorax as characters separating *Afromantispa* Snyman & Ohl, 2012 from *Mantispa*. The distal third of the antennae of the fossil appears to be lighter in colour as preserved and the texture of the prothorax seems to lack an obvious ornamentation, yet in fact both aspects remain unclear due to preservation, mostly because of the presence of Verlumung. Moreover, the integrity of *Afromantispa* has been put into question (Monserrat 2014). On the other hand, the inability to access the hind wing and the genitalia of the specimen would preclude a certain generic assignment of the present fossil for the sake of caution. In sum, the most conservative stance is to tentatively classify our specimen within *Mantispa*. We hope that future conspecific material can shed light on the present species, including a possible character gradation between *Mantispa* and *Afromantispa* as currently understood.

Mantispa? damzenogedanica sp. nov. represents the first record of an adult mantis lacewing in Baltic amber. The only two previous records of Mantispidae from Baltic amber were first-instar larvae (Ohl 2011, Wunderlich 2012). One was attached by its head to the pedicel of a spider, likely displaying what is termed 'boarding' behaviour (Ohl 2011, Jepson 2015). This circumstance explains why that fossil immature was interpreted as a representative of Mantispinae, as spider-boarding is known to only take place among larvae of this group at present. Otherwise, the morphology of the first instar did not allow for a more detailed interpretation (Ohl 2011). It is also impossible to determine whether the adult reported here is conspecific with the previously described larvae (Ohl 2011, Jandausch et al. 2018).

The new species is among the oldest representatives of Mantispinae currently known, certainly the oldest adult of the group described in amber. The previously oldest representative of Mantispinae, *Vectispa relicta* Cockerell, 1921, is from the Priabonian (upper Eocene) Bembridge marls, UK (Cockerell 1921, Jarzembowski 1980). The remaining fossils of the group described are either from the Oligocene, i.e., *Prosagittalata oligocenica* Nel, 1988 (Céreste, France, middle Oligocene) and *Climaciella? henrotayi* Nel, 1988 (Dauphin, France, middle Oligocene) (Nel 1988), or Miocene, i.e., *Dicromantispa electromexicana* Engel & Grimaldi, 2007 (Mexican amber, Burdigalian to Serravallian), *Dicromantispa moronei* Engel & Grimaldi, 2007 and *Feroseta prisca* Poinar, 2006 (Dominican amber, Burdigalian) (Poinar 2006, Engel and Grimaldi 2007). When compared to these other fossils of Mantispinae, *Mantispa? damzenogedanica* differs from (1) *V. relicta* in the pterostigma distally ending at the mid-length of cell 3r (ending at the distal part of that cell in *V. relicta*) and the presence of a fully closed cell 4r (Jarzembowski 1980); from (2) *P. oligocenica* in the longer pronotum (3.3× as long as wide in the Oligocene species), a higher number of posterior RP branches, and a different shape of the cell 4r (Nel 1988); from (3) *C.? henrotayi* (assuming it corresponds to a forewing) in the general wing shape, the shape of the radial cells, and the lower number of posterior RP branches (Nel 1988); from (4) *F. prisca* in the gradually tapering last flagellomere (abruptly changing in diameter in that species), pronotum lacking an anterior constriction (present immediately before the pronotal prozone in *F. prisca*), and a pterostigma well sclerotised (apparently not sclerotised on the Oligocene species) (Poinar 2006); and from both (5) *D. electromexicana* and *D. moronei* in its diagnostic stouter pronotal setation (these two species presumably lacking that sort of setation on the occiput as well), and considerably shorter pronotum than that of *D. electromexicana* (3× longer than the maximum width, vs 10× longer than the maximum width in *D. electromexicana*) (Engel and Grimaldi 2007).

4.2. Scarcity of Mantispidae in Baltic amber

The fact that the present specimen is the first record of an adult mantis lacewing from Baltic amber is remarkable taking into account that the latter is among the most intensively studied ambers worldwide (Weitschat and Wichard 2002). There are over a dozen adults of Mantispidae known from Cretaceous ambers (Poinar and Buckley 2011, Pérez-de la Fuente and Peñalver 2019, Lu et al. 2020, Shi et al. 2020a, b), and three records from Miocene ambers (Poinar 2006, Engel and Grimaldi 2007). In many instances, Baltic amber has yielded significantly more specimens than are known from Miocene ambers (e.g., Haug et al. 2020a, 2021b). The lower number of specimens of Mantispidae in Baltic amber compared to that of Cretaceous ambers could be explained by the overall decline of Neuroptera during at least the last 100 million years (e.g., Aspöck and Aspöck 2007). Yet, this cannot account for differences to Miocene ambers. In the latter, the three species known from Dominican amber do not seem to suggest much difference with the modern diversity of Mantispidae on present-day Hispaniola. Today, the fauna of Hispaniola includes at least five species of Mantispidae (Perez-Gelabert 2008, Hoffman et al. 2017). Modern Europe also has about five species of Mantispidae, but unlike Hispaniola where the current tropical environment is very similar to that of the Miocene, the regional climate of Europe has transitioned from a paratropical landmass and bordering archipelagos in the Eocene to a cooler temperate today. Thus, the potential for significant faunal alteration is greater. Nonetheless, given that mantis lacewings are generally more diverse and abundant in warmer habitats, one would presume that the Eocene fauna of Mantispidae in Baltic amber would be more prevalent than that of present-day Europe. In any case, there is an emerging understanding of the Baltic amber forest as a warm-temperate to temperate environment rather than a tropical forest (Kaasalainen et al. 2017, Sadowski et al. 2017, Rikkinen and Schmidt 2018). Thus, a more temperate climate in the area of Baltic amber deposition might partly explain the lower abundance of mantis lacewings in this deposit.

4.3. Changes on morphological diversity over time in Mantispidae

Already on a qualitative level, it is quite apparent that a significant loss in morphological diversity within Mantispidae has taken place since the Cretaceous (Lu et al. 2020). Our quantitative analysis of the raptorial appendages provides further support to that view. The Cretaceous specimens span a large area of the morphospace, while modern forms are restricted to a significantly smaller area. Hence, a significant part of the morphospace became lost over time in the group regarding one of their defining features, the raptorial foreleg, as well as their corresponding potential biologies. Furthermore, all the specimens from the Miocene plot within the area occupied by modern representatives of Mantispidae. This indicates that, already by the Miocene, the morphospace was restricted in a manner similar to that of modern diversity, although the rather low sample size makes this statement less conclusive. Regarding the Eocene specimens, the species described herein plots within the area of modern mantis lacewings, not far from extant species of *Mantispa*. Close, on the upper right of the new fossil plots a specimen of *Mantispilla perla* (from Lucchese 1956); even closer, on the lower right to the new fossil, plots a specimen of *Mantispa styriaca* (from Poivre 1974); right under it a specimen of *Anchieta fumosella* (from Alvim et al. 2019); to the lower left a specimen of *Plega* (species unknown; from Reynoso-Velasco and Contreras-Ramos 2008); to the upper left *Symphrasis varia* (from Tjeder 1959). It is important to note that the low resolution of the time bins in our analysis prevents us from inferring if the decline in the diversity of mantispid raptorial appendages was steady or more irregular.

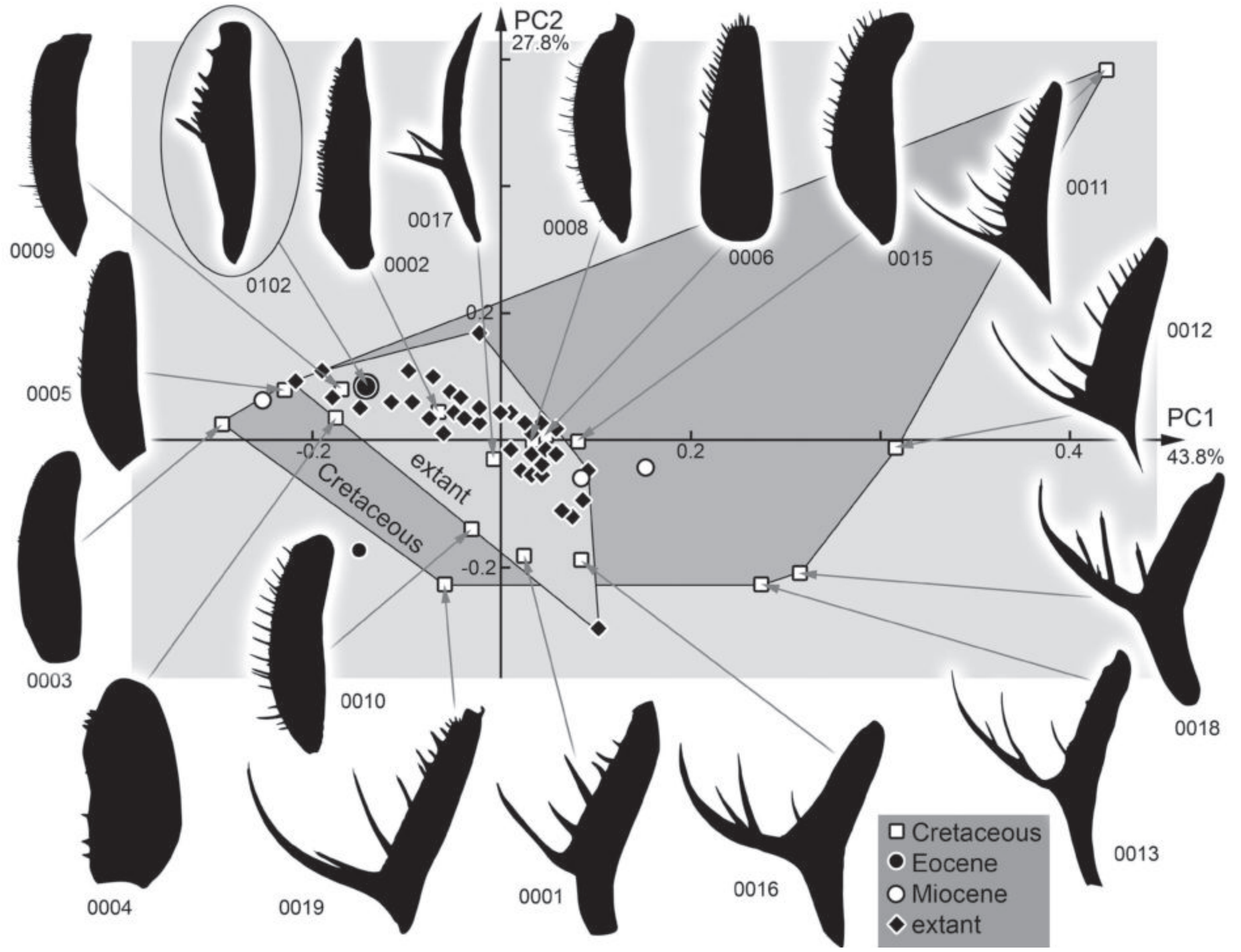

Figure 5. Morphospace occupied by the femora of raptorial legs of extant and fossil adult representatives of Mantispidae. The profemur of the new species has been circled. Total captured variation = 71.6%; 43.8% at PC1 and 27.8% at PC2. Numbers refer to Suppl. material 2: Table S1 (https://github.com/chironomus/Mantispidae-shape-analysis/blob/main/_CLEANED_FOR_EOCENE_Raptorial_Neuropterans.xls).

Although Winterton et al. (2018) and Ardila-Camacho et al. (2021) recovered Symphrasinae as sistergroup to Rhachiberothidae, with the latter work considering Symphrasinae as an ingroup of Rhachiberothidae, we prefer to follow here the classic view considering Symphrasinae as an ingroup of Mantispidae pending more supporting data. Note that even if Symphrasinae was not considered in the quantitative analysis this would not impact the overall results, as extinct species of Symphrasinae fall within or very close to extant representatives in the morphospace.

Although *Whalfera venatrix* was originally described as a representative of Mantispidae (Whalley 1983), subsequent works have generally regarded the species as a representative of Rhachiberothidae based on characters such as the protibia and protarsus being longer than the profemoral length, the presence of a first protarsal process, and the type of integumentary processes present in a dense group (Engel 2004, Wedmann and Makarkin 2007, Makarkin and Kupryjanowicz 2010, Pérez-de la Fuente and Peñalver 2019, Nakamine et al. 2020). However, universal consensus would appear to still be lacking, mostly related to the inability to ascertain several diagnostic characters from the holotype (see Jepson 2015). The fact that *W. venatrix* plots out of the morphospace of even extinct forms of Mantispidae (see black circle in Fig. 5 and Suppl. material 1: Fig. S2) further supports regarding the species as a representative of Rhachiberothidae.

Mantispa? damzenogedanica sp. nov. represents the sole definitive Eocene adult of Mantispidae preserved in amber. As the species is well circumscribed within modern morphospace, it tends to support the notion that declines in diversity of Mantispidae occurred prior to the Eocene, differing in this respect from what has been inferred to occur in some other neuropteran lineages where comparable quantitative data are available, at least from larvae (e.g., Aspöck and Aspöck 2007, Wang et al. 2016, Liu et al. 2016, 2018, Badano et al. 2018, Haug et al. 2019a, 2020a, b, c, Zippel et al. 2021). Admittedly, though, given the small sample for Eocene individuals of Mantispidae (n = 3), such a conclusion might just as likely represent an extreme sampling artefact. Thus, considerable exploration for further Cenozoic adults of Mantispidae is needed to enrich the available data from which patterns of diversity might be observed and conclusions on mantis lacewing evolution inferred.

5. Conclusions

The record presented herein illustrates a striking decline in the Mantispidae morphological diversity over the course of the Cretaceous and Cenozoic. This trend illustrates yet another case of the drastic decline of the morphological diversity in an ingroup of Neuroptera (Haug et al. 2021c).

Data availability

All data and results are presented in the main text, tables, figures and supplement. (https://github.com/chironomus/Mantispidae-shape-analysis/blob/main/_CLEANED_FOR_EOCENE_Raptorial_Neuropterans.xls).

Author contributions

Conceptualization: VB, RPF, ME, VB, JTH; Methodology:VB, RPF, ME, JTH; Formal analysis and investigation: RPF, ME, JTH, VB Writing – original draft preparation: JVB, ME, RPF, JTH; Writing – review and editing: all authors; Image preparation : JUH, JTH, CH, PGP, CK, MKH, CS, VB, ME, RPF; Analysis: JTH; Funding acquisition: JTH, VB, CH, JUH. Resources: JTH, VB, JUH.

Competing interests

The authors declare that they have no conflict of interest.

Acknowledgements

We are grateful to Mr. Jonas Damzen (Vilnius, Lithuania) for preparing the specimen and bringing it to our attention. We extend our gratitude to the editor and the reviewers, Michael Ohl and Louwtjie Snyman, for their insightful comments and edits. This project is supported by the Volkswagen Foundation in the frame of a Lichtenberg Professorship (J.T.H.). This study is also a contribution to the AEI/FEDER, UE project CRE CGL2017-84419 (R.P.-d.l.F.). V.B. was supported by the LMU Excellence Initiative via a LMU Junior Researcher Fund. R.P.-d.l.F. is funded by a Museum Research Fellowship from the Oxford University Museum of Natural History, UK. CK is currently funded by the Landesgraduiertenförderung MV. P.G.P. is funded by CAPES (Process 88887.161379/2017–00). Scanning of the specimen was supported by the DESY Block Allocation Group project "Scanning the past – Reconstructing the diversity in million years old fossil amber specimens using SRμCT" at PETRA III.

References

Alvim BGC, Machado RJP, Krolow TK (2019) Mantidflies (Neuroptera, Mantispidae) from Tocantins state (Brazil): distribution and identification key. Check List 15: 275–285. https://doi.org/10.15560/15.2.275

Ardila-Camacho A, Martins CC, Aspöck U, Contreras-Ramos A (2021) Comparative morphology of extant raptorial Mantispoidea (Neuroptera: Mantispidae, Rhachiberothidae) suggests a non-monophyletic Mantispidae and a single origin of the raptorial condition within the superfamily. Zootaxa 4992(1): 1–89. https://doi.org/10.11646/zootaxa.4992.1.1

Aspöck U, Aspöck H (2007) Verbliebene Vielfalt vergangener Blüte. Zur Evolution, Phylogenie und Biodiversität der Neuropterida (Insecta: Endopterygota). Denisia 20: 451–516.

Badano D, Engel MS, Basso A, Wang B, Cerretti P (2018) Diverse Cretaceous larvae reveal the evolutionary and behavioural history of antlions and lacewings. Nature Communications 9: e3257. https://doi.org/10.1038/s41467-018-05484-y

Baranov VA, Schädel M, Haug JT (2019) Fly palaeo-evo-devo: immature stages of bibionomorphan dipterans in Baltic and Bitterfeld amber. PeerJ 7: e7843. https://doi.org/10.7717/peerj.7843

Breitkreuz LCV, Winterton SL, Engel MS (2017) Wing tracheation in Chrysopidae and other Neuropterida (Insecta): a resolution of the confusion about vein fusion. American Museum Novitates 3890: 1–44. https://doi.org/10.1206/3890.1

Cockerell TDA (1921) LVII. Fossil arthropods in the British Museum. VI. Oligocene insects from Gurnet Bay, Isle of Wight. Annals and Magazine of Natural History 7: 453–480. https://doi.org/10.1080/00222932108632550

Engel MS (2004) Thorny lacewings (Neuroptera: Rhachiberothidae) in cretaceous amber from Myanmar. Journal of Systematic Palaeontology 2: 137–140. https://doi.org/10.1017/S1477201904001208

Engel MS, Grimaldi DA (2007) The neuropterid fauna of Dominican and Mexican amber (Neuropterida, Megaloptera, Neuroptera). American Museum Novitates 3587: 1–58. https://doi.org/10.1206/0003-0082(2007)3587[1:TNFODA]2.0.CO;2

Engel MS, Winterton SL, Breitkreuz LC (2018) Phylogeny and evolution of Neuropterida: where have wings of lace taken us? Annual Review of Entomology 63: 531–551. https://doi.org/10.1146/annurev-ento-020117-043127

Green T (2014) Praying Mantis Ultimate Care Guide. World Ideas Ltd., 134 pp.

Haug C, Shannon KR, Nyborg T, Vega FJ (2013a) Isolated mantis shrimp dactyli from the Pliocene of North Carolina and their bearing on the history of Stomatopoda. Boletín de la Sociedad Geológica Mexicana 65: 273–284. https://doi.org/10.18268/BSGM2013v65n2a9

Haug C, Herrera-Flórez AF, Müller P, Haug, JT (2019a) Cretaceous chimera – an unusual 100-million-year old neuropteran larva from the "experimental phase" of insect evolution. Palaeodiversity 12: 1. https://doi.org/10.18476/pale.v12.a1

Haug C, Haug GT, Baranov VA, Solórzano-Kraemer MM, Haug JT (2021b) An owlfly larva preserved in Mexican amber and the Miocene record of lacewing larvae. Boletín de la Sociedad Geológica Mexicana 73: A271220. https://doi.org/10.18268/BSGM2021v73n3a271220

Haug GT, Haug C, Pazinato P, Braig F, Perrichot V, Gröhn C, Müller P, Haug JT (2020a) The decline of silky lacewings and morphological diversity of long-nosed antlion larvae through time. Palaeontologia Electronica 23: a39. https://doi.org/10.26879/1029

Haug GT, Haug C, van der Wal S, Müller P, Haug JT (2021c) Split-footed lacewings declined over time: indications from the morphological diversity of their antlion-like larvae. PalZ online first. https://doi.org/10.1007/s12542-021-00550-1

Haug JT, Müller CHG, Sombke A (2013b) A centipede nymph in Baltic amber and a new approach to document amber fossils. Organisms Diversity & Evolution 13: 425–432. https://doi.org/10.1007/s13127-013-0129-3

Haug JT, Müller P, Haug C (2018) The ride of the parasite: a 100-million-year old mantis lacewing larva captured while mounting its spider host. Zoological Letters 4: 31. https://doi.org/10.1186/s40851-018-0116-9

Haug JT, Müller P, Haug C (2019b) A 100-million-year old slim insectan predator with massive venom-injecting stylets – a new type of neuropteran larva from Burmese amber. Bulletin of Geosciences 94: 431–440. https://doi.org/10.3140/bull.geosci.1753

Haug JT, Baranov V, Schädel M, Müller P, Gröhn C, Haug C (2020b) Challenges for understanding lacewings: how to deal with the incomplete data from extant and fossil larvae of Nevrorthidae? (Neuroptera). Fragmenta Entomologica 52: 137–168. https://doi.org/10.4081/fe.2020.472

Haug JT, Pazinato PG, Haug GT, Haug C (2020c) Yet another unusual new type of lacewing larva preserved in 100-million-year old amber from Myanmar. Rivista Italiana di Paleontologia e Stratigrafia 126: 821–832. https://doi.org/10.13130/2039-4942/14439

Haug JT, Haug GT, Zippel A, van der Wal S, Müller P, Gröhn C, Wunderlich J, Hoffeins C, Hoffeins H-W, Haug C (2021a) Changes in the morphological diversity of larvae of lance lacewings, mantis lacewings and their closer relatives over 100 million years. Insects 12: 860. https://doi.org/10.3390/insects12100860

Haug JT, Engel MS, Mendes dos Santos P, Haug GT, Müller P, Haug C (In press) Declining morphological diversity in snakefly larvae during last 100 million years. PalZ.

Hoffman KM, Flint OS, Perez-Gelabert DE (2017) The Mantispidae of the West Indies with special reference to the Dominican Republic (Neuroptera: Mantispidae). Insecta Mundi 0559: 1–15.

Hörnig MK, Sombke A, Haug C, Harzsch S, Haug JT (2016) What nymphal morphology can tell us about parental investment – a group of cockroach hatchlings in Baltic amber documented by a multi-method approach. Palaeontologia Electronica 19: 6A. https://doi.org/10.26879/571

Jandausch K, Beutel RG, Pohl H, Gorb SN, Büsse S (2018) The legs of “spider associated” parasitic primary larvae of *Mantispa aphavexelte* (Mantispidae, Neuroptera)–Attachment devices and phylogenetic implications. Arthropod Structure and Development 47(5): 449–456. https://doi.org/10.1016/j.asd.2018.06.002

Jarzembowski EA (1980) Fossil insects from the Bembridge Marls, Palaeogene of the Isle of Wight, southern England. Bulletin of the British Museum (Natural History) 33: 237–293.

Jepson JE (2015) A review of the current state of knowledge of fossil Mantispidae (Insecta: Neuroptera). Zootaxa 3964: 419–432. https://doi.org/10.11646/zootaxa.3964.4.2

Jepson JE, Heads SW, Makarkin VN, Ren D (2013) New fossil mantidflies (Insecta: Neuroptera: Mantispidae) from the Mesozoic of north-eastern China. Palaeontology 56: 603–613. https://doi.org/10.1111/pala.12005

Iwata H, Ukai Y (2002) SHAPE: A computer program package for quantitative evaluation of biological shapes based on elliptic Fourier descriptors. Journal of Heredity 9: 384–385. https://doi.org/10.1093/jhered/93.5.384

Kaasalainen U, Schmidt AR, Rikkinen J (2017) Diversity and ecological adaptations in Palaeogene lichens. Nature Plants 3(5): 1–8. https://doi.org/10.1038/nplants.2017.49

Kasiński JR, Kramarska R, Słodkowska B, Sivkov V, Piwocki M (2020) Paleocene and Eocene deposits on the eastern margin of the Gulf of Gdańsk (Yantarny P-1 borehole, Kaliningrad region, Russia). Geological Quarterly 64(1): 29–53. https://doi.org/10.7306/gq.1513

Lambkin KJ (1986) A revision of the Australian Mantispidae (Insecta: Neuroptera) with a contribution to the classification of the family. I. General and Drepanicinae. Australian Journal Zoology Supplements 3: 1–142. https://doi.org/10.1071/AJZS116

Liu X, Zhang W, Winterton SL, Breitkreuz LCV, Engel MS (2016) Early morphological specialization for insect-spider associations in Mesozoic lacewings. Current Biology 26: 1590–1594. https://doi.org/10.1016/j.cub.2016.04.039

Liu X, Shi G, Xia F, Lu X, Wang B, Engel MS (2018) Liverwort mimesis in a Cretaceous lacewing larva. Current Biology 28: 1475–1481. https://doi.org/10.1016/j.cub.2018.03.060

Lu X, Wang B, Zhang W, Ohl M, Engel MS, Liu X (2020) Cretaceous diversity and disparity in a lacewing lineage of predators (Neuroptera: Mantispidae). Proceedings of the Royal Society B: Biological Sciences 287: 20200629. https://doi.org/10.1098/rspb.2020.0629

Limaye A (2012) Drishti: a volume exploration and presentation tool. Developments in X-ray Tomography VIII. Proceedings of the Society of Photo-Optical Instrumentation Engineers (SPIE) 8506: 85060X. https://doi.org/10.1117/12.935640

Lytaev P, Hipp A, Lottermoser L, Herzen J, Greving I, Khokhriakov I, Meyer-Loges S, Plewka J, Burmester J, Caselle M, Vogelgesang M, Chilingaryan S, Kopmann A, Balzer M, Schreyer A, Beckmann F (2014) Characterization of the CCD and CMOS cameras for grating-based phase-contrast tomography. Developments in X-Ray Tomography IX: 921218. https://doi.org/10.1117/12.2061389

Machado RJP (2007) Taxonomia e sazonalidade das espécies de Mantispidae (Insecta: Neuroptera) da Amazônia Brasileira, Master thesis, Instituto Nacional de Pesquisas da Amazônia, Brazil, 127 pp.

Makarkin VN, Kupryjanowicz J (2010) A new mantispid-like species of Rhachiberothinae (Neuroptera: Berothidae) from Baltic amber, with a critical review of the fossil record of the subfamily. Acta Geologica Sinica 84: 655–664. https://doi.org/10.1111/j.1755-6724.2010.00238.x

McMongile O (2013) Keeping the Praying Mantis: Mantodean Captive Biology, Reproduction, and Husbandry, Coachwhip Publications, 202 pp.

Monserrat VJ (2014) Los mantíspidos de la Península Ibérica y Baleares (Insecta, Neuropterida, Neuroptera, Mantispidae). Graellsia 70(2): 1–52. https://doi.org/10.3989/graellsia.2014.v70.115

Moosmann J, Ershov A, Weinhardt V, Baumbach T, Prasad MS, LaBonne C, Xiao X, Kashef J, Hoffmann R (2014) Time-lapse X-ray phase-contrast microtomography for in vivo imaging and analysis of morphogenesis. Nature Protocols 9: 294–304. https://doi.org/10.1038/nprot.2014.033

Nakamine H, Yamamoto S, Takahashi Y (2020) Hidden diversity of small predators: new thorny lacewings from mid-Cretaceous amber from northern Myanmar (Neuroptera: Rhachiberothidae: Paraberothinae). Geological Magazine 157: 1149–1175. https://doi.org/10.1017/S0016756820000205

Nel A (1988) Deux nouveaux Mantispidae (Planipennia) fossils de l'Oligocene du sud-ouest de la France. Neuroptera International 5: 103–109.

Ohl M (2011) Aboard a spider – a complex developmental strategy fossilized in amber. Naturwissenschaften 98: 453–456. https://doi.org/10.1007/s00114-011-0783-2

Perez-Gelabert DE (2008) Arthropods of Hispaniola (Dominican Republic and Haiti): A checklist and bibliography. Zootaxa 1831: 1–530. https://doi.org/10.11646/zootaxa.1831.1.1

Pérez-de la Fuente R, Peñalver E (2019) A mantidfly in Cretaceous Spanish amber provides insights into the evolution of integumentary specialisations on the raptorial foreleg. Scientific Reports 9: 13248. https://doi.org/10.1038/s41598-019-49398-1

Poinar G (2006) *Feroseta priscus* (Neuroptera: Mantispidae), a new genus and species of mantidflies in Dominican amber. Proceedings of the Entomological Society of Washington 108: 411–417.

Poinar G, Buckley R (2011) *Doratomantispa burmanica* n. gen., n. sp. (Neuroptera: Mantispidae), a new genus of mantidflies in Burmese amber. Historical Biology 23: 169–176. https://doi.org/10.1080/08912963.2010.505024

Poivre C (1976) Observations sur la biologie, le comportement et le phénomène de convergence chez les Mantispidés [Planipennes]. Entomologiste 32: 2–19.

Rikkinen J, Schmidt AR (2018) Morphological convergence in forest microfungi provides a proxy for Paleogene forest structure. In: Krings M, Harper CJ, Cúneo NR, Rothwell GW (Eds) Transformative Paleobotany, Papers to Commemorate the Life and Legacy of Thomas N. Taylor, 527–549. https://doi.org/10.1016/B978-0-12-813012-4.00022-X

Sadowski EM, Schmidt AR, Seyfullah LJ, Kunzmann L (2017) Conifers of the Baltic amber forest and their palaeoecological significance. Stapfia 106: 1–73.

Schindelin J, Arganda-Carreras I, Frise E, Kaynig E, Longair M, Pietzsch T, Preibisch S, Rueden C, Saalfeld S, Schmid B, Tinevez JY, White DJ, Hartenstein V, Eliceiri K, Tomancak P, Cardonaet A (2012) Fiji: an open-source platform for biological-image analysis.Nature Methods 9: 676–682. https://doi.org/10.1038/nmeth.2019

Shi C, Yang Q, Shih C, Labandeira CC, Pang H, Ren D (2020a) Cretaceous mantid lacewings with specialized raptorial forelegs illuminate modification of prey capture (Insecta: Neuroptera). Zoological Journal of the Linnean Society 190: 1054–1070. https://doi.org/10.1093/zoolinnean/zlaa096

Shi C, Yang Q, Winterton SL, Pang H, Ren D (2020b) Stem-group fossils of Symphrasinae shed light on early evolution of Mantispidae (Insecta, Neuroptera), Papers in Palaeontology 6: 143–154. https://doi.org/10.1002/spp2.1265

Snyman LP, Ohl M, Mansell MW, Scholtz C (2012) A revision and key to the genera of Afrotropical Mantispidae (Neuropterida, Neuroptera), with the description of a new genus. ZooKeys 184: 67–93. https://doi.org/10.3897/zookeys.184.2489

Snyman LP, Sole CL, Ohl M (2015) On *Afromantispa* and *Mantispa* (Insecta, Neuroptera, Mantispidae): elucidating generic boundaries. ZooKeys 523: 89–97. https://doi.org/10.3897/zookeys.523.6068

Snyman LP, Sole CL, Ohl M (2018) A revision of and keys to the genera of the Mantispinae of the Oriental and Palearctic regions (Neuroptera: Mantispidae). Zootaxa 4450(5): 501–549. https://doi.org/10.11646/zootaxa.4450.5.1

Snyman LP, Ohl M, Pirk CWW, Sole CL (2020) A review of the biology and biogeography of Mantispidae (Neuroptera). Insect Systematics & Evolution 1: 1–42. https://doi.org/10.1163/1876312X-bja10002

Van Aarle W, Palenstijn WJ, De Beenhouwer J, Altantzis T, Bals S, Batenburg KJ, Sijbers J (2015) The ASTRA Toolbox: A platform for advanced algorithm development in electron tomography. Ultramicroscopy 157: 35–47. https://doi.org/10.1016/j.ultramic.2015.05.002

Van Aarle W, Palenstijn WJ, Cant J, Janssens E, Bleichrodt F, Dabravolski A, De Beenhouwer J, Batenburg KJ, Sijbers J (2016) Fast and flexible X-ray tomography using the ASTRA toolbox. Optics Express 24: 25129–25147. https://doi.org/10.1364/OE.24.025129

Wang B, Xia F, Engel MS, Perrichot V, Shi G, Zhang H, Chen J, Jarzembowski EA, Wappler T, Rust J (2016) Debris-carrying camouflage among diverse lineages of Cretaceous insects. Science Advances 2: e1501918. https://doi.org/10.1126/sciadv.1501918

Wedmann S, Makarkin VN (2007) A new genus of Mantispidae (Insecta: Neuroptera) from the Eocene of Germany, with a review of the fossil record and palaeobiogeography of the family. Zoological Journal of the Linnean Society 149: 701–716. https://doi.org/10.1111/j.1096-3642.2007.00273.x

Weitschat W, Wichard W (2002) Atlas of Plants and Animals in Baltic Amber. Verlag Dr. Friedrich Pfeil, Munich, Germany, 256 pp.

Whalley PES (1983) *Fera venatrix* gen. and sp. n. (Neuroptera, Mantispidae) from amber in Britain. Neuroptera International 2: 229–233.

Willmann R (1994) Die phylogenetische Position ursprünglicher Mantispidae (Insecta, Planipennia) aus dem Mesozoikum und Alt-Tertiär. Verhandlungen des Naturwissenschaftlichen Vereins in Hamburg (NF) 34: 177–203.

Winterton SL, Lemmon AR, Gillung JP, Garzon IJ, Badano D, Bakkes DK, Breitkreuz LCV, Engel MS, Moriarty Lemmon E, Liu X, Machado RJP, Skevington JH, Oswald JD (2018) Evolution of lacewings and allied orders using anchored phylogenomics (Neuroptera, Megaloptera, Raphidioptera). Systematic Entomology 43(2): 330–354. https://doi.org/10.1111/syen.12278

Wunderlich J (2012) "Frozen behaviour" in "vampires" of spiders – fossil insect larvae of the family Mantispidae (Neuroptera) as parasites of sac spiders (Araneae: Clubionidae) in Eocene Baltic amber. In: Wunderlich J (Ed.) Fifteen papers on extant and fossil spiders (Araneae) Hirschberg, Germany, 150–156.

Zippel A, Kiesmüller C, Haug GT, Müller P, Weiterschan T, Haug C, Hörnig MK, Haug JT (2021) Long-headed predators in Cretaceous amber – fossil findings of an unusual type of lacewing larva. Palaeoentomology 4(5): 475–498. https://doi.org/10.11646/palaeoentomology.4.5.14

Supplementary material 1

Graphical representation of the PC's correspondence to morpholog

Authors: Viktor Baranov, Ricardo Pérez-de la Fuente, Michael S. Engel, Jörg U. Hammel, Christine Kiesmüller, Marie K. Hörnig, Paula G. Pazinato, Corleone Stahlecker, Carolin Haug, Joachim T. Haug

Data type: figures

Explanation note: Figure S1. Shape-drivers of the principal components in the PCA analysis. Figure S2. Numbered specimens used in the analysis. Legend to the numbers in the Suppl. material 2: Table S1 (https://github.com/chironomus/Mantispidae-shape-analysis/blob/main/_CLEANED_FOR_EOCENE_Raptorial_Neuropterans.xls).

Link: https://doi.org/10.3897/fr.25.80134.suppl1

Supplementary material 2

Table S1. Cleaned for eocene Raptorial Neuropterans

Authors: Viktor Baranov, Ricardo Pérez-de la Fuente, Michael S. Engel, Jörg U. Hammel, Christine Kiesmüller, Marie K. Hörnig, Paula G. Pazinato, Corleone Stahlecker, Carolin Haug, Joachim T. Haug

Data type: table

Link: https://doi.org/10.3897/fr.25.80134.suppl2

Fossil Record 25 (1) 2022, 25–41 | DOI 10.3897/fr.25.80211

Deciphering the morphological variation and its ontogenetic dynamics in the Late Devonian conodont *Icriodus alternatus*

Catherine Girard[1], Anne-Lise Charruault[1], Thomas Gluck[1], Carlo Corradini[2], Sabrina Renaud[3]

1 *Institut des Sciences de l'Evolution de Montpellier (ISEM), Univ Montpellier, CNRS, EPHE, IRD, Montpellier, France*
2 *Università degli Studi di Trieste, Dipartimento di Matematica e Geoscienze, Trieste, Italy*
3 *Laboratoire de Biométrie et Biologie Evolutive, UMR 5558, CNRS, Université Claude Bernard Lyon 1, Université de Lyon, 69622, Villeurbanne, France*

http://zoobank.org/1DC16A46-9FFC-4388-87D7-F84E2B9FD714

Corresponding author: Catherine Girard (catherine.girard@umontpellier.fr)

Academic editor: Florian Witzmann ♦ **Received** 5 November 2021 ♦ **Accepted** 6 January 2022 ♦ **Published** 7 February 2022

Abstract

Identification of relevant taxonomic and evolutionary units is a recurrent issue in the fossil record, and all the more for ancient fossils devoid of modern equivalents such as conodonts. Extensive morphological variation has often led to the description of numerous species, subspecies or morphotypes, which may correspond to end-member morphologies reached through ontogeny. The platform elements of the Late Devonian conodont species *Icriodus alternatus* were characterized by rows of denticles coming into occlusion between opposite elements; each element grew by the incremental addition of lamellae and by the addition of successive triads during ontogeny. During the late Frasnian and the early Famennian, the important morphological variation within this species led to the description of three subspecies. An extensive sample of early Famennian *Icriodus alternatus* was quantified using 2D biometric measurements and denticle counts on 2D pictures, showing that the subspecies mainly differed in their size range but not in their general morphology. A 3D morphometric analysis was further performed on a subsample to characterize the shape of the ontogenetically older part of the elements. During ontogeny, early valleys between denticles tended to be filled, and the asymmetry between the inner and outer side of the element increased. These ontogenetic trends are responsible for the morphologies formerly described as the subspecies *Ic. alt. mawsonae* and *Ic. alt. helmsi*. Slight discrepancies between temporal ranges of the subspecies may be achieved through variations in range of size reached by the elements as a response to environmental changes. Disparity along ontogeny seems to follow an "hourglass model" suggesting a shift from relatively loose developmental constraints to a pattern of growth modulated by functional constraints during occlusion.

Key Words

Devonian, disparity, geometric morphometrics, hourglass model, *Icriodus alternatus*

1. Introduction

Conodonts are long extinct animals known from the Cambrian to the end-Triassic, without modern equivalent. These early vertebrates were an important part of the nektonic fauna increasing in richness through the Paleozoic era (Purnell 1995). They had a well-developed feeding apparatus composed of several tooth-like elements of complex shapes. Anterior elements formed a trapping structure, whereas posterior platform elements processed food items (Aldridge et al. 1987, Purnell and Donoghue 1997). These elements functioned in occlusion between right and left elements and displayed a complex morphology, sometimes even allowing a molar-like occlusion (Donoghue and Purnell 1999). This allowed conodont animals to exploit niches of first level consumers (Balter et al. 2019). The morphological complexity of the posterior platform elements, together with their rapid temporal evolution made, them efficient stratigraphic tools for the Paleozoic and Triassic eras.

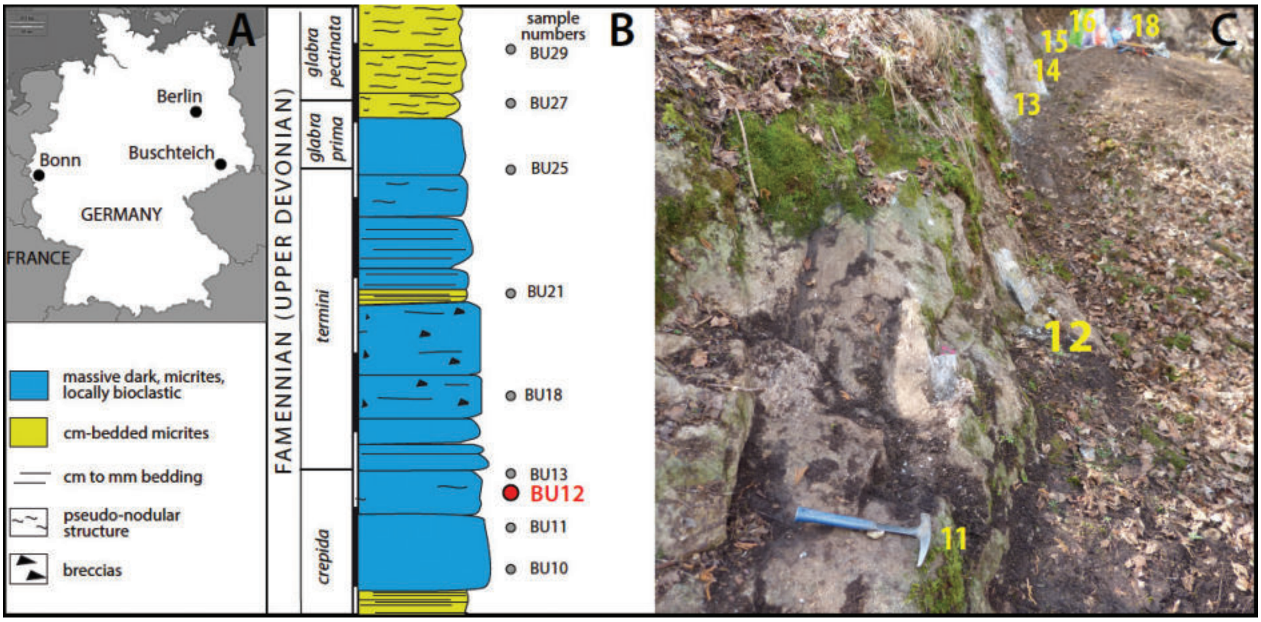

Figure 1. A. Location of the Buschteich section (Germany). **B.** Section log of the Lower Famennian in the Buschteich section and position of the studied sample, BU12 in bold (after Girard et al. 2017); **C.** Lower Famennian rocks succession in the Buschteich section.

This morphological diversity repeatedly raised the question of how to deal with an extensive phenotypic variation, leading description of numerous species, subspecies, or morphotypes (Philip and Jackson 1967, Sandberg and Ziegler 1973, Ziegler and Sandberg 1990). In the context of long extinct organisms, these concepts are not necessarily related to their meaning regarding modern animals for which genetics and behavior are crucial components to support the concept of species. As a consequence, the level to be considered as a relevant operational evolutionary unit is matter of debate (Girard et al. 2004, Girard and Renaud 2011). Conodont elements grew by the adjunction of lamellae through all the life of the animal, leading to larger elements in older animals (Donoghue 1998). Diagnostic features, and more generally, morphological variation, are also likely to increase along this continuous ontogeny, due to the fact that slight variation among individuals in the zones of preferential accretion will lead to an increasingly large phenotypic signature along growth. Considering such end-member phenotypes of a continuous variation as taxonomic units (Girard et al. 2004) might artificially inflate biodiversity estimates, and would not correspond to relevant units for evolutionary studies. Deciphering how the morphological diversity, as described by taxonomic units such as subspecies, develop along ontogeny may thus shed precious light on the operational units to be considered for evolutionary studies.

The genus *Icriodus* is documented from the Lower Devonian up to the Upper Devonian period. *Icriodus*, as many other genera, has a cosmopolitan distribution but several endemisms at specific level have been documented (Klapper and Johnson 1980, Clark 1984). Several apparatuses were described (Lange 1968, Nicoll 1982, Serpagli 1983, Simpson 1998, Suttner et al. 2017), that show a composition of twelve coniform elements and one pair of platform “Icriodontan” (I) elements. The Icriodontan elements are the characteristic feature for the description of *Icriodus* phenotypic diversity. Several species (e.g., *Ic. praealternatus*, *Ic. alternatus*, *Ic. deformatus*, *Ic. iowanensis*, *Ic. symmetricus*) have been described around the Frasnian – Famennian boundary (F/F), (numerical age 372.2; Cohen et al. 2013 updated). Despite the one of the major mass extinctions in Earth’s history (McGhee 1996), pronounced temperature decrease, and sea-level fall (Joachimski and Buggisch 2002, Girard and Renaud 2007), all four species survived the crisis (Dreesen and Houllenberghs 1980, Sandberg and Dreesen 1984, Spalletta et al. 2017). Morphological diversity even led to the description of subspecies which also survived to the crisis period, questioning whether they did correspond to relevant evolutionary units. The present study aims at quantifying the morphological variation within the most abundant *Icriodus* species at that time, *Icriodus alternatus* Branson and Mehl 1934, based on material from the Buschteich section (Thuringia, Germany) (Fig. 1). The samples, include the three subspecies *Ic. alternatus alternatus*, *Ic. alt. helmsi*, and *Ic. alt. mawsonae*. These taxa were analyzed using an extensive 2D biometric analysis complemented by a 3D biometric and geometric morphometric analysis. The hypothesis to be tested was that the subspecies corresponded to end-member phenotypes of a continuous variation generated through ontogeny.

2. Presentation of *Icriodus alternatus* and taxonomic background

One natural cluster of *Icriodus alternatus* has been described (Lange 1968), but the in-vivo position and orientation of

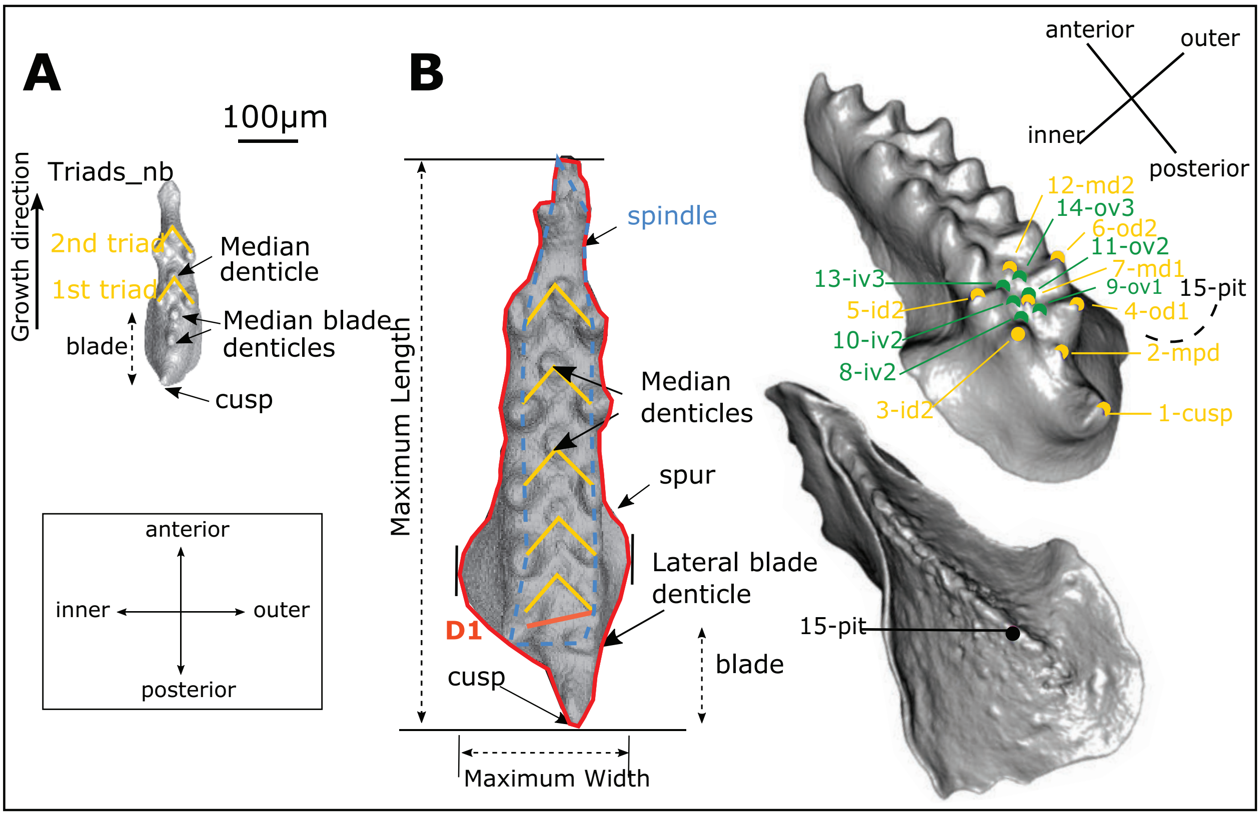

Figure 2. Morphological descriptors of I elements of *Icriodus alternatus*. **A.** “Small” specimen (UM BUS 031), upper (occlusal) view. 2D counts: Number of triads (Triads_nb): estimation of the number of triads, based on the presence of the pair of outer and inner denticles; Number of median denticles on the spindle area (Med_dent_nb); Number of lateral denticle on the blade area (Lat_blade_dent); Number of median denticle on the blade area (Med_blade_dent). **B.** *Icriodus alternatus helmsi* (UM BUS 035), upper (occlusal) view. Biometric measurements (D1, MaxLength, MaxWidth, area and spindle area). Triads in yellow; spindle area in blue dotted line, area of the 2D specimen in red, D1 distance between the inner and the outer denticles of the first triad in orange. **C.** *Icriodus alternatus alternatus* (UM BUS 033), upper and lower views (not to scale) with the position of the 3D landmarks (3D measurements). In green the valleys; in yellow the denticles.

Icriodontan elements within the animal mouth remains unknown. Therefore, the conventional nomenclature for the description of the elements (“anterior”, “posterior”, “inner” and “outer” side) (Branson and Mehl 1934, Sandberg and Dreesen 1984) has been retained.

The ontogenetic growth of Icriodontan elements, as described based on the species *Icriodus expansus* (Nicoll 1982), occurs through the successive addition of “triads”, consisting of one median denticle and a pair of lateral denticles (Fig. 2A). The first ontogenetic stage consists of a short blade with two or three denticles and one triad. The subsequent triads are added “anteriorly”, away from the blade. This ontogenetic process leads to the characteristic morphological feature of Icriodontan elements: the presence of three longitudinal rows of denticles forming a spindle (Figs 2B, 3).

Icriodus alternatus was initially characterized as bearing “denticles of the median row (…) small, rounded and isolated, alternating with the lateral denticles in position” (Branson and Mehl 1934, p. 226), with a “lachrymiform” basal cavity extending over the entire length of the element but larger in the posterior part. The authors also observed the “inconspicuousness of the median row of denticles” in *Ic. alternatus* compared to the strong denticles occurring in *Ic. symmetricus*. The reduction of the median row denticles was later emphasized by Klapper (in Ziegler 1975, p. 69), who noted that “the most distinctive aspect of the denticulation of I elements of *Ic. alternatus* is the extreme lateral compression and/or weak development of the middle row denticles. It is this feature that characterizes *Ic. alternatus*, rather than the alternation of the middle row denticles with those of the lateral rows, a denticulation common to other species of the genus”.

These characteristics are highlighted in the revised diagnosis of the species (Sandberg and Dreesen 1984, p. 157). *Icriodus alternatus* was described as “A species […] in which the longitudinal axis of the I element is nearly straight and the denticles of the medial and lateral rows alternate longitudinally. The medial-row denticles are strongly reduced in height and diameter relative to the lateral-row denticles, or they are obsolescent”. These authors discriminated two subspecies based on the position of the cusp, a conelike structure at the posterior extremity of the element (Fig. 2): the cusp is aligned with the median row of denticles in the nominal subspecies *alternatus*, whereas the cusp is aligned with one of the lateral rows in the subspecies *helmsi* (Sandberg and Dreesen 1984). The authors further observed that a reduction of the median denticles, leading to a “trough” between the lateral rows of denticles, a reduction most pronounced in stratigraphically more recent specimens (Sandberg and Dreesen 1984, p. 159).

A third subspecies, *Ic. alt. mawsonae*, was later introduced by Yazdi (1999) introduced, as “a subspecies […] with a row of very weakly expressed nodes located in a central trough between lateral rows of nodes. The basal cavity follows the shape of the spindle, expanding posteriorly” (Yazdi 1999, p. 197). The author interprets the new subspecies as an “aberrant form of *Ic. alt. alternatus* with the central nodes poorly developed”, and stated that *Ic. alt. mawsonae* had a “somehow larger basal” cavity than *Ic. alt. alternatus*. The characteristics of *Ic. alt. mawsonae* resemble those described by Sandberg and Dreesen (1984) for the stratigraphically late specimens of *Ic. alt. helmsi*. Indeed, the Icriodontan elements described by Yazdi (1999) come from only one sample from the upper part of an undifferentiated *crepida* Zone, that corresponds to the highest occurrence of *Ic. alt. helmsi*.

However, according to the recent revision of the Famennian conodont zonation (Spalletta et al. 2017), the three subspecies have a close stratigraphic distribution. Both *Ic. alt. alternatus* and *Ic. alt. helmsi* appeared during the Upper *rhenana* Zone (= FZ 12), whereas earliest *Ic. alt. mawsonae* are reported slightly later, during the late part of the *linguiformis* Zone (= FZ13c) (Ziegler and Sandberg 1990, Girard et al. 2005, Klapper and Kirchgasser 2016). The last occurrence (LO) of *Ic. alt. alternatus* is dated to the *Pa. gl. pectinata* (= Uppermost *crepida*) Zone, LOs of *Ic. alt. helmsi* and *Ic. alt. mawsonae* are observed slightly earlier during the *Pa. glabra prima* (= Upper *crepida*) Zone.

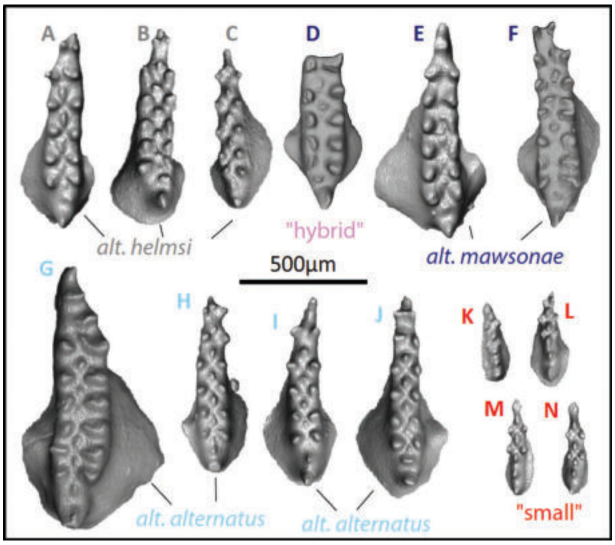

Figure 3. Morphological variation within the species *Icriodus alternatus*. Note the “hybrid” with morphological characteristic of both *helmsi* and *mawsonae*. **A.** UM BUS 034; **B.** UM BUS 035; **C.** UM BUS 036; **D.** UM BUS 037; **E.** UM BUS 038; **F.** UM BUS 039; **G.** UM BUS 033; **H.** UM BUS 040; **I.** UM BUS 041; **J.** UM BUS 042; **K.** UM BUS 043; **L.** UM BUS 044; **M.** UM BUS 045; **N.** UM BUS 031.

3. Material

The Buschteich outcrop (Thuringia, Germany), is a condensed pelagic section entirely composed of limestones (Fig. 1A, B). It contains a diverse and very abundant conodont fauna allowing the establishment of a fine biostratigraphic scheme (Girard et al. 2017). The section ranges from uppermost Frasnian to uppermost Famennian. Along this record, the present study focuses on specimens sampled from interval BU12, a level very rich in *Icriodus* elements (Girard et al. 2017), dated to the *Palmatolepis crepida* conodont Zone of Spalletta et al. (2017) (Fig. 1B, C).

Conodonts were extracted from the limestone samples following the classical procedure. Rock material was dissolved using diluted formic acid (10%). Residues were rinsed through 100 µm and 1 mm sieves; the fraction in between was dried and the conodonts were picked using a Nikon stereomicroscope. All P1 elements attributed to *Icriodus alternatus sensu lato*, hence including *Ic. alt. helmsi* and *Ic. alt. mawsonae*, were selected for the present study. Specimens with 3 triads or less were considered separate in a “small” elements group.

4. Methods

4.1. Data acquisition

4.1.1. 2D counts and measurements

A total of 191 elements were deemed to be in a suitable preservation state for a 2D quantitative study realized on SEM (Scanning Electron Microscope) pictures. Variables included the following counts (Fig. 2A):

- Number of triads (Triads_nb): estimation of the number of triads, based on the presence of the pair of outer and inner denticles;
- Number of median denticles on the spindle area (Med_dent_nb);
- Number of lateral denticle on the blade area (Lat_blade_dent);
- Number of median denticle on the blade area (Med_blade_dent).

Among these counts, the number of lateral and median denticles on the blade area were designed to characterize the *helmsi* morphotype, whereas the number of median denticles on the spindle area relative to the number of triads should characterized the *mawsonae* morphotype.

Furthermore, several 2D quantitative measurements were taken on 2D pictures of the upper (occlusal) surface of these 191 specimens using an image analysis device (Nikon NIS Elements software), in to describe the general size and shape of the elements (Fig. 2B):

- Maximum Length (MaxLength): maximum antero-posterior length of the element;

- Square root of the area of the 2D surface of the element in occlusal view (sqrtArea);
- Square root of the area of the spindle surface in occlusal view (sqrtSpinArea);
- Maximum Width (MaxWidth): largest inner-outer distance of the element;
- D1: distance between the inner and outer denticle of the first triad.

For 133 of these elements, measurements were taken on MEB pictures. A subset of 58 elements was µCT-scanned and measurements were taken on 2D snapshots of the 3D surface oriented with the occlusal surface up as for MEB pictures. The total sampling included 95 *Ic. alt. alternatus* s.s., 36 *Ic. alt. helmsi*, 17 *Ic. alt. mawsonae*, and 42 "small" specimens. One specimen displayed characters typical of both, *Ic. alt. helmsi* (most posterior denticle shifted towards the inner line of denticles) and of *Ic. alt. mawsonae* (absence of expressed first median denticle, md1) (Fig. 3D). Since the anterior was broken, it was discarded for most analyses, but was otherwise included in the *mawsonae* group.

4.1.2. Acquisition and extraction of 3D surfaces

A subset of 58 elements were glued on a toothpick and scanned at a cubic voxel resolution of ~1 µm using Phoenix Nanotom S microtomograph (µCT) on the AniRA-ImmOs platform of the SFR Biosciences, Ecole Normale Supérieure, Lyon (France). The scanning parameters were as follow: 100 kV, 70 µA, 3000 projections at 360° with no filter. The surface of the element was extracted semi-automatically using the thresholding tool in Avizo (v. 9.1—Visualization Science Group, FEI Company).

These elements were selected to document the morphological variation over a broad range of ontogenetic stages (from two to eight triads) and across subspecies. Most corresponded to *alternatus* specimens (N = 29), but the sampling included the *helmsi* (N = 11) and *mawsonae* (N = 5) subspecies. One specimen displayed characters typical of both, *helmsi*-like with the most posterior denticle shifted towards the inner row of denticles and of *mawsonae* with absence of expressed first median denticle, md1; it was depicted as "hybrid" but attributed to the subspecies *mawsonae* in statistical analyses (Fig. 3D). In the 2D analyses, "small" specimens were those with three or less triads (N = 12). Specimens with little or no damage were preferentially selected, but several broken elements were included because of their interest in documenting the morphological variation. Three specimens were anteriorly broken, hindering the measurements of their length.

All the specimens are housed in the collections of the University of Montpellier. The reconstructed 3D surfaces of the specimens illustrated on Fig. 2 and Fig. 3 (collection numbers UM BUS 031 to UM BUS 045) have been deposited in MorphoMuseuM (Girard et al. 2022).

4.1.3. Length, width and 3D landmarks

3D surfaces of the left elements, spur to the right when the element is seen in occlusal view), were subjected to a mirror transformation and measured as right elements. Length, measured as the greatest antero-posterior distance, and width, the largest inner-outer dimension, were manually measured on the 3D surfaces using Avizo. Fifteen 3D landmarks (Suppl. material 1: Table S1, Fig. 2C) were manually positioned on the surface of each element using IDAV Landmark Editor v.3.6 (Wiley et al. 2005). They document the "core" area of the element, including the blade and first two triads: being located on the first parts to develop along the ontogeny, these landmarks can be identified on all specimens including small ones. They corresponded to the tip of the cusp, the most posterior denticle (mpd) following the cusp, the tip of the inner, outer and median denticles of the first two triads, as well as the valleys between the median and lateral denticles. The pit was also documented. Defined as the deepest point of the basal cavity, its position was difficult to assess in a comparable manner in all elements, because of the occurrence of more posterior secondary "pits" in some elements. The "pit" landmark was thus taken as the deepest point in the vicinity of the first median denticle (md1).

4.2. Analysis of counts and 2D measurements

Correlations involving counts were assessed using Kendall's rank order test; correlations between numerical variables were assessed using the Pearson correlation coefficient. Differences between the *alternatus*, *helmsi*, *mawsonae*, and small groups were tested using non-parametric Kruskal-Wallis tests and pairwise Wilcoxon comparisons.

Linear models using Maximum Length as the independent variable were used to assess relationships of the different variables along ontogenetic growth, and to provide size-corrected residuals. Models including Maximum Length and group as factor were also performed. They allowed to test the significance of the differences between groups while taking size into account; the interaction between both factors indicated whether slopes were similar in the different groups.

All these tests were performed using R (R Core Team 2017).

4.3. Analyses of the 3D dataset: distances, heights, and geometric morphometrics

4.3.1. Length and width

The relationship between element length and width was assessed using a linear regression. Since width was available for all elements, the relationship length ~ width was used to interpolate length values for the three anteriorly broken specimens.

4.3.2. Characterization of the element geometry using interlandmark distances

In order to document the growth of the different parts of the elements, inter-landmark distances were calculated from the landmark coordinates. The following distances were considered:

- dlat1, distance between the inner and outer denticles of the 1st triad [= d(id1, od1)]. This distance is the equivalent in 3D of the distance D1 in 2D, but incorporates differences in height between the two lateral denticles of the triad;
- dlat2, distance between the inner and outer denticles of the 2nd triad [= d(id2, od2)]; this is the equivalent for the second triad of dlat1;
- d(cusp, mpd), distance between the cusp and the most posterior denticle following it;
- d(mpd, md1), distance from mpd to the median denticle of the 1st triad md1;
- d(mpd, id1) and d(mpd, od1), distances from mvd to the inner and outer denticles of the 1st triad, respectively.

How these distances varied along the ontogeny was investigated using linear regression of each distance *vs* element length. Interpolated values were used for visual representations but were not included in the calculation of the regressions.

4.3.3. Denticle height and pit depth: estimation by the triangle geometry

In order to estimate the height of the denticles above the valleys, geometric properties of the triangle were used. For any triangle, the semi-perimeter (p) and the area (S) can be derived can be calculated from the sides of the triangle a, b, and c, following to the two equations $p = (a + b + c) / 2$ and $S = \text{sqrt}[p (p-a) (p-b) (p-c)]$. The altitude h at the summit A (opposed to side a) can then be obtained as $h = 2S/a$.

According to these formulas, the height of md1 can be approximated as the altitude of a triangle defined by the tip of the denticle (md1) and the two valleys surrounding it along a same line (iv1 and ov2, or alternatively ov1 and iv2) (Suppl. material 3: Fig. S1), the sides of the triangles being calculated as the corresponding inter-landmark distances. The height of md1 was thus calculated using the triangles md1-iv1-od2 and md1-od1-iv2 and assessed as the mean of both estimates. A similar procedure allowed the depth of the pit to be estimated from the same valley points.

The height of the outer and inner denticles were assessed using the valleys along the same line: h-id1, based on the triangle id1-iv1-ov2; h-od1 based on od1-ov1-iv2; h-id2 based on id2-iv2-ov1, and h-od2 based on od2-ov2-iv1.

The relationship of denticle height and pit depth with element length was assessed using linear regression. Linear models including, groups and their interaction were further investigated.

4.3.4 3D geometric morphometrics

The configurations of the fifteen 3D landmarks were superimposed using a generalized Procrustes analysis (GPA) standardizing size, position, and orientation while retaining the geometric relationships between specimens (Rohlf and Slice 1990). The aligned coordinates constituted the shape variables for further analyses. The size of the landmark configuration was estimated by the centroid size where CS: square root of the sum of squared distances from the landmarks and semi-landmarks to the centroid).

Size-related variations in shape and differences between groups (*alternatus*, *helmsi*, *mawsonae* and “small” groups were investigated using Procrustes ANOVA. With this approach, the Procrustes distances among specimens are used to quantify the components of shape variation, which are statistically evaluated via permutation, here, 9999 permutations (Adams and Otarola-Castillo 2013). The allometric relationship was visualized as the common allometric component (CAC) derived from an analysis of the aligned coordinates vs. size (Adams et al. 2013). Procrustes ANOVA were also used to assess models including size, groups, and their interaction as factors.

The Procrustes superimposition, allometric analysis, and Procrustes ANOVA were performed using the R package geomorph (Adams and Otarola-Castillo 2013).

5. Results

5.1. 2D morphological variation: overall changes with size and localized differences between subspecies

The 2D sampling included elements with two to eight triads (Fig. 4A). Maximum length increased with the number of triads (Kendall’s Tau = 0.7928004, $p < 2.2e-16$). Groups were different for their maximum length (Kruskal-Wallis $p < 2.2e-16$), taken as a proxy of size. The subspecies *alternatus* covered a large size range whereas *helmsi* and *mawsonae* were both characterized by a similar large size (Fig. 4B, Table 1).

All variables, being counts or numeric measurements, were significantly related together (Fig. 5, Suppl. material 2: Table S2). Continuous measurements were particularly highly correlated with each other (e.g. Fig. 6), due to an overall increase in all dimensions when triad number increases. The distance between the inner and outer denticle of the first triad, D1, was the less strongly correlated to the other measurements. Among counts, the number of lateral denticles on the blade was the less strongly associated with other variables. One noticeable exception emerged in this pattern: the number of median denticle on the blade was significantly related with the other variables, but it decreased with triad number and overall size.

The variables specifically designed to capture the characteristics of the subspecies indeed showed significant

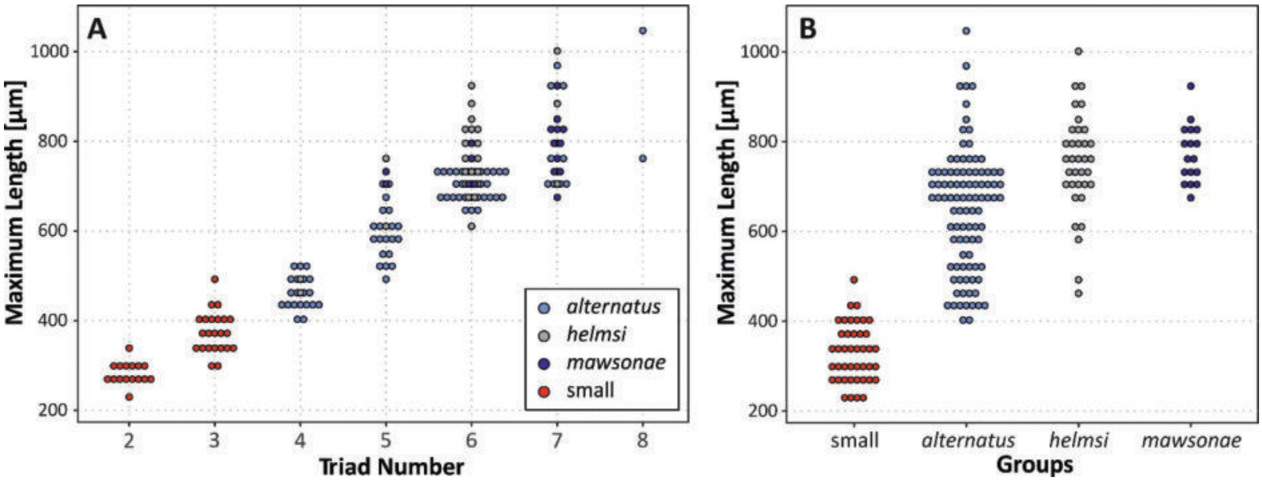

Figure 4. Maximum length of *Icriodus* elements along triad numbers (**A**) and among the subspecies (**B**) represented as dot plots. Each dot corresponds to one observation (specimen); dots within a given bin width are stacked. Here, bin width = 30.

Table 1. Differences between subspecies, for maximum length, ratio between the number of median denticles and triad number, the number of lateral denticles on the blade, and the residuals of √Area, √Spindle Area, maximum width and distance D1 vs. maximum length. KW: p-value of a Kruskal-Wallis test; if significant, p-values of pairwise Wilcoxon tests are provided below. In bold, p-value < 0.001, in italics p-value < 0.05.

Maximum Length		KW	**< 2.2e-16**
	small	**alternatus**	**helmsi**
alternatus	**< 2e-16**	-	-
helmsi	**< 2e-16**	**9.2e-05**	-
mawsonae	**2.9e-14**	**9.2e-05**	0.5
Med_dent_nb/Triad_nb		KW	**3.804e-06**
	small	alternatus	helmsi
alternatus	*0.0068*	-	-
helmsi	*0.0038*	0.2104	-
mawsonae	**5.2e-05**	*0.0017*	*0.0437*
Lat_Blade_Dent_nb		KW	**< 2.2e-16**
	small	alternatus	helmsi
alternatus	0.1370	-	-
helmsi	**6.9e-14**	**< 2e-16**	-
mawsonae	*0.0140*	0.106	**6.9e-06**
residuals sqrtArea		KW	0.1367
residuals sqrtSpinArea		KW	0.2194
residuals Max Width		KW	0.1759
Residuals D1		KW	0.6757

differences. The number of median denticles on the spindle area of course increased with triad number, but to a lesser degree for *mawsonae* (Fig. 7A). As a consequence, the ratio of the median denticles number vs triad number differed between groups (Table 1).

The number of median blade denticles decreases with triad numbers (Fig. 7B), but concomitantly, the number of lateral blade denticles tends to increase, particularly in *helmsi* (Fig. 7C). As a consequence, the number of lateral blade denticles, differed between *helmsi* and the other groups (Table 1). In contrast, the subspecies did not differ in the numeric variables when the effect of size increase was taken out by considering residuals *vs.* maximum length (Table 1).

The homogeneity of the subspecies when considering their general aspect was confirmed using linear models including maximum length and groups as factors (Table 2). While maximum length always displayed a highly significant effect, the group effect was significant only for √Spindle Area and maximum width, with no significant interaction showing that the four groups shared similar slopes of variation with maximum length. However, when excluding the "small" group, the group effect was not significant anymore, showing that the three subspecies *Ic. alt. alternatus*, *Ic. alt. helmsi* and *Ic. alt. mawsonae* did not differ in their overall dimensions, when taking out the general size increase.

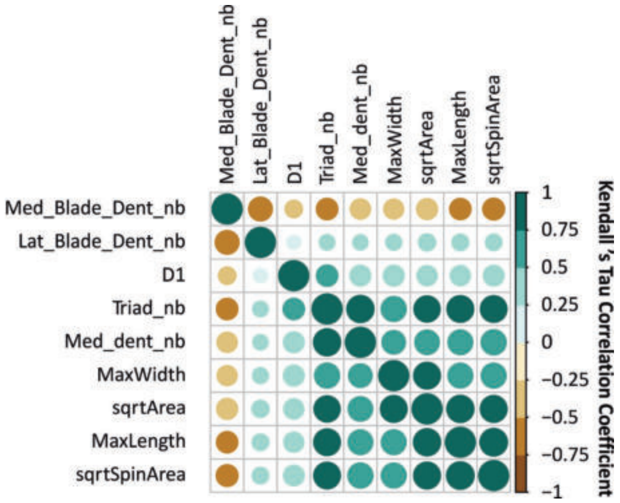

Figure 5. Correlogram of the relationship between each pair of counts and numeric variables in the *Icriodus* dataset. Size of the circle is proportional to the strength of the correlation, color varies with the value of the correlation. Kendall's tau correlation coefficient has been used for the representation. Variables are ordered according to a hierarchical clustering of the correlations.

5.2. Disparity through ontogeny

In order to assess how morphological disparity varied along ontogeny, the variance of the different variables was assessed for each triad number. Triads 1 and 2, and

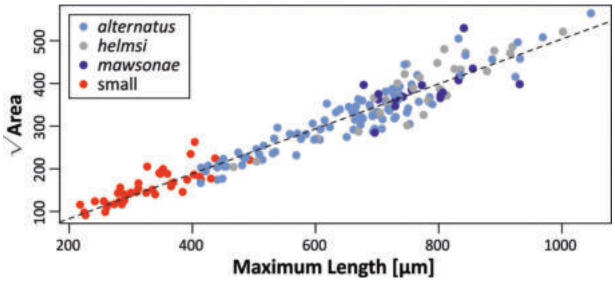

Figure 6. Relationship between maximum length and the square root of total area across the four groups of *Icriodus*. The dotted line represents the linear correlation between both variables (Pearson correlation coefficient = 0.9598, p-value < 2.2e-16).

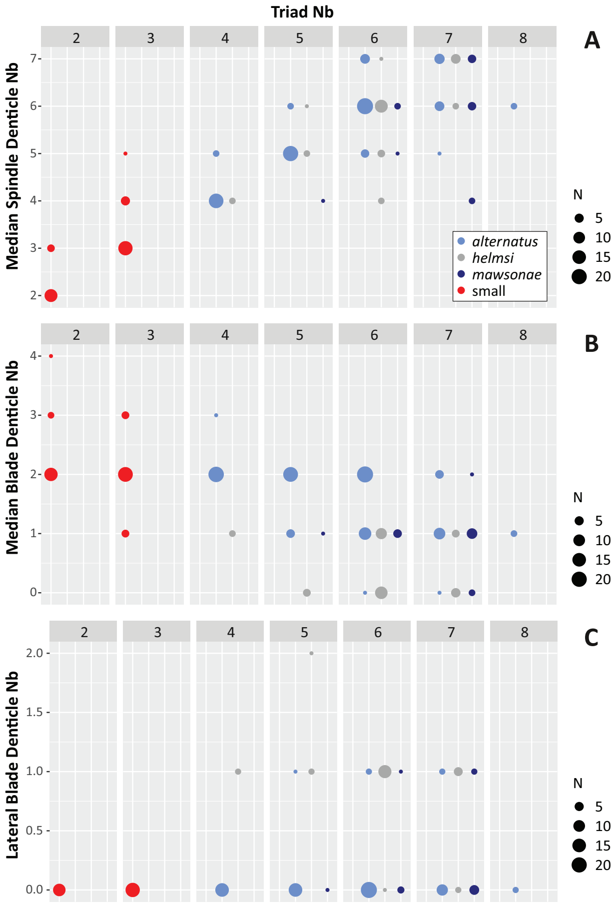

Figure 7. Number of median denticles on the spindle area (**A**), of median blade denticles (**B**) and of lateral blade denticles (**C**) along triad numbers in the four groups. The size of the symbols is proportional to the number of observations (N).

7-8, were grouped together because of insufficient data. The relative number of median denticles (Med_Dent_nb/Triads_nb) was considered together with maximum length and width, √ of the total area and spindle area, the distance between the inner and outer denticles of the first triad (D1), and the number of lateral and median denticles on the blade. To level out the effect of different scales and of size increase, variables were centered to the mean and divided by the standard deviation).

Table 2. Effects of maximum length and subspecies (Ssp) on total area (√), spindle area (√), maximum width and the distance between the inner and outer denticle of the first triad (D1). P-values of linear models including maximum length and groups are given; left, including the four groups; right, excluding the “small” group.

	Four groups		Large only	
sqrtArea				
MaxLength	< 2e-16	***	< 2e-16	***
Ssp	0.05268		0.5478	
ML:Ssp	0.16214		0.1800	
sqrtSpinArea				
MaxLength	< 2e-16	***	< 2e-16	***
Ssp	0.03443	*	0.7423	
ML:Ssp	0.08720		0.3426	
MaxWidth				
MaxLength	< 2e-16	***	< 2e-16	***
Ssp	0.03522	*	0.9998	
ML:Ssp	0.66452		0.7563	
D1				
MaxLength	< 2e-16	***	8.632e-09	***
Ssp	0.27271		0.4680	
ML:Ssp	0.06596		0.0228	*

The patterns of variance through ontogeny were compared using Kendall rank order tests (Fig. 8A), showing little congruence except for maximum length, √Area, and √Spindle Area. However, all variables showed a minimum variance at the stage Triad 4 (Fig. 8B), to the exception of the number of lateral denticles on the blade, showing little variance in triads 1-2-3, but starting to increase in variance at triad 4. On the contrary, the variance in relative numbers of median denticles on the spindle was high in the first triads (1-2-3), decreased abruptly at triad 4, then re-increasing gently thereafter.

5.3. Variations in 3D distances and denticle heights

Length vs width in the 3D dataset

When focusing on the 3D subset, length and width measured on the 3D surfaces were strongly related (Pearson’s product-moment correlation R = 0.920, p-value: < 2.2e-16), with the length increasing 1.5 faster than the length (slope of the regression: 1.509) (Suppl. material 4: Fig. S2). This regression provided interpolated length values for the three elements that have a missing anterior part.

5.4. Distances, denticle height and pit depth as a function of growth

The analysis of the heights and distances focused on the most posterior part of the element, including the first triad, because these features can be measured in almost all specimens, including small ones, and document the growth of the elements. Most variables increase with growth as indicated by increasing length (Table 3, Fig. 9). The distance between the tip of two lateral denticles of the first triad (dlat1) shows the

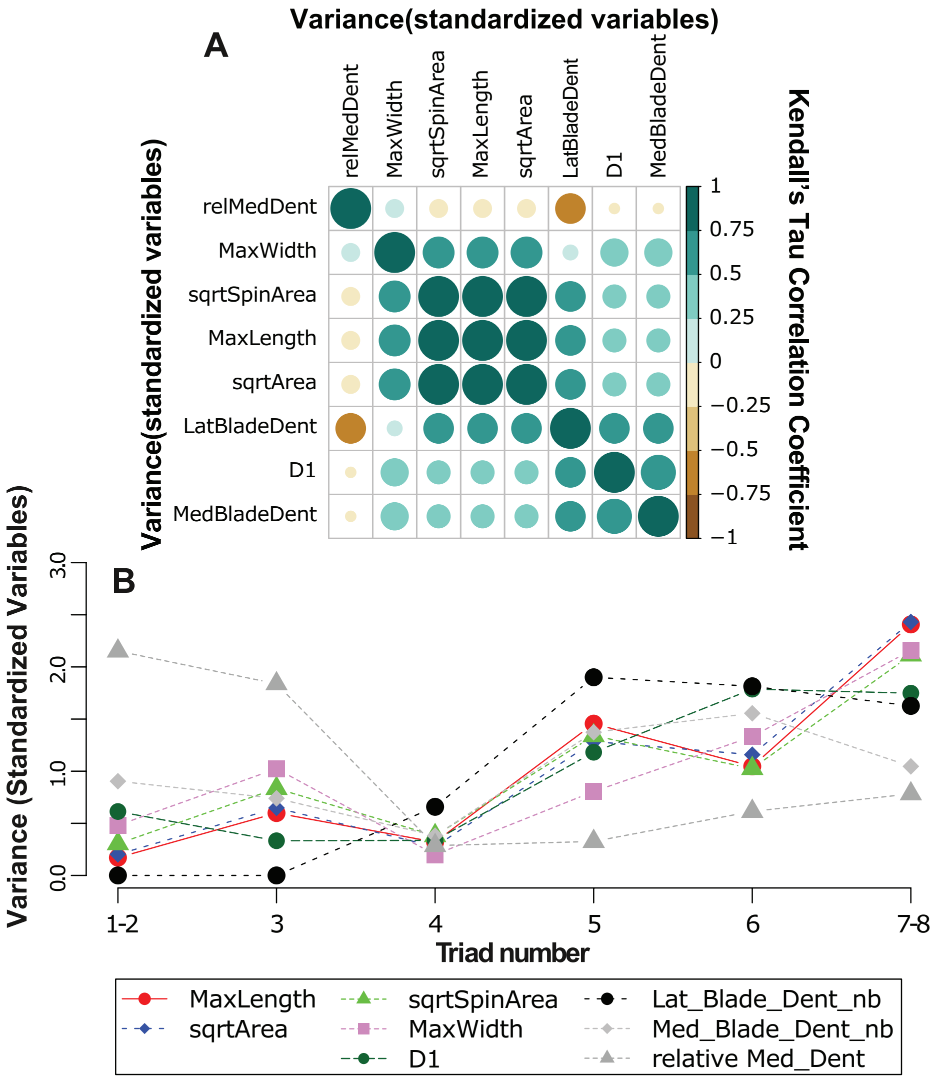

Figure 8. Disparity through ontogeny. The variance of the different reduced-centered variables was estimated for each triad number (triads 1-2 and 7-8 grouped). **A.** Correlogram showing the congruence of the pattern between variables, estimated using Kendall's tau coefficient; **B.** Change in the level of variance through ontogeny. The variance of each variable has been scaled by its mean in order to represent the different lines on a single graph. Variables considered were: MaxLength: maximum length, sqrtArea: √ of the total area of the element; sqrtSpindleArea: √ of the spindle area; MaxWidth: maximum width; D1: distance between the inner and outer denticles of the first triad; LatBladeDent: number of lateral denticles on the blade; MedBladeDent: number of median denticles on the blade; relMedDent: number of median denticles on the spindle, divided by triad number.

Table 3. Relationship of element length with inter-landmark distances, denticle height and pit depth. Above, linear model of variable vs length: R, Pearson's product-moment correlation R, associated p-value, and slope of the regression. Below, p-values of linear models with two factors: length, group [*alternatus*, *helmsi*, *mawsonae* {including the "hybrid"}, small {three or less developed triads}], and their interaction. In bold p-values < 0.001, in italics p < 0.01.

	Pit depth	Height md1	dlat1	dlat2	Height id1	Height od1	d(mpd, id1)	d(mpd, od1)	d(mpd, md1)	d(cusp, mpd)
p-value lm(~ Length)										
R	0.661	-0.639	0.896	0.797	0.434	0.599	-0.018	0.468	0.104	0.690
p-value	**4.02e-08**	**1.49e-07**	**<2.2e-16**	**3.32e-13**	**0.0009**	**1.38e-06**	0.8962	**0.0003**	0.4498	**5.70e-09**
Slope	0.06	-0.04	0.11	0.11	0.03	0.04	0.00	0.03	0.01	0.07
p-value lm(~ Length * Group)										
Length	**2.25e-08**	**1.65e-07**	**<2e-16**	**1.20e-12**	*0.0013*	**8.66e-07**	0.8968	**0.0006**	0.4298	**6.12e-09**
Group	0.0796	0.7163	0.1306	0.7346	0.4869	0.3032	0.2930	0.6098	0.1266	0.1992
*	0.2868	0.1185	0.5474	0.2235	0.8240	0.0982	0.6529	0.9989	0.1875	0.3448

tightest correlation with length, followed by the equivalent for the second triad (dlat2). The first outer denticle (od1) shows a more pronounced growth than the inner one (id1).

Three variables clearly depart from this general growth pattern. Two distances involving the most posterior denticle show no relationship with length: distance from mpd to od1 and md1. Most strikingly, the

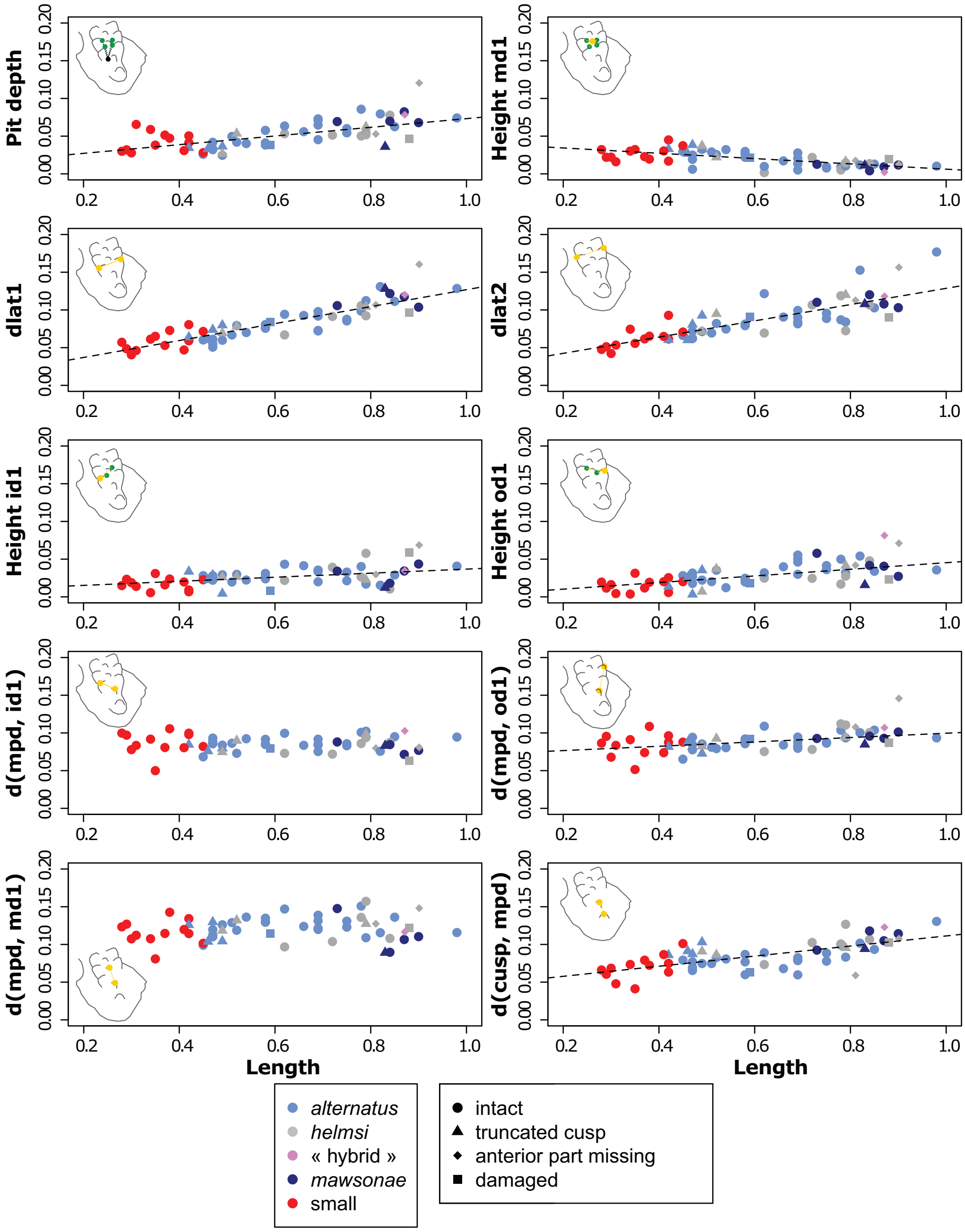

Figure 9. Relationship between Length (x-axis on all plots) and various inter-landmark distances, denticle height and pit depth. Dotted lines: significant linear relations. Interpolated values of length for the three elements with the anterior part missing (diamond symbol) are used for visualization but are not included in the regressions.

height of the first median denticle (md1) is not only stable through growth, but even decreases. Concomitantly, pit depth increases slightly faster than the height of md1. Pit depth roughly assesses the thickness of the element in the vicinity of md1, from the same valley points from which md1 height is calculated. The balance between increasing pit depth and decreasing md1 height may therefore be largely due to a filling of the valleys, ultimately leading to a md1 which is not visible anymore.

Variables can thus be associated according to the way they covary (Fig. 10). A first block of variables shows a pronounced association with length: dlat1, dlat2, pit depth, and od1 height; md1 height is also strongly associated with length, but in a negative way. The distance of the most posterior denticle (mpd) to id1 and md1 is not related to length, but is associated with other variables related to distance from mpd to the pit and to od1. The height of id1, id2 and od2 are relatively loosely related to the other variables.

These analyses were complemented by linear models including length, groups, and their interaction, in order to assess whether the growth dynamics differed between *alternatus*, *helmsi*, *mawsonae*, and the small specimens (Table 3). For all variables which were significantly related to length with a simple regression, this relation was confirmed and no difference between groups was indicated.

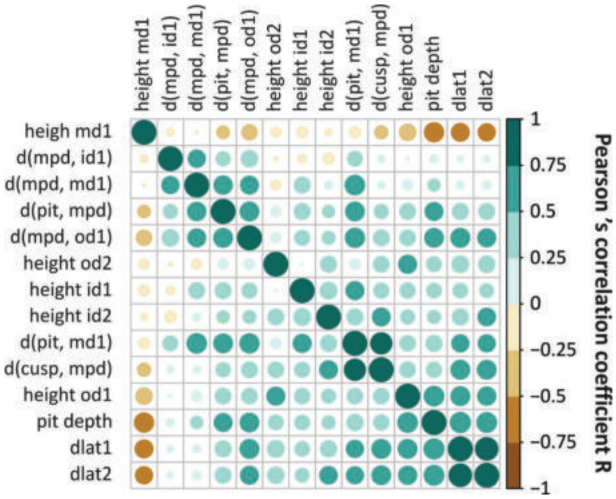

Figure 10. Correlations between univariate variables: element length (including the three interpolated values), denticle height, pit depth, and distances between denticles. In each case, the diameter of the circle and its color is proportional to the strength of the correlation, estimated using the Pearson coefficient. Variables are order to a hierarchical clustering approach.

5.5. 3D Geometric morphometrics

The Procrustes superimposition delivered the centroid size of the configurations as another proxy of element size, which was related to element length (Pearson's product-moment correlation R = 0.673, p-value = 1.811e-08) (Suppl. material 5: Fig. S3).

The morphometric analysis of the 3D shape showed along the first axis of the PCA on the aligned coordinates (PC1 = 35.2%), an opposition between small elements, towards negative scores, and *helmsi*, and especially *mawsonae*, tending to display high positive scores (Fig. 11). Scores on PC1 were highly correlated with element size (correlation with Length, including interpolated values: R = 0.891, p-value < 2.2e-16).

Therefore, the variation along PC1 mostly depicts the growth of the element. Towards negative scores corresponding to small elements, outer and inner denticles are close to and approximately at the same distance from the median axis of the element (Fig. 11B). The first median denticle is the highest, and the pit is located relatively posteriorly. Towards positive scores (Fig. 11D), in contrast, the pit is shifted towards a more anterior position. Inner and outer denticles grew in height and centrifugally from the median axis of the element; the centrifugal growth of the outer denticles being more pronounced than for the inner ones, the element acquired a torsion with an increased outer component. The most posterior denticle, maintaining its distance to the first outer and median denticles, tends to grow with an inner component. The height of the first median denticle is greatly reduced, a trend shared by the second median denticle, but to a lesser degree.

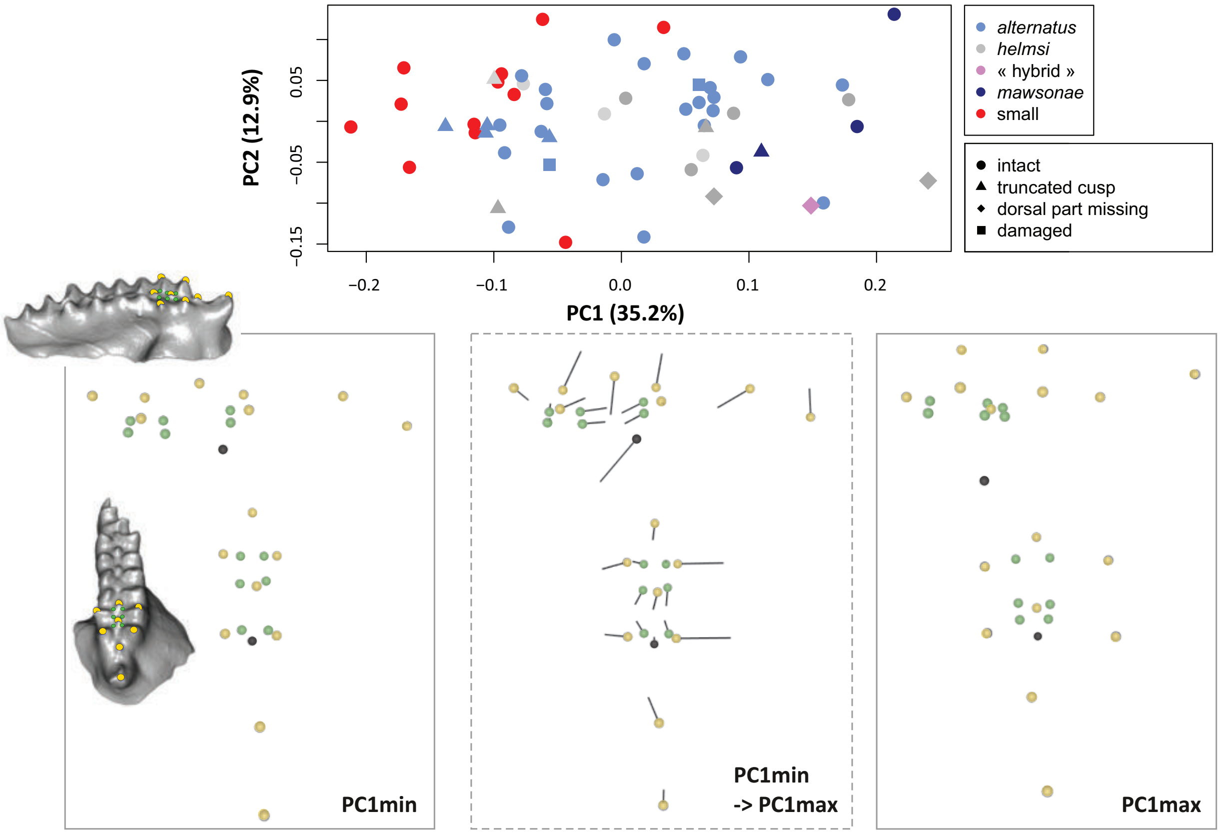

Figure 11. 3D Geometric morphometric analysis of *Icriodus alternatus* shape variation; **A.** First two axes of a PCA on the aligned coordinates; **B, C, D.** Visualization of the deformation in profile and oral view; in yellow tip of the denticles, in green valley landmarks, in black the pit; **B.** Configuration corresponding to the minimum score along PC1; **C.** Shape change from the minimum (dots) to the maximum (tip of the vectors) scores along PC1; **D.** Configuration corresponding to the maximum score along PC1.

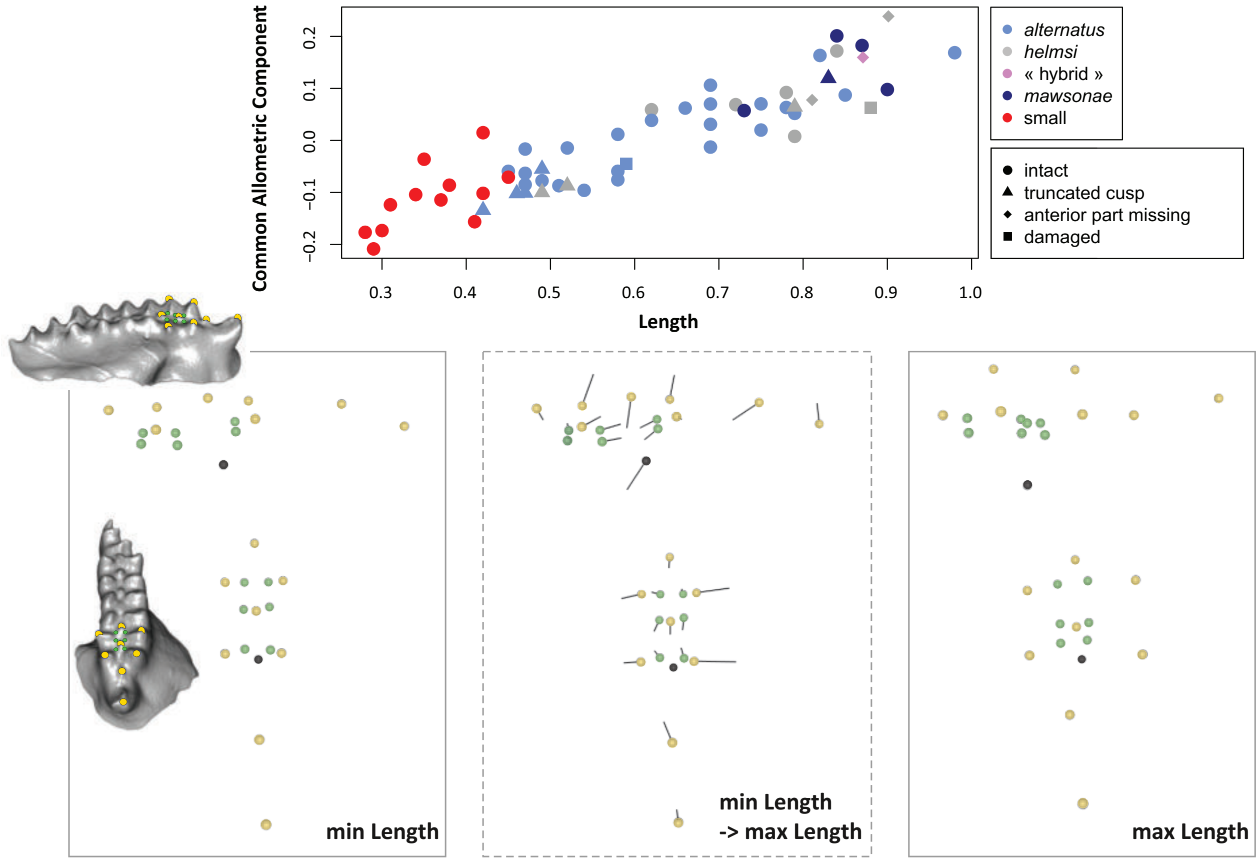

Figure 12. Allometric shape variation in *Icriodus alternatus*; **A.** Relationship between the total length of the element and the Common Allometric Component, based on the aligned coordinates of the posterior part of the element; **B, C, D.** Visualization of the deformation in profile and oral view, corresponding to extreme size values; in yellow tip of the denticles, in green valley landmarks, in black the pit; **B.** Configuration corresponding to the minimum length; **C.** Shape change from the minimum (dots) to the maximum (tip of the vectors) length; **D.** Configuration corresponding to the maximum length.

The relationship of shape with size and groups were investigated using Procrustes ANOVA. As expected, the size / shape relationship was very strong (Procrustes ANOVA, shape ~ Length including interpolated values: $P = 0.0001$) (Suppl. material 5: Fig. S3). When including groups as cofactors, Length remained the prominent factor, the grouping effect being close to the significance threshold (Procrustes ANOVA, shape ~ Length * Groups: $P_{Length} = 0.0001$, $P_{Groups} = 0.0627$, $P_{interaction} = 0.3435$). This difference between groups disappeared when small elements were grouped with *alternatus* ($P_{Length} = 0.0001$, $P_{Groups} = 0.3516$, $P_{interaction} = 0.3900$).

The allometric size/shape relationship can be visualized using scores along the Common Allometric Component, which highly resembles scores on PC1 (Pearson's product-moment correlation R = 0.998, p-value < 2.2e-16), underlining the importance of the allometric signal in the total shape variation. Accordingly, shape deformation associated with allometry (Fig. 12) resembles those expressed along PC1. Small specimens are characterized by shallow inner and outer denticles, organized symmetrically on both sides of the median axis of the element; the pit is shallow as well. Large elements are characterized by a deep pit, as well as elevated inner and outer denticles, the outer one being more centrifugal relative to the median axis of the element than the inner one.

6. Discussion

6.1. Subspecies describe an ontogenetic-driven morphological variation

The 3D analysis was focused on the posterior, ontogenetically oldest part of the Icriodontan element. Results showed that independently of the addition of new triads along ontogeny, the geometry of this posterior part changed deeply along growth, the main components being: (1) a growth of the inner and outer first denticles with both, a vertical and lateral component, the centrifugal growth being more pronounced for the outer denticles; (2) a growth of the cusp towards a more posterior direction, increasing its distance from the first triad; (3) a shift of the pit towards a more anterior position, together with an increase in the thickness of the element between the pit and the valleys surrounding the first median denticle; (4) a decrease in height of the first median denticle, up to its disappearance in most extreme cases. (5) In contrast, the zone comprising the most posterior denticle, the first median denticle and inner denticle, which seem to form a "core" area of the element in which the geometry, designed early during ontogeny, is little affected later on.

The subspecies *Ic. alt. alternatus*, *Ic. alt. helmsi*, and *Ic. alt. mawsonae* appeared to share the same ontogenetic trajectory, and once size-related variation is accounted for, they did not differ in any quantitative variable describing their general shape or the relationships between posterior denticles. The most prominent criterion distinguishing *Ic. alt. helmsi* and *Ic. alt. mawsonae* is their large size, suggesting that actually, these subspecies simply represent end-member geometries achieved at late growth.

The *Ic. alt. helmsi* subspecies has been characterized by the alignment of the most posterior denticle with the inner row of denticles. This morphology is achieved due to pronounced centrifugal growth of the outer denticles. Combined with the invariant relationships between the most posterior denticle and the first inner one, this trend tends to twist the shape of the large elements, up to orienting the most posterior denticle with the inner row in the most extreme cases.

As for the *Ic. alt. mawsonae* subspecies, it corresponds to an end-member of the trend of decreasing height of the first median denticles along ontogeny. Since the removal of material from a denticle seems unlikely, this decreasing height, together with the increasing thickness of the element at the vertical of the first median denticle expressed by the increase in pit depth, suggest a progressive filling of the initial deep valleys. Without a concomitant growth of the median denticle, this leads to a progressive reduction, up to its disappearance. In agreement with this interpretation of the subspecies as part of a morphological continuum including all *Ic. alternatus* subspecies, several specimens first identified as *Ic. alt. mawsonae* displayed "clear" traces of the first median denticle on the 3D scans. Furthermore, at least one specimen displayed the diagnostic features of both *Ic. alt. helmsi* and *Ic. alt. mawsonae*.

As a consequence, the described subspecies appear to belong to a single, homogeneous taxonomic and evolutionary unit, corresponding to the species *Ic. alternatus*. Although they can be seen as a way of describing an extensive morphological variation, the use of the "subspecies" concept in this context is misleading. For modern organisms, this notion corresponds to geographically isolated pools (Mayr 1963), implying some degree of gene flow breakdown. This is clearly not the case for *Ic. alt. alternatus*, *Ic. alt. helmsi* and *Ic. alt. mawsonae*, and the terminology of "subspecies" should be avoided since all can be found in the same time and place, indicating shared gene pool simply corresponding to *Icriodus alternatus*. If ever, the term "morphotype" should be preferred to describe this morphological variation, avoiding the risk to count such units in diversity analyses.

Variation in the oldest, posterior part of the element: a general feature of the genus *Icriodus*

The posterior part of the platform Icriodontan element is the first to be formed in ontogeny. As such, it is exposed to remodeling during all subsequent growth, consequently being the most variable zone in different *Icriodus* species. A morphotype differing in the expression of the denticles in the posterior area of the spindle middle row, hence similar to *Ic. alt. mawsonae*, has been described in *Icriodus subterminus* (Middle-Late Devonian) (Narkiewicz and Bultynck 2010). In another species, *Icriodus* sp. cf *Ic. brevis* (van den Boogaard 1983), the posterior denticles of the spindle, being progressively covered by new lamellae, become progressively less sharply separated from each other. The trend culminates for the three posteriormost denticles of the median row that become almost completely fused into a crest.

The blade, the other part of the element that composes the initial growth stage, displays similar trends of denticle progressive disappearance or fusion, as shown by the progressive diminution of blade denticle number along growth in *Ic. alternatus* (Dreesen and Houllenbergs 1980).

6.2. A potential for temporal changes along the ontogenetic pattern

Slight discrepancies exist in the temporal extension of the "subspecies" *Ic. alt. alternatus*, *Ic. alt. helmsi* and *Ic. alt. mawsonae*, apparently arguing for them being distinct evolutionary units. *Icriodus alternatus* as a whole appeared during a period marked by a succession of environmental perturbations. The mass extinction marking the Frasnian – Famennian boundary was the culmination of the Upper Kellwasser event materialized by anoxic deposits in many marine environments: it was associated with a pronounced temperature decrease and sea-level fall biosphere (Joachimski and Buggisch 2002, Girard and Renaud 2007). This event was preceded, *ca*. 1 myrs before, by the Lower Kellwasser event, episode of similar nature but of lesser impact on the biosphere (Joachimski and Buggisch 2002, Girard and Renaud 2007). A temperature decrease associated with a sea-level shallowing occurred towards the end of the LKE. The typical *Ic. alt. alternatus* form, together with *Ic. alt. helmsi*, appeared just after the LKE, whereas *mawsonae* appeared shortly before the UKE. Reversely, *Ic. alt. helmsi* and *Ic. alt. mawsonae* went extinct slightly before the typical *Ic. alt. alternatus* form during the early Famennian. Trends of size variation have been documented during this time period (Girard and Renaud 1996) that can explain these discrepancies. *Icriodus alternatus* displayed an increase in size in the interval between both Kellwasser events, a trend that should have promoted the apparition of *Ic. alt. mawsonae*, characterized by the largest size. Reversely, a decrease in size shortly before the species extinction might explain the disappearance of *Ic. alt. helmsi* and *Ic. alt. mawsonae* large-sized forms slightly before the final disappearance of the species. This suggests that *Icriodus alternatus* responded to environmental variations by shifts along a conserved ontogenetic trajectory, an interpretation supported by the allometric relationship between size and shape documented across the UKW and the Frasnian – Famennian crisis (Renaud and Girard 1999).

6.3. Morphological disparity along ontogeny: hint of changing constraints?

The ontogenetic pattern of *Icriodus alternatus* I elements further displayed heterogeneous disparity, with minimum morphological variance at the stage of four triads. This pattern is reminiscent of the "hourglass" developmental model (Irie and Kuratani 2014), stating that the most conserved embryonic stage is not the earliest but a mid-embryonic period called the 'phylotypic period'. This pattern has been interpreted as due to a maximum of molecular integration leading to high developmental canalization at the stage when common anatomical features of the basic body plan are defined. Regarding Icriodontan elements, this would correspond to relatively poorly constrained initial stages of development, when the earliest triads are added to the blade, converging towards the typical phenotype of the species, before that continuous growth and remodeling generate extensive morphological variation when late triads are added. Indeed, surprisingly high phenotypic variation has been found early during embryonic tooth development (Hayden et al. 2020) despite canalized adult phenotypes. Such early variation may be favored because the tooth-like structures are not yet functional. Later on, functioning may itself contribute to generate phenotypic variation in feeding structures. The morphology of Icriodontan elements suggests that the denticles were interlocked during occlusion; strong canalization would be required so that the opposite denticles would match with each other. The movement of occlusion seems to have incorporated some rotational dynamics, not only along the antero-posterior axis of the element, but also along the inner-outer axis (Suttner et al. 2017). Possibly, the addition of lamellae during late growth was influenced by the physical pressures exerted during occlusion, thus fostering the increasing asymmetry between the inner and outer denticles of the element. The "hourglass" pattern of morphological disparity along ontogeny thus suggests a shift from relatively loose developmental constraints to a pattern of growth modulated by functional constraints during occlusion. As recently suggested for the conodont genera *Polygnathus* (Renaud et al. 2021) and *Palmatolepis* (Renaud, Girard and Dufour in press), patterns of morphological variance, and not only shape itself, may be enlightening for deciphering the functional constraints related to occlusion on the platform element geometry.

7. Conclusions

2D and 3D biometric and geometric morphometric analyses have shown here that the platform (Icriodontan) elements of *Icriodus alternatus* display two major morphological trends along ontogeny, besides the addition of successive triads elongating the element: (1) a filling of the initially deep valleys between denticles on the posterior part of the element, leading to the progressive disappearance of the first median denticle on the spindle; and (2) an increasing asymmetry between the inner and outer denticles of a same triad, due to a more pronounced centrifugal growth of the outer denticle. These results suggest that the subspecies of *Icriodus alternatus* described for the end Frasnian and early Famennian constitute end-member morphologies characterizing the different growth stages. *Icriodus alternatus helmsi* and especially *Ic. alt. mawsonae* represent phenotypes achieved when large element sizes are reached, due to remodeling in relation with the continuous growth. *Icriodus alternatus alternatus* included smaller forms along the same ontogenetic trajectory. The term "subspecies" should thus be avoided to prevent the risk of artificially inflating biodiversity estimates.

Morphological disparity seems not to be homogeneous along the ontogenetic trajectory, following an "hourglass" pattern, suggesting loose developmental constraints at the beginning of the development, and increasing variance in late stages, due to continuous remodeling possibly modulated by occlusal functioning. In between, morphological variance reaches a minimum for elements with four triads. This stage may represent a "phylotypic" stage characterized by the highest canalization and hence the most discriminant between species. Taxonomic efforts should concentrate on such stages to identify relevant evolutionary relevant taxonomic units.

Data availability

Depending on the journal, the morphological data will be deposited in Dryad or as Supplementary Files. Illustrated specimens (collection numbers UM BUS 031 to UM BUS 045) are available in MorphoMuseuM.

Author contribution

CG initiated and coordinated the study. CG, ALC and CC were responsible for all aspects relevant to paleontological and geological expertise (sampling, picking, identification, dating). TG and CG acquired the 2D measurements, CG and SR analyzed the corresponding data. SR performed the 3D analyses. CG and SR wrote the first draft and all authors contributed and approved the final version of the manuscript.

Competing interest

The authors declare that they have no conflict of interest.

Acknowledgments

We acknowledge Jeff Over (Geneseo, NY) and Tomas Kumpan (Masaryck, Czech Republic) for their comments on the manuscript, and the contribution of SFR Biosciences

(UMS3444/CNRS, US8/Inserm, ENS de Lyon, UCBL) AniRa-ImmOs facility, and we particularly thank Mathilde Bouchet and Louise Souquet for their kind assistance during the scanning sessions. This work was supported by the ANR Project ECODEV (ANR-13-BSV7-005; 2014–2017) and the LabEx CeMEB project MARCON (2018–2020). This is publication ISEM 2022-003.

References

Adams CD, Otarola-Castillo E (2013) geomorph: an R package for the collection and analysis of geometric morphometric shape data. Methods in Ecology and Evolution 4: 393–399. https://doi.org/10.1111/2041-210X.12035

Aldridge RJ, Smith MP, Norby RD, Briggs DEG (1987) The architecture and function of Carboniferous polygnathacean conodont apparatus. In: Aldridge RJ (Ed.) Palaeobiology of conodonts. Ellis Horwood, Chichester, England, 63–76.

Balter V, Martin J, Tacail T, Suan G, Renaud S, Girard C (2019) Ca stable isotopes place Devonian conodonts as first level carnivores. Geochemical Perspectives Letters 10: 36–39. https://doi.org/10.7185/geochemlet.1912

Branson EB, Mehl MG (1934) Conodont studies number three. The University of Missouri studies, A quarterly of research VIII: 171–259.

Clark DL (1984) Conodont biofacies and provincialism. Geological Society of America special Paper 196, 340 pp.

Cohen KM, Finney SC, Gibbard PL, Fan J-X (2013 [updated]) The ICS International Chronostratigraphic Chart. Episodes 36: 199–204. https://doi.org/10.18814/epiiugs/2013/v36i3/002

Donoghue PCJ (1998) Growth and patterning in the conodont skeleton. Philosophical Transactions of the Royal Society London B 353: 633–666. https://doi.org/10.1098/rstb.1998.0231

Donoghue PCJ, Purnell MA (1999) Mammal-like occlusion in conodonts Paleobiology 25(1): 58–74. https://doi.org/10.1017/S0022336000031292

Dreesen R, Houllebreghs E (1980) Evolutionary trends of Famennian icriodids in the Dinant and Vestre Basins (Conodonts, Belgian Upper Devonian). Annales de la Société de Géologie de Belgique 103: 111–141.

Girard C, Charruault A-L, Gluck T, Corradini C, Renaud S (2022) 3D models related to the publication: Deciphering the morphological variation and its ontogenetic dynamics in the Late Devonian conodont *Icriodus alternatus*. MorphoMuseum. https://doi.org/10.18563/journal.m3.161

Girard C, Cornée J-J, Charruault A-L, Corradini C, Weyer D, Bartzsch K, Joachimski MM, Feist R (2017) Conodont biostratigraphy and palaeoenvironmental trends during the Famennian (Late Devonian) in the Thuringian Buschteich section (Germany), Newsletters on Stratigraphy 50(1): 71–89. https://doi.org/10.1127/nos/2016/0318

Girard C, Klapper G, Feist R (2005) Subdivision of the terminal Frasnian *linguiformis* conodont Zone, revision of the correlative interval of Montagne Noire Zone 13, and discussion of stratigraphically significant associated trilobites. In: Over DJ, Morrow JR, Wignall PB (Eds) Understanding Late Devonian and Permian-Triassic Biotic and Climatic Events: Towards an integrated approach. Devonian Palaeontological Stratigraphical Series, 181–198. https://doi.org/10.1016/S0920-5446(05)80007-X

Girard C, Renaud S (1996) Size variations in conodonts in response to the Upper Kellwasser crisis (Upper Devonian of the Montagne Noire, France). Comptes Rendus de l'Académie des Sciences, Paris 323(série IIa): 435–442.

Girard C, Renaud S (2007) Quantitative conodont-based approaches for correlation of the Late Devonian Kellwasser anoxic events. Palaeogeography Palaeoclimatology Palaeoecology 250: 114–125. https://doi.org/10.1016/j.palaeo.2007.03.007

Girard C, Renaud S (2011) The species concept in a long-extinct fossil group, the conodonts. Comptes rendus Palevol 10: 107–115. https://doi.org/10.1016/j.crpv.2010.10.009

Girard C, Renaud S, Sérayet A (2004) Morphological variation of *Palmatolepis* Devonian conodonts: species vs. genus. Comptes rendus Palevol 3: 1–8. https://doi.org/10.1016/j.crpv.2003.09.008

Hayden L, Lochovska L, Sémon M, Renaud S, Delignette-Muller M-L, Vicot M, Peterková R, Hovorakova M, Pantalacci S (2020) Developmental variability channels mouse molar evolution. eLife 9: e50103. https://doi.org/10.7554/eLife.50103

Irie N, Kuratani S (2014) The developmental hourglass model: a predictor of the basic body plan? Developmental Biology 141: 4649–4655. https://doi.org/10.1242/dev.107318

Joachimski M, Buggisch W (2002) Conodont apatite $\delta^{18}O$ signatures indicate climatic cooling as a trigger of the Late Devonian mass extinction. Geology 30(8): 711–714. https://doi.org/10.1130/0091-7613(2002)030%3C0711:CAOSIC%3E2.0.CO;2

Klapper G (1989) The Montagne Noire Frasnian (Upper Devonian) conodont succession. In: McMillan NJ, Embry AF, Glass DJ (Eds) Devonian of the World. Paleontology, Paleoecology, Biostratigraphy, Canadian Society of Petroleum Geologists, Memoir 14, Calgary, 449–468.

Klapper G, Johnson JG (1980) Endemism and dispersal of Devonian conodonts. Journal of Paleontology 54(2): 400–455. http://www.jstor.org/stable/1304071

Klapper G, Kirchgasser WT (2016) Frasnian Late Devonian conodont biostratigraphy in New York: graphic correlation and taxonomy. Journal of Paleontology 90: 525–554. https://doi.org/10.1017/jpa.2015.70

Lange FG (1968) Conodonten-Gruppenfunde aus Kalken des tieferen Oberdevon. Geologica et Palaeontologica 1: 97–114.

Mayr E (1963) Animal Species and Evolution, Mass. Belknap Press, Cambridge. https://doi.org/10.4159/harvard.9780674865327

McGhee GRJ (1996) The Late Devonian Mass Extinction – The Frasnian/Famennian crisis. Columbia University Press, New York, 303 pp.

Narkiewicz K, Bultynck P (2010) The Upper Givetian (Middle Devonian) *subterminus* conodont Zone in North America, Europe and North Africa. Journal of Paleontology 84(4): 588–625. https://doi.org/10.1666/10-029.1

Nicoll RS (1982) Multielement composition of *Icriodus expansu*s Branson and Mehl from the Upper Devonian of the Canning basin, Western Australia. BMR Journal of Australian Geology and Geophysics 7: 197–213.

Philip GM, Jackson JH (1967) Lower Devonian subspecies of the conodont *Polygnathus linguiformis* Hinde from Southern Australia Journal of Paleontology 41(5): 1262–1266. http://www.jstor.org/stable/1302097

Purnell MA (1995) Microwear on conodont elements and macrophagy in the first vertebrates. Nature 374: 798–800. https://doi.org/10.1038/374798a0

Purnell MA, Donoghue PCJ (1997) Architecture and functional morphology of the skeletal apparatus of ozarkodinid conodonts. Philosophical Transactions of the Royal Society of London 352: 1545–1564. https://doi.org/10.1098/rstb.1997.0141

R Core Team (2017) R: A Language and Environment for Statistical Computing. In: R. F. f. S. Computing (Ed.) Vienna, Austria. https://www.R-project.org

Renaud S, Ecalle B, Claisse P, Charruault A-L, Ledevin R, Girard C (2021) Patterns of bilateral asymmetry and allometry in Late Devonian *Polygnathus* conodonts. Palaeontology 64(1): 137–159. https://doi.org/10.1111/pala.12513

Renaud S, Girard C (1999) Strategies of survival to extreme environmental perturbations: evolution of conodonts in response to the Kellwasser crisis (Upper Devonian). Palaeogeography Palaeoclimatology Palaeoecology 146: 19–32. https://doi.org/10.1016/S0031-0182(98)00138-2

Renaud S, Girard C, Dufour A-B (2021) Morphometric variance, evolutionary constraints and their change through time in Late Devonian *Palmatolepis* conodonts. Evolution 75–11: 2911–2929. https://doi.org/10.1111/evo.14330

Rohlf FJ, Slice D (1990) Extensions of the Procrustes method for the optimal superimposition of landmarks. Systematic Biology 39(1): 40–59. https://doi.org/10.2307/2992207

Sandberg CA, Dreesen RMJ (1984) Late Devonian icriodontid biofacies models and alternate shallow water conodont zonation. In Clark DL (Ed.) Conodont biofacies and provincialism. Geological Society of America Special Papers, Boulder/Colorado, 143–178. https://doi.org/10.1130/SPE196-p143

Sandberg CA, Ziegler W (1973) Refinement of standard Upper Devonian conodont zonation based on sections in Nevada and West Germany. Geologica et Palaeontologica 7: 97–122.

Serpagli E (1983) The conodont apparatus of *Icriodus woschmidti woschmidti*. Fossils and Strata 15: 155–161.

Simpson A (1998) Apparatus structure of the latest Silurian to Early Devonian conodont *Icriodus woschmidti hesperius* Klapper and Murphy, and some comments on phylogeny. Palaeontologica Polonica 58: 153–169. http://www.palaeontologia.pan.pl/Archive/1998-58_153-169.pdf

Spalletta C, Perri MC, Over DJ, Corradini C (2017) Famennian (Upper Devonian) conodont zonation: revised global standard. Bulletin of Geosciences 92(1): 1–27. https://doi.org/10.3140/bull.geosci.1623

Suttner TJ, Kido E, Briguglio A (2018) A new icriodontid conodont cluster with specific mesowear supports an alternative apparatus motion model for Icriodontidae. Journal of Systematic Palaeontology 16(11): 909–926. https://doi.org/10.1080/14772019.2017.1354090

van den Boogaard M (1983) Conodont faunas from Portugal and southwestern Spain. Part 7. A Frasnian conodont fauna near the Estação de Cabrela (Portugal). Scripta Geologica 69: 1–10.

Wiley DF, Amenta N, Alcantara DA, Deboshmita G, Kil YJ, Delson E, Harcourt-Smith W, Rohlf FJ, St John K, Hamann B (2005) Evolutionary morphing, VIS 05. IEEE Visualization. IEEE.

Yazdi M (1999) Late Devonian-Carboniferous conodonts from Eastern Iran. Rivista Italiana Paleontologica et Stratigraphica 105(2): 167–200.

Ziegler W (1975) Catalogue of conodonts. Vol. V. E. Schweizcrbart'sche Verlagsbuchhandlung, 399 pp.

Ziegler W, Sandberg CA (1990) The late Devonian standard conodont zonation. Courier Forschung-Institut Senckenberg 121: 1–115.

Supplementary material 1

Table S1

Authors: Catherine Girard, Anne-Lise Charruault, Thomas Gluck, Carlo Corradini, Sabrina Renaud

Data type: table

Explanation note: Description of the 15 landmarks.

Link: https://doi.org/10.3897/fr.25.80211.suppl1

Supplementary material 2

Table S2

Authors: Catherine Girard, Anne-Lise Charruault, Thomas Gluck, Carlo Corradini, Sabrina Renaud

Data type: table

Explanation note: Correlations between variables, tested using Kendall rank order tests. Below the diagonal, Kendall's tau correlation coefficient, above the diagonal, p-value. In bold, $p < 0.001$, in italics $p < 0.05$.

Link: https://doi.org/10.3897/fr.25.80211.suppl2

Supplementary material 3

Figure S1

Authors: Catherine Girard, Anne-Lise Charruault, Thomas Gluck, Carlo Corradini, Sabrina Renaud

Data type: figure

Explanation note: Illustration of the calculation of md1 height by the geometry of the triangle iv1-md1-ov2.

Link: https://doi.org/10.3897/fr.25.80211.suppl3

Supplementary material 4

Figure S2

Authors: Catherine Girard, Anne-Lise Charruault, Thomas Gluck, Carlo Corradini, Sabrina Renaud

Data type: figure

Explanation note: Relationship between width and length of the elements. The regression (dotted line) allowed for the interpolation of the length for the three elements with their anterior part missing (pointed by arrows on the graph).

Link: https://doi.org/10.3897/fr.25.80211.suppl4

Supplementary material 5

Figure S3

Authors: Catherine Girard, Anne-Lise Charruault, Thomas Gluck, Carlo Corradini, Sabrina Renaud

Data type: figure

Explanation note: Relationship between length and geometric morphometrics of the posterior part of the element. A, Length vs Centroid Size of the posterior part. B, Length vs PC1 based on the aligned coordinates. Symbols with the thick black outline correspond to the interpolated length values.

Link: https://doi.org/10.3897/fr.25.80211.suppl5

Fossil Record 25 (1) 2022, 43–63 | DOI 10.3897/fr.25.79958

Hypothesis testing on the planktic foraminiferal survival model after the KPB mass extinction: evidence from Tunisia and Algeria

Ignacio Arenillas[1], José A. Arz[1], Fariza Metsana-Oussaid[2], Vicente Gilabert[1], Djelloul Belhai[2]

1 *Departamento de Ciencias de la Tierra, and Instituto Universitario de Investigación en Ciencias Ambientales de Aragón (IUCA), Universidad de Zaragoza, E-50009, Spain*

2 *Faculté des Sciences de la Terre, de Géographie et de l'Aménagement du Territoire (FSTGAT), Université des Sciences et de la Technologie Houari Boumediene (USTHB), Algeria*

http://zoobank.org/0471341F-0C2F-42A1-A333-327904E59803

Corresponding author: Ignacio Arenillas (ias@unizar.es)

Academic editor: Florian Witzmann ♦ **Received** 27 August 2021 ♦ **Accepted** 13 January 2022 ♦ **Published** 7 February 2022

Abstract

A historical review of the extinction, survival, and evolutionary models of planktic foraminifera proposed for the Cretaceous/Paleogene boundary (KPB) mass extinction event sometimes leaves the impression that there is still no conclusive evidence to support any single one of them. Two main models have been put forward: i) catastrophic mass extinction, almost total for some authors, compatible with the geologically instantaneous paleoenvironmental effects of a large meteorite impact (Chicxulub impact, Mexico); and ii) gradual mass extinction, compatible with the paleoenvironmental effects of massive, long-lasting volcanism (Deccan Traps, India). Over the years, a lot of evidence has been proposed supporting one hypothesis or the other, highlighting isotopic ($\delta^{18}O$, $\delta^{13}C$, $^{87}Sr/^{86}Sr$) as well as taphonomic, biostratigraphic, quantitative (relative and/or absolute abundance), phylogenetic, and even teratological. We review previous planktic foraminiferal and stable isotope studies, and provide new quantitative and statistical tests from two pelagic sections: the El Kef section (Tunisia), recognized as the most continuous and expanded lowermost Danian section worldwide, and the Sidi Ziane section (Algeria), affected by relevant hiatus in the lower Danian. The results indicate that all the latest Maastrichtian planktic foraminiferal species except those of *Guembelitria* went extinct exactly at the KPB, supporting the hypothesis of an almost total extinction. In the light of this new evidence, we maintain that the Maastrichtian planktic foraminiferal specimens found worldwide in lower Danian samples could be the result of similar reworking and vertical mixing processes to those at El Kef and Sidi Ziane.

Key Words

catastrophic mass extinction, biostratigraphy, Danian, Maastrichtian, reworking

1. Introduction

The accuracy of planktic foraminiferal extinction models across the Cretaceous/Paleogene boundary (KPB) has been a matter of controversy since the 1980s. The mass extinction event was initially described in the Caravaca (Spain) and El Kef (Tunisia) sections as being sudden and almost total (Smit 1982), except for the survival of the disaster opportunist *Guembelitria cretacea*. The near-complete extinction model was questioned by Keller (1988), who pointed out that, at El Kef, 12 Maastrichtian species went extinct before the KPB, 31 species disappeared near the KPB, and at least 11 species survived into the early Danian. To resolve the dispute, four specialists (Canudo 1997; Masters 1997; Olsson 1997; Orue-Etxebarria 1997) blindly examined unlabeled samples from the El Kef stratotype (Smit and Nederbragt 1997). The El Kef blind test was an admirable attempt to resolve the controversy (Lipps 1997; Ginsburg 1997a). However, both Smit (Smit and Nederbragt 1997) and Keller (Keller 1997) claimed that the outcome supported their own views. Ginsburg (1997b) concluded that the blind test had failed, among other reasons, due to differences in the taxonomic naming of the species among those carrying out the test, as well as an inability to discriminate between in situ and ex situ (reworked) specimens.

In accordance with Smit (1982, 1990), the so-called catastrophist hypothesis was supported by many other specialists in planktic foraminifera in the 1990s (KPB–catastrophists from now on), albeit proposing slightly different extinction models in which a greater number of surviving species were suggested (e.g., Arz et al. 1996b, 1999a; Huber 1996; Koutsoukos 1996; Molina et al. 1996, 1998; Apellaniz et al. 1997; Kaiho and Lamolda 1999). KPB–catastrophists argue that a geologically instantaneous extinction can only be explained by the abrupt environmental effects caused by the impact of a large asteroid, which is linked to the Chicxulub impact in the Yucatan Peninsula, Mexico (see Hildebrand et al. 1991; Schulte et al. 2010 and references therein).

After defending the idea that a wider range of Maastrichtian species went extinct before or after the KPB, the supporters of so-called gradualist hypothesis (KPB–gradualists from now on) suggest that a gradual mass extinction can only be explained by long-lasting environmental changes not directly related to the Chicxulub impact (e.g., Keller et al. 1993, 1995; MacLeod and Keller 1994; Luciani 1997). A gradual extinction extending for hundreds of thousands of years across the KPB would be more consistent with the hypothesis of global climate changes triggered by massive volcanism linked to the flood basalt emplacement of the Deccan Traps in west-central India (Officer and Drake 1985; Courtillot et al. 1988; Keller et al. 2010, and references herein). Alternatively, KPB–gradualists have proposed the hypothesis of multiple causes, which combines the three major extinction factors postulated for that time: massive volcanism, a sea-level fall, and a large meteorite impact, via climate change (Canudo et al. 1991; Li and Keller 1998).

KPB–catastrophists have pointed out that the latest Maastrichtian planktic foraminiferal extinctions are in fact an artefact of the Signor–Lipps effect, due to the low intensity in the search for the scarcest species (Signor and Lipps 1982; Molina 1995). The Signor–Lipps effect might lead to the erroneous interpretation that the stratigraphic ranges of some Maastrichtian planktic foraminiferal species do not reach the KPB. Nevertheless, KPB–gradualists have continued to hold that the micropaleontological data agreed with their claim that the extinction began in the last 500 kyr of the Maastrichtian and continued in the earliest Danian (Keller 2001, and references herein). On the other hand, Smit (1982, 1990) warned that the presence of Maastrichtian species in Danian samples may be the result of reworking processes, and not the result of their survival from the KPB extinction. However, KPB–gradualists considered these to be surviving species (Keller 2001, and references herein). In the 1990s, $\delta^{18}O$ and $\delta^{13}C$ analyses of Maastrichtian planktic foraminiferal species identified in the lower Danian also failed to distinguish clearly between the surviving taxa and reworked specimens (e.g., Stott and Kennett 1990; Zachos et al. 1992; Keller et al. 1993; Barrera and Keller 1994; Kaiho and Lamolda 1999), so the debate on the magnitude and extension of the KPB mass extinction event seemed to resist all attempts at solution.

In the last twenty years, KPB specialists have focused on determining which of two alleged factors (asteroid impact or massive volcanism) was the main contributor to the extinction (Keller et al. 2010, 2020; Schulte et al. 2010; Vellekoop et al. 2014, 2016; Arenillas et al. 2018; Lowery et al. 2018, 2020; MacLeod et al. 2018; Renne et al. 2018; Henehan et al. 2019; Hull et al. 2020; Gilabert et al. 2021a, 2021b), as well as ascertaining the precise timing of both the Chicxulub impact and the main Deccan volcanic phases (Renne et al. 2013, 2015; Schoene et al. 2015, 2019; Sprain et al. 2019; Gilabert et al. 2022). Because the dispute among KPB specialists focused on the controversy over the causes of the extinction, the debate on the presence of "reworked specimens vs. survivor taxa" in lowermost Danian samples waned in the 2000s, and virtually nothing else was published in the 2010s, with only a few exceptions (e.g., Gallala et al. 2009; Gallala 2013, 2014; Punekar et al. 2014; Molina 2015). However, this is a relevant issue both for the verification or refutation of the two main hypotheses about the causes of the KPB extinction (asteroid impact vs. massive volcanism) and for the reconstruction of the phylogenetic relationships among early Danian planktic foraminifera (e.g., Koutsoukos 2014). In order to provide new evidence that might clear up how many species survived the KPB mass extinction event, we have first reviewed biostratigraphic and isotopic studies of planktic foraminifera previously carried out in some relevant KPB pelagic sections and Ocean Drilling Program (ODP) sites around the world (Fig. 1). In addition, we have quantitatively and statistically analyzed the planktic foraminiferal survival patterns after the KPB extinction in two western Tethyan localities: El Kef (Tunisia) and Sidi Ziane (Algeria).

2. Geographical and geological setting

The El Kef section is located 5–6 km southwest of the city of El Kef, northwestern Tunisia. The KPB lies in the upper Maastrichtian to Paleocene El Haria Formation (Salaj 1974). It was chosen to define the Global Boundary Stratotype Section and Point (GSSP) for the base of the Danian Stage, or KPB, because it is the most continuous, complete, and expanded section worldwide (Remane et al. 1999; Molina et al. 2006). The GSSP for the KPB was defined as the lowermost part of what is informally known as the dark KPB Clay, specifically as the base of a 2–5 mm thick rust clay layer (airfall layer) that has anomalous iridium concentrations and is rich in impact ejecta (impact glasses, Ni-spinels, shocked quartz, etc.). The base of this airfall layer at El Kef is the same stratigraphic level as the planktic foraminiferal extinction horizon (Arenillas et al. 2000b; Molina et al. 2006).

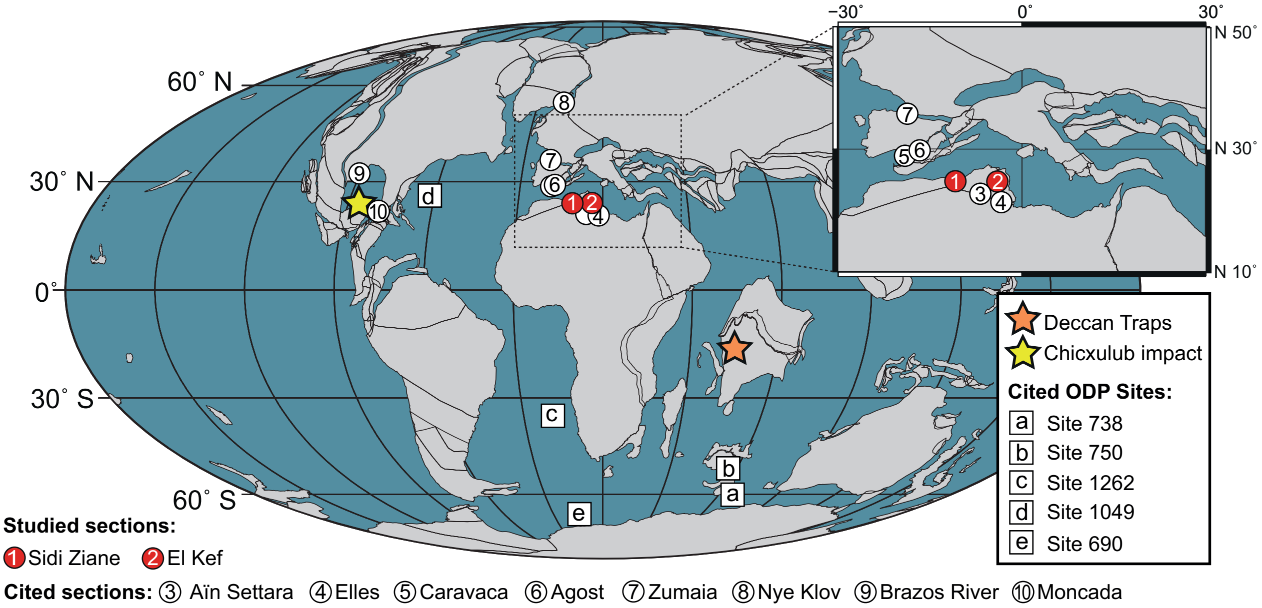

Figure 1. Paleogeographic reconstruction of the KPB (66.00 Ma), with the localities cited in this study (after https://www.odsn.de/odsn/services/paleomap/adv_map.html). ODP – Ocean Drilling Program.

The Sidi Ziane section is located 4 km south of the village of Sidi Ziane in the Souagui District of Médéa Province, northern Algeria, which is approximately 75 km southwest of Algiers and 47 km southeast of Médéa, the capital city of the province of the same name. The area is characterized by thick allochthonous deposits of Cretaceous to Eocene age (Kieken 1974). The KPB lies in Unit I of Kieken (1974), consisting of clayey marls in the upper Maastrichtian and an alternation of clayey marls and marly limestones in the lower Danian. The thickness of the last planktic foraminiferal biozone of the Maastrichtian (*Plummerita hantkeninoides* Zone) at Sidi Ziane is 13.5 m, making it one of the thickest identified to date, suggesting that the uppermost Maastrichtian is complete and continuous. Based on graphic correlation, it has been determined that the sedimentation rate of the Maastrichtian in Sidi Ziane is 8.98 cm/kyr, which is comparable with the most expanded and continuous sections worldwide, such as the El Kef and Aïn Settara sections in Tunisia (Metsana-Oussaid et al. 2019). However, the absence of the dark KPB Clay and the first Danian biozones at Sidi Ziane indicates a hiatus affecting the first few hundred thousand years of the Danian (Metsana-Oussaid et al. 2019).

3. Material and methods

For biostratigraphic and taphonomic interpretations, we selected 40 samples from El Kef and 47 samples from Sidi Ziane across the critical KPB interval from the set of samples collected in both sections. All studied rock samples were disaggregated in water with diluted H_2O_2, washed through a 63 µm sieve, and then oven dried at 50 °C. The planktic foraminiferal species of the upper Maastrichtian were intensively searched in all samples from the ≥ 63 µm size fraction in order to minimize the Signor–Lipps effect. The quantitative analyses (relative abundance counts at species level) were based on representative aliquots, obtained by microsplitter, of approximately 300 specimens per sample (Suppl. material 2: Table S1, Suppl. material 3: Table S2). Some relevant planktic foraminiferal specimens were picked from the residues and selected for scanning electron microscopy (SEM), using a Zeiss MERLIN FE-SEM of the Electron Microscopy Service of the Universidad de Zaragoza (Spain). SEM photographs of some species are provided in Figs 2–4.

In order to minimize the reworking effect and determine the planktic foraminiferal survival patterns at El Kef and Sidi Ziane, we drew on quantitative and statistical analyses. For these analyses, we followed two methods.

First, we performed nonlinear regression analyses using least squares to find equations/functions that fit two data sets of the lowermost Danian in both the El Kef and Sidi Ziane sections: y = relative abundance (%) of Maastrichtian specimens with respect to the total planktic foraminiferal specimens, and x = number of sample (cm above the KPB). The data were fitted by a method of successive approximations, following Levenberg-Marquardt optimization. In order to select which function or model best fits the x-y data, the Akaike Information Criterion (Akaike IC) was used; lower values for the Akaike IC imply a better fit. Two nonlinear functions were selected: exponential and power functions. Other nonlinear functions were also tested, but they did not give good results since very high Akaike IC values were obtained. To fit data to exponential functions (exponential curve $y = ae^{bx} + c$), an initial guess by linearization (log-transforming y), followed by nonlinear optimization, was performed. To fit data to power functions (power curve $y = ax^b + c$), an initial guess by log-log transformation and linear regression, i.e. $c = 0$, followed by nonlinear optimization,

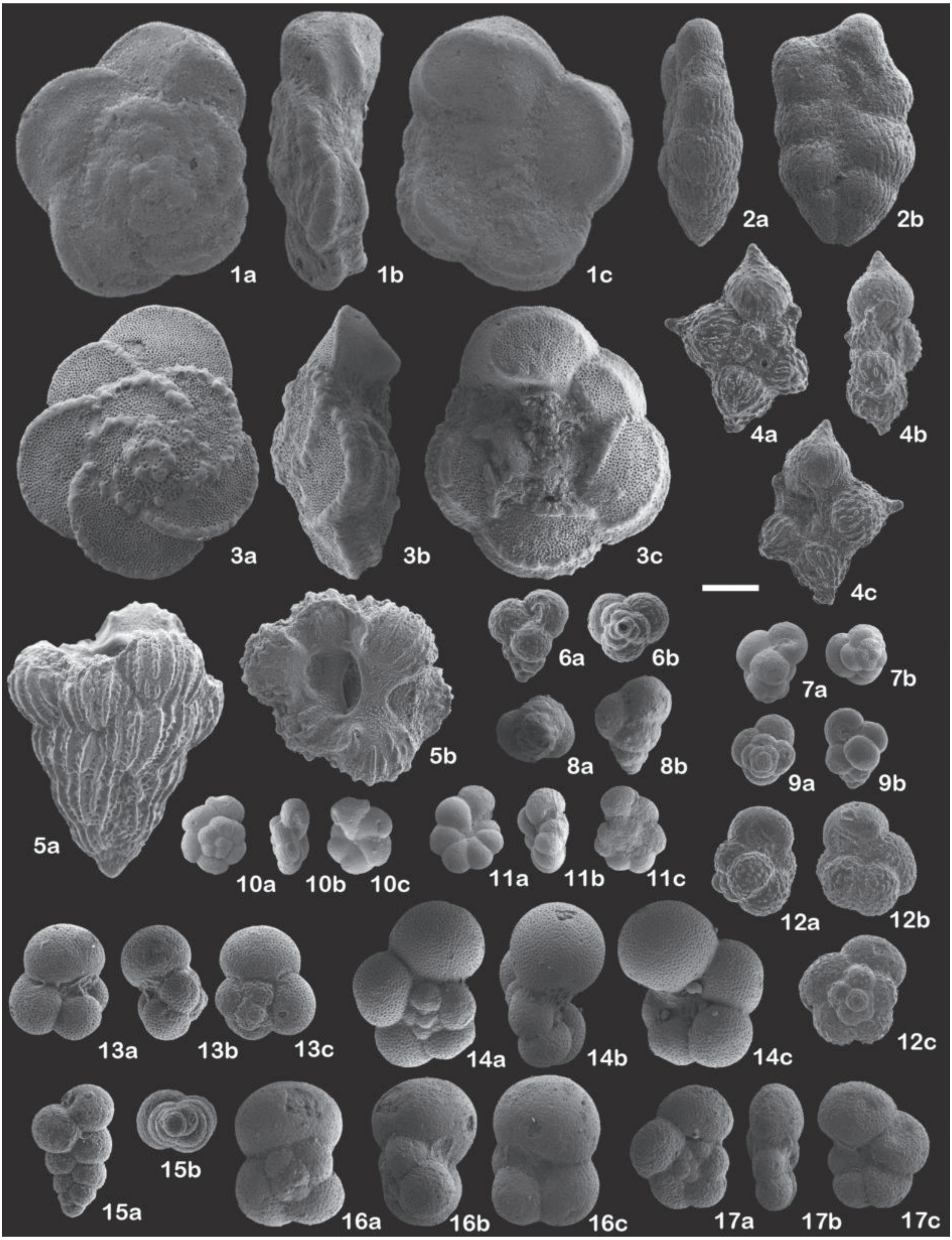

Figure 2. SEM photographs of the planktic foraminiferal index species and some other relevant species from the Maastrichtian and Danian. Samples K and SZ numbered in cm from the KPB. **1.** *Abathomphalus mayaroensis* (SZ-350); **2.** *Pseudoguembelina hariaensis* (SZ-1550); **3.** *Globotruncana arca* (K-1200); **4.** *Plummerita hantkeninoides* (sample K-400); **5.** *Racemiguembelina fructicosa* (K-400); **6.** *Guembelitria cretacea* (K-100); **7.** *Pseudocaucasina antecessor* (K+70); **8.** *Chiloguembelitria danica* (SZ+1); **9.** *Palaeoglobigerina alticonusa* (K+450); **10.** *Parvularugoglobigerina longiapertura* (K+100); **11.** *Parvularugoglobigerina eugubina* (K+200); **12.** *Trochoguembelitria liuae* (K+850); **13.** *Eoglobigerina simplicissima* (sample K+550); **14.** *Parasubbotina pseudobulloides* (K+1110); **15.** *Woodringina hornerstownensis* (K+650); **16.** *Subbotina triloculinoides* (SZ+30); **17.** *Globanomalina compressa* (SZ+445). Scale bar: 100 µm.

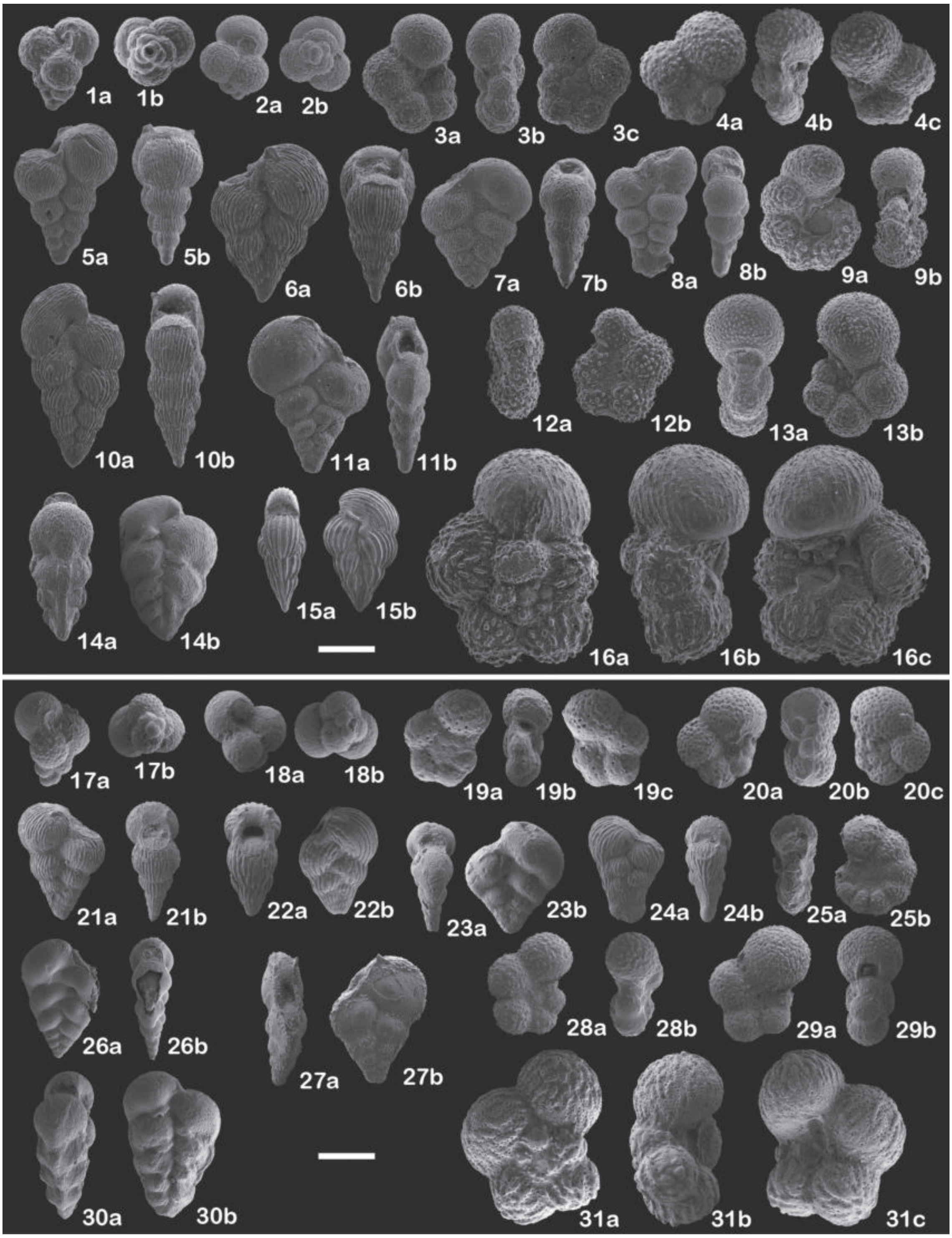

Figure 3. SEM photographs of the Maastrichtian planktic foraminiferal species usually considered to be putative survivors of the KPB extinction. Specimen comparison from upper Maastrichtian and lower Danian samples at El Kef. Samples K numbered in cm from the KPB. Specimens in Maastrichtian samples: **1.** *Guembelitria cretacea* (K-100); **2.** *Guembelitria blowi* (K-750); **3.** *Muricohedbergella holmdelensis* (K-400); **4.** *Muricohedbergella monmouthensis* (K-70); **5.** *Heterohelix globulosa* (K-400); **6.** *Heterohelix labellosa* (K-400); **7.** *Heterohelix planata* (K-400); **8.** *Heterohelix navarroensis* (K-400); **9.** *Globigerinelloides yaucoensis* (K-400); **10.** *Pseudoguembelina costulata* (sample K-400); **11.** *Laeviheterohelix glabrans* (K-400); **12.** *Globigerinelloides prairiehillensis* (K-1100); **13.** *Globigerinelloides volutus* (sample K-400); **14.** *Pseudoguembelina kempensis* (sample K-400); **15.** *Pseudoguembelina costulata* (K-400); **16.** *Rugoglobigerina rugosa* (K-400). Specimens in Danian samples: **17.** *Guembelitria cretacea* (K+5); **18.** *Guembelitria blowi* (K+5); **19.** *Muricohedbergella holmdelensis* (K+5); **20.** *Muricohedbergella monmouthensis* (K+70); **21.** *Heterohelix globulosa* (K+5); **22.** *Heterohelix labellosa* (K+5); **23.** *Heterohelix planata* (K+20); **24.** *Heterohelix navarroensis* (K+5); **25.** *Globigerinelloides yaucoensis* (K+5); **26.** *Laeviheterohelix pulchra* (K+5); **27.** *Laeviheterohelix glabrans* (K+5); **28.** *Globigerinelloides prairiehillensis* (K+10); **29.** *Globigerinelloides volutus* (K+5); **30.** *Pseudoguembelina kempensis* (K+10); **31.** *Rugoglobigerina rugosa* (K+5). Scale bars: 100 μm.

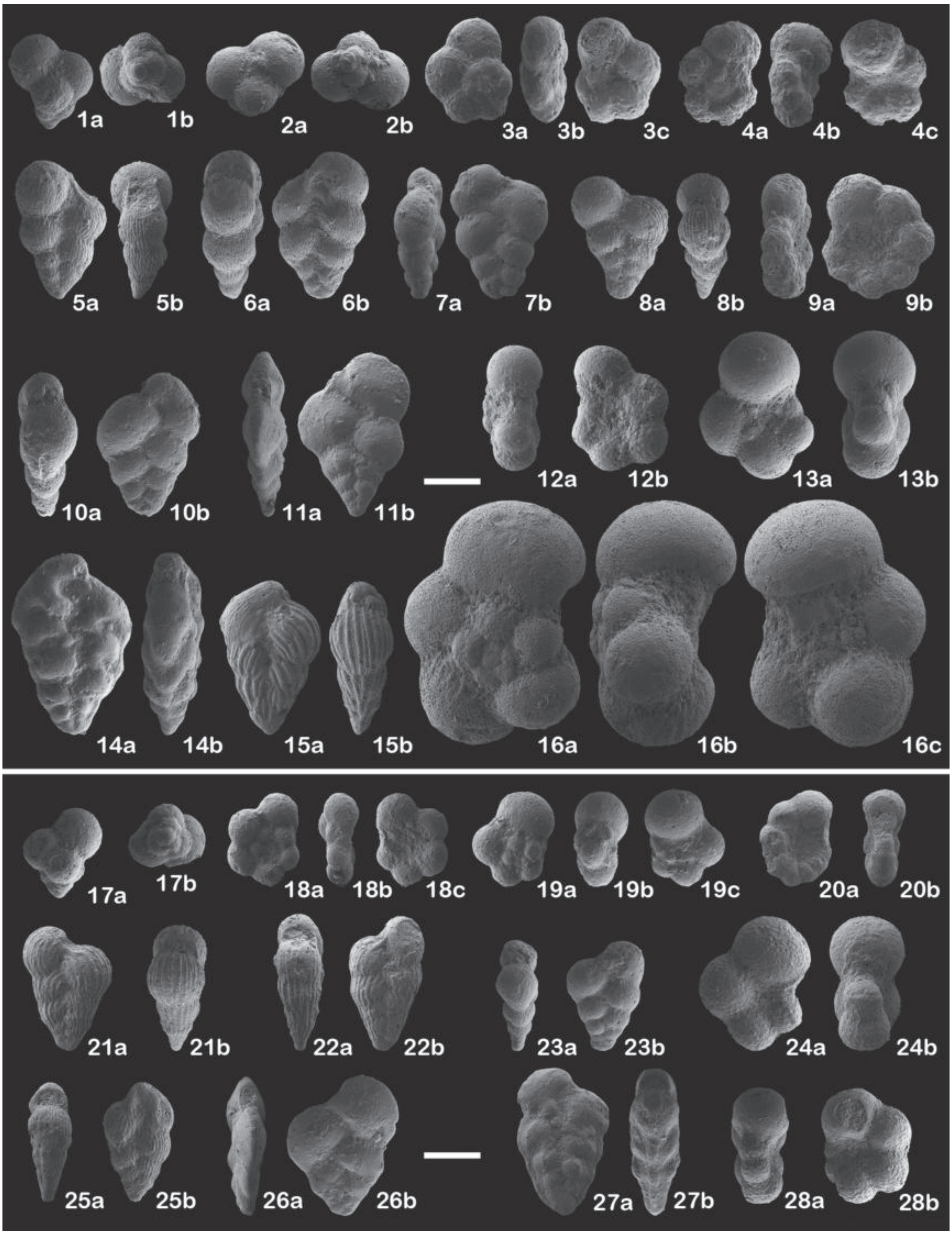

Figure 4. SEM photographs of the Maastrichtian species usually considered to be putative survivors of the KPB extinction. Specimen comparison from upper Maastrichtian and lower Danian samples at Sidi Ziane. Samples SZ numbered in cm from the KPB. Specimens in Maastrichtian samples: **1.** *Guembelitria cretacea* (SZ-40); **2.** *Guembelitria blowi* (SZ-40); **3.** *Muricohedbergella holmdelensis* (SZ-40); **4.** *Muricohedbergella monmouthensis* (SZ-850); **5.** *Heterohelix globulosa* (SZ-40); **6.** *Heterohelix labellosa* (SZ-40); **7.** *Heterohelix planata* (SZ-40); **8.** *Heterohelix navarroensis* (SZ-40); **9.** *Globigerinelloides yaucoensis* (SZ-820); **10.** *Laeviheterohelix pulchra* (SZ-40); **11.** *Laeviheterohelix glabrans* (SZ-40); **12.** *Globigerinelloides prairiehillensis* (SZ-40); **13.** *Globigerinelloides volutus* (SZ-40); **14.** *Pseudoguembelina kempensis* (SZ-40); **15.** *Pseudoguembelina costulata* (SZ-40); **16.** *Rugoglobigerina rugosa* (SZ-80). Specimens in Danian samples (from *Globanomalina compressa* Subzone, or Subbiozone P1c): **17.** *Guembelitria cretacea* (SZ+1); **18.** *Muricohedbergella holmdelensis* (SZ+1); **19.** *Muricohedbergella monmouthensis* (SZ+1); **20.** *Globigerinelloides yaucoensis* (SZ+1); **21.** *Heterohelix globulosa* (SZ+1); **22.** *Heterohelix labellosa* (SZ+1); **23.** *Heterohelix navarroensis* (SZ+1); **24.** *Globigerinelloides volutus* (SZ+1); **25.** *Pseudoguembelina costulata* (SZ+1); **26.** *Laeviheterohelix glabrans* (SZ+1); **27.** *Pseudoguembelina kempensis* (SZ+1); **28.** *Globigerinelloides prairiehillensis* (SZ+1). Scale bars: 100 µm.

was performed. 95% confidence intervals, based on 1999 bootstrap replicates, were calculated and added in scatter graphs of both exponential and power curves. The software used was the program PAST, version 4.04 for Mac (Hammer et al. 2001).

Second, we used counts of the average relative abundance (%) of the most relevant and/or abundant Maastrichtian planktic foraminiferal taxa in uppermost Maastrichtian and lowermost Danian samples from both the El Kef and Sidi Ziane sections (Suppl. material 2: Table S1, Suppl. material 3: Table S2). These counts were carried out at the genus and species levels and were used to determine the relative abundance distribution (RAD) of Maastrichtian species and genera in both upper Maastrichtian and lower Danian samples. Incoming Danian taxa were excluded from the calculation of the relative abundances in Danian samples. For the lower Danian, average relative abundances were calculated for two sample sets: i) all Danian samples, and ii) samples from the first 20 cm of Danian. In the El Kef section, average relative abundances of *Guembelitria* in the lower Danian were calculated with respect to: i) the total specimen number of both Maastrichtian and Danian species, and ii) the total specimen number of only Maastrichtian species.

4. Planktic foraminiferal biostratigraphy and biochronology

The stratigraphic ranges of planktic foraminiferal species in the El Kef section (Fig. 5) are based on Arenillas et al. (2000b) and subsequent revisions (see Arenillas and Arz 2017). Here we include data from the uppermost Maastrichtian biozone (Biozone CF1 of Li and Keller 1998, or *Plummerita hantkeninoides* Subzone of Arz and Molina 2002) and the first Danian biozones. The latter include the *Guembelitria cretacea* Zone (*Muricohedbergella holmdelensis* and *Parvularugoglobigerina longiapertura* Subzones), the *Parvularugoglobigerina eugubina* Zone (*Parvularugoglobigerina sabina* and *Eoglobigerina simplicissima* Subzones), and the *Parasubbotina pseudobulloides* Zone (*Eoglobigerina trivialis*, *Subbotina triloculinoides*, and *Globanomalina compressa* Subzones) of Arenillas et al. (2004). These are approximately equivalent to the most standardized Biozones P0 and Pα, and Subbiozones P1a, P1b, and P1c of Wade et al. (2011). According to Gilabert et al. (2022), the *Plummerita hantkeninoides* Subzone spans the last 99 kyr of the Maastrichtian. The bases of the lower Danian subzones of Arenillas et al. (2004) have recently been astronomically calibrated by Gilabert et al. (2022) to 0, 7, 18, 26, 68, 210, and 473 kyr after the KPB, respectively. The dark bed of the KPB Clay roughly coincides with the *Muricohedbergella holmdelensis* Subzone (Biozone P0). The stratigraphic ranges of planktic foraminiferal species in the Sidi Ziane section (Fig. 6) are based on Metsana-Oussaid et al. (2019), who recognized a relevant hiatus in the lower Danian, affecting the *Gb. cretacea* and *Pv. eugubina* Zones and *E. trivialis* and *S. triloculinoides* Subzones. According to the age model of Gilabert et al. (2022), the hiatus at Sidi Ziane spans approximately the first 500 kyr of the Danian.

5. Isotopic evidence a proxy for distinguishing of reworked specimens vs. survivor taxa

To infer the survival pattern that best fits what is observed in each KPB section, and before inferring the global survival model, which is part of the extinction model, the species that survived the KPB mass extinction must be identified. With a few exceptions, taphonomic evidence is hard to recognize in planktic foraminiferal specimens in lowermost Danian samples because it is difficult to find a simple visual criterion to distinguish reworked specimens. Only a few criteria have been cited, such as the differences in the preservation and coloration of reworked specimens compared to those of in situ specimens (Zumaia; Arz et al. 1999b), or the differences in the coloration of test infill in reworked specimens (ODP Site 1049; Huber et al. 2002). Isotopic evidence has been considered the most objective tool for testing the hypotheses on planktic foraminiferal extinction and survival models across the KPB. Comparison of the values of planktic foraminiferal $\delta^{18}O$, $\delta^{13}C$, and $^{87}Sr/^{86}Sr$ in Maastrichtian and Danian samples makes it possible to discern whether the Maastrichtian specimens found above the KPB are in situ or ex situ. If the tests of a particular Maastrichtian species have a Danian isotopic signal, differing significantly from the one they have in the Maastrichtian, they can be considered specimens in situ and consequently survivors, unless the isotopic signal is altered by diagenesis.

The first species to be considered a survivor based on isotopic evidence was *Heterohelix globulosa*, after analysis of its $\delta^{18}O$ and $\delta^{13}C$ values in both Maastrichtian and Danian from Brazos River (Barrera and Keller 1990; MacLeod and Keller 1994) and Nye Klov (Keller et al. 1993; Barrera and Keller 1994). However, other specialists raised doubts about this evidence, since the *H. globulosa* $\delta^{13}C$ values in the Maastrichtian and the Danian exhibited great similarity at ODP Sites 690 (Maud Rise; South Atlantic) and 750 (Kerguelen Plateau; Indian Ocean), suggesting that *H. globulosa* specimens are reworked in the Danian samples (Stott and Kennett 1990; Zachos et al. 1992). Barrera and Keller (1994) admitted that such isotopic similarity also occurred at ODP Site 738.

The second species to be recognized as a potential survivor based on isotopic evidence was *Rugoglobigerina rugosa*, following its isotopic analysis at Nye Klov (Keller et al. 1993). However, as in the case of *H. globulosa*, subsequent stable isotope studies again called this evidence into question (Huber 1996; MacLeod and Huber 1996; Kaiho and Lamolda 1999). For example, Huber (1996) noted that the $\delta^{13}C$ values of the *R. rugosa* (as well as *H. globulosa*) reported at Nye Klov by Keller et al.

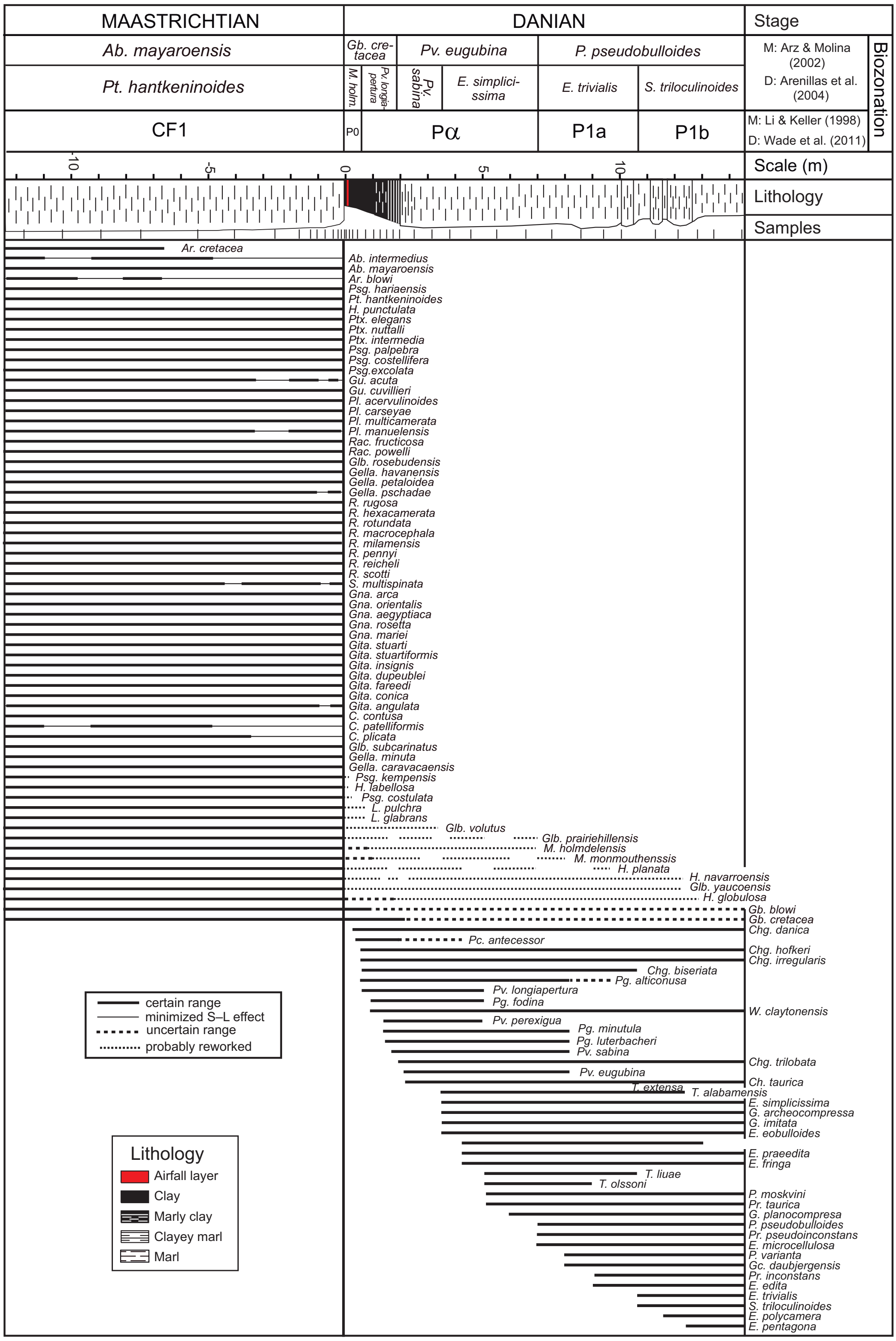

Figure 5. Stratigraphic ranges of the planktic foraminiferal species across the KPB in the El Kef section. Certain range = known stratigraphic range according to Arenillas et al. (2000b); minimized S-L effect = stratigraphic range after minimizing the Signor–Lipps effect and comparing with the stratigraphic ranges from other sections; uncertain range = doubtful stratigraphic ranges according to Arenillas and Arz (2017) and Arenillas et al. (2008); probably reworked = stratigraphic range based on probably reworked specimens (identified in the representative aliquot). M: Biozonation for the upper Maastrichtian; D: Biozonation for the lower Danian. Ar. – *Archaeoglobigerina*; Ab. – *Abathomphalus*; Psg. – *Pseudoguembelina*; Pt. – *Plummerita*; H. – *Heterohelix*; Ptx. – *Pseudotextularia*; Gu. – *Gublerina*; Pl. – *Planoglobulina*; Rac. – *Racemiguembelina*; Glb. – *Globigerinelloides*; Gella. – *Globotruncanella*; R. – *Rugoglobigerina*; S. – *Schackoina*; Gna. – *Globotruncana*; Gita. – *Globotruncanita*; C. – *Contusotruncana*; L. – *Laeviheterohelix*; M. – *Muricohedbergella*; Gb. – *Guembelitria*; Chg. – *Chiloguembelitria*; Pc. – *Pseudocaucasina*; Pg. – *Palaeoglobigerina*; Pv. – *Parvularuoglobigerina*; W. – *Woodringina*; T. – *Trochoguembelitria*; E. – *Eoglobigerina*; G. – *Globanomalina*; P. – *Parasubbotina*; Gc. – *Globoconusa*; Pr. – *Praemurica*; S. – *Subbotina*.

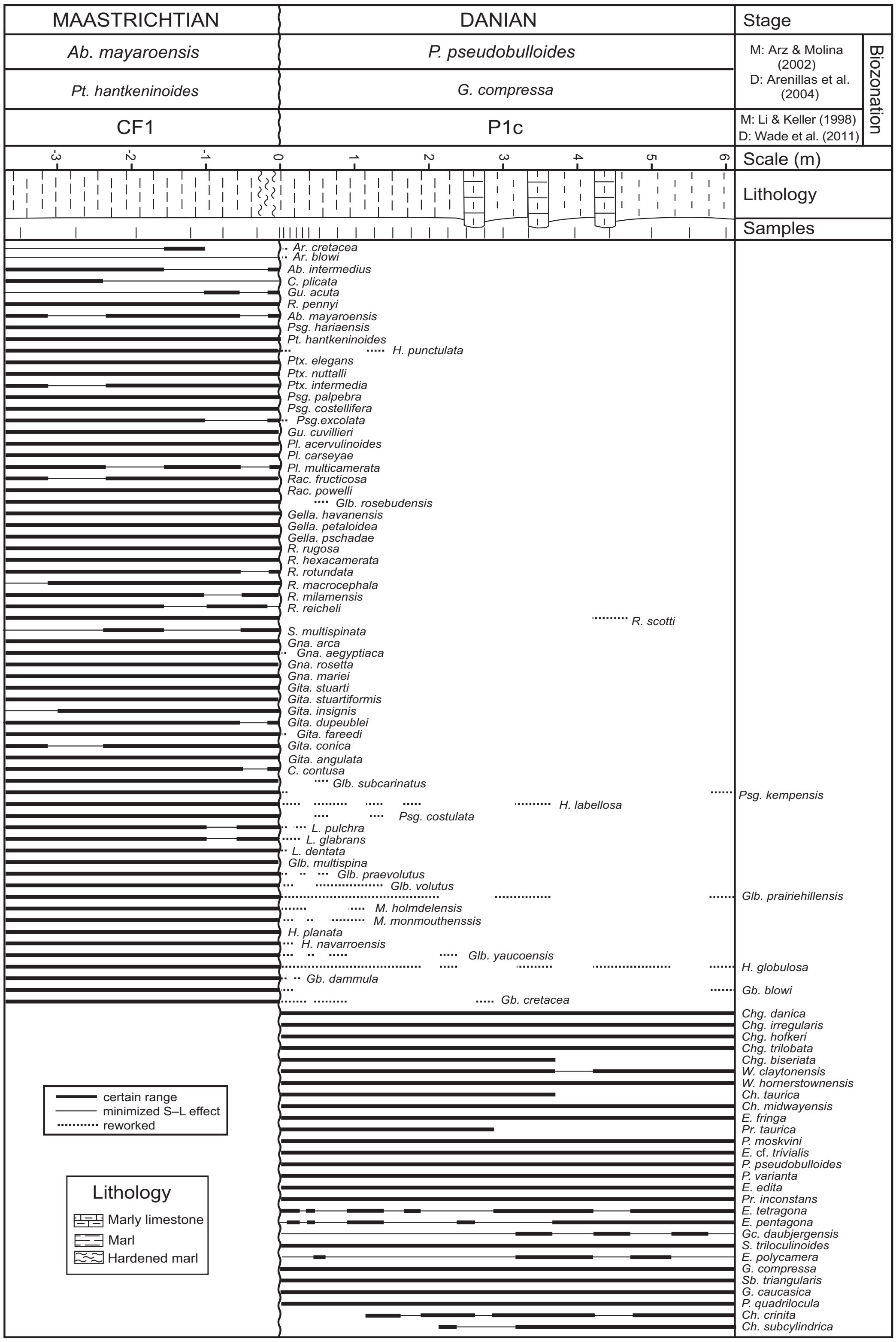

Figure 6. Stratigraphic ranges of the planktic foraminiferal species across the KPB in the Sidi Ziane section. Certain range = known stratigraphic range based on Metsana-Oussaid et al. (2019); minimized S-L effect = stratigraphic range after minimizing the Signor–Lipps effect and comparing with the stratigraphic ranges from other sections; reworked = stratigraphic range based on reworked Maastrichtian specimens (identified in the representative aliquot). M: Biozonation for the upper Maastrichtian; D: Biozonation for the lower Danian. Ar. – *Archaeoglobigerina*; Ab. – *Abathomphalus*; Psg. – *Pseudoguembelina*; Pt. – *Plummerita*; H. – *Heterohelix*; Ptx. – *Pseudotextularia*; Gu. – *Gublerina*; Pl. – *Planoglobulina*; Rac. – *Racemiguembelina*; Glb. – *Globigerinelloides*; Gella. – *Globotruncanella*; R. – *Rugoglobigerina*; S. – *Schackoina*; Gna. – *Globotruncana*; Gita. – *Globotruncanita*; C. – *Contusotruncana*; L. – *Laeviheterohelix*; M. – *Muricohedbergella*; Gb. – *Guembelitria*; Chg. – *Chiloguembelitria*; Pc. – *Pseudocaucasina*; Pg. – *Palaeoglobigerina*; Pv. – *Parvularuoglobigerina*; W. – *Woodringina*; T. – *Trochoguembelitria*; E. – *Eoglobigerina*; G. – *Globanomalina*; P. – *Parasubbotina*; Gc. – *Globoconusa*; Pr. – *Praemurica*; S. – *Subbotina.*

(1993) and Barrera and Keller (1994) do not exhibit any significant change across the KPB.

The next species to be isotopically proposed as survivors were those belonging to disaster opportunist *Guembelitria*. At Nye Klov, Barrera and Keller (1994) suggested that *Gb. cretacea*, *Gb. blowi* (called *Gb. trifolia* by these authors), and *Gb. dammula* (called *Gb. danica* by these authors) are survivors. Given that all planktic foraminiferal taxonomists and biostratigraphers agree that *Guembelitria* survived (Smit 1982; Keller 1988; Molina et al. 1996; Olsson et al. 1999; Arenillas et al. 2000a, 2000b, 2006, 2018; Huber et al. 2002; Keller and Pardo 2004; Birch et al. 2016; Lowery et al. 2018, 2020), this isotopic evidence can be considered a verification. However, we must note some taxonomic details. Arz et al. (2010) and Arenillas et al. (2017) warned of the existence of pseudocryptic species in the lowermost Danian among *Guembelitria* and *Chiloguembelitria* (*Gb. cretacea* vs. *Chg. danica*; *Gb. blowi* vs. *Chg. trilobata*; *Gb. dammula* vs. *Chg. hofkeri*), which are only differentiated by the position of the aperture and mainly by the wall texture. Therefore, many isotopic analyses on putative *Guembelitria* tests of the lower Danian were most likely performed on *Chiloguembelitria* tests. For this reason, Arenillas et al. (2017) raised doubts as to whether at least one of the *Guembelitria* species, *Gb. dammula*, was indeed a survivor.

Another species to be recognized as a survivor was *Zeauvigerina waiparaensis* (Huber and Boersma 1994; Olsson et al. 1999). Barrera and Keller (1994) obtained isotopic evidence at ODP Site 738 (Kerguelen Plateau; Indian Ocean), where *Z. waiparaensis*, which they called *Chiloguembelina waiparaensis*, became the dominant species of the early Danian foraminiferal assemblages. However, there are many doubts as to whether this species is planktic or benthic (Arenillas 2012; Lowery et al. 2020). Its planktic life-form was inferred by Huber and Boersma (1994) based on relative abundance counts, after discovering that, in the pelagic sections they studied, the relative abundance of *Z. waiparaensis* was higher than that of all the benthic species (see also Olsson et al. 1999). However, Huber and Boersma (1994) indicated that *Z. waiparaensis* yields stable isotopic values that are closer to benthic foraminiferal values than to planktic ones, raising doubts about its planktic life-form. Barrera and Keller (1994) also reported that the *Z. waiparaensis* $\delta^{13}C$ values are similar to benthic foraminiferal ones, although they used them as evidence of its deeper water habitat. These isotopic data could be more compatible with the hypothesis that *Z. waiparaensis* had a benthic life-form and was a disaster opportunist. A similar case could be *Rectoguembelina cretacea*, which is also considered a planktic species that survived the extinction event (Huber and Boersma 1994; Olsson et al. 1999).

Furthermore, Huber (1996) noted that, in addition to *Gb. cretacea* and *Z. waiparaensis*, there are other Maastrichtian species, such as *Muricohedbergella holmdelensis* and *Muricohedbergella monmouthensis*, that are considered survivors and ancestral to Cenozoic planktic foraminiferal lineages (Liu and Olsson 1992, 1994; Olsson et al. 1992, 1999; Aze et al. 2011; Lowery et al. 2018, 2020). Recently, Birch et al. (2016) contributed to the discussion by demonstrating with isotopic evidence that *M. holmdelensis* was a survivor. After reporting a relevant decrease in the $\delta^{13}C$ values of its test after the KPB at ODP Site 1262 (Walvis Ridge; South Atlantic), they concluded that the specimens of *M. holmdelensis* above the KPB had a Danian isotopic signal. Nevertheless, this evidence was based on a very low-resolution sampling, taking measurements on just four samples, of which only one was from the lowermost Danian. Consequently, more isotopic evidence will be needed before it can be concluded that *Muricohedbergella* was a Maastrichtian survivor like *Guembelitria*.

Subsequently, Keller (1997) also claimed to have isotopically demonstrated that *Globigerinelloides asper* was a survivor, although we have not been able to find any such evidence in the references cited by the author (Barrera and Keller 1990; Keller 1993; Keller et al. 1993). The latter only reported the high abundance of this species in the lower Danian of Brazos River, Nye Klov, and ODP Site 738C as evidence of its survival. Keller (1988, 1989a, 1989b), Huber (1991), and Barrera and Keller (1994) also noted the high relative abundance of other species of *Globigerinelloides*, such as *Glb. multispinus*, in the lower Danian, which could indicate that these survived the KPB extinction. However, Stott and Kennett (1990), Zachos et al. (1992), Barrera and Keller (1994), and Huber (1996) ruled this out, because the isotopic values showed very little difference below and above the KPB in the studied localities and were consistently very different from in situ specimens of co-occurring Danian species.

Most of the $\delta^{18}O$ and $\delta^{13}C$ studies have not been able to demonstrate that the Maastrichtian species found in Danian samples, except for *Gb. cretacea* and the allegedly planktic *Z. waiparaensis* and *Rec. cretacea*, were survivors. Conversely, there is much isotopic evidence showing that most of the Maastrichtian specimens found in the lowermost Danian are reworked (e.g., Stott and Kennett 1990; Zachos et al. 1992; Barrera and Keller 1994; Huber 1996; MacLeod and Huber 1996). The most extensive isotopic analysis of taxon-specific tests across the KPB was probably that conducted by Kaiho and Lamolda (1999) at Caravaca. They analyzed $\delta^{13}C$ values from specimens of 12 Maastrichtian species belonging to the genera *Globotruncana*, *Rugoglobigerina* (including *R. rugosa*), *Racemiguembelina*, *Pseudotextularia*, *Pseudoguembelina*, *Globigerinelloides* (including *Glb. asper*), and *Heterohelix* (including *H. globulosa*), which constituted > 99% of the total specimens (in the ≥ 63 μm size fraction) collected across the KPB. Their results were similar to those obtained by Zachos et al. (1992) and Huber (1996) for *H. globulosa* and *Globigerinelloides* spp. at ODP Sites 690, 738, and 750. Based on this isotopic evidence and the sharp decline in the relative and absolute abundance of these species, Kaiho and Lamolda (1999) concluded that most planktic foraminiferal species, except *Gb. cretacea*, did not survive and abruptly went extinct at the KPB.

Complementary studies of the $^{87}Sr/^{86}Sr$ ratios of taxon-specific tests at ODP Site 738 suggested an extensive and pervasive reworking across the KPB and led to the conclusion that there were likely to be few, if any, survivors after the KPB extinction event (MacLeod and Huber 1996). The results also implied that several methods for evaluating survival patterns (e.g., Keller 1993; Keller et al. 1993; MacLeod and Keller 1994) are flawed insofar as they fail to recognize extensive reworking.

In summary, isotopic evidence has been used to support both catastrophic and gradual hypotheses on planktic foraminiferal extinction and survival patterns across the KPB. This evidence may be flawed for several main reasons. First, diagenesis may have destroyed the original geochemical signature of the calcareous tests, and samples may not be suitable for isotopic studies. Second, the lower Danian specimens of Maastrichtian species used for isotopic analysis could be small, juvenile forms due to taphonomic selection by size, as already pointed out by Smit and Nederbragt (1997). In this case, they will always yield a different isotopic signal from those of the Maastrichtian regardless of whether they are survivors or reworked. Third, taxonomic assignment errors could lead to the use of specimens belonging to Danian species for isotopic analysis after erroneously assigning them to the analyzed Maastrichtian species, especially when the selection of tests was performed in samples from the < 63 µm size fraction.

6. Quantitatively and statistically testing the survival model

Quantitative data on relative abundances have also been used as a criterion to ascertain the survival model. The relative abundances of all Maastrichtian species except those of *Guembelitria* consistently decrease in the first cm of Danian in pelagic sections, so this could be used as a criterion for recognizing reworked specimens (e.g., Olsson 1997; Arenillas et al. 2000a, 2000b, 2006, 2016; Krahl et al. 2017; Gilabert et al. 2021b, 2022). However, because there are no incoming Danian species or their abundance is still very low, Maastrichtian species remain proportionally dominant in the basal part of the Danian, so this has also been used as evidence of survival (Keller 1988; Keller et al. 1995; Orue-Etxebarria 1997).

At Elles (Tunisia), Agost (Spain), and Caravaca (Spain), Arz et al. (1999a, 2000) observed in the lower Danian a sharp decrease in the relative abundance of all Maastrichtian species with the exception of *Guembelitria* spp. The decreases in these sections fitted well with a polynomial function, following a descending curve that they called the RASCS curve (Relative Abundance of the "Surviving" Cretaceous Species, or *ARECS* in the Spanish acronym). Arz et al. (1999a) interpreted the RASCS curve from Elles and Agost as the product of the progressive decrease in the abundance of Maastrichtian survivors as they were gradually replaced by the incoming Danian species. However, Arz et al. (2000) were not able to confirm the validity of this interpretation with dependable evidence at Caravaca. The late Maastrichtian species identified in the lower Danian samples were precisely the most abundant species in the Maastrichtian, and they seemed to disappear in an order corresponding almost exactly to their relative abundance in the late Maastrichtian, leading the authors to suspect the existence of a statistical relationship between the two terms (Arz et al. 1999a). The RASCS curves might simply represent the progressive decline of reworked Maastrichtian specimens across the lowermost Danian.

To delve further into this topic, we propose two types of tests to verify or refute whether the Maastrichtian species found in the lower Danian of El Kef and Sidi Ziane are in situ or ex situ: a statistical test based on nonlinear regression analyses to find equations that fit the downward curves of relative abundance in Maastrichtian specimens, and a quantitative test to calculate the average relative abundance distribution (RAD) of Maastrichtian species in both upper Maastrichtian and lower Danian samples.

6.1. Statistical tests (comparison of RASCS curves)

At El Kef, the asymptotic decrease in the relative abundance of Maastrichtian specimens, excluding *Guembelitria* spp., across the lower Danian (the RASCS curve) fits better with an exponential function (Akaike IC = 457.74) than a power function (Akaike IC = 5340.7). The RASCS curve at El Kef is fitted with the exponential equation $y = 105.63\ e^{-0.041314x} + 1.0737$ (Fig. 7A) and the power equation $y = 9313.9\ x^{-0.0011128} - 9247$ (Suppl. material 1:

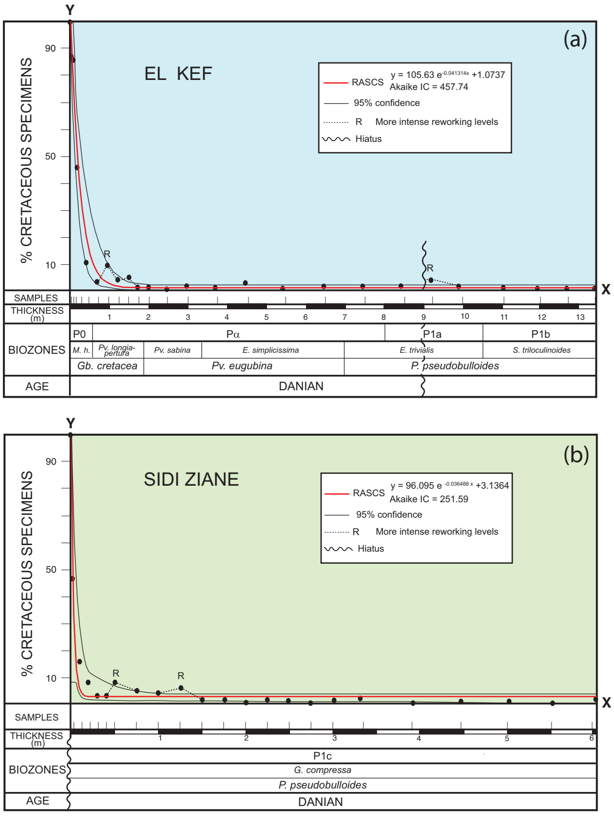

Figure 7. RASCS curves (relative abundance of the "surviving" Cretaceous species), fitted to an exponential function, across the lower Danian at **(A)** El Kef and **(B)** Sidi Ziane.

Fig. S1A). In both cases, but especially for the exponential model, all the *x-y* data fall within the 95% confidence interval, except the sample to 9.25 m above the KPB, which belongs to the *E. trivialis* Subzone (~ Subbiozone P1a). This sample appears to represent a level of more intense reworking and may be related to an erosive hiatus (Fig. 7A and Suppl. material 1: Fig. S1A). The thickness of the *E. trivialis* Subzone at El Kef is proportionally less than in other Tethyan localities (see Arenillas et al. 2004, and Molina et al. 2009), which could corroborate the existence of this short hiatus at El Kef. In the nearby Elles section, Arz et al. (1999a) also identified a hiatus affecting the *E. trivialis* Subzone, which is absent.

As at El Kef, the RASCS curve at Sidi Ziane is also better fitted to an exponential function (Akaike IC = 251.59) (Fig. 7B) than to a power function (Akaike IC = 455.09) (Suppl. material 1: Fig. S1B). It is fitted with the exponential equation $y = 96.095\ e^{-0.34886x} + 3.1364$ and the power equation $y = 63.925\ x^{-0.15091} - 26.598$. In both cases, but especially for the power model, all the *x-y* data fall within the 95% confidence interval, except for two samples in the lower part of the *G. compressa* Subzone (~ Subbiozone P1c), which have been attributed to levels of more intense reworking (Fig. 7B and Suppl. material 1: Fig. S1B).

As suggested by Arz et al. (1999a) for Elles and Agost, the RASCS curves (exponential and power) from El Kef could still be interpreted as the result of the gradual decline of Maastrichtian species due to their progressive replacement by the incoming Danian species, which were probably better adapted to the new and stressed environmental conditions after the KPB. However, this hypothesis is impossible to apply to the RASCS curves from Sidi Ziane, which are suspiciously similar to those of El Kef, both being better fitted with an exponential function. The RASCS curves in the Sidi Ziane section undoubtedly reflect the decrease in abundance of reworked Maastrichtian specimens in the Danian samples, including, unlike at El Kef, those of *Guembelitria*. This is so because the biostratigraphic interval that includes the *Gb. cretacea* Zone, the *Pv. eugubina* Zone, the *E. trivialis* Subzone and a large part of the *S. triloculinoides* Subzone, in which the extinctions of all supposedly surviving Maastrichtian species are recorded (e.g., Olsson et al. 1999; Arenillas et al. 2017, 2018), is missing at Sidi Ziane. The similarity of the RASCS curves in both sections suggests that those from El Kef are also the result of the progressive decrease in abundance of reworked Maastrichtian specimens in the lower Danian samples, i.e., in the time interval in which the planktic foraminiferal assemblages were progressively recovering and contributing more and more tests to the ocean bottom.

This interpretation was already suggested by Olsson (1997), who noted that, after the KPB catastrophic mass extinction event, the seafloor would be littered with Maastrichtian planktic foraminiferal tests, which would be easily remobilized until their final burial in Danian samples. Based on the vertical mixing model of Berger and Health (1968) for pelagic sediments, Olsson (1997) observed that the asymptotic decrease in the abundance of Maastrichtian species in the lowermost Danian (similar to the RASCS curves, but in terms of absolute abundance) fits with the mixing curve expected from reworking. Given certain assumptions for their model, Berger and Health (1968) demonstrated that the specimen concentration of a particular species decreases gradually in pelagic sediments upon its extinction, following an approximately exponential function.

6.2. Quantitative tests (comparison of RADs)

This type of test aims to quantitatively compare the Maastrichtian assemblages present in upper Maastrichtian samples and those present in lower Danian samples in order to identify differences or similarities in their relative abundance distribution (RAD). The RADs were estimated at genus and species levels, analyzing especially those genera and species that are more abundant or more relevant to the debate on the relative importance of reworked reworked specimens vs. survivor taxa (Suppl. material 2: Table S1, Suppl. material 3: Table S2). If numerous Maastrichtian species survived, the sudden environmental crisis triggered by the Chicxulub impact and its aftermath would have forced a sharp change in their RAD after the KPB boundary. We can assume therefore that, if the RADs are very similar before and after the KPB, the Maastrichtian specimens found in lowermost Danian samples were reworked as a result of vertical mixing by remobilization from older sediments. Additionally, bioturbation can foster the redistribution of microfossils, as well as abiotic components, in burrows further down or even up the KPB, which can influence interpretation of the extinction/survivorship patterns (Rodríguez-Tovar and Uchman 2008).

At El Kef (Arenillas et al. 2000b, 2018), the Maastrichtian species identified in lowermost Danian samples with a relative abundance high enough to be considered survivors were, ordered according to their alleged extinction horizon, the following: *Pseudoguembelina kempensis*, *Heterohelix labellosa*, *Pseudoguembelina costulata*, *Laeviheterohelix pulchra*, *L. glabrans*, *Globigerinelloides volutus*, *Glb. prairiehillensis*, *Muricohedbergella holmdelensis*, *M. monmouthensis*, *H. planata*, *H. navarroensis*, *Glb. yaucoensis*, *H. globulosa*, *Guembelitria blowi*, and *Gb. cretacea* (Figs 3, 5). Additionally, we have included *R. rugosa* because it is also frequently identified in lower Danian samples. The rest of the species are either very scarce or absent in the representative aliquot studied in each Danian sample (i.e., they can only be found after an intensive search to minimize the Signor–Lipps effect), so their presence in the Danian of El Kef was eliminated from Fig. 5. At Sidi Ziane, the Maastrichtian species identified in lowermost Danian samples are similar to those identified at El Kef (Fig. 6). The differences in the lower Danian stratigraphic ranges of the Maastrichtian species presumed surviving appear to be a reflection of the different Maastrichtian RADs between the two sections (Suppl. material 2: Table S1, Suppl. material 3: Table S2). The abundance of all the Maastrichtian genera identified in the upper Maastrichtian and the lower Danian samples is shown in Fig. 8 in order to visualize the RADs of Maastrichtian genera in the three chosen stratigraphic intervals (upper Maastrichtian, first 20 cm of Danian, and lower Danian).

The quantitative data show that at El Kef (Fig. 8; Suppl. material 2: Table S1) the late Maastrichtian assemblages are dominated by *Heterohelix* (72.4% average), followed by *Globigerinelloides* (9.8% average) and *Muricohedbergella* (5.3% average). The relative abundance of each other genus is always < 3% average, including *Guembelitria*, *Pseudoguembelina*, and *Rugoglobigerina*. In terms of species (Fig. 9; Suppl. material 2: Table S1), the most abundant by far is *Heterohelix. globulosa* (61.6% average), followed by *H. navarroensis* (6.2% average), *Globigerinelloides prairiehillensis* (4% average), and *Muricohedbergella holmdelensis* (3.8% average). At Sidi Ziane (Fig. 8; Suppl. material 3: Table S2), the late Maastrichtian assemblages exhibit some differences with respect to those at El Kef. *Heterohelix* is also the predominant genus (41.3% average), but the relative abundances of *Globigerinelloides* (21.3% average) and *Guembelitria* (18.6% average) are proportionally much higher. The rest of the genera have an average abundance similar to those at El Kef, albeit slightly higher in *Muricohedbergella* (5.7% average), *Pseudoguembelina* (3.9% average), and *Rugoglobigerina* (2.9% average).

When the upper Maastrichtian and lower Danian RADs of Maastrichtian species are compared, a strong similarity can be observed in both sections (Figs 8, 9; Suppl. material 2: Table S1, Suppl. material 3: Table S2), indicating that all the Maastrichtian specimens are reworked in the Danian samples, except those of *Guembelitria* at El Kef.

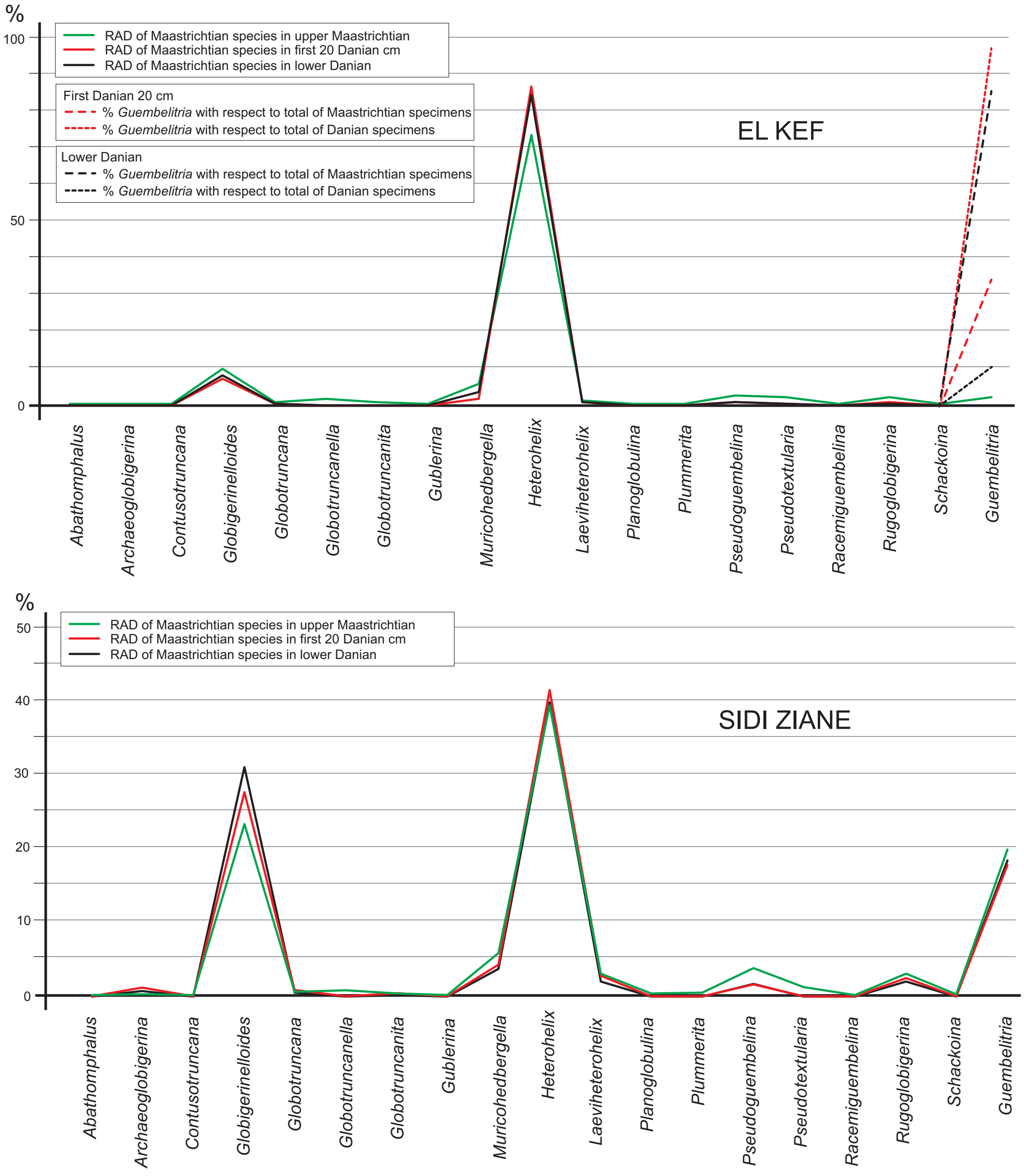

Figure 8. Comparison of the relative abundance distributions (RADs) of Maastrichtian genera in Maastrichtian (green color) and Danian (red-black colors) samples from El Kef and Sidi Ziane.

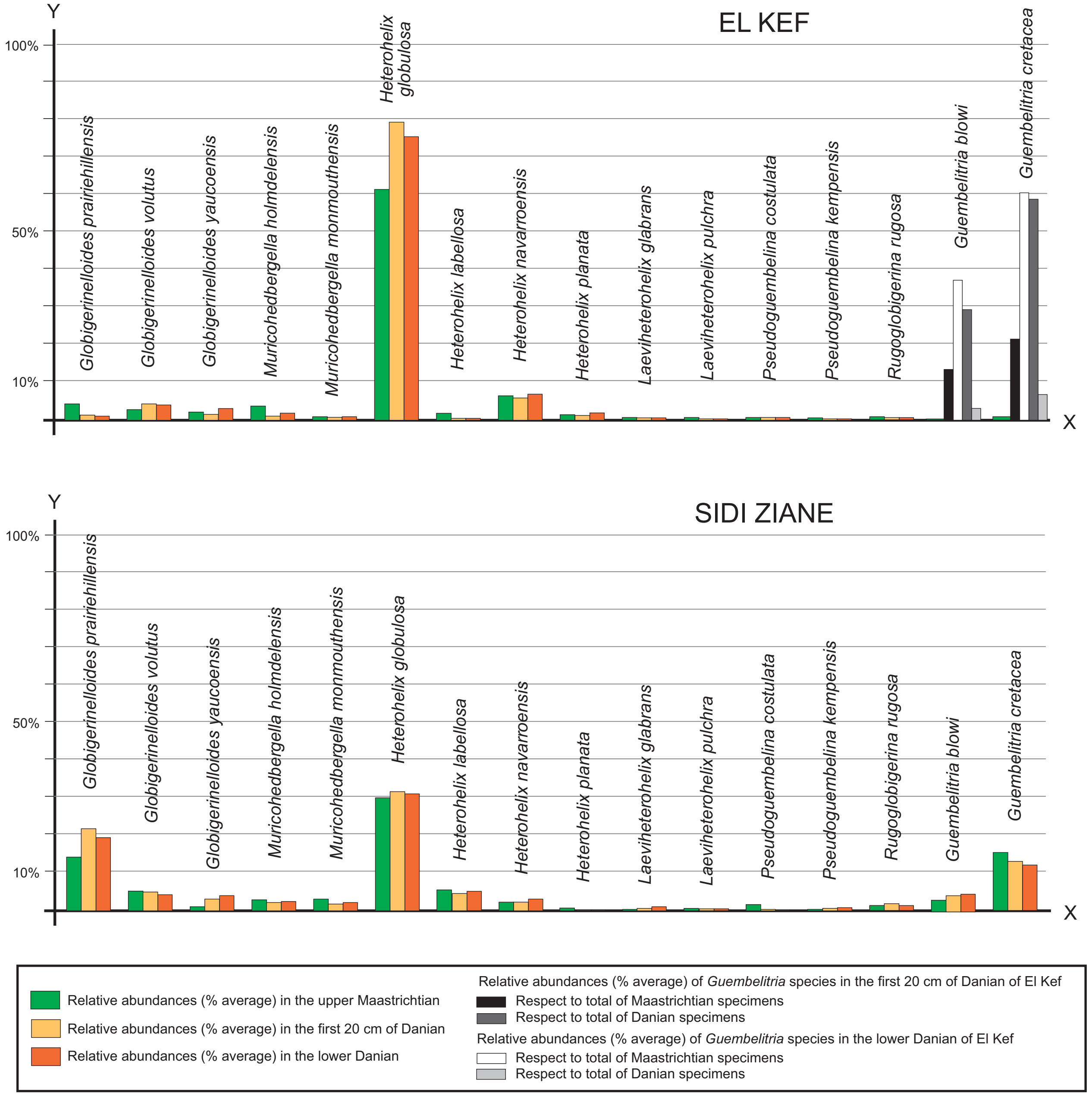

Figure 9. Comparison of the relative abundance of some Maastrichtian species in Maastrichtian and Danian samples from El Kef and Sidi Ziane. At El Kef, *Guembelitria* spp. were excluded from the count in Danian samples.

7. Evidence for the survival of Maastrichtian taxa

Many biostratigraphers have concluded that, if the aforementioned Signor–Lipps and reworking effects are minimized, the planktic foraminiferal extinction model is more compatible with a catastrophic mass extinction event occurring exactly at the KPB (e.g., Smit 1990; Molina et al. 1996, 1998; Olsson 1997; Smit and Nederbragt 1997; Arenillas et al. 2000a, 2000b; Arz et al. 2000; Koutsoukos 2014; Molina 2015; Lowery et al. 2018; Gilabert et al. 2021b, 2022). Next, we analyze the genera that are most often considered to be survivors, especially *Guembelitria*, *Heterohelix* s.l., and *Muricohedbergella*, with a view to verifying or refuting the catastrophic hypothesis. All the average relative abundances mentioned below are exclusively with respect to the total Maastrichtian planktic foraminiferal specimens (excluding the incoming Danian taxa), both in Maastrichtian and Danian samples.

7.1. Survival of *Guembelitria*

Guembelitria was undoubtedly a survivor given the amount of evidence that has been reported, not only isotopic (Barrera and Keller 1994; Birch et al. 2016) but also quantitative and phylogenetic. Two of its species, *Gb. cretacea* and *Gb. blowi*, may in fact be the only species surviving the KPB extinction event (Arenillas and

Arz 2017; Arenillas et al. 2018). It has also been widely demonstrated that the abundance of *Guembelitria* increased after the KPB (e.g., Smit 1982; Molina et al. 1996; Smit and Nederbragt 1997; Arenillas et al. 1998, 2000a, 2000b; Punekar et al. 2014; Lowery et al. 2018; Krahl et al. 2020; Gilabert et al. 2021b, 2022). In addition, *Guembelitria* played a relevant role in the phylogeny of Danian taxa (Olsson et al. 1999), having been widely shown to be the ancestor, through *Chiloguembelitria*, of two Danian lineages: the biserial lineage that groups together *Woodringina* and *Chiloguembelina*, and the trochospiral lineage that groups *Trochoguembelitria* and *Globoconusa* (see Arenillas and Arz 2017).

The survival of *Guembelitria* is again verified in the quantitative analysis carried out at El Kef. Its relative abundance increases abruptly in the first 20 cm of Danian, with an average of 34.3% if we only take Maastrichtian species into account, or 97.1% if we only take Danian species into account, which contrasts with its average relative abundance (1.8%) in the upper Maastrichtian (Fig. 8; Suppl. material 2: Table S1). If we consider all the samples from the lower Danian, the average relative abundance of *Guembelitria* increases to 86.6% for the total Maastrichtian specimens but drops to 10.2% when we consider only Danian specimens. There are two reasons for the latter: i) incoming Danian taxa increase in abundance across the lower Danian, and ii) the genus *Chiloguembelitria* has been taxonomically differentiated from *Guembelitria*. At Sidi Ziane, unlike at El Kef, the average relative abundances of *Guembelitria* both in the lower Danian (18.4%) and the first 20 cm of Danian (17.7%) are very similar to those in the upper Maastrichtian (18.6%) (Fig. 9; Suppl. material 3: Table S2), evidencing that, as expected given the hiatus in the lower Danian, the *Guembelitria* specimens found in the Danian of Sidi Ziane are reworked.

7.2. Survival of *Heterohelix* s.l.?

One of the genera most commonly considered a survivor is *Heterohelix* s.l. (*Heterohelix* and *Laeviheterohelix*), especially *H. globulosa* but also *H. navarroensis*, *H. planata*, *H. labellosa*, *L. pulchra*, and *L. glabrans*. Phylogenetic evidence has been proposed to support this, since *Heterohelix* has on occasion been considered the ancestor of the Paleogene genus *Chiloguembelina* (e.g., Apellaniz et al. 2002). However, this proposal has been rejected in most phylogenetic studies (e.g., Olsson et al. 1999), since it has been demonstrated that *Chiloguembelina* is a descendant of *Woodringina*, and this in turn of *Chiloguembelitria* (Arenillas et al. 2017).

The high relative abundance of *Heterohelix* s.l. in lowermost Danian samples has been put forward as among the strongest evidence for its survival (e.g., Pardo and Keller 2008). Here, however, we refute this evidence. In both El Kef and Sidi Ziane, the average relative abundance of *Heterohelix* s.l. in the Danian samples is similar to, or only slightly higher than, that in the Maastrichtian samples, both in the first 20 cm of Danian and in the Danian interval studied as a whole. At El Kef, its average relative abundance goes up slightly to ~ 85% but, at Sidi Ziane, it remains stable at around 40% (Fig. 8; Suppl. material 2: Table S1). This quantitative pattern across the KPB is repeated when we observe the average relative abundances of the dominant species *H. globulosa* (Fig. 9). At Sidi Ziane, the average relative abundance of *Heterohelix* s.l. in lower Danian samples seems to reflect that of the total Maastrichtian samples (Fig. 8; Suppl. material 3: Table S2). The survival of *Heterohelix* s.l. appears to be refuted since its quantitative pattern across the KPB in El Kef is very similar to that in Sidi Ziane, where it is obvious that the *Heterohelix* s.l. specimens are reworked.

7.3. Survival of *Muricohedbergella*?

Another of the genera whose survival has been most frequently asserted is *Muricohedbergella* (Huber 1996; Olsson 1997; Olsson et al. 1999; Huber et al. 2002; Koutsoukos 2014; Birch et al. 2016; Lowery et al. 2018, 2020), including the species *M. holmdelensis* and *M. monmouthensis*. *Muricohedbergella* is also commonly considered the ancestor of two Danian lineages (e.g., Olsson et al. 1999; Aze et al. 2011): the spinose lineage that groups together *Eoglobigerina*, *Parasubbotina*, and *Subbotina*, and the non-spinose lineage that groups *Globanomalina* and *Praemurica*. As in the case of *Gb. cretacea*, Huber (1996), Olsson (1997) and Koutsoukos (2014) proposed that *Muricohedbergella* should also be considered a survivor based on this phylogenetic evidence, by contrast with the original proposal made by Smit (1982). After ascertaining that the biostratigraphic ranges of *Muricohedbergella* and the spinose and non-spinose lineages do not overlap in the lower Danian (Arenillas et al. 2000a, 2000b), Arenillas and Arz (2000) disproved the claim that *Muricohedbergella* was the ancestral form of these lineages, proposing instead that it was the ancestor of parvularugoglobigerinids. However, this latter phylogenetic proposal was also refuted by Arenillas and Arz (2017). Based on Brinkhuis and Zachariasse (1988), these authors proposed that the parvularugoglobigerinids, which are the most probable ancestor of the spinose and non-spinose lineages (Arenillas et al. 2018, and references herein), evolved from the benthic genus *Caucasina*, which exhibits a similar microperforate, smooth wall texture, *Pseudocaucasina antecessor* being its first representative. If verified, this hypothesis implies not only that the main Cenozoic lineages of trochospiral planktic foraminifera, whose descendants have reached the present day, could have a benthic origin after the KPB, but also that the phylogenetic evidence for the survival of *Muricohedbergella* is disproved.

The new quantitative data obtained at El Kef likewise appear not to support the survival of *Muricohedbergella*. At El Kef (Figs 8, 9; Suppl. material 2: Table S1), the average relative abundance of *Muricohedbergella* decreases in Danian samples (3.5%) relative to the Maastrichtian (5.3%), especially in the first 20 cm of Danian (2%). If incoming Danian species are taken into account, the relative abundance of *Muricohedbergella* tends to zero in the first 20 cm of Danian, as with the other Maastrichtian genera except *Guembelitria*. At Sidi Ziane (Figs 8, 9; Suppl. material 3: Table S2), the abundance of *Muricohedbergella* in Danian samples also decreases, albeit more slightly (from 5.6% to ~ 4%). This very similar quantitative pattern in both sections seems to refute the idea that *Muricohedbergella* was a survivor. Unlike *Guembelitria*, the relative and/or absolute abundance of *Muricohedbergella* declined abruptly after the KPB until its supposed extinction in the earliest Danian, just the opposite of what might be expected of generalist taxa in a period of environmental recovery (Arenillas et al. 2000a, 2000b, 2018).

7.4. Survival of other Maastrichtian taxa?

Interpretations similar to those for *Heterohelix* s.l. and *Muricohedbergella* are derived from the quantitative patterns for *Globigerinelloides*, *Pseudoguembelina*, and *Rugoglobigerina* at El Kef and Sidi Ziane. In both sections, their average relative abundances in Danian sediments are similar to those in Maastrichtian sediments (Figs 8, 9; Suppl. material 2: Table S1, Suppl. material 3: Table S2). Only of *Globigerinelloides* does the relative abundance appear to increase significantly at Sidi Ziane in Danian samples (~ 30%) with respect to Maastrichtian samples (~ 23%). However, this increase may be due to the significantly higher abundance of this genus in the last 400 Maastrichtian centimeters (Suppl. material 3: Table S2). There is also no quantitative evidence of survival at El Kef and Sidi Ziane for other Maastrichtian genera such as *Abathomphalus*, *Archaeoglobigerina*, *Contusotruncana*, *Globotruncana*, *Globotruncanella*, *Globotruncanita*, *Gublerina*, *Planoglobulina*, *Plummerita*, *Pseudotextularia*, *Racemiguembelina*, and *Schackoina*, and the species they contain (Figs 8, 9; Suppl. material 2: Table S1, Suppl. material 3: Table S2).

The quantitative and statistical evidence from El Kef and Sidi Ziane refuting the survival of all the Maastrichtian taxa except *Guembelitria* agrees with independent quantitative evidence reported by Arenillas et al. (2018) from El Kef and Aïn Settara (Tunisia), based on calculations of the relative abundance of specimens with abnormal morphologies. The authors observed in the lowermost Danian a strong increase in aberrant forms (> 10%) among *Guembelitria* and incoming Danian species, and attributed this to huge environmental changes induced mainly by the Chicxulub impact. Gilabert et al. (2021b) reported similar increases in aberrant forms of *Guembelitria* and other Danian species in the lowermost Danian of Caravaca. These findings contrasted with very low percentages (< 1%) of aberrant Maastrichtian specimens, including those of *Heterohelix* s.l. and *Muricohedbergella*, in the lowermost Danian samples, which were very similar to the percentages of aberrant specimens estimated in Maastrichtian samples. This teratological evidence suggests that, except for *Guembelitria*, all Maastrichtian specimens (aberrants and non-aberrants alike) found in the lowermost Danian of El Kef, Aïn Settara, and Caravaca are in fact reworked.

The hypothesis of a single surviving genus (*Guembelitria*) is also in agreement with the biostratigraphic data reported by Arenillas et al. (2016) in the Moncada section (Cuba), which was located in the middle to upper slope of the eastern Yucatan continental margin when the Chicxulub asteroid impacted (Tada et al. 2002). This KPB section is characterized by a 2 m thick, ejecta-rich clastic deposit, locally named the Moncada Formation, which disconformably overlies the Albian micritic limestones of the Pons Formation, and unconformably underlies the earliest Danian marly limestones of the Ancón Formation (Tada et al. 2002; Arenillas et al. 2016). The Moncada section offered an excellent opportunity to test the survival of Maastrichtian taxa because it is continuous and complete in the lowermost Danian, and the underlying Upper Cretaceous sediments were removed by the huge Chicxulub impact-triggered debris flow, which transported them towards deeper locations. After analyzing the first 125 cm of Danian of the Moncada section in detail, Arenillas et al. (2016) revealed the lack of Maastrichtian taxa in the Danian samples, including the generalist and cosmopolitan *Heterohelix* s.l. and *Muricohedbergella*, unlike what happens in most pelagic sections worldwide such as El Kef and Sidi Ziane. Only specimens of the opportunist *Guembelitria* were found in the Danian, its relative abundance reaching 100% of the planktic foraminiferal assemblages. The previous erosion and disappearance of Maastrichtian deposits by the Chicxulub-linked sedimentological disturbances at the eastern Yucatan continental margin may have minimized the tendency for reworked Maastrichtian specimens to arrive in the Moncada area, preventing their presence in the lowermost Danian. This finding was relevant because it supports the hypothesis that only *Guembelitria* survived the KPB mass extinction triggered by the Chicxulub impact.

8. Conclusions

After reviewing the planktic foraminiferal extinction models and the causes proposed for the Cretaceous/Paleogene boundary (KPB) mass extinction event, it can give the wrong impression that there is still no conclusive evidence to support any single one of them. One of the main disputes focuses on the severity of the KPB extinction, i.e. on the proportion of surviving species after the KPB event (survival model). This dispute is grounded in the controversy over the relative importance of "reworked specimens vs. survivor taxa", i.e. the question how many Maastrichtian species identified in the lower Danian of pelagic sections were survivors and how many were the result of reworking processes. New quantitative and statistical evidence from the El Kef stratotype section (Tunisia), recognized as the most continuous, complete, and expanded lower Danian section worldwide, and the Sidi Ziane section (Algeria), affected by a relevant hiatus in the lower Danian, supports the notion that all the latest Maastrichtian species, except those of *Guembelitria*, went extinct exactly at the KPB. Nonlinear regression analyses indicate that the equation that best fits the asymptotically decreasing curve of the relative abundance of Maastrichtian specimens in lower Danian samples (the RASCS curve) is an exponential equation in both El Kef and Sidi Ziane, adjusting well to the vertical mixing curve expected by reworking processes. The similar relative abundance distribution (RAD) of the Maastrichtian planktic foraminiferal assemblages recorded in the upper Maastrichtian and the lower Danian of El Kef and Sidi Ziane indicates that all the Maastrichtian specimens found in Danian samples, except those of *Guembelitria*, are reworked. The obvious Maastrichtian paleobiological signal of the RADs of the Maastrichtian species in the lower Danian of El Kef leads one to conclude that the survival model of the Maastrichtian planktic foraminiferal species after the KPB event is definitely compatible with a model of almost total catastrophic extinction caused by the Chicxulub impact.

Data availability

All data and supplementary figures are included as supplementary materials.

Author contributions

IA led the writing and organization of the manuscript. IA and JAA performed the biostratigraphy and quantitatively analyzed the micropaleontological samples from El Kef and Sidi Ziane. FMD and DB sampled and stratigraphically analyzed the Sidi Ziane section. VG provided magnetochronological and astronomical calibrations and reviewed the quantitative and statistical analyses. All co-authors assisted with the conceptualization and writing of the manuscript.

Competing interests

The authors declare that they have no conflict of interest.

Acknowledgements

We thank Guilherme Krahl and Andrew Fraass for their constructive reviews. This work was supported by the Ministerio de Ciencia, Innovación y Universidades (MCIU) / Agencia Estatal de Investigación (AEI) / European Regional Development Fund (ERDF) (grant PGC2018-093890-B-I00), and by the Aragonese Government / ERDF (grant DGA group E33_20R). V. Gilabert is supported by the Spanish Ministry of Economy and Competitiveness (MINECO) (FPI grant BES-2016-077800). We thank R. Glasgow for improving the English text.

References

Apellaniz E, Baceta JI, Bernaola-Bilbao G, Nuñez-Betelu K, Orue-Extebarria X, Payros A, Pujalte V, Robin E, Rocchia R (1997) Analysis of uppermost Cretaceous–lowermost Tertiary hemipelagic successions in the Basque Country (Western Pyrenees): Evidence for a sudden extinction of more than half planktic foraminifer species at the K/T boundary. Bulletin de la Société Géologique de France 168(6): 783–793.

Apellaniz E, Orue-Etxebarria X, Luterbacher HP (2002) Evolution of the early Paleocene planktonic foraminifera: A Basque point of view. Neues Jahrbuch für Geologie und Palaontologie – Abhandlungen 225(2): 157–194. https://doi.org/10.1127/njgpa/225/2002/157

Arenillas I (2012) Patterns of spatio-temporal distribution as criteria for the separation of planktic foraminiferal species across the Danian-Selandian transition in Spain. Acta Palaeontologica Polonica 57(2): 401–422. https://doi.org/10.4202/app.2010.0076

Arenillas I, Arz JA (2000) *Parvularugoglobigerina eugubina* type-sample at Ceselli (Italy): Planktic foraminiferal assemblage and lowermost Danian biostratigraphic implications. Rivista Italiana di Paleontologia e Stratigrafia 106(3): 379–390. https://doi.org/10.13130/2039-4942/6152

Arenillas I, Arz JA (2017) Benthic origin and earliest evolution of the first planktonic foraminifera after the Cretaceous/Paleogene boundary mass extinction. Historical Biology 29(1): 17–24. https://doi.org/10.1080/08912963.2015.1119133

Arenillas I, Arz JA, Molina E (1998) El límite Cretácico/Terciario de Zumaya, Osinaga y Músquiz (Pirineos): control bioestratigráfico y cuantitativo de hiatos con foraminíferos planctónicos. Revista de la Sociedad Geológica de España 11(1–2): 127–138.

Arenillas I, Arz JA, Molina E, Dupuis C (2000a) The Cretaceous/Paleogene (K/P) boundary at Aïn Settara, Tunisia: Sudden catastrophic mass extinction in planktic foraminifera. Journal of Foraminiferal Research 30: 202–218. https://doi.org/10.2113/0300202

Arenillas I, Arz JA, Molina E, Dupuis C (2000b) An independent test of planktonic foraminiferal turnover across the Cretaceous/Paleogene (K/P) boundary at El Kef, Tunisia: Catastrophic mass extinction and possible survivorship. Micropaleontology 46: 31–49.

Arenillas I, Arz JA, Molina E (2004) A new high-resolution planktic foraminiferal zonation and subzonation for the lower Danian. Lethaia 37: 79–95. https://doi.org/10.1080/00241160310005097

Arenillas I, Arz JA, Grajales-Nishimura JM, Murillo-Muñetón G, Alvarez W, Camargo-Zanoguera A, Molina E, Rosales-Domínguez C (2006) Chicxulub impact event is Cretaceous/Paleogene boundary in age: new micropaleontological evidence. Earth and Planetary Science Letters 249: 241–257. https://doi.org/10.1016/j.epsl.2006.07.020

Arenillas I, Arz JA, Grajales-Nishimura JM, Rojas-Consuegra R (2016) The Chicxulub impact is synchronous with the planktonic foraminifera mass extinction at the Cretaceous/Paleogene boundary: New evidence from the Moncada section, Cuba. Geologica Acta 14(1): 35–51. https://doi.org/10.1016/j.epsl.2006.07.020

Arenillas I, Arz JA, Gilabert V (2017) Revalidation of the genus *Chiloguembelitria* Hofker: Implications for the evolution of early Danian planktonic foraminifera. Journal of African Earth Sciences 134: 435–456. https://doi.org/10.1016/j.jafrearsci.2017.07.011

Arenillas I, Arz JA, Gilabert V (2018) Blooms of aberrant planktic foraminifera across the KPB in the Western Tethys: Causes and evolutionary implications. Paleobiology 44(3): 460–489. https://doi.org/10.1017/pab.2018.16

Arz JA, Molina E (2002) Bioestratigrafía y cronoestratigrafía con foraminíferos planctónicos del Campaniense superior y Maastrichtiense de latitudes subtropicales y templadas (España, Francia y Tunicia). Neues Jahrbuch für Geologie und Palaontologie – Abhandlungen 224: 161–195. https://doi.org/10.1127/njgpa/224/2002/161

Arz JA, Arenillas I, Molina E, Dupuis C (1999a) Los efectos tafonómico y "Signor–Lipps" sobre la extinción en masa de foraminíferos planctónicos en el límite Cretácico/Terciario de Elles (Tunicia). Revista de la Sociedad Geológica de España 12(2): 251–268.

Arz JA, Arenillas I, Molina E (1999b) Extinción de foraminíferos planctónicos en el tránsito Cretácico-Terciario de Zumaya (Guipúzcoa): ¿supervivencia o reelaboración? Revista Española de Micropaleontología 33(3): 297–304.

Arz JA, Arenillas I, Molina E, Sepúlveda R (2000) La estabilidad faunística de foraminíferos planctónicos en el Maastrichtiense superior y su extinción en masa catastrófica en el límite K/T de Caravaca, España, Revista Geológica de Chile 27: 27–47. https://doi.org/10.4067/S0716-02082000000100003

Arz JA, Arenillas I, Náñez C (2010) Morphostatistical analysis of Maastrichtian populations of *Guembelitria* from El Kef, Tunisia. Journal of Foraminiferal Research 40(2): 148–164. https://doi.org/10.2113/gsjfr.40.2.148

Aze T, Ezard THG, Purvis A, Coxall H, Stewart DRM, Wade BS, Pearson PN (2011) A phylogeny of Cenozoic macroperforate planktonic foraminifera from fossil data. Biological Reviews 86: 900–927. https://doi.org/10.1111/j.1469-185X.2011.00178.x

Barrera E, Keller G (1990) Stable isotope evidence for gradual environmental changes and species survivorship across the Cretaceous/Tertiary boundary. Paleoceanography 5: 867–890. https://doi.org/10.1029/PA005i006p00867

Barrera E, Keller G (1994) Productivity across the Cretaceous–Tertiary boundary in high latitudes. Geological Society of America Bulletin 106: 12547–1266. https://doi.org/10.1130/0016-7606(1994)106%3C1254:PATCTB%3E2.3.CO;2

Berger WH, Health GR (1968) Vertical mixing in pelagic sediments. Journal of Marine Research 2: 134–143.

Birch HS, Coxall HC, Pearson PN, Kroon D, Schmidt DN (2016) Partial collapse of the marine carbon pump after the Cretaceous–Paleogene boundary. Geology 44(4): 287–290. https://doi.org/10.1130/G37581.1

Brinkhuis H, Zachariasse WJ (1988) Dinoflagellate cysts, sea level changes and planktonic foraminifers across the Cretaceous–Tertiary boundary at El Haria, Northwest Tunisia. Marine Micropaleontology 13: 153–191. https://doi.org/10.1016/0377-8398(88)90002-3

Canudo JI (1997) El Kef blind test I results, Marine Micropaleontology 29(2): 73–76. https://doi.org/10.1016/S0377-8398(96)00040-0

Canudo JI, Keller G, Molina E (1991) Cretaceous/Tertiary boundary extinction pattern and faunal turnover at Agost and Caravaca, SE Spain, Marine Micropaleontology 17: 319–341. https://doi.org/10.1016/0377-8398(91)90019-3

Courtillot VE, Feraud G, Maluski H, Vandamme D, Moreau MG, Besse J (1998) Deccan flood basalts and the Cretaceous/Tertiary boundary. Nature 333: 843–846. https://doi.org/10.1038/333843a0

Gallala N (2013) Planktonic foraminiferal biostratigraphy and correlation across the Cretaceous-Paleogene transition at the Tethyan and the Atlantic realms. Paleontology Journal 2013: e643278. https://doi.org/10.1155/2013/643278

Gallala N (2014) Biostratigraphie, paléoécologie et zones d'acmé des foraminifères planctoniques au passage Crétacé-Paléogène dans la Téthys (Tunisie et Espagne) et l'Atlantique (France). Annales de Paléontologie 100(3): 193–215. https://doi.org/10.1016/j.annpal.2013.11.005

Gallala N, Zaghbib-Turki D, Molina E, Arenillas I, Arz JA (2009) Catastrophic mass extinction and assemblage evolution in planktic foraminiferal across the Cretaceous/Paleogene (K/Pg) boundary at Bidart (SW France). Marine Micropaleontology 72: 196–209. https://doi.org/10.1016/j.marmicro.2009.05.001

Gilabert V, Arz JA, Arenillas I, Robinson SA (2021a) Influence of the Latest Maastrichtian Warming Event on planktic foraminiferal assemblages and ocean carbonate saturation at Caravaca, Spain. Cretaceous Research 125: 104844. https://doi.org/10.1016/j.cretres.2021.104844

Gilabert V, Arenillas I, Arz JA, Batenburg SJ, Robinson SA (2021b) Multiproxy analysis of paleoenvironmental, paleoclimatic and paleoceanographic changes during the Early Danian in the Caravaca section (Spain). Palaeogeography Palaeoclimatology Palaeoecology 576: 110513. https://doi.org/10.1016/j.palaeo.2021.110513

Gilabert V, Batenburg SJ, Arenillas I, Arz JA (2022) Contribution of orbital forcing and Deccan volcanism to global climatic and biotic changes across the KPB at Zumaia, Spain. Geology 50(1): 21–25. https://doi.org/10.1130/G49214.1

Ginsburg RN (1997a) An attempt to resolve the controversy over the end-Cretaceous extinction of planktic foraminifera at El Kef, Tunisia using a blind test. Introduction: background and procedures. Marine Micropaleontology 29(2): 67–68. https://doi.org/10.1016/S0377-8398(96)00038-2

Ginsburg RN (1997b) Perspectives on the blind test. Marine Micropaleontology 29(2): 101–103. https://doi.org/10.1016/S0377-8398(96)00046-1

Hammer Ø, Harper DAT, Ryan PD (2001) PAST: Paleontological Statistics Software Package for Education and Data Analysis. Palaeontologia Electronica 4(1): 1–9.

Henehan MJ, Ridgwell A, Thomas E, Zhang S, Alegret L, Schmidt DN, Rae JWB, Witts JD, Landman NH, Greene SE, Huber BT, Super JR, Planavsky NJ, Hull PM (2019) Rapid ocean acidification and protracted Earth system recovery followed the end-Cretaceous Chicxulub impact. Proceedings of the National Academy of Sciences of the United States of the America 116: 22500–22504. https://doi.org/10.1073/pnas.1905989116

Hildebrand AR, Penfield GT, Kring DA, Pilkington M, Camargo A, Jacobsen SB, Boynton WV (1991) Chicxulub crater: a possible Cretaceous/Tertiary boundary impact crater on the Yucatan Peninsula, Mexico. Geology 19: 867–871. https://doi.org/10.1130/0091-7613(1991)019%3C0867:CCAPCT%3E2.3.CO;2

Huber BT (1991) Maestrichtian planktonic foraminifer biostratigraphy and the Cretaceous/Tertiary boundary at Hole 738C, (Kerguelen plateau, Southern Indian Ocean). Proceedings of the Ocean Drilling Program Scientific Report 119: 451–465. https://doi.org/10.2973/odp.proc.sr.119.143.1991

Huber BT (1996) Evidence for planktonic foraminifer reworking versus survivorship across the Cretaceous–Tertiary boundary at high latitudes. Geological Society of America Special Paper 307: 319–334. https://doi.org/10.1130/0-8137-2307-8.319

Huber BT, Boersma A (1994) Cretaceous origination of *Zeauvigerina* and its relationship to Paleocene biserial planktonic foraminifera. Journal of Foraminiferal Response 24(4): 268–287. https://doi.org/10.2113/gsjfr.24.4.268

Huber BT, MacLeod KG, Norris R (2002) Abrupt extinction and subsequent reworking of Cretaceous planktonic foraminifera across the Cretaceous/Tertiary boundary: Evidence for the subtropical North Atlantic. Geological Society of America Special Paper 356: 277–290. https://doi.org/10.1130/0-8137-2356-6.277

Hull PM, Bornemann A, Penman DE, Henehan M, Norris RD, Wilson PA, Blum P, Alegret L, Batenburg SJ, Bown PR, Bralower TJ, Cournede C, Deutsch A, Donner B, Friedrich O, Jehle S, Kim H, Kroon D, Lippert PC, Loroch D, Moebius I, Moriya K, Peppe DJ, Ravizza GE, Röhl U, Schueth JD, Sepúlveda J, Sexton PF, Sibert EC, Śliwińska KK, Summons RE, Thomas E, Westerhold T, Whiteside JH, Yamaguchi T, Zachos JC (2020) On impact and volcanism across the Cretaceous–Paleogene boundary. Science 367: 266–272. https://doi.org/10.1126/science.aay5055

Kaiho K, Lamolda MA (1999) Catastrophic extinction of planktonic foraminifera at the Cretaceous–Tertiary boundary evidenced by stable isotopes and foraminiferal abundance at Caravaca, Spain. Geology 27: 355–358. https://doi.org/10.1130/0091-7613(1999)027%3C0355:CEOPFA%3E2.3.CO;2

Keller G (1988) Extinction, survivorship and evolution of planktic foraminifera across the Cretaceous/Tertiary boundary at El Kef, Tunisia. Marine Micropaleontology 13: 239–263. https://doi.org/10.1016/0377-8398(88)90005-9

Keller G (1989a) Extended Cretaceous/Tertiary boundary extinctions and delayed population change in planktonic foraminiferal faunas from Brazos River, Texas. Paleoceanography 4: 287–332. https://doi.org/10.1029/PA004i003p00287

Keller G (1989b) Extended period of extinctions across the Cretaceous/Tertiary boundary in planktonic foraminifera of continental-shelf sections: Implications for impact and volcanism theories. Geological Society of America Bulletin 101: 1408–1419. https://doi.org/10.1130/0016-7606(1989)101%3C1408:EPOEAT%3E2.3.CO;2

Keller G (1993) The Cretaceous–Tertiary boundary transition in the Antarctic Ocean and its global implications, Marine Micropaleontology 21: 1–45. https://doi.org/10.1016/0377-8398(93)90010-U

Keller G (1997) Analysis of El Kef blind test I. Marine Micropaleontology 29: 89–93. https://doi.org/10.1016/S0377-8398(96)00044-8

Keller G (2001) The end-cretaceous mass extinction in the marine realm: Year 2000 assessment. Planetary and Space Science 49: 817–830. https://doi.org/10.1016/S0032-0633(01)00032-0

Keller G, Pardo A (2004) Disaster opportunists Guembelitrinidae: Index for environmental catastrophes. Marine Micropaleontology 53: 83–116. https://doi.org/10.1016/j.marmicro.2004.04.012

Keller G, Barrera E, Schmitz B, Mattson E (1993) Long-term oceanic instability but no mass extinction or major $\delta^{13}C$ shift in planktic foraminifera across the Cretaceous/Tertiary boundary in Northern high latitudes: Evidence from Nye Klov, Denmark. Geological Society of America Bulletin 105: 979–997. https://doi.org/10.1130/0016-7606(1993)105%3C0979:GMESSA%3E2.3.CO;2

Keller G, Li L, MacLeod N (1995) The Cretaceous/Tertiary boundary stratotype sections at El Kef, Tunisia: How catastrophic was the mass extinction? Palaeogeography, Palaeoclimatology, Palaeoecology 119(3–4): 221–254. https://doi.org/10.1016/0031-0182(95)00009-7

Keller G, Adatte T, Pardo A, Bajpai S, Khosla A, Samant B (2010) Cretaceous Extinctions: Evidence Overlooked. Science 328: 974–975. https://doi.org/10.1126/science.328.5981.974-a

Keller G, Mateo P, Monkenbusch J, Thibault N, Punekar J, Spangenberg JE, Abramovich S, Ashckenazi-Polivoda S, Schoene B, Eddy MP, Samperton KM, Khadri SFR, Adatte T (2020) Mercury linked to Deccan Traps volcanism, climate change and the end-Cretaceous mass extinction. Global and Planetary Change 194: 103312. https://doi.org/10.1016/j.gloplacha.2020.103312

Kieken M (1974) Etude géologique du Hodna, du Titteri et de la partie occidentale des Biban (Dépt. D'Alger-Algérie). PhD thesis, Alger, Algeria: Service géologique de l'Algérie.

Krahl G, Koutsoukos EAM, Fauth G (2017) Paleocene planktonic foraminifera from DSDP Site 356, South Atlantic: Paleoceanographic inferences. Marine Micropaleontology 135: 1–14. https://doi.org/10.1016/j.marmicro.2017.07.001

Krahl G, Bom MHH, Kochhann KGD, Souza LV, Savian JF, Fauth G (2020) Environmental changes occurred during the Early Danian at the Rio Grande Rise, South Atlantic Ocean. Global and Planetary Change 191: 103197. https://doi.org/10.1016/j.gloplacha.2020.103197

Koutsoukos EAM (1996) Phenotypic experiments into new pelagic niches in early Danian planktonic foraminifera: aftermath of the K/T boundary event. In: Hart MB (Ed.) Biotic Recovery from Mass Extinctions Events. Geological Society Special Publications, London 102: 319–335. https://doi.org/10.1144/GSL.SP.1996.001.01.24

Koutsoukos EAM (2014) Phenotypic plasticity, speciation, and phylogeny in early Danian planktic foraminifera. Journal of Foraminiferal Research 44(2): 109–142. https://doi.org/10.2113/gsjfr.44.2.109

Lipps JH (1997) The Cretaceous–Tertiary boundary: The El Kef blind test. Marine Micropaleontology 29: 65–66. https://doi.org/10.1016/S0377-8398(96)00037-0

Li L, Keller G (1998) Maastrichtian climate, productivity and faunal turnovers in planktic foraminifera in South Atlantic DSDP sites 525A and 21. Marine Micropaleontology 33: 55–86. https://doi.org/10.1016/S0377-8398(97)00027-3

Liu C, Olsson RK (1992) Evolutionary radiation of microperforate planktonic foraminifera following the K/T mass extinction event. Journal of Foraminiferal Research 22: 328–346. https://doi.org/10.2113/gsjfr.22.4.328

Liu C, Olsson RK (1994) On the origin of Danian normal perforate planktonic foraminifera from *Hedbergella*. Journal of Foraminiferal Research 24: 61–74. https://doi.org/10.2113/gsjfr.24.2.61

Lowery CM, Bralower TJ, Owens JD, Rodríguez-Tovar J, Jones H, Smit J, Whalen MT, Claeys P, Farley K, Gulick SPS, Morgan JV, Green S, Chenot E, Christeson GL, Cockell CS, Coolen MJL, Ferrière L, Gebhardt C, Goto K, Kring DA, Lofi J, Ocampo-Torres R, Perez-Cruz L, Pickersgill AE, Poelchau MH, Rae ASP, Rasmussen C, Rebolledo-Vieyra M, Riller U, Sato H, Tikoo SM, Tomioka N, Urrutia-Fucugauchi J, Vellekoop J, Wittmann A, Xiao L, Yamaguchi KE, Zylberman W (2018) Rapid recovery of life at ground zero of the end-Cretaceous mass extinction. Nature 558: 288–291. https://doi.org/10.1038/s41586-018-0163-6

Lowery CM, Bown PR, Fraass AJ, Hull PM (2020) Ecological Response of Plankton to Environmental Change: Thresholds for Extinction. Annual Review of Earth and Planetary Sciences 48: 403–429. https://doi.org/10.1146/annurev-earth-081619-052818

Luciani V (1997) Planktonic foraminiferal turnover across the Cretaceous–Tertiary boundary in the Vajont valley (Southern Alps, northern Italy). Cretaceous Research 18: 799–821. https://doi.org/10.1006/cres.1997.0088

MacLeod KG, Huber BT (1996) Strontium isotopic evidence for extensive reworking in sediments spanning the Cretaceous–Tertiary boundary at ODP Site 738. Geology 24(5): 463–466. https://doi.org/10.1130/0091-7613(1996)024%3C0463:SIEFER%3E2.3.CO;2

MacLeod KG, Quinton P, Sepúlveda J, Negra M (2018) Postimpact earliest Paleogene warming shown by fish debris oxygen isotopes (El Kef, Tunisia). Science 360: 1467–1469. https://doi.org/10.1126/science.aap8525

MacLeod N, Keller G (1994) Comparative biogeographic analysis of planktic foraminiferal survivorship across the Cretaceous/Tertiary (K/T) boundary. Paleobiology 20(2): 143–177. https://doi.org/10.1017/S0094837300012653

Masters BA (1997) El Kef blind test II results. Marine Micropaleontology 29(2): 77–79. https://doi.org/10.1016/S0377-8398(96)00041-2

Metsana-Oussaid F, Belhai D, Arenillas I, Arz JA, Gilabert V (2019) New sections of the Cretaceous–Paleogene transition in the southwestern Tethys (Médéa, northern Algeria): planktic foraminiferal biostratigraphy and biochronology. Arabian Journal of Geosciences 12(217): 1–34. https://doi.org/10.1007/s12517-019-4402-4

Molina E (1995) Modelos y causas de extinción masiva. Interciencia 20(2): 83–89.

Molina E (2015) Evidence and causes of the main extinction events in the Paleogene based on extinction and survival patterns of foraminifera. Earth-Science Reviews 140: 166–181. https://doi.org/10.1016/j.earscirev.2014.11.008

Molina E, Arenillas I, Arz JA (1996) The Cretaceous/Tertiary boundary mass extinction in planktic foraminifera at Agost (Spain). Revue de Micropaléontologie 39(3): 225–243. https://doi.org/10.1016/S0035-1598(96)90075-6

Molina E, Arenillas I, Arz JA (1998) Mass extinction in planktic foraminifera at the Cretaceous/Tertiary boundary in subtropical and temperate latitudes. Bulletin de la Société Géologique de France 169(3): 351–363.

Molina E, Alegret L, Arenillas I, Arz JA, Gallala N, Hardenbol J, von Salis K, Steurbaut E, Vandenberghe N, Zaghbib-Turki D (2006) The Global Stratotype Section and Point of the Danian Stage (Paleocene, Paleogene, "Tertiary", Cenozoic) at El Kef, Tunisia: Original definition and revision. Episodes 29(4): 263–278. https://doi.org/10.18814/epiiugs/2009/v32i2/002

Molina E, Alegret L, Arenillas I, Arz JA, Gallala N, Grajales-Nishimura M, Murillo-Muñetón G, Zaghbib-Turki D (2009) The Global Boundary Stratotype Section and Point for the base of the Danian Stage (Paleocene, Paleogene, "Tertiary", Cenozoic): auxiliary sections and correlation. Episodes 32(2): 84–95. https://doi.org/10.18814/epiiugs/2009/v32i2/002

Officer CB, Drake CL (1985) Terminal Cretaceous environmental events. Science 277: 1161–1167. https://doi.org/10.1126/science.227.4691.1161

Olsson RK (1997) El Kef blind test III results, Marine Micropaleontology 29(2): 80–84. https://doi.org/10.1016/S0377-8398(96)00042-4

Olsson RK, Hemleben C, Berggren WA, Liu C (1992) Wall texture classification of planktonic foraminifera genera in the lower Danian. Journal of Foraminiferal Research 22: 193–213. https://doi.org/10.2113/gsjfr.22.3.195

Olsson RK, Hemleben C, Berggren WA, Huber BT (1999) Atlas of Paleocene Planktonic Foraminifera. Smithsonian Contributions to Paleobiology 85: 1–252. https://doi.org/10.5479/si.00810266.85.1

Orue-Etxebarria X (1997) El Kef blind test IV results, Marine Micropaleontology 29(2): 85–88. https://doi.org/10.1016/S0377-8398(96)00043-6

Pardo A, Keller G (2008) Biotic effects of environmental catastrophes at the end of the Cretaceous and Early Tertiary: *Guembelitria* and *Heterohelix* blooms. Cretaceous Research 29: 1058–1073. https://doi.org/10.1016/j.cretres.2008.05.031

Punekar J, Keller G, Khozyem H, Hamming C, Adatte T, Tantawy AA, Spangenberg JE (2014) Late Maastrichtian–early Danian high-stress environments and delayed recovery linked to Deccan volcanism. Cretaceous Research 49: 63–82. https://doi.org/10.1016/j.cretres.2014.01.002

Remane J, Keller G, Hardenbol J, ben Haj Ali M (1999) International workshop on Cretaceous-Paleogene transitions in Tunisia: The El Kef stratotype for the Cretaceous-Paleogene boundary reconfirmed. Episodes 22(1): 47–48.

Renne PR, Deino AL, Hilgen FJ, Kuiper KF, Mark DF, Mitchell WS, Morgan LE, Mundil R, Smit J (2013) Time scales of critical events around the Cretaceous–Paleogene boundary. Science 339: 684–687. https://doi.org/10.1126/science.1230492

Renne PR, Sprain CJ, Richards MA, Self S, Vanderkluysen L, Pande K (2015) State shift in Deccan volcanism at the Cretaceous–Paleogene boundary, possibly induced by impact. Science 350: 76–78. https://doi.org/10.1126/science.aac7549

Renne PR, Arenillas I, Arz JA, Vajda V, Gilabert V, Bermúdez HD (2018) Multi-proxy record of the Chicxulub impact at the Cretaceous–Paleogene boundary from Gorgonilla Island, Colombia. Geology 46: 547–550. https://doi.org/10.1130/G40224.1

Rodríguez-Tovar FJ, Uchman A (2008) Bioturbational disturbance of the Cretaceous–Palaeogene (K–Pg) boundary layer: Implications for the interpretation of the K–Pg boundary impact event. Geobios 48: 661–667. https://doi.org/10.1016/j.geobios.2008.01.003

Salaj J (1974) Proposition pour des hypostratotypes du Danien et du Paléocène (Localité type de la formation El Haria: le Kef, Tunisie septentrionale). Notes Service Géologique Tunisie 41: 1–14.

Schoene B, Samperton KM, Eddy MP, Keller G, Adatte T, Bowring SA, Khadri SFR, Gertsch B (2015) U–Pb geochronology of the Deccan Traps and relation to the end-Cretaceous mass extinction. Science 347: 182–184. https://doi.org/10.1126/science.aaa0118

Schoene B, Eddy MP, Samperton KM, Keller CB, Keller G, Adatte T, Khadri SFR (2019) U–Pb constraints on pulsed eruption of the Deccan Traps across the end-Cretaceous mass extinction. Science 363: 862–866. https://doi.org/10.1126/science.aau2422

Schulte P, Alegret L, Arenillas I, Arz JA, Barton PJ, Bown PR, Bralower TJ, Christeson GL, Claeys P, Cockell CS, Collins GS, Deutsch A, Goldin TJ, Goto K, Grajales-Nishimura JM, Grieve RAF, Gulick SPS, Johnson KR, Kiessling W, Koeberl C, Kring DA, MacLeod KG, Matsui T, Melosh J, Montanari A, Morgan JV, Neal CR, Nichols DJ, Norris RD, Pierazzo E, Ravizza G, Rebolledo-Vieyra M, Reimold WU, Robin E, Salge T, Speijer, RP, Sweet AR, Urrutia-Fucugauchi J, Vajda V, Whalen MT, Willumsen PS (2010) The Chicxulub asteroid impact and mass extinction at the Cretaceous–Paleogene boundary. Science 327: 1214–1218. https://doi.org/10.1126/science.1177265

Signor III PW, Lipps JH (1982) Sampling bias, gradual extinction patterns and catastrophes in the fossil record. Geological Society America Special Paper 190: 291–296. https://doi.org/10.1130/SPE190-p291

Smit J (1982) Extinction and evolution of planktonic foraminifera after a major impact at the Cretaceous/Tertiary boundary. Geological Society America Special Paper 190: 329–352. https://doi.org/10.1130/SPE190-p329

Smit J (1990) Meteorite impact, extinctions and the Cretaceous–Tertiary boundary. Geologie en Mijnbouw 69: 187–204.

Smit J, Nederbragt AJ (1997) Analysis of the El Kef blind test II. Marine Micropaleontology 29: 95–100. https://doi.org/10.1016/S0377-8398(96)00045-X

Sprain CJ, Renne PR, Vanderkluysen L, Pande K, Self S, Mittal T (2019) The eruptive tempo of Deccan volcanism in relation to the Cretaceous–Paleogene boundary. Science 363: 866–870. https://doi.org/10.1126/science.aav1446

Stott LD, Kennett JP (1990) The paleoceanographic and climatic signature of the Cretaceous/Paleogene boundary in the Antarctic: Stable isotopic results from ODP Leg 113. In: Baker PF, Kennett JP, and others (Eds) Ocean Drilling Program, scientific results, Leg 113: College Station, Texas, 113: 829–848. https://doi.org/10.2973/odp.proc.sr.113.158.1990

Tada R, Nakano Y, Iturralde-Vinent MA, Yamamoto S, Kamata T, Tajika E, Toyoda K, Kiyokawa S, Delgado DG, Oji T, Goto K, Takayama H, Rojas-Consuegra R, Matsui T (2002) Complex tsunami waves suggested by the Cretaceous/Tertiary boundary deposit at the Moncada section, western Cuba. In: Koeberl C, Macleod G (Eds) Catastrophic Events and Mass Extinctions: Impact and Beyond, Geological Society of America Special Paper 356: 109–123. https://doi.org/10.1130/0-8137-2356-6.109

Wade BR, Pearson PN, Berggren WA, Pälike H (2011) Review and revision of Cenozoic tropical planktonic foraminiferal biostratigraphy and calibration to the geomagnetic polarity and astronomical time scale. Earth-Science Reviews 104: 111–142. https://doi.org/10.1016/j.earscirev.2010.09.003

Vellekoop J, Sluijs A, Smit J, Schouten S, Weijers JWH, Sinninghe-Damsté JS, Brinkhuis H (2014) Rapid short-term cooling following the Chicxulub impact at the Cretaceous–Paleogene boundary. Proceedings of the National Academy of Sciences of the United States of the America 111: 7537–7541. https://doi.org/10.1073/pnas.1319253111

Vellekoop J, Esmeray-Senlet S, Miller KG, Browning JV, Sluijs A, van de Schootbrugge B, Sinninghe Damsté JS, Brinkhuis H (2016) Evidence for Cretaceous–Paleogene boundary bolide "impact winter" conditions from New Jersey. Geology 44(8): 619–622. https://doi.org/10.1130/G37961.1

Zachos JC, Berggren WA, Aubry MP, Mackensen A (1992) Chemostratigraphy of the Cretaceous/Paleocene boundary at Site 750, southern Kerguelen Plateau, In: Schlich R, Wise Jr SW, and others (Eds) Ocean Drilling Program, scientific results, Leg 119: College Station, Texas, Ocean Drilling Program, 120: 961–977. https://doi.org/10.2973/odp.proc.sr.120.188.1992

Supplementary material 1

Figure S1

Authors: Ignacio Arenillas, José A. Arz, Fariza Metsana-Oussaid, Vicente Gilabert, Djelloul Belhai

Data type: pdf file

Explanation note: RASCS curves (relative abundance of the "surviving" Cretaceous species), fitted to a power function, across the lower Danian at (A) El Kef and (B) Sidi Ziane.

Link: https://doi.org/10.3897/fr.25.79958.suppl1

Supplementary material 2

Table S1

Authors: Ignacio Arenillas, José A. Arz, Fariza Metsana-Oussaid, Vicente Gilabert, Djelloul Belhai

Data type: Quantitative dataset Table

Explanation note: Relative abundance of Maastrichtian planktic foraminiferal species and genera in both Maastrichtian and Danian samples of the El Kef section.

Link: https://doi.org/10.3897/fr.25.79958.suppl2

Supplementary material 3

Table S2

Authors: Ignacio Arenillas, José A. Arz, Fariza Metsana-Oussaid, Vicente Gilabert, Djelloul Belhai

Data type: Quantitative dataset Table

Explanation note: Relative abundance of Maastrichtian planktic foraminiferal species and genera in both Maastrichtian and Danian samples of the Sidi Ziane section.

Link: https://doi.org/10.3897/fr.25.79958.suppl3

Fossil Record 25 (1) 2022, 65–74 | DOI 10.3897/fr.25.81054

First fossil species of ship-timber beetles (Coleoptera, Lymexylidae) from Eocene Rovno amber (Ukraine)

Shûhei Yamamoto[1], Vitaly Yu. Nazarenko[2], Dmitry V. Vasilenko[3,4], Evgeny E. Perkovsky[2]

1 *The Hokkaido University Museum, Hokkaido University, Kita 8, Nishi 5, Kita-ku, Sapporo 060-0808, Japan*
2 *Schmalhausen Institute of Zoology, National Academy of Sciences of Ukraine, B. Khmelnitskogo 15, Kiev 01030, Ukraine*
3 *Borissiak Paleontological Institute, Russian Academy of Sciences, Profsoyuznaya 123, 117868 Moscow, Russia*
4 *Cherepovets State University, Lunacharsky prospect 5, Cherepovets 162600, Vologda region, Russia*

http://zoobank.org/B6791E34-7D6E-4956-9E8C-BED11F2CFA6F

Corresponding authors: Shûhei Yamamoto (s.yamamoto.64@gmail.com), Evgeny E. Perkovsky (perkovsk@gmail.com)

Academic editor: Carolin Haug ♦ **Received** 28 June 2021 ♦ **Accepted** 19 January 2022 ♦ **Published** 7 February 2022

Abstract

A new lymexylid fossil species, †*Raractocetus sverlilo* Nazarenko, Perkovsky & Yamamoto, **sp. nov.**, is described from late Eocene Rovno amber of Ukraine. This new species is similar to species of the recent genera *Atractocerus* Palisot de Beauvois and *Raractocetus* Kurosawa in the ship-timber beetle subfamily Atractocerinae, but differs in pronotal and elytral features. Notably, the new species is one of the smallest atractocerines known to date. This is the first member of the family Lymexylidae found in Rovno amber. Our finding sheds further light on the paleodiversity of atractocerine beetles, highlighting a peculiar distribution during the Eocene. Only one extant atractocerine specimen has been reported from Europe (Greece), while three species from Eocene European amber forests with equable climate are known now, including two species from the otherwise tropical genus *Raractocetus*. Our finding of the *Raractocetus* beetle from Rovno amber is of significant biogeographically because it indicates the wide distribution of the genus in the Eocene European amber forests.

Key Words

Atractocerinae, Lymexyloidea, new species, paleobiogeography, paleoclimate, paleodiversity, *Raractocetus*, systematics

Introduction

Extant ship-timber beetles (Lymexylidae) include approximately 70 species of 12 genera in four subfamilies (Lawrence 2020), including 17 Palaearctic species and only 5 known in Europe (Cuccodoro 2007). Currently, Lymexylidae are placed within the cucujiformian superfamily Tenebrionoidea (e.g. Lawrence 2020) or in its own superfamily Lymexyloidea (e.g. Bouchard et al. 2010; Zhang et al. 2018). All known members of the family develop in wood as larvae and mutualism with fungi has been reported for a few species (Batra and Francke-Grosmann 1961; Wheeler 1986; Young 2002; Lawrence 2010; Casari and Albertoni 2013; Toki 2021), although more rigorous study and evidence are needed if the other unstudied lymexylid beetles are strongly connected with fungi (Lawrence 2010). Recently, Peris et al. (2021) discussed a potentially crucial role of the lymexylids as wood-boring insects, with a special emphasis on the insect–fungus mutualism, more specifically the cultivate ambrosia fungi and their associations. Moreover, Peris et al. (2021) considered that Lymexylidae might actually be one of the ambrosia beetles based on the fact that some of their larvae feed primarily on symbiotic ambrosia fungi in tunnels or caves in woody tissues following the criteria by Kirkendall et al. (2015).

The fossil records of Lymexylidae are relatively rare and scarce, mostly known from fossiliferous resins (e.g. Heer 1865; Wickham 1911; Kirejtshuk 2008; Wolf-Schwenninger 2011; Chen 2019; Yamamoto 2019; Chen and Zhang 2020; Nazarenko et al. 2020). The earliest Lymexylidae fossil is known from the Lower

Cretaceous Crato Formation in Brazil (Wolf-Schwenninger 2011). Five species in four genera of the subfamily Atractocerinae have recently been described from mid-Cretaceous Burmese (Kachin) amber (Chen 2019; Yamamoto 2019; Chen and Zhang 2020), with some unstudied material (e.g. Peris 2020, 2021; Yamamoto, pers. obs.). The family is relatively rare in Eocene Baltic amber and is represented definitively only by adults (Kirejtshuk 2008; Yamamoto 2019). So far, three extinct species of the recent atractocerine genus *Raractocetus* Kurosawa have been described from Kachin and Eocene Baltic ambers (Yamamoto 2019).

Late Eocene Rovno amber from Ukraine is the southern coeval of the famous Baltic amber (Sokoloff et al. 2018), and more than 300 arthropod species have already been described from there (Perkovsky 2018; Bukejs et al. 2020; Colombo et al. 2021a, 2021b; Khaustov et al. 2021a, 2021b and references therein). Fewer than 48% of Rovno hymenopteran species (Simutnik et al. 2020, 2021; Colombo et al. 2021a, 2021b, 2021c; Radchenko et al. 2021, our data), 32% of caddisfly species (Melnitsky et al. 2021a, 2021b, 2021c), 24% of Nematocera (Giłka et al. 2021), and less than 15% of beetle species (Legalov et al. 2021a, 2021b; Kirichenko-Babko et al. 2021, 2022; Kupryjanowicz et al. 2021; Lyubarsky and Perkovsky 2021; Telnov et al. 2021; Tshernyshev and Perkovsky 2021; Perkovsky et al. 2022; this paper) are shared with Baltic amber fauna. Nearly all studied Rovno amber inclusions from the Rovno Region were collected from Klesov and the Horyn River Basin (Perkovsky et al. 2010; Perkovsky 2017a; Mitov et al. 2021), except new collections from Varash District (former Vladimirets and Zarechnoye Districts) in the Rovno Region and the former Manevichi District in the Volyn Region (Styr, Veselukha, and Stokhod River Basins). These new collections (mostly from Kuchotskaya Volya, Voronki, and Velyki Telkovichi) revealed a number of new species of hymenopterans, termites, cockroaches, caddisflies, beetles, neuropterans, and snakeflies (e.g. Jałoszyński and Perkovsky 2019, 2021; Legalov et al. 2019, 2021b; Perkovsky and Makarkin 2019, 2020; Makarkin and Perkovsky 2020; Lyubarsky and Perkovsky 2020; Perkovsky et al. 2020; Anisyutkin and Perkovsky 2021; Melnitsky et al. 2021a; Matalin et al. 2021; Perkovsky and Nel 2021, etc.) and some species recorded previously from Baltic amber (Perkovsky and Olmi 2018; Martynova et al. 2019; Mamontov et al. 2020; Simutnik et al. 2020) or from both Baltic and Bitterfeld ambers (Radchenko and Perkovsky 2018, 2020).

Here, we describe a new *Raractocetus* species for the first time from Rovno amber from the Varash District, Ukraine. We discuss paleobiogeographical, paleoecological, and morphological features based on the new species.

Material and methods

The amber fossil studied here came from Voronki (former Vladimirets District), Rovno Region, Ukraine. The holotype of †*Raractocetus sverlilo* sp. nov. is relatively well preserved, embedded in a parallelogram-shaped piece of amber (53 × 46 × 13 mm). Recent studies suggested the late Eocene age of Rovno amber, with a different geological background from Baltic amber (Perkovsky 2016a, 2018; Mänd et al. 2018). The generic classification of Atractocerinae generally follows that of Yamamoto (2019) and Lawrence (2020). The holotype of †*R. sverlilo* sp. nov. is deposited in the I.I. Schmalhausen Institute of Zoology (SIZK), National Academy of Sciences of Ukraine, Kiev, Ukraine, with the assigned number SIZK L-814. We compared the new species with the previously described three fossil species of *Raractocetus* by Yamamoto (2019), of which deposited in the insect collection of the Gantz Family Collections Center, Field Museum of Natural History (FMNH), Chicago, IL, USA, with consecutive numbers from FMNHINS-3965988 to FMNHINS-3965991. Observations were made using MBS-9 and Leica M165C stereomicroscopes. Images were taken with a Leica M165C equipped with a Canon EOS 500D or Leica Z16 APO stereomicroscope equipped with a Leica DFC 450, and later processed with Helicon Focus for focus stacking. The figures were edited and assembled using Photoshop Elements 15. This published work and the nomenclatural acts it contains have been registered in ZooBank, the proposed online registration system for the International Code of Zoological Nomenclature (ICZN). The ZooBank Life Science Identifiers (LSIDs) can be resolved and the associated information viewed through any standard web browser by appending LSID to the prefix 'http://zoobank.org/'. The LSIDs for this publication are: urn:lsid:zoobank.org:pub:B6791E34-7D6E-4956-9E8C-BED11F2CFA6F; urn:lsid:zoobank.org:act:CBAD43C7-ECAF-4637-BC1E-67E23F216E7E.

Systematic paleontology

Superfamily Lymexyloidea Fleming, 1821
Family Lymexylidae Fleming, 1821
Subfamily Atractocerinae Laporte, 1840
Genus *Raractocetus* Kurosawa, 1985

†*Raractocetus sverlilo* Nazarenko, Perkovsky & Yamamoto, sp. nov.

http://zoobank.org/CBAD43C7-ECAF-4637-BC1E-67E23F216E7E
Figs 1–4A, C, D

Holotype. SIZK L-814, female. The beetle inclusion can be observed from multiple angles, except obliquely. Near the inclusion there are cracks that partially cover the lower part of the body. Syninclusions: Scraptiidae (Coleoptera), Mymaridae (Hymenoptera), 3 Dolichopodidae (Diptera), larva of Syrphidae (Diptera), Lepidoptera, and Acari.

Etymology. The name of the species is derived from the Russian name, сверлило (sverlilo), for Lymexylidae.

Type strata. Rovno amber, Upper Eocene.

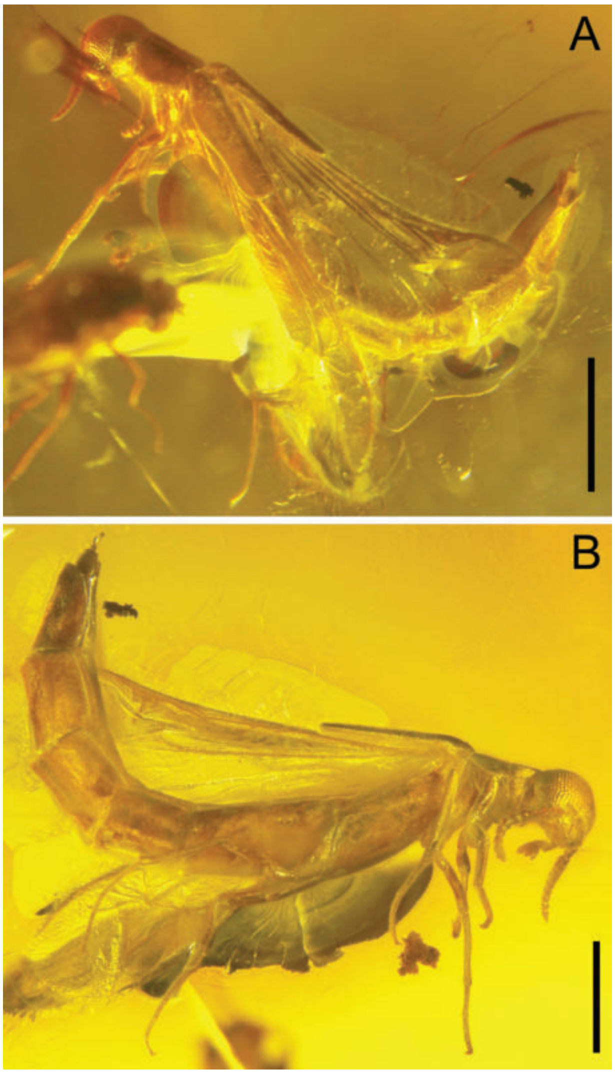

Figure 1. †*Raractocetus sverlilo* sp. nov., female, holotype, SIZK L-814. **A.** General habitus, dorsolateral view; **B.** General habitus, ventrolateral view. Scale bars: 1.0 mm.

Type locality. Voronki locality (Varash district), Rovno Region, Ukraine.

Description. Measurements: body length ca. 7.1 mm, head length 0.60 mm, head width 0.70 mm, pronotum length 0.60 mm; elytra length 1.30 mm, elytra width 0.41 mm, hindwing length ca. 4.20 mm, hindwing width 1.10 mm; length of protibia 0.37 mm, mesotibia 0.67 mm, metatibia 0.78 mm; length of protarsus ca. 0.44 mm, mesotarsus 0.71 mm, metatarsus 1.10 mm; lengths of 4–7th sternites, respectively 0.77 mm, 0.86 mm, 0.80 mm and 0.86 mm.

Female. Body small, narrowly elongate, abdomen arcuate dorsally curved. Color uniformly yellowish brown, in some areas with cuticles darker. Surface leathery, covered with dense, very short protruding pubescence in most areas; legs and thoracic sternites mostly covered with dense setae.

Head broadly oval, rather vertical, 1.3 times shorter than pronotum, slightly wider than prothorax. Eyes large, nearly contiguous, occupying almost entire visible surface of head capsule; anterior margin cut out, covering partly of antennal insertion; vertex areas each diverging to form rather triangle shape of eyes. Antennae 11-segmented, relatively short and thick, 1.2 times as long as head and 1.5 times as long as pronotum; left antenna fully visible and observable, whereas right one partially appressed with only 7 last antennomeres clearly visible; first two antennomeres each slightly transverse, rounded, similar in shape and size, with visible part of first antennomere 1.6 times as wide as its length, of second 1.3 times; 3rd to 11th antennomeres forming flagellum with somewhat fusiform club; 3rd antennomere 1.25 times wider than second, its length almost equal to its width, next two antennomeres approximately equal to it in width, fourth 1.5 times wider than its length, fifth 2 times wider than its length, sixth 1.1 times narrower than 5th, 1.3 times wider than its length, its width slightly decreasing towards apex, seventh 1.14 times narrower than sixth and 1.17 times wider its length, 8th approximately equal in length and width, 1.14 times narrower than 7th, 9th almost same width, 1.17 times wider than its length, 10th 1.1 times narrower than 9th, 1.17 times as long as wide, 11th cone-shaped, pointed, 1.18 times narrower than 10th and 2 times as long as wide. Mouthparts partially visible. Clypeus transverse. Mandibles small, inconspicuous. Maxillary palpus with at least 7 short branched appendages (i.e., maxillary palporgan *sensu* Wheeler 1986), each slightly to moderately longer than penultimate maxillary palpomere.

Pronotum short, without maculation, anterior margin rounded; complete longitudinal groove along midline present, but with interruption just behind middle of furrow (see Fig. 4A, C, *ipf*). Mesoscutellum relatively narrow, details not visible.

Mid- and hindlegs somewhat long, slender; forelegs rather short, robust, moderately thickened, profemora, protibiae, and protarsi approximately equal in length; protibiae without spur, mesotibiae and metatibiae each with one spur (indistinct on mesotibia); procoxae thick, robust, more or less cylindrical; protibiae robust, 4 times as long as wide, protarsi 1.1 times as long as protibiae, 1.35 times as long as pronotum; mesofemora 0.38 times narrower than profemora; mid- and hindlegs long and thin; mesotibiae and metatibia 1.1 times longer than pronotum and 1.8 times as long as protibiae; metacoxae strongly projecting posteriorly, metatibiae feebly curved externally. Tarsi 5-segmented, metatarsi slightly longer than metatibiae; protarsi with 1st and 5th protarsomeres very long, 2nd and 3rd short and inconspicuous, approximately equal in length, 4th protarsomere shorter than each of them; meso- and metatarsi with first segments longest, second ones about 2.3 times shorter than them, 3rd and 5th segments slightly shorter than 2nd, 4th about 1.8 times shorter than 3rd. Claws simple, widely separated.

Elytra short, 2.45 times as long as pronotum, and 3.4 times as long as its maximum width, each nearly subparallel sided, exposing most part of abdomen; outer elytral margins gently arcuate each with very shallow median emargination (Fig. 4D, *eoe*), whereas inner margin

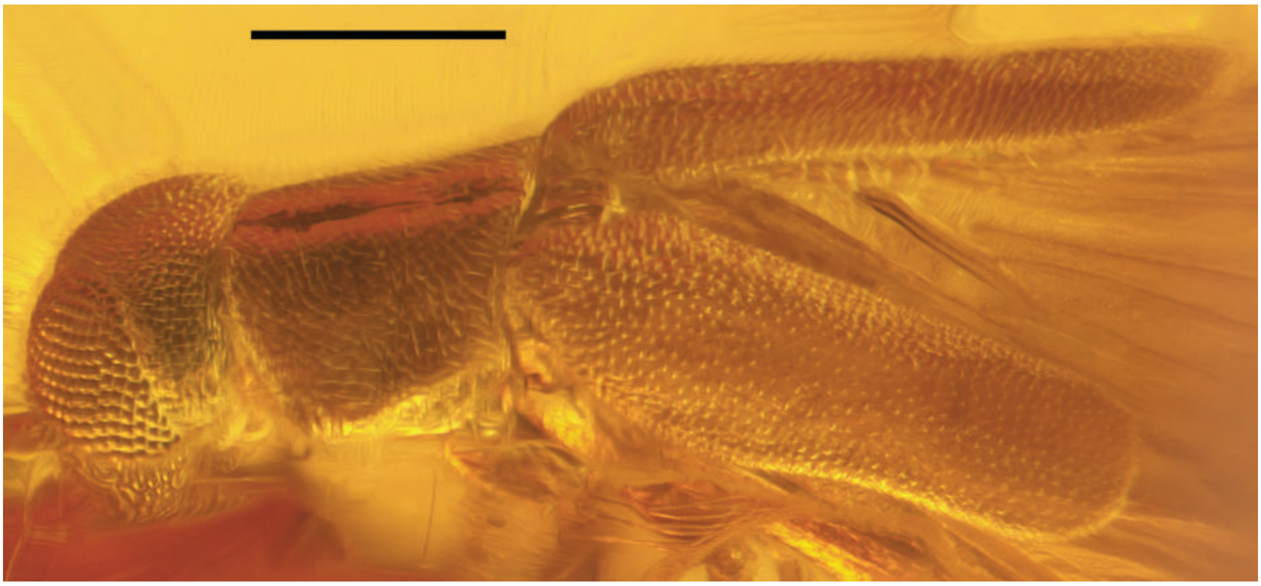

Figure 2. †*Raractocetus sverlilo* sp. nov., female, holotype, SIZK L-814: forebody, dorsolateral view. Scale bar: 0.5 mm.

straight, not extending beyond metacoxae; surface covered with dense, short obliquely protruding pubescence.

Hindwings fully developed, entire, 2.7 times as long as elytra; their apices not covering last two visible abdominal tergites; venation with details remaining unclear, but with visible veins of C-Sc-R, radial-medial (r-m), medial and cubital veins, and part of anal veins. Metaventrite distinctly elongate.

Abdomen narrowly elongate, nearly subparallel-sided, weakly tapering posteriorly, uniformly bent dorsally as preserved; abdominal segments II–VII visible. Abdominal segment VIII and ovipositor partially protruding. Styli exposed, weakly clavate, their apices with sparse long bristles.

Male unknown.

Comparison. †*Raractocetus sverlilo* Nazarenko, Perkovsky & Yamamoto, sp. nov. can be assigned to Atractocerinae based on the markedly reduced brachelytrous elytra with largely exposed hindwings, large bulging eyes, and distinctly modified maxillary palporgan in the female (Paulus 2004; Yamamoto 2019). The new fossil species is placed in the genus *Raractocetus* by having a rather vertical head, which is slightly wider than the pronotum, and large and subcontiguous eyes in the frontal view (Kurosawa 1985; Paulus 2004). This new species is similar to described fossil representatives of the genus from Eocene Baltic amber and mid-Cretaceous Burmese (Kachin) amber based on the strongly projecting metacoxae, length and shape of the pronotum, elytral shape, wing venation, antennal details and appendages of the maxillary palps of the female (Yamamoto 2019), and possibly its smaller body size as well. Interestingly, †*R. sverlilo* sp. nov. has a much smaller body (ca. 7.1 mm) than recent atractocerine species (less than half in body length, see Lawrence 2020), but it is similar in size to the mid-Cretaceous species †*R. fossilis* Yamamoto, 2019 (ca. 7.6 mm). Nevertheless, the individual size of adult ship-timber beetles may depend of larval feeding and therefore, the reason for such the small sizes in the fossil lymexylid species are still unclear. More study is needed to discuss the possible miniaturization phenomenon as seen in the extinct ship-timber beetles. The new species differs from the three extinct species currently assigned to *Raractocetus* mainly by the pronotal and elytral shapes, together with the structures of a longitudinal furrow along midline of the pronotal disc. It is readily distinguished from †*R. balticus* Yamamoto, 2019 from Baltic amber, by its markedly smaller body (†*R. balticus*, ca. 11.1 mm body length), the presence of the interruption on the pronotal furrow (see Fig. 4A, C, *ipf* vs. †*R. balticus* in Fig. 4B), non-linear (i.e., shallowly emarginate) outer margins of the elytra (Fig. 4D, *eoe*) and possibly by seemingly thicker antennae. Furthermore, †*R. sverlilo* sp. nov. is distinguished from †*R. extinctus* Yamamoto, 2019 and †*R. fossilis* from Kachin amber by having a smaller body size (†*R. extinctus* ca. 13.4 mm body length), simple coloration without any types of maculation, rounded anterior margin of the pronotum, more conspicuous and deeper longitudinal pronotal furrow, the presence and straight elytral inner edges with their different shapes of elytral emargination along outer margins of elytra, additionally by seemingly thicker antennae and protibiae.

Discussion

Here, we described the first lymexylid beetle from the Ukrainian Rovno amber. Our discovery of the atractocerine genus *Raractocetus* in Rovno amber suggests a potentially widespread distribution of this genus in the late Eocene in Europe, as previously suggested by Yamamoto (2019) based on †*R. balticus* from Baltic amber. The only two recent species of *Raractocetus* are distributed in the Oriental Region and Australia respectively (Lawrence 2020). The entire subfamily

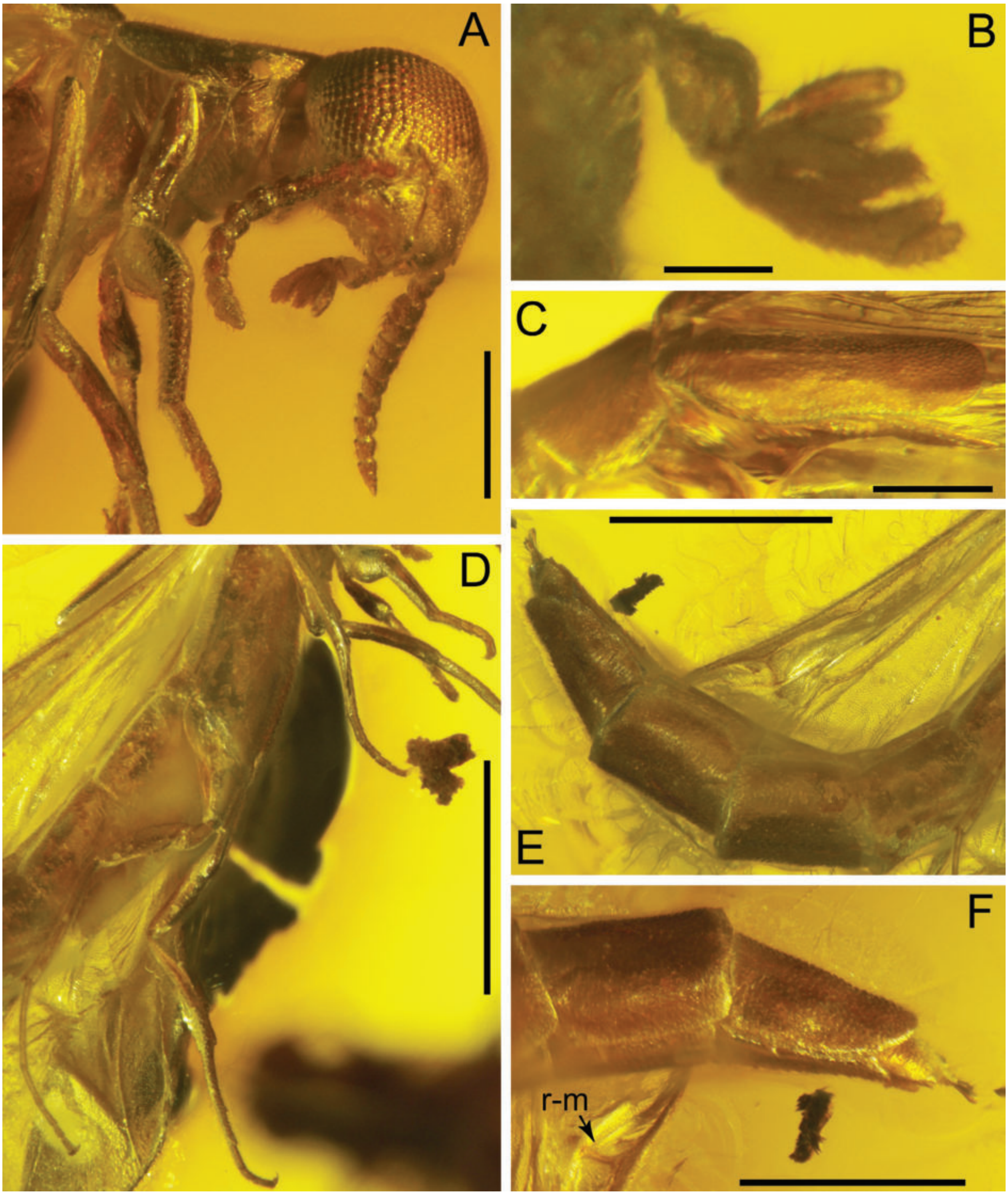

Figure 3. †*Raractocetus sverlilo* sp. nov., female, holotype, SIZK L-814. **A.** Head and prothorax, dorsoventral view; **B.** Maxillary palporgan with branches; **C.** Pronotum and left elytron, dorsolateral view; **D.** Metaventrite and legs, ventrolateral view; **E.** Abdomen in posterior half, ventrolateral view; **F.** Abdominal terminalia with styli, lateral view. Scale bars: 0.5 mm (**A**, **C**); 0.1 mm (**B**); 1.0 mm (**D–F**). Abbreviation: r-m, radial-medial vein.

Atractocerinae is represented now in Europe by the single species *Urtea graeca* Paulus, 2004 from Greece only (Paulus 2004). Hence, finding *Raractocetus* in European ambers is of great significance when considering the paleobiogeography of the genus and subfamily. Extant *Raractocetus* feed on both living (Lawrence 2020) and dead trees. In addition, a scraptiid syninclusion may indicate that the new species possibly fed on dead trees because nearly all the members of Scraptiidae develop in dead wood. Numerous scraptiid larvae in Rovno amber (V. K. Odnosum, Kiev, pers. com.) were also found together in the same amber with larvae and adults of the

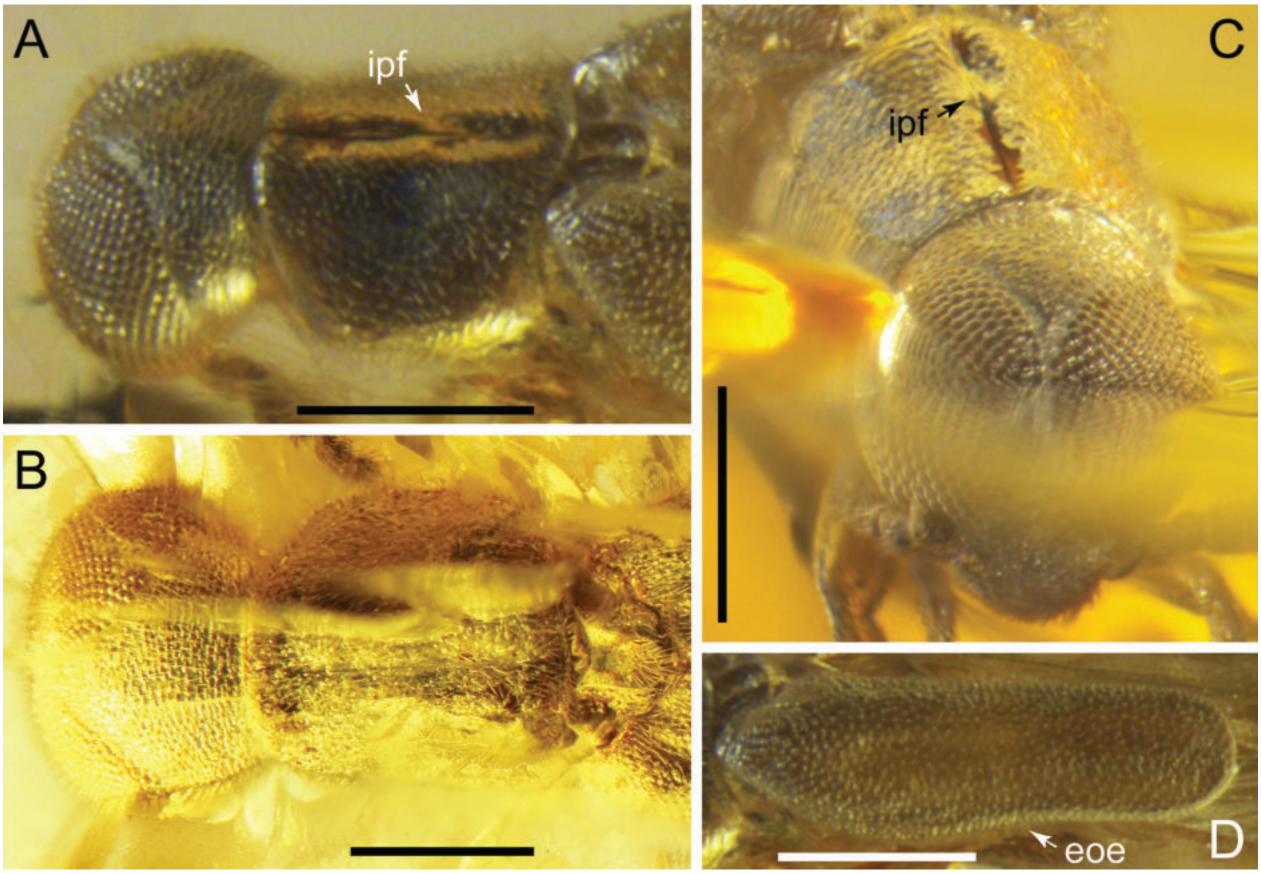

Figure 4. Morphological comparison of two Eocene *Raractocetus* species. †*Raractocetus sverlilo* sp. nov., female, holotype, SIZK L-814 (**A**, **C**, **D**) and †*R. balticus* in Eocene Baltic amber, female, holotype, FMNHINS-3965991 (**B**). **A.** Head, pronotum and mesoscutellum, dorsolateral view; **B.** Head, pronotum and mesoscutellum, dorsal view; **C.** Head and pronotum, frontal view; **D.** Elytron, dorsolateral view. Scale bars: 0.5 mm (**A**–**D**). Abbreviations: eoe, shallow median emargination along outer elytral margin; ipf, interrupted longitudinal furrow on pronotum.

wood-boring Micromalthidae beetle, *Micromalthus priabonicus* Perkovsky, 2016 (Perkovsky 2016b).

The Oriental species of *Raractocetus* occurs in tropical India, Sri Lanka, Myanmar, Thailand, Sumatra, Java, Sulawesi, Sarawak and the Philippines (Wheeler 1986 and references therein) and in subtropical Taiwan (Kurosawa 1985); it was reported to feed on the oriental plants *Buchanania latifolia* Roxb. (Anacardiaceae) and *Dipterocarpus zeylanicus* Thwaites (Dipterocarpaceae) (Wheeler 1986 and references therein). Australian species feeds in Western Australia on the several myrtaceous trees, mostly *Eucalyptus* (Clarke 1925; Lawrence 2020) and was most important pest for commercial timber there (Clarke 1925). All localities of Australian species (Lawrence 2020) have a cold month mean temperature (CMMT) higher than 11 °C, except the Australian Capital Territory and a nearby (70 km) locality in New South Wales with a CMMT = 5.5 °C and a single locality in South Australia with a CMMT = 7.4 °C. The Baltic amber forest is thought to have grown in a climate with mild winters (Archibald and Farrell 2003), although extant Holarctic genera prevail in its entomofauna (Perkovsky 2017b; Radchenko and Perkovsky 2021 and references therein). As the CMMT was lower than 5.5 °C, this might account for Baltic amber *Raractocetus* being so rare; for comparison, in Arnaia (Chalkidiki, Greece), where the holotype of *Urtea graeca* was found, the CMMT is 5 °C, and still only the holotype of this species has been reported. The climate of the Rovno amber forest was warmer than that of the Baltic (Perkovsky 2017b, 2018; Mänd et al. 2018), and therefore, it could be possible to speculate that *Raractocetus* as well as many other thermophilic beetles, e. g. Smicripidae (Kupryjanowicz et al. 2019), should have been more common in the amber-producing forest but more evidence is needed to assess this hypothesis.

The morphology of †*R. sverlilo* sp. nov. generally agrees well with the three fossil *Raractocetus* species from Baltic and Kachin amber, more than with the extant species, which have different geographical and geological backgrounds. For example, they share similar structures in the metacoxae and its inner areas strongly project posteriorly (Fig. 3D). In most primitive Atractocerinae, the metacoxae project very strongly posteriorly (see also Paulus 2004), such as in the fossils *Cratoatractocerus* (Wolf-Schwenninger 2011) and *Vetatractocerus* (Yamamoto 2019) and the extant *Urtea* Paulus, *Fuscicornis* Philippi (Chile) and *Leptonetron* Lawrence (Tasmania, in continental Australia outside of Victoria and New South

Wales known only from Brisbane (Queensland) and Pemberton in extreme southwestern Western Australia). The very strongly projecting metacoxae in Cenozoic Atractocerinae correlate with seasonal subtropical and even temperate climate and importance of the shorter pupal stage. This stimulates premature eclosion of adult that in turn results in imaginal juvenilization which is accompanied with elongation of metacoxae in Polyphaga (Tikhomirova 1991). A pair of elytra of Eocene species also remarkably reduced as in the extant species (also a possible result of juvenalization, as a retention of pupal short elytra, cf Tikhomirova 1991: fig. 10, *9*), and the elytra shows species-specific variation in shape and size (Yamamoto 2019; this study). Compared to the Kachin amber taxa, the specimens from European ambers lack distinct colored markings, maculation, or patterns on the head, pronotum, and elytra (Yamamoto 2019; this study). Of note, such color patterns appear to play a role in the mimicry of various Hymenoptera, particularly certain nocturnal wasps (Kurosawa 1985). If correct, then the ecological and behavioral strategies of species from European and Kachin ambers might differ. Such color patterns are sometimes not preserved in fossils or even appeared as artefact. Nevertheless, it is noteworthy to mention here that Eocene species had no evident color pattern as seen in the Myanmar amber fossils (Yamamoto 2019; this study). The discovery of †*R. sverlilo* sp. nov. opens a new window on the paleobiogeography and paleoecology of lymexylid beetles.

Data availability

The sole fossil material (holotype) of †*Raractocetus sverlilo* sp. nov. described in the paper is deposited in the I.I. Schmalhausen Institute of Zoology, National Academy of Sciences of Ukraine, Kiev, Ukraine (SIZK). The remaining material of the other three fossil species of *Raractocetus* are deposited in the insect collection of the Gantz Family Collections Center, Field Museum of Natural History (FMNH), Chicago, IL, USA. All data are included in the description. Higher-resolution images are also available through the Zenodo repository (https://doi.org/10.5281/zenodo.5913279).

Author contributions

SY and EEP designed the study. SY, EEP and VYN identified and described the specimen. SY and VYN produced the photos. SY edited and assembled the figures. SY, VYN, DVV and EEP prepared the paper and contributed to the editing.

Competing interests

The authors declare that they have no conflict of interest.

Financial support

This research has been supported by the Grant-in-Aid for JSPS Fellows given to SY (20J00159) from the Japan Society for the Promotion of Science (JSPS), Tokyo, Japan.

Acknowledgements

EEP thanks Alexandr P. Rasnitsyn (Borissiak Paleontological Institute RAS, Moscow, Russia) and Kirill V. Makarov (Moscow State Pedagogical University, Moscow, Russia) for discussion and Lynne G. Forster (University of Tasmania, Hobart, Australia) for providing literature. We also thank Nikolai R. Khomich for his help in obtaining the specimen. SY thanks John F. Lawrence for providing literature. We are grateful to Vitalii I. Alekseev and two anonymous reviewers for their helpful comments and suggestions regarding an earlier version of this manuscript.

References

Anisyutkin LN, Perkovsky EE (2021) *Periplaneta* (?) *perialla* sp. nov., a cockroach larva of the subfamily Blattinae (Dictyoptera, Blattidae) from Rovno amber. Paleontological Journal 55: 294–300. https://doi.org/10.1134/S0031030121030047

Archibald SB, Farrell BD (2003) Wheeler's dilemma. Acta Zoologica Cracoviensia 46: 17–23.

Batra LR, Francke-Grosmann H (1961) Contributions to our knowledge of ambrosia fungi. I. *Ascoidea hylecoeti* sp. nov. (Ascomycetes). American Journal of Botany 48: 453–456. https://doi.org/10.1002/j.1537-2197.1961.tb11668.x

Bouchard P, Bousquet Y, Davies AE, Alonso-Zarazaga MA, Lawrence JF, Lyal CHC, Newton AF, Reid CAM, Schmitt M, Ślipiński SA, Smith AB (2011) Family-group names in Coleoptera (Insecta). ZooKeys 88: 1–972. https://doi.org/10.3897/zookeys.88.807

Bukejs A, Háva J, Alekseev VI (2020) A new fossil species of *Attagenus* Latreille (Coleoptera: Dermestidae) in Rovno and Baltic ambers, with a brief review of known fossil beetles from the Rovno amber Lagerstätte. Fossil Record 23: 95–104. https://doi.org/10.5194/fr-23-95-2020

Casari SA, Albertoni FF (2013) First instar larva of *Atractocerus brasiliensis* (Lepeletier & Audinet-Serville, 1825) (Lymexylidae, Atractocerinae). Papeis Avulsos de Zoologia (São Paulo) 53: 359–372. https://doi.org/10.1590/S0031-10492013002700001

Chen X-Y (2019) A new genus and species of Lymexylidae (Insecta: Coleoptera) from mid-Cretaceous amber of northern Myanmar. Paleontological Journal 53: 1203–1205. https://doi.org/10.1134/S003103011911008X

Chen X-Y, Zhang H-C (2020) A new fossil record of Lymexylidae (Insecta: Coleoptera) from mid-Cretaceous amber of northern Myanmar. Zootaxa 4878: 195–200. https://doi.org/10.11646/zootaxa.4878.1.11

Clark J (1925) Forests pests. The Pin-hole borer (Atractocerus Kreuslerae Pasc.). Journal of the Department of Agriculture of Western Australia 2: 138–142.

Colombo WD, Gobbi FT, Perkovsky, EE, Azevedo CO (2021a) Synopsis of the fossil Pristocerinae (Hymenoptera, Bethylidae), with description of two new genera and six species from Burmese, Taimyr, Baltic and Rovno ambers. Historical Biology 33: 1736–1752. https://doi.org/10.1080/08912963.2020.1733551

Colombo WD, Perkovsky EE, Vasilenko DV (2021c) The first sclerodermine flat wasp (Hymenoptera: Bethylidae) from the upper Eocene Rovno amber, Ukraine. Alcheringa: An Australasian Journal of Palaeontology 45: 429–434. https://doi.org/10.1080/03115518.2021.2006311

Colombo WD, Perkovsky EE, Waichert C, Azevedo CO (2021b) Synopsis of the fossil flat wasps Epyrinae (Hymenoptera, Bethylidae), with description of three new genera and 10 new species. Journal of Systematic Palaeontology 19: 39–89. https://doi.org/10.1080/14772019.2021.1882593

Cuccodoro G (2007) Family Lymexylidae Fleming, 1821. In: Löbl I, Smetana A (Eds) Catalogue of Palaearctic Coleoptera. Vol. 4. Elateroidea–Derodontoidea–Bostrichoidea–Lymexyloidea–Cleroidea–Cucujoidea. Apollo Books, Stenstrup, Denmark, 362–363.

Giłka W, Harbach RE, Perkovsky EE (2021) Mosquitoes (Diptera: Culicidae) in Eocene amber from the Rovno region, Ukraine. Zootaxa 5016: 257–270. https://doi.org/10.11646/zootaxa.5016.2.6

Heer O (1865) Die Urwelt der Schweiz. Friedrich Schulthess, Zürich, 622 pp.

Jałoszyński P, Perkovsky EE (2019) The Mastigitae genus †*Baltostigus* in Upper Eocene Rovno amber (Coleoptera: Staphylinidae: Scydmaeninae). Zootaxa 4661: 594–600. https://doi.org/10.11646/zootaxa.4661.3.12

Jałoszyński P, Perkovsky EE (2021) A new bizarre species of *Euconnus* (*Cladoconnus*) in Upper Eocene Rovno amber (Coleoptera: Staphylinidae: Scydmaeninae). Zootaxa 5004: 395–400. https://doi.org/10.11646/zootaxa.5004.2.8

Khaustov AA, Vorontsov DD, Perkovsky EE, Lindquist EE (2021a) Review of fossil heterostigmatic mites (Acari: Heterostigmata) from late Eocene Rovno Amber. I. Families Tarsocheylidae, Dolichocybidae and Acarophenacidae. Systematic & Applied Acarology 26: 33–61. https://doi.org/10.11158/saa.26.1.3

Khaustov AA, Vorontsov DD, Perkovsky EE, Klimov PB (2021b) First fossil record of mite family Barbutiidae (Acari: Raphignathoidea) from late Eocene Rovno Amber, with a replacement name *Hoplocheylus neosimilis* nomen novum (Tarsocheylidae). Systematic & Applied Acarology 26: 973–980. https://doi.org/10.11158/saa.26.5.12

Kirejtshuk AG (2008) A new genus and species of timber beetle (Coleoptera: Lymexylidae) from the Baltic amber. Paleontological Journal 42: 63–65. https://doi.org/10.1007/s11492-008-1010-2

Kirichenko-Babko M, Perkovsky EE, Vasilenko DV (2021) A new genus and species of Lebiini (Coleoptera: Carabidae) from late Eocene Rovno amber. Historical Biology, 1–7. https://doi.org/10.1080/08912963.2021.1924701

Kirichenko-Babko M, Perkovsky EE, Vasilenko DV (2022) †*Antephilorhizus zerovae* sp. nov. (Carabidae: Lebiini), the second ground beetle species from Rovno amber. Historical Biology, 1–6. https://doi.org/10.1080/08912963.2021.2018686

Kirkendall LR, Biedermann PHW, Jordal BH (2015) Evolution and diversity of bark and ambrosia beetles. In: Vega FE, Hofstetter RW (Eds) Bark Beetles: Biology and Ecology of Native and Invasive Species. Academic Press, London, 85–156. https://doi.org/10.1016/B978-0-12-417156-5.00003-4

Kupryjanowicz J, Lyubarsky GY, Perkovsky EE (2019) A new species of the family Smicripidae (Coleoptera: Cucujoidea) from Rovno amber. Paleontological Journal 53: 165–171. https://doi.org/10.1134/S0031030119020059

Kupryjanowicz J, Lyubarsky GY, Perkovsky EE (2021) *Heterhelus buzina* sp.n. (Coleoptera: Kateretidae) from Rovno amber: the first proxy for *Sambucus* in the Eocene of Eastern Europe. Invertebrate Zoology 18: 16–24. https://doi.org/10.15298/invertzool.18.1.02

Kurosawa Y (1985) Revisional notes on the family Lymexylonidae (Coleoptera) in Eastern and Southeastern Asia. Bulletin of the National Science Museum – Series A, Zoology 11: 109–119.

Lawrence JF (2010) 8. Lymexloidae Fleming, 1821. In: Leschen RAB, Beutel RG, Lawrence JF (Eds) Handbook of Zoology. Arthropoda: Insecta. Coleoptera. Beetles. Vol. 2: Morphology and systematics (Elateroidea, Bostrichiformia, Cucujiformia partim). Walter de Gruyter, Berlin, Germany, 229–235. https://doi.org/10.1515/9783110911213.229

Lawrence JF (2020) The Australian Lymexylidae (Coleoptera: Tenerionoidea) with one new genus and two genera new to Australia. Zootaxa 4895: 211–238. https://doi.org/10.11646/zootaxa.4895.2.3

Legalov AA, Nazarenko VY, Perkovsky EE (2019) New weevils (Coleoptera: Curculionidae) from the Rovno amber. Paleontological Journal 53: 1045–1059. https://doi.org/10.1134/S0031030119100101

Legalov AA, Nazarenko VY, Perkovsky EE (2021a) A new species of the genus *Glaesotropis* Gratshev and Zherikhin, 1995 (Coleoptera, Anthribidae) from Rovno amber. Fossil Record 24: 1–7. https://doi.org/10.5194/fr-24-1-2021

Legalov AA, Nazarenko VY, Vasilenko DV, Perkovsky EE (2021b) *Ceutorhynchus* Germar (Coleoptera, Curculionidae) as proxy for Eocene core Brassicaceae: first record of the genus from Rovno amber. Journal of Paleontology, 1–8. https://doi.org/10.1017/jpa.2021.82

Lyubarsky GY, Perkovsky EE (2020) First Rovno amber species of the genus *Telmatophilus* (Coleoptera: Clavicornia: Cryptophagidae) from Veselukha floodplain. Invertebrate Zoology 17: 25–35. https://doi.org/10.15298/invertzool.17.1.03

Lyubarsky GY, Perkovsky EE (2021) New findings of Cryptophagidae (Coleoptera: Clavicornia) from Baltic amber in the unbiased collection of the Paleontological Institute of RAS. Russian Entomological Journal 30: 282–287. https://doi.org/10.15298/rusentj.30.3.05

Makarkin VN, Perkovsky EE (2020) A new species of *Proneuronema* (Neuroptera, Hemerobiidae) from the late Eocene Rovno amber. Zootaxa 4718: 292–300. https://doi.org/10.11646/zootaxa.4718.2.11

Mamontov YS, Atwood JJ, Perkovsky EE, Ignatov MS (2020) Hepatics from Rovno amber (Ukraine): *Frullania pycnoclada* and a new species, *F. vanae*. Bryologist 123: 421–430. https://doi.org/10.1639/0007-2745-123.3.421

Mänd K, Muehlenbachs K, McKellar RC, Wolfe AP, Konhauser KO (2018) Distinct origins for Rovno and Baltic ambers: evidence from carbon and hydrogen stable isotopes. Palaeogeography, Palaeoclimatology, Palaeoecology 505: 265–273. https://doi.org/10.1016/j.palaeo.2018.06.004

Martynova KV, Perkovsky EE, Olmi M, Vasilenko DV (2019) New records of Upper Eocene chrysidoid wasps (Hymenoptera: Chrysidoidea) from basins of Styr and Stokhod rivers (Rovno amber). Paleontological Journal 53: 998–1023. https://doi.org/10.1134/S0031030119100125

Matalin AV, Perkovsky EE, Vasilenko DV (2021) First record of tiger beetles (Coleoptera, Cicindelidae) from Rovno amber with the description of a new genus and species. Zootaxa 5016: 243–256. https://doi.org/10.11646/zootaxa.5016.2.5

Melnitsky SI, Ivanov VD, Perkovsky EE (2021a) A new species of *Plectrocnemia* (Trichoptera: Polycentropodidae) from Rovno amber. Zootaxa 5006: 106–109. https://doi.org/10.11646/zootaxa.5016.2.5

Melnitsky SI, Ivanov VD, Perkovsky EE (2021b) A new species of the fossil genus *Electrotrichia* (Insecta: Trichoptera: Hydroptilidae) from Rovno amber (Zhytomyr region, Olevsk locality). Palaeoentomology 4: 421–424. https://doi.org/10.11646/palaeoentomology.4.5.4

Melnitsky SI, Ivanov VD, Perkovsky EE (2021c) A new species of the genus *Holocentropus* (Trichoptera: Polycentropodidae) from Rovno amber. Zoosystematica Rossica 30: 298–302. https://doi.org/10.31610/zsr/2021.30.2.298

Mitov PG, Perkovsky EE, Dunlop JA (2021) Harvestmen (Arachnida: Opiliones) in Eocene Rovno amber (Ukraine). Zootaxa 4984: 43–72. https://doi.org/10.11646/zootaxa.4984.1.6

Nazarenko VY, Perkovsky EE, Vasilenko DV (2020) New genus and species of Lymexylidae (Coleoptera) from Baltic amber. Paleontological Journal 54: 1395–1399. https://doi.org/10.1134/S0031030120120035

Paulus HF (2004) *Urtea graeca* nov. gen. et nov. spec., der erste Vertreter der tropischen Atractocerinae in Europa sowie eine Beschreibung von *Hymaloxylon aspoecki* nov. spec. aus Yunnan (China) (Coleoptera, Cucujiformia, Lymexylidae, Atractocerinae nov. status). Denisia 13: 277–290.

Peris D (2020) Coleoptera in amber from Cretaceous resiniferous forests. Cretaceous Research 113: 104484. https://doi.org/10.1016/j.cretres.2020.104484

Peris D, Delclòs X, Jordal B (2021) Origin and evolution of fungus farming in wood-boring Coleoptera – a palaeontological perspective. Biological Reviews 96: 2476–2488. https://doi.org/10.1111/brv.12763

Perkovsky EE (2016a) Tropical and Holarctic ants in Late Eocene ambers. Vestnik Zoologii 50: 111–122. https://doi.org/10.1515/vzoo-2016-0014

Perkovsky EE (2016b) A new species of Micromalthidae (Coleoptera) from the Rovno amber: 1. Adult morphology. Paleontological Journal 50: 293–296. https://doi.org/10.1134/S0031030116030047

Perkovsky EE (2017a) Rovno amber caddisflies (Insecta, Trichoptera) from different localities, with information about three new sites. Vestnik Zoologii 51: 15–22. https://doi.org/10.1515/vzoo-2017-0003

Perkovsky EE (2017b) Comparison of biting midges of the Early Eocene Cambay amber (India) and Late Eocene European ambers supports the independent origin of European ambers. Vestnik Zoologii 51: 275–284. https://doi.org/10.1515/vzoo-2017-0033

Perkovsky EE (2018) Only a half of species of Hymenoptera in Rovno amber is common with Baltic amber. Vestnik Zoologii 52: 353–360. https://doi.org/10.2478/vzoo-2018-0037

Perkovsky EE, Makarkin VN (2019) A new species of *Succinoraphidia* Aspöck and Aspöck, 2004 (Raphidioptera: Raphidiidae) from the late Eocene Rovno amber, with venation characteristics of the genus. Zootaxa 4576: 570–580. https://doi.org/10.11646/zootaxa.4576.3.9

Perkovsky EE, Makarkin VN (2020) A new species of *Sympherobius* Banks (Neuroptera: Hemerobiidae) from the late Eocene Rovno amber. Palaeoentomology 3: 196–203. https://doi.org/10.11646/palaeoentomology.3.2.9

Perkovsky EE, Nel A (2021) A new Rovno amber termite genus (Isoptera, Rhinotermitidae) from Styr River basin. Palaeontologia Electronica 24: a05. https://doi.org/10.26879/1127

Perkovsky EE, Odnosum VK, Nazarenko VY, Vasilenko DV (2022) First record of the genus *Cyrtanaspis* Emery (Insecta: Coleoptera: Scraptiidae) from Baltic amber. Paleontological Journal 56: in press.

Perkovsky EE, Olmi M (2018) Discovery of the first pincer wasp (Hymenoptera, Dryinidae) from Rovno amber. Zootaxa 4457: 296–304. https://doi.org/10.11646/zootaxa.4457.2.5

Perkovsky EE, Olmi M, Vasilenko DV, Capradossi L, Guglielmino A (2020) The first species of *Bocchus* Ashmead (Hymenoptera: Dryinidae) from Upper Eocene Rovno amber: *B. schmalhauseni* sp. nov. Zootaxa 4819: 544–556. https://doi.org/10.11646/zootaxa.4819.3.6

Perkovsky EE, Rasnitsyn AP, Vlaskin AP, Taraschuk MV (2007) A comparative analysis of the Baltic and Rovno amber arthropod faunas: representative samples. African Invertebrates 48: 229–245.

Perkovsky EE, Zosimovich VY, Vlaskin AP (2010) Chapter 7: Rovno amber. In: Penney D (Ed.) Biodiversity of fossils in amber from the major world deposits. Siri Scientific Press, Manchester, 116–136.

Radchenko AG, Perkovsky EE (2018) First record of fossil ant species *Eocenomyrma rugosostriata* (Mayr) (Hymenoptera: Formicidae) from the Rovno amber. Russian Entomological Journal 27: 285–288. https://doi.org/10.15298/rusentj.27.3.08

Radchenko AG, Perkovsky EE (2020) New finds of the fossil ant genus *Prionomyrmex* Mayr (Hymenoptera, Formicidae, Myrmeciinae) from Late Eocene European ambers. Paleontological Journal 54: 617–626. https://doi.org/10.1134/S0031030120060088

Radchenko AG, Perkovsky EE (2021) Wheeler's dilemma revisited: first *Oecophylla-Lasius* syninclusion and other ants syninclusions in the Bitterfeld amber (late Eocene). Invertebrate Zoology 18: 47–65. https://doi.org/10.15298/invertzool.18.1.02

Radchenko AG, Perkovsky EE, Vasilenko DV (2021) *Formica* species (Hymenoptera, Formicidae, Formicinae) in late Eocene Rovno amber. Journal of Hymenoptera Research 82: 237–251. https://doi.org/10.3897/jhr.82.64599

Simutnik SA, Perkovsky EE, Vasilenko DV (2020) First record of *Leptoomus janzeni* Gibson (Hymenoptera, Chalcidoidea) from Rovno amber. Journal of Hymenoptera Research 80: 137–145. https://doi.org/10.3897/jhr.80.58882

Simutnik SA, Perkovsky EE, Khomych MR, Vasilenko DV (2021) First record of the *Sulia glaesaria* Simutnik, 2015 (Hymenoptera, Chalcidoidea, Encyrtidae) from Rovno amber. Journal of Hymenoptera Research 88: 85–102. https://doi.org/10.3897/jhr.88.75941

Sokoloff DD, Ignatov MS, Remizowa MV, Nuraliev MS, Blagoderov V, Garbout A, Perkovsky EE (2018) A male flower of *Prunus* s. l. (Rosaceae) from Eocene Rovno amber (Ukraine). Journal of Plant Research 131: 925–943. https://doi.org/10.1007/s10265-018-1057-2

Telnov D, Perkovsky EE, Vasilenko DV, Yamamoto S (2021) The first fossil Coleoptera record from the Volyn Region, Ukraine, with description of a new *Glesoconomorphus* (Coleoptera, Mycteridae) in syninclusion with Winterschmidtiidae (Acari) and a key to species. ZooKeys 1068: 189–201. https://doi.org/10.3897/zookeys.1068.75391

Tikhomirova AL (1991) Ontogeny transformation as a mechanism of the insect evolution. Nauka, Moscow, 168 pp. [in Russian]

Toki W (2021) A single case study of mycetangia-associated fungi and their abilities to assimilate wood-associated carbon sources in the ship timber beetle *Elateroides flabellicornis* (Coleoptera: Lymexylidae) in Japan. Symbiosis 83: 173–181. https://doi.org/10.1007/s13199-021-00745-9

Tshernyshev SE, Perkovsky EE (2021) *Protomauroania mikhailovi* – a new species of malachite beetles (Coleoptera, Dasytidae) in Rovno amber. Zootaxa 5006: 189–194. https://doi.org/10.11646/zootaxa.5006.1.20

Wheeler QD (1986) Revision of the genera of Lymexylidae (Coleoptera: Cucujiformia). Bulletin of the American Museum of Natural History 183: 113–210.

Wickham HF (1911) Fossil Coleoptera from Florissant, with descriptions of several new species. Bulletin of the American Museum of Natural History 30: 53–69.

Wolf-Schwenninger K (2011) The oldest fossil record of Lymexylidae (Insecta: Coleoptera) from the Lower Cretaceous Crato Formation of Brazil. Insect Systematics & Evolution 42: 205–212. https://doi.org/10.1163/187631211X578352

Yamamoto S (2019) Fossil evidence of elytra reduction in ship-timber beetles. Scientific Reports 9: e4938. https://doi.org/10.1038/s41598-019-41310-1

Young DK (2002) 71. Lymexylidae Fleming 1821. In: Arnett Jr RH, Thomas MC, Skelley PE, Frank HJ (Eds) American Beetles. Vol. 2. Polyphaga: Scarabaeoidea through Curculionoidea. CRC Press, Boca Raton, FL, USA, 261–262. https://doi.org/10.1201/9781420041231.ch4

Zhang S-Q, Che L-H, Li Y, Liang D, Pang H, Ślipiński A, Zhang P (2018) Evolutionary history of Coleoptera revealed by extensive sampling of genes and species. Nature Communications 9: e205. https://doi.org/10.1038/s41467-017-02644-4

Fossil Record 25 (1) 2022, 75–82 | DOI 10.3897/fr.25.81862

Bizarre egg structure uncovers a new family of Plecoptera (Insecta) from mid-Cretaceous Burmese amber

Zhi-Teng Chen[1]

[1] *School of Grain Science and Technology, Jiangsu University of Science and Technology, Zhenjiang, 212004, China*

http://zoobank.org/C905FCB0-7880-4990-931D-8BCC98CD85C3

Corresponding author: Zhi-Teng Chen (741208116@qq.com)

Academic editor: Carolin Haug ♦ **Received** 29 November 2021 ♦ **Accepted** 8 February 2022 ♦ **Published** 15 February 2022

Abstract

A new fossil stonefly, *Perspicuusoperla lata* **gen.** et **sp. nov.**, is described and illustrated based on a well-preserved female adult and its eggs in mid-Cretaceous Burmese amber. The new taxon exhibits a combination of diagnostic morphologies, such as two crossveins between anterior radius (RA) and posterior radius (RP), broad subgenital plate exceeding abdomen tip, and entirely membranous eggs that cannot be incorporated into any known stonefly families. Perspicuusoperlidae, fam. nov. is established based on *Perspicuusoperla* gen. nov. and its systematic position is preliminarily discussed based on morphological comparison with other stoneflies. Palaeobiological implications are inferred from the egg morphology. This study represents the earliest known and best-preserved fossil record of extinct stonefly eggs.

Key Words

Burmese amber, Perspicuusoperlidae, Plecoptera, stonefly

1. Introduction

Plecoptera, also called stoneflies, are a basal, aquatic insect order distributed on all continents and most major islands except Antarctica (Steward 2009). Stoneflies are hemimetabolous, with egg, nymph, and adult life stages. They are typically associated with running water and waterside microhabitats. Plecoptera is supported as a monophyletic order according to a series of anatomical characters and also molecular evidence (Zwick 2000; Terry and Whiting 2005). There are more than 4100 species recorded in Plecoptera, including over 300 fossil species (DeWalt et al. 2021). The current classification system of Plecoptera comprises 16 extant families under two suborders (Zwick 2000). The suborder Arctoperlaria is largely distributed in the Northern Hemisphere except the family Notonemouridae, which occurs in the Southern Hemisphere. Arctoperlaria is further divided into two groups/infraorders, Euholognatha (including six families: Capniidae, Leuctridae, Nemouridae, Taeniopterygidae, Scopuridae and Notonemouridae) and Systellognatha (including six families Pteronarcyidae, Peltoperlidae, Styloperlidae, Perlidae, Perlodidae and Chloroperlidae). The other suborder Antarctoperlaria is exclusively restricted to the Southern Hemisphere, containing four families: Austroperlidae, Diamphipnoidae, Eustheniidae, and Gripopterygidae. The 16 extant families of Plecoptera can be readily divided by their unique morphology concerning mouthparts, gills, wings, tarsi, genitalia, cerci, and other characters (Stewart and Stark 2008; Chen and Du 2018).

Plecoptera comprises relatively rich fossil record, with the oldest Pennsylvanian representative *Gulou carpenteri* Béthoux et al. (2011) from the Tupo Formation of China (Béthoux et al. 2011). Numerous younger fossils have been described with ages ranging from Permian to Pliocene (Liu and Ren 2006). In recent years, mid-Cretaceous Kachin amber is attracting lots of interest from the researchers. Three families of stoneflies are known from Kachin amber, including Perlidae, extinct family Petroperlidae, and Peltoperlidae (Latreille 1802; Claassen 1931; Sroka et al. 2018; Chen and Xu 2020). These extinct stoneflies have exhibited a series pf specially modified external structures which are probably associated with mating behavior (Chen and Xu 2021).

Egg morphology of Plecoptera is very informative from species level to subordinal level delimitation and has obvious oviposition-related biological implications (Hynes 1976; Zwick 2000; Mtow and Machida 2018; Mtow et al. 2021). However, eggs are rarely reported from fossil materials, merely with simple egg description from Tertiary Dominican amber (Stark and Lentz 1992). In this study, a new stonefly that represents a new extinct family is described based on a well-preserved female specimen from the mid-Cretaceous Kachin amber. The description and analysis are provided for the female and its well-preserved egg mass.

2. Materials and methods

The Burmese amber studied in this study was obtained from Kachin, Hukawng Valley (26°20'N, 96°36'E) of northern Myanmar (precise locality in Kania et al. 2015: fig. 1). The age was dated and widely accepted as the earliest Cenomanian (98.79 ± 0.62 Ma) of mid-Cretaceous (Shi et al. 2012; Yu et al. 2019). The amber is deposited in the Insect Collection of Jiangsu University of Science and Technology (**ICJUST**, No. CZT-PLE-MA11), Jiangsu Province, China. Examination and measurements were conducted with a SDPTOP SZM45 stereomicroscope. Photographs were taken by a Canon EOS 6D digital camera equipped with a Canon MP-E 65 mm 5× macro lens. Photographs and line drawings were adjusted and optimized with Adobe Photoshop CS6. Wing venation nomenclature follows Béthoux (2005).

3. Systematic palaeontology

Order Plecoptera Burmeister, 1839
Suborder Arctoperlaria Zwick, 1973

Perspicuusoperlidae, fam. nov.

http://zoobank.org/3B3C915F-BB52-4A6B-BAF0-BAB42239D696

Type genus. *Perspicuusoperla* gen. nov.

Etymology. The first part of the compound noun refers to the transparent egg and is derived from Latin 'perspicuus'; the second part 'perlidae' refers to the stonefly family Perlidae Latreille, 1802.

Diagnosis. Triocellate; maxillary palp slender, apical segment unmodified; labial palp short, apical segment slightly shortened; cervical gills invisible. Legs with two giant apical tibial spurs; first two tarsal segments shortest, with developed euplantulae; arolium without setae. In forewings, ScP joining into RA after ra-rp; h stout and with regular obliquity; RA not reaching wing apex; RP originating at basal ⅓ of RA and with three branches; two crossveins present between RA and RP; CuA with four branches, two posterior branches fused basally; CuP and AA1 simple; AA2 appears unforked and abruptly curved backwards at apical half; hind wings with extremely broad and multifolded anal area. Abdominal segments unmodified; paraprocts sclerotized and thumb-shaped; subgenital plate broad, exceeding posterior margin of tergum 10. Cerci slender, membranous and with multiple segments. Egg mass with dozens of uniformly oriented cylindrical eggs; each egg with very short collar, membranous and transparent chorion, without anchor and pedicel.

Perspicuusoperla gen. nov.

http://zoobank.org/D44F3A06-90E9-49FC-A85C-5F35D2C36C2D

Type species. *Perspicuusoperla lata* gen. et sp. nov.

Etymology. The genus name is a combination of the words *Perspicuuso* and *perla*; the first word is derived from Latin 'perspicuus', meaning 'transparent' and refers to the transparent egg; the second word refers to the stonefly genus *Perla* Geoffroy, 1762.

Diagnosis. By monotypy, as for the type species.

Perspicuusoperla lata sp. nov.

http://zoobank.org/D6B8C72C-2175-49E4-9B03-56C4DDDA509A
Figs 1–5

Etymology. The specific epithet means 'broad' and is derived from Latin 'lata', refers to the broad female subgenital plate.

Type material. Holotype male (No. CZT-PLE-MA11), deposited in the Insect Collection of Jiangsu University of Science and Technology (ICJUST). The specimen is well preserved, but its hindwings are covered by forewings.

Type locality. Hukawng Valley, southwest Maingkhwan, Kachin State (26°20N, 96°36E), Myanmar, uppermost Albian-lowermost Cenomanian (mid-Cretaceous).

Description. Macropterous (Fig. 1A–C); body long and stout, length (excluding antennae and cerci) ca. 7.5 mm, generally brown.

Head (Figs 1, 2A–C) short and wide, width three times longer than length, mostly dark brown, anterolateral and posterior margins pale. Triocellate, anterior ocellus large and elevated. Compound eye large, oval and strongly protruded laterad. Antenna brown and filiform, with 25 segments preserved, basal segments much shorter than wide, each antennal segment covered with dense short hairs. Maxillary palp slender, with five segments, apical segment unmodified. Labial palp short, length near 2/3 of maxillary palp, three-segmented, apical segment slightly shorter than second segment. Cervical gills invisible.

Pronotum (Figs 1A–B, 2A–B) slightly narrower than head, transversely kidney-shaped, anterior margin longer than posterior margin, surface densely pubescent, with thick rugosity. Meso- and metanota mostly sclerotized, nearly as wide as pronotum. Legs mostly dark brown, femur longer and thicker than tibia (Fig. 1); two giant tibial spurs present ventrally; first two tarsal segments shortest (Fig. 2D–F), euplantulae developed; third tarsal segment apically with long bristles; arolium without setae.

Wings (Figs 1, 3) hyaline, veins dark brown. Forewings length ca. 10.0 mm. In right forewing (Fig. 3), ScP

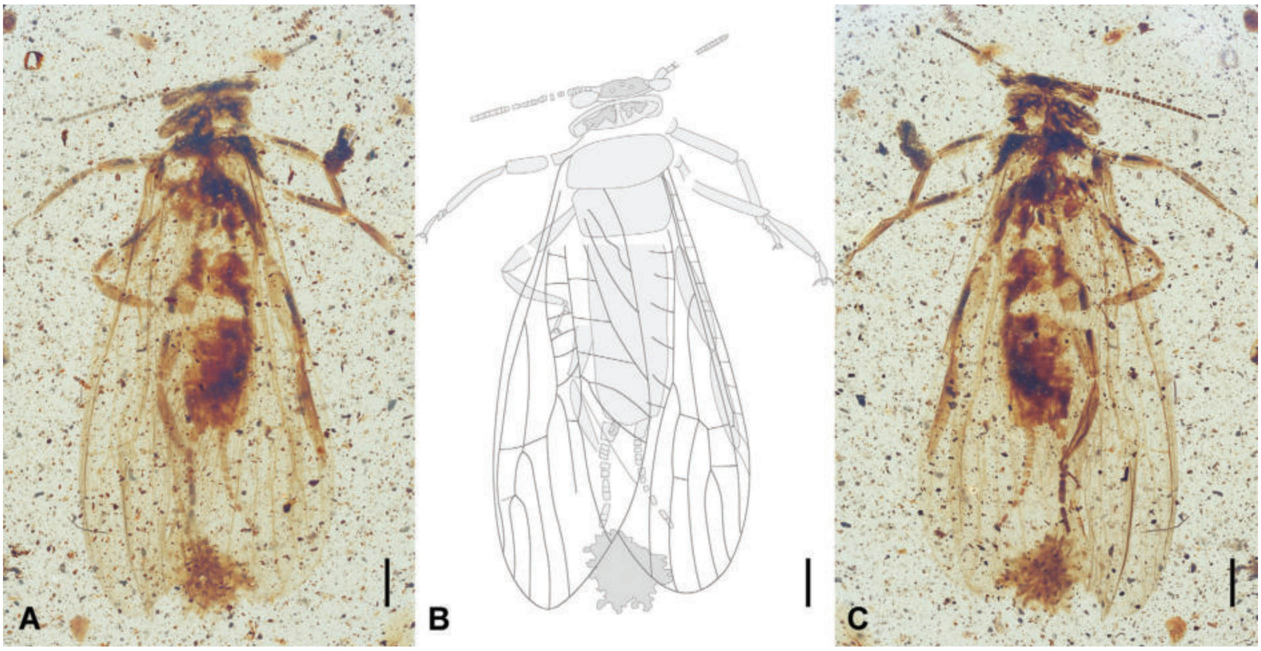

Figure 1. *Perspicuusoperla lata* gen. et sp. nov., holotype female (CZT-PLE-MA11): **A.** Habitus photo, dorsal view; **B.** Drawing of habitus, dorsal view; **C.** Habitus photo, ventral view. Scale bars: 1.0 mm.

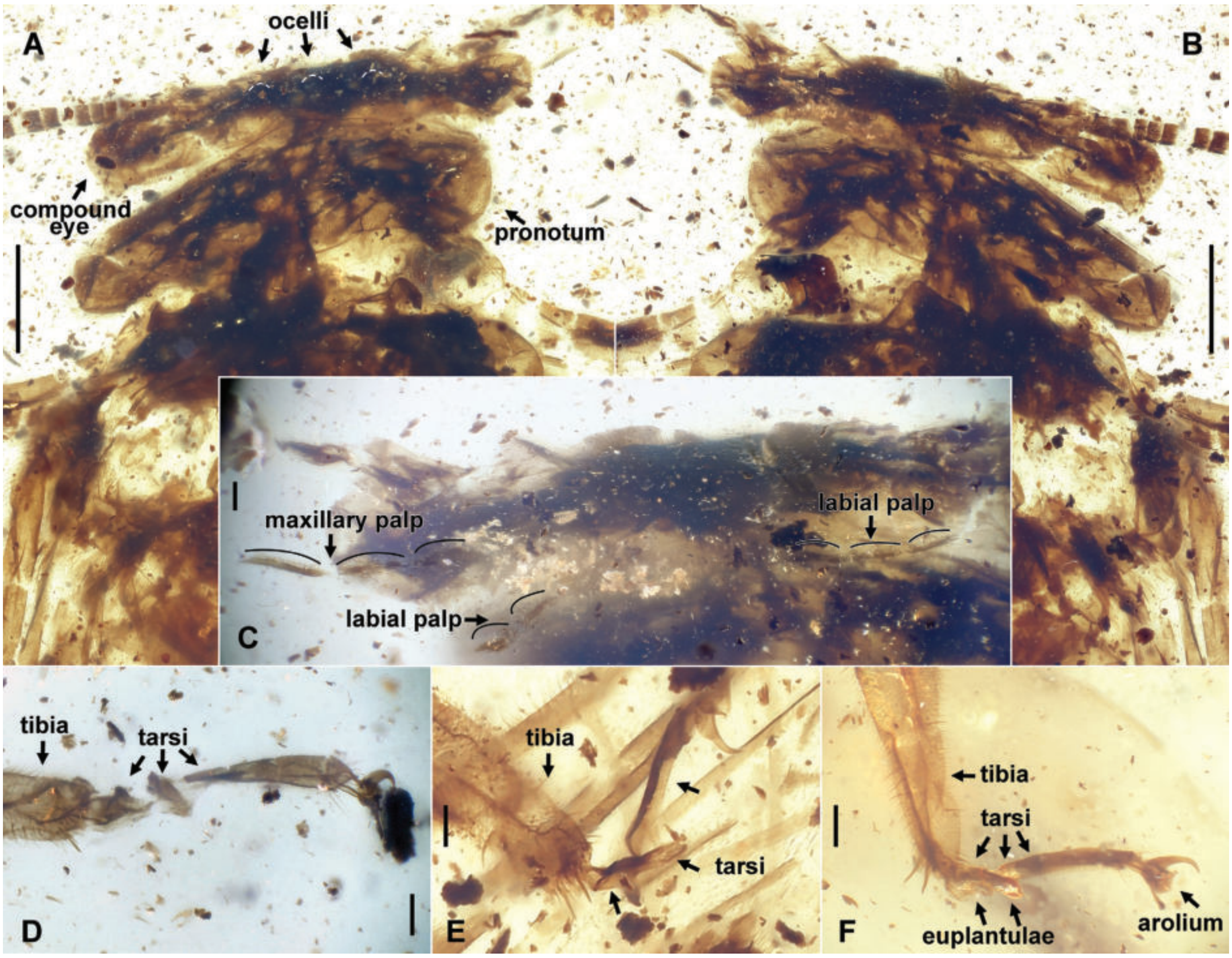

Figure 2. *Perspicuusoperla lata* gen. et sp. nov., holotype female (CZT-PLE-MA11): **A.** Head and thorax, dorsal view; **B.** Head and thorax, ventral view; **C.** Head, ventral view; **D.** Tarsi of left foreleg, ventral view; **E.** Tarsi of left midleg, ventral view; **F.** Tarsi of left hindleg, ventral view. Scale bars: 0.5 mm (**A, B**), 0.1 mm (**D–F**).

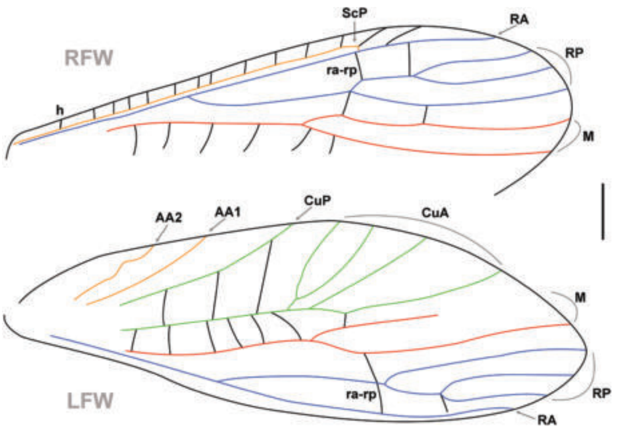

Figure 3. *Perspicuusoperla lata* gen. et sp. nov., holotype female (CZT-PLE-MA11): drawing of forewings, dorsal view. Abbreviations: RFW, right forewing; LFW, left forewing; h, humera; ScP, posterior subcosta; RA, anterior radius; RP, posterior radius; M, media; CuA, anterior cubitus; CuP, posterior cubitus; AA1, first anterior analis; AA2, second anterior analis; ra-rp, crossvein between RA and RP. Scale bar: 1.0 mm.

reaching RA after ra-rp; h stout and with regular obliquity, another 12 crossveins present between Sc and the anterior margin; one extra crossvein present beyond ScP; RA not reaching wing apex; RP originating at basal ⅓ of RA and with three branches; two crossveins present between RA and RP; M forked at near half of wing length; at least six crossveins present between M and CuA; other longitudinal veins invisible. In left forewing (Fig. 3), RA, RP and M similar to right forewing; two crossveins present between RA and RP; single crossvein present between RP and M; area between M and CuA with seven crossveins; CuA with four branches, two posterior branches fused basally; three crossveins present between CuA and CuP; CuP and AA1 simple; AA2 seems unforked and abruptly curved backwards at apical half. Hind wings length ca. 9.0 mm, veins invisible; anal area extremely broad, with multiple folds.

Abdomen (Figs 1, 4) length ca. 4.5 mm, stout, generally brown. Abdominal terga unmodified; posterior margin of tergum 10 near truncate (Fig. 1A–B). Paraproct strongly sclerotized, thumb-shaped, two times longer than wide, apex blunt and curved (Fig. 4A–C). Subgenital plate originating

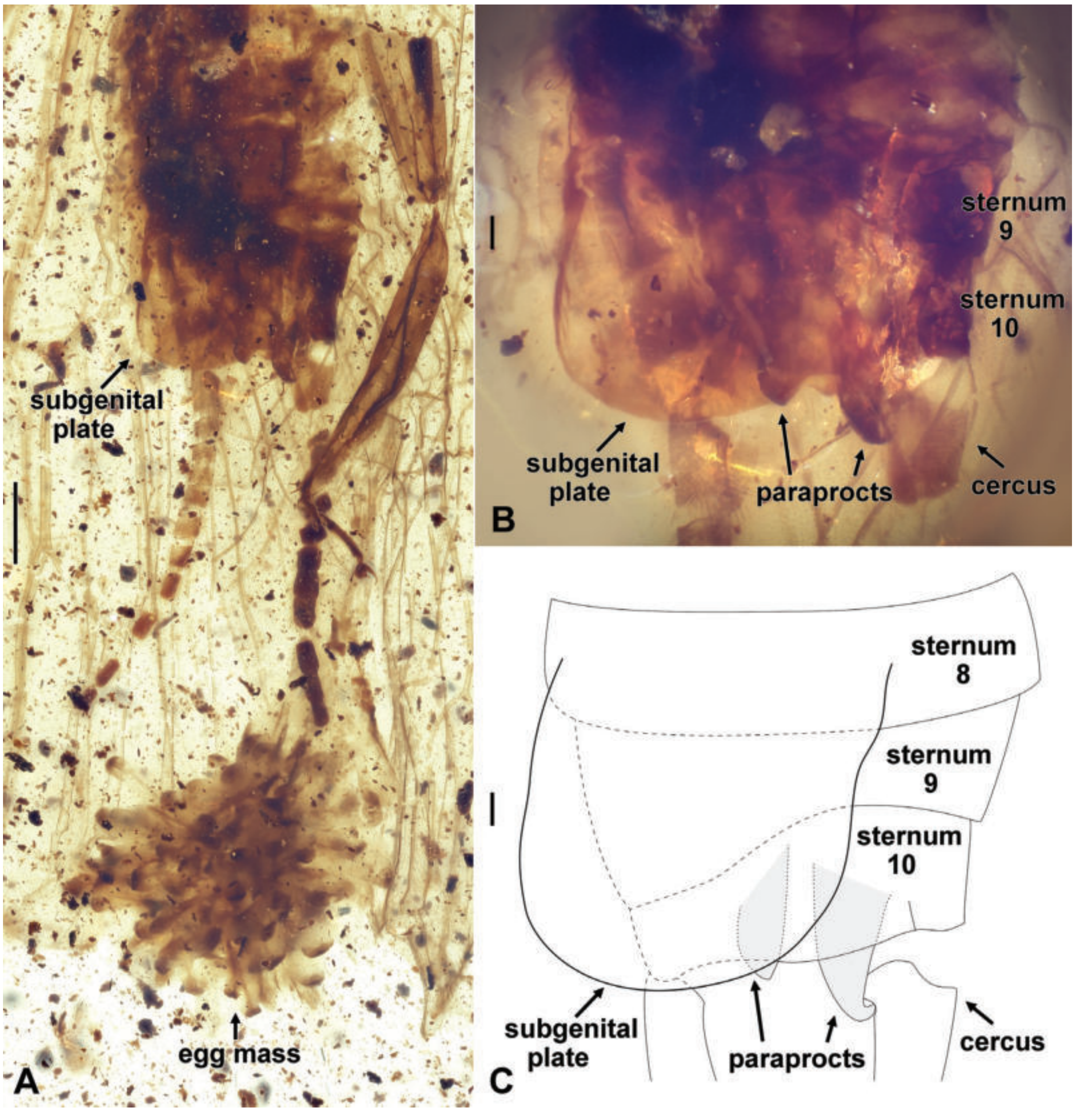

Figure 4. *Perspicuusoperla lata* gen. et sp. nov., holotype female (CZT-PLE-MA11): **A.** Photo of abdomen and egg mass, ventral view; **B.** Photo of terminalia, ventral view; **C.** Drawing of terminalia, ventral view. Scale bars: 0.5 mm (**A**), 0.1 mm (**B, C**).

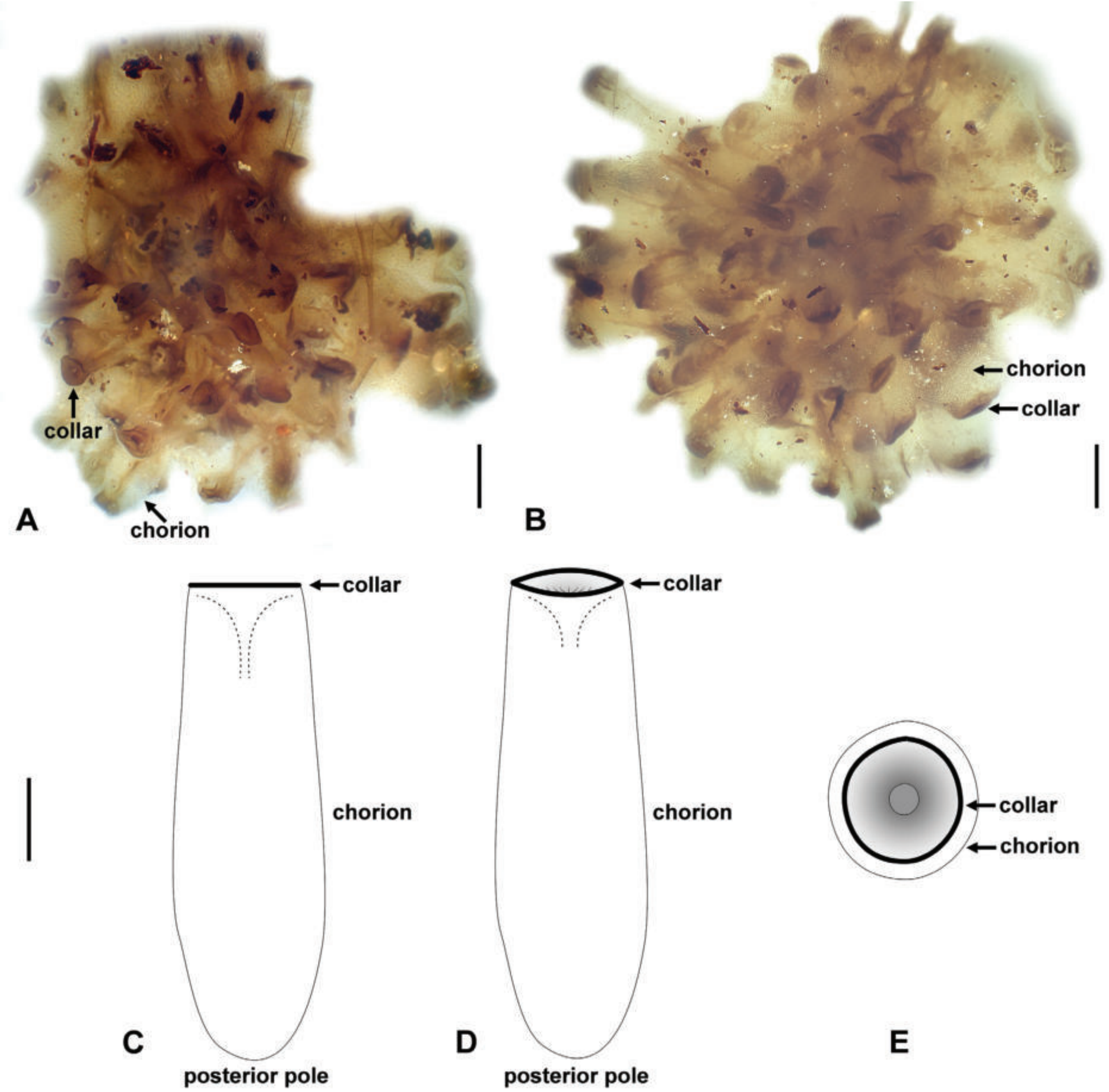

Figure 5. *Perspicuusoperla lata* gen. et sp. nov., holotype female (CZT-PLE-MA11): **A.** Photo of egg mass, dorsal view; B. Photo of egg mass, ventral view; **C.** Drawing of single egg, lateral view; **D.** Drawing of single egg, anteriolateral view; **E.** Drawing of single egg, anterior view. Scale bars: 0.2 mm (**A, B**), 0.1 mm (**C–E**).

from sternum 8, broad and rounded, lateral margins near parallel at anterior half; posterior margin of subgenital plate extended beyond posterior margin of tergum 10 (Fig. 4A–C). Cerci (Fig. 4A) membranous and dark brown, with 12 segments preserved; each segment covered with dense, moderately long bristles; boundaries of segments clear.

Egg mass (Figs 1, 4A, 5A–B) composed of dozens of cylindrical eggs, diameter ca. 1.2 mm; posterior poles of all eggs stuck together in the center of egg mass, whereas collars of anterior poles pointing outward. Egg length ca. 0.75 mm, slender, slightly enlarged at middle (Fig. 5A–E). Chorion entirely membranous, transparent and smooth. Collar very short, narrow, simple and weakly sclerotized, boundary with chorion inconspicuous, inner area circular and medially depressed, forming a funnelform median channel (Fig. 5C–E). Anchor and pedicel absent.

4. Discussion

4.1. Systematic position

The monophyly of Arctoperlaria is supported by drumming behavior and related male abdominal structures such as ventral lobe, hammer, vesicle or hair brush (Zwick 2000). However, the female holotype does not allow a convenient subordinal assignment by drumming related male structures.

Antarctoperlaria: Egg structure and wing venation of Perspicuusoperlidae apparently distinguish from those of the four antarctoperlarian families. The completely membranous egg chorion of Perspicuusoperlidae differs from the sclerotized chorion in most Antarctoperlaria except for Austroperlidae (Hynes 1974; Zwick 2000; Mtow et al. 2021). The absence of net-like venation, namely multiple crossveins in apical half of forewings excludes its assignment to Austroperlidae, Diamphipnoidae and Eustheniidae (Illies 1960, 1969; Riek 1973; Zwick 1979; McLellan 2001; Béthoux 2005). ScP joining into RA instead of running free from RA until reaching the anterior wing margin excludes its assignment in Gripopterygidae (McLellan 1977; Béthoux 2005; McLellan et al. 2007).

Euholognatha of Arctoperlaria: Although the soft egg chorion is considered apomorphic in the infraorder Euholognatha (Zwick 2000), the assignment of Perspicuusoperlidae to Euholognatha is easily excluded by the presence of euplantulae on first two tarsal segments and the multiple branches of CuA in forewings (Nelson 2009; Cui et al. 2014). The presence of well-developed wings and absence of thoracic notal projections exclude Perspicuusoperlidae from the apterous family Scopuridae (Jin and Bae 2005). The two shortest basal tarsomeres and absence of setiform basipulvilli on pretarsus exclude Perspicuusoperlidae from superfamily Nemouroidea (Zwick 2000; Nelson 2009). The presence of more than one crossvein in the distal half of RA–RP area in forewings also denied the assignment of Perspicuusoperlidae to most Nemouroidea except some Taeniopterygidae (Chen 2021).

Systellognatha of Arctoperlaria: The absence of setae on the arolium, the completely membranous egg chorion, and the basal crossvein of the costal field equal in size to the remaining crossveins and with normal regular obliquity all together excluded Perspicuusoperlidae from the infraorder Systellognatha (Zwick 2000; Nelson 2009; Cui et al. 2014). Specifically, Perspicuusoperlidae differs from Pteronarcyidae by absence of numerous crossveins in wings and absence of gill remnants on abdominal segments (Nelson 1988; Chen and Du 2018); from Peltoperlidae by the presence of two crossveins between RA and RP (Chen and Xu 2020); from Styloperlidae by the presence of three well-developed ocelli, giant tibial spurs, and absence of numerous crossveins between RA and M (Uchida and Isobe 1989); from Perlidae by absence of thoracic gill remnants (Zwick 2000) and presence of sclerotized paraprocts in female; from the three recognized tribes (Arcynopterygini, Diploperlini, Perlodini) of perlodid subfamily Perlodinae by the apparently different shape and structure of eggs (Stark and Szczytko 1984), from another perlodid subfamily Isoperlinae by the extremely large female subgenital plate exceeding end of sternum 10 in combination with the three-branched RP in forewing (Zwick and Surenkhorloo 2005; Szczytko and Kondratieff 2015a, 2015b); from Chloroperlidae by the stout body, broad anal region in forewing and unmodified apical maxillary palpal segment (Zwick 2000, 2006); from the recently proposed Kathroperlidae by absence of strongly elongated head, and by two crossveins between RA and RP (South et al. 2021).

The wing venation, especially the presence of two crossveins between RA and RP in forewings of Perspicuusoperlidae apparently differs from all other extinct stoneflies described from mid-Cretaceous Kachin amber, but is reminiscent of the Late Permian fossil family Palaeoperlidae (Sinitshenkova 1987, 2013). However, the combination of wing characters, including ScP reaching RA after ra-rp, RP with three branches and CuA with four branches can separate Perspicuusoperlidae from Palaeoperlidae (Sinitshenkova 1987, 2013).

As a result, it's currently difficult to conclude the exact systematic position of Perspicuusoperlidae in lack of male characters. Perspicuusoperlidae is confidently excluded from suborder Antarctoperlaria by exhibiting no resemblance concerning body pattern and shape to any of the four extant families; the completely membranous egg chorion further suggests that Perspicuusoperlidae is not an antarctoperlarian group. Similarly, in Arctoperlaria, Perspicuusoperlidae cannot be reliably placed in any of the two infraorders (Euholognatha and Systellognatha) nor any of the families according to the characters discussed above. The general body characters (body shape, color, wing venation, tarsal structures, etc.) of Perspicuusoperlidae resemble those of Systellognatha, whereas the soft egg chorion is more close related to Euholognatha. Zwick (2000) suggested that sclerotized hard egg chorion is a groundplan character of Plecoptera whereas the soft chorion is probably apomorphy for Euholognatha. Perspicuusoperlidae is herein proposed as the stem group of Euholognatha + Systellognatha based on the following characters: soft egg chorion (apomorphy of Euholognatha); absence of anchor plate in eggs (opposed to the apomorphy of Systellognatha); presence of collar in eggs (apomorphy of Systellognatha), although not well defined; short first tarsomere (apomorphy of Systellognatha); presence of euplantulae on basal two tarsomeres (plesiomorphy of Systellognatha); absence of setae on arolium (opposed to the apomorphy of Systellognatha); forewing with numerous crossveins in costal field (plesiomorphy of Systellognatha); basal crossvein in the costal field of forewing similar to the remaining crossveins (opposed to the apomorphy of Systellognatha).

4.2. Palaeobiological implications

The eggs of Plecoptera are too small to be noticed and can hardly be preserved in fossil impressions, leaving the merely available description for *Dominiperla antigua* Stark & Lentz, 1992 (Plecoptera: Perlidae) from Tertiary Dominican amber (Stark and Lentz 1992). The eggs of *D. antigua* were bullet-shaped with one pole sharp and another pole enlarged. Herein, we reported the oldest stonefly's eggs, which perfectly preserved details for the extinct Plecoptera.

Several interesting characters are found in these eggs of Perspicuusoperlidae. Firstly, the egg mass comprises only dozens of eggs. The number of stonefly eggs in a mass is highly variable, ranged from only a few hundred in large species to over 1400 in small winter species (Jewett 1959). The egg masses immediately disintegrate very quickly under water (Hynes 1976). In Perspicuusoperlidae, the egg mass is considerably small, with no more than 100 eggs. According to the study of *Taeniopteryx nebulosa* (Linnaeus, 1758) in Brittain (1977), the low number of eggs per egg mass might suggest a low water temperature (lower than 10 °C) in the habitat area.

Whereas in the biological study of *Nemoura cinerea* (Retzius, 1783), the number of eggs per mass has no significant relationship with temperature (Ebrittain and Lillehammer 1987). A fixed level of available natural resource could lead to a tradeoff between egg size and egg number (Smith and Fretwell 1974), the apparently large individual eggs of Perspicuusoperlidae might result in the less number in the mass (Berrigan 1991). Another plausible hypothesis proposed by the author is that, the ancient Burmese forest streams were small in size, slow-flowing or even fragmented, which could not bear a high-density population as big rivers or streams and partially contributed to the low number of eggs in Perspicuusoperlidae.

Secondly, the eggs of Perspicuusoperlidae are completely membranous in lack of complicated external structures, and the egg mass is composed of uniformly arranged individual eggs. Eggs of stoneflies are highly variable in size, shape, and chorionic modification. Several main types of eggs are introduced by Hynes (1976): eggs with an anchor plate to adhere firmly to substrates under water (as in some Systellognatha); eggs with sticky membranous or gelatinous surface coverings that swell rapidly in water and stick to substrates (as in Euholognatha and some Systellognatha); eggs with filament-like projections with hooked tips (as in *Perlesta* Banks, 1906); eggs not sticky and simply fall into interstices of stream bed (as in most Antarctoperlaria). However, the eggs of Perspicuusoperlidae have no anchor plates, sticky membranous or gelatinous surface, or any filament-like projections. Dissolution of these structures during the fossil formation is less possible since the surface and outline of all visible eggs are uniformly clearly recognized without any remnants of above mentioned structures. Two potential strategies might be used by eggs of Perspicuusoperlidae: simply fall and scatter in water; or use the multiple concave collar areas arranged outside the egg mass as sucking discs to adhere to substrates. The latter assumption seems more reasonable since the egg masses of extant stoneflies usually stick together with random orientation for each egg, whereas the eggs of Perspicuusoperlidae uniformly project the collar areas outward. Such ordered arrangement of eggs should be functional.

Data availability

All material included in this paper is deposited in the Insect Collection of Jiangsu University of Science and Technology, Jiangsu Province, China.

Author contributions

ZTC produced the photos and prepared the paper.

Competing interests

The authors declare that they have no conflict of interest.

Acknowledgements

The author thanks the editor and reviewers for helpful comments. This work is funded by the Natural Science Foundation of Jiangsu Province (No. BK20201009), Start-up Funding of Jiangsu University of Science and Technology (No. 1182931901), and the support of the Museum für Naturkunde Berlin.

References

Berrigan D (1991) The allometry of egg size and number in insects. Oikos 60(3): 313–321. https://doi.org/10.2307/3545073

Burmeister H (1839) Zweite Halfte. Neuroptera. Handbuch der Entomologie. Reimer, Berlin, 863 pp.

Brittain JL (1977) The effect of temperature on the egg incubation period of *Taeniopteryx nebulosa* (Plecoptera). Oikos 29(2): 302–305. https://doi.org/10.2307/3543618

Banks N (1906) Notes on the Classification of the Perlidae. Canadian Entomologist 38: 221–224. https://doi.org/10.4039/Ent38221-7

Béthoux O (2005) Wing venation pattern of Plecoptera (Neoptera). Illiesia 1: 52–81.

Béthoux O, Cui YY, Kondratieff B, Stark B, Ren D (2011) At last, a Pennsylvanian stem-stonefly (Plecoptera) discovered. BMC Evolutionary Biology 11: e248. https://doi.org/10.1186/1471-2148-11-248

Claassen PW (1931) Plecoptera nymphs of American (north of Mexico). The Thomas Say Foundation 3: 1–199.

Cui YY, Béthoux O, Kondratieff B, Liu YS, Ren D (2014) *Sinosharaperla zhaoi* (Insecta: Plecoptera; Early Cretaceous), a Gondwanian element in the northern hemisphere, or just a misplaced species? Systematic Palaeontology 13: 883–889. https://doi.org/10.1080/14772019.2014.960903

Chen ZT (2021) Discovery of *Mesyatsia karakorum* (Šámal, 1935) (Plecoptera: Taeniopterygidae) in Yunnan Province of China. Aquatic Insects: 1–10. https://doi.org/10.1080/01650424.2021.1967401

Chen ZT, Du YZ (2018) A checklist and adult key to the Chinese stonefly (Plecoptera) genera. Zootaxa 4375(1): 59–74. https://doi.org/10.11646/zootaxa.4375.1.2

Chen ZT, Xu CP (2020) First Peltoperlidae (Insecta: Plecoptera) from mid-Cretaceous Burmese amber. Cretaceous Research 114: 104506. https://doi.org/10.1016/j.cretres.2020.104506

Chen ZT, Xu CP (2021) New perlid stonefly (Insecta: Plecoptera) from mid-Cretaceous Burmese amber. Cretaceous Research 127: 104954. https://doi.org/10.1016/j.cretres.2021.104954

DeWalt RE, Maehr MD, Hopkins H, Neu-Becker U, Stueber G (2021) Plecoptera Species File Online. http://Plecoptera.SpeciesFile.org

Ebrittain J, Lillehammer A (1987) Variability in the rate of egg development of the stonefly, *Nemoura cinerea* (Plecoptera). Freshwater Biology 17: 565–568. https://doi.org/10.1111/j.1365-2427.1987.tb01077.x

Geoffroy EL (1762) Histoire abrégée des insectes qui se trouvent aux environs de Paris; dans laquelle ces animaux sont rangés suivant un órdre méthodique, Vol. 2. Durand, Paris, 690 pp. https://doi.org/10.5962/bhl.title.154842

Hynes HBN (1974) Observations on the adults and eggs of Australian Plecoptera. Australian Journal of Zoology, Supplement 29: 37–52.

Hynes HBN (1976) Biology of Plecoptera. Annual Review of Entomology 21(1): 135–153. https://doi.org/10.1146/annurev.en.21.010176.001031

Illies J (1960) Archiperlaria, eine neue Unterordnung der Plecopteren. Beiträge zur Entomologie 10(7–8): 661–697.

Illies J (1969) Revision der Plecopteren familie Austroperlidae. Entomologisk Tidskrift 90(1–2): 19–51.

Jewett SG (1959) The Stoneflies (Plecoptera) of the Pacific Northwest. Oregon State College, Corvallis, 95 pp.

Jin YH, Bae YJ (2005) The wingless stonefly family Scopuridae (Plecoptera) in Korea. Aquatic Insects 27(1): 21–34. https://doi.org/10.1080/01650420400021417

Kania I, Wang B, Szwedo J (2015) Dicranoptycha Osten Sacken, 1860 (Diptera, Limoniidae) from the earliest Cenomanian Burmese amber. Cretaceous Research 52: 522–530. https://doi.org/10.1016/j.cretres.2014.03.002

Linnaeus C (1758) Systema natura per regna tria naturae secundum classes, ordines, genera, species, cum characteribus, differentiis, synonymis, locis, 10th edn., Vol. 1. Laurentii Salvii, Holmiae, 824 pp. https://doi.org/10.5962/bhl.title.542

Latreille PA (1802) Histoire naturelle, générale et particulière des crustacés et des insectes: ouvrage faisant suite aux oeuvres de Leclerc de Buffon, et partie du cours complet d'histoire naturelle rédigé 3. De L'imprimerie de Crapelet, Paris, 467 pp. https://doi.org/10.5962/bhl.title.15764

Liu YS, Ren D (2006) Progress in the study of Plecoptera fossils. Acta Zootaxonomica Sinica 31(4): 758–768.

McLellan ID (1977) New alpine and southern Plecoptera from New Zealand, and a new classification of the Gripopterygidae. New Zealand Journal of Zoology 4(2): 119–147. https://doi.org/10.1080/03014223.1977.9517945

McLellan ID (2001) A revision of South American Austroperlidae (Plecoptera). Aquatic Insects 23(3): 233–251. https://doi.org/10.1076/aqin.23.3.233.4891

McLellan ID, Zwick P (2018) New species of and keys to South American Gripopterygidae (Plecoptera). Illiesia 3(4): 20–42.

Mtow S, Machida R (2018) Egg structure and embryonic development of arctoperlarian stoneflies: a comparative embryo-logical study (Plecoptera). Arthropod Systematics & Phylogeny 76(1): 65–86.

Mtow S, Smith BJ, Machida R (2021) Egg structure of five antarctoperlarian stoneflies (Insecta: Plecoptera, Antarctoperlaria). Arthropod Structure & Development 60: 101011. https://doi.org/10.1016/j.asd.2020.101011

Nelson CH (1988) Note on the phylogenetic systematics of the family Pteronarcyidae (Plecoptera), with a description of the eggs and nymphs of the Asian species. Annals of the Entomological Society of America 81(4): 560–576. https://doi.org/10.1093/aesa/81.4.560

Nelson CH (2009) Surface ultrastructure and evolution of tarsal attachment structures in Plecoptera (Arthropoda: Hexapoda). Aquatic Insects 31(sup1): 523–545. https://doi.org/10.1080/01650420802598210

Retzius AJ (1783) Caroli Lib. Bar. De Geer, genera et species insectorum e generosissimi auctoris scriptis extaxit, digessit, latine quoad partem reddidit, et terminologiam insectorum Linneanam addidit. Siegfried Lebrecht Crusium, Lipsiae, 220 pp.

Riek EF (1973) The genera of Australian Austroperlidae (Insecta: Plecoptera). Australian Journal of Entomology 12(4): 289–295. https://doi.org/10.1111/j.1440-6055.1973.tb01675.x

Stark BP, Lentz DL (1992) *Dominiperla antigua* (Plecoptera: Perlidae), the first stonefly from Dominican amber. Journal of the Kansas Entomological Society 65(1): 93–96.

Stark BP, Szczytko SW (1984) Egg morphology and classification of Perlodinae (Plecoptera: Perlodidae). Annales de Limnologie 20(1–2): 99–103. https://doi.org/10.1051/limn/1984029

Smith CC, Fretwell SD (1974) The optimal balance between size and number of offspring. The American Naturalist 108(962): 499–506. https://doi.org/10.1086/282929

South EJ, Skinner RK, DeWalt RE, Davis MA, Johnson KP, Teslenko VA, Lee JJ, Malison RL, Hwang JM, Bae YJ, Myers LW (2021) A new family of stoneflies (Insecta: Plecoptera), Kathroperlidae, fam. n., with a phylogenomic analysis of the Paraperlinae (Plecoptera: Chloroperlidae). Insect Systematics and Diversity 5(4): 1–27. https://doi.org/10.1093/isd/ixab014

Shi G, Grimaldi DA, Harlow GE, Wang J, Wang J, Wang M, Lei W, Li Q, Li X (2012) Age constraint on Burmese amber based on U-Pb dating of zircons. Cretaceous Research 37: 155–163. https://doi.org/10.1016/j.cretres.2012.03.014

Stewart KW (2009) Plecoptera: stoneflies. In: Resh VH, Cardé RT (Eds) Encyclopedia of Insects. Academic Press, San Diego, 810–813. https://doi.org/10.1016/B978-0-12-374144-8.00214-9

Stewart KW, Stark BP (2008) Plecoptera. In: Merritt RW, Cummins KW, Berg MB (Eds) An introduction to the aquatic insects of North America, 4th edn. Kendall/Hunt Publishing Company, Dubuque, 311–384.

Sinitshenkova ND (1987) Istopicheskoe razvitie vesiyanok. Akademiya Nauk SSSR. Trudy Paleontologicheskogo Instituta 221: 1–142.

Sinitshenkova ND (2013) A new stonefly assemblage (Insecta: Perlida = Plecoptera) from the Upper Permian deposits of northern European Russia. Paleontological Journal 47: 766–782. https://doi.org/10.1134/S0031030113020135

Sroka P, Staniczek AH, Kondratieff BC (2018) 'Rolling' stoneflies (Insecta: Plecoptera) from mid-Cretaceous Burmese amber. PeerJ 6: e5354. https://doi.org/10.7717/peerj.5354

Szczytko SW, Kondratieff BC (2015a) Photographic atlas of the eastern Nearctic Isoperlinae (Plecoptera: Perlodidae) species. Monographs of Illiesia 2: 1–124.

Szczytko SW, Kondratieff BC (2015b) A review of the Eastern Nearctic Isoperlinae (Plecoptera: Perlodidae) with the description of twenty-two new species. Monographs of Illiesia 1: 1–289.

Terry MD, Whiting MF (2005) Mantophasmatodea and phylogeny of the lower neopterous insects. Cladistics 21: 240–257. https://doi.org/10.1111/j.1096-0031.2005.00062.x

Uchida S, Isobe Y (1989) Styloperlidae, stat. nov. and Microperlinae, subfam. nov. with a revised system of the family group Systellognatha (Plecoptera). Spixiana 12(2): 145–182.

Yu T, Kelly R, Mu L, Ross A, Kennedy J, Broly P, Xia F, Zhang H, Wang B, Dilcher D (2019) An ammonite trapped in Burmese amber. Proceedings of the National Academy of Sciences of the United States of America 116: 11345–11350. https://doi.org/10.1073/pnas.1821292116

Zwick P (1973) Insecta: Plecoptera. Phylogenetisches system und katalog. Das Tierreich 94: 1–465.

Zwick P (1979) Revision of the stonefly family Eustheniidae (Plecoptera), with emphasis on the fauna of the Australian region. Aquatic Insects 1(1): 17–50. https://doi.org/10.1080/01650427909360975

Zwick P (2000) Phylogenetic system and zoogeography of the Plecoptera. Annual Review of Entomology 45: 709–746. https://doi.org/10.1146/annurev.ento.45.1.709

Zwick P (2006) New family characters of larval Plecoptera, with an analysis of the Chloroperlidae: Paraperlinae. Aquatic Insects 28(1): 13–22. https://doi.org/10.1080/01650420500400552

Zwick P, Surenkhorloo P (2005) The Mongolian species of Isoperlinae (Plecoptera: Perlodidae). Acta Zoologica Academiae Scientiarum Hungaricae 51(3): 253–276.

Fossil Record 25 (1) 2022, 83–98 | DOI 10.3897/fr.25.83081

Fossil assemblage from the Khok Pha Suam locality of northeastern, Thailand: an overview of vertebrate diversity from the Early Cretaceous Khok Kruat Formation (Aptian-Albian)

Sita Manitkoon[1,2], Uthumporn Deesri[1,2], Komsorn Lauprasert[2], Prapasiri Warapeang[1,2], Thanit Nonsrirach[1,2], Apirut Nilpanapan[2], Kamonlak Wongko[3], Phornphen Chanthasit[4]

1 *Palaeontological Research and Education Centre, Mahasarakham University, Khamriang, Maha Sarakham, 44150, Thailand*
2 *Faculty of Science, Mahasarakham University, Khamriang, Maha Sarakham, 44150, Thailand*
3 *Mineral Resources Office Region 1, Department of Mineral Resources, 414 moo 3, Sala, Ko Kha, Lampang, 52130, Thailand*
4 *Sirindhorn Museum, Department of Mineral Resources, Sahatsakhan, Kalasin, 46140, Thailand*

http://zoobank.org/F338D097-44EC-48FC-96E1-B1A295CA3FDA

Corresponding author: Sita Manitkoon (sita.m@msu.ac.th)

Academic editor: Johannes Müller ♦ **Received** 22 August 2021 ♦ **Accepted** 4 March 2022 ♦ **Published** 23 March 2022

Abstract

The Khok Pha Suam locality in the province of Ubon Ratchathani, northeastern, Thailand, is known as “the last home of Thai dinosaurs”, because it belongs to the Lower Cretaceous Khok Kruat Formation (Aptian-Albian) which is currently the youngest Mesozoic vertebrate fossil producing formation in the Khorat Group. Here, we describe a diverse vertebrate assemblage, including hybodonts, ray-finned fishes, turtles, crocodyliforms, pterosaurs, and dinosaurs from the Khok Pha Suam locality. The updated data on the Khok Kruat fauna provides a better understanding of the variety and distribution of Early Cretaceous continental ecosystems, which are useful for palaeoenvironmental reconstruction. In addition to consolidating unincorporated data on fauna, this study also provides the palaeontological data necessary to illustrate the palaeoecosystem to the general public, as well as improving the academic value of the Pha Chan-Sam Phan Bok Geopark.

Key Words

Aptian-Albian, Khorat Group, Lower Cretaceous, Pha Chan-Sam Phan Bok Geopark, Vertebrates

1. Introduction

The Mesozoic Khorat Group is composed of non-marine sedimentary rocks ranging from the Upper Jurassic to Lower Cretaceous in northeastern Thailand. Three of the formations (Phu Kradung, Sao Khua, and Khok Kruat) have yielded rich vertebrate remains including selachians, actinopterygians, sarcopterygians, temnospondyl amphibians, turtles, crocodyliformes, pterosaurs, non-avian dinosaurs, and birds (Fig. 1) (Buffetaut and Suteethorn 1998; Buffetaut et al. 2003b, 2005, 2006). The Khok Kruat Formation is the youngest Mesozoic vertebrate-bearing formation of Thailand (Buffetaut et al. 2005) named after the Ban Khok Kruat locality in Nakhon Ratchasima Province (commonly known as Khorat Province). The Khok Kruat Formation also crops out in several other areas of northeast Thailand notably in Kalasin, Nakhon Phanom, Khon Kaen, Chaiyaphum, and Ubon Ratchathani Provinces (Buffetaut and Suteethorn 1992; Buffetaut et al. 2005; Shibata et al. 2015; Wongko et al. 2019) The Khok Kruat Formation is well-distributed in the outer rims of the Phu Phan mountain range and separated from the overlying Maha Sarakham Formation by an unconformity forming a sharp contact with basal anhydrite (Sattayarak et al. 1991; Racey et al. 1996; Jin-Geng and Meesook 2013). The Khok Kruat Formation consists mainly of reddish brown, fine- to medium-grained sandstones with minor siltstones, mudstones and conglomerates (Jin-Geng and Meesook

2013). The Khok Kruat Formation is considered the lateral equivalent to the Grès Supérieurs Formation of southern Laos. Both are considered as Aptian-Albian in age based on their vertebrate assemblages, bivalves, and palynomorphs (Cappetta et al. 1990; Buffetaut et al. 2005; Racey 2009; Allain et al. 2012). In contrast to the Barremian Sao Khua Formation, which contains no evidence of ornithischians, three taxa of hadrosauroid iguanodontians and a basal ceratopsian have been described from the Khok Kruat Formation (Buffetaut et al. 2005; Shibata et al. 2015).

Khok Pha Suam is part of the Pha Chan-Sam Phan Bok Geopark. It is the third national geopark that has been created after the Satun Global Geopark (Satun Province) and the Khorat Geopark (Nakhon Ratchasima Province). This geopark has many outstanding geological sites and contains three main spots: ‘land of the last Thai dinosaurs’ in the Khok Pha Suam locality; unique natural places such as Pha Chan (high cliffs above the Mekong River), the Sam Pan Bok (known as the ‘Grand Canyon of Thailand’, which consists of extensive bedrock with many potholes outcropping in the Mekong River), Pha Taem (ancient cliff paintings in the Pha Taem National Park); and the two-color river viewpoint where the blue water of the Mun River mixes with the brown water of the Mekong River (Singtuen and Won-in 2019; Department of Mineral Resources 2021). The creation of a geopark will help to promote trade investment and tourism, improve the quality of its inhabitants, strengthen communities, and contribute substantially to both geoconservation and geotourism by promoting a new type of tourism in Thailand (Singtuen and Won-in 2019). This study summarises the palaeontological data that illustrates to the general public what Khok Pha Suam looked like a hundred million years ago, and will also improve the academic interest of the geopark.

2. Institutional abbreviations

PRC	Palaeontological Research and Education Centre, Mahasarakham University, Thailand;
SM	Sirindhorn Museum, Kalasin Province, Thailand.

3. Geological settings and palaeoenvironment

Khok Pha Suam is located in the Na Kham Subdistrict, Si Muang Mai District, Ubon Ratchathani Province. The outcrop was discovered in 1993 by villagers near the forested area maintained by the Na Kham Subdistrict Administrative Organization. The site has been extensively eroded by water into a badlands-type landscape (Cappetta et al. 2006).

The thickness of the lithostratigraphic section is about 4 meters (Fig. 2c). The exposed deposits are composed of siltstone and very fine sandstone with some carbonate

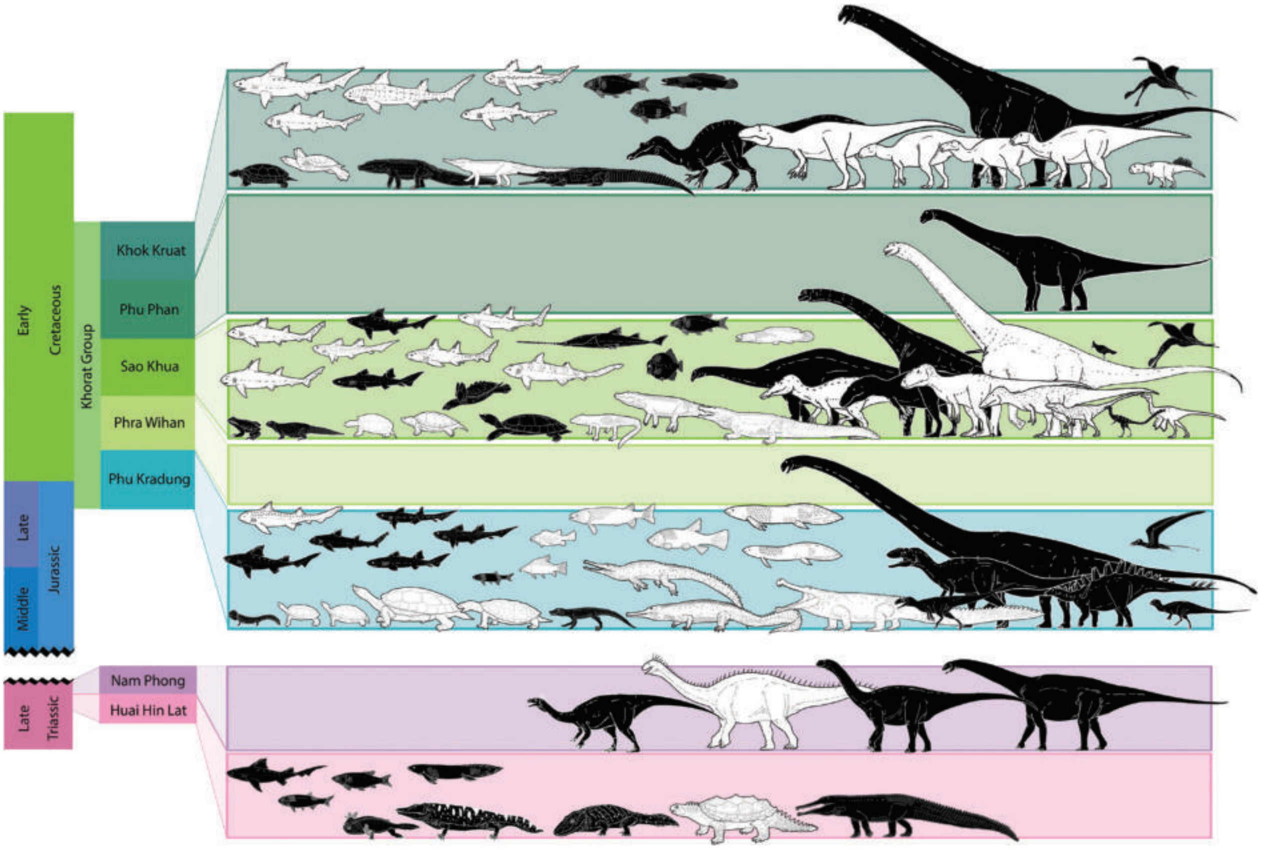

Figure 1. Mesozoic vertebrate fauna from the Indochina Terrane of NE Thailand, species-level identified taxa shown in white silhouettes, tentatively identified taxa in black silhouettes, further details in Suppl. material 1 (Modified from Lionel Cavin: All not to scale).

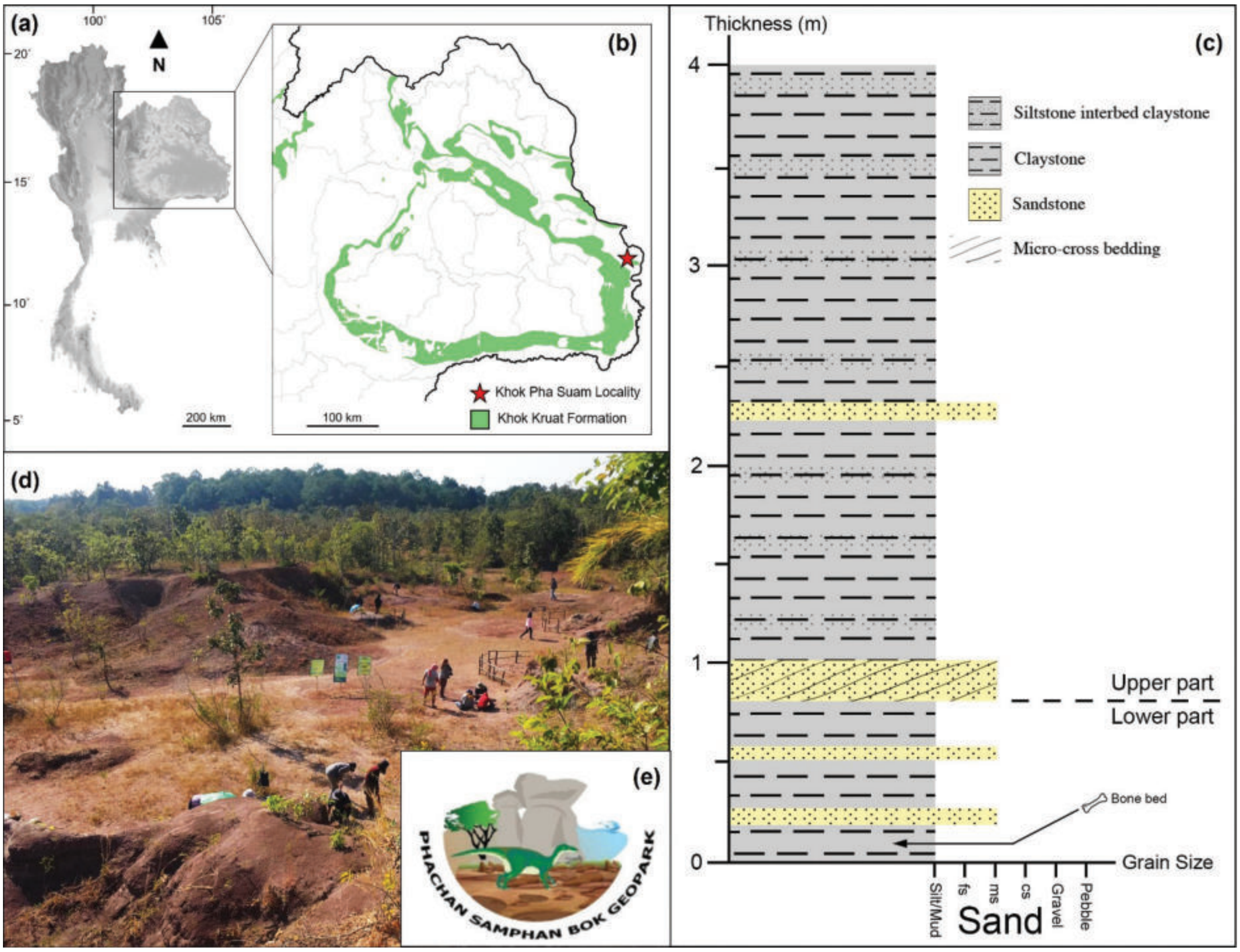

Figure 2. Locality map and Lithostratigraphic section of Khok Pha Suam locality. **a.** Map of Thailand, showing the location of the Khorat Plateau; **b.** Distribution of the Khok Kruat Formation in northeastern Thailand (green color; modified from DMR, 2004), location of Khok Pha Suam locality (red star); **c.** Stratigraphic column of Khok Pha Suam, d, a photograph of the excavation site; **e.** Logo of The Pha Chan-Sam Phan Bok Geopark.

caliche pebble conglomerates. The fining-upward sequence is pale red to grayish-red and reddish brown. The dip of the strata is 10/135 to the south-east. The lower part is 1 meter thick and consists of reddish brown very thin to thin bedded claystone grading up to thin bedded siltstone interbedded with fine-grained sandstone. The fragile vertebrate remains are found on the eroded surface of this layer which can be collected directly. The upper part is 3 meters thick and consists of reddish-brown, thin-to medium bedded, medium-grained sandstones interbedded siltstones, claystones. A calcrete horizon (palaeosol) has been found at the top of the succession (Wongko 2018; Wongko et al. 2019).

The bonebed presents lithostratigraphic and sedimentary structures composed of fining-upward sequences, carbonate caliche horizon, micro cross-bedding, load-cast and rip-up clasts, micaceous fine sand and silt which also form scattered thin lenticular beds and laminated carbonaceous shale in the sequences. These features indicate low-energy current, floodplain deposits. Fossil remains consist of isolated or fragmentary elements indicating transport under high energy conditions and deposition on floodplains. It could correspond to an arid or semi-arid subtropical climate, as indicated by the caliche pebble conglomerate (Fig. 6) (Wongko 2018; Wongko et al. 2019).

4. Material

The specimens were collected from Khok Pha Suam locality, Na Kham Subdistrict, Si Muang Mai District, Ubon Ratchathani Province (Fig. 2) and are now housed in the collections of the Palaeontological Research and Education Centre, Mahasarakham University and Sirindhorn Museum. This work includes a review of published specimens and new records from recent discoveries.

5. Vertebrate palaeontology

The vertebrates found at the Khok Pha Suam locality comprise five taxa of hybodont sharks, at least two taxa of ginglymodians, a sinamiid fish, carettochelyid and adocid turtles, neosuchian crocodyliforms, pterosaurs, dinosaurs (iguanodontians, sauropods, and at least two taxa of theropods). The faunal diversity described in this article together with additional data from other localities allows us to propose a preliminary reconstruction of the Early Cretaceous Khok Kruat Formation ecosystem (Fig. 6).

5.1 Selachians

Class Chondrichthyes Huxley, 1880
Euselachii Hay, 1902
Hybodontiformes Patterson, 1966
Family Thaiodontidae Cuny, Suteethorn, Khamha & Buffetaut, 2008
***Thaiodus ruchae* Cappetta, Buffetaut, & Suteethorn, 1990 (Fig. 3a)**

T. ruchae possesses asymmetric teeth with an occlusal crest displaced lingually. Its serrated teeth are strongly interlocked, which usually indicates preference in hunting large prey and possibly occasional scavenging via the ability to cut tough meat (Cuny et al. 2008). *T. ruchae* is also found in the Ban Sam Ran locality (Khon Kaen Province), Lam Pao Dam (Kalasin Province), Ban Khok Kruat and Ban Sapan Hin localities (Nakhon Ratchasima Province) (Cuny et al. 2007, 2008; Wongko 2018).

***Khoratodus foreyi* Cuny, Suteethorn, Khamha & Buffetaut, 2008 (Fig. 3b)**

K. foreyi teeth are very elongated, flattened, and rod shaped. *Thaiodus* and *Khoratodus* teeth show common features in addition to their asymmetry, such as the ornamentation restricted to the upper half of the crown and they also show a common vascularization pattern of the root and an interlocking system between the teeth which is unusual among hybodonts. These genera are included in the family Thaiodontidae, which appear to be restricted to Asia (Cuny et al. 2008).

“*Hybodus*” *aequitridentatus* Cuny, Suteethorn, Khamha, and Buffetaut., 2008 (Fig. 3c)

“*H.*” *aequitridentatus* teeth are probably adapted towards an opportunistic feeding method, but the low and blunt cusps indicate some specialization towards hard-shelled preys (Cuny et al. 2008). Based on new material found in the Xinlong Formation (Guangxi Province, southern China), Cuny et al. (2017) proposed that this species does not belong to the genus *Hybodus* but to a new genus of the family Thaiodontidae.

Family incertae sedis
***Heteroptychodus steinmanni* Yabe & Obata, 1930 (Fig. 3d)**

H. steinmanni is quite abundant at Khok Pha Suam. Its teeth are typically broad, with a low crown densely and are strongly ornamented, which indicates specialization towards a durophagous diet (Cuny et al. 2008). *H. steinmanni* occur also in other Khok Kruat Formation outcrops including Ban Sam Ran, Wat Wang Sai (Khon Kaen Province), Lam Pao Dam, and Ban Sapan Hin (Cuny et al. 2007, 2008; Wongko 2018). Moreover, A single tooth of *Heteroptychodus* sp. was discovered in Ban Pha Nang Sua (Chaiyaphum Province) (Department of Mineral Resources Division of Fossil Protection 2016).

Besides the Khok Kruat Formation, *H. steinmanni* was also discovered from various localities of the Sao Khua Formation (Cuny et al. 2007). Another species, *H. kokutensis* have been reported from Ko Kut, Trat Province, which is likely correlated with the Sao Khua Formation (Cuny et al. 2010). *Heteroptychodus* sp. have been reported from the Phu Kradung Formation in Chong Chat, Nong Bua Lamphu Province, and Kham Phok, Mukdahan Province (Cuny et al. 2007).

Family incertae sedis
***Acrorhizodus khoratensis* Cappetta, Buffetaut, Cuny & Suteethorn, 2006 (Fig. 3e)**

A. khoratensis teeth possess a high root with a U-shaped longitudinal crest, except in the posterior teeth. The crown is broadly rectangular in apical view. A blunt cusp is also observed on the labial side that is almost as wide as the crown. The tooth morphology indicates adaptations towards various food source, in a way probably similar to *H. aequitridentatus* (Cuny et al. 2008).

5.2. Actinopterygians

Isolated remains of actinopterygians (ray-finned fishes) preserved in the Khok Pha Suam locality usually consist of vertebral centra, fragments of skull bones, fragments of jaws, isolated teeth, and numerous scales.

Holostei Müller, 1844 sensu Grande, 2010
Ginglymodi Cope, 1872 sensu Grande, 2010
Lepisosteiformes Hay, 1929 sensu López-Arbarello, 2012
Family incertae sedis (Fig. 3f–g)

Two taxa of ginglymodians can be separated by the ornamentation of their ganoid scales (Cavin et al. 2009). Ginglymodi type I (Fig. 3f) is represented by scales with a smooth surface whereas Ginglymodi type II (Fig. 3g) possess slightly larger scales with parallel ridges on the surface.

***Lanxangichthys* sp. Cavin, Deesri, Veran, Khentavong, Jintasakul, Chanthasit & Allain, 2018**

So far, only one genus of ginglymodian, *Lanxangichthys*, has been identified on the basis of fossil material from the Khok Kruat Formation and from the Grès supérieurs Formation in Laos. Isolated skull remains from Ban Sapan Hin and Khok Pha Suam localities present strong

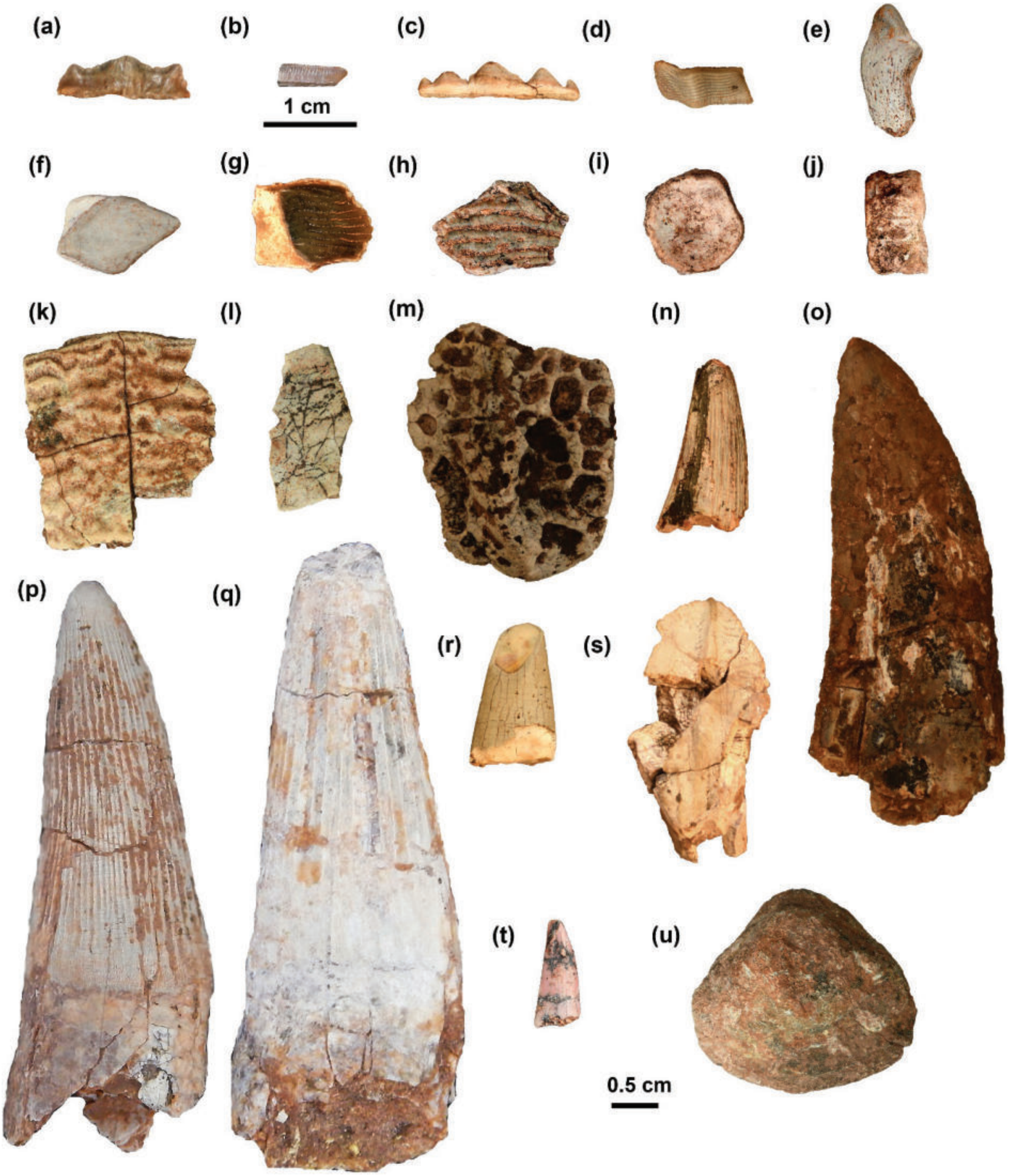

Figure 3. Isolated microremains from Khok Pha Suam locality. *Thaiodus ruchae* tooth (**a.** PRCMR301) in labial view, *Khoratodus foreyi* tooth (**b.** PRCMR302) in lingual view, "*Hybodus*" *aequitridentatus* tooth (**c.** PRCMR303) in labial view, *Heteroptychodus steinmanni* tooth (**d.** PRCMR304) in apical view, *Acrorhizodus khoratensis* tooth (**e.** PRCMR305) in mesio-lingual or disto-lingual view, ginglymodian external side scales with ganoin, uncovered field and bone on the anterior margin (**f–g.** PRCMR305-306) in dorsal view, ginglymodian external side of the dermal bone (**h.** PRCMR307) in dorsal view, sinamiid centrum (**i–j.** PRCMR308) in anterior (**i.**) and dorsal (**j.**) views, carettochelyid shell fragment (**k.** PRCMR309) in dorsal view, adocid shell fragment (**l.** PRCMR310) in ventral view, neosuchian osteoderm (**m.** PRCMR311) in dorsal view, neosuchian tooth (**n.** PRCMR312) in lingual view, theropod tooth (**o.** SM2016-1-155), spinosaurid tooth morphotype I (**p.** PM2016-1-003) in anterior view, spinosaurid tooth morphotype II (**q.** PM2016-1-006) in anterior view, sauropod tooth (**r.** PRCMR315) in lingual view, iguanodontian tooth (**s.** SM2021-1-121), pterosaur tooth (**t.** PRCMR317), and bivalve mold right valve of articulated shell (**u.** PRCMR318) in external view. Scale bars: 0.5 cm (**a, c–s**); 1 cm (**b**).

ornamentation of ganoin forming radiating and tuberculate patterns similar to the ornamentation of non-weathered bones of a single articulated skull of the holotype of *L. alticephalus* from the Savannakhet Basin in Laos. As the Grès supérieurs Formation from the Savannakhet Basin are regarded as an equivalent to the Khok Kruat Formation, the isolated ornamented cranial remains from Khok Kruat Formation are referred, with caution, to *Lanxangichthys* sp. (Cavin et al. 2018). In regard to the body shape of *Lanxangichthys*, the scales type II from the Khok Pha Suam locality probably belongs to the genus *Lanxangichthys* as the scale itself are deep.

Amiiformes sensu Grande & Bemis, 1998
Halecomorphi Cope, 1872
Family Sinamiidae Berg, 1940
cf. *Siamamia* Cavin, Suteethorn, Buffetaut, Claude, Cuny, Le Loeuff & Tong, 2007 (Fig. 3i–j)

Vertebral centra are referred to a sinamiid together with fragments of dentaries, a premaxilla, possible fragments of maxillae and many scale types from the Khok Pha Suam locality. The material shows similarities with *Siamamia naga* from the older Sao Khua Formation (Cavin et al. 2009; Deesri et al. 2017). For instance, the scales are much smaller and thinner than those of the two different ginglymodian scales whereas the isolated fragment of jaws are obviously similar in each. In 2018, another sinamiid specimen was discovered during a Thai-Japan joint excavation in the Ban Krok Duean Ha locality, Nakhon Ratchasima province. This sub-complete and articulated specimen is significantly different from *S. naga*, and possibly represents a new species or even a new genus (Deesri et al. 2021).

5.3. Turtles

Testudines Cope, 1868
Cryptodira Cope, 1868
Trionychoidae Fitzinger, 1826 sensu Gaffney & Meylan, 1988
Family Adocidae Cope, 1870 (Fig. 3k)
Family Carettochelyidae Boulenger, 1887 (Fig. 3l)

Two different families of trionychoids have been collected from the Khok Pha Suam locality, each identified by the ornamentation pattern of their shell fragments: the carettochelyid fragment is covered with strong ornamentation (Fig. 3k), while the adocid fragment is covered with tiny pits (Fig. 3l). Although turtle remains are quite abundant in Khok Pha Suam, they are too fragmentary for in-depth identification. Two genera of trionychoids have been reported from the Khok Kruat Formation, the carettochelyid *Kizylkumemys khoratensis* from Ban Sapan Hin (Nakhon Ratchasima), and the adocids *Shachemys laosiana* from the Grès Supérieurs Formation of southern Laos and *Shachemys* sp. from Ban Sapan Hin (Tong et al. 2005, 2009).

5.4. Crocodyliforms

Crocodylomorpha Walker, 1970
Crocodyliformes Hay, 1929
Neosuchia Benton & Clark, 1988
Family incertae sedis (Fig. 3m–n)

Osteoderms (Fig. 3m) and teeth (Fig. 3n) of neosuchian crocodyliforms have been collected on the outcrop surface and are rather poorly preserved. The teeth sample can be divided into four morphotypes: morphotype I is robust, high and conical; morphotype II is slender and conical; morphotype III is roughly triangular; morphotype IV is relatively short and robust (Lauprasert 2006).

Family Goniopholididae Cope, 1875 (Fig. 4)

A nearly complete left mandible of goniopholidid (SM2021-1-112: Fig. 4), 327 mm in length, consists of a dentary, splenial, surangular and angular. The anterior extremity to the second alveolus of the specimen is lacking. The dentary is elongated and about 285 mm in length. In dorsal view, 23 dentary alveoli, the second to the 24th ones, can be counted. The dentary alveoli are separated by equal interalveolar septum 2 mm long, except between the second and the third, the fourth and the fifth ones, which show slightly wider spaces of about 5 mm. The ventral surface of the specimen is strongly convex transversally. Above this convexity, the base of the root of the second dentary tooth is observed *in situ*, below the level of the third dentary alveolus. The preserved tooth is slightly curved lingually and has an oval cross-section. In dorsal view, the lateral margin of the specimen exhibits three convexities. The first convexity is situated at the level of the fourth dentary alveolus, suggesting the position of the largest tooth on the dentary. The second convexity reaches its maximum at the level of the 16th dentary alveolus while the third convexity is located at the level of the anterodorsal extremity of the surangular. The dentary floor is partly preserved at the medial margin of the fourth to the sixth dentary alveoli. Because the splenial is crushed and distorted, a part of its medial surface is visible in dorsal view only from the sixth to the 17th dentary alveoli. A row of vascular foramina is visible in the medial margin of the tooth row, each about 1–2 mm in diameter. Posteriorly, the 18th to the 24th dentary alveoli are worn but parts of their labial edges remain partially intact. In lateral view, the dorsal margin of the specimen presents two convexities. The first convexity rises to the level of the third and fourth dentary alveoli. The dorsal margin becomes strongly concave and reaches its maximum concavity at the level of the 10th and 11th dentary alveoli. The second convexity reaches the maximum curvature at the level of the 18th dentary alveolus. These convexities are about twice as high as the maximum of the concavity.

This left mandible of SM2021-1-112 cannot be compared with the slender-snouted neosuchian crocodyliform *Khoratosuchus jintasakuli* (Lauprasert et al. 2009), from the Khok Kruat Formation of Nakhon Ratchasima, which is only known by a partial skull without mandible.

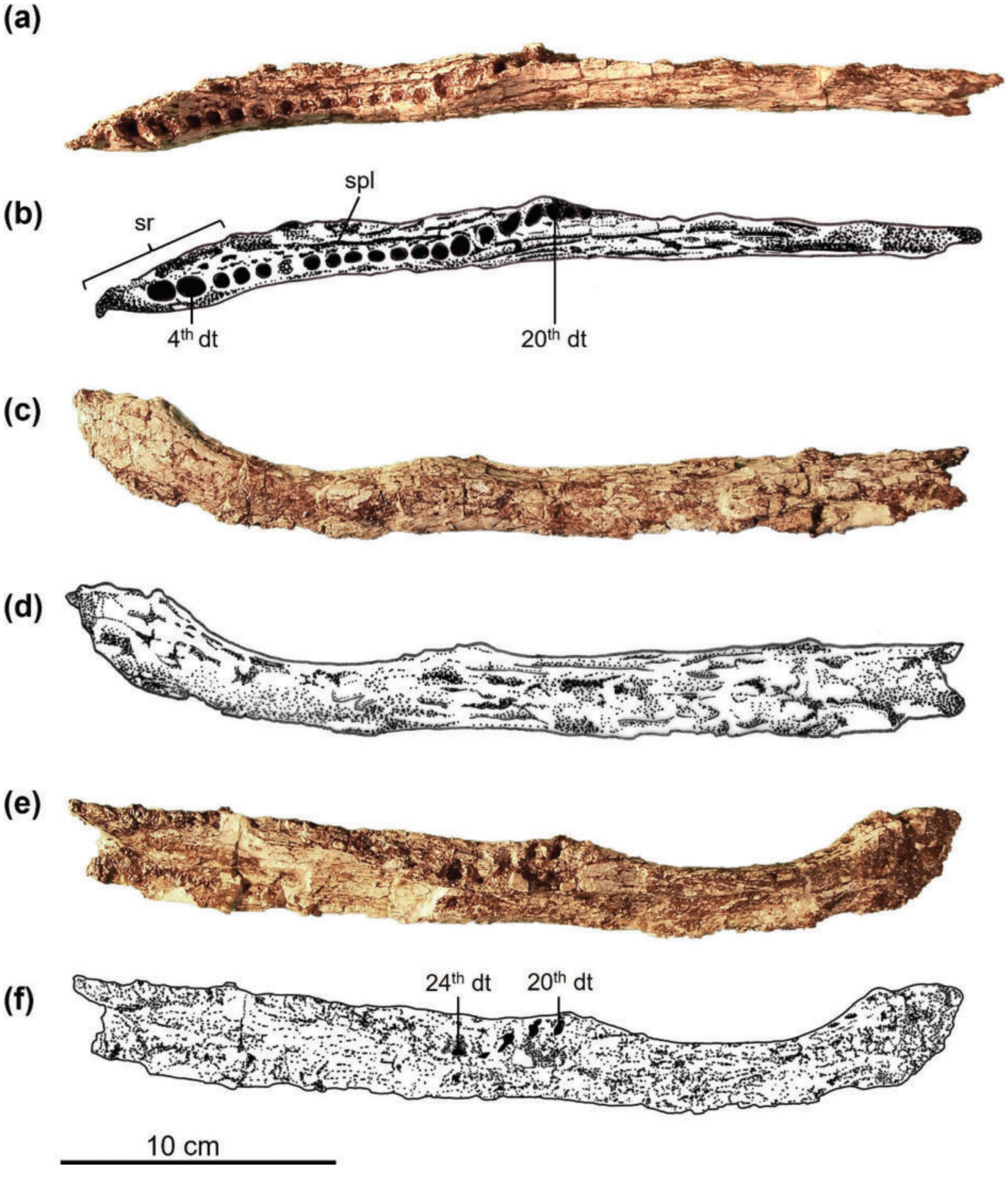

Figure 4. Photos and drawing of a nearly complete left mandible of Goniopholididae indet. from Khok Pha Suam (SM2021-1-112) in dorsal (**a, b**), lateral (**c, d**) and lingual (**e, f**) views. Abbreviation: dt, dentary tooth; spl, splenial; sr, symphyseal region.

However, the presence of a short dentary symphysis and the number of preserved dentary teeth indicate that SM2021-1-112 is also a short-snouted crocodyliform. Moreover, the presence of the enlarged and contiguous third and fourth dentary alveoli reinforces the idea that SM2021-1-112 belongs to the family Goniopholididae (Buffetaut and Ingavat 1983). It is quite difficult to distinguish the goniopholidid genera from only a part of the lower jaw. Short-snouted crocodyliforms have been reported from the older Sao Khua Formation, including "*Goniopholis*" *phuwiangensis* (Buffetaut and Ingavat 1983), which cannot be confidently attributed to the genus *Goniopholis* (Lauprasert 2006; Andrade et al. 2011) and *Siamosuchus phuphokensis* (Lauprasert et al. 2007). The latter taxon is known only from a upper jaw and postcranial material. However, more material is needed in order to confirm the exact taxonomic status of SM2021-1-112.

On the contrary, SM2021-1-112 shows a combination of characters on the dentary that have been described in "*G.*" *phuwiangensis*, which are: 1) anterior portion of the tooth row with no marked angulation; 2) absence of a strong outward protrusion of the lateral margin at the level of the third and the fourth dentary alveoli and 3) presence of dentary curvatures in both lateral and vertical planes. However, based on the strong undulation of its lateral margin on a vertical plane, SM2021-1-112 can be distinguished from "*G.*" *phuwiangensis*. The first and the second convexities of SM2021-1-112 are about twice as high as its concavity, whereas in "*G.*" *phuwiangensis*, the proportion between the maximum height of convexity and concavity is significantly less than that of SM2021-1-112. Additionally, the ornamentation on the lateral surface of SM2021-1-112 is faintly sculptured whereas that of "*G.*" *phuwiangensis* is heavily sculptured. These two characters, therefore, are sufficient to validate SM2021-1-112 as a species different from "*G.*" *phuwiangensis*.

Based on the obscured relationships of the Thai, European and North American *Goniopholis* as well as the absence of the lower jaw of *Siamosuchus*, it should be suitable for the time being to consider SM2021-1-112 as an uncertain genus in the family Goniopholididae until further studies can accurately evaluate the internal relationships of Thai goniopholidids.

5.5. Sauropods

Dinosauria Owen, 1842
Saurischia Seeley, 1888
Sauropoda Marsh, 1878
Neosauropoda Bonaparte, 1986
Macronaria Wilson & Sereno, 1998 (Fig. 3r)

Sauropod remains are rare in Khok Pha Suam. A small femur approximately 40 cm in length of a probable juvenile sauropod is an exhibit at the local museum under the supervision of Na Kham Subdistrict Administrative Organization. Some isolated teeth have been found but are very fragile. A peg-shaped tooth (PRCMR315, Fig. 3r), missing half its proximal portion shows a nearly cylindrical crown and symmetrical D-shaped cross-section and possesses an apical wear facet on the lingual side, suggesting that it is an upper tooth based on comparisons with *Nemegtosaurus mongoliensis* (Wilson 2005). The ridges on both the mesial and distal edges are notable. The tooth is lingually curved with a smooth grey enamel on the crown surface except for the wear facet. Thai sauropod teeth can be divided into two morphotypes; spoon-shaped teeth were discovered from the Late Jurassic Phu Kradung Formation and the Early Cretaceous Sao Khua Formation whereas peg-shaped teeth were discovered from the Sao Khua and Khok Kruat Formations. Peg-shaped sauropod dentition tend to be associated with Diplodocoidea and Titanosauriformes (Macronaria) (Upchurch 1995, 1998; Wilson and Sereno 1998). The Khok Pha Suam teeth are reminiscent of *Phuwiangosaurus sirindhornae*, a basal titanosauriform from the Sao Khua Formation (Buffetaut et al. 2005; Suteethorn et al. 2009).

5.6. Theropods

Theropoda Marsh, 1881
Superfamily Allosauroidea Marsh, 1878 (Fig. 3o)

Several teeth of theropod dinosaurs differing in size have been collected and can be divided into Allosauroidea and Spinosauridae. The allosauroid teeth (Fig. 3o) resembles the Khok Kruat basal carcharodontosaurian *Siamraptor suwati* (Chokchaloemwong et al. 2019). Teeth are ziphodont (blade-shaped and serrated) with subquadrangular denticles (serration) on both margins, lenticular shaped in crown cross-section, and with arcuate enamel wrinkles that extend across the labial and lingual margins, which is a feature shared with other members of Allosauroidea (Brusatte et al. 2007; Hendrickx et al. 2015).

Family Spinosauridae Stromer, 1915 (Fig. 3p–q)

Spinosaurid teeth exhibit conical crown and extremely reduced serrations, a morphology reminiscent of crocodilian teeth. The teeth of Khok Kruat spinosaurids can be categorized into two sub-morphotypes (Wongko et al. 2019), both found in the Khok Pha Suam locality. Sub-morphotype I (Fig. 3p) presents a smooth enamel surface of the crown and possesses more than 20 fine ridges on each side. Sub-morphotype II (Fig. 3q) shows a wrinkled enamel surface of the crown and no more than 16 coarse ridges on each side, which is similar to *Siamosaurus suteethorni* from the Sao Khua Formation.

The spinosaurid *Ichthyovenator laosensis* (Allain et al. 2012) has been described from Laos on the basis of skeletal remains, and post-cranial elements of an indeterminate spinosaurid have been reported from Ban Sam Ran (Buffetaut et al. 2005), but no bones of spinosaurid have been found so far in the locality of Khok Pha Suam.

5.7. Iguanodontians

Onithischia Seeley, 1888
Neornithischia Cooper, 1985
Ornithopoda Marsh, 1881
Iguanodontia Dollo, 1888 (Fig. 3s and Fig. 5)

Teeth of iguanodontian dinosaurs are common and show a heavy degree of wear. SM2021-1-121 (Fig. 3s) is the largest one collected presently. It resembles the dentary tooth of *Sirindhorna khoratensis* (Shibata et al. 2015), with a leaf-shape and enamel-covering on the lingual surface of the tooth. A strong primary ridge runs along the entire height of the crown. At least two weak secondary ridges are present on the mesial side and one on the distal side. Denticles are present on both mesial and distal crown borders. The lower part of the crown possesses a facet for an adjacent tooth allowing the formation of a complex dental battery.

Although Khok Pha Suam vertebrates are mostly known from microremains and fragmentary larger remains, some

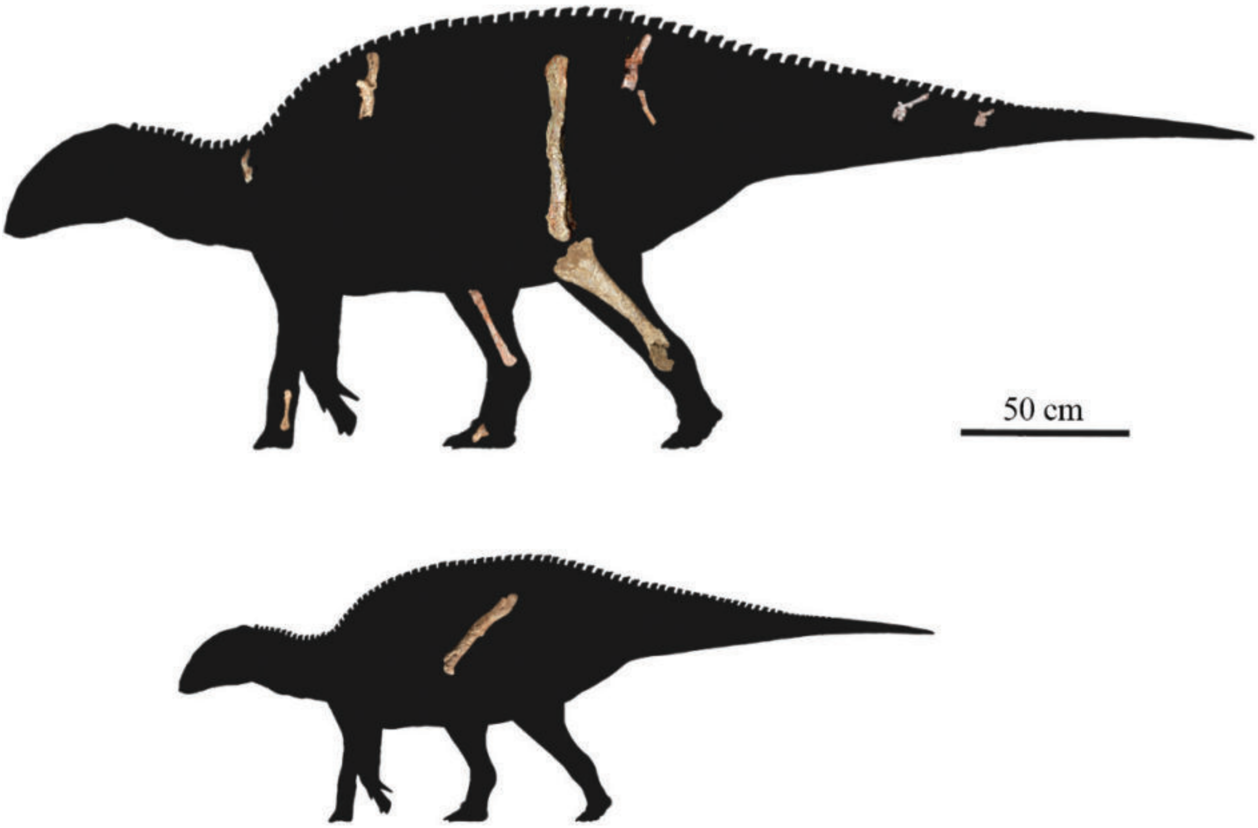

Figure 5. Tentative reconstruction of Khok Pha Suam iguanodontian indet. showing recovered bones in left lateral view

isolated postcranial bones belonging to iguanodontians were discovered (Fig. 5), including vertebrae and limb bones from different individuals. For this reason, these herbivores are outstanding from all the other tetrapods of the Khok Pha Suam locality, becoming therefore an iconic symbol of Pha Chan-Sam Phan Bok Geopark (Fig. 2c).

Three taxa of hadrosauroids have been described from the Khok Kruat Formation in Nakhon Ratchasima Province, including *Siamodon nimngami* (Buffetaut and Suteethorn 2011), *Ratchasimasaurus suranareae* (Shibata et al. 2011), and *Sirindhorna khoratensis* (Shibata et al. 2015). Material of *S. nimngami* and *R. suranareae* encompass only a left maxilla and a left dentary, respectively. However, *S. khoratensis* is the best-preserved iguanodontian ornithopod in Southeast Asia, described from a composite individual including skull and mandible, as well as postcranial elements (Shibata et al. 2018). Therefore it is necessary to compare the postcranial material between Khok Pha Suam taxa and *S. khoratensis* in our further research.

5.8. Pterosaurs

Pterosauria Kaup, 1834
Pterodactyloidea Plieninger, 1901 (Fig. 3t)

Pterosaur teeth in Thailand are very scarce. An isolated Ornithocheirid tooth has been reported from the Sao Kua Formation in northeastern Thailand (Buffetaut et al. 2003a). A well-preserved tooth (Fig. 3t) from Khok Pha Suam presents a slender crown with an oval cross-section, pointed apex and no carinae on both margins. The labial and lingual sides are slightly convex, moderately recurved mesiodistally, and nearly straight labiolingually. The enamel surface is smooth without ridges on the labial and lingual sides. The enamel covering the apex to the base on both surfaces indicates that this specimen is the tip of the crown (Wellnhofer and Buffetaut 1999). The Khok Pha Suam pterosaur is probably related to ornithocheiroids based on the mentioned characters (Alves et al. 2007). Teeth of Khok Kruat pterosaur are also found in Nakhon Ratchasima. They are on exhibit at the Northeastern Research Institute of Petrified Wood & Mineral Resources (In Honor of His Majesty the King) Nakhon Ratchasima Rajabhat University.

6. Overview of other Khok Kruat localities

The sedimentology of Khok Kruat localities shows that the vertebrate fossils were deposited in a fluvial system including flood plains and channels of meandering rivers. At Ban Saphan Hin, Nakhon Ratchasima Province, various vertebrate remains were found scattered and fragmented in a medium to thick-bedded reddish-brown conglomerates. The conglomerates are locally cross-bedded. These elements indicate that the fossils were transported with medium to high energy and deposited in the channel. Carbonate clasts are commonly found and well cemented by calcite. These shreds of evidence

Figure 6. Palaeoenvironmental interpretation of the Early Cretaceous (Aptian-Albian) Khok Pha Suam Locality. Drawing by Sakka Weerataweemat.

suggest a semi-arid environment. This locality has yielded *Thaiodus ruchae*, *Heteroptychodus steinmanni*, *Lanxangichthys* sp., *Shachemys* sp., *Kizylkumemys khoratensis*, *Khoratosuchus jintasakuli*, Eusuchian indet., *Sirindhorna khoratensis*, *Siamraptor suwati* (Tong et al. 2005; Cuny et al. 2008; Lauprasert et al. 2009; Shibata et al. 2015; Cavin et al. 2018; Kubo et al. 2018; Chokchaloemwong et al. 2019).

Many groups of vertebrates have been found in the Sam Ran locality, Khon Kaen Province, including teeth of two hybodont taxa (incl. *H. steinmanni*, and *T. ruchae*), ganoid scales of actinopterygians (Ginglymodi type II), turtle shell fragments, teeth of crocodyliforms, teeth of large theropods and partial postcranial bones of spinosaurid indet. The presence of sedimentary structures such as fining upward, planar cross-bedding, load casted, rip-up clasts indicate meandering channel deposits and crevasse splay sequences. The very good preservation of the vertebrate fossils, notably the partial skeleton of a spinosaurid indet. is likely a result of a low-energy current system. The calcisol with pedogenetic carbonates is an indication of a semi-arid climate (Wongko 2018). Unfortunately, this locality has been transformed due to land use making further excavation attempts more difficult.

Lam Pao Dam locality in Kalasin Province has poor fossil preservation. This locality has yielded the teeth of hybodonts (incl. *H. steinmanni*, *T. ruchae* and possibly *K. foreyi*), teeth and scales of ginglymodians, teeth of crocodyliforms and theropods. Trace fossils, such as theropod footprint, *Lockeia*, *Phycodes*, *Planolites*, and *Skolithos* indicate a moderately to well-drained floodplain. It could have been arid or semi-arid in a subtropical climate, as indicated by the caliche-siltstone granule calcareous sandstone deposits. The presence of lithostratigraphic and sedimentary structures such as stacked fining-upward sequences, small scale cross-bedding, rip-up clasts, and conglomerates at the base of sequences indicate high-energy current, meandering channel conglomerate deposits or point-bar deposits (Wongko 2018).

The fossil remains from Ban Pha Nang Sua locality, Chaiyaphum Province are found in reddish-brown sandstones and siltstones in the lower part of the sequence which is interpreted as a crevasse splay deposit. Most of the specimens belong to a giant titanosauriforms indet., associated with some teeth of hybodonts, crocodyliforms, and theropods (Department of Mineral Resources Division of Fossil Protection 2016).

7. Discussion

The vertebrate fauna from Khok Pha Suam represents the richest assemblage at the generic level within the Khok Kruat Formation (Table 1). Although there are similarities when compared to the Barremian Sao Khua Formation, the existence of ornithischian dinosaurs is an important difference between the two formations.

Hundreds of isolated teeth and many dorsal fin spine fragments of hybodonts representing up to five different genera have been recovered so far. Pattern and form variation of these shark teeth show adaptations towards various diets: cutting (*Thaiodus*), crushing (*Khoratodus*, “*Hybodus*” and *Acrorhizodus*), and grinding (*Heteroptychodus*) (Cuny et al. 2017). Bivalve internal molds (Fig. 3u) which have been found in Khok Pha Suam resemble *Trigonioides trigonus* (Hoffet 1937) from the Grès Supérieurs Formation of southern Laos and *Pseudohyria* (*Matsumotoina*) *somanai* (Tumpeesuwan et al. 2010) from the older Sao Khua Formation based only on comparisons with external shell morphology. Additional

Table 1. List of vertebrate faunas from Khok Pha Suam locality with other taxa from the Khok Kruat Formation (*The Grès Supérieurs Formation of southern Laos is laterally considered an equivalent to the Khok Kruat Formation).

Taxa	Khok Pha Suam	References	Khok Kruat (other localities)	References
Ornithopods	Iguanodontian indet.	(Buffetaut et al. 2003b, 2005)	*Mandschurosaurus laosensis* (Laos*)	(Hoffet 1944)
			Siamodon nimngami (Nakhon Ratchasima)	(Buffetaut and Suteethorn 2011)
			Ratchasimasaurus suranareae (Nakhon Ratchasima)	(Shibata et al. 2011)
			Sirindhorna khoratensis (Nakhon Ratchasima)	(Shibata et al. 2015)
Ceratopsians			*Psittacosaurus sattayaraki* (Chaiyaphum)	(Buffetaut and Suteethorn 1992)
			Psittacosaurid indet. (Khon Kaen & Laos*)	(Buffetaut et al. 2007)
Spinosaurids	Spinosaurid type I	(Wongko et al. 2019)	*Ichthyovenator laosensis* (Laos*)	(Allain et al. 2012)
	Spinosaurid type II	(Wongko et al. 2019)	Spinosaurid indet. (Khon Kaen, Kalasin & Chaiyaphum)	(Buffetaut et al. 2005; Department of Mineral Resources 2016)
Allosauroids	Carcharodontosaurian indet.	(Buffetaut et al. 2005)	*Siamraptor suwati* (Nakhon Ratchasima)	(Chokchaloemwong et al. 2019)
Sauropods	Titanosauriforms indet.	(Buffetaut et al. 2005)	*Tangvayosaurus hoffeti* (Laos*)	(Allain et al. 1999)
			Titanosauriforms indet. (Chaiyaphum & Khon Kaen)	(Khansubha et. al. 2017)
Pterosaurs	Pterodactyloid indet.	In this paper	Pterosaur indet. teeth (Nakhon Ratchasima)	
Crocodyliforms	Goniopholidid indet.	(Lauprasert 2006)	*Khoratosuchus jintasakuli* (Nakhon Ratchasima)	(Lauprasert et al. 2009)
			Eusuchian indet. (Nakhon Ratchasima)	(Kubo et al. 2018)
	Neosuchian indet.		Neosuchian indet. (Khon Kaen, Kalasin & Chaiyaphum)	(Department of Mineral Resources 2016; Wongko 2018)
Turtles	Carettochelyid indet.	(Tong et al. 2009)	*Kizylkumemys khoratensis* (Nakhon Ratchasima)	(Tong et al. 2005)
			Carettochelyid indet. (Kalasin, Khon Kaen)	(Wongko 2018)
	Adocid indet.	(Tong et al. 2009)	*Shachemys laosiana* (Laos*)	(de Lapparent de Broin 2004)
			Shachemys sp. (Nakhon Ratchasima & possibly Khon Kaen)	(Tong et al. 2009; Wongko 2018)
Halecomorphs	cf. *Siamamia* indet.	(Deesri et al. 2017)	Sinamiidae indet. (Nakhon Ratchasima)	(Deesri et al. 2021)
Ginglymodians	*Lanxangichthys* sp.	(Cavin et al. 2018)	*Lanxangichthys alticephalus* (Laos*)	(Cavin et al. 2018)
	Ginglymodi type I	(Wongko 2018)	*Lanxangichthys* sp. (Nakhon Ratchasima)	(Cavin et al. 2018)
	Ginglymodi type II	(Wongko 2018)	Ginglymodi type I (Kalasin)	(Wongko 2018)
			Ginglymodi type II (Kalasin & Khon Kaen)	(Wongko 2018)
Hybodontiforms	*Heteroptychodus steinmanni*	(Cuny et al. 2003)	*Heteroptychodus steinmanni* (Kalasin, Khon Kaen, Nakhon Ratchasima & probably Chaiyaphum)	(Cuny et al. 2007; Department of Mineral Resources 2016; Wongko 2018)
	Thaiodus ruchae	(Cappetta et al. 1990)		
	"*Hybodus*" *aequitridentatus*	(Cuny et al. 2008)		
	Khoratodus foreyi	(Cuny et al. 2008)	*Thaiodus ruchae* (Nakhon Ratchasima,Khon Kaen, & Kalasin)	(Cappetta et al. 1990; Cuny et al. 2003; Cuny et al. 2007)
	Acrorhizodus khoratensis	(Cappetta et al. 2006)		

comparisons of hinge teeth characters are needed to establish more taxonomic precision. These bivalves could potentially have been food for *H. steinmanni*. The five species of hybodonts from the same assemblage have also been found in the Xinlong Formation in southern China (Cuny et al. 2017). They are indeed endemic to Southeast Asia and South China, four of them (*Acrorhizodus*, "*H.*" *aequitridentatus*, *Thaiodus* and *Khoratodus*) are restricted to the Aptian-Albian interval (Cuny 2012). The fifth genus, *Heteroptychodus* is currently restricted to Thailand, Japan, Kyrgyzstan, South China and Mongolia, and is the most common hybodont species found in the Khorat Group (Cuny et al. 2008, 2014), exhibiting a large stratigraphic distribution, from the Upper Phu Kradung Formation to the Khok Kruat Formation (Cuny et al. 2014). Three species are currently recognized including *H. steinmanni*, *H. kokutensis*, and *H. chuvalovi* (Cuny et al. 2008). It is important to note, that Khok Pha Suam has yielded few large teeth compared to the number of small ones, contrary to Ban Saphan Hin, where only large teeth are recovered. If we consider the large teeth as belonging to adult specimens, small ones to juveniles, then Khok Pha Suam may appear as a potential nursery for these sharks.

Among the thousands of dinosaur bones from the Sao Khua Formation that belong to sauropods and theropods, there is so far no evidence of any ornithischians. In the Khok Kruat Formation, the diversity of sauropods appears to be greatly diminished with the appearance of basal ceratopsians and advanced iguanodontians (Buffetaut and Suteethorn 1998; Buffetaut et al. 2005, 2006). The possible palaeobiogeographical reasons for this change are still unclear. The Khok Kruat sauropods are still poorly known although these long-necked plant-eating dinosaurs are very abundant from the older non-marine Mesozoic formations in northeastern Thailand. Khok Pha Suam sauropods are probably closely related to the very large undescribed titanosauriform sauropod (known from a dorsal vertebra, sacral vertebrae, pelvic girdle, humerus, femur, and ribs) from the dinosaur site in the vicinity of Ban Pha Nang Sua, Nong Bua Rawe District, Chaiyaphum Province of Thailand (Khansubha et al. 2017) and from *Tangvayosaurus hoffeti* from the Grès supérieurs Formation of Savannakhet Province in Laos (Allain et al. 1999).

The teeth of Khok Kruat spinosaurids can be categorized into two morphotypes (Wongko et al. 2019) and indicate that two distinct spinosaurid taxa potentially occur in the Albian-Aptian of Thailand. If these morphotypes are not related to differences between taxa, they are due to dimorphism within a single species. However, there are evidences of several spinosaurid taxa in the same area from many formations such as *Spinosaurus aegyptiacus* and *Sigilmassasaurus brevicollis* from the Cenomanian Kem Kem beds of Morocco and *Ceratosuchops inferodios* and *Riparovenator milnerae* from the Barremian Wessex Formation of UK (Richter et al. 2013; Hendrickx et al.

2016; Barker et al. 2021). This suggests the possibility of a co-occurrence of two distinct spinosaurid taxa in the Khok Kruat Formation.

It is worth noting that the material of psittacosaurids seems to be the only group of Khok Kruat animals that have never been discovered in Khok Pha Suam (Table 1). Although psittacosaurids were abundant in the Early Cretaceous of Eastern Asia (especially China, Mongolia, and Siberia), they appear to be scarce in Southeast Asia (Buffetaut and Suteethorn 1992; Buffetaut et al. 2007). Specimens of *Psittacosaurus* are often found in lacustrine deposits (Averianov et al. 2006; Buffetaut et al. 2007). Moreover, an exceptionally well-preserved specimen of *Psittacosaurus* sp. from the Jehol biota of China shows countershade adaptations for closed habitat with an evergreen canopy (Vinther et al. 2016). This differs greatly from the reconstructed palaeoenvironment of the Khok Kruat Formation and the Grès Supérieurs Formation which are fluvial deposits with an arid or -semi-arid subtropical climate (Racey et al. 1996; Wongko 2018). Both factors, depositional environment and palaeoclimate, may provide an explanation for the scarcity of psittacosaurid materials uncovered in Thailand and Laos.

Another noteworthy point is the absence of amphibians from the Khok Kruat Formation (Fig. 1). Mesozoic Thai amphibian remains are assigned to temnospondyls (Cyclotosauridae, Plagiosauridae, and Brachyopoidea) and Anura, which have been discovered from three formations of the Indochina Terrane ranging from the Upper Triassic to the Lower Cretaceous (Nonsrirach et al. 2021). The Upper Triassic Huai Hin Lat Formation, which is mainly formed by fluvio-lacustrine deposits, has yielded the most amphibian specimens so far in terms of generic-level diversity and numerical abundance (including *Cyclotosaurus*, Plagiosauridae, and Stereospondyli indet.) (Ingavat and Janvier 1981; Suteethorn et al. 1988; Racey et al. 1996; Meesook 2000; Nonsrirach et al. 2021). However, the younger formations show a marked decrease in the number of temnospondyls. Brachyopoids have been found in the Upper Jurassic Phu Kradung Formation that was deposited in a lacustrine-dominated alluvial floodplain (Meesook 2000; Racey 2009; Nonsrirach et al. 2021). A few fragments of frogs have been found in the Early Cretaceous Sao Khua Formation that was deposited in an alluvial floodplain and meandering river (Racey et al. 1996; Buffetaut and Suteethorn 1999; Meesook 2000; Nonsrirach et al. 2021). Temnospondyls reached worldwide very high diversity in the Early Triassic, then gradually decreased during the Middle to Late Triassic (Ruta and Benton 2008). With the rise of the crocodyliforms in the middle Triassic that would have competed with them, only Brachyopoidea were able to surive into the Jurassic to Early Cretaceous deposits across Asia and Australia (Ruta and Benton 2008). The giant *Koolasuchus cleelandi* is the youngest known brachyopoid from the Aptian of Australia inhabiting a polar environment too cold in the winter for crocodyliforms to survive (Warren et al. 1991; Rich and Rich 2014). Although no fossils of anura were found in the Khok Kruat Formation, it cannot be concluded that they did not exist -taphonomy of amphibians in a semi-arid meandering river may affect fossilization.

8. Conclusions

The Khok Pha Suam locality has yielded vertebrates from the Aptian-Albian stages. It represents one of the most diverse vertebrate assemblages in the Khok Kruat Formation of Thailand and the laterally equivalent Grès Supérieurs Formation of Laos. The site is characterized by the dominance of hybodont teeth and iguanodont postcranial material. This study underlines the palaeontological value of this site, which is an essential feature of the Pha Chan-Sam Phan Bok Geopark. The locality improves our knowledge of the diversity of Early Cretaceous vertebrate faunas and provides a useful point of comparison with other East and Southeast Asian taxa.

Acknowledgements

We would like to thank many colleagues for useful suggestions and comments; Clive Burrett, Bouziane Khalloufi and Thitiwoot Sethapanichsakul for their help with the English language. Sukboworn Tumpeesuwan, Suchada Khamha, Wilailuck Naksri, Sasa-On Khansubha, Kantanat Trakunweerayut, and Tapanan Sunipan for providing data on bivalves, hybodonts, turtles, sauropods, maps, and the history of Khok Pha Suam respectively. Nareerat Boonchai, Paul Grote, and Marc Phillipe for discussion about plants and palaeoenvironmental reconstruction. Witaya Nimgnam for data on hybodonts from the Ban Sapan Hin locality. The Khok Pha Suam ecosystem is illustrated by Sakka Weerataweemat. The stratigraphic column of Khok Pha Suam is from Wongwech Chowchuvech. We are grateful to the staff of the Palaeontological Research and Education Centre of Mahasarakham University, Sirindhorn Museum, and Na Kham Subdistrict Administrative Organization, who took part in our fieldwork and helped during visits to the collection. This research project has been supported by Mahasarakham University (First International Publication 2021). Sita Manitkoon was financially supported by the Mahasarakham University Development Fund for the international symposium presentation.

References

Allain R, Taquet P, Battail B, Dejax J, Richir P, Véran M, Limon-Duparcmeur F, Vacant R, Mateus O, Sayarath P, Khenthavong B, Phouyavong S (1999) Un nouveau genre de dinosaure sauropode de la formation des Grès supérieurs (Aptien-Albien) du Laos. Comptes Rendus de l'Académie de Sciences – Serie IIa: Sciences de la Terre et des Planètes 329: 609–616. https://doi.org/10.1016/S1251-8050(00)87218-3

Allain R, Xaisanavong T, Richir P, Khentavong B (2012) The first definitive Asian spinosaurid (Dinosauria: Theropoda) from the Early Cretaceous of Laos. Naturwissenschaften 99: 369–377. https://doi.org/10.1007/s00114-012-0911-7

Alves F, Elias FA, Bertini RJ, Alfredo M, Medeiros A (2007) Pterosaur teeth from the Laje do Coringa, Middle Cretaceous, São Luís- Grajaú basin, Maranhão state, Northern-Northeastern Brazil. Revista Brasileira de Geociências 37: 1–9. https://doi.org/10.25249/0375-7536.20073744760668676

Andrade MB, Edmonds R, Benton MJ, Schouten R (2011) A new Berriasian species of *Goniopholis* (Mesoeucrocodylia, Neosuchia) from England, and a review of the genus. Zoological Journal of the Linnean Society 163: 66–108. https://doi.org/10.1111/j.1096-3642.2011.00709.x

Averianov AO, Voronkevich AV, Leshchinskiy SV, Fayngertz AV (2006) A ceratopsian dinosaur *Psittacosaurus sibiricus* from the Early Cretaceous of West Siberia, Russia and its phylogenetic relationships. Journal of Systematic Palaeontology 4: 359–395. https://doi.org/10.1017/S1477201906001933

Barker CT, Hone DWE, Naish D, Cau A, Lockwood JAF, Foster B, Clarkin CE, Schneider P, Gostling NJ (2021) New spinosaurids from the Wessex Formation (Early Cretaceous, UK) and the European origins of Spinosauridae. Scientific Reports 11: e19340. https://doi.org/10.1038/s41598-021-97870-8

Benton MJ, Clark JM (1988) Archosaur phylogeny and the relationships of the Crocodilia. In: Benton MJ (Ed.) The Phylogeny and Classification of the Tetrapods, Vol. 1. Clarendon Press, Oxford, 295–338.

Berg LS (1940) The classification of fishes, both Recent and fossil. Trudy Zoologicheskogo lnstituta Akademiia nauk SSSR 5: 87–517.

Bonaparte JF (1986) The early radiation and phylogenetic relationships of sauropod dinosaurs, based on vertebral anatomy. In: Padian K (Ed.) The Beginning of the Age of Dinosaurs. Cambridge University Press, Cambridge, 247–258.

Boulenger GA (1887) On a new family of Pleurodiran turtles. The Annals and Magazine of Natural History Series 5, 19: 170–172. https://doi.org/10.1080/00222938709460223

Brusatte SL, Benson RBJ, Carr TD, Williamson TE, Sereno PC (2007) The systematic utility of theropod enamel wrinkles. Journal of Vertebrate Paleontology 27: 1052–1056. https://doi.org/10.1671/0272-4634(2007)27[1052:TSUOTE]2.0.CO;2

Buffetaut E, Ingavat R (1983) *Goniopholis phuwiangensis* nov. sp., a new mesosuchian crocodile from the Jurassic of northeastern Thailand. Geobios 16: 79–91. https://doi.org/10.1016/S0016-6995(83)80048-5

Buffetaut E, Suteethorn V (1992) A New Species of the Ornithischian Dinosaur *Psittacosaurus* from the Early Cretaceous of Thailand. Palaeontology 35: 801–812. https://a1992ke44400004

Buffetaut E, Suteethorn V (1998) The biogeographical significance of the Mesozoic vertebrates from Thailand. Biogeography and Geological Evolution of SE Asia: 83–90.

Buffetaut E, Suteethorn V (1999) The dinosaur fauna of the Sao Khua Formation of Thailand and the beginning of the Cretaceous radiation of dinosaurs in Asia. Palaeogeography, Palaeoclimatology, Palaeoecology 150: 13–23. https://doi.org/10.1016/S0031-0182(99)00004-8

Buffetaut E, Suteethorn V (2011) A new iguanodontian dinosaur from the Khok Kruat Formation (Early Cretaceous, Aptian) of northeastern Thailand. Annales de Paleontologie 97: 51–62. https://doi.org/10.1016/j.annpal.2011.08.001

Buffetaut E, Suteethorn V, Tong H (2006) Dinosaur Assemblages from Thailand: a Comparison with Chinese Faunas. In: Lu JC, Kobayashi Y, Huang D, Lee Y-N (Eds) Papers from the 2005 Heyuan International Dinosaur Symposium. Geological Publishing House, Beijing, 19–37.

Buffetaut E, Suteethorn V, Khansubha S (2007) The ceratopsian dinosaur *Psittacosaurus* in the Early Cretaceous of Southeast Asia: a review of old and recent finds. In: GEOTHAI'07 International Conference on Geology of Thailand: Towards Sustainable Development and Sufficiency Economy, 338–343.

Buffetaut E, Suteethorn V, Tong H, Cuny G, Cavin L (2003a) A Pterodactyloid Tooth from the Sao Khua Formation (Early Cretaceous) of Thailand. 1st International Conference on Palaeontology of Southeast Asia Mahasarakham University Journal 22: 92–98.

Buffetaut E, Suteethorn V, Le Loeuff J, Khansubha S, Tong H, Wongko K (2005) The Dinosaur Fauna from the Khok Kruat Formation (Early Cretaceous) of Thailand. International Conference on Geology, Geotechnology and Mineral Resources of Indochina (GEOINDO 2005): 575–581.

Buffetaut E, Suteethorn V, Cuny G, Khansubha S, Tong H, Le Loeuff J, Cavin L (2003b) Dinosaurs in Thailand. Maha Sarakham University Journal, Special Issue: 69–82.

Cappetta H, Buffetaut E, Suteethorn V (1990) A new hybodont shark from the Lower Cretaceous of Thailand. Neues Jahrbuch für Geologie und Paläontologie, Monatshefte 11: 659–666. https://doi.org/10.1127/njgpm/1990/1990/659

Cappetta H, Buffetaut E, Cuny G, Suteethorn V (2006) A new elasmobranch assemblage from the Lower Cretaceous of Thailand. Palaeontology 49: 547–555. https://doi.org/10.1111/j.1475-4983.2006.00555.x

Cavin L, Deesri U, Suteethorn V (2009) The Jurassic and Cretaceous bony fish record (Actinopterygii, Dipnoi) from Thailand. Geological Society, London, Special Publications 315: 125–139. https://doi.org/10.1144/SP315.10

Cavin L, Suteethorn V, Buffetaut E, Claude J, Cuny G, Le Loeuff J, Tong H (2007) The first sinamiid fish (holostei, halecomorpha) from southeast Asia (Early Cretaceous of Thailand). Journal of Vertebrate Paleontology 27: 827–837. https://doi.org/10.1671/0272-4634(2007)27[827:TFSFHH]2.0.CO;2

Cavin L, Deesri U, Veran M, Khentavong B, Jintasakul P, Chanthasit P, Allain R (2018) A new Lepisosteiformes (Actinopterygii: Ginglymodi) from the Early Cretaceous of Laos and Thailand, SE Asia. Journal of Systematic Palaeontology 17(5): 393–407. https://doi.org/10.1080/14772019.2018.1426060

Chokchaloemwong D, Hattori S, Cuesta E, Jintasakul P, Shibata M, Azuma Y (2019) A new carcharodontosaurian theropod (Dinosauria: Saurischia) from the Lower Cretaceous of Thailand. PLoS ONE 14: 1–43. https://doi.org/10.1371/journal.pone.0222489

Cooper MR (1985) A revision of the ornithischian dinosaur *Kangnasaurus coetzeei* Haughton, with a classification of the ornithischia. Annals of the South African Museum 95: 281–317.

Cope ED (1868) On the origin of genera. Proceedings of the Academy of Natural Sciences of Philadelphia 20: 242–30.

Cope ED (1870) On the Adocidae. Proceedings of the American Philosophical Society 11: 547–553.

Cope ED (1872) Observations on the systematic relations of the fishes. Proceedings of the American Association for the Advancement of Science 20: 317–343.

Cope ED (1875) 2 Report of the U.S. Geological Survey of the territories (F.V. Hayden) The vertebrata of the Cretaceous formations of the West. 303 pp. https://doi.org/10.5962/bhl.title.61834

Cuny G, Suteethorn V, Buffetaut E, Philippe M (2003) Hybodont sharks from the Mesozoic Khorat Group of Thailand. Mahasarakham University Journal 22: 49–68.

Cuny G (2012) Freshwater hybodont sharks in Early Cretaceous ecosystems: A review. In: Godefroit P (Ed.) Bernissart Dinosaurs and Early Cretaceous Terrestrial Ecosystems. Indiania University Press, Bloomington, 518–529.

Cuny G, Suteethorn V, Khamha S, Buffetaut E (2008) Hybodont sharks from the lower Cretaceous Khok Kruat Formation of Thailand, and hybodont diversity during the Early Cretaceous. Geological Society of London 295: 93–107. https://doi.org/10.1144/SP295.7

Cuny G, Laojumpon C, Cheychiw O, Lauprasert K (2010) Fossil vertebrate remains from Kut Island (Gulf of Thailand, Early Cretaceous). Cretaceous Research 31: 415–423. https://doi.org/10.1016/j.cretres.2010.05.007

Cuny G, Suteethorn V, Kamha S, Lauprasert K, Srisuk P, Buffetaut E (2007) the Mesozoic Fossil Record of Sharks in Thailand. In: GEOTHAI'07 International Conference on Geology of Thailand: Towards Sustainable Development and Sufficiency Economy. Department of Mineral Resources, Bangkok, Thailand, 349–354.

Cuny G, Liard R, Deesri U, Liard T, Khamha S, Suteethorn V (2014) Shark faunas from the Late Jurassic—Early Cretaceous of northeastern Thailand. Palaontologische Zeitschrift 88: 309–328. https://doi.org/10.1007/s12542-013-0206-0

Cuny G, Mo J, Amiot R, Buffetaut E, Suteethorn S, Suteethorn V, Tong H (2017) New data on Cretaceous freshwater hybodont sharks from Guangxi Province, South China. Research & Knowledge 3: 11–15.

Deesri U, Wongko K, Cavin L (2017) Taxic diversity and ecology of Mesozoic bony fish assemblages from the Khorat Group, NE Thailand. Research & Knowledge 3: 18–22.

Deesri U, Naksri W, Jintasakul P, Yoshikazu N, Hirokazu Y, Cavin L (2021) New sinamiid fish (Actinopterygii: Halecomorphi) from the Early Cretaceous of northeastern Thailand. In: Current studies on past biodiversity in South-East Asia, 19–20.

Department of Mineral Resources (2021) Pha Chan – Sam Phan Bok Geopark. https://www.geopark-thailand.org

Department of Mineral Resources Division of Fossil Protection (2016) The Cretaceous Giant Sauropod from the Khok Kruat Formation at Ban Pha Nang Sua, Nong Bua Rawe District, Chaiyaphum Province, Northeastern Thailand: a preliminary report. Technical Report DFP 1: 1–90.

Dollo L (1888) Iguanodontidae et Camptonotidae. Comptes rendus l'Academie des Sci 106.

Fitzinger LJ (1826) Entwurf einer systematischen Anordnung der Schildkröten nach Grundsätzen der natürlichen Methode. Annalen des Wiener Museums der Naturgeschichte 1: 105–105.

Gaffney ES, Meylan PA (1988) The Phylogeny and Classification of the Tetrapods, Vol. 1, Amphibians, Reptiles, Birds. In: Benton MJ (Ed.) Clarendon Press, Oxford, 157–219.

Grande L (2010) An empirical synthetic pattern study of gars (Lepisosteiformes) and closely related species, based mostly on skeletal anatomy: the resurrection of Holostei. In: American Society of Ichthyologists and Herpetologists. Special Publication, 871 pp.

Grande L, Bemis WE (1998) A Comprehensive Phylogenetic Study of Amiid Fishes (Amiidae) Based on Comparative Skeletal Anatomy. An Empirical Search for Interconnected Patterns of Natural History. Journal of Vertebrate Paleontology 18: 1–690. https://doi.org/10.1080/02724634.1998.10011114

Hay OP (1902) Bibliography and catalogue of the fossil vertebrate of North America. Bulletin of the United States Geological Survey 179: 1–868. https://doi.org/10.5962/bhl.title.20094

Hay OP (1929) Second bibliography and catalogue of the fossil Vertebrata of North America. Carnegie Institution of Washington publication 390.

Hendrickx C, Mateus O, Araujo R (2015) A proposed terminology of theropod teeth (Dinosauria, Saurischia). Journal of Vertebrate Paleontology 35(5): e982797. https://doi.org/10.1080/02724634.2015.982797

Hendrickx C, Mateus O, Buffetaut E (2016) Morphofunctional analysis of the quadrate of Spinosauridae (Dinosauria: Theropoda) and the presence of Spinosaurus and a second spinosaurine taxon in the Cenomanian of North Africa. PLoS ONE 11: 1–49. https://doi.org/10.1371/journal.pone.0144695

Hoffet JH (1944) Description des ossements les plus caractéristiques appartenant à des Avipelviens du Sénonien du Bas-Laos [Description of the most characteristic bones belonging to bird-hipped dinosaurs from the Senonian of Lower Laos]. Comptes Rendus des Séances du Conseil des Recherches Scientifiques de l'Indochine.

Hoffet JH (1937) Les lamellibranches saumatres du Senonien de Muong Phalane (Bas-Laos). Bulletin du Service Geologique de l' Indochine 29: 12–20.

Huxley TH (1880) On the application of the Laws of Evolution to the Arrangement of the Vertebrata. In: The Zoological Societyand more particularly of the Mammalia, 649–662.

Ingavat R, Janvier P (1981) *Cyclotosaurus* cf. *posthumus* Fraas (Capitosauridae, Stereospondyli) from the Huai Hin Lat Formation (Upper Triassic), northeastern Thailand, with a note on capitosaurid biogeography. Geobios 14: 711–725. https://doi.org/10.1016/S0016-6995(81)80149-0

Jin-Geng S, Meesook A (2013) Non-Marine Cretaceous Bivalve Biostratigraphy of Thailand and Southern Lao PDR. The 2nd Lao-Thai Technical Conference on Geology and Mineral Resources: 17–18. http://library.dmr.go.th/Document/DMR_Technical_Reports/2013/36767.pdf

Kaup J (1834) Versuch einer Eintheilung der Säugethiere in 6 Stämme und der Amphibien in 6 Ordnungen. Isis von Oken 3: 311–315.

Khansubha S, Othichaiya C, Rugbumrung M, Meesook A (2017) The gigantic titanosauriform sauropod from the Early Cretaceous Khok Kruat Formation in the northeastern of Thailand: a preliminary report. In: Society of Vertebrate Paleontology 2017, 141–142.

Kubo T, Shibata M, Naksri W, Jintasakul P, Azuma Y (2018) The earliest record of Asian Eusuchia from the Lower Cretaceous Khok Kruat Formation of northeastern Thailand. Cretaceous Research 82: 21–28. https://doi.org/10.1016/j.cretres.2017.05.021

de Lapparent de Broin F (2004) A new Shachemydinae (Chelonii, Cryptodira) from the Lower Cretaceous of Laos: Preliminary data. Comptes Rendus – Palevol 3: 387–396. https://doi.org/10.1016/j.crpv.2004.05.004

Lauprasert K (2006) Evolution and palaeoecology of crocodiles in the Mesozoic of Khorat plateau, Thailand. Chulalongkorn University.

Lauprasert K, Cuny G, Thirakhupt K, Suteethorn V (2009) *Khoratosuchus jintasakuli* gen. et sp. nov., an advanced neosuchian crocodyliform from the Early Cretaceous (Aptian-Albian) of NE Thailand. Geological Society Special Publication 315: 175–187. https://doi.org/10.1144/SP315.13

Lauprasert K, Cuny G, Buffetaut E, Suteethorn V, Thirakhupt K (2007) *Siamosuchus phuphokensis*, a new goniopholidid from the Early Cretaceous (ante-Aptia) of northeastern Thailand. Bulletin de la Societe Geologique de France 178: 201–216. https://doi.org/10.2113/gssgfbull.178.3.201

López-Arbarello A (2012) Phylogenetic interrelationships of ginglymodian fishes (Actinopterygii: Neopterygii). PLoS ONE 7: e39370. https://doi.org/10.1371/journal.pone.0039370

Marsh OC (1878) Principal characters of American Jurassic dinosaurs. Part I. American Journal of Science and Arts 16: 411–416. https://doi.org/10.2475/ajs.s3-16.95.411

Marsh OC (1881) Principal characters of American Jurassic dinosaurs. Part V. The American Journal of Science and Arts 3–21: 417–423. https://doi.org/10.2475/ajs.s3-21.125.417

Meesook A (2000) Cretaceous environments of North- eastern Thailand. In: Okada H, Mateer NJ (Eds) Cretaceous Environments of Asia. Elsevier, Amsterdam, 207–223. https://doi.org/10.1016/S0920-5446(00)80023-0

Müller J (1844) Über den Bau und die Grenzen der Ganoiden und über das natürliche System der Fishe. Bericht Akademie der Wiessenschaften Berlin: 416–422.

Nonsrirach T, Manitkoon S, Lauprasert K (2021) First occurrence of brachyopid temnospondyls in Southeast Asia and review of the Mesozoic amphibians from Thailand. Fossil Record 24: 33–47. https://doi.org/10.5194/fr-24-33-2021

Owen R (1842) British Association for the Advancement of Science, Annual Report for 1841 Report on British Fossil Reptiles. Part II. London.

Patterson C (1966) British Wealden sharks. Bulletin of the British Museum of Natural History (Geology) 11: 283–350. https://doi.org/10.5962/p.150189

Plieninger F (1901) Beiträge zur Kenntnis der Flugsaurier. Palaeontographica 48: 65–90.

Racey A (2009) Mesozoic red bed sequences from SE Asia and the significance of the Khorat Group of NE Thailand. Geological Society, London, Special Publications 315: 41–67. https://doi.org/10.1144/SP315.5

Racey A, Love MA, Canham AC, Goodall JGS, Polachan S, Jones PD (1996) Stratigraphy and reservoir potential of the Mesozoic Khorat group, NE Thailand Part 1: Stratigraphy and Sedimentary Evolution. Journal of Petroleum Geology 19: 5–40. https://doi.org/10.1021/id500025n

Rich VP, Rich TH (2014) Dinosaurs of Polar Australia. Scientific American 23: 46–53. https://doi.org/10.1038/scientificamericandinosaurs0514-46

Richter U, Mudroch A, Buckley LG (2013) Isolated theropod teeth from the Kem Kem Beds (Early Cenomanian) near Taouz, Morocco. Palaontologische Zeitschrift 87: 291–309. https://doi.org/10.1007/s12542-012-0153-1

Ruta M, Benton MJ (2008) Calibrated diversity, tree topology and the mother of mass extinctions: The lesson of temnospondyls. Palaeontology 51: 1261–1288. https://doi.org/10.1111/j.1475-4983.2008.00808.x

Sattayarak N, Srigulawong S, Patarametha M (1991) Subsurface stratigraphy of the non-marine Mesozoic Khorat Group, northeastern Thailand. In: Proceedings of GEOSEA 7th Conference, Bangkok, 5–8 November 1991, 36.

Seeley HG (1888) On the classification of the fossil animals commonly named Dinosauria. Proceedings of the Royal Society of London 43: 165–171. https://doi.org/10.1098/rspl.1887.0117

Shibata M, Jintasakul P, Azuma Y (2011) A New Iguanodontian Dinosaur from the Lower Cretaceous Khok Kruat Formation, Nakhon Ratchasima in Northeastern Thailand. Acta Geologica Sinica – English Edition 85: 969–976. https://doi.org/10.1111/j.1755-6724.2011.00530.x

Shibata M, Jintasakul P, Azuma Y, You H-L (2015) A New Basal Hadrosauroid Dinosaur from the Lower Cretaceous Khok Kruat Formation in Nakhon Ratchasima Province, Northeastern Thailand. PLoS ONE 10(12): e0145904. https://doi.org/10.1371/journal.pone.0145904

Shibata M, Jintasakul P, Azuma Y, Chokchaloemwong D, Kawabe S (2018) All about *Sirindhorna khoratensis* (Ornithopoda; Hadrosauroidea). In: Te 6th International Symposium of International Geoscience Programme IGCP Project 608, 4–5.

Singtuen V, Won-in K (2019) Geoheritage Sites and Geoconservation at Pha Chan – Sam Phan. Geoconservation Research 2: 12–25. https://doi.org/10.30486/gcr.2019.664490

Stromer E (1915) Ergebnisse der Forschungsreisen Prof. E. Stromers in den Wüsten Ägyptens. II. Wirbeltier-Reste der Baharije-Stufe (unterstes Cenoman). 3. Das Original des Theropoden *Spinosaurus aegyptiacus* nov. gen., nov. spec. Abhandlungen der Königlich Bayerischen Akademie der Wissenschaften, Mathematisch-physikalische Klasse (in German) 28: 1–32.

Suteethorn S, Le Loeuff J, Buffetaut E, Suteethorn V, Talubmook C, Chonglakmani C (2009) A new skeleton of *Phuwiangosaurus sirindhornae* (Dinosauria, Sauropoda) from NE Thailand. Geological Society Special Publication 315: 189–215. https://doi.org/10.1144/SP315.14

Suteethorn V, Janvier P, Morales M (1988) Evidence for a Plagiosaurid amphibian in the Upper Triassic Huai Hin Lat Formation of Thailand. Jornal of Southeast Asian Earth Sciences 2: 185–187. https://doi.org/10.1016/0743-9547(88)90029-3

Tong H, Suteethorn V, Claude J, Buffetaut E, JintasakulL P (2005) The turtle fauna from the Khok Kruat Formation (Early Cretaceous) of Thailand. Proceedings of the International Conference on Geology, Geotechnology and Mineral Resources of Indochina (GEOINDO 2005): 610–614.

Tong H, Claude J, Suteethorn V, Naksri W, Buffetaut E (2009) Turtle assemblages of the Khorat Group (Late Jurassic - Early Cretaceous) of NE Thailand and their palaeobiogeographical significance. Geological Society Special Publication 315: 141–152. https://doi.org/10.1144/SP315.11

Tumpeesuwan S, Sato Y, Nakhapadungrat S (2010) A New Species of *Pseudohyria* (Matsumotoina) (Bivalvia: Trigonioidoidea) from the Early Cretaceous Sao Khua Formation, Khorat Group, Northeastern Thailand. Tropical Natural History 10: 93–106.

Upchurch P (1995) The evolutionary history of sauropod dinosaurs. Philosophical Transactions of the Royal Society B: Biological Sciences 349: 365–390. https://doi.org/10.1098/rstb.1995.0125

Upchurch P (1998) The phylogenetic relationships of sauropod dinosaurs. Zoological Journal of the Linnean Society 124: 43–103. https://doi.org/10.1006/zjls.1997.0138

Vinther J, Nicholls R, Lautenschlager S, Pittman M, Kaye TG, Rayfield E, Mayr G, Cuthill IC (2016) 3D Camouflage in an Ornithischian Dinosaur. Current Biology 26: 2456–2462. https://doi.org/10.1016/j.cub.2016.06.065

Walker AD (1970) A revision of the Jurassic reptile Hallopus victor (MARSH) with remarks on the classification of the crocodiles. Philosophical Transactions of the Royal Society of London. Series B 257: 323–372. https://doi.org/10.1098/rstb.1970.0028

Warren AA, Kool L, Cleeland M, Rich TH, Rich P V (1991) An Early Cretaceous labyrinthodont. Alcheringa 15: 327–332. https://doi.org/10.1080/03115519108619027

Wellnhofer P, Buffetaut E (1999) Pterosaur remains from the Cretaceous of Morocco. Paläontologische Zeitschrift 73: 133–142. https://doi.org/10.1007/BF02987987

Wilson JA (2005) Redescription of the mongolian sauropod *Nemegtosaurus mongoliensis* nowinski (Dinosauria: Saurischia) and comments on Late Cretaceous sauropod diversity. Journal of Systematic Palaeontology 3: 283–318. https://doi.org/10.1017/S1477201905001628

Wilson JA, Sereno PC (1998) Early Evolution and Higher-Level Phylogeny of Sauropod Dinosaurs. Journal of Vertebrate Paleontology 18: 1–79. https://doi.org/10.1080/02724634.1998.10011115

Wongko K (2018) Spinosaurid Diversity and Depositional Environment of the Khok Kruat Fomation from Northeastern Thailand. Mahasarakham University.

Wongko K, Buffetaut E, Khamha S, Lauprasert K (2019) Spinosaurid theropod teeth from the Red Beds of the Khok Kruat Formation (Early Cretaceous) in Northeastern Thailand. Tropical Natural History 19: 8–20.

Yabe H, Obata T (1930) On some fossil fishes from the Cretaceous of Japan. Japanese Journal of Geology and Geography 8: 1–8.

Supplementary material 1

Mesozoic vertebrate fauna from the Indochina Terrane of Thailand and additional photos

Authors: Sita Manitkoon, Uthumporn Deesri, Komsorn Lauprasert, Prapasiri Warapeang, Thanit Nonsrirach, Apirut Nilpanapan, Kamonlak Wongko, Phornphen Chanthasit

Data type: Images

Explanation note: Fig. S1. Mesozoic vertebrate fauna from the Indochina Terrane of Thailand. Figs S2–S5. Additional photos were mentioned in the article.

Link: https://doi.org/10.3897/fr.25.83081.suppl1

Fossil Record 25 (1) 2022, 99–145 | DOI 10.3897/fr.25.83781

Amphibian and reptilian fauna from the early Miocene of Echzell, Germany

Davit Vasilyan[1,2], Andrej Čerňanský[3], Zbigniew Szyndlar[4], Thomas Mörs[5,6]

1 *JURASSICA Museum, Route de Fontenais 21. 2900 Porrentruy, Switzerland*
2 *Department of Geosciences, University of Fribourg, Chemin du musée 6, 1700, Fribourg, Switzerland*
3 *Department of Ecology, Laboratory of Evolutionary Biology, Faculty of Natural Sciences, Comenius University in Bratislava, Mlynská dolina, Ilkovičova 6, 842 15 Bratislava, Slovakia*
4 *Institute of Systematics and Evolution of Animals, Polish Academy of Sciences, Slawkowska 17, 31-016 Kraków, Poland*
5 *Department of Palaeobiology, Swedish Museum of Natural History, P.O. Box 50007, 104 05 Stockholm, Sweden*
6 *Bolin Centre for Climate Research, Stockholm University, Stockholm, Sweden*

http://zoobank.org/7A16698D-4F18-48D2-9D96-51A6E0CC15AC

Corresponding author: Davit Vasilyan (davit.vasilyan@jurassica.ch)

Academic editor: Florian Witzmann ◆ **Received** 13 October 2021 ◆ **Accepted** 3 May 2022 ◆ **Published** 10 May 2022

Abstract

The present study describes a rich amphibian and reptilian assemblage from the early Miocene locality Echzell, Germany. It consists of one allocaudate, five salamander, five frog, one gecko, chamaeleonids, anguine lizards, one lacertid, one skink and five snake taxa. The entire herpetofauna of Echzell is represented by genera and/or families very broadly known from the early Miocene of Europe. Contrary to other early Miocene herpetofaunas, the Echzell assemblage includes surprisingly only one form of crocodile-newts (*Chelotriton*). The Echzell *Palaeobatrachus robustus* represents the youngest record of the species and extends its stratigraphic range to the late early Miocene. Regarding chameleons, the frontal is partly preserved, but represents the first described frontal of the extinct species *Chamaeleo andrusovi*. The only anguine lizard that can be identified in the assemblage is represented by a new genus and species *Smithosaurus echzellensis.* Our phylogenetic analyses consistently recovered it as the sister taxon to either [*Ophisauriscus quadrupes* + *Ophisaurus holeci*] + [*Anguis* + *Ophisaurus*] (in the first analysis) or [*Anguis* + *Ophisaurus*] (in the second analysis). However, the results are based on limited fossil material – the parietal – and the support for the clade is very low. Thus, the interpretation of the *Smithosaurus* relationship among anguines needs to be taken with caution and has to be tested in further studies. Among snakes, *Natrix longivertebrata* represents the oldest record of the species and extends the stratigraphic range of this fossil snake back to the early Miocene. In addition, we provide here a broader comparison of the Echzell amphibian and reptilian assemblage with their European records for the MN3 and MN4 biostratigraphical units. Besides that, the entire herpetofauna of Echzell includes very broadly known early Miocene European forms. Remains of other groups of the same period such as Bufonidae, Hylidae, Pelodytidae, Amphisbaenia, Varanidae, Cordylidae, *Pseudopus*, are not found in the material available to us. We also conclude that the amphibian and reptilian fossil record across MN3–MN4 is significantly biased by taphonomic and/or environmental conditions. The amphibian and reptilian assemblage of Echzell is rich in forms living in humid and warm environments with forested areas, permanent water bodies and also some open habitats. The following climatic parameters can be reconstructed based on the herpetofauna: a mean annual temperature of 17.4–28.8 °C, minimal warm month temperature 18–28.3 °C, minimal cold month temperature 8–22.2 °C, and mean annual precipitation with a value of 791±254 mm.

Key Words

early Miocene, frogs, Germany, lizards, salamanders, snakes

Introduction

The early Miocene of the European continent is characterised by a number of faunistic changes, which in turn are caused by palaeogeographic and climatic reorganisations (Rössner and Heissig 1999; Steinthorsdottir et al. 2021). While the mammalian record is better studied, the fossil record of other tetrapod groups, such as amphibians, reptiles and birds, has received less attention. During recent years, research focussed on the early Miocene herpetofauna has been intensified and a number of studies documented so far poorly known fossil records of amphibians and reptiles (Ivanov 2008; Čerňanský et al. 2015; Čerňanský 2016; Villa et al. 2021). A better understanding of the faunistic evolution of those groups through time can be provided, taking into account the known fossil record. In the present study, we aim to describe amphibian and reptilian fossil material from the Echzell locality, which is so far known for its mammalian fauna (Fig. 1, see references below). Further, we aim also to provide a faunistic comparison of the studied groups across the MN3–MN4 zones.

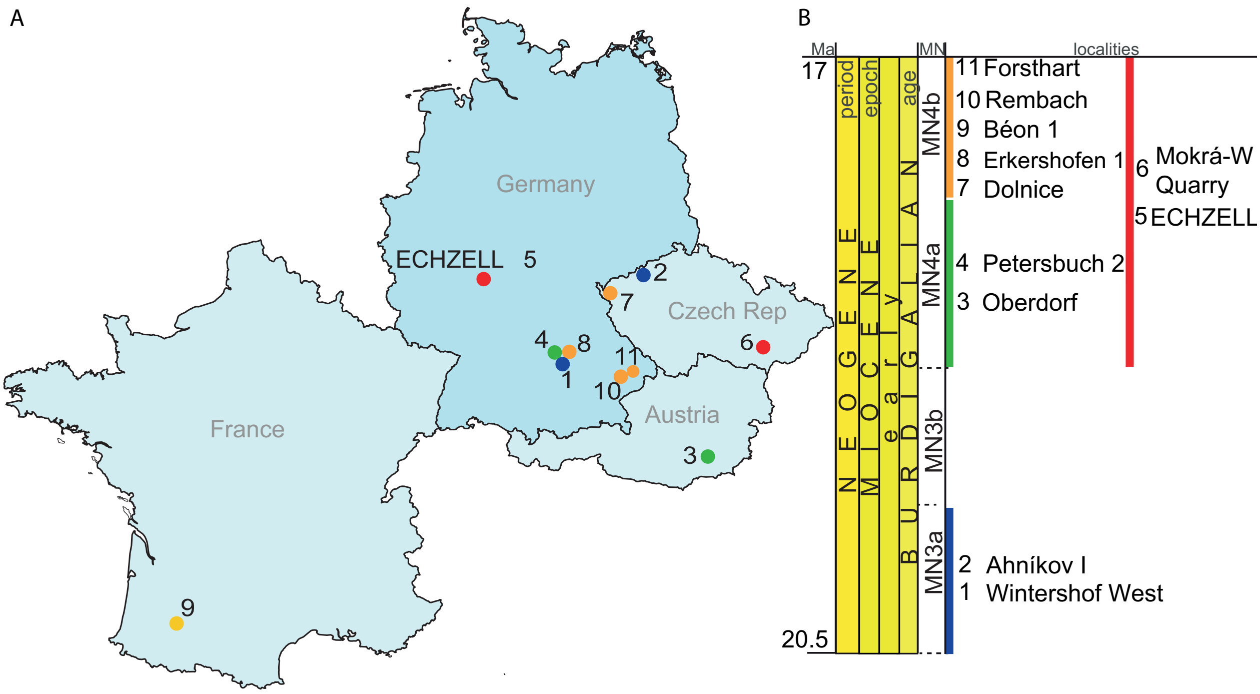

Figure 1. A. Partial map of Europe indicating Burdigalian (MN3–MN4) localities with well-represented amphibian and reptilian faunas including the Echzell locality. The colour of the circles indicating the localities corresponds to the vertical balks in (**B**); **B.** Temporal and biochronologic assignments of the fossil localities, the vertical balks in different colour correspond to MN (sub) zones (e.g. the localities Echzell and Mokrá-W Quarry belong to the MN4 zone where the former is located biochronologically older than the latter withing the same MN4 zone).

Echzell locality and biostratigraphic setting

Echzell is located approximately 30 km NNE of Frankfurt am Main at the eastern edge of the Horloff Graben, which cuts into the southwestern part of the basaltic Vogelsberg volcanic complex. The Vogelsberg was active during the entire Miocene and covered an area of 2,500 km^2. Some diatomitic maar lake deposits and reworked basaltic ashes produced Miocene vertebrate remains (for references, see Mörs 2010), but the disintegrated volcanic tuffs of the Echzell locality are most fossiliferous (Tobien 1954, 1982; Pineker and Mörs 2011; Mörs and Flink 2018; Jovells Vaqué and Mörs 2022). The Echzell fauna is dominated by small mammals (Table 1). Additionally, Tobien (1954, 1982) reported among large mammals *Gomphotherium angustidens*, *Bunolistriodon*, small ruminants, a rhinocerotid and a large amphicyonid.

Tobien (1954, 1982) also mentioned shell plates of testudinid tortoises, osteoderms of the anguine *Ophisaurus*, and metapodials of anurans. Unfortunately, the turtle material is missing, but we can add here a single tooth fragment of the alligator *Diplocynodon* and bone fragments of passeriform songbirds. Echzell represents an early Miocene, more specific a middle Orleanian fauna that can be correlated with the Mammalian Neogene unit MN4. The biostratigraphic setting is framed by taxa that have in Central Europe their last appearance datum (LAD) or first appearance datum (FAD) in MN4: *Pseudotheridomys parvulus* (LAD), *Ligerimys florancei* (LAD), *Democricetodon franconicus* (FAD), *Eumyarion weinfurteri* (FAD), *Melissiodon dominans* (LAD), *Neocometes similis* (FAD). *Anomalomys minor* (FAD) and *Gomphotherium angustidens* (FAD). Additionally, the evolutionary stage of *N. similis* is

Table 1. The Miocene small mammal fauna of Echzell.

MARSUPIALIA
Herpetotheriidae: *Amphiperatherium frequens*
LIPOTYPHLA
Erinaceidae: *Galerix* sp.
Talpidae: *Proscapanus* sp., *Mygalea antiqua*
Dimylidae: *Plesiodimylus hürzeleri*, *Chainodus intercedens*, *Lacrimodon vandermeuleni*, Dimylidae indet.
Soricidae: "*Sorex*" sp.
Heterosoricidae: *Dinosorex* sp., *Heterosorex neumeyrianus*
CHIROPTERA
Megadermatidae: *Megaderma franconica*
RODENTIA
Sciuridae: *Miopetaurist dehmi*, *Heteroxerus hürzeleri*, *Spermophilinus bredai*, *Palaeosciurus sutteri*
Gliridae: *Myoglis antecedens*, *Glirudinus undosus*, *G. gracilis*, *Glirulus diremptus*, *Peridyromys murinus*, *Bransatoglis cadeoti*, *Miodyromys aegercii*, *Microdyromys koenigswaldi*
Eomyidae: *Pseudotheridomys parvulus*, *Ligerimys florancei*, *Apeomys oldrichi*, *Megapeomys lindsayi*
Cricetidae: *Democricetodon franconicus*, *Eumyarion weinfurteri*, *Melissiodon dominans*
Platacanthomyidae: *Neocometes similis*
Anomalomyidae: *Anomalomys minor*
LAGOMORPHA
Ochotonidae: *Prolagus* sp.

very similar to the material from the MN4 locality Erkertshofen 2 (Fejfar 1999; Fejfar and Kalthoff 1999; Pineker and Mörs 2011; Steinthorsdottir et al. 2021), and the derived evolutionary stage of *Apeomys oldrichi* and *Megapeomys lindsayi* is very similar to material from the MN4 localities Dolnice 1 and Petersbuch 2 (Mörs and Flink 2018).

Material and methods

The vertebrate remains have been obtained from disintegrated volcanic tuffs by screen washing (Tobien 1954). Two fossiliferous layers, one at 2.20 m depth which yielded remains of both large and small mammals, and one at 11.0 m depth which produced the majority of the small mammals, were excavated by the Geological Department of the Hessisches Landesmuseum, Darmstadt, HLMD in September 1953 (Tobien 1954).

The fossil material has been photographed using a Hitachi S-4300 field emission scanning-electron microscope at the Swedish Museum of Natural History (Stockholm) and a Keyence VHX970 digital light microscope at the JURASSICA Museum (Porrentruy). Most photographs of fossil lizards from Echzell (except Gekkota and a parietal from Gratkorn) were taken using a Leica M205 C binocular microscope with an axially mounted DFC 290 HD camera at the Comenius University in Bratislava; software: LAS (Leica Application Suite) 4.1.0 (build 1264). For comparisons, the osteological collections of amphibians and reptiles at the JURASSICA Museum (MJSN), and specimens of extant species of chameleons deposited in the collections of the Department of Ecology, Comenius University in Bratislava, Faculty of Natural Sciences have been used.

The reconstruction of the climatic parameters follows the actualistic approach (Mörs et al. 2020). Temperature values have been reconstructed based on the climatic spaces of given reptilian taxa according to Haller-Probst (1997). The palaeoprecipitation value has been estimated using the herpetofaunistic assemblage of the locality according to Böhme et al. (2006). The ecophysiological indices for each taxon are given in Table 2. The present-day value of the nearest climatic station has been taken from Wetter und Klima – Deutscher Wetterdienst (www.dws.de). Standard anatomical orientation system is used throughout this paper, and terminology for describing individual bone structures is based on Rage and Augé (2010) and Čerňanský (2010, for acrodont lizards). For amphibians, terminology is directly indicated in the description.

This published work and the containing nomenclatural acts have been registered in ZooBank (www.zoobank.org) on https://doi.org/10.5194/fr-24-1-202 and under LSID number urn:lsid:zoobank.org:act:7A16698D-4F18-48D2-9D96-51A6E0CC15AC.

Phylogenetic analysis for the new anguine taxon

A morphological data matrix (see Suppl. material 1: Appendix S1) was developed and modified using characters taken primarily from Klembara et al. (2019). We added four characters of relevance for Anguimorpha (see Suppl. material 2: Appendix S2).

The matrix comprises 40 characters scored for 6 extant (*Ophisaurus harti*, *O. koellikerii*, *O. ventralis*, *Pseudopus apodus*, *Anguis fragilis*, *Xenosaurus grandis*) and 8 extinct (*Odaxosaurus piger*, *Ophisauriscus quadrupes*, *Ophisaurus holeci*, *Ophisaurus roqueprunensis*, *Pseudopus pannonicus*, *P. laurillardi*, *P. ahnikoviensis* and *Peltosaurus granulosus*) anguimorph taxa in addition to the new fossil anguine taxon described here. *Shinisaurus crocodilurus* was used as an outgroup taxon. The principal goal of this analysis is to understand the relationship of the new Miocene

Table 2. Overview of amphibian and reptilian faunas from MN3–MN4 sites. Each large taxonomic group is highlighted in different color. The herpetofaunistic record follows for: Wintershof West – Böhme and Ilg (2003); Ahníkov 1 (= Merkur North) – Čerňanský (2010a), Čerňanský and Bauer (2010), Čerňanský et al. (2015), Klembara et al. (2010), Villa and Delfino (2019a, b); Oberdorf – Čerňanský (2016), Čerňanský et al. (2020b), Sanchíz (1998), Szyndlar (1998), Villa and Delfino (2019a); Petersbuch 2 – Čerňanský (2011), Ivanov (2001), Klembara et al. (2010), Szyndlar and Schleich (1993), Szyndlar and Rage (2002), Szyndlar and Rage (2003), Villa and Delfino (2019a), Villa et al. (2018); Echzell – present study; Mokrá-W Q 1/2001 and Mokrá-W Q 2/ 2001 – Ivanov (2008), Ivanov et al. (2020); Dolnice – Böhme and Ilg (2003), Čerňanský (2010b), Fejfar and Roček (1986), Klembara (2015), Szyndlar (1987), Villa and Delfino (2019a); Erkertshofen 1 – Klembara et al. (2010); Beon 1 – Rage and Bailon (2005); Rembach – Klembara et al. (2010); Forsthart – Klembara et al. (2010). The ecophysiological indices for Echzell assemblage are given for each taxon as well as the calculated precipitation values and errors are calculated according to Böhme et al. (2006).

		taxon	**Wintershof West**	**Ahníkov 1 (=Merkur North)**	**Oberdorf**	**Petersbuch 2**	**Echzell**	**Mokrá-W Q 1/2001**	**Mokrá-W Q 2/2001**	**Dolnice**	**Erkertshofen 1**	**Béon 1**	**Rembach**	**Forsthart**
			MN3a	**MN 3a**	**MN4**	**MN4a**	**MN4**	**MN4**	**MN4**	**MN 4b**	**MN 4b**	**MN 4b**	**MN 4b**	**MN 4b**
Allocaudata	Albanerpetonidae	*Albanerpeton inexpectatum*	+	cf.	+	+	**0.0917**				+			
Urodela	Cryptobranchidae	*Andrias scheuchzeri*		+										
	Proteidae	*Mioproteus* sp.							+					
	Salamandridae	*Salamandrina* sp.				+								
		Chioglossa meini				+			+		+			
		Chioglossa sp.			+		**0.9768**							
		Mertensiella mera							+					
		Mertensiella sp.	+	+		+	**0.9768**		+					
		Salamandra sansaniensis	+		+	+					+			
		Salamandra sp.					**0.3918**							
		Chelotriton paradoxus	+			+								
		Chelotriton aff. *pliocaenicus*				+								
		Chelotriton sp.	+	+	+		**0.3918**				+	cf.		
		Chelotriton sp. 1						+	+					
		Chelotriton sp. 2						+	+					
		Triturus cf. *marmoratus*						+	+			+		
		Triturus ex. gr. *cristatus*							+					
		Triturus (*marmoratus* group) sp.				+								
		Lissotriton cf. *helveticus*				+						+		
		Lissotriton roehsi			+			+	+					
		Lissotriton aff. *roehsi*						+						
		Lissotriton sp.					**0.3918**							
		Triturus/Lissotriton sp.		+										
		Triturus aff. *vittatus*				+								
		Ichthyosaura alpestris												
		Ichthyosaura wintershofi	+											
Anura	Alytidae	*Latonia gigantea*								+				
		Latonia ragei	+	+	+	+								
		Latonia cf. *ragei*	+									+		
		Latonia sp.					**0.3918**							
	Palaeobatrachidae	*Palaeobatrachus robustus*					**1**							
		Palaeobatrachus sp.		+	+									
		Palaeobatrachidae sp. 1				+								
		Palaeobatrachidae sp. 2				+								
	Bufonidae	*Bufo* sp.							+					
		Bufotes (cf.) *viridis*				+					+			
	Ranidae	*Pelophylax* sync *esculenta*						+	+					
		Pelophylax sp.		+	+	+	**0.513**			+	+	+		
		Rana sp.	+				**0.3918**							+
	Pelodytidae	*Pelodytes* sp.	+	+	+						+			
	Pelobatidae	*Eopelobates* sp.	+	+						+				
		Pelobates sanchizi			+		**0.0917**	+	+					
		Pelobates sp.			+	+					+			+
		Pelobates sp. nov.				+								
	Hylidae	*Hyla* sp.			+					+				
Crocodylia		*Diplocynodon* sp.		+						+		+		
Testudines		*Ptychogaster* sp.	+			+				+	+	+		
		Ptychogaster buechelbergense		+						cf.				
		Testudo rectangularis												+
		Testudo sp.				+				+	+	+		+
		Geochelone/Ergilemys sp.				+						+		
		aff. *Clemmydopsis* sp.											+	
Serpentes	Colubridae	*Natrix longivertebrata*					+					cf.		
		Natrix merkurensis		+								aff.		

		taxon	Wintershof West	Ahníkov 1 (=Merkur North)	Oberdorf	Petersbuch 2	Echzell	Mokrá-W Q 1/2001	Mokrá-W Q 2/2001	Dolnice	Erkertshofen 1	Béon 1	Rembach	Forsthart
			MN3a	**MN 3a**	**MN4**	**MN4a**	**MN4**	**MN4**	**MN4**	**MN 4b**	**MN 4b**	**MN 4b**	**MN 4b**	**MN 4b**
Serpentes	Colubridae	*Natrix sansaniensis*		+		+						+		
		Natrix sp.						+	+					
		cf. *Neonatrix* sp.			+	+								
		Palaeonatrix lehmani				+				+		aff.		
		Neonatrix nova								+				
		Neonatrix europaea										+		
		Neonatrix natricoides										+		
		Palaeonatrix sp.			+									
		Natricinae indet.		+		+		+	+					
		Coluber caspioides		+	cf.	+								
		Coluber dolnicensis		+						+				
		Coluber pouchetii										+		
		Coluber suevicus		+										
		Coluber sp.						+	+					
		Texasophis meini										+		
		Texasophis bohemicus								+				
		Elaphe sp.		+										
		Colubrinae indet.		+			+							
		Colubrinae indet. 1						+	+					
		Colubrinae indet.	+						+					
		Colubrinae indet. A			+									
		Colubrinae indet. B			+									
		Colubridae indet.		+				+	+					
		Colubroidea indet.					+							
	Viperidae	*Vipera antiqua*				+				+				
		Vipera platyspondyla				+				+				
		Vipera aspis complex										+		
		Daboia/oriental *Vipera* complex										+		
		Viper sp.		+	+				+					
		Viperidae indet.						+	+					
		Viperinae indet.						+	+					
	Elapidae	*Naja romani*				+								
		Naja cf. *romani*					+							
		Micrurus gallicus				+						+		
		Elapidae indet.		+				+				+		
		Elapidae/Natricinae indet.			+									
	Boidae	*Bavarioboa hermi*				+		+		+				
		Bavarioboa cf. *hermi*					**0.0917**	+						
		Bavarioboa sp.		+										
		cf. *Bavarioboa* sp.			+									
		Pyton europaeus										+		
		Pyton sp.						+						
		Falseryx petersbuchi				+								
		Bransateryx septentrionalis				+				+				
		Bransateryx sp.												
		Scolecophidia indet.										+		
	Aniliidae	*Eoanilus* sp.				+								
		Serpentes indet.	+	+										
Iguania	Chamaeleonidae	*Chamaeleo* sp.				+							+	
		Chamaeleo andrusovi					**0.0917**			+				
		Chamaeleo caroliquarti	+							+	+			
		Chamaeleonidae indet.		+	?	+	+							
Gekkota	Gekkonidae	*Euleptes gallica*		+										
		Gekkota indet.	+	+	+		**0.0917**					+	+	
Amphisbaenia	Blanidae	*Blanus* sp.								+			+	
		Blanus thomaskelleri		+										
	Amphisbaenidae	Amphisbaenidae indet.									+	+		
		Amphisbaenia indet.							+					
Lacertiformata	Lacertidae	*Lacerta* cf. *L. poncenatensis*			+									
		Lacerta ex. gr. *L. viridis*								+				
		Lacerta sp.		+	+	+				+	+		+	
		Lacerta sp. 1	+											+
		Lacerta sp. 2	+											+
		Miolacerta tenuis								+				
		Miolacerta sp.				+							+	
		Janoskia sp.				+								
		Ambyolacerta dolnicensis								+				

		taxon	Wintershof West	Ahníkov 1 (=Merkur North)	Oberdorf	Petersbuch 2	Echzell	Mokrá-W Q 1/2001	Mokrá-W Q 2/2001	Dolnice	Erkertshofen 1	Béon 1	Rembach	Forsthart
			MN3a	MN 3a	MN4	MN4a	MN4	MN4	MN4	MN 4b	MN 4b	MN 4b	MN 4b	MN 4b
Lacertiformata	Lacertidae	*Ambyolacerta* sp.									+			
		Lacertidae indet.		+	+		**0**	+	+	+		+		+
		Lacertidae indet. 1										+		
		Lacertidae indet. 2										+		
		Lacertoidea indet.							+					
Scinciformata	Scincidae	*Eumeces* sp.									+			
		Bavariascincus mabuyaformis				+							+	+
		Chalcides augei			+									
		cf. *Chalcides* sp.					**0**							
		Scincidae indet.				+	+			+	+			
	Cordylidae	*Palaeocodylus bohemicus*								+				
		aff. *Palaeocodylus bohemicus*		+										
		Cordylidae indet.		?	+	+								
		Scincoidea indet.			+				+					
Anguimorpha	Varanidae	*Varanus mokrensis*						+	+					
		Varanus hofmanni				+								
		Varanus sp.									+	+		
		cf. *Varanus* sp.				+								
	Shinisauridae	*Merkurosaurus ornatus*		+										
		Shinisauridae indet.	+											
	Anguidae	*Pseudopus laurillardi*				+		+	+		+	+		
		Pseudopus confertus		+										
		Pseudopus ahnikoviensis		+						+				
		Pseudopus sp.	+					+	+	+			+	+
		Smithosaurus echzellensis					+							
		Anguis sp.								+				
		Ophisaurus fejfari				+				+				
		Ophisaurus cf. *O. fejfari*	+											
		Ophisaurus spinari		+						+				
		Ophisaurus cf. *O. spinari*			+									
		Ophisaurus robustus								+				
		Ophisaurus aff. *O. robustus*									+			
		Ophisaurus holeci		+						+				
		Ophisaurus sp.		+	+	+		+		+		+		+
		Ophisaurus sp. 1		+						+			+	
		Ophisaurus sp. 2		+						+			+	
		Anguinae indet.					+	+	+					
		Anguidae indet.			+	+	+						+	
		Squamata indet.					+							
		Squamata indet. 1			+									
		Squamata indet. 2			+									
		Squamata indet. 3			+									
		average ecophysiological index					0.344							
		MAP					791							
		recent MAP (in mm)					630							
		95 % prediction interval - error (in mm)					254							
		(near) city/town of the value or recent MAP					Frankfurt a. M.							
		MAP/MAPrecent (in %)					125.5036157							

taxon described here among Anguinae. The data matrix was analysed using maximum parsimony as an optimality criterion in the program TNT and the NT (New Technology) search (with ratchet) and 1000 iterations (Goloboff et al. 2008). All characters were treated as unordered and were equally weighted. Support was estimated through Bremer support indices (Bremer 1994). Mesquite v.2.75 was used to visualize all trees (build 566; Maddison and Maddison, D. R. et al. 2011). In the second analysis, the heuristic traditional search in TNT was also used to observe and compare the potential results.

Systematic Paleontology

Lissamphibia Haeckel, 1866
Allocaudata Fox & Naylor, 1982
Albanerpetontidae Fox & Naylor, 1982
***Albanerpeton* Estes & Hoffstetter, 1976**

Albanerpeton inexpectatum Estes & Hoffstetter, 1976

Fig. 2

Material and horizon. One frontal HLMD-Ez 2004, four praemaxillae HLMD-Ez 2005–2008, nine maxillae

HLMD-Ez 2009–2016, ten dentaries HLMD-Ez 2017–2027, one vertebra HLMD-Ez 2028.

Description. Frontal: Frontal is partly preserved. It is triangular in shape and as wide as long (Fig. 2A). The entire preserved dorsal surface of the bone is covered by moderately deep polygonal pits limited from each other by rather low ridges. The anterolateral processes are missing. The anteriorly-projecting internasal is rather narrow and elongated. In ventral view, its spike-like outline is more evident (Fig. 2B). Only the anteromedial slot is preserved. It is long, low and not deep. In ventral view, the ventrolateral crest is broad, concave and in transverse view, triangular in outline. It starts at the base of the preserved portion of the anterolateral process and projects posterolaterally, reaching the posterior lateral tips of the frontal. The crest becomes thinner laterally. The ventral surface of the frontal, between the posterolateral crests, is flat.

Praemaxilla: Available four praemaxillae show different preservation and are not fused. The medial surface of the bone, where two praemaxillae connect with each other, possesses grooves and flanges (Fig. 2G). The width of the bone, measured along the tooth row, ranges from 1–1.5 mm. The pars dorsalis is elongated and long. In lateral view, it is curved. The laterodorsal notch is weakly developed. The pars dorsalis at its middle part extends slightly laterally, which in large-sized bones is stronger developed than in the small-sized ones. The labial surface of the bone is covered by different structures (Fig. 2C, F). The ventral portion, corresponding to the pars dentalis, is nearly smooth. The middle part of the surface, making the most of the pars dorsalis, is pierced by nutrition foramina. The tip of the pars dorsalis possesses the boss. Pustular structures and polygonal-shaped pits cover it. In labial view, the maxillary process of praemaxilla projects laterally behind the pars dorsalis. In lingual view, the well-developed suprapalatal pit at the medial base of the pars dorsalis is present (Fig. 2D, H). It has an elongate outline and reopens ventrally as a palatal foramen in the ventral surface of the pars palatinum. In medial view, the pars palatinum is curved. Distinct vomerine and maxillary processes are visible on the pars palatinum. The maxillary process is stronger developed than the vomerine one. Six to seven pleurodont teeth are attached to the pars dentalis.

Maxilla: In total, eight maxillae with different preservation are available. The pars dentalis in most well-preserved specimens possesses 13–14 teeth or tooth bases. In lingual view, the pars dentalis is high anteriorly and reduces in height posteriorly (Fig. 2J, M, P). The pars palatinum is well-developed and curved. In the middle part of the bone, it reaches its most width. The anterior tip of the pars palatinum extends anteromedially and forms a distinct process (Fig. 2J, P). The premaxillary process is well developed (Fig. 2M, P). The distinct nasal process projects anterodorsally (Fig. 2J, M). Both the dorsal and labial surfaces of the maxillae are pierced by short rows of up to three nutrition foramina, which are limited to the area around the nasal process (Fig. 2N, L, Q).

Dentary: All eleven dentaries are only partially preserved. No dentary with a fully preserved tooth row (pars dentalis) is available in the material to count the tooth number. The teeth reduce in height posteriorly. The Meckelian groove is closed and form a canal. The dental shelf is moderately broad, and its lingual margin is angular (Fig. 2R, V). The symphyseal articulation surfaces are flat and vertical. Lingually, it possesses two distinct prongs (Fig. 2R, S). The dorsal prong is long and oriented anterodorsally. The ventral one is smaller and anteroventrally oriented. The ventral prong and the main symphyseal surface are separated with a moderately deep depression, which is pierced by the anterior opening of the Meckelian groove. The latter opens posteriorly with two large ventral and small dorsal (“opening for an unnamed canal” sensu Szentesi et al. (2015); fig. 8) openings. Taking into account the “natural” cross-sections of the bones (Fig. 2U, X, Z), the split of the Meckelian canal into two branches already at the sixth tooth position can be stated. The small dorsal branch runs below the tooth row, whereas the large ventral one is enclosed in the ventral portion of the bone. The labial surface of the dentary is smooth. A row of labial foramina of different sizes is arranged along the midline of the dentary (Fig. 2T, W, Y).

Dentition: The teeth on premaxillae, maxillae. and dentary have similar morphology. All teeth are pleurodont and closely located. The tip of teeth is tricuspid with a main central large cuspid and two lateral small cuspids, which are sometimes nearly absent. The tooth pedicles are compressed anterodorsally. The tooth tip is round in cross-section. They reduce in size posteriorly.

Remarks. The fossil remains can be assigned to the genus *Albanerpeton* considering the presence of the following autapomorphies (Venczel and Gardner 2005): 1) dorsal/ventral outlines of fused frontals are triangular (Character state 21(1) in Venczel and Gardner (2005)); 2) ratio of midline length of fused frontals to the width across posterior edge of bone, between lateral edge of the ventrolateral crest, is as wide as long (1:1) (Character state 22(1) in Venczel and Gardner (2005)); 3) path followed by canal through pars palatinum in praemaxillae, between dorsal and ventral openings of palatal foramen, is vertical (Character 27(1) in Venczel and Gardner (2005)). Among the species of the genus, two apomorphies of *A. inexpectatum* are such as; 1) the pustular ornament pattern of labial surface of premaxillary (Character 8(1) in Venczel and Gardner (2005)) and 2) form of ventrolateral crest on large, fused frontals wide and triangular in transverse view, with strongly concave ventral surface (Character 24(2) in Venczel and Gardner (2005)). Further, two character states [16(1), 17(1)] of Venczel and Gardner (2005) cannot be observed due to poor preservation of the material. The Echzell remains can be clearly distinguished from the second available European Tertiary albanerpetontid species *Albanerpeton pannonicum* by: 1) lack of

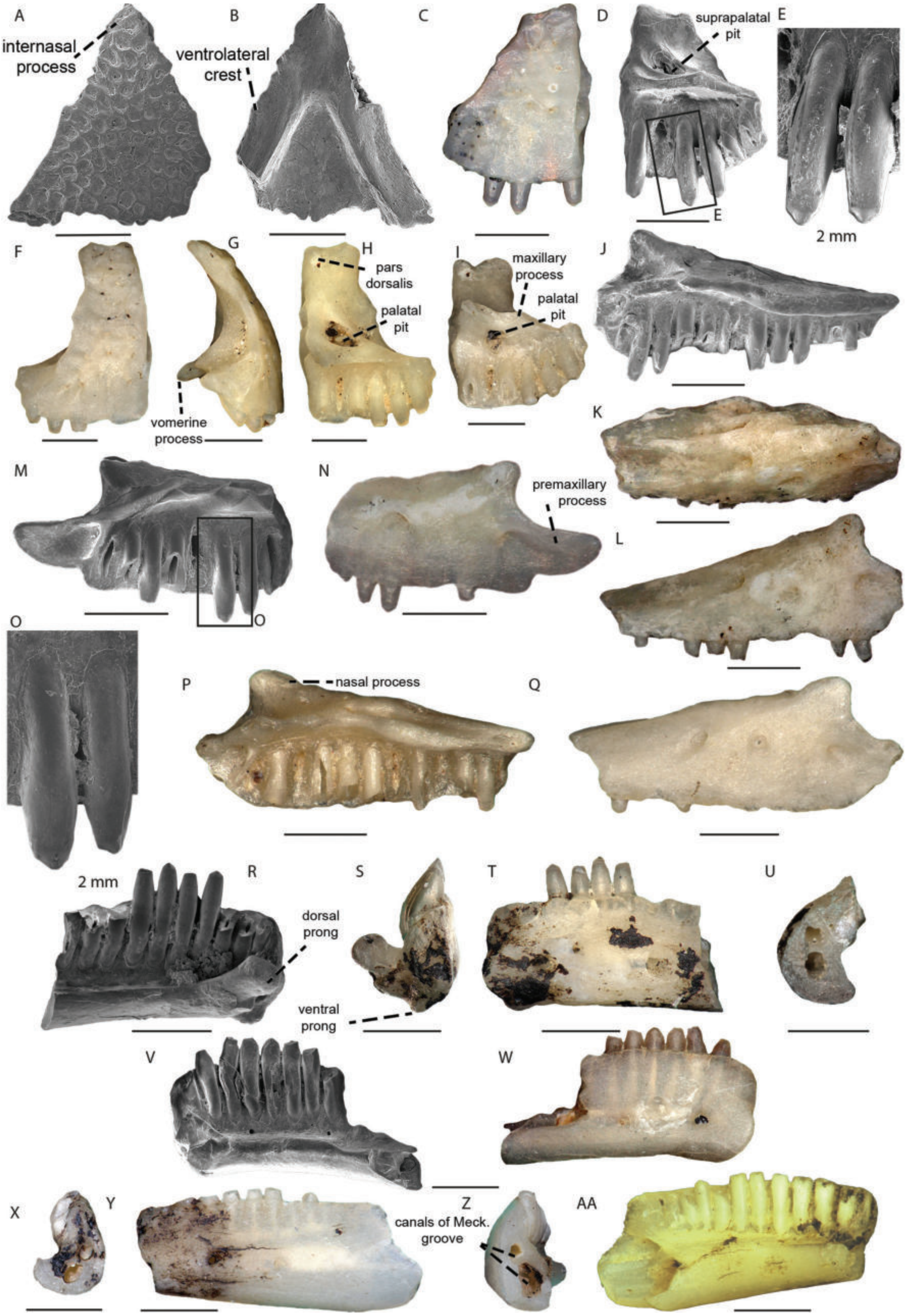

Figure 2. *Albanerpeton inexpectatum* from the Echzell locality. Frontal (**A, B.** HLMD-Ez 2004). Premaxillae (**C–E.** HLMD-Ez 2161; **F–I.** HLMD-Ez 2005). Maxillae (**J–L.** HLMD-Ez 2009; **M–O.** HLMD-Ez 2010; **P, Q.** HLMD-Ez 2012). The bones are figured in (**A, K**) dorsal, (**B**) ventral, (**C, F, L, N, Q, T, W, Y**) labial, (**D, E, H, J, M, O, P, R, V, AA**) lingual, (**I**) ventroposterior, (**S, X**) medial, (**G, U, Z**) posterior views. Where not indicated, the scale bar equals 5 mm.

the ventromedial keel on frontals (vs. present in *A. pannonicum*); 2) labial pustulate ornament on premaxilla is not restricted to the boss but also cover the surface of the bone ventrally from the boss. The presence of boss on praemaxilla has been suggested as a characteristic for *A. pannonicum* and should be absent in *A. inexpectatum* (e.g., Venczel and Gardner 2005; Szentesi et al. 2015). The structures on the dorsolabial surface of the pars dorsalis on the studied material is interpreted as boss and most probably, suggesting the character to be shared between two species.

Urodela Dumériel, 1806
Caudata Scopoli, 1777
Salamandridae Goldfuss, 1820
Mertensiella Wolterstorff, 1925

Mertensiella sp.

Fig. 3A–G

Material. Five trunk vertebrae, HLMD-Ez 2039–2041.

Description. The vertebrae are elongated and have opistocoelous centra (Fig. 3B, C). The pre- and postzygapophyses are elliptical and extended anteriorly. The condyle is rounded and has a clear constriction at its base. The cotyle is larger in diameter than the condyle. The neural arch is moderately high. In anterior view, the neural canal is slightly dorsoventrally flattened. The neural spine is high (observable in the rather well-preserved specimen (Fig. 3B)). The anterior tip of the neural spine is located behind the posterior margin of the prezygapophyses. Posteriorly the neural spine does not reach the posterior margin of the pterygapophysis. The zygapophyseal crest is absent (four vertebrae) or extremely poorly developed. The transverse processes are poorly preserved; however, distinct dia- and parapophysis can be observed (Fig. 3B, C). The anterior and posterior alar processes (anterior and posterior ventral crests sensu Venczel and Hír (2013)) connecting the parapophysis with the centrum are rather well developed.

Remarks. See the remarks in *Chioglossa* sp.

Chioglossa Bocage, 1864

Chioglossa sp.

Fig. 3H–I

Material. Ten trunk vertebrae, HLMD-Ez 2042–2045.

Description and remarks. The vertebra morphology is nearly identical to *Mertensiella* sp. The following differences from it can be observed on the available material: 1) the lack or extremely poor development of the posterior alar process (vs. rather well-developed in *Mertensiella*); 2) the anterior zygapophyseal crest is well developed (vs. absent in *Mertensiella*) (Sanchíz and Młynarski 1979; Hodrová 1984; Ivanov 2008). The orientation of the dia- and parapophysis, the shape of the pterygapophyses have been mentioned as further characters allowing to distinguish these two genera (Hodrová 1984; Sanchíz 1998). However, due to poor preservation of the material, neither these characters can be evaluated nor any further identification at the species level can be done.

Lissotriton Bell, 1839

Lissotriton sp.

Fig. 4

Material. Six vertebrae, HLMD-Ez 2047–2050.

Description. The preserved small-sized trunk vertebrae have opistocoelous centra measuring up to 2 mm in length. The condyle is shorter and slightly smaller than the cotyle. The pericondylar constriction is well pronounced. The anteriorly oriented prezygapophyses have an oval outline. In dorsal view, the neural arch has a weakly-pronounced sandglass shape, where the narrowest part is located behind the prezygapophyses. The posterior margin of the neural arch is either flat or slightly bifurcated. The posterior notch is well preserved and visible on HLMD-Ez 2047 (Fig. 4E). The neural spine starts behind the anterior margin of the neural arch and reaches the posterior tip of the latter (Fig. 4B, G). The neural spine is always missing; however, where it is preserved, no ornamentation can be observed on it, and its rather large height can be suggested. The pre- and postzygapophyses are connected by a well-pronounced (nearly) horizontal interzygapophyseal crest, which covers slightly the proximal part of the transverse process (Fig. 4B). The transverse process is composed of the dia- and parapophysis, which in turn are connected by an osseous lamina along their length. In ventral view, the anterior and poster processes form a distinct ventral lamina of triangular to irregular rhomboidal shape (Fig. 4C, H). It is pierced by two smaller subcentral foramina near the center of the vertebra centrum. The anterior alar process is larger than the posterior one. The opening of the spinal nerve is visible behind the transverse process at the base of the neural arch. In anterior view, the neural canal is large (larger than the diameter of the condyle) and has a round or slightly expressed pentagonal outline (Fig. 4D, I). In posterior view, the neural canal is also large and has a round or slightly elliptical outline (Fig. 4E, J).

Remarks. The remains can be clearly assigned to the genus *Lissotriton* considering their small sizes; the lack of the dorsal widening or any structures on the neural spine; the presence of a well-pronounced rhomboid/triangular ventral lamina on the vertebral centrum (Ivanov 2008; Georgalis et al. 2019). On the one hand, poor and partial preservation of vertebrae and, on the other hand, not adequate knowledge of the osteology of the *Lissotriton* genus does not allow any further allocation at species or species group levels.

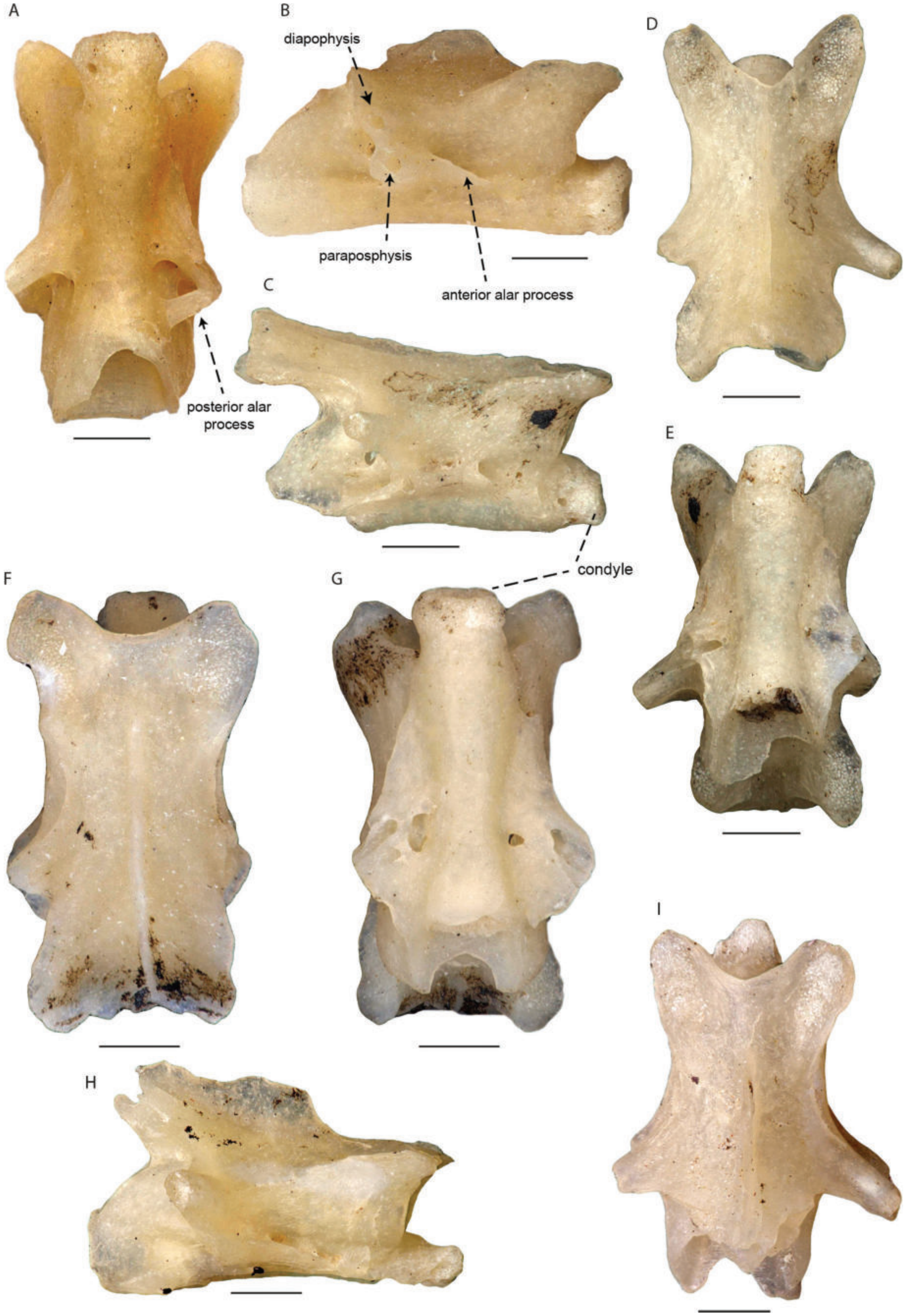

Figure 3. Vertebrae of *Chioglossa* sp. (**A, B.** HLMD-Ez 2042; **C, D.** HLMD-Ez 2043; **F, G.** HLMD-Ez 2044; **E.** HLMD-Ez 2043) and *Mertensiella* sp. (**H, I.** HLDM-Ez 2039) from the Echzell locality in (**A, C, E, H**) dorsal, (**B, D, F**) lateral and (**D, G, I**) ventral views. Scale bars: 0.5 mm.

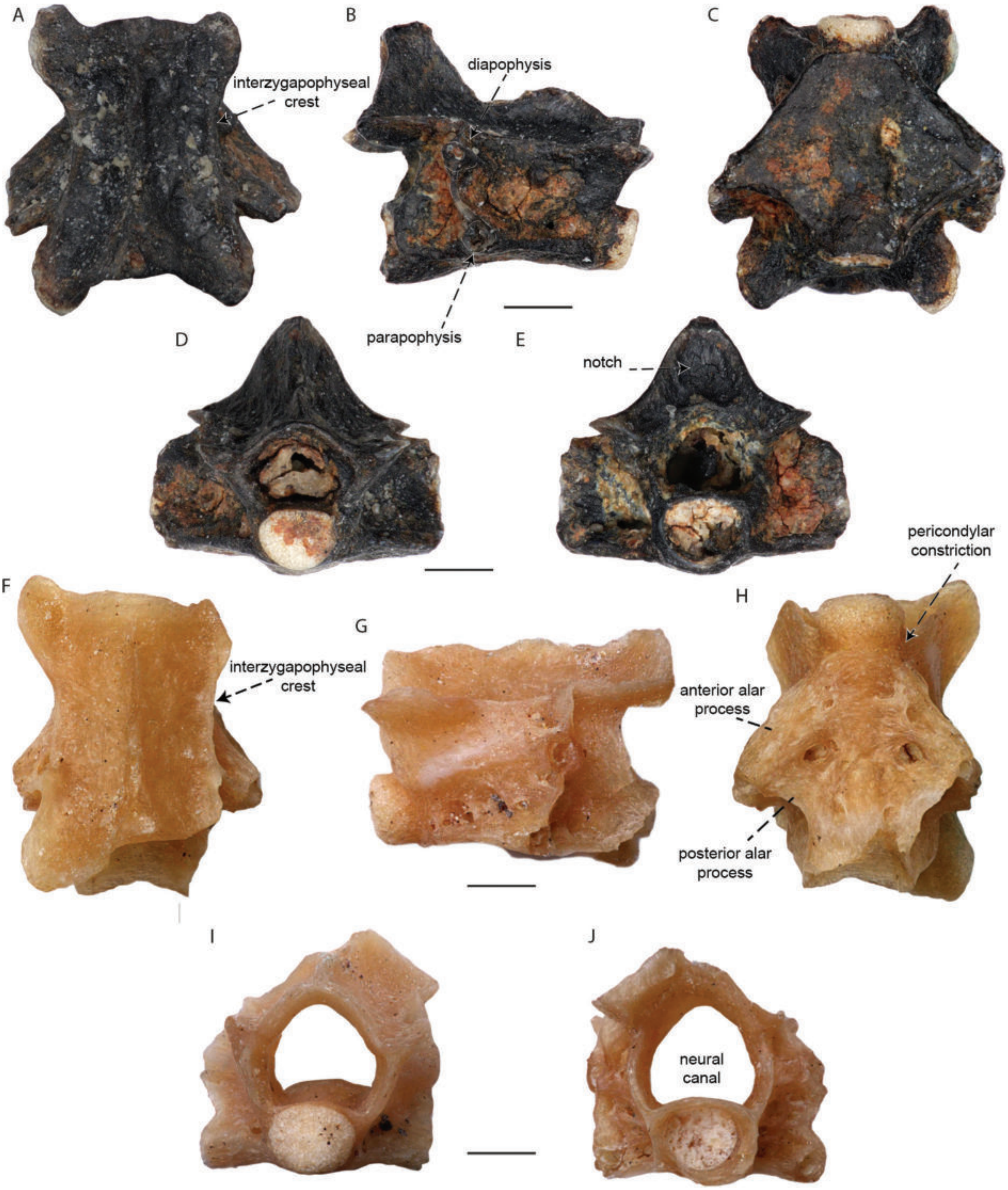

Figure 4. Vertebrae of *Lissotriton* sp. (**A–E.** HLDM-Ez 2047; **F–J.** HLDM-Ez 2048) from the Echzell locality in (**A, F**) dorsal, (**B, G**) lateral, (**C, H**) ventral, (**D, I**) anterior and (**E, J**) posterior views. Scale bars: 0.5 mm.

Salamandra Garsault et al., 1764

Salamandra sp.

Fig. 5A–F

Material. Five trunk vertebrae, HLMD-Ez 2029–2033.

Description. The vertebrae are opistocoelous and dorsoventrally flattened. They are large in size (5–7 mm). In dorsal view, the neural arch is broad and has an outline of a rectangle (HLMD-Ez 2029, Fig. 5A) or square (HLMD-Ez 2031, Fig. 5F). The prezygapophyses have round outlines and project anterolaterally. The neural arch between the prezygapophysese is flat. The neural spine starts behind this short flat surface and posteriorly does not reach the posterior tip of the pterygapophysis. In lateral view, the neural spine is low. It is highest at its middle point. The posterior margin of the pterygapophysis can be bifurcated. Its posterior surface possesses two distinct notches of variable sizes and dimensions. In anterior view, the neural canal is dorsoventrally flattened. In HLMD-Ez 2029, the bases of the prezygapophyses are pierced by the subzygapophyseal (sensu Vasilyan et al. 2017) or anterior (sensu Tissier et al. 2015) foramen. Other vertebrae do not have this character. The arterial canal with large and/or smaller openings runs across the base of the transverse process. The latter is fully preserved only in HLMD-Ez 2029. It projects posterolaterally and is composed of dia- and parapophysis, which are connected with a thin lamina at their medial half (Fig. 5B); otherwise, they are free laterally. Additionally, the parapophysis is connected with the centrum anteriorly and posteriorly by anterior and posterior alar processes, respectively. They build a triangular-shaped lamina (Fig. 5C). In lateral view, a well-pronounced horizontal interzygapophyseal ridge connects the prezygapophysis with diapophysis, whereas the horizontal dorsal lamina connects the diapophysis with postzygapophysis. The centrum is flattened dorsoventrally and arched.

Remark. The general morphology and large size of remains, including the dorsoventrally compressed ophistocoelous vertebrae, broad and low neural arch as well as arched vertebra centrum allow assigning the remains to the genus *Salamandra* (Estes and Hoffstetter 1976). HLMD-Ez 2029 shows a slightly different morphology (presence of subprezygaphyseal foramen vs. its lack; square outline of the vertebra in dorsal view vs. rectangular outline) than the other available vertebrate. Comparable morphology is observable in the second vertebrae of *Salamandra salamandra* (see the morphosource link https://www.morphosource.org/concern/parent/000S44906/media/000165871). Thus, the HLMD-Ez 2029 can interpreted as an anterior vertebra.

Chelotriton Pomel, 1853

Chelotriton sp.

Figs 5G–6M

Material. Four frontals HLMD-Ez 2070–2073, four prefrontals HLMD-Ez 2068–2069, one nasal HLMD-Ez 2058, seven maxillae HLMD-Ez 2063–2065, two squamosals HLMD-Ez 2066–2067, one dentary HLMD-Ez 2057, five trunk vertebrae HLMD-Ez 2059–2061, ten ribs HLMD-Ez 2053–2056.

Description. Frontal: All four frontals are fragmentarily preserved. They represent individuals of different sizes. The frontal is widest at its most complete posterior portion. Its dorsal surface is covered by dermal ornamentation (Fig. 5G, I, K). The bone is slightly bent along its midline between the fronto-squamosal arch (sensu Ivanov 2008) and the rest of the bone. The fronto-squamosal arch projects posteriorly behind the main part of the bone. In ventral view, the partes contactae are reduced and run parallel along the anteroposterior axis of the bone. The braincase roof, located medially from the pars contacta, is delimited by a low crest of a semilunar outline (Fig. 5H, J, L).

Prefrontal: The prefrontals are wing-shaped bones, anteriorly broad and posteriorly narrowing to a sharp tip (Fig. 5M–N). The lateral margin (margo orbitalis) of the bone forms the anterodorsal wall of the orbit. The anterior corner of the margo orbitalis is pierced by the foramina of the V nerve. In ventral view, the ventral vertical wall separates the margo orbitalis from the rest of the bone. The articulation surface with the frontal bone, located at the posterolateral margin of the bone, is massive and more strongly developed than any other margin of the bone.

Nasal: The nasal bone has a nearly rectangular outline (Fig. 5O–P). All its margins are flat, without any concave outlines. Its dorsal surface is slightly rounded and possesses dermal ornamentation. In ventral view, parallel to the medial margin of the bone a ridge for articulation with the premaxillae is present.

Maxilla: only the posterior portions of the bone without dentition are present in the material. In dorsal view, the bone is narrow and a thin-walled horizontal pterygoid process projects lingually (Fig. 5S, U). In lateral view, the bone surface is covered by dermal ornamentation made of a dense network of small pits and pustules. Posteriorly the bone increase in height. In lingual view, the bone surface is smooth (Fig. 5R, T). The articulation surface with the quadratojugal bone is located on the posterodorsal surface of the bone. The size and dimensions of the articulation surface vary among available maxillae.

Squamosal: Two squamosals are partially preserved. In dorsal view, the HLMD-Ez 2066 is nearly semilunar in outline (Fig. 5V). The frontal process is curved slightly medially and possesses a vertical and almost flat articulation surface with the frontal. The lateral margin of the bone is rounded. The dorsal surface of the bone is somewhat horizontal and is covered by dermal ornamentation similar to other skull bones. The parietal process (in HLMD-Ez 2067, Fig. 5X) has a horizontal surface. It is slightly shorter but broader than the frontal process. In ventral view, a medioposteriorly oriented ridge, corresponding to the base of the ventral process of the bone, is visible. Posteriorly from the ridge, the bone surface is moderately concave.

Dentary: The fragmentary-preserved dentary is 1.7 mm in height. In lingual view, it shows a very low dental shelf with traces of the tooth pedicles. The preserved portion of the Meckelian groove is narrow and rather shallow (Fig. 5Z). Another but smaller groove is observable below the posterior half of the Meckelian groove, resembling most probably the articulation surface with the coronoid. In lateral view, the dentary is heavily ornamented by pits and pustules (Fig. 5Y). A remarkable concave surface separates the portion of the dental shelf from the rest of the bone.

Trunk vertebrae: the vertebrae are robust. The opistocoelous vertebra centrum is massive and slightly dorsoventrally flattened. The neural crest is nearly as high as the vertebra centrum (Fig. 6B, I). In dorsal view, its dorsal surface possesses a flat and (elongate) triangular

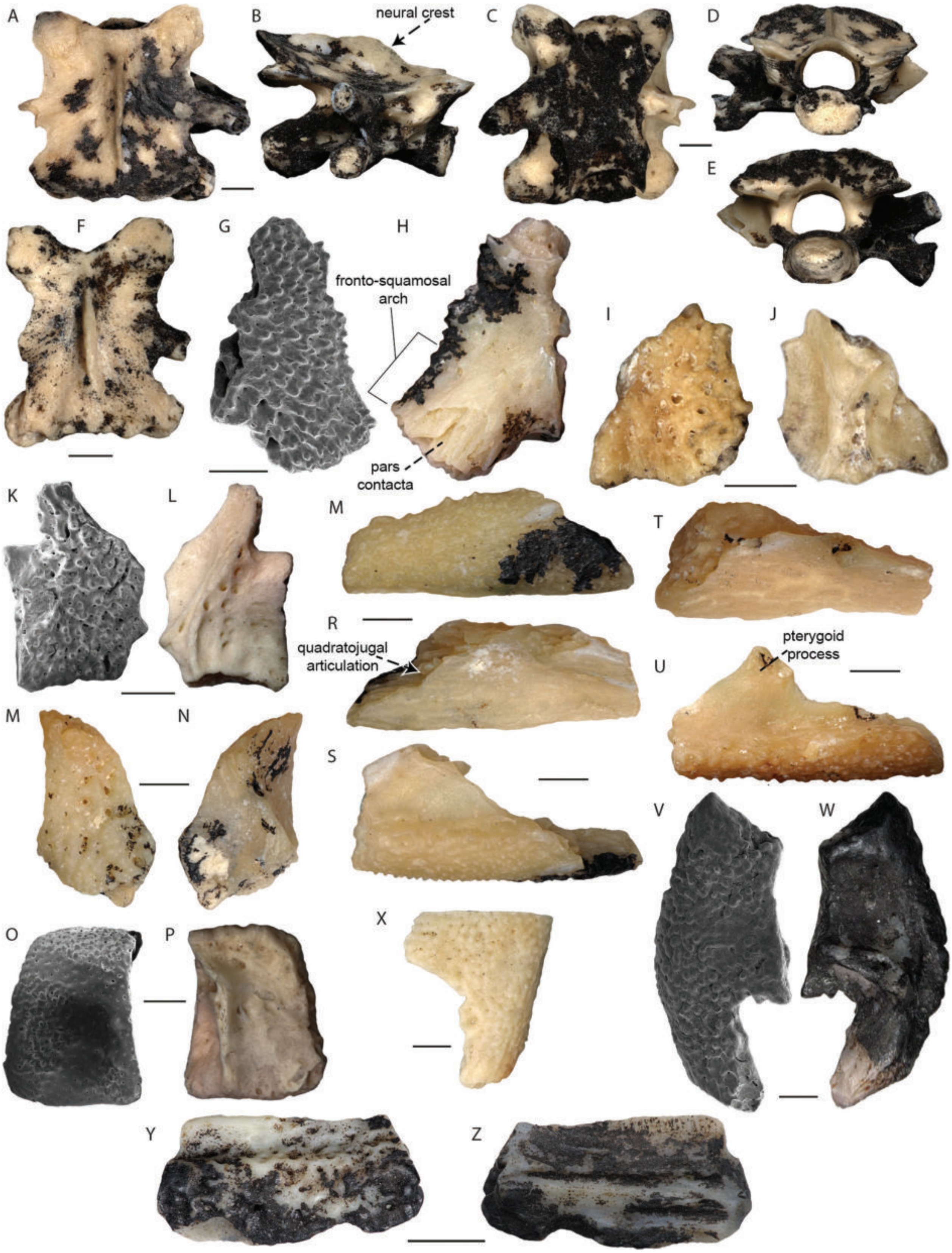

Figure 5. Vertebrae of *Salamandra* sp. (**A–E.** HLDM-Ez 2029; **F.** HLDM-Ez 2031) and (**G–Z**) cranial bones of *Chelotriton* sp. from the Echzell, including frontals (**G, H.** HLDM-Ez 2070; **I–J.** HLDM-Ez 2071; **K, L.** HLDM-Ez 2072), prefrontal (**M, N.** HLDM-Ez 2068), nasal (**O, P.** HLDM-Ez 2058), maxillae (**Q–S.** HLDM-Ez 2063; **T–U.** HLDM-Ez 2064), squamosals (**X.** HLDM-Ez 2067; **V, W.** HLDM-Ez 2066) and dentary (**Y, Z.** HLDM-Ez 2057). The bones are figures in dorsal (**A, F, G, I, K, M, O, S, X, V**) dorsal, (**B**) lateral, (**C, H, J, L, N, P, W**) ventral, (**D**) anterior, (**E**) posterior, (**Q, Y**) labial and (**R, T, Z**) lingual views. Scale bars: 1 mm.

Figure 6. Vertebrae (**A–E.** HLDM-Ez 2059; **F–J.** HLDM-Ez 2060) and ribs (**K.** HLDM-Ez 2054; **L.** HLDM-Ez 2053; **M.** HLDM-Ez 2055) of *Chelotriton* sp. Frontal (**N, O.** HLDM-Ez 2038) and ribs (**P, Q.** HLDM-Ez 2036; **R, S.** HLDM-Ez 2037) remains of Salamandridae indet. from Echzell. Bones in (**A, H, N**) dorsal, (**B, I**) lateral, (**C, J, O**) ventral, (**D, F**) anterior, (**E, G**) posterior, (**K, L, M, P, S**) posterior/anterior and (**Q, R**) medial views. Scale bars: 1 mm.

in outline plate, which is covered by a dermal ornamentation made of deep pits and low pustules (Fig. 5A, H). This place can be well developed and projects over the neural arch. Anteriorly, the neural crest does not reach the anterior tip of the neural arch (Fig. 6D, F). The pre- and postzygapophyses are round or elongated and project (latero-)anteriorly. The neural arch between the anterior half of the prezygapophyses has a smooth and convex surface. In anterior view, the neural canal is rounded or nearly triangular in outline (Fig. 6F). The condyle has a dorsoventrally flattened oval shape.

Small subprezygapophyseal foramina (sensu Vasilyan et al. 2017) can be present at the basis of the prezygapophyses. In lateral view, the transverse process is connected with the postzygapophysis by a clearly visible dorsal lamina (Fig. 6B, I). The posterior alar process connecting the parapophysis with the cotyle is smaller than the dorsal lamina. The prezygapophysis is connected with the parapophysis by a well-developed accessory alar process. A very thin anterior alar process connects the base of the prezygapophysis with the parapophysis of the transverse process. In ventral view, rather large-sized subcentral foramina and rather smaller foramina are visible on the ventral surface of vertebrae. The transverse process consists of para- and diapophysis, which, though located close to each other, are separated by a thin lamina (Fig. 6B). In posterior view, the pterygapophysis possesses two distinct notches.

Ribs: All ribs are fragmentarily preserved. The articulation joints with the transverse process of the vertebrae are bicapitate. Both articulation heads are rounded and connected with a thin bone lamina (HLMD-Ez 2053, Fig. 6L). The dorsal surface of all ribs possesses two (HLMD-Ez 2054, Fig. 6K) to five (HLMD-Ez 2055, Fig. 6M) spines of different sizes and orientations.

Remarks. Based on the combination of the following characters, the described fossil remains can be attributed to the genus *Chelotriton*, broadly known from the Cenozoic deposits of Europe: 1) the presence of the characteristic dorsal ornamentation on skull bones and the horizontal plate of the neural spine of vertebrae; 2) the pterygoid process of the maxillae connected with the pterygoid; 3) the presence of spines on the ribs and 4) general morphology and dimensions of the bones (Ivanov 2008; Schoch et al. 2015; Vasilyan 2020). The remains cannot be clearly assigned to any known species of the genus due to the lack of a comprehensive understanding of the taxonomic diversity within the *Chelotriton* genus. However, some comparative remarks can be given below. The described skull bones differ significantly from all so far known *Chelotriton* records. For example, the frontal shows an intermediate morphology observable in *Chelotriton* sp 1. and sp. 2 from Mokrá-Western Quarry, Czech Republic, early Miocene (Ivanov 2008) and *Chelotriton paradoxus* from the Enspel Maar, Germany, late Oligocene, and Randecker Maar, Germany, early Miocene (Schoch et al. 2015). The shape of the squamosal in the Echzell material can be found only in *Chelotriton* sp. from Orsberg, Germany, late Oligocene (Marjanović and Witzmann 2015), where a bone of a similar shape is named as a quadratojugal-quadrate bone. The nasal from Echzell (nearly rectangular in outline) can be clearly distinguished from that of all known forms in which the form varies from irregular-shaped one (e.g. in *Chelotriton paradoxus* from Enspel, Roček and Wuttke 2010) to trapezoid-shaped in *Chelotriton* sp. form Orsberg (Marjanović and Witzmann 2015). Most probable, the suggested high variability of the skull bone (Schoch et al. 2015) can be explained by uncovered high specific diversity of *Chelotriton*. Thus, at this stage of knowledge, we describe the fossil remains of *Chelotriton* with an open nomenclature.

Salamandridae indet.

Fig. 6N–S

Material. One frontal, HLMD-Ez 2038, seven trunk vertebrae, HLMD-Ez 2034, 20 caudal vertebrae, HLMD-Ez 2035, nine vertebrae, HLMD-Ez 2051, 2052, 2062, two ribs HLMD-Ez 2036, HLMD-Ez 2037, two extremity bones HLMD-Ez 2052.

Description and remarks. A single frontal, with a length of 6 mm, displays a flat dorsal surface (Fig. 6N). In dorsal view, the most anterior portion of the bone possesses an articulation facet with the parietal that is covered by parallel to each other ridges. Comparison with recent similar-sized species shows most similarities with *Salamandra salamandra* (MJSN-OS 806). However, due to the lack of comprehensive studies of the skull bones among salamandrids, an allocation of the bone to the family Salamandridae is more appropriate.

The vertebrae are poorly preserved. They show ophistocoelous morphology partially with complex structures of haemal and neural processes, characteristic of the caudal region of the vertebral column (Duellman and Trueb 1994). On the one hand, the poor preservation and, on the other hand, the poor knowledge on osteological differences of the caudal region in *Chelotriton* and *Salamandra* genera (both present in the fossil locality) make it at the moment impossible to identify the vertebrae correctly.

Nine small-sized opistocoelous vertebrae are available in the material. They have variable preservation; however, a large number of structures/characters are missing for further identification. Considering the vertebra sizes as well as available similar-sized salamander taxa present in the material, most probably, they represent remains of *Lissotriton*, *Mertensiella* or *Chioglossa*. The juvenile and most distal caudal vertebra of *Salamandra* and *Chelotriton* can be excluded because in the former form the juvenile vertebrae are not fully ossified, whereas in the latter the dorsal tip of the neural crest possesses a ornamented surface, which is missing here.

Two bicapitate rips are present (Fig. 6P–S). Their lateral portion does not possess any process, which allows to exclude them from *Chelotriton*. Most probable, they should belong to the genus *Salamandra*, which has a similar rib morphology and is represented in the material by large-sized individuals as well.

Anura Fischer, 1813
Pelobatidae Bonaparte, 1850
Pelobates Wagler, 1830

Pelobates sanchizi Venczel, 2004

Fig. 7

Material. Four frontoparietals HLMD-Ez 2107–2110, 13 squamosals HLMD-Ez 2104–2106, one premaxilla HLMD-Ez 2098, 48 maxillae HLMD-Ez 2095–2097, 38 fragments of skull bones HLMD-Ez 2103, three presacral HLMD-Ez 2098, 2099, 2102 and two sacral vertebrae HLMD-Ez 2100, 2101, 11 ilia HLMD-Ez 2111–2115.

Description. Frontoparietals: Fragmentarily preserved remains are covered dorsally with the characteristic pit-and-ridge style sculpture as well as low spines (Fig. 7A, H). The tectum supraorbitale is moderately broad. In dorsal view, the lateral superior process is longer than broad. The articulation surface with the squamosal is well-developed, concave and oriented fully laterally (Fig. 7A). Neither incrassation

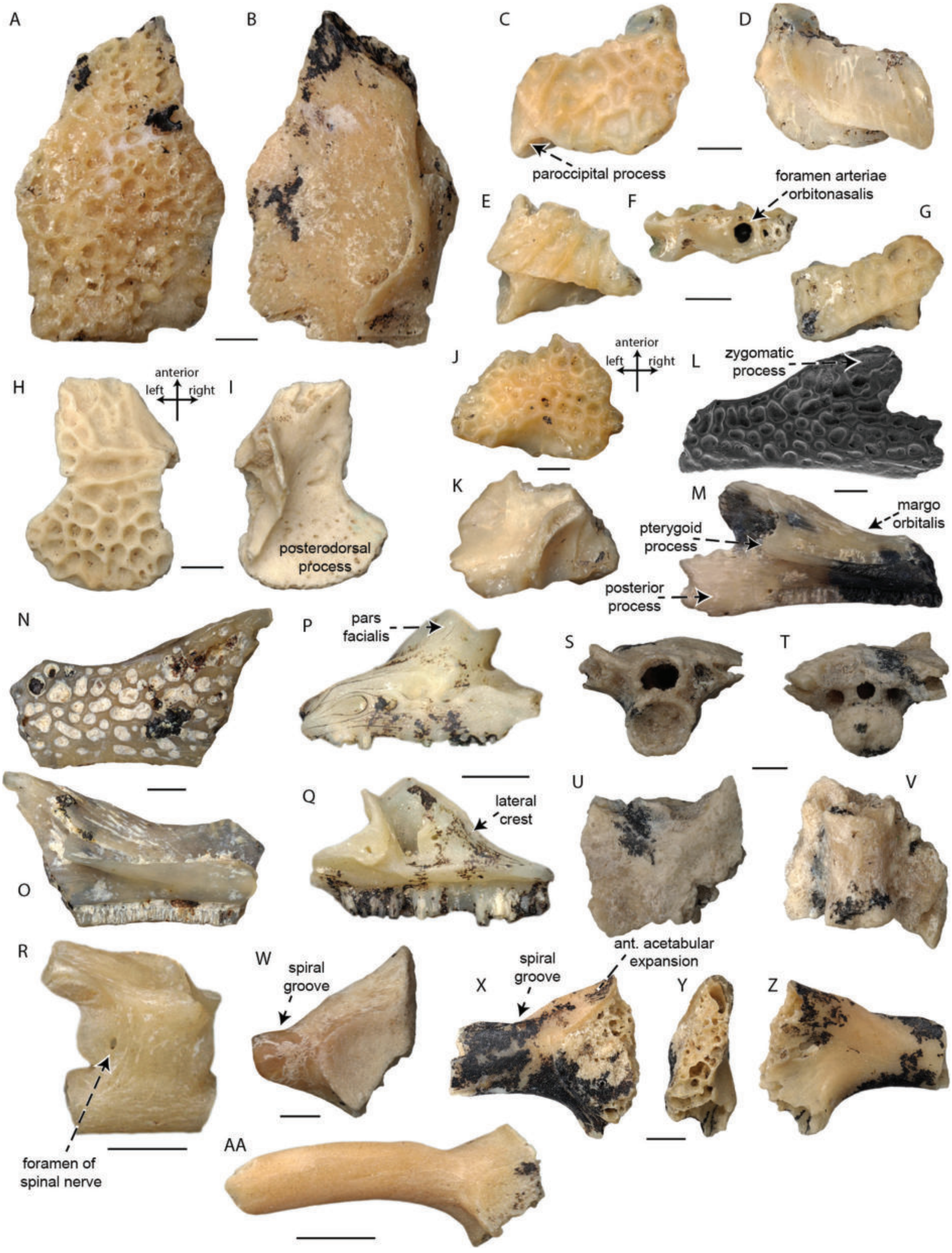

Figure 7. *Pelobates sanchizi* from the Echzell locality. Frontoparietals HLDM-Ez 2109 (**A, B**), HLDM-Ez 2107 (**C, D**), HLDM-Ez 2108 (**E–G**). Squamosals HLDM-Ez 2105 (**H, I**), HLDM-Ez 2106 (**J, K**). Maxillae HLDM-Ez 2077 (**L, M**), HLDM-Ez 2097 (**N, O**). Premaxilla HLDM-Ez 2098 (**P, Q**). Vertebrae HLDM-Ez 2101 (**S–V**), HLDM-EZ 2099 (r). Ilia HLDM-Ez 2113 (**W**), HLDM-Ez 2111 (**X–Z**), HLDM-Ez 2112 (**AA**). Bones figures in (**A, C, E, G, H, J, U**) dorsal, (**B, D, I, K, V**) ventral, (**F, T, Y**) posterior, (**L, N, P**) labial, (**M, O, Q**) lingual, (**S**) anterior, (**R, W, X, AA**) lateral and (**z**) medial views. Scale bars: 1 mm.

frontoparietalis nor the margins are preserved/observable in the remains. The paroccipital process is reduced, but its dorsal surface possesses a distinct crest. The medial base of the paroccipital process is pierced by the occipital arterial foramen, which is covered dorsally by the posterior margin of the frontoparietal and, thus, not visible in dorsal view (Fig. 7E). The fragmentarily preserved parts of the inferior superior process suggest that it was not longer than the lateral superior process. However, its lateral and slightly ventrally bending can be assumed. The arteria orbitonasalis opens ventrally on the supraorbital tectum (Fig. 7F).

Squamosals: The dorsal surface is covered by a similar to frontoparietal pit-and-ridge sculpture. The bone remains are fragmentarily preserved. Only in HLMD-Ez 2105 (Fig. 7H, I), an intact posterodorsal process lamina is present, and shows rounded posterior margin. The dorsal and zygomatic processes are broken. However, considering the presence of intact and concave bone margins between the preserved bases of these processes, we can suggest that they were delimited from each other. In ventral view, lamellar structures at the base of the posterolateral processes are observable (Fig. 7I, K). However, they are incomplete for any further description.

Maxillae: The labial surface of the bone is covered by a dense network of moderately deep to deep pits-and-ridge sculpture. The distinct zygomatic process extends posterodorsally and has a rounded posterior tip (Fig. 5L). The posterior process projects backwards. It is separated clearly from the zygomatic process by a deep concavity and projects much posteriorly. The orbital margin is concave. In lingual view, the pterygoid process projects posteromedially (Fig. 7M, O). Anteriorly, it is connected with the dorsally oriented lamella above the horizontal lamina.

Premaxilla: In anterior view, the pars dentalis is low but broad. Its surface is covered by rugose structures (Fig. 7P), which recalls the pit-and-ridge sculpture of, e.g., frontoparietal and maxilla. The pars facialis is broken, but its preserved base suggests a L-shaped form. Medially from this process, another shorter and posteromedially oriented process is present. The lateral crest (sensu Venczel 2004) is moderately developed. The dental crest possesses 15 tooth pedicles (Fig. 7Q).

Vertebrae: three presacral and two sacral vertebrae are present. The vertebra centrum is procoelous (four vertebrae, HLMD-Ez 2098, 2100–2102) or amphicoelous (one vertebra, HLMD-Ez 2099, Fig. 7R). The HLMD-Ez 2099 represents a small-sized individual that, most probably, does not have fully ossified joints. In presacral vertebrae, the neural arch is high; and the neural canal is large. The foramina for the spinal nerve are present slightly above the posterior bases of the neural arch. In presacral vertebrae, they are visible in lateral view, whereas in sacral ones – in posterior views (Fig. 7T). The sacral vertebrae have a broad and flattened transverse process.

Ilium: Though all ilia are very fragmentarily preserved, the following characters can be observed on the material: the acetabular region triangular; the acetabulum itself has round outline; the dorsal prominence low and covered by rare irregular structures; the dorsal protuberance absent; the moderately deep spiral groove extends from ventrolateral to dorsomedial direction in the region of the fusion of iliac shaft and acetabulum (Fig. 7W–AA); in medial view, the ilioischiatic juncture is covered by elongated striae (Fig. 7Z); the dorsal acetabular expansion larger than the ventral one.

Remarks. The described remains can be assigned to the genus *Pelobates* based on the following combination of characters: 1) azygous frontoparietals articulating with the squamosals; 2) well-pronounced pit-and-ridge style sculpture with pustular structures on frontoparietal, squamosal and maxillae; 3) the presence of the spinal nerve foramina in vertebrae; 4) the presence of the moderately deep spiral groove on ilium, etc. (e.g., Venczel 2004; Roček et al. 2014). The fossil material of *Pelobates* can be allocated to the species *P. sanchizi* considering: 1) the presence of moderately broad tectum supraorbitale; 2) the occipital arterial foramen not visible in dorsal view; 3) the arteria orbitonasalis opening ventrally on the supraorbital tectum; 4) delimited posterior and posterodorsal processes of squamosal (Venczel 2004)

Comparison of our material with other fossil species of *Pelobates* (Böhme et al. 1982; Khozatskiy 1985; Böhme 2010; Roček et al. 2014) allowed to suggest further diagnostic features for *P. sanchizi* such as: 1) the lateral superior process of the frontoparietal is longer than broad; 2) articulation surface on frontoparieals with squamosal well-developed, concave and oriented fully laterally.

The single premaxilla from Echzell shows a remarkable feature: ornamented on the anterior surface of the bone, recalling the pit-and-ridge sculpture of, e.g., frontoparietal and squamosal. Comparable ornamentation has not been ever described for the genus *Pelobates* and in *P. sanchizi* from other Miocene localities. Only for *Eopelobates deani* (Roček et al. 2014), a moderated rugose outer surface has been mentioned.

Alytidae Fitzinger, 1843
Latonia von Meyer, 1843

Latonia sp.

Fig. 8

Material. 76 maxillae HLMD-Ez 2130–2135, seven frontoparietals HLMD-Ez 2141–2144, one prooticoccipital HLMD-Ez 2127, six atlases HLMD-Ez 2116–2117, 23 presacral HLMD-Ez 2118–2120 and 22 sacral vertebrae HLMD-Ez 2121–2123, two costae (ribs) HLMD-Ez 2128, 23 urostyles 2124–2126, 58 ilia HLMD-Ez 2136–2140.

Description. Frontoparietals: All bones are very fragmentarily preserved, and all of them possess ornamentation made of a dense network of tubercles (Fig. 8A, C, E). In ventral view, a number of ridges and structures are visible (Fig. 8B, D, F); however, due to their preservation, any further description/anatomical identification is impossible.

Figure 8. *Latonia* sp. from Echzell. Frontoparietals HLMD-Ez 2141 (**A, B**), HLMD-Ez 2142 (**C, D**), HLMD-Ez 2143 (**E, F**). Maxilla HLMD-Ez 2133. Prooticoccipital HLMD-Ez 2127 (**I–L**). Atlas HLMD-Ez 2116 (**M, N**). Presacral vertebrae HLMD-Ez 2118 (**O, P**) and HLMD-Ez 2119 (**Q–T**). Sacral verterba HLMD-Ez 2122 (**W–Y**). Urostyle HLMD-Ez 2124 (**Z**) and HLMD-Ez 2125 (**AA**). Ilia HLMD-Ez2137 (**AB**), HLMD-Ez2138 (**AC–AE**), HLMD-Ez 2140 (**AF**) and HLMD-Ez2139 (**AG–AI**). Bones are figures in (**A, C, E, L, O, T, X, Z, AA**) dorsal, (**B, D, F, K, M, R**) ventral, (**G**) labial, (**H**) lingual, (**I, Q, Y, Ad, Ah**) posterior, (**J, N, P, S, W**) anterior and (**AB, AC, AE, AF, AG, AI**) lateral views. Scale bars: 1 mm.

Maxillae: All bones are fragmentarily preserved. Their labial surface is smooth and does not possess any ornamentation (Fig. 8G). Only in (HLMD-Ez 2132), the labial surface is covered by some irregularities. In lingual view, the horizontal lamina has a rounded surface and reduces height anteriorly (Fig. 8H). Posteriorly, it terminates with a medioposteriorly projecting pterygoid process. The posterior depression is moderately developed. The margo orbitalis is slightly concave.

Prooticoccipital: One preserved prooticoccipital (HLMD-Ez 2127) consists of both fused prootic and lateral occipital processes (Fig. 8I–L). It displays a distinct supracondylar depression. The prominentia ductus semicircularis posterioris is present as a distinct crest. It starts at the base of the lateral prootic process and projects medioanteriorly until the articulation surface with the frontoparietal. A foramen is present at the ventral base of the lateral prootic process. The sulcus venae jugularis is present as a horizontal groove. The fenestra ovalis is massive (Fig. 8K).

The atlas has a dorsoventrally flattened centrum (HLMD-Ez 2116, Fig. 8N). The neural arch is not preserved. The crista ventralis is well developed. The condyloid fossae are separated from each other by a notch. The opisthocoelous presacral vertebrae have massive, slightly dorsally compressed centrum. The transverse processes project laterally. The neural arch in a small-sized vertebra projects posterodorsally (HLMD-Ez 2118), and the neural spine is clearly visible (Fig. 8O, P). The sacral vertebrae have one anterior and two posterior condyles with very rounded external surfaces (Fig. 8X, Y). The neural arch is short. It measures as long as the bases of the transverse processes. The latter widens laterally and project lateroposteriorly. The prezygapophyses in both presacral and sacral vertebrae project laterodorsally (Fig. 8S, W).

The urostyle possesses two condyloid fossae and two lateroposteriorly bending transverse processes (Fig. 8Z, AA). The opening of the neural canal is rounded. The neural canal opens dorsally behind the transverse processes in the form of a narrow and long strip.

The preserved ilia have low or moderately developed dorsal prominence. The dorsal protuberance has a flat surface and shows high variation in shape and size. It can be very reduced in the form of a small protuberance (HLMD-Ez 2137, Fig. 8AB) or rather well-developed elongate (HLMD-Ez 2140, Fig. 8AF) or short drop-shaped (HLMD-Ez 2140–2141, Fig. 8AF) structure. It is connected with the lateromedially compressed iliac shaft by a thin lamina which reduces in height anteriorly behind the dorsal protuberance. The acetabular region is well developed. The dorsal acetabular expansion is well-developed and has a triangular outline. The ventral acetabular expansion is rather reduced and widens ventrally, expanding below the ventral margin of the acetabular crest. The ventral portion of the acetabular crest is well developed and projects ventrolaterally. The supraacetabular fossa is absent or, if present, weakly developed. A distinct tubercular fossa is visible in the corner between dorsal prominence and iliac shaft. In both medial (Fig. 8AE, AI) and posterior views (Fig. 8AH), a well-developed interiliac tubercle is visible. In posterior view, the ilioischiatic juncture can be clearly divided into a massive ventral and a slender dorsal portions, which are delimited in the medial surface by a deep groove.

Remarks. The herein described remains can be assigned to the genus *Latonia* based on the presence of the following features: 1) frontoparietal with the characteristic tubercular sculpture; 2) prooticooccipital bone with a distinct supracondylar depression; 3) atlas possessing ventral crest; 4) urostyle with lateroposteriorly projecting transverse processes; 5) the general morphology of ilium and presence of the interiliac tubercle etc. (Roček 1994). Due to the poor preservation of the material, any further taxonomic identification is impossible.

Ranidae Rafinesque, 1815
Pelophylax Fitzinger, 1843

Pelophylax sp.

Fig. 9A–D

Material. Four ilia HLMD-Ez 2088–2091.

Description. All ilia are fragmentary. The iliac shaft and most proximal portions are missing. The dorsal prominence is well developed; it is high, in lateral view projects anterodorsally, whereas in posterior view, it has a medially curved outline. The dorsal protuberance is massive, drop-shaped, with a rounded surface (Fig. 9D). The supraacetabular fossa is moderately developed and located posteriorly from the ventral base of the dorsal prominence. The acetabular ridge is ventrally significantly higher than dorsally (Fig. 9C, D). The iliac shaft is rather thin and round in cross-section. The iliac shaft and the dorsal prominence are connected by a high and thin bone lamina.

Remarks. See remarks of *Rana* sp.

Rana Linnaeus, 1758

Rana sp.

Fig. 9E–H

Material. Three ilia HLMD-Ez 2092–2094.

Description. The best-preserved ilium (HLMD-Ez 2094, Fig. 9G, H) shows a well-developed (rather narrow and high) dorsal acetabular expansion and a reduced (broad and low) ventral acetabular expansion. The dorsal prominence is not very high. It is oriented rather anteriorly than anterodorsally. The dorsal protuberance has an oval outline. Its surface is either smooth (HLMD-Ez 2094, Fig. 9G) or possesses muscle scars (HLMD-Ez 2093, Fig. 9E). The iliac shaft is rather thin and round in cross-section. A low and thin bone lamina connects the iliac shaft and the dorsal prominence. In posterior view, the dorsal prominence projects laterodorsally. The ilioischiatic juncture is narrow (Fig. 9H).

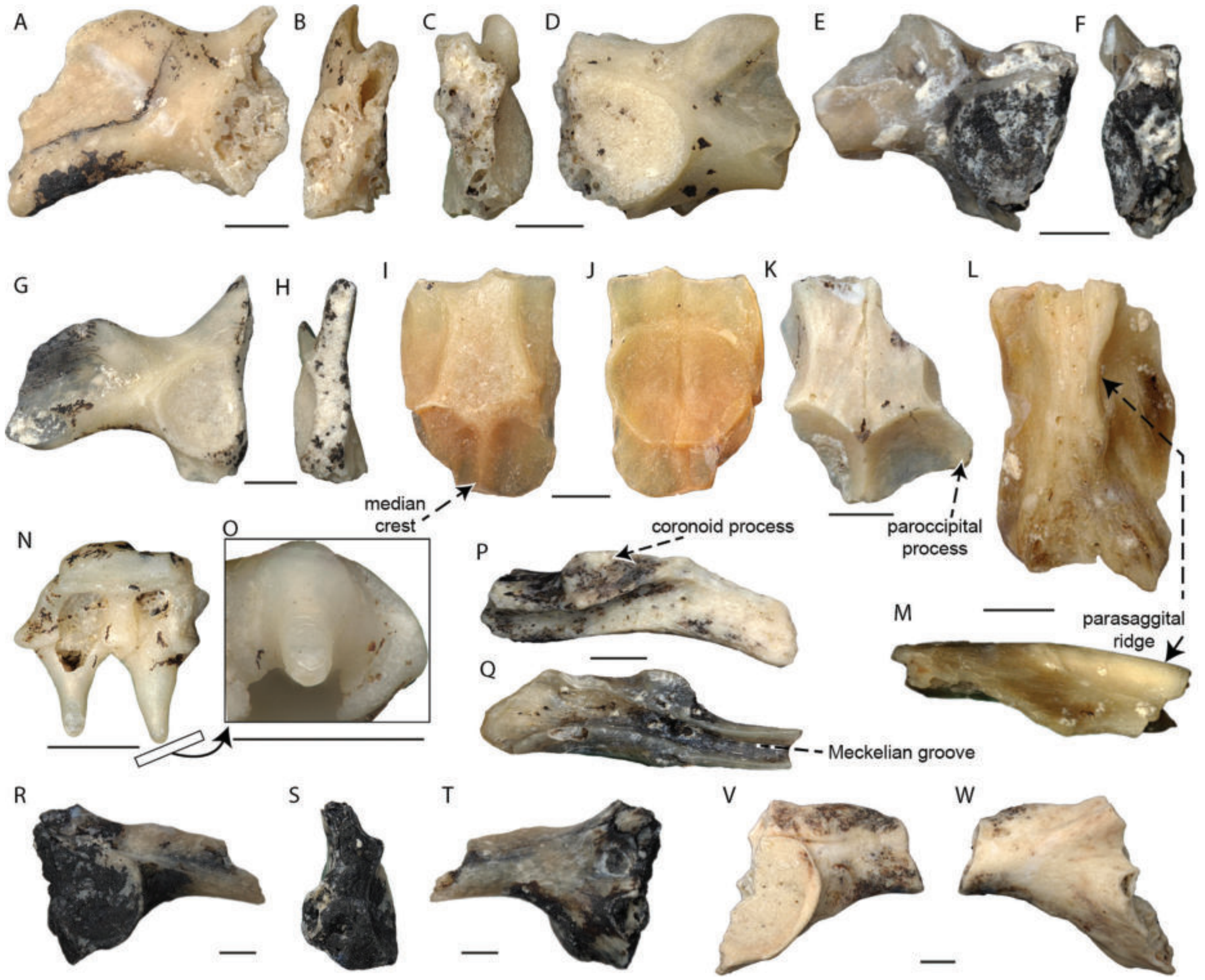

Figure 9. Frogs from Echzell locality. Ilia of *Pelophylax* sp. HLMD-Ez 2089 (**A, B**) and HLMD-Ez 2090 (**C, D**). Ilia of *Rana* sp. HLMD-Ez 2093 (**E, F**) and HLMD-Ez 2094 (**G, H**). *Palaeobatrachus robustus* (**I–W**). Frontoparietals HLMD-Ez 2077 (**I, J**), HLMD-Ez 2078 (**K**) and HLMD-Ez 2076 (**L, M**). Jaw bone HLMD-Ez 2084 (**N, O**). Angulars HLMD-Ez 2083 (**P**) and HLMD-Ez 2082 (**Q**). Ilia HLMD-Ez 2079 (**R–T**) and HLMD-Ez 2080 (**V, W**). Bones are figured in (**A, D, E, G, M, R, V**) lateral, (**B, C, F, H, S**) posterior, (**I, K, L, P, Q**) dorsal, (**J, O**) ventral, (**N**) labial and (**T, W**) medial views. Scale bars: 1 mm.

Remarks. Echzell frog ilia can be clearly assigned to green *Pelophylax* and brown *Rana* frogs based on the following characters. The genus *Pelophylax* is characterised by: anterodorsally oriented, high, large and dorsomedially curved dorsal prominence and protuberance; the dorsal protuberance has a smooth surface; whereas the genus *Rana* by in lateral view anterodorsally and in posterior view laterodorsally oriented, rather low and reduced dorsal prominence and protuberance, the dorsal protuberance has smooth or irregular surface (Böhme 1977; Blain et al. 2007).

Palaeobatrachidae Cope, 1865
Palaeobatrachus Tschudi, 1838 (sensu Wuttke et al. 2012)

Palaeobatrachus robustus Hossini & Rage, 2000

Fig. 9I–W

Material. Four frontoparietals HLMD-Ez 2076–2078, five ilia HLMD-Ez 2079–2081, two angulars HLMD-Ez 2082, 2083, five jaw bones HLMD-Ez 2084, 2085.

Description. Frontoparietals are flat and thin. They represent small-sized individuals. The parasagittal ridges are well-developed and build the limit between the flat dorsal surface of the bones and somewhat concave orbital margins. The parasagittal ridges are very closely located near the midpoint of the bone and form a sandglass shape at the dorsal surface of the bone. The dorsal surface of the bone between the parasagittal ridges is irregular and pierced by small foramina (pineal foramen sensu Villa et al. 2016) and pits (Fig. 9L). Posteriorly, the surface of the frontoparietal table is flat and rather smooth. The irregularities, if present, are weakly pronounced. The parasagittal ridges reach the paroccipital processes posteriorly (Fig. 9I, K). The latter are not fully preserved. Only their bases are observable, which in turn, possess a crest. A smaller posterior median crest is present along the anteroposterior axis of the bone which starts from the posterior margin of the frontoparietal table. The posterior margin of the bone between the median margin and paroccipital process is arched and forms a “bilobed” outline

(Fig. 9K). The median crest is lower than the paroccipital processes. Judging from the preserved portions of the paroccipital process and posterior median process, a shorter length of the former in comparison to the latter can be assumed. In ventral view, the frontoparietal incrassation, visible only in HLMD-Ez 2077 (Fig. 9J), representing the posterior portion of the bone, has a round outline with slightly prominent margins. No structure similar to the lanceolate area (sensu Roček et al. 2015) is observable on the available frontoparietals.

Premaxillae, maxillae, vomer: all three bones are fragmentarily preserved and do not allow any detailed description. The preserved teeth and tooth pedicles display diagnostic characters, such as the conical and slightly lingually bent ankylosed teeth. At the tooth basis, large and deep pits are preserved. The bicuspid tooth has a small labial and large apical cusps (Fig. 9N, O, HLMD-Ez 2084).

Angulars: in total, two angulars can be clearly assigned to this taxon. They are elongated and curved bones. The coronoid process is compact and can be oval to drop-shape (Fig. 9P, Q). Its surface is concave, rather smooth and can possess tubercles (muscle scars). The Meckelian groove behind the coronoid process is broad and opens dorsally, whereas anteriorly, it is open laterally or slightly dorsolaterally.

Ilium: The acetabular region of the ilium is robust. The dorsal prominence (sensu Gómez and Turazzini 2015) is not well-developed. The drop-shape dorsal protuberance (sensu Gómez and Turazzinin 2015) is large (Fig. 9R) and can be weakly to moderately developed (Fig. 9V). Its surface is rather smooth, and its small posterior portion is located above the anterior margin of the acetabular crest. The ventral acetabular expansion (also known as pars descendens) does not project ventrally, but it is massive in ventral/dorsal views (Fig. 9R). The dorsal acetabular expansion (also known as pars ascendens), even if only fragmentarily preserved, is moderately developed. The ventral half of the acetabular fossa is massive. The well-developed ventral portion of the acetabular crest projects laterally and contributes to the ventroanterior surface of the acetabular region of the ilia. In larger individuals (e.g. HLMD-Ez 2080), an oval knob-like flat surface is present in the lateroventral cornet between the iliac shaft and acetabulum (Fig. 9V). It represents most probably the attachment surface for the muscle iliacus internus (sensu Gómez and Turazzini 2015). In posterior view, the well-pronounced interiliac groove and laterally projecting acetabular crest are observable. The iliac shaft is moderately developed, lateromedially flattened and has a rather smooth surface.

Remarks. The fossil remains display characteristic features of the genus *Palaeobatrachus* as well as the family Palaeobatrachidae such as: 1) azygous frontoparietal with a flat dorsal surface; 2) angular coronoid process smooth and/or covered by muscle scars; 3) anteroventrally extending large acetabulum; 4) acetabular area strongly protruding; 5) well-pronounced interiliac groove (Wuttke et al. 2012) and 6) paroccipital processes do not extend probably beyond the level of posterior median process (Roček et al. 2015; see characters 12, table 2). Among the material available bones, only the frontoparietal can be used for the species-level identification since other elements such as ilium, angular do not contain sufficient diagnostic characters. The *Palaeobatrachus* frontoparietal from Echzell can be distinguished from other Miocene forms, e.g. *P. hiri* (locs. Bátraszölos and Sámsonhaza, Venczel 2004), and *P.* sp. A (loc. Rudabanya, Roček 2005) by the sculptured frontoparietal (vs. unsculptured in *P. hiri* and *P.* sp. A) and weakly developed frontoparietal incrassation (vs. strongly developed, in form of crests in *P. hiri* and *P.* sp. A). The Echzell frontoparietals strongly resemble the morphology of the *P. robustus* from the early Miocene (MN2) of France (loc. Laugnac, Hossini and Rage 2000), in having 1) a comparable sculpture on dorsal surface of the bone; 2) the skull table narrows in the midpoint of the bone, giving a sandglass shape; 3) weakly developed, rounded frontoparietal incrassation. We did not compare with *P. hauffianus* from Randecker Maar, Germany (middle Miocene) (Roček et al. 2006) which taxonomic status still needs revision.

Anura indet.

Material. Six angulars HLMD-Ez 2086, eight premaxillae HLMD-Ez 2129, 38 humeri HLMD-Ez 2087, a number of bone fragments HLMD-Ez 2145.

Remarks. The bones are either very fragmentarily preserved or do not possess characters useful for further identification.

Squamata Oppel, 1811
Gekkota Cuvier, 1816–1817

Gekkota indet.

Fig. 10

Material. One right dentary HLMD-Ez 1958, one vertebra HLMD-Ez 1959.

Description. Dentary: Only a fragment of the right mid-dentary region is preserved (Fig. 10A, B). It bears 16 tooth positions that are densely spaced. Unfortunately, all teeth are broken off and missing, except for two preserved tooth bases. The dentary is slender (note, however, that the alveolar crest is high). In medial view, it gradually widens posteriorly and Meckel`s groove is fully closed. The ventral margin of the dentary is slightly concave. Besides three labial foramina, the external surface of the bone is smooth.

Vertebra: Only one isolated dorsal vertebra is preserved (Fig. 10C–G). The vertebra is small, lightly built and anteroposteriorly elongated. It is amphicoelous with the centrum pierced by a notochordal canal. On the dorsal surface of the low neural arch, a straight dorsal and longitudinal, almost indistinct crest is present along the surface of the neural spine. The neural spine is weak, and it does not rise dorsally. However, the posterior region of this area is damaged, and the right postzygapophysis is broken off. On the anterior side, a deep and wedge-shaped notch is present (note, that it is unclear how much its contour is a result of potential breakage and/or normal state). Both pre- and postzygapohyses are almost anteriorly and posteriorly directed. The neural canal is large and heart-shaped because of the rounded centrum that is located ventrally. In lateral view, there is an elliptical synapophysis. In this view, the centrum has a concave ventral margin. In ventral view, the lateral margins of the centrum are concave as well. In the central region, a short ridge is developed between the anterior and posterior portions of the centrum. Laterally from the ridge, the surface is pierced by a pair of subcentral foramina.

Remarks. In the European Miocene, the sphaerodactylid genus *Euleptes* is often present (see e.g., Daza et al. 2014; Čerňanský et al. 2018). Extinct genera of Gekkota are represented by *Gerandogekko*, which has been identified as closely related to *Euleptes* (Daza et al. 2014) and *Palaeogekko* (Schleich 1987). The material from Echzell is, however, too fragmentary for a generic assignment.

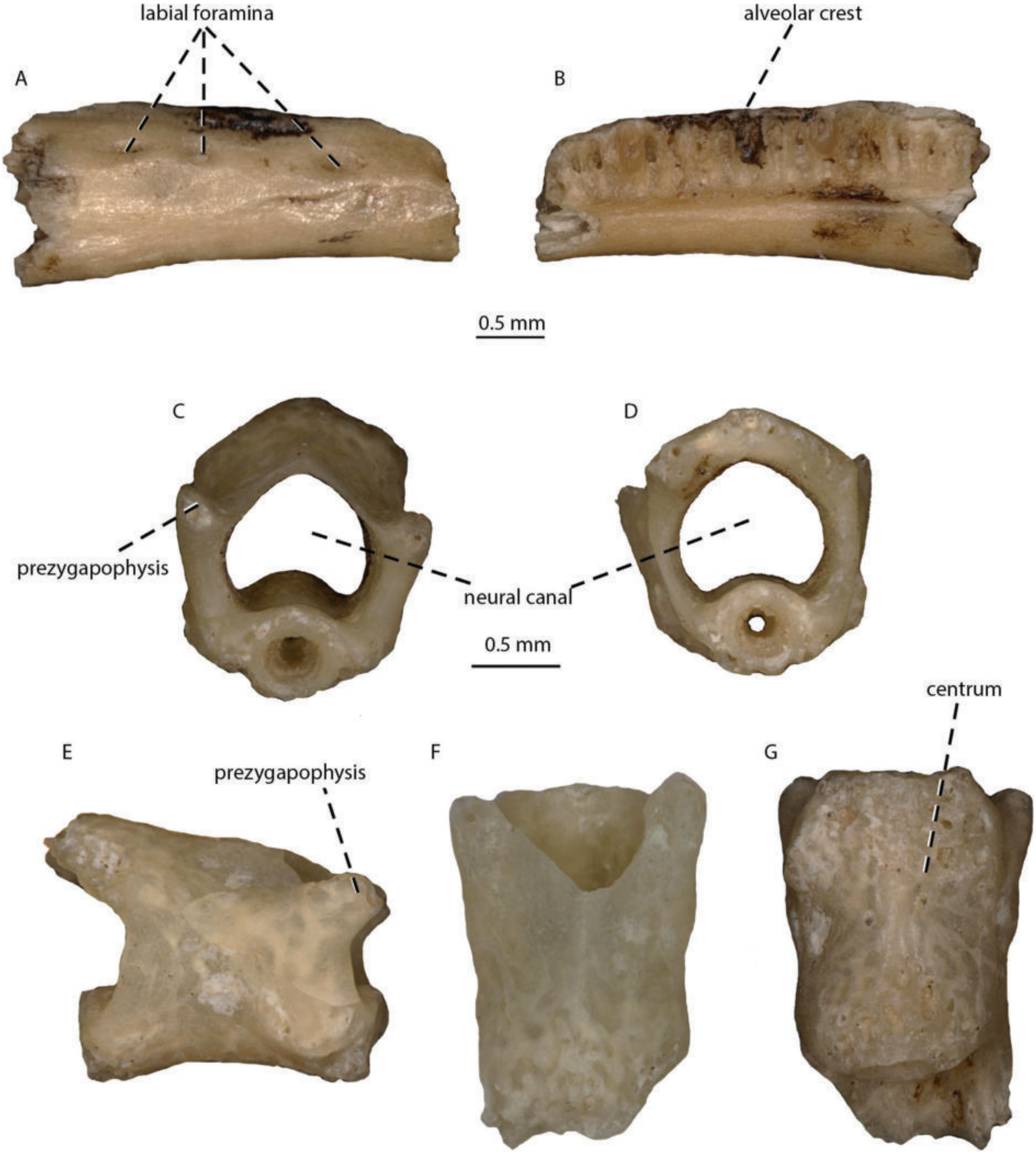

Figure 10. Gekkota indet. from the Echzell locality. right dentary HLMD-Ez 1958 in (**A**) lateral and (**B**) medial views. Vertebra HLMD-Ez 1959 in (**C**) anterior, (**D**) posterior, (**E**) lateral, (**F**) dorsal and (**G**) ventral views.

Iguania Cope, 1864
Acrodonta Cope, 1864
Chamaeleonidae Gray, 1825
Chamaeleo Linnaeus, 1758–1759

Chamaeleo andrusovi Čerňanský, 2010b
Fig. 11A, B

Material. One frontal HLMD-Ez 1960.

Description. Frontal: The frontal is partly preserved. Only its posterior region around the parietal foramen (sensu Gauthier et al. 2012: character 105) is available. The dorsal surface possesses well-developed ornamentation formed by large, robustly developed, and distinctly pustular protuberances (Fig. 11A). Only four are preserved (note, however, most of the dorsal surface of two of them is damaged). In the posterior region, the protuberances are large and somewhat anteroposteriorly elongated. They appear to be moderately spaced with a more-or-less complex structure (somehow resembling gomphothere molars). The internal surface of the frontal (Fig. 11B) is pierced by a small, elliptical foramen. It opens a canal that continues anterodorsally (note that the preserved dorsal surface is not pierced by it). Lateral to it, rounded, dorsally sloped ridges are well-developed. They form the border between the central, bulged region with its central shallow longitudinal depression and two additional distinct depressions located lateral to the central region. These lateral depressions become more distinct anteriorly, being gradually more recessed (in other words, the central region is deeper relative to the lateral areas). In the central region, another hole is preserved, which was most probably caused by damage.

Remarks. Similar depressions located laterally from the central area with a foramen and being more anteriorly recessed, whereas the foramen opens a canal which continues anterodorsally, can be observed in extant *Chamaeleo chamaeleon* as well. The typical ornamentation formed by distinctly developed and complicated pustular protuberances, which are moderately spaced and not arranged in a ridge here, allows allocation of this cranial bone to the European Miocene chameleon *Chamaeleo andrusovi* Čerňanský 2010b. This species was initially described from the early Miocene of the Czech Republic (Čerňanský 2010b) and later recognized from other areas of Europe (e.g., Georgalis et al. 2016; Čerňanský et al. 2017).

Chamaeleonidae indet.
Fig. 11C–M

Material. Two right maxillae HLMD-Ez 1961–1962, two left dentaries HLMD-Ez 1963–1964.

Description. Maxilla: The specimen HLMD-Ez 1961 (Fig. 11C–E) represents the anterior maxillary section. It bears five small teeth. The fragment is relatively massively built with a slight medial curvature at its anterior end. The bone rises dorsally, but only the base of the facial process is preserved. In medial view, the anterior internal dorsal margin has a rough surface. It can be most likely interpreted as a facet for the premaxilla. The supradental shelf is thin in medial view. However, this structure is well-expanded medially, being broad in ventral view. The external surface of the preserved section of the bone is smooth. The specimen HLMD-Ez 1962 (Fig. 11F, G) represents a posterior maxillary section – a part of the posteroventral process. It bears four teeth. In medial view, the supradental shelf is well-developed. Dorsally from this structure, the maxilla forms a longitudinal depression; a facet for the jugal is present here. The lateral surface of this fragment is smooth.

Dentary: Both dentaries are fragmentarily preserved. The specimen HLMD-Ez 1963 (Fig. 11H–J) represents the anterior portion of the left dentary. The anterior end of the dentary is curved medially, and a large elliptical symphysis is located here. This dentary fragment bears six teeth, although it should be noted that the anterior tooth is broken off. Ventrally to it, the dental groove is present, being shallow rather than deep. The well-developed and straight supra-alveolar ridge floors it. Most of the ventral portion of the Meckel`s groove is damaged. The external surface is pierced by a labial foramen located closed to the ventral margin. The specimen HLMD-Ez 1964 (Fig. 11K–M) bears only two teeth. Its lateral surface shows well-developed triangular interdental grooves (two are preserved), which incline anteroventrally.

Dentition: The tooth implantation is acrodont. Tooth size increases more-or-less posteriorly, but the dentary specimen HLMD-Ez 1964 and maxillary specimen HLMD-Ez 1962 show that at least the last posterior tooth is smaller than the adjacent anterior (probably penultimate) one. The teeth are triangular, with a low degree of tricuspidity – the central cusp is distinctly dominant. The teeth are compressed mediolaterally. The sizes of the inter-dental gaps are small in the anterior region and distinctly widen posteriorly. The large posterior teeth have wide interdental gaps. Thus, their bases are not in contact. On the posterior region of the maxilla, however, the size of the inter-dental gap between the last and the penultimate tooth is small.

Remarks. The absence of pleurodont dentition in the anterior section of the tooth row allows the allocation to Chamaeleonidae without doubts (Čerňanský 2010b; Čerňanský et al. 2020a). In contrast to chamaeleonids, agamids retain a trace of the primitive pleurodont condition in the anterior region (often in caniniform anterior teeth; Moody 1978).

Lacertoidea Estes, Queiroz & Gauthier, 1988
Lacertidae Oppel, 1811

Lacertidae indet.
Fig. 12A, B

Material. Right dentary HLMD-Ez 1992.

Description. Dentary: The description is based on a right dentary that represents the anterior section (Fig. 12A, B). The specimen bears 13 tooth positions with

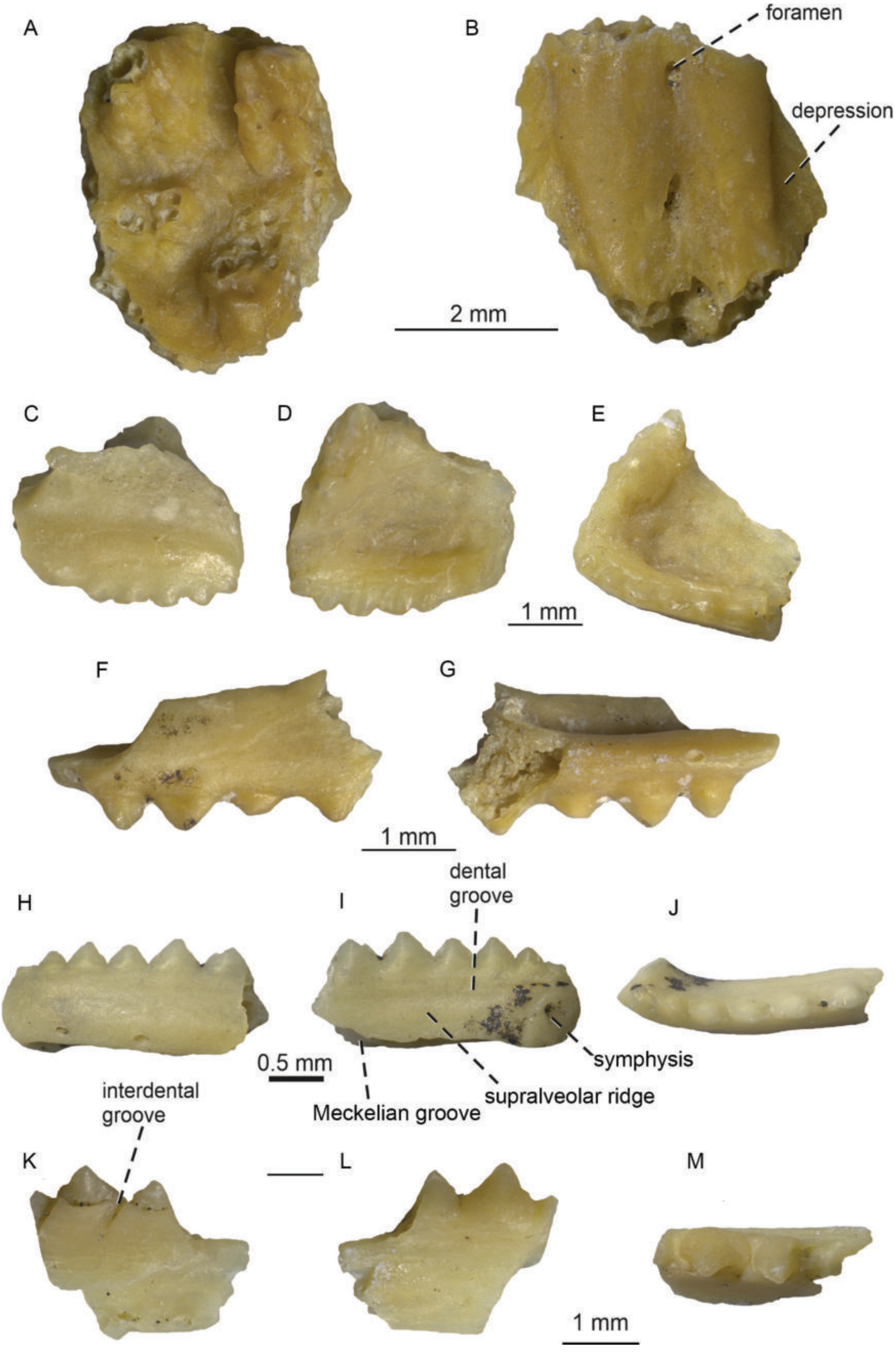

Figure 11. *Chamaeleo andrusovi* (**A, B**) and Chamaeleonidae indet. (**C–M**) from the Echzell locality. Frontal HLMD-Ez 1960 in (**A**) dorsal and (**B**) ventral views. Right maxilla HLMD-Ez 1961 in (**C**) lateral, (**D**) medial and (**E**) ventral views. Right maxilla HLMD-Ez 1962 in (**F**) lateral, and (**G**) medial views. Left dentary HLMD-Ez 1963 in (**H**) lateral, (**I**) medial, and (**J**) dorsal views. Left dentary HLMD-Ez 1964 in (**K**) lateral, (**L**) medial, and (**M**) dorsal views.

nine teeth still attached. However, its posterior region is broken off and the real tooth number is undoubtedly higher. The preserved portion of the dentary is more-or-less robust, anteroposteriorly elongated. The bone gradually narrows anteriorly. In dorsal view, its anterior portion has a small medial curvature. The otherwise smooth lateral surface is pierced by several labial foramina located in the mid-portion of the bone (five are preserved). In medial view, the Meckel`s groove is narrow, entirely open and gradually widens posteriorly. The subdental shelf is medially protruded and robust, especially in the anterior region. It narrows posteriorly because of the presence of the splenial articulation facet. The symphysis is rectangular.

Dentition. The tooth implantation is pleurodont. The teeth are conical and high. They are bicuspid with a dominant distal cusp and smaller accessory mesial cusp. However, the anteriormost dentary teeth are monocuspid, becoming bicuspid starting from the sixth to seventh tooth position. The lingual aspect of the tooth crowns has very fine vertical striations, and the tooth necks bulge slightly medially, with small interdental gaps.

Scinciformata Vidal & Hedges, 2005
Scincidae Gray, 1825
Chalcides Laurenti, 1768

cf. *Chalcides* sp.

Fig. 12C–H

Material. Right maxilla HLMD-Ez 1990, six right dentaries HLMD-Ez 1993–1998, one left dentary HLMD-Ez 1999.

Description. Maxilla: One fragment of a right maxilla is preserved. The specimen HLMD-Ez 1990 (Fig. 12C, D) represents the posterior region of the maxilla. The lateral surface of this specimen is completely smooth. This maxillary fragment bears eight tooth positions with five teeth still attached). The nasal process is partly preserved. Note, however, that the dorsoventral height of the posteriorly located posteroventral process of the maxilla is still significant. Thus, it forms the wall along the entire length of the process here rather than narrowing posteriorly into a tip. Moreover, the shallow notch is developed posteriorly between the dental crest supporting teeth and the dorsally located wall. Although the posterior portion of this dorsal wall is broken off, it can be estimated that, when completely preserved, it exceeds the dental part posteriorly. The dorsal margin of the posteroventral process is slightly damaged, but this portion has a thicker appearance than the ventrally located region possessing a longitudinal depression. This depression partly forms a jugal facet. The ventrally located supradental shelf is thin and expands laterally. It is dorsally convex, but only a small portion is completely preserved. No alveolar superior foramen is preserved here. This highlights a possible anterior position of this foramen.

Dentary: The description is based on several fragments (Fig. 12E–H), most of which represent more-or-less anterior sections. The most complete specimen bears 20 tooth positions; however, its posterior region is broken off. The real tooth number is undoubtedly slightly higher. The dentary is slender, anteroposteriorly elongated. The bone gradually narrows anteriorly. In dorsal view, its anterior portion has a small medial curvature. The otherwise smooth lateral surface is pierced by several labial foramina located in the mid-portion of the bone. In medial view, the Meckel`s groove is narrow, but entirely open. The subdental shelf is medially protruded and robust, especially in the anterior region. It narrows posteriorly because of the presence of the splenial articulation facet. The symphysis is small, rectangular and somewhat narrow.

Dentition: The tooth implantation is pleurodont. The teeth are conical and high. They are closely spaced with small interdental gaps. The tooth crowns are mediolaterally compressed. Thus, the necks have a slightly lingually enlarged appearance. The tooth crowns have blunt apices. In medial view, they have a labial and lingual cusp. The lingual side, bordered by the culmen lateralis posterior and anterior, has striation formed by apicobasal ridges. They are more-or-less parallel to each other and their number usually varies from around five to eight. The labial aspect of the teeth appears smooth. Resorption pits pierce the tooth bases of some teeth.

Remarks. All scincid elements here are assigned to one species based on the significant similarity in the dentition. Moreover, all elements are from the same locality and comparable in size. Besides tooth morphology (see Kosma 2004), the Echzell skink material can be allocated to the clade Scincidae (sensu Hedges 2014; Scincinae sensu Estes et al. 1988) based on the narrow but fully open Meckelian groove in the dentary. This is present in members of the Scincidae clade and in, e.g., *Ateuchosaurus*, whereas it is closed in members of Acontiidae, Sphenomorphidae, Eugongylidae, Lygosomidae, Egerniidae and Mabuyidae (see, e.g., Greer 1970, 1974; Evans 2008; Hutchinson and Scanlon 2009; Čerňanský et al. 2020b; Čerňanský and Syromyatnikova 2021).

The specimens resemble members of the genus *Chalcides*. The Miocene species of this taxon is represented by *Chalcides augei* (see Čerňanský et al. 2020b) and the Echzell material shows similarities to this taxon. Note that usually five striations are reported in *Ch. augei*, it can range from five to seven, and the small variation in the number of striae (from five to seven ot eight) can be seen in specimens from Austria as well (Čerňanský 2016). However, the limitation of the Echzell material does not allow alpha taxonomy and caution is needed here.

Anguimorpha Fürbinger, 1900
Anguidae Gray, 1825
Anguinae Gray, 1825

Smithosaurus gen. nov.

http://zoobank.org/4D22CE09-4ABF-438A-8870-230F484F5D5D

Fig. 13

Etymology. We name this genus in honour of American paleoherpetologist Krister T. Smith for his valuable contributions to vertebrate paleontology and particularly

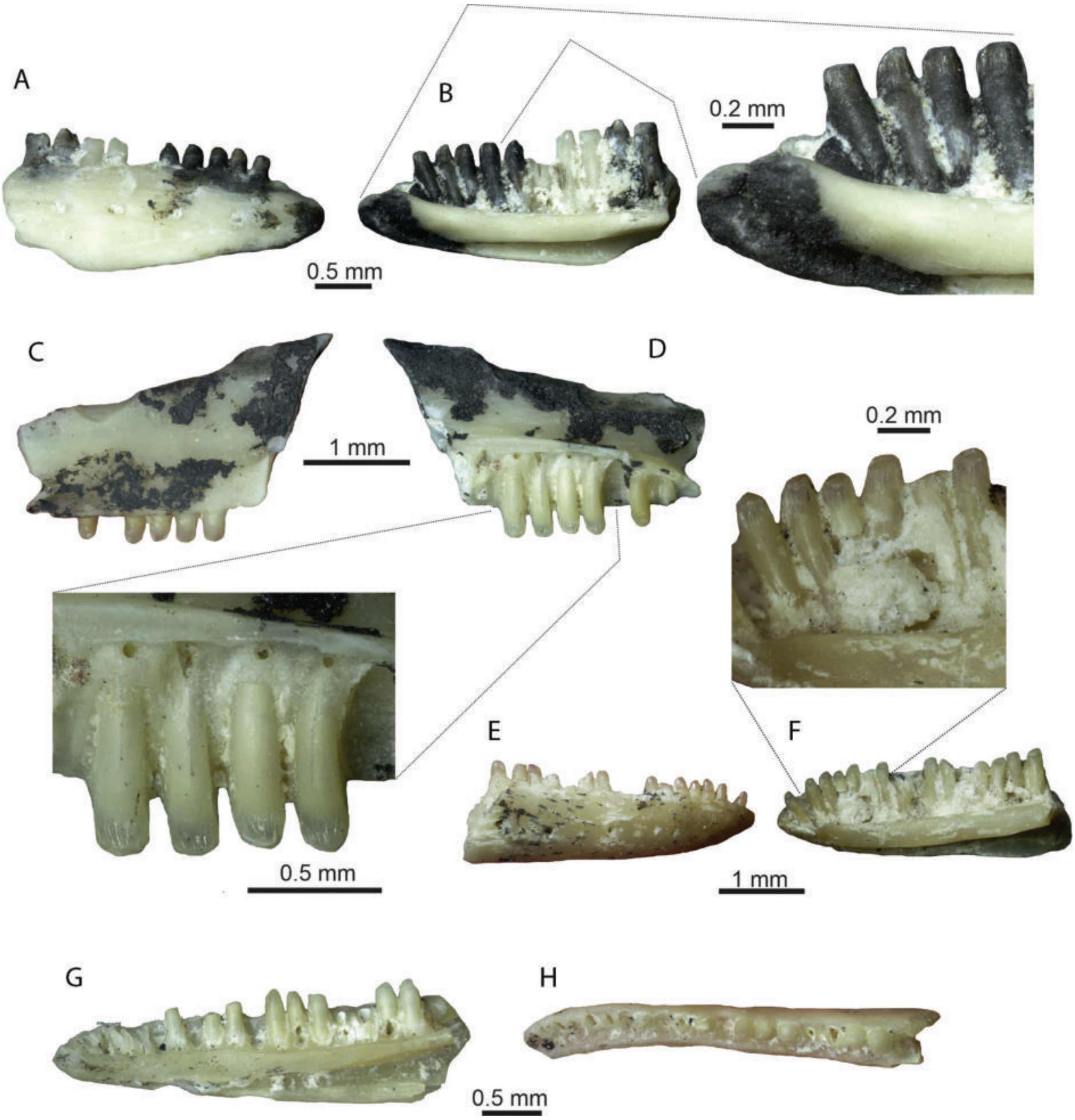

Figure 12. Lacertidae indet. (**A, B**) and cf. *Chalcides* sp. (**C–H**) from the Echzell locality. Right dentary HLMD-Ez 1992 in (**A**) lateral and (**B**) medial views with a detail of dentition. Right maxilla HLMD-Ez 1990 in (**C**) lateral and (**D**) medial views with a detail of dentition. Right dentary HLMD-Ez 1994 in (**E**) lateral and (**F**) medial views with a detail of dentition. Right dentary HLMD-Ez 1993 in (**G**) lateral, and (**H**) medial views.

to squamate morphology and evolution; and from Greek σαύρα [saura], lizard.

Diagnosis. As for *Smithosaurus echzellensis*, the only known species.

***Smithosaurus echzellensis* gen. et sp. nov.**

http://zoobank.org/ED8797D9-46FE-4462-BA43-A32D16934582

2014 *Ophisaurus spinari* – Böhme and Vasilyan: p. 29, fig. 3f.

Etymology. Based on the locality Echzell in Germany – one of two known localities, where this taxon occurred.

Holotype. One parietal UMJGP 204.749.

Paratype. One parietal HLMD-Ez 1965.

Range. Germany (Echzell), early Miocene; Austria (Gratkorn), late middle Miocene.

Remarks. Both parietals – HLMD-Ez 1965 from the early Miocene Echzell locality and UMJGP 204.749 from the late middle Miocene Gratkorn locality in Austria (see Böhme and Vasilyan 2014; fig. 3f), exhibit the same unique combination of features and can be placed to a single taxon without any doubts. Because the parietal UMJGP 204.749 (Fig. 13A, B) is better preserved than HLMD-Ez 1965 (Fig. 13C, F), it has been designated as the holotype for the new taxon.

Diagnosis. Anguine lizard distinguishable from *Anguis*, *Pseudopus* and *Ophisaurus* by two autapomorphic features:

(1) the parietal table gradually expands laterally in the anterior direction in an extreme way; thus, it appears to be distinctly constricted at the level of the parietal foramen or slightly posterior to it. The lateral margins of the table markedly diverge anterolaterally from this point, inclining at an angle of about 30° from the median plane. Posteriorly located lateral margins diverge gradually posterolaterally and continue to more-or-less straight supratemporal processes. Due to the lateral expansion of the parietal table, the anterolateral corner of the parietal table reaches further laterally than the supratemporal process. The ornamented surface on the dorsal side of the bone gradually widens anteriorly as well (in contrast to being rectangular);

(2) the parietal cranial crests diverge in the anterior direction to form a V that separates the cranial vault from the muscular surface laterally (the anteriormost section of the crests bents laterally rather than medially).

Besides these two autapomorphic features, this taxon is characterized by the unique combination of the following characters: (1) the occipital shield is large, its anteroposterior length is longer than the length of the posteriorly located smooth area; (2) a narrow muscular surface is present; (3) a short postfoveal crest is present; (4) anterior end of the ventrolateral ridge of the supratemporal process joins the parietal cranial crest at the level anterior to the posteromedial margin of the floor of the parietal fossa. The parietal crest is sharp in the area of the junction; (5) the virtual line, continuing from the ventrolateral ridge of the supratemporal process to the anterior margin of the parietal table, reaches the level as the lateral margin of the parietal foramen here; (6) the supratemporal process has a smooth ventrolateral surface, which fluently continues anteriorly to the muscular surface of the parietal table; and (7) the supratemporal process is straight.

Description. Parietal: The parietal UMJGP 204.749 (Fig. 13A, B) from Gratkorn is fairly preserved, whereas HLMD-Ez 1965 (Fig. 13C, D) from Echzell represents the posterior half of the parietal table, with the left supratemporal process being, however, only partly preserved. The description is therefore based mostly on the holotype UMJGP 204.749. The ornamented surface of several fused headshield osteoderms covers most of the parietal table. The ornamentation consists of well-developed foramina and pits of various sizes, being densely distributed. At the periphery of the ornamented surface, radiated grooves and ridges are developed. The interparietal shield is well recognized in both specimens. This region is pierced by the large anteroposteriorly elongated parietal foramen. Unfortunately, its anterior margin is not preserved. The occipital shield is very large. Its anteroposterior length is twice as long as the length of the posteriorly located smooth area. The parietal notch is well developed. The lateral (=parietal) shields are preserved (but note that the almost entire lateral margins of the parietal table in HLMD-Ez 1965 are damaged). The arcuate edge runs on the dorsal surface of the bases of the supratemporal processes and diminishes laterally. The right supratemporal process is almost completely preserved, being straight. The parietal table extremely widens anteriorly – so it appears to be distinctly constricted at the level of the parietal foramen or slightly posterior to it. Thus, the lateral margins of the table markedly diverge anterolaterally from this point, inclining at an angle of about 30° from the median plane. Due to the lateral expansion of the parietal table, the anterolateral corner of the parietal table reaches further laterally than the supratemporal process. The anterolateral corners protrude into anterolateral processes. The ornamented surface is not rectangular but gradually widens anteriorly as well. The anterior end of the interparietal sulcus lies medial to the anterolateral corner of the ornamented surface.

On the ventral surface, many diagnostic features can be recognized. The oval parietal fossa is small, located in the central posteriormost region of the parietal table. The short postfoveal crests are well developed. In ventral view, both cranial crests are preserved, especially the complete right one, including the anterior portions missing in the Echzell specimen. The cranial crests are sharp. They diverge anteriorly, forming a V-shaped outline that separates the cranial vault from the muscular surface laterally. The muscular surface is narrow, but present. The virtual line, continuing from the ventrolateral ridge of the supratemporal process to the anterior margin of the parietal table, reaches the level as the lateral margin of the parietal foramen here. The ventrolateral ridge of the supratemporal process is well developed and preserved on the right side in UMJGP 204.749 and left side in HLMD-Ez 1965. Its anterior end joins the parietal cranial crest at the level anterior to the posteromedial margin of the parietal fossa. The cranial crest is sharp in this region. The root portion of the supratemporal process is broad. The other distal portion distinctly narrows posteriorly. The ventrolateral ridge is well developed. The supratemporal articulation extends anteriorly, being well visible on the lateral surface of the supratemporal process. Anteriorly to it, between the most anterior portion of the ventrolateral ridge and the anterolateral margin of the supratemporal process, a short ventrolateral surface can be recognized. This surface lies posterior to the parietal cranial crest-supratemporal process junction (note that it is broadly damaged in the Echzell specimen).

Remarks. See the discussion part.

Phylogenetic analysis of *Smithosaurus echzellensis*. The phylogenetic trees presented here are based on limited fossil material – the parietal, and thus more complete fossil specimens of this taxon are needed to draw more robust conclusions. However, in both two analyses, *Smithosaurus echzellensis* is consistently recovered as the sister taxon to either [*Ophisauriscus quadrupes* + *Ophisaurus holeci*] + [*Anguis* + *Ophisaurus*] (in the first analysis) or [*Anguis* + *Ophisaurus*] (in the second analysis). In overall, the support for the clade is very low (no strict synapomorphy; the calculating Bremer supports

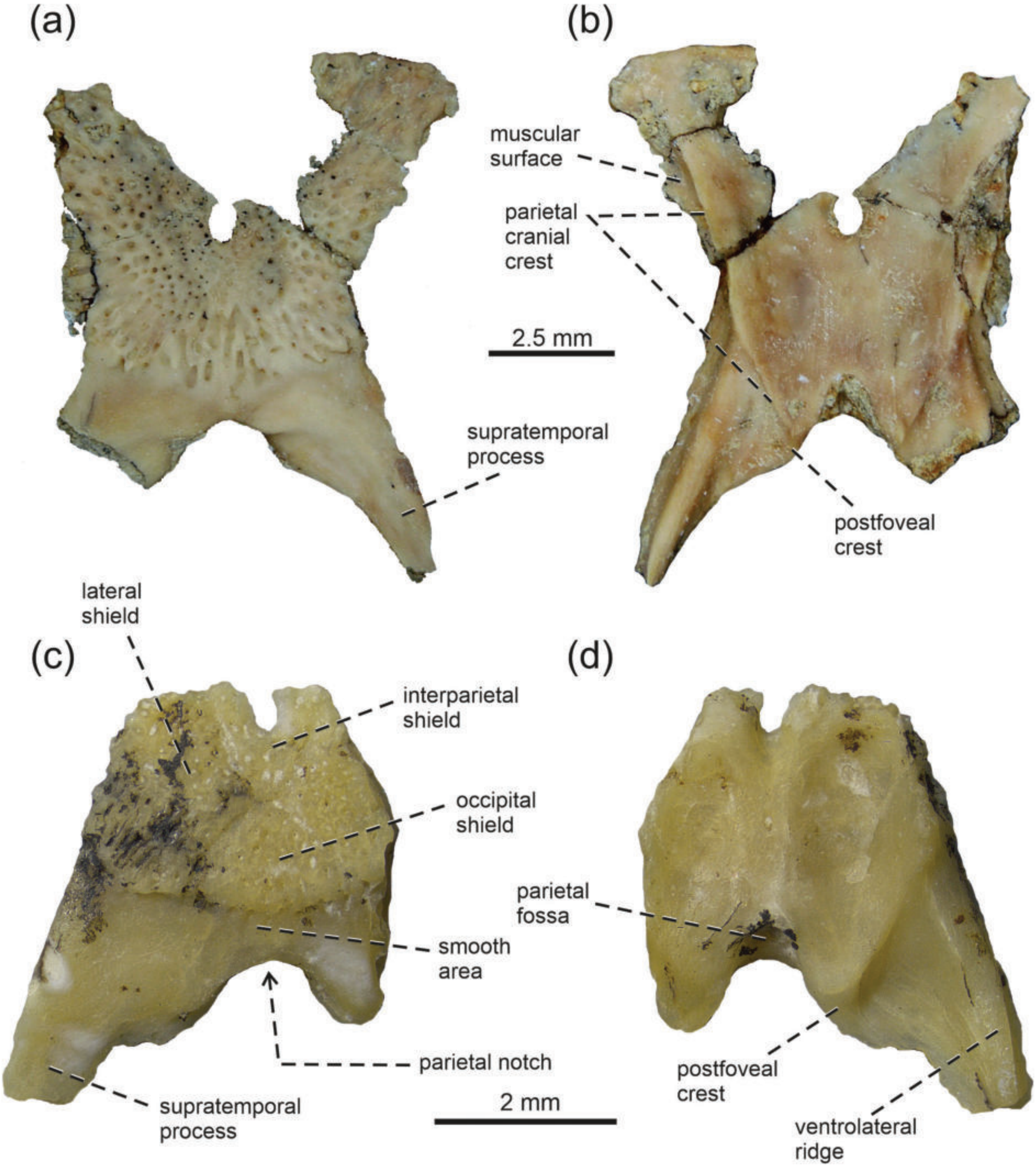

Figure 13. *Smithosaurus echzellensis* gen. et sp. nov. Holotypic parietal UMJGP 204.749 from the Gratkorn locality in (**A**) dorsal, and (**B**) ventral views. Paratypic parietal HLMD-Ez 1965 from the Echzell locality in (**C**) dorsal and (**D**) ventral views.

collapsed the node into polytomy, see below) and thus, the interpretation of the *Smithosaurus* relationship among anguines needs to be met with caution.

1. A New Technology (NT) search in TNT produced a single tree (Fig. 14A). The position of *Smithosaurus echzellensis* is recovered as being sister to the clade [[*Ophisauriscus quadrupes* + *Ophisaurus holeci*] + [*Anguis* + *Ophisaurus* (all others except of *O. holeci*)]]. The calculating Bremer supports collapsed the node (Bremer value 1, relative Bremer 25; Fig. 14B), with the relationship among *Smithosaurus echzellensis* and the clades [*Ophisauriscus quadrupes* + *Ophisaurus holeci*] (Bremer value 3, relative Bremer 50) and [*Anguis* + *Ophisaurus*] (Bremer 2, relative Bremer 50) being unresolved.
2. The heuristic search in TNT produced two equally parsimonious trees. In both,

Smithosaurus echzellensis is recovered as sister to [*Anguis* + *Ophisaurus* (all others except of *O. holeci*)], whereas *Ophisauriscus quadrupes* and *Ophisaurus holeci* are sister to the clade formed by *Smithosaurus*, *Anguis* and *Ophisaurus* (all others except of O. *holeci*). This is contrary to the results from the NT analysis (see above). In the strict consensus tree, however, the position of *Smithosaurus* is unresolved among [*Ophisauriscus quadrupes* + *Ophisaurus holeci*] and [*Anguis* + *Ophisaurus* (all others except of *O. holeci*)], although all these taxa together form a clade. Thus, the topology of examined taxa in this strict consensus tree is identical to that figured in Fig. 14B.

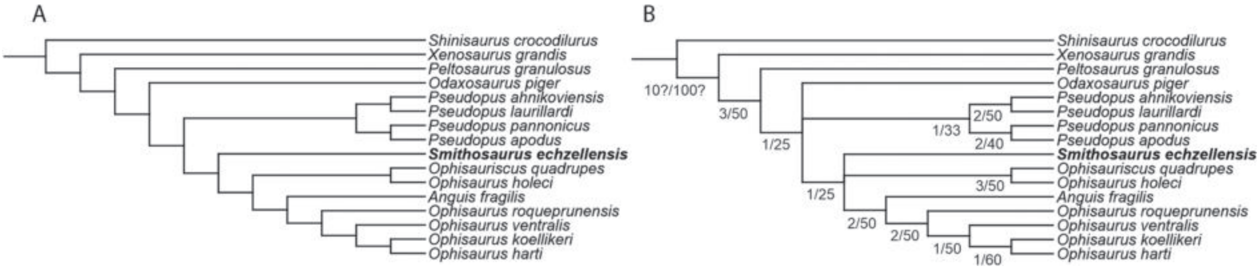

Figure 14. Phylogenetic position of *Smithosaurus echzellensis*. **A.** Single parsimonious tree recovered by TNT using NT (New Technology) search (with ratchet) and 1000 iterations; **B.** Tree showing Bremer / relative Bremer values at nodes recovered by TNT.

Anguinae indet.

Fig. 15

Material. One right maxilla HLMD-Ez 1966, one right and one left dentaries HLMD-Ez 1967–1968, 12 dorsal vertebrae HLMD-Ez 1969–1980.

Description. Maxilla: Only a fragment of the right maxilla is preserved (Fig. 15A, B). It represents the area around the superior alveolar foramen plus the section of the posteroventral process. This maxillary fragment bears eight tooth positions (one tooth is still attached). The otherwise smooth lateral surface is pierced by the labial foramina – three and a half are preserved. The medial side bears the well-developed supradental shelf. At the level of the fifth tooth position (counted from posterior), the shelf expands medially to form the palatine articulation. At this level, the superior alveolar foramen is located on the dorsal side of the shelf. Only the base of the nasal process is preserved; the rest of the bone is broken off. The posterior portion gradually narrows into the posteroventral process. Its dorsal margin smoothly decreases ventrally without being stepped.

Dentary**:** Two dentary fragments are preserved, both representing only the posterior portions (Fig. 15C–F). The right one (HLMD-Ez 1967) possesses five tooth positions, where the penultimate and fourth (counted from posterior) are still partly preserved. Except for two labial foramina, the lateral surface is smooth (only one foramen is preserved in HLMD-Ez 1968). The medial surface exhibits open Meckel`s groove, which narrows anteriorly. It is roofed by the concave, shallow subdental shelf. The position of the anterior inferior alveolar foramen between the dentary and a splenial can be recognized at the level of the fifth tooth position, but this area appears to be eroded. The alveolar foramen is located at the level of the third tooth position. The intramandibular septum, which separates the alveolar canal from Meckel`s groove, is completely fused with the body of the dentary (the free ventral portion is absent). The surangular spine is damaged, so only its root portion can be recognized. The angular process is broken off. The other posterior processes are damaged. The left dentary HLMD-Ez 1968 represents a specimen with four tooth positions – only one complete tooth and the base of another one are still preserved. The position of the anterior inferior alveolar foramen can be still recognized on the subdental shelf. The splenial spine is absent in both specimens. Due to poor preservation of this area, however, this appears to represent a postmortal damage only.

Dentition: The tooth implantation is shallowly pleurodont. The teeth are large, well exposed over the dorsal crest, which supports them laterally. They are conical and distinctly recurved. Their tips are pointed. The mesial and distal cutting edges are well developed. The tooth bases are broad, being pierced by resorption pits. In most cases, the pits are located slightly posterior to the tooth axis. The dentary teeth are smooth by weathering (or affected by digestive process of carnivores), the maxillary tooth crown possesses fine but dense striations on both labial and lingual sides.

Dorsal vertebra: The description is based on the well-preserved specimen HLMD-Ez 1969 (Fig. 15G–J). The vertebral centrum is anteroposteriorly elongated. The height of the vertebra gradually increases posteriorly. The neural spine is low, however, its dorsal portion is broken off. It forms a ridge running along almost the entire length of the dorsal section of the neural arch. In dorsal view, the ridge is thin, becoming less distinct in the anterior section. In the posterior third of its length, it is well defined and widens at its posterior end. The neural canal is high and well arched dorsally. The cotyle is depressed, being mediolaterally expanded and broader than the neural canal. However, the maximum height of the cotyle is

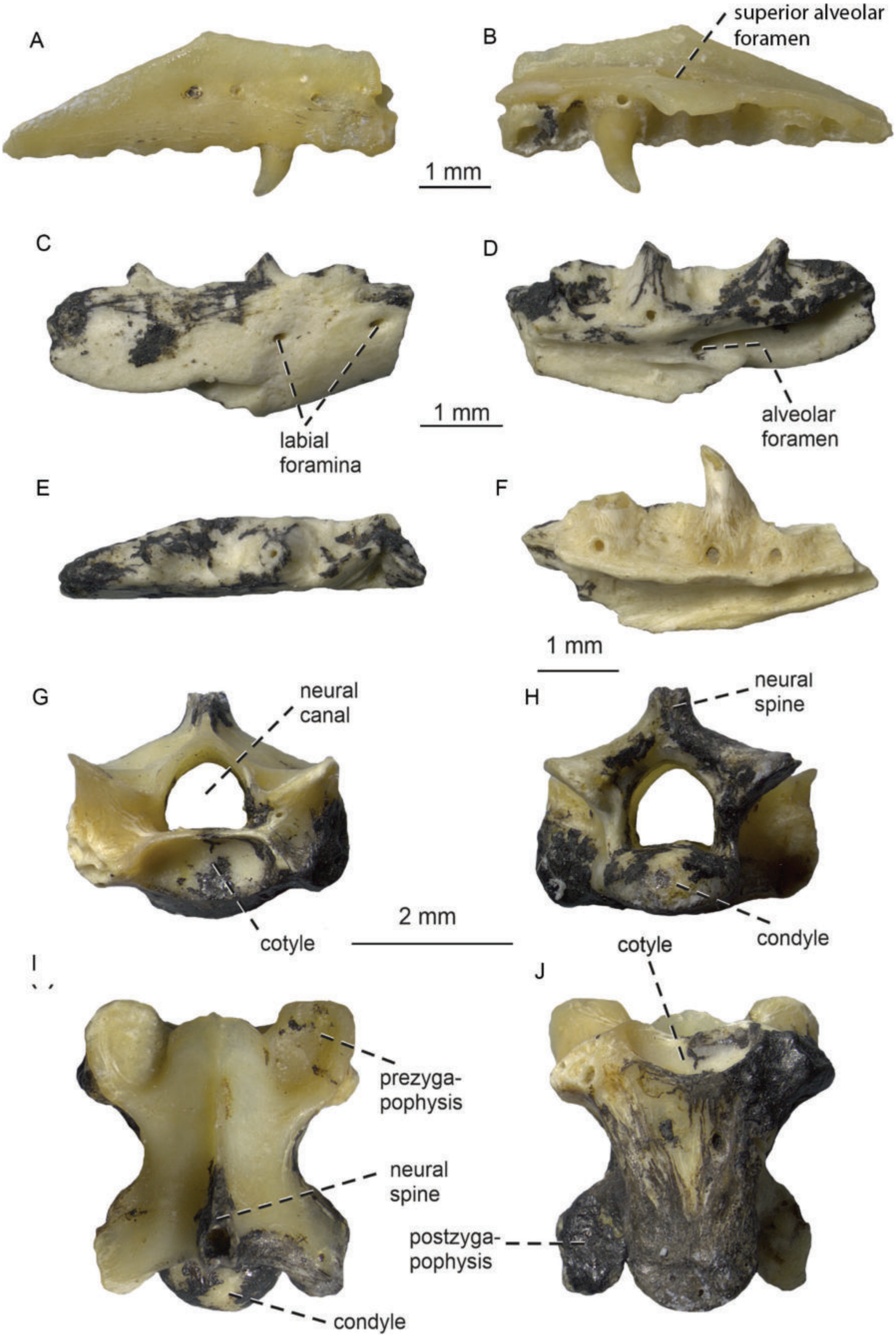

Figure 15. Anguinae indet. from the Echzell locality. Right maxilla HLMD-Ez 1966 in (**A**) lateral, and (**B**) medial views. Right dentary HLMD-Ez 1967 in (**C**) lateral, (**D**) medial and (**E**) dorsal views. Left dentary HLMD-Ez 1968 in (**F**) medial view. Dorsal vertebra HLMD-Ez 1969 in (**G**) anterior, (**H**) posterior, (**I**) dorsal and (**J**) ventral views.

lower than the maximum dorsoventral height of the neural canal. The pre- and postzygapophyses are well expanded laterally; a well-developed interzygapophyseal constriction is located between them. The pre- and postzygapophyses have elliptical articulation surfaces, oriented more or less anteroposteriorly. The prezygapophyses are inclined from the horizontal plane at an angle of approximately 30°. The synapophyses are protruding laterally, being square in shape. The condyle, which is well-protruded posteriorly, is markedly depressed as well as the above-mentioned cotyle. The ventral surface of the centrum is flat. It is pierced by two subcentral foramina in the anterior one-third of the centrum. The lateral margins of the centrum have a concave course, running more anterolaterally from the level of the subcentral foramina.

Remarks. Among extant anguine genera, the morphology of herein described vertebrae resembles that of *Ophisaurus* (Čerňanský et al. 2019). The maxilla with markedly recurved teeth and vertebrae similar to those from Echzell have been described also from Gratkorn (see Böhme and Vasilyan 2014). Such a distinct tooth curvature is not very typical among members of extant *Ophisaurus* (see Klembara et al. 2014), but can be found in fossil species, e.g. in *O. acuminatus* (see Klembara and Čerňanský 2020). However, it should be noted that some features in the dentary, such as the presence of a splenial spine, cannot be supported with confidence due to poor preservation. Moreover, another crucial reason exists why the allocation of this material to *Ophisaurus* might be problematic – the occurrence of a new taxon *Smithosaurus echzellensis* in both Echzell and Gratkorn localities. We cannot entirely exclude the very plausible option that some of those specimens (if not all) belong to this newly described taxon. For this reason, we allocated this material only as Anguinae indet. Caution is also needed in regards to interpretations of isolated jaw fragments and isolated vertebrae from other European Miocene localities, where such incomplete and fragmentary materials are often described as *Ophisaurus*. More complete and articulated material of *Smithosaurus echzellensis*, in which bones can be associated together to observe the anatomy of this taxon, is crucial to resolve this problem.

Anguidae indet.

Fig. 16

Material. Four caudal vertebrae HLMD-Ez 1981–1984, 73 osteoderms HLMD-Ez 1985–1987 (figured ones), HLMD-Ez 1988 (the remaining osteoderms).

Description. Caudal vertebra: The caudal vertebrae (Fig. 16A–E) are elongate and narrow. Both pre- and postzygapophyses are small; thus, there is a typical tendency toward the elongation of the centra in caudal vertebrae and a relative reduction of all processes. The cotyle and condyle are dorsoventrally depressed. The neural canal is a tunnel-like structure here. The haemapophyses are fused to the posterior portion of the centrum, but, unfortunately, their ends are broken off. Only the bases of the anteroventrally oriented transverse processes (pleurapophyses) are preserved, being dorsoventrally slightly flattened. They are pierced by a foramen. The distal portions are, however, broken off. The neural spine is posterodorsally oriented, rather slim and pointed. The transverse autotomic split is present.

Remarks. The presence of an autotomic split indicates that we can exclude *Pseudopus*, in which only autotomic foramina are developed (see Čerňanský et al. 2019). In contrast, the autotomic split is present in both *Anguis* and *Ophisaurus* (see Hoffstetter and Gasc 1969).

Osteoderm: A large number of osteoderms of several types are preserved in the material. The first type represents wide, rectangular osteoderms (e.g., HLMD-Ez 1985, Fig. 16G–F). There is a low medial ridge running along their central regions. However, the ridge is almost indistinctive and restricted only to the sculptured region. The anterior overlap surface is large and occupies about one-third of the external surface. The lateral bevel is the highest close to the overlap surface. The posterior portion of the external surface is ornamented. The ornamentation is formed by several tubercles, pits, long grooves, and ridges diverging from the central region. Three foramina pierce the central part of the internal surface. The second type (and the most common, as represented by HLMD-Ez 1986, Fig. 16H) includes slender osteoderms. In those, the medial ridge runs along the entire external surface, including both ornamented and anterior overlap surface. The third type (rare, HLMD-Ez 1987, Fig. 16I) is represented by a flat and wide osteoderm without a medial ridge.

The differences might very likely represent individual variability and a different body topology from where osteoderms originated (e.g., ventral vs. dorsal armour; see, e.g., Čerňanský and Klembara 2017). Their determination to the alpha taxonomy level is currently impossible. Nevertheless, they resemble osteoderms of *Ophisaurus*, but other taxa cannot be excluded.

Squamata indet.

Fig. 17A–F

Material. One premaxilla HLMD-Ez 1989, right quadrate HLMD-Ez 2002, left pterygoid HLMD-Ez 2003, two osteoderms HLMD-Ez 2000–2001.

Description. Premaxilla: Premaxilla HLMD-Ez 1989 (Fig. 17A–C) represents a small element, although with a more-or-less robust appearance. It is almost fully preserved. It is a single, unpaired T-shaped element (note, a groove or break is running through the midline, see remarks). The premaxilla bears seven-tooth positions with three teeth still attached to the dental parapet. The laterally extended maxillary processes are well developed. They are rather short than long. They possess an articulation facet for the maxilla on their dorsolateral surfaces. The fragmentarily preserved nasal process is wide, its external surface is flat. Here, a few small vestiges of osteoderms attached to the bone are present. In anterior and posterior views, the base of the nasal process

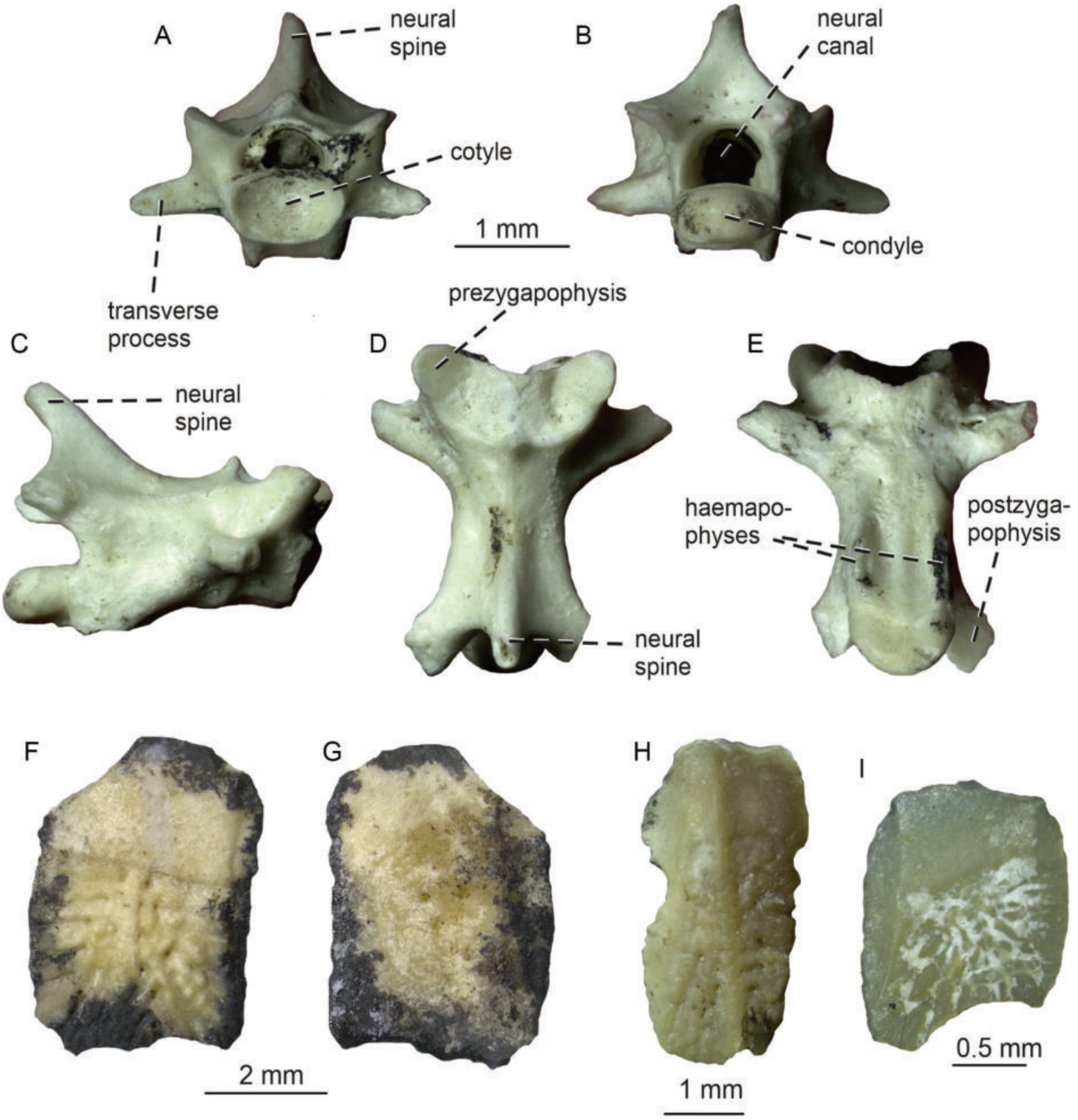

Figure 16. Anguidae indet. from the Echzell locality. Caudal vertebra HLMD-Ez 1981 in (**A**) anterior, (**B**) posterior, (**C**) lateral, (**D**) dorsal and (**E**) ventral views. Osteoderms HLMD-Ez 1985 (**G**), HLMD-Ez 1986 (**E**) and HLMD-Ez 1987 (**I**) in (**F, H, I**) external and (**G**) internal views.

is laterally constricted. Thus, the lateral margins in the lowest region of the process are rounded, having a cut-out like appearance. Dorsally, this region is wide, having more-or-less parallel lateral margins. The most dorsal preserved portion of the process narrows abruptly again, but the rest of the process – the posterodorsal portion with a termination - is broken off. On the internal side, there is a sagittal ridge running along the entire length of the preserved nasal process. It separates the facet for the nasals on both sides. On the lateral side, the ethmoidal foramen is located close to the base of the nasal process. The supradental shelf is formed by two segments, which are well expanded posteriorly. The dorsal side bears the vomerine process, which forms a small bulge. The short, weakly bilobed median incisive process is located ventral to the supradental shelf.

Remarks. Although the right and left premaxillae are fused, note that there is a fracture-like structure (or a tiny groove) running through the central portion of the element. However, it is unclear whether this is postmortal damage only or reflects the fusion of the right and left premaxillae during ontogeny. Even if it is only a fracture

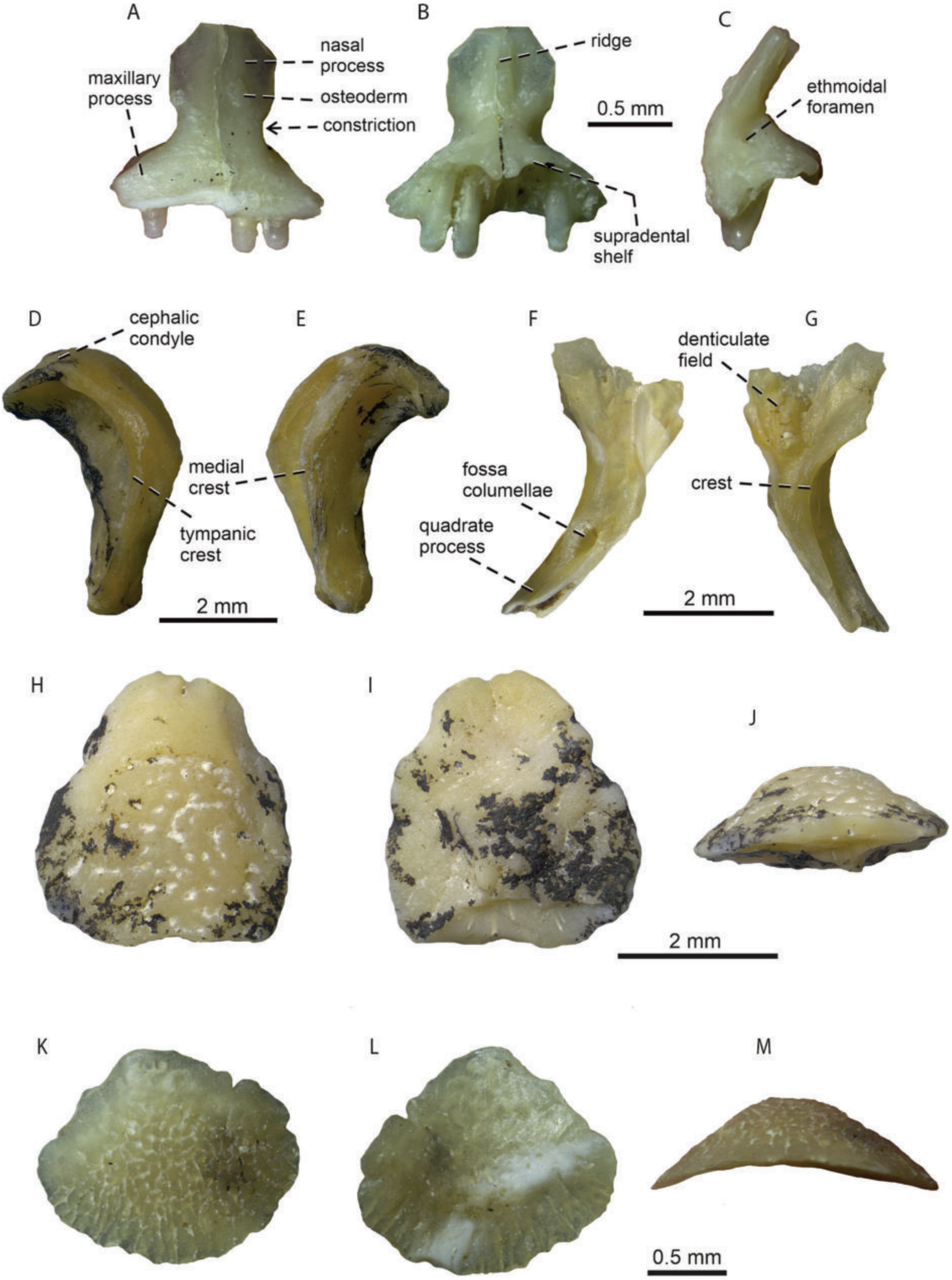

Figure 17. Squamata indet. from the Echzell locality. Premaxilla HLMD-Ez 1989 in (**A**) anterior, (**B**) posterior, and (**C**) lateral views. Right quadrate HLMD-Ez 2002 in (**D**) lateral, and (**E**) medial views. Left pterygoid HLMD-Ez 2003 in (**F**) dorsal and (**G**) ventral views. Osteoderms HLMD-Ez 2000 (**H–J**) and 2001 (**K–M**) in (**H, K**) external, (**I, L**) internal and (**J, M**) posterior views.

caused by damage, the central region might be weaker due to the late fusion and, thus, prone to breakage when pressure is applied. Among *Chalcides* species, a groove indicating a fusion is often present in various degrees (for *Ch. ocellatus*, see Digimorph.org 2002–2012; in some, e.g., *Ch. polylepis*, the right and left premaxillae are separated; see, e.g., Caputo (2004); pers. obs. of A.Č.). However, its lacertid affinity can not be excluded. The premaxilla of lacertids is formed by a single element (see, e.g., Čerňanský and Syromyatnikova 2019). If the specimen HLMD-Ez 1989 represents a lacertid, the present groove is caused by postmortal damage only. In any case, we decided to allocate this specimen to Squamata indet.

Quadrate: A right quadrate is available in the material (Fig. 17D, E). It is a slender, dorsoventrally elongated element. In lateral view, the quadrate is anteroposteriorly narrow, with an anteriorly expanded, rounded anterior margin. Here, the sharp and laterally expanded tympanic crest is present. This crest is continuous from the cephalic to the mandibular condyle. The crest is slightly angled approximately in the mid-region. Further dorsally, it fluently and gradually continues without being distinctly separated by a sharp angle from the portion formed by the cephalic condyle. The dorsal portion of the cephalic condyle protrudes slightly posteriorly. The ventral half of the quadrate narrows gradually ventrally. The ventral region ends with the saddle-shaped mandibular condyle. It is slightly smaller than the cephalic condyle. The medial surface possesses a distinct medial crest. Posterior to this crest, the bone is pierced by a quadrate foramen located in the ventral one-third of the dorsoventral height of the element.

Remarks. The morphology of the quadrate HLMD-Ez 2002 is similar to that of lacertids (see e.g., Čerňanský and Syromyatnikova 2019) rather than anguids. Note, however, that the general shape of the lacertid quadrate resembles that of scincids (see Villa and Delfino 2019b),

Pterygoid: The left pterygoid is incompletely preserved (Fig. 17F, G). It is a tri-radiate, Y-shaped element. Its ventral portion bears a distinct dentition located in the central region. Only the base of the ectopterygoid process is preserved, being broad. From its posterior region, a sharp crest runs to the quadrate process. Here, the crests border a fossa located laterally on the process. The quadrate process is long but note that its end is broken off. The fossa columellae (= epipterygoid fossa), which is present on the dorsal side, is large and elliptical.

Identification of isolated elements as pterygoids is problematic and caution is needed. However, the morphology of HLMD-Ez 2003, e.g., the absence of the obtuse process (ventromedial process sensu Conrad 2008), indicates that we can exclude Anguidae here. Its morphology, including the crests bordering a fossa located laterally on the quadrate process, resembles skinks. Although note that dentition is absent in e.g., *Chalcides occelatus*, but present in, e.g., *Plestiodon fasciatus* (see Caputo 2004; Digimorph.org 2002–2012).

Osteoderm: Two osteoderms are available in the material. The larger osteoderm HLMD-Ez 2000 (Fig. 17H–J) is roughly trapezoidal in shape. It is thick, with distinct external bulging. Its external surface expands in the anterior direction, being gradually more pronounced. This gives a convex appearance in cross-section. The whole osteoderm gradually narrows anteriorly. Here, the well-developed anterior overlap surface is located, forming one-third of the entire anteroposterior length of the osteoderm. Its anterior mid-region bears a short groove, which is present on the internal side as well. The region posterior to the overlap surface bears ornamentation. The ornamentation appears to be rather weak and not dense, being formed mostly by ridges and pits, connected by short grooves in some cases. The medial ridge is absent. The internal aspect of the osteoderm is not flat, but is rough. It has several irregularly distributed pits, foramina, and a few grooves near the posterior end.

The smaller specimen HLMD-Ez 2001 (Fig. 17K–M) is wide. Its width is slightly greater than its anteroposterior length. The anterior portion, which bears a narrow overlap surface, is triangular, whereas the posterior portion has a round margin. The osteoderm is thick, although note that it is narrower relative to its size if compared to the larger one. Here, the internal surface of the smaller osteoderms is slightly concave. The ornamentation of the external surface is formed by densely spaced ridges and grooves running from the ossification centre; those ones located on the periphery are prolonged.

The differences in these two osteoderms can be caused by ontogeny and different origins regarding the body topology. Overall, this type of osteoderms resembles the osteoderms described by Čerňanský (2016; fig. 11) as Squamata indet. 2 from the lower Miocene of the Austrian locality Oberdorf. They might very likely belong to skink.

Serpentes Linnaeus, 1758
Boidae Gray, 1825
Bavarioboa Szyndlar & Schleich, 1993
Bavarioboa hermi Szyndlar & Schleich, 1993

Bavarioboa cf. *hermi*

Fig. 18A–E

Material. Forty-two trunk vertebrae HLMD-Ez 2146–2148, one cloacal vertebra HLMD-Ez 2149, four caudal vertebrae HLMD-Ez 2150 and HLMD-Ez 2150a.

Description. Trunk vertebrae: All but one trunk vertebrae come from the middle trunk portion of the column. Some of them are preserved in relatively good condition, perhaps due to their robust morphology as characteristic of constrictors. In lateral view, these vertebrae are as high as long. In dorsal and ventral views, they are distinctly wider than long. In the largest and best-preserved vertebra HLMD-Ez 2148, the centrum length measures 5.7 mm, centrum width – 7.2 mm, centrum length/centrum

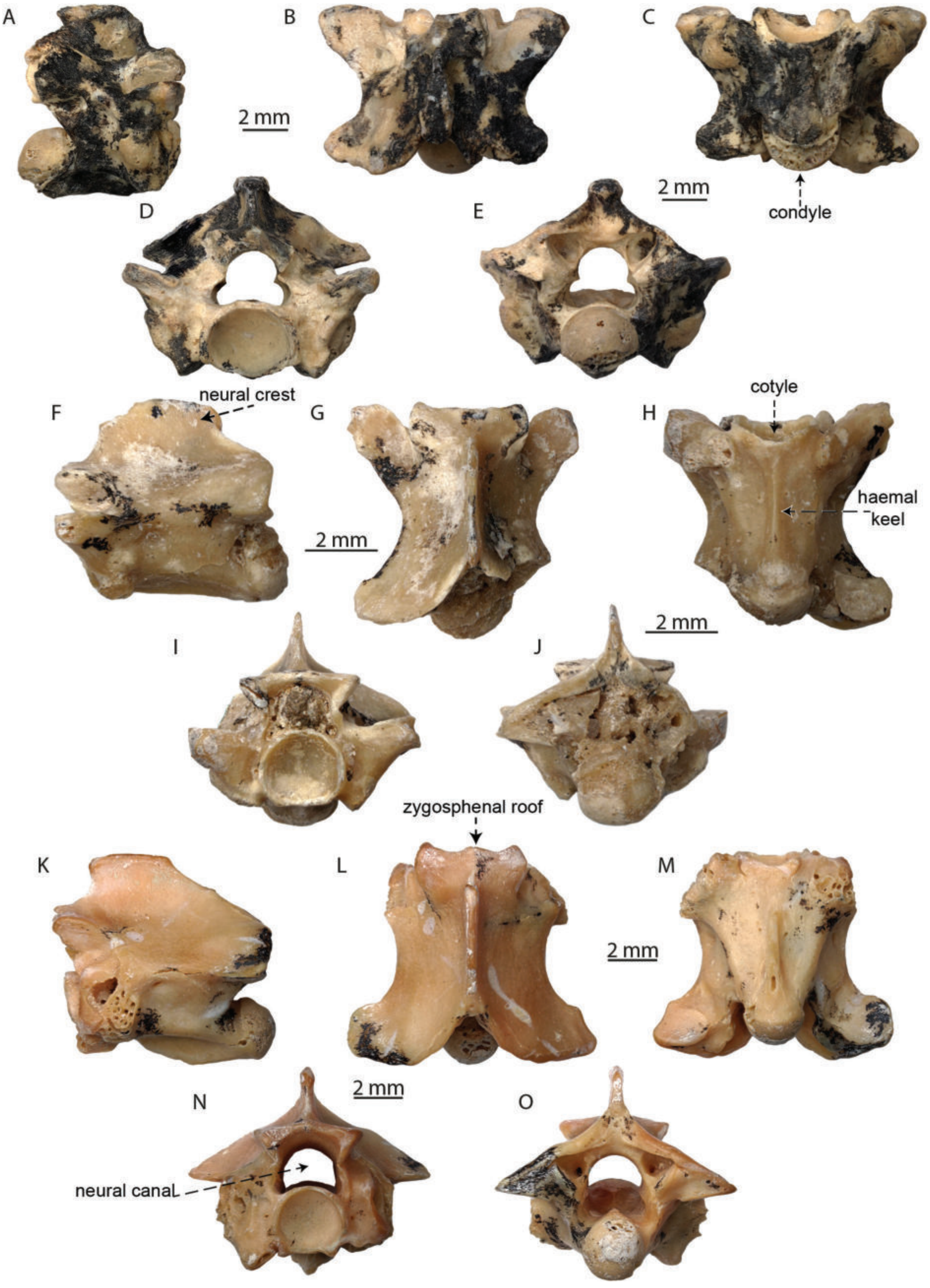

Figure 18. Snakes from the Echzell. **A–E.** *Bavarioboa* cf. *hermi* (HLMD-Ez 2148), middle trunk vertebra; **F–J.** "Colubrinae" indet. (HLMD-Ez 2159), middle trunk vertebra; **K, L.** *Naja* cf. *romani* (HLMD-Ez 2151), middle trunk vertebra. All vertebrae in (**A, F, K**) lateral, (**B, G, L**) dorsal, (**C, H, M**) ventral, (**D, I, N**) anterior and (**E, J, O**) posterior views.

width equals 0.8. The interzygapophyseal constriction, especially in larger vertebrae, is weakly expressed. The centrum is subtriangular in shape. The haemal keel is prominent, broad and slightly broadening posteriorly. In a few vertebrae, however, the keel looks like a biconcave lens owing to the presence of a distinct constriction, located at the level of the subcentral foramina, and prominent broadenings at the anterior and posterior ends. The subcentral grooves and subcentral ridges are prominent. The neural arch is moderately depressed. The neural spine is very low (approximately three times longer than high), thick, and widening posteriorly (Fig. 18A). It occupies more than one half the length of the neural arch and begins immediately behind the zygosphenal articular facets. The zygosphenal roof is slightly convex or roughly straight in dorsal view. The prezygapophyseal and postzygapophyseal articular facets are usually subsquare in shape. The prezygapophyseal processes (if preserved) are very short and hardly visible dorsally. The paradiapophyses are subsquare in outline, higher than long, with indistinct subdivision into para- and diapophyseal portions. The cotyle and condyle are slightly flattened. The subcentral and lateral foramina are large. The paracotylar foramina are absent (Fig. 18D).

In the sole anterior trunk vertebra HLMD-Ez 2146, the haemal keel is replaced by a ventrally directed hypapophysis (its distal portion is broken). The neural spine of this vertebra is very short and relatively high in lateral view. Apart from these characteristics, the anterior trunk vertebra does not differ significantly from the middle trunk vertebrae.

Cloacal vertebra: One cloacal vertebra HLMD-Ez 2149, as characteristic for the sacral portion of the column, is provided with paired lymphapophyses (their distal ends are broken). The centrum length measures 3.4 mm, centrum width – 4.1 mm, centrum length / centrum width equals 0.8. Surprisingly, located on the ventral side of the centrum, minute but distinct paired haemapophyses are present, thus far the trait unknown in the genus *Bavarioboa* (see below).

Caudal vertebrae: Four caudal vertebrae are provided with paired pleurapophyses (missing or partly missing in some vertebrae). In the largest caudal vertebra HLMD-Ez 2150, the centrum length is 4.0 mm, centrum width 4.5 mm, centrum length / centrum width 0.9. Situated on the ventral side of the centrum, are short but distinct paired haemapophyses (partly broken).

Remarks. The constrictor from Echzell displays clearly diagnostic features of the genus *Bavarioboa*, so among others: mid-trunk vertebrae distinctly wider than long; the interzygapophyseal constriction well expressed; the neural arch moderately depressed; the neural spine approximately as high as long, occupying one half the length of the neural arch; the haemal keel prominent; the zygosphene usually roughly straight; the prezygapophyses located clearly above the floor of the neural canal; the long axis of prezygapophyseal facets oblique in dorsal view; the prezygapophyseal processes weakly developed; the paradiapophyses subsquare in shape, with indistinct subdivision into para- and diapophyseal portions (Szyndlar and Rage 2003). By their morphological characteristics and also relatively large size, the vertebrae are similar to those of the type species, *Bavarioboa hermi*, occurring in the German and Czech late early Miocene (Szyndlar and Schleich 1993; Szyndlar and Rage 2003; Ivanov et al. 2020). However, the peculiar hourglass-shaped haemal keels observed in a few trunk vertebrae suggest affinities with *Bavarioboa crocheti* from the French late Oligocene. Interestingly, the sole mid-trunk vertebra of *Bavarioboa* reported from Turkey by Szyndlar and Hoşgör (2012) was provided with a similar (i.e., *crocheti*-like) keel. Nonetheless, other morphological traits of the vertebrae from Echzell suggest that the snake represented *Bavarioboa hermi* or a closely related form.

There is yet another strange anatomical peculiarity observed in the sole cloacal vertebra of *Bavarioboa* from Echzell, namely the presence of the paired haemapophyses. This is surprising, because, in virtually all recent genera of the Boinae, haemapophyses are absent in the sacral region of the column as well as they are absent in the anterior caudals. Exactly the same morphological pattern was observed in some species of *Bavarioboa*, whose vertebrae coming from the sacral / anterior caudal portion of the column of which were available (Szyndlar and Rage 2003). However, there is at last one exception from this tendency in the Boinae, namely, the presence of haemapophyses was confirmed in the posterior cloacal vertebrae (as well in the anterior caudals) in the living boine *Epicrates cenchria* (Szyndlar, unpublished observation).

Colubridae Oppel, 1811
Natrix Laurenti, 1768

Natrix longivertebrata Szyndlar, 1984

Fig. 19

Material. One basisphenoid HLMD-Ez 2158.

Description. The basiphenoid is fragmentary. Its anterior portion, at the level of the anterior orifices of the Vidian canals approximately, is missing. The maximum width of the bone, measured between distal tips of the basipterygoid processes, is 3.7 mm. In ventral view, the basisphenoid crest is absent (Fig. 18A, B). The basipterygoid processes are distinct. Their posterior margins are strongly extended posteriorly covering the recess housing the posterior foramina of the Vidian canals. However, a tiny proximal fragment of the left basipterygoid process is broken off, owing to which the posterior orifice of the Vidian canal as well as the cerebral foramen (for palatine branch of facial nerve, VII) are clearly visible in ventral view.

In dorsal view, several foramina are visible, distributed typically of higher snakes (Fig. 18C, D). The paired largest foramina, located at the midway between the posterior border of the bone itself and the posterior border of the pituitary fossa (sella turcica), are posterior openings for the abducens nerves (VI). The anterior openings for these nerves are situated near the postero-lateral corners of the pituitary fossa. The sympathetic nerve foramina (not visible on the right side) are located directly anterior to the pituitary fossa. The paired openings piercing the basipterygoid processes, laterally to the abducens nerve foramina, are tentatively interpreted as the deep petrosal nerve foramina (both visible on the left side only).

Seen in left lateral view, an opening located directly above the posterior orifice of the Vidian canal and partly hidden beneath the basipterygoid process, is interpreted as a foramen for re-entry of the constrictor internus dorsalis branch (cid) of the trigeminal nerve (V_4) on its way from the prootic (Fig. 19E, F). The location of the exit of the latter nerve (either within the basisphenoid or in a suture between the basisphenoid and parietal) remains unknown owing to the damage of the bone anterior to the basipterygoid processes.

Remarks. Apart from the basisphenoid, the available snake material from Echzell does not contain any other elements, in particular vertebrae, identifiable as belonging to natricine snakes. This absence of any vertebrae is astonishing, considering that in virtually all fossil sites, if they yield snake cranial remains, the latter are typically accompanied by vertebrae. Unfortunately, this is not the case of the material from Echzell. Theoretically, some vertebral fragments classified here as "Colubroides indet." could belong to natricines, but it cannot be proved on the studied material.

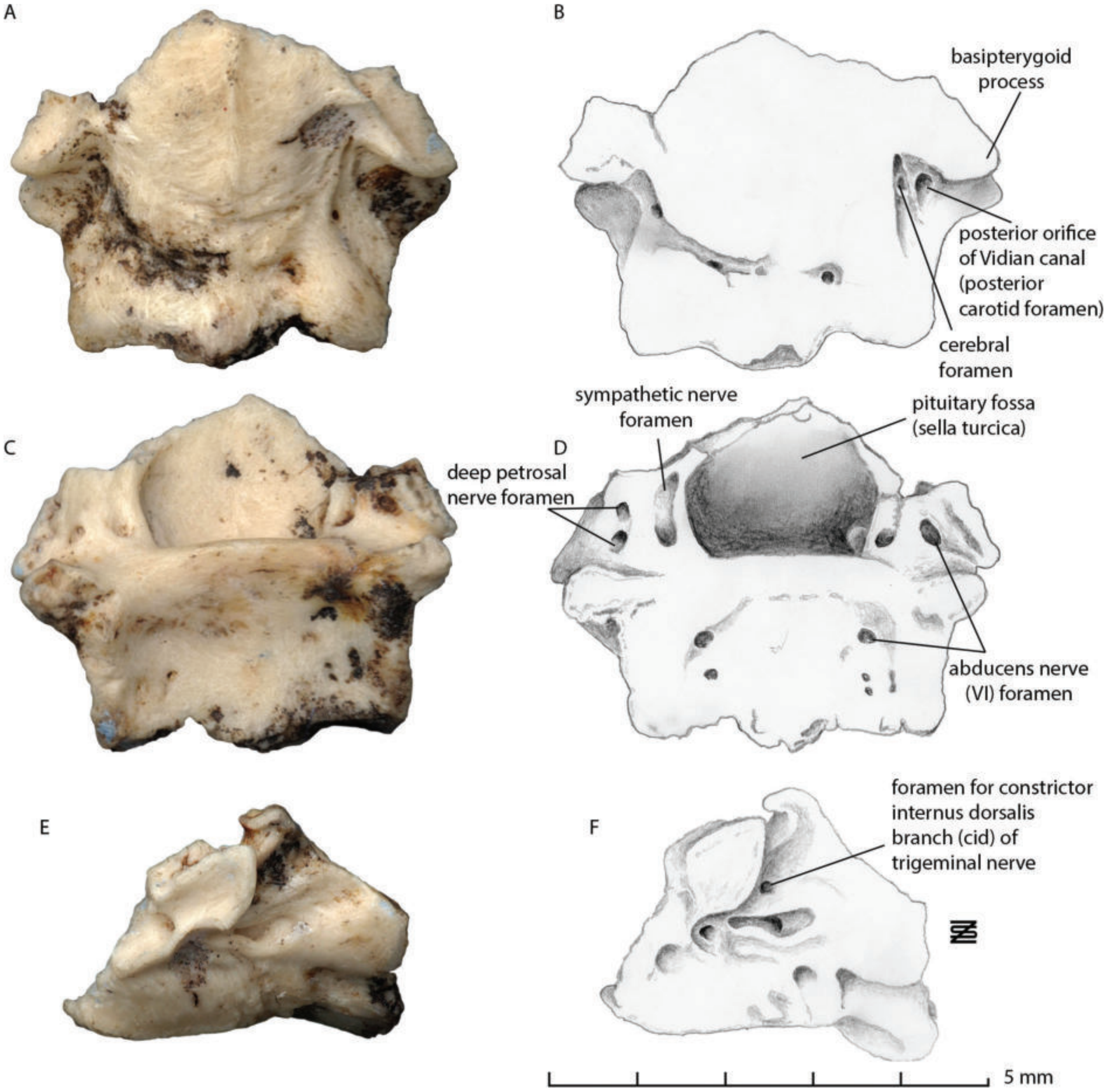

Figure 19. Basisphenoid of *Natrix longivertebrata* (HLMD-Ez 2158) in (**A, B**) dorsal, (**C, D**) ventral and (**E, F**) left lateral views.

The basisphenoid from Echzell is clearly referable to the extinct snake *Natrix longivertebrata*. By its peculiar morphology, it significantly differentiates not only from basisphenoids of other natricines (except for *N. astreptophora*, see below) but also from those belonging to members of other ophidian families (Szyndlar, unpublished observations).

“Colubrinae” indet.

Fig. 18F–J

Material. Seventy trunk vertebrae HLMD-Ez 2159 and HLMD-Ez 2159a.

Description. Vertebrae: All vertebrae classified here as “Colubrinae” are preserved in more or less fragmentary state; most are badly preserved. The largest vertebra, coming from the middle trunk portion of the column HLMD-Ez 2159 (Fig. 18F–J), belonged to a relatively small-sized snake (centrum length measures 4.5 mm, centrum width – 3.6, centrum length / centrum width ratio equals 1.25). It lacks both prezygapophyseal processes and right postzygapophysis. The centrum of most vertebrae is subtriangular in ventral view and slightly longer than wide in the largest vertebrae. In a number of smaller vertebrae, interpreted as posterior trunk vertebrae, the centrum is more elongated. The subcentral ridges are well developed. The haemal keel is distinct and slightly widening before reaching the condyle base. The neural arch is moderately vaulted, not accompanied by any epizygapophyseal spine. The neural spine (partly preserved in few vertebrae only) is twice longer than high approximately. The zygosphenal roof (preserved in few vertebrae) is roughly straight or consisting of three indistinct lobes. The prezygapophyseal articular facets are oval (Fig. 18G), the postzygapophyseal facets are usually subsquare in shape (Fig. 18H). The prezygapophyseal processes are damaged in all vertebrae. Remnants of the processes preserved in one (?posterior) vertebra indicate that the apophyses may have been slender and relatively long (as long or almost as long as the prezygophyseal articular facets). The paradiapophyses (usually eroded) are moderately developed, with the dia- and parapophyseal portions of roughly equal length (Fig. 18I). The cotyle and condyle are slightly depressed dorso-ventrally. The lateral, subcentral and paracotylar foramina are small but distinct.

Remarks. Owing to the bad preservation state of the aforementioned remains, we refrain from identifying the fossil snake to the genus level. The remains resemble roughly those of a number of small “colubrines” (i.e., “Colubridae” devoid of hypapophyses throughout the column) reported from several early Miocene sites (Szyndlar 2012). We cannot exclude the possibility that the fossils belonged to more than one taxon, but it cannot be proved.

Elapidae Boie, 1827
Naja Laurenti, 1768
Naja romani (Hoffstetter, 1939)

Naja cf. *romani*

Fig. 18K–O

Material. Four fangs HLMD-Ez 2157, 50 trunk vertebrae HLMD-Ez 2151–5156.

Description. Fangs: Four isolated teeth are venomous fangs. They are tubular, with acute distal tips. The discharge orifice, located on the anterior surface of each fang, is elongate and gladiate-shaped. The discharge orifice extends, towards the proximal end, in the form of a visible suture. The latter condition is characteristic of elapid snakes, whereas in viperids the anterior surface of the fang is generally smooth. Relatively small dimensions of the fangs suggest that they either belonged to juvenile / subadult individuals or were replacement (non-functional) fangs.

Vertebrae: Most vertebrae come from the middle trunk portion of the column. In the largest (but partly damaged) vertebra (HLMD-Ez 2151, Fig. 18K–O), centrum length measures 7.1 mm, centrum width – 5.7 mm, and centrum length / centrum width ratio equals 1.25. At least in large vertebrae, the centrum is triangular in ventral view, with a flat or slightly concave ventral surface. The subcentral ridges are well developed, especially behind the paradiapophyses. The hypapophysis, preserved partly in few vertebrae, is thick, strongly inclined posteriorly and shows a straight anteroventral margin. The neural arch is rather depressed. The neural spine, preserved partly in few vertebrae, is approximately twice longer than high. Its anterior margin is straight. The shape of the posterior margin is unknown. The paradiapophyses are well developed with short but distinct parapophyseal processes (the latter is preserved only in two vertebrae). The zygosphenal roof is almost straight or slightly convex in dorsal view. The prezygapophyseal and postzygapophyseal articular facets are relatively small and oval-shaped. The prezygapophyseal process (preserved only on the left side of one vertebra) is well developed, somewhat shorter than the articular facet and possesses also a moderately obtuse tip. The cotyle and condyle are suborbicular or slightly depressed. The subcentral, lateral, and paracotylar foramina are distinct (Fig. 18K–M).

A few trunk vertebrae coming from the posterior trunk portion of the vertebral column are more elongated than those from the middle portion. One vertebra (HLMD-Ez 2154; centrum length 4.1 mm, centrum width is 3.0 mm, centrum length / centrum width ratio 1.4) is provided with a completely preserved hypapophysis. The hypapophysis is dagger-shaped and directed posteriorly.

Remarks. Based on the overall vertebral morphology, cobras can be rather easily differentiated from other European fossil snakes. The vertebrae of cobras “mimic” the morphological pattern characteristic of large-sized "colubrines" but, unlike the latter, they are provided with hypapophyses throughout the trunk portion of the column. The vertebrae described above generally display the anatomical features characteristic (e.g., dagger-shaped and posteriorly directed hypapophysis) of the extinct species *Naja romani* (Szyndlar 2005). Considering the fragmentary state of preservation of the fossils, we prefer to use the species name with the qualifier "cf.".

Colubroides indet.

Material. Fifty-seven caudal vertebrae HLMD-Ez 2160.

Remarks. The caudal vertebrae (all damaged, in most cases badly preserved) belong most likely to small-sized advanced snakes (i.e., different than *Bavarioboa*). Because of the poor preservation, the vertebrae were not identified to the family level.

Serpentes indet.

Material. Fifty-six vertebrae HLMD-Ez 2161.

Remarks. All these elements are minute vertebral fragments (rather than fragmentary vertebrae). They display ophidian characteristics, but besides more precise identification is not realizable.

Discussion

The Echzell fauna consists of one allocaudate – *Albanerpeton inexpectatum*, five salamanders – *Chioglossa* sp., *Mertensiella* sp., *Lissotriton* sp., *Salamandra* sp., *Chelotriton* sp., five frogs – *Latonia*, *Palaeobatrachus robustus*, *Pelophylax* sp., *Rana* sp., *Pelobates sanchizi*, a gecko – Gekkota indet., a chameleon *Chamaeleo andrusovi*, and anguine lizards, also represented by a new genus and species, – *Smithosaurus echzellensis*, a lacertid, a skink – cf. *Calcides* sp., four snakes – *Natrix longivertebrata*, "Colubrinae" indet., *Naja* cf. *romani*, *Bavarioboa* cf. *hermi.* In addition to them, Tobien (1954) mentioned also shell plates of testudinid tortoises which, unfortunately, could not be relocated in the collection of the HLMD and made available for our study. Clearly, the Echzell assemblage does not include the primary paleofauna and thus, a better picture of the fauna as well as our interpretations can be improved by further material collection. For the palaeobiogeographic analysis of the Echzell herpetofauna, we provide an overview of the well-documented amphibian and reptilian assemblages from European localities of the MN3–MN4 zones. The record of amphibians and reptiles follows the references cited in the caption of Table 2. The entire herpetofauna of Echzell is represented by genera very broadly known in the early Miocene of Europe.

The analysis suggests that fossil records of higher taxonomic groups are significantly biased by taphonomic and/or environmental conditions. For instance, the lack of *Latonia* from both localities of Mokrá-Western Quarry is interpreted by Ivanov (2008) to be a result of the depositional environment. Testudinids are entirely missing in e.g. Oberdorf, Austria, whereas for Mokrá-Western Quarry, Czech Republic they have not been studied yet (Table 2). Moreover, many lizard groups, which often occur in other European localities, are missing in Echzell (see below).

We have compared the early Miocene European herpetofauna (Table 2) with the Anatolian one (Vasilyan et al. 2019) as much as the taxonomy of the latter record allows it. The over-regional scale comparison suggests similar frog (*Latonia*, Palaeobatrachidae, Pelobatidae, Bufonidae) and salamander (*Salamandra*) faunas, whereas the lacertids are quite diverse in comparison to Europe. The taxonomic assignment of the anguids from Anatolia does not allow any comparison with the European record. Other groups are missing from the fossil assemblages, or the identification is not as precise as necessary to compare.

Amphibians

The amphibian assemblage of Echzell is represented by characteristic forms commonly known from the (early) Miocene of Europe, e.g. *A. inexpectatum*, *Chioglossa*, *Mertensiella*, *Salamandra*, *Latonia*, *Palaeobatrachus* etc. (Table 2). The remains of *Chelotriton* are the most abundant, whereas *Albanerpeton*, *Chioglossa*, *Mertensiella*, *Salamandra* are less abundant. The genera *Chioglossa* and *Mertensiella*, being phylogenetically sister groups (Pyron and Wiens 2011), have rather synchronous and exclusively European fossil occurrence since the late Oligocene – early Miocene (Böhme and Ilg 2003). Their recent areas are limited to humid forested regions of Western Europe (*Chioglossa*) and Western Asia (*Mertensiella*) (Sparreboom 2014). Surprisingly, in a number of Western and Central European early Miocene localities, they have sympatric occurrences (e.g., see Table 2). Osteologically, the genera can be distinguished by few characters of trunk vertebra, see, e.g. Ivanov (2008), Hodrová (1984). Most probably, Western and Central European early Miocene *Chioglossa* and *Mertensiella* represent the earliest forms of the genera and suggest a European origin of the clade *Chioglossa*+*Mertensiella*. However, due to recent advances in molecular phylogeny (e.g., Wielstra et al. 2010; Recuero and García-París 2011), a better understanding of the diversity of these genera as well as other recent genera, e.g., *Salamandra*, *Lissotriton*, *Triturus* is available. A detailed osteological study (including other skeletal elements than vertebra) of the recent forms, taking into account the current knowledge of molecular studies, will enable more precise identification of the fossil material, for instance, at the species or species-group level.

Among other salamanders, it is interesting to note that the Echzell assemblage includes only one form of *Chelotriton* contrary to, e.g. both localities of Mokrá Western Quarry

(Ivanov 2008). As discussed before, the Echzell *Chelotriton* sp. differs morphologically from all other forms of the genus from MN3–MN4 localities. This has been already observed earlier and interpreted as interspecific variability (Schoch et al. 2015) or uncovered high specific or generic diversity (Vasilyan 2020) for the genus. The second option seems rather probable, considering the present-day biodiversity of the genus *Tylototriton* (Hernandez 2016), a genus most probably related to the European fossil *Chelotriton*.

Two of the five frog taxa, *Latonia* and *Pelobates*, are most abundant in the Echzell assemblage. The species *P. sanchizi* is commonly found in the middle to early late Miocene European localities. So far, the species *P. sanchizi* has been described only from two MN4 localities Mokrá-Western Quarry 1/2001 and 2/2001 and from other younger localities correlated to MN6 and younger zones. A gap in the stratigraphic occurrence at the transition of the early-middle Miocene is "filled" by another species, *P. fahlbuschi* from Sandelzhausen, Germany (Böhme 2010). *P. sanchizi* from Echzell, representing one of the oldest fossil records of the species, extends its geographic occurrence during the early Miocene (MN4) of Europe.

Palaeobatrachus robustus from Echzell extends the stratigraphic occurrence of the species, so far limited to MN2. It was confidently known from the early Miocene (MN2) locality Laugnac, France (Hossini and Rage 2000). Another probable occurrence has been mentioned for the late Oligocene of Germany (loc. Oberleichtersbach; Böhme 2008), where a fragmentary frontoparietal has been identified as *Palaeobatrachus* sp., showing affinities with *P. robustus*. The figured Oberleichtersbach specimen of *Palaeobatrachus* sp. aff. *P. robusutus* in Böhme (2008; plate 3, fig. 7) resembles the morphology of Echzell frontoparietals. The taxonomic identification of the palaeobatrachids both at the generic and species level relies on the frontoparietal morphology (Wuttke et al. 2012; Roček et al. 2015). Unfortunately, this bone has very limited preservation potential in the fossil record, which hinders species-level identification of the material and a better understanding of the stratigraphic occurrence of the species. Nevertheless, the Echzell record of the species suggests a longer presence of the species in Europe during the Miocene.

The other two frog taxa, *Pelophylax* sp. and *Rana* sp., are represented by very few remains. These two genera are also commonly found in all localities of similar age. In general, the comparison of anuran assemblages of MN3–MN4 localities (Table 2) suggests that representatives of the Bufonidae, Hylidae, Pelodytidae families are rarely found. It could be related to the absence of environments, e.g., dry habitats for *Bufotes*, or in general rare occurrences of those clades in the amphibian assemblages.

Lizards

Although the Echzell lizard material is only fragmentarily preserved, it provides essential information on the paleobiodiversity and spatial distribution of lizard taxa in the early Miocene. Several major clades can be recognized: Gekkota, Chamaeleonidae, Anguidae and Scincidae. Overall, the Echzell lizard assemblage is similar to other European localities from MN4, e.g., Dolnice and Mokrá Western-Quarry in the Czech Republic (see Roček 1984; Čerňanský 2010b, 2010c; Ivanov et al. 2020) and Oberdorf in Austria (Čerňanský 2016) (see Table 2). Interestingly, amphisbaenians, varanids, cordylids and the genus *Pseudopus* were not recognized in the material available to us. Lacertids are very limited in Echzell based on the material available to us, although they are very abundant in other localities of this age (Čerňanský 2010c, 2016; Ivanov et al. 2020). The missing group represents large-sized animals, which might point to potential taphonomic and/or sampling biases. However, an environmental bias cannot be excluded since a large size animal (testudinid tortoises) has been reported with one fragment from the locality.

Regarding chameleons, the frontal is partly preserved. The bone described here, although preserved only as a fragment, represents the first described frontal of the extinct species *Chameleo andrusovi* Čerňanský, 2010b.

Regarding the parietal bone, three genera of anguines (where this element can be studied) are recognized in the Neogene of Europe until now: *Pseudopus*, *Anguis* and *Ophisaurus* (including problematic *O. holeci*, see below). Note that these taxa also represent extant lineages. However, the parietals from Echzell and Gratkorn have unique features (plus combination of other character states, see diagnosis) which do not allow to allocate them to any of the currently known genera. Therefore, we have erected a new taxon, *Smithosaurus echzellensis*. The parietal UMJGP 204.749 from Gratkorn was originally allocated to *Ophisaurus spinari* (Böhme and Vasilyan 2014; note that originally three other parietals from Gratkorn were erroneously assigned to anguines) but Klembara and Rummel (2018) recognized its unique morphology in regard to other taxa. The occurrence of a new genus in the Neogene of Europe shows a greater diversity of anguines than previously thought. Besides the clear autapomorhic features typical for this new taxon, it exhibits interestingly a mixture of features of *Ophisaurus*, *Anguis* and *Pseudopus*: (1) a short postfoveal crest – this character state is typical for *Pseudopus* (and present also in the fossil taxon *Ophisaurus holeci*, but absent in *Anguis* and all other *Ophisaurus*; see Klembara 2015; Čerňanský and Klembara 2017; Čerňanský et al. 2019); (2) narrow muscular surface – the large muscular surface is present in *Pseudopus* (a narrow one is developed in some large individuals of *O. holeci* as well, see Klembara et al. 2019); (3) a large occipital shield, its anteroposterior length is longer than the length of the posteriorly located smooth area. This is typical for *Anguis* (Klembara and Rummel 2018; Čerňanský et al. 2020a); (4) the parietal notch present – this can be seen in *Anguis* and *Ophisaurus* (e.g., Čerňanský et al. 2015; Klembara et al. 2019); (5) the supratemporal process with a smooth ventrolateral surface, which fluently continues anteriorly to the muscular surface of the parietal table (a typical character state in *Pseudopus* (see e.g., Klembara et al. 2017; Klembara and Rummel 2018)); (6) a straight supratemporal process – this is present in *Pseudopus*, but not in *Anguis* and all other *Ophisaurus* species studied except of *O. holeci* (see e.g., Čerňanský and Klembara 2017; Klembara et al. 2019); (7) the anterior end of the ventrolateral ridge of the supratemporal process joining the parietal cranial crest at the level anterior to the posteromedial margin of the floor of the parietal fossa. The parietal crest is sharp in the area of junction. This is in contrast to *O. holeci*, *O. roqueprunensis* and *Pseudopus pannonicus* (Čerňanský and Klembara 2017; Klembara and Rummel 2018; Klembara et al. 2019).

The typical, anteriorly diverging parietal cranial crests in *Smithosaurus* can be seen outside of the Anguinae. It is present, although not developed to such a degree, in e.g., *Elgaria* (Gerrhonotinae; see Bhullar 2011; fig. 35b; Ledesma and Scarpetta 2018; fig. 18b) and in some xenosaurs (Bhullar 2011; fig. 36b).

The results of the phylogenetic analyses, although based only on the limited data, recovered *Smithosaurus echzellensis* as sister to the clade formed by *Ophisaurus* and *Anguis* (or to the larger clade formed by these and *Ophisauriscus quadrupes* + *Ophisaurus holeci*). This reflects the primitive character states of the new taxon in regard to anguines (and/or eventually, the combination of character states is present in the other anguines studied here). Although the position on the tree represents a relative degree of evolutionary relationships rather than reflecting the process of phylogeny (i.g., a sequence of ancestors and descendants), such a result might point to the existence of potentially archaic lineage(s), persisting into the Miocene. Another example in this regard is *Ophisaurus holeci* (see Klembara et al. 2019). As stated above, however, all conclusions are based strictly on the parietal features only and need to be met with caution. Only future studies of complete material can shed light on anguine phylogeny.

Snakes

The genus *Bavarioboa* is an extinct representative of the subfamily Boinae, the group today absent in the Old World continents. *Bavarioboa*, represented by several species, belonged to the commonest European snakes in the second half of the Oligocene. Remains of this snake, of late Oligocene / early Miocene age, were also found in Turkey (Szyndlar and Hoşgör 2012; Syromyatnikova et al. 2019). *Bavarioboa* reappeared in Europe at the end of the early Miocene (Ivanov 2002; Szyndlar and Rage 2003). The geologically youngest remains of *Bavarioboa* were reported from the middle Miocene of Germany (Ivanov and Böhme 2011).

Natrix longivertebrata was described, as a new species, from the late Pliocene of Poland by Szyndlar (1984), based on a large number of diverse bones including several basisphenoids. Later, fossil remains (exclusively vertebrae) referred to this species (usually with qualifiers 'cf.' or 'aff.') were reported from several European sites, dated from late Miocene to late Pliocene, by various authors (see Szyndlar 2005, and references therein). It is doubtful that all these remains belong to *N. longivertebrata*. The turning point in studies on this species was the discovery of several basisphenoids (along with other bones) among ophidian remains coming from the middle Miocene of France (identified as *N.* aff. *longivertebrata*), making *N. longivertebrata* a snake with one of the longest known stratigraphic ranges. *N. longivertebrata* was considered to be morphologically closer to the living *N. natrix* than to any other extant members of the genus *Natrix* and, eventually, it was considered a direct ancestor of *N. natrix* (Rage and Szyndlar 1986; Szyndlar 1991).

The key differences between *N. longivertebrata* and *N. natrix* can be observed in the basicranium, in particular in the posteriormost area of the basisphenoid. In *N. longivertebrata* the posterior margins of the basipterygoid processes of the basisphenoid are strongly extended posteriorly so that the posterior orifices of the Vidian canals are hidden inside bony recesses and hence invisible in ventral aspect. In *N. natrix* (excluding *N. n. astreptophora*, which cranial osteology remained unstudied yet in the early 1990s), the posterior margins of the basipterygoid processes are oriented anteromesially, so that the posterior foramina of the Vidian canals, usually shifted forwards from the posterior border of the bone, are well exposed in ventral view. The former condition was termed "ancient", while the latter was termed "modern" (Szyndlar 1991). The "ancient" pattern is the only condition observed in *N. longivertebrata*, but it occurred very rarely in populations of *N. natrix* from the Polish early and middle Pleistocene: altogether, 3 "ancient" versus 136 "modern" basisphenoids (Szyndlar 1991: table 1). The gradual change in the frequency of the two different basicranial morphological patterns ("ancient" vs. "modern" basisphenoids and also other cranial characteristics) was the basis for Szyndlar (1991) hypothesis of the transformation of the *N. longivertebrata* lineage into *N. natrix*. Clearly, the greatest weakness of the above hypothesis is the lack of any basicranial elements referable to natricine snakes from the long period between the middle Miocene and late Pliocene.

Rage and Szyndlar (1986: 60) mentioned that "in recent snakes, this character [i.e., the "ancient" pattern] has been noted only in one specimen from Spain" (*Natrix natrix*, MNCN 820924). Unfortunately, they did not connect the variability of the basiphenoid with the geographic distribution of different populations (subspecies) of the living grass snake. In 1996, Stefan Müller-Champrenaud (unpublished observations, see Szyndlar 2012 for details) first noticed that the "ancient" pattern of *N. longivertebrata* is also characteristic of a living subspecies of *N. natrix*, namely *N. n. astreptophora*, inhabiting today Iberia and southern France. The taxonomic status of the latter snake was then discussed by Pokrant et al. (2016), who raised *astreptophora*, mainly based on genetic characters, to the species level. Apart from the molecular evidence, these authors presented also some observations on the cranial osteology of *N. astreptophora* and, eventually, made some comments with reference to *N. longivertebrata*.

Although Pokrant et al. (2016; fig. 2) seemed to appreciate the significance of the basisphenoid morphology, the bone has been missed for *N. astreptophora* when depicting it in ventral aspects for a few subspecies of *Natrix natrix*. Pokrant et al. (2016: 875) argued that Szyndlar (1991) for "contradicting basic phylogenetic principles", without explaining why both "ancient" and "modern" basiphenoid patterns occur together in Pleistocene ophidian assemblages. They claimed (ibidem: 875) that the "re-examination of Szyndlar's material revealed that his only three specimens of *N. natrix* sharing the character state of the fossil *N. longivertebrata* (Szyndlar 1991) belong to [sic!] *N. n. astreptophora*". As mentioned above, these three "ancient" (or *astreptophora*-like) basisphenoids were found in two Polish Pleistocene localities along with more numerous "modern" basisphenoids and, consequently, all remains were identified as belonging to *N. natrix* (Szyndlar 1991; table 1). Such a variability of the skull bone one can interpret as a polymorphism, which has not been considered by Pokrant et al. (2016).

Finally, Pokrant et al.: 885 (2016) observed that "the same character state as in *Natrix longivertebrata* and *N. n. astreptophora* [i.e., the "ancient" basisphenoid pattern] is also found in *N. maura*". The above statement cannot be supported, as the basisphenoid of the latter snake depicted by these authors (ibidem; fig. 2F) represents apparently the "modern" pattern. Similarly, the basisphenoid of another specimen of *N. maura* (MNCN 824272), examined and illustrated by Szyndlar (1984; fig. 28: 7), displays clearly the "modern" pattern, as well. In the light of these facts, Pokrant et al. (2016) conclusions resulting from the osteological observations needs to be critically considered. In particular, the suggestion that homoplasy explains "the occurrence of identical basisphenoid patterns in certain *Natrix* taxa" (ibidem: 884–885) remains unproven.

As mentioned above, based on the cranial osteology (in particular basisphenoids), Rage and Szyndlar (1986) hypothesized that the living species *Natrix natrix* was a direct descendant of the Neogene extinct species *N. longivertebrata*. Based on our current knowledge of the osteology of *N. astreptophora*, we propose to modify this hypothesis and consider *N. natrix* and *N. astreptophora* as descendants of *N. longivertebrata*. If this supposition is correct, the divergence into two extant species must have taken place between the middle Miocene and late Pliocene (indeed, based on molecular data, Kindler et al. (2017; fig. S1) estimated that the split into *N. astreptophora* and *N. natrix* took place between 9.6 and 10.6 Ma, i.e., early late Miocene). Unfortunately, owing to the lack of any fossil record (basisphenoids) from this very long period, more precise dating based on paleontological data is not possible. The proposed hypothesis does not contradict Pokrant et al. (2016; p. 884) conviction "of the unambiguous molecular evidence for the monophyly of *N. natrix* (inclusive of *N. n. astreptophora*)". Last but not least, detailed comparative studies of skulls of *N. natrix* and *N. astreptophora* woud be desired. Concluding, the present discovery of the basisphenoid from Echzell, clearly referable to *Natrix longivertebrata*, extends back the stratigraphic range of this fossil species to the early Miocene.

Naja romani was first described as a member of the extinct genus *Palaeonaja*, from the French middle Miocene (Hoffstetter 1939). Rage and Szyndlar (1990), who revised the entire fossil record of the European cobras, synonymized *Palaeonaja* with the extant genus *Naja*. Remains of *N. romani*, in some cases abundant and perfectly preserved, were reported from several European sites, ranging in age from early to late Miocene (see Szyndlar 2005, and references therein). Additionally, a number of vertebrae identified as *Naja* sp. were reported from some other localities representing the same time span.

Palaeoenvironmental and -climatic implications

The amphibian and reptilian assemblage of Echzell is rich in forms living in humid and warm environments. Thus, the presence of amphibian genera such as *Chioglossa*, *Mertensiella*, *Lissotriton*, *Latonia*, *Pelobates*, and the reptile *Chamaelaeo* suggest in general humid and warm forested environments, whereas *Palaeobatrachus*, *Pelophylax*, *Natrix* indicate the presence of permanent water bodies. Other taxa, including the genus *Rana*, skinks and the remaining snake taxa, allows also concluding about open habitats. The presence of Chamaeleonidae in Echzell allows to reconstruct palaeotemperature. Haller-Probst (1997) suggested that the chamaeleonid occurrence indicates a range of the mean annual temperature of 17.4–28.8 °C, minimal warm month temperature 18–28.3 °C, minimal cold month temperature 8–22.2 °C (Haller-Probst 1997). This is also supported by the presence of the clade Gekkota, which are distributed worldwide in warm temperate to tropical areas (Bauer 2013; Meiri 2020). The mean annual precipitation (MAP) value has been estimated using the bioclimatic analysis of the amphibian and reptilian assemblage of Böhme et al. (2006). The analysis suggests a MAP value of 791±254 mm (Table 2) for Echzell, which is 126% wetter than the present-day value (Table 2).

Sample availability the studied fossils are deposited at the Hessisches Landesmuseum, Darmstadt (HLMD), Germany.

Author contribution

DV and TM designed the project and all authors carried it out. All authors prepared the manuscript with contributions from all co-authors. DV edited the text. All authors read and approved the text.

Competing interests

The authors declare that they have no conflict of interest.

Acknowledgements

The authors thank Oliver Sandrock (Hessisches Landesmuseum Darmstadt) for making the material available for study. A.Č. acknowledges financial support from the Scientific Grant Agency of the Ministry of Education of the Slovak Republic and Slovak Academy of Sciences, Grant Nr. 1/0191/21. T.M. acknowledges financial support from the Bolin Center for Climate Research, Stockholm University (RA6 grant).

References

Bell T (1839) A History of British Reptiles, John van Voorst, London, 142 pp. https://doi.org/10.5962/bhl.title.10835

Bhullar B-AS (2011) The power and utility of morphological characters in systematics: A fully resolved phylogeny of *Xenosaurus* and its fossil relatives (Squamata: Anguimorpha). Bulletin of the Museum of Comparative Zoology160: 65–181. https://doi.org/10.3099/0027-4100-160.3.65

Blain H-A, Bailon S, Agustí J (2007) Anurans and squamate reptiles from the latest early Pleistocene of Almenara-Casablanca-3 (Castellón, East of Spain). Systematic, climatic and environmental considerations. Geodiversitas 29: 269–295.

Bocage JVB (1864) Note sur un nouveau batracien du Portugal, *Chioglossa lusitanica*, et sur une grenouille nouvelle de l´Afrique occidentale. Revue et Magasin de Zoologie Pure et Appliquée, Serie 2, 16: 248–253.

Böhme G (1977) Zur Bestimmung quartärer Anuren Europas an Hand von Skelettelementen. Wissenschaftliche Zeitschrift der Humboldt-Universität zu Berlin, Mathematisch-Naturwissenschaftliche Reihe 26: 283–299.

Böhme M (2008) Ectothermic vertebrates (Teleostei, Allocaudata, Urodela, Anura, Testudines, Choristodera, Crocodylia, Squamata) from the Upper Oligocene of Oberleichtersbach (Northern Bavaria, Germany). Courier Forschungsinstitut Senckenberg 260: 161–183.

Böhme M (2010) Ectothermic vertebrates (Actinopterygii, Allocaudata, Urodela, Anura, Crocodylia, Squamata) from the Miocene of Sandelzhausen (Germany, Bavaria) and their implications for environment reconstruction and palaeoclimate. Paläontologische Zeitschrift 84: 3–41. https://doi.org/10.1007/s12542-010-0050-4

Böhme M, Ilg A (2003) fosFARbase. [Available at] www.wahre-staerke.com

Böhme M, Vasilyan D (2014) Ectothermic vertebrates from the late Middle Miocene of Gratkorn (Austria, Styria). Palaeobiodiversity and Palaeoenvironments 94: 21–40. https://doi.org/10.1007/s12549-013-0143-7

Böhme M, Ilg A, Ossig A, Küchenhoff H (2006) New method to estimate paleoprecipitation using fossil amphibians and reptiles and the middle and late Miocene precipitation gradients in Europe. Geology 34: 425–428. https://doi.org/10.1130/G22460.1

Böhme W, Roček Z, Špinar ZV (1982) On *Pelobates decheni* Troschel, 1961, and *Zaphrissa eurypelis* Cope, 1866 (Amphibia: Pelobatidae) from the early Miocene of Rott near Bonn West Germany. Journal of Vertebrate Paleontology 2: 1–7. https://doi.org/10.1080/02724634.1982.10011913

Boié F (1827) Bemerkungen über Merrem's Versuch eines Systems der Amphibien: 1ste Lieferung. Isis von Oken, Leipzig, 508–566.

Bonaparte CL (1850) Conspectus systematum. Mastozoölogiae. Ornithologiae. Herpetologiae et Amphibiologiae. Ichthyologiae, E. J. Brill, Lugduni Batavorum.

Bremer K (1994) Branch support and tree stability. Cladistics 10: 295–304. https://doi.org/10.1111/j.1096-0031.1994.tb00179.x

Caputo V (2004) The cranial osteology and dentition in the scincid lizards of the genus *Chalcides* (Reptilia, Scincidae). Italian Journal of Zoology 71: 35–45. https://doi.org/10.1080/11250000409356604

Čerňanský A (2011) A revision of the chameleon species *Chamaeleo pfeili* Schleich (Squamata; Chamaeleonidae) with description of a new material of chamaeleonids from the Miocene deposits of southern Germany. Bulletin of Geosciences 86: 275–282. https://doi.org/10.3140/bull.geosci.1259

Čerňanský A (2010a) Albanerpetontid amphibian (Lissamphibia: Albanerpetontidae) from the Early Miocene of the locality Merkur–North (north-west of the Czech Republic): data and a description of a new material. Acta Geologica Slovaka 2: 113–116.

Čerňanský A (2010b) A revision of chamaeleonids from the Lower Miocene of the Czech Republic with description of a new species of *Chamaeleo* (Squamata, Chamaeleonidae). Geobios 43: 605–613. https://doi.org/10.1016/j.geobios.2010.04.001

Čerňanský A (2010c) Earliest world record of green lizards (Lacertilia, Lacertidae) from the Lower Miocene of central Europe. Biologia 64: 737–741. https://doi.org/10.2478/s11756-010-0066-y

Čerňanský A (2016) Another piece of the puzzle: The first report on the Early Miocene lizard fauna from Austria (Ottnangian, MN 4; Oberdorf locality). Paläontologische Zeitschrift 90: 723–746. https://doi.org/10.1007/s12542-016-0329-1

Čerňanský A, Bauer AM (2010) *Euleptes gallica* Müller (Squamata: Gekkota: Sphaerodactylidae) from the Lower Miocene of North-West Bohemia, Czech Republic. Folia zoologica 59: 323–328. https://doi.org/10.25225/fozo.v59.i4.a8.2010

Čerňanský A, Klembara J (2017) A skeleton of *Ophisaurus* (Squamata: Anguidae) from the middle Miocene of Germany, with a revision of the partly articulated postcranial material from Slovakia using micro-computed tomography. Journal of Vertebrate Paleontology 37: e1333515. https://doi.org/10.1080/02724634.2017.1333515

Čerňanský A, Syromyatnikova EV (2019) The first Miocene fossils of *Lacerta* cf. *trilineata* (Squamata, Lacertidae) with a comparative study of the main cranial osteological differences in green lizards and their relatives. PLoS ONE 14: e0216191. https://doi.org/10.1371/journal.pone.0216191

Čerňanský A, Syromyatnikova EV (2021) The first pre-Quaternary fossil record of the clade Mabuyidae with a comment on the enclosure of the Meckelian canal in skinks. Papers in Palaeontology 7: 195–215. https://doi.org/10.1002/spp2.1279

Čerňanský A, Daza JD, Bauer AM (2018) Geckos from the middle Miocene of Devínska Nová Ves (Slovakia): new material and a review of the previous record. Swiss Journal of Geosciences 111: 183–190. https://doi.org/10.1007/s00015-017-0292-1

Čerňanský A, Rage JC, Klembara J (2015) The Early Miocene squamates of Amöneburg (Germany): the first stages of modern squamates in Europe. Journal of Systematic Palaeontology 13: 97–128. https://doi.org/10.1080/14772019.2014.897266

Čerňanský A, Szyndlar Z, Mörs T (2017) Fossil squamate faunas from the Neogene of Hambach (northwestern Germany). Palaeobiodiversity and Palaeoenvironments 97: 329–354. https://doi.org/10.1007/s12549-016-0252-1

Čerňanský A, Herrel A, Kibii JM, Anderson CV, Boistel R, Lehmann T (2020a) The only complete articulated early Miocene chameleon skull (Rusinga Island, Kenya) suggests an African origin for Madagascar's endemic chameleons. Scientific Reports 10: e109. https://doi.org/10.1038/s41598-019-57014-5

Čerňanský A, Syromyatnikova EV, Kovalenko ES, Podurets KM, Kaloyan AA (2020b) The Key to Understanding the European Miocene *Chalcides* (Squamata, Scincidae) Comes from Asia: The Lizards of the East Siberian Tagay Locality (Baikal Lake) in Russia. The Anatomical Record 303: 1901–1934. https://doi.org/10.1002/ar.24289

Čerňanský A, Yaryhin O, Ciceková J, Werneburg I, Hain M, Klembara J (2019) Vertebral Comparative Anatomy and Morphological Differences in Anguine Lizards With a Special Reference to *Pseudopus apodus*. The Anatomical Record 302: 232–257. https://doi.org/10.1002/ar.23944

Cope ED (1865) Sketch of the primary groups of Batrachia Salientia. Natural history review 5: 97–120.

Cuvier G (1816–1817) Le Règne Animal distribué d'après son organisation pour servir de base à l'histoire naturelle des animaux et d'introduction à l'anatomie comparée. Avec Figures, dessinées d'après nature, Contenant Les reptiles, les poissons, les mollusques et les annélides., Deterville, Paris, [i–xviii +] 532 pp.

Daza JD, Bauer AM, Snively ED (2014) On the Fossil Record of the Gekkota. The Anatomical Record 297: 433–462. https://doi.org/10.1002/ar.22856

Digimorph.org (2002–2012): Digital morphology: a national science foundation digital library at the University of Texas at Austin. http://www.digimorph.org/index.phtml

Duellman WE, Trueb L (1994) Biology of Amphibia. The Johns Hopkins University Press, Baltimor-London, 670 pp.

Duméril AMC (1806) Zoologie analytique, ou méthode naturelle de classification des animaux, rendue plus facile à l'aide de tableaux synoptiques. H. L. Perronneau, Paris, 344 pp. https://doi.org/10.5962/bhl.title.44835

Estes R, Hoffstetter R (1976) Les Urodèles du Miocène de la Grive-Saint-Alban (Isère, France). Bulletin du Muséum National d'Histoire Naturelle, 3e Série, Science de la Terre 57: 297–343.

Estes R, Queiroz K, Gauthier J (1988) Phylogenetic relationships within Squamata. In: Estes R, Pregill G (Eds) Phylogenetic relationships of the lizard families. Stanford University Press, Stanford, California, 119–281.

Evans SE (2008) The skull of lizards and tuatara. In: Gans C (Ed.) The skull of Lepidosauria. Society for the Study of Amphibians and Reptiles, Ithaca, 1–347.

Fejfar O (1999) Subfamily Platacanthomyinae. In: Rössner G, Heissig K (Eds) The Miocene Land Mammals of Europe. Dr. Friedrich Pfeil, München, 389–394.

Fejfar O, Kalthoff D (1999) Aberrant cricetids (Platacanthomyines, Rodentia, Mammalia) from the Miocene of Eurasia. Berliner geowissenschaftliche Abhandlungen E 30: 191–206.

Fejfar O, Roček Z (1986) The Lower Micoene vertebrate fauna of Dolnice, Cheb Basin (Western Bohemia, Czechoslovakie). Acta Universitatis Carolinae – Geologica 2: 233–249.

Fischer G (1813) Zoognosia. Tabulis Synopticis Illustrata, in Usum Prælectionum Academiæ Imperialis Medico-Chirurgicæ Mosquensis Edita, 3rd ed., 1. Typis Nicolai Sergeidis Vsevolozsky, Moscow, 465 pp.

Fitzinger L (1843) Systema Reptilium. Fasciculus Primus, Braumüller et Seidel, Wien, 106 pp. https://doi.org/10.5962/bhl.title.4694

Fox RC, Naylor BG (1982) A reconsideration of the relationships of the fossil amphibian *Albanerpeton*. Canadian Journal of Earth Sciences 33: 1–107. https://doi.org/10.1139/e82-009

Fürbinger M (1900) Zur Vergleichenden Anatomie des Brustschulterapparates und der Schultermuskeln. Jenaische Zeitschrift für Naturwissenschaft 34: 215–718. https://doi.org/10.5962/bhl.title.52377

Garsault FAd, Defehrt AJ, Prévost BL, Duflos P, Martinet FN, Geoffroy ÉF (1764) Les figures des plantes et animaux d'usage en medecine décrits dans La matiere medicale de Mr. Geoffroy medecin, Chez l'auteur rue St. Dominique porte St. Jacques, Paris, 644–729. https://doi.org/10.5962/bhl.title.49481

Gauthier JA, Kearney M, Maisano JA, Rieppel O, Behlke AD (2012) Assembling the squamate tree of life: perspectives from the phenotype and the fossil record. Bulletin of the Peabody Museum of Natural History 53: 3–308. https://doi.org/10.3374/014.053.0101

Georgalis GL, Villa A, Delfino M (2016) First description of a fossil chamaeleonid from Greece and its relevance for the European biogeographic history of the group. Die Naturwissenschaften 103: e12. https://doi.org/10.1007/s00114-016-1336-5

Georgalis G, Villa A, Ivanov M, Vasilyan D, Delfino M (2019) Fossil amphibians and reptiles from the Neogene locality of Maramena (Greece), the most diverse European herpetofauna at the Miocene/Pliocene transition boundary. Palaeontologia Electronica 22(3): 1–99. https://doi.org/10.26879/908

Goldfuss GA (1820) Handbuch der Zoologie. Bd. 2. J. L. Schrag, Nürnberg, 510 pp.

Goloboff PA, Farris JS, Nixon KC (2008) TNT, a free program for phylogenetic analysis. Cladistics 24: 774–786. https://doi.org/10.1111/j.1096-0031.2008.00217.x

Gómez RO, Turazzini GF (2015) An overview of the ilium of anurans (Lissamphibia, Salientia), with a critical appraisal of the terminology and primary homology of main ilial features. Journal of Vertebrate Paleontology 36(1): e1030023. https://doi.org/10.1080/02724634.2015.1030023

Gray JE (1825) A synopsis of the genera of reptiles and Amphibia, with a description of some new species. Annals of Philosophy London 10: 193–217.

Greer AE (1970) A subfamilial classification of scincid lizards. Bulletin of the Museum of Comparative Zoology 139(3): 151–183.

Greer AE (1974) The genetic relationships of the Scincid lizard genus *Leiolopisma* and its relatives. Australian Journal of Zoology Supplementary Series 22(31): 1–67. https://doi.org/10.1071/AJZS031

Haeckel E (1866) Generelle Morphologie der Organismen. Georg Reimer, Berlin, 574 pp. https://doi.org/10.1515/9783110848281

Haller-Probst MS (1997) Die Verbreitung der Reptilia in den Klimazonen der Erde: Unter Berücksichtigung Känozoischer Vorkommen Europas. Courier Forschungsinstitut Senckenberg 203: 1–147.

Hedges SB (2014) The high-level classification of skinks (Reptilia, Squamata, Scincomorpha). Zootaxa 3765: 317–338. https://doi.org/10.11646/zootaxa.3765.4.2

Hernandez A (2016) Crocodile newts: The primitive Salamandridae of Asia (genera *Echinotriton* and *Tylototriton*). Frankfurter Beiträge zur Naturkunde 62: 1–415.

Hodrová M (1984) Salamandridae of the Upper Pliocene Ivanovce locality (Czechoslovakia). Acta Universitatis Carolinae – Geologica 4: 331–352.

Hoffstetter R (1939) Contribution à l'étude des Elapidae actuels et fossiles et de l'ostéologie des Ophidiens. Archives du Muséum d'Histoire Naturelle de Lyon 15: 1–78. https://doi.org/10.3406/mhnly.1939.980

Hoffstetter R, Gasc JP (1969) Vertebrae and rips of modern reptiles. In: Gans C (Ed.) Biology of the Reptilia Morphology A. Academic Press, London, New York, 201–310.

Hossini S, Rage JC (2000) Palaeobatrachid frogs from the earliest Miocene (Agenian) of France, with description of a new species. Geobios 33: 223–231. https://doi.org/10.1016/S0016-6995(00)80019-4

Hutchinson MN, Scanlon JD (2009) New and Unusual Plio-Pleistocene Lizard (Reptilia: Scincidae) from Wellington Caves, New South Wales, Australia. Journal of Herpetology 43: 139–147. https://doi.org/10.1670/08-126R.1

Ivanov M (2001) Changes in the composition of the European snake fauna during the Early Miocene and at the Early / Middle Miocene transition. Palaeontologische Zeitschrift 74: 563–573. https://doi.org/10.1007/BF02988162

Ivanov M (2002) The oldest known Miocene snake fauna from Central Europe: Merkur–North locality, Czech Republic. Acta Palaeontologica Polonica 47: 513–534.

Ivanov M (2008) Early Miocene Amphibians (Caudata, Salientia) from the Mokrá-Western Quarry (Czech Republic) with comments on the evolution of Early Miocene amphibian assemblages in Central Europe. Geobios 41: 465–492. https://doi.org/10.1016/j.geobios.2007.11.004

Ivanov M, Böhme M (2011) Snakes from Griesbeckerzell (Langhian, Early Badenian), North Alpine Foreland Basin (Germany), with comments on the evolution of snake faunas in Central Europe during the Miocene Climatic Optimum. Geodiversitas 33: 411–449. https://doi.org/10.5252/g2011n3a2

Ivanov M, Čerňanský A, Bonilla-Salomón I, Luján ÀH (2020) Early Miocene squamate assemblage from the Mokrá-Western Quarry (Czech Republic) and its palaeobiogeographical and palaeoenvironmental implications. Geodiversitas 42: 343–376. https://doi.org/10.5252/geodiversitas2020v42a20

Jovells Vaqué S, Mörs T (2022) The aberrant hamster Melissiodon (Cricetidae, Rodentia) from the early Miocene of Echzell and other German and French localities. Historical Biology. https://doi.org/10.1080/08912963.2022.2067758

Khozatskiy LI (1985) A new species of *Pelobates* from the Pliocene of Moldova. In: Negadaev-Nikonov KN (Ed.) Fauna and flora of Late Cenozoic of Moldova. Shtiintsa, Kishinev, 59–72.

Kindler C, Chèvre M, Ursenbacher S, Böhme W, Hille A, Jablonski D, Vamberger M, Fritz U (2017) Hybridization patterns in two contact zones of grass snakes reveal a new Central European snake species. Scientific Reports 7: e7378. https://doi.org/10.1038/s41598-017-07847-9

Klembara J (2015) New finds of anguines (Squamata, Anguidae) from the Early Miocene of Northwest Bohemia (Czech Republic). Paläontologische Zeitschrift 89: 171–195. https://doi.org/10.1007/s12542-014-0226-4

Klembara J, Čerňanský A (2020) Revision of the cranial anatomy of *Ophisaurus acuminatus* Jörg, 1965 Anguimorpha, Anguidae) from the late Miocene of Germany. Geodiversitas 42: 539–557. https://doi.org/10.5252/geodiversitas2020v42a28

Klembara J, Rummel M (2018) New material of *Ophisaurus*, *Anguis* and *Pseudopus* (Squamata, Anguidae, Anguinae) from the Miocene of the Czech Republic and Germany and systematic revision and palaeobiogeography of the Cenozoic Anguinae. Geological Magazine 155: 20–44. https://doi.org/10.1017/S0016756816000753

Klembara J, Dobiašová K, Hain M, Yaryhin O (2017) Skull Anatomy and Ontogeny of Legless Lizard *Pseudopus apodus* (Pallas, 1775): Heterochronic Influences on Form. The Anatomical Record 300: 460–502. https://doi.org/10.1002/ar.23532

Klembara J, Böhme M, Rummel M (2010) Revision of the Anguine Lizard *Pseudopus laurillardi* (Squamata, Anguidae) from the Miocene of Europe, with Comments on Paleoecology Journal of Paleontology 84: 159–196. https://doi.org/10.1666/09-033R1.1

Klembara J, Hain M, Čerňanský A (2019) The first record of anguine lizards (Anguimorpha, Anguidae) from the early Miocene locality Ulm – Westtangente in Germany. Historical Biology 31: 1016–1027. https://doi.org/10.1080/08912963.2017.1416469

Klembara J, Hain M, Dobiašová K (2014) Comparative anatomy of the lower jaw and dentition of *Pseudopus apodus* and the interrelationships of species of subfamily Anguinae (Anguimorpha, Anguidae). The Anatomical Record 297: 516–544. https://doi.org/10.1002/ar.22854

Laurenti JN (1768) Specimen medicum, exhibens synopsin reptilium emendatum cum experimentis circa venena et antidota Reptilium Austriacorum. Typ. Joan. Thom. nob. de Trattnern, Viennae, 214 pp. https://doi.org/10.5962/bhl.title.5108

Ledesma DT, Scarpetta SG (2018) The skull of the gerrhonotine lizard *Elgaria panamintina* (Squamata: Anguidae). PLoS ONE 13: e0199584. https://doi.org/10.1371/journal.pone.0199584

Linnaeus C (1758) Systema naturae per regna tria naturae, secundum classes, ordines, genera, species, cum characteribus, differentiis, synonymis, locis. L. Salvi, Stockholm, 823 pp. https://doi.org/10.5962/bhl.title.542

Maddison WP, Maddison DR (2011) Mesquite: a modular system for evolutionary analysis.

Marjanović D, Witzmann F (2015) An Extremely Peramorphic Newt (Urodela: Salamandridae: Pleurodelini) from the Latest Oligocene of Germany, and a New Phylogenetic Analysis of Extant and Extinct Salamandrids. PLoS ONE 10: e0137068. https://doi.org/10.1371/journal.pone.0137068

Meyer von H (1843) Mittheilung an Professor Bronn gerichtet. Neues Jahrbuch für Geologie und Paläontologie, Geognasie, Geologie und Petrefactenkunde, 579–590.

Moody S (1978) The phylogenetic relationships of taxa within the lizards family Agamidae. PhD thesis, University of Michigan at Ann Arbor, Michigan, USA.

Mörs T (2010) Wirbeltiere aus dem Miozän von Homberg/Ohm (Vogelsberg, Hessen). Geologisches Jahrbuch Hessen 136: 109–119.

Mörs T, Flink T (2018) Large apeomyine rodents (Mammalia, Eomyidae) from the early Miocene of Echzell, Germany. Historical Biology 30: 1102–1111. https://doi.org/10.1080/08912963.2017.1338695

Mörs T, Reguero M, Vasilyan D (2020) First fossil frog from Antarctica: implications for Eocene high latitude climate conditions and Gondwanan cosmopolitanism of Australobatrachia. Scientific Reports 10: e5051. https://doi.org/10.1038/s41598-020-61973-5

Oppel M (1811) Die Ordnungen, Familien und Gattungen der Reptilien als Prodrom einer Naturgeschichte derselben. Joseph Lindauer, München, 87 pp. https://doi.org/10.5962/bhl.title.4911

Pineker P, Mörs T (2011) *Neocometes* (Rodentia, Platacanthomyinae) from the early Miocene of Echzell, Germany. Geobios 44: 279–287. https://doi.org/10.1016/j.geobios.2010.12.001

Pokrant F, Kindler C, Ivanov M, Cheylan M, Geniez P, Böhme W, Fritz U (2016) Integrative taxonomy provides evidence for the species status of the Ibero-Maghrebian grass snake *Natrix astreptophora*. Biological Journal of the Linnean Society 118: 873–888. https://doi.org/10.1111/bij.12782

Pomel A (1853) Catalogue méthodique et descriptif des vertébrés fossiles découverts dans le bassin hydrographique supérieur de la Loire. J. B. Baillières, Paris, 193 pp.

Pyron AR, Wiens JJ (2011) A large-scale phylogeny of Amphibia including over 2800 species, and a revised classification of extant frogs, salamanders, and caecilians. Molecular Phylogenetics and Evolution 61: 543–583. https://doi.org/10.1016/j.ympev.2011.06.012

Rafinesque CS (1815) Analyse de Nature, ou Tableau de l'Universe et des Corps Organisés. Jean Barravecchia, Palermo, 224 pp. https://doi.org/10.5962/bhl.title.106607

Rage JC, Augé ML (2010) Squamate reptiles from the middle Eocene of Lissieu (France). A landmark in the middle Eocene of Europe. Geobios 43: 253–268. https://doi.org/10.1016/j.geobios.2009.08.002

Rage JC, Bailon S (2005) Amphibians and squamate reptiles from the late early Miocene (MN 4) of Béon 1 (Montréal-du-Gers, southwestern France). Geodiversitas 27: 413–441.

Rage JC, Szyndlar Z (1986) *Natrix longivertebrata* from the European Neogene, a snake with one of the longest known stratigraphic ranges. Neues Jahrbuch für Geologie und Paläontologie - Monatshefte 1986: 56–64. https://doi.org/10.1127/njgpm/1986/1986/56

Rage JC, Szyndlar Z (1990) West Palearctic cobras of the genus *Naja* (Serpentes: Elapidae): interrelationships among extinct and extant species. Amphibia-Reptilia 11: 385–400. https://doi.org/10.1163/156853890X00078

Recuero E, García-París M (2011) Evolutionary history of *Lissotriton helveticus*: multilocus assessment of ancestral vs. recent colonization of the Iberian Peninsula. Molecular Phylogenetics and Evolution 60: 170–182. https://doi.org/10.1016/j.ympev.2011.04.006

Roček Z (1984) Lizards (Reptili: Sauria) from the Lower Miocene locality Dolnice (Bohemia, Czechoslovakia). Řada matematických a přirodních věd 94: 4–69.

Roček Z (1994) A Review of the fossil Caudata of Europe. Abhandlungen und Berichte für Naturkunde 17: 51–56.

Roček Z (2005) Late Miocene Amphibia from Rudabánya. Palaeontographia Italica 90: 11–29.

Roček Z, Wuttke M (2010) Amphibia of Enspel (Late Oligocene, Germany). Palaeobiodiversity and Palaeoenvironments 90: 321–340. https://doi.org/10.1007/s12549-010-0042-0

Roček Z, Boistel R, Lenoir N, Mazurier A, Pierce SE, Rage JC, Smirnov SV, Schwermann AH, Valentin X, Venczel M, Wuttke M, Zikmund T (2015) Frontoparietal Bone in Extinct Palaeobatrachidae (Anura): Its Variation and Taxonomic Value. The Anatomical Record: Advances in Integrative Anatomy and Evolutionary Biology 298: 1848–1863. https://doi.org/10.1002/ar.23203

Roček Z, Böttcher R, Wassersug R (2006) Gigantism in tadpoles of the Neogene frog *Palaeobatrachus*. Paleobiology 32: 666–675. https://doi.org/10.1666/05073.1

Roček Z, Wuttke M, Gardner J, Singh Bhullar BA (2014) The Euro-American genus *Eopelobates*, and a re-definition of the family Pelobatidae (Amphibia, Anura). Palaeobiodiversity and Palaeoenvironments 94: 529–567. https://doi.org/10.1007/s12549-014-0169-5

Rössner G, Heissig K (1999) The Miocene Land Mammals of Europe. Dr. Friedrich Pfeil, München, 516 pp.

Sanchíz B (1998) Vertebrates from the Early Miocene lignite deposits of the opencast mine Oberdorf (Western Styrian Basin, Austria). Annalen des Naturhistorischen Museums in Wien 99A: 13–29.

Sanchíz B, Młynarski M (1979) Pliocene salamandrids (Amphibia, Caudata) from Poland. Acta zoologica cracoviensia 24: 175–188.

Schleich HH (1987) Neue Reptilienfunde aus dem Tertiär Deutschlands 7. Erstnachweis von Geckos aus dem Mittelmiozän Süddeutschlands: *Palaeogekko risgoviensis* nov. gen., nov. spec. (Reptilia, Sauria, Gekkonidae)[1]). Mitteilungen der Bayerischen Staatssammlung für Paläontologie und historische Geologie 27: 67–96.

Schoch RR, Poschmann M, Kupfer A (2015) The salamandrid *Chelotriton paradoxus* from Enspel and Randeck Maars (Oligocene–Miocene, Germany). Palaeobiodiversity and Palaeoenvironments 95: 77–86. https://doi.org/10.1007/s12549-014-0182-8

Scopoli GA (1777) Introductio ad historiam naturalem, sistens genera lapidum, plantarum et animalium hactenus detecta, caracteribus essentialibus donata, in tribus divisa, subinde ad leges naturae. Apud Wolfgangum Gerle, Prague, 506 pp. https://doi.org/10.5962/bhl.title.10827

Sparreboom M (2014) Salamanders of the Old World: The salamanders of Europe, Asia and northern Africa, First edition. KNNV Publishing, Zeist, 431 pp. https://doi.org/10.1163/9789004285620

Steinthorsdottir M, Coxall HK, Boer AM, Huber M, Barbolini N, Bradshaw CD, Burls NJ, Feakins SJ, Gasson E, Henderiks J, Holbourn AE, Kiel S, Kohn MJ, Knorr G, Kürschner WM, Lear CH, Liebrand D, Lunt DJ, Mörs T, Pearson PN, Pound MJ, Stoll H, Strömberg CAE (2021) The Miocene: The Future of the Past. Paleoceanographica and Paleoclimatology 36: e2020PA004037. https://doi.org/10.1029/2020PA004037

Syromyatnikova E, Georgalis GL, Mayda S, Kaya T, Saraç G (2019) A new early Miocene herpetofauna from Kilçak, Turkey. Russian Journal of Herpetology 26: 205. https://doi.org/10.30906/1026-2296-2019-26-4-205-224

Szentesi Z, Pazonyi P, Mészáros L (2015) Albanerpetonidae from the late Pliocene (MN 16A) Csarnóta 3 locality (Villany Hills, South Hungary) in the collection of the Hungarian Natural History Museum. Fragmenta Palaeontologica Hungarica 32: 49–66. https://doi.org/10.17111/FragmPalHung.2015.32.49

Szyndlar Z (1984) Fossil snakes from Poland. Acta zoologica cracoviensia 28: 1–156.

Szyndlar Z (1987) Snakes from the Lower Miocene Locality of Dolnice (Czechoslovakia). Journal of Vertebrate Paleontology 7: 55–71. https://doi.org/10.1080/02724634.1987.10011637

Szyndlar Z (1991) Ancestry of the Grass Snake (*Natrix natrix*): Paleontological Evidence. Journal of Herpetology 25: 412–418. https://doi.org/10.2307/1564762

Szyndlar Z (1998) Vertebrates from the Early Miocene lignite deposits of the opencast mine Oberdorf (Western Styrian Basin, Austria). 3. Reptilia, 2: Serpentes. Annalen des Naturhistorischen Museums in Wien, Series A 99A: 31–38.

Szyndlar Z (2005) Snake fauna from the Late Micoene of Rudabánya. Palaeontographia Italica 90: 31–52.

Szyndlar Z (2012) Early Oligocene to Pliocene Colubridae of Europe: a review. Bulletin de la Société Géologique de France 183: 661–681. https://doi.org/10.2113/gssgfbull.183.6.661

Szyndlar Z, Hoşgör I (2012) *Bavarioboa* sp. (Serpentes, Boidae) from the Oligocene / Miocene of eastern Turkey with comments on connections between European and Asiatic snake faunas. Acta Palaeontologica Polonica 57: 667–671. https://doi.org/10.4202/app.2011.0075

Szyndlar Z, Rage JC (2002) Fossil record of the true vipers. In: Schütt GW, Höggren M, Douglas ME, Greene HW (Eds) Biology of the Vipers. Eagle Mountain Publishing, Eagle Mountain, 419–444.

Szyndlar Z, Rage JC (2003) Non-erycine Booidea from the Oligocene and Miocene of Europe. Institute of Systematics and Evolution of Animals Polish Academy of Sciences, Kraków, 109 pp.

Szyndlar Z, Schleich HH (1993) Description of Miocene Snakes from Petersbuch 2 with Comments on the Lower and Middle Miocene

Ophidian Faunas of Southern Germany. Stuttgarter Beiträge zur Naturkunde. Serie B (Geologie und Paläontologie) 192: 1–47.

Tissier J, Rage JC, Boistel R, Fernandez V, Pollet N, Garcia G, Laurin M (2015) Synchrotron analysis of a 'mummified' salamander (Vertebrata: Caudata) from the Eocene of Quercy, France. Zoological Journal of the Linnean Society 171(1): 147–164. https://doi.org/10.1111/zoj.12341

Tobien H (1954) Eine miozäne Säugerfauna aus vulkanischen Tuffen des Vogelsberges (Vortragsbericht). Zeitschrift der deutschen geologischen Geselschaft 105: 588–588. https://doi.org/10.1127/zdgg/105/1955/588

Tobien H (1982) 1200 Jahre Echzell: 782 - 1982; Ursprung, Epochen u. Strukturen e. Dörfergemeinschaft, Ahnert, Echzell, 400 pp.

Tschudi JJ (1838) Classification der Batrachier, Mit Berucksichtigung der fossilen Thiere dieser Abtheilung der Reptilien. Petitpierre, Neuchâtel, 100 pp. https://doi.org/10.5962/bhl.title.4883

Vasilyan D (2020) Fish, amphibian and reptilian assemblage from the middle Miocene locality Gračanica—Bugojno palaeolake, Bosnia and Herzegovina. Palaeobiodiversity and Palaeoenvironments 100: 437–455. https://doi.org/10.1007/s12549-019-00381-8

Vasilyan D, Roček Z, Ayvazyan A, Claessens LPAM (2019) Fish, amphibian and reptilian faunas from latest Oligocene to middle Miocene localities from Central Turkey. Palaeobiodiversity and Palaeoenvironments 99: 723–757. https://doi.org/10.1007/s12549-019-00405-3

Vasilyan D, Zazhigin VS, Böhme M (2017) Neogene amphibians and reptiles (Caudata, Anura, Gekkota, Lacertilia, Testudines) from south of Western Siberia, Russia and Northeastern Kazakhstan. PeerJ 5: e3025. https://doi.org/10.7717/peerj.3025

Venczel M (2004) Middle Miocene anurans from the Carpathian Basin. Palaeontographica Abteilung A 271: 151–174. https://doi.org/10.1127/pala/271/2004/151

Venczel M, Gardner JD (2005) The geologically youngest Albanerpetontid Amphibian, from the Lower Pliocene of Hungary. Palaeontology 48: 1273–1300. https://doi.org/10.1111/j.1475-4983.2005.00512.x

Venczel M, Hír J (2013) Amphibians and Squamates from the Miocene of Felsötárkány Basin, N-Hungary, Palaeontographica Abteilung A 300: 117–147. https://doi.org/10.1127/pala/300/2013/117

Vidal N, Hedges SB (2005) The phylogeny of squamate reptiles (lizards, snakes, and amphisbaenians) inferred from nine nuclear protein-coding genes. Comptes rendus biologies 328: 1000–1008. https://doi.org/10.1016/j.crvi.2005.10.001

Villa A, Delfino M (2019a) Fossil lizards and worm lizards (Reptilia, Squamata) from the Neogene and Quaternary of Europe: an overview. Swiss Journal of Palaeontology 138: 177–211. https://doi.org/10.1007/s13358-018-0172-y

Villa A, Delfino M (2019b) A comparative atlas of the skull osteology of European lizards (Reptilia: Squamata). Zoological Journal of the Linnean Society 187: 829–928. https://doi.org/10.1093/zoolinnean/zlz035

Villa A, Gobbi S, Delfino M (2021) Additions to the early Miocene herpetofauna of Weisenau (Germany): urodeles and squamates from a rediscovered historical collection in Italy. Paläontologische Zeitschrift 96: 113–127. https://doi.org/10.1007/s12542-021-00571-w

Villa A, Kosma R, Čerňanský A, Delfino M (2018) Taxonomic assessment of '*Bavaricordylus*' Kosma, 2004 (Reptilia, Squamata). Journal of Vertebrate Paleontology 38: 1–4. https://doi.org/10.1080/02724634.2018.1487844

Villa A, Roček Z, Tschopp E, Van den Hoek Ostende LW, Delfino M (2016) *Palaeobatrachus eurydices* sp. nov. (Amphibia, Anura), the last western European palaeobatrachid. Journal of Vertebrate Paleontology 36: e1211664. https://doi.org/10.1080/02724634.2016.1211664

Wagler JG (1830) Natürliches System der Amphibien, mit vorangehender Classification der Säugethiere und Vögel Ein Beitrag zur vergleichenden Zoologie. J.G. Cotta, München-Stuttgart-Tübingen, 354 pp. https://doi.org/10.5962/bhl.title.58730

Wetter und Klima (undated) Wetter und Klima - Deutscher Wetterdienst. https://www.dwd.de/

Wielstra B, Themudo GE, Güçlü O, Olgun K, Poyarkov NA, Arntzen JW (2010) Cryptic crested newt diversity at the Eurasian transition: the mitochondrial DNA phylogeography of Near Eastern *Triturus* newts. Molecular Phylogenetics and Evolution 56: 888–896. https://doi.org/10.1016/j.ympev.2010.04.030

Wolterstorff W (1925) Katalog der Amphibien-Sammlung im Museum für Natur- und Heimkunde zu Magdeburg: Erster Teil, Apoda, Caudata. Abhandlungen und Berichte für Naturkunde aus dem Museum für Natur- und Heimkunde 4: 231–310.

Wuttke M, Přikryl T, Ratnikov VY, Dvořák Z, Roček Z (2012) Generic diversity and distributional dynamics of the Palaeobatrachidae (Amphibia: Anura). Palaeobiodiversity and Palaeoenvironments 92: 367–395. https://doi.org/10.1007/s12549-012-0071-y

Supplementary material 1

Appendix S1

Authors: Davit Vasilyan, Andrej Čerňanský, Zbigniew Szyndlar, Thomas Mörs

Data type: nexus file of the phylogenetic analysis

Explanation note: Updated phylogenetic matrices in TNT. file format used for the phylogenetic analyses in this study.

Link: https://doi.org/10.3897/fr.25.83781.suppl1

Supplementary material 2

Appendix S2

Authors: Davit Vasilyan, Andrej Čerňanský, Zbigniew Szyndlar, Thomas Mörs

Data type: list of characters

Explanation note: List of characters used for analysis.

Link: https://doi.org/10.3897/fr.25.83781.suppl2

Fossil Record 25 (1) 2022, 147–172 | DOI 10.3897/fr.25.84604

Mid-Cretaceous coastal amber forest palaeoenvironment revealed by exceptionally preserved ostracods from an extant lineage

He Wang[1], Renate Matzke-Karasz[2], David J. Horne[3]

1 *Nanjing Institute of Geology and Palaeontology Chinese Academy of Sciences, 39 East Beijing Road, Nanjing 210008, China*
2 *Department of Earth and Environmental Sciences, Palaeontology and Geobiology, Ludwig-Maximilians-Universität München, Richard-Wagner-Strasse 10, 80333 München, Germany*
3 *School of Geography, Queen Mary University of London, Mile End Road, London E1 4NS, UK*

http://zoobank.org/91C70EDD-7ACE-492E-AA7F-1CE884018AE6

Corresponding author: He Wang (hwang@nigpas.ac.cn); Renate Matzke-Karasz (matzke-karasz@lmu.de)

Academic editor: Alexander Schmidt ♦ **Received** 30 March 2022 ♦ **Accepted** 11 May 2022 ♦ **Published** 1 June 2022

Abstract

As a famous fossil Lagerstätte, the mid-Cretaceous (ca. 100 Ma) amber from Kachin, northern Myanmar, harbors one of the most diverse Mesozoic palaeobiotas yet discovered. Over the past few years, reports of organisms trapped in Kachin amber have increased exponentially. Ostracods, as fully aquatic animals, are so far represented in Kachin amber by two records of specimens without soft parts (1 valve and two carapaces) as well as an exceptional assemblage with well-preserved soft parts comprising 39 specimens of three species assigned to the families Candonidae and Loxoconchidae. Since the last-mentioned focused on the exceptional preservation of giant sperm and reproductive organs in only one species, we here present in-depth morphological descriptions of all three species including a new genus: *Myanmarcypris hui* Wang et al., 2020, *Electrocypria burmitei* **gen. et sp. nov.**, and *Sanyuania* sp. We further describe taphonomic traits indicating that the studied ostracods were quickly surrounded by resin and instantly immobilized. The palaeoenvironment is considered to be a vegetated brackish (mesohaline-oligohaline) lagoon.

Key Words

Candonidae, Kachin amber, Loxoconchidae, ostracods, palaeoenvironment, taphonomy

1. Introduction

Calcified bivalved carapaces of ostracods (Crustacea) have a high potential to be preserved as microfossils, and consequently ostracods have been the most common fossil arthropods since the Ordovician (Rodriguez-Lazaro and Ruiz-Muñoz 2012). However, ostracod soft parts (body and appendages) are rarely fossilized (Matzke-Karasz and Smith 2020). Furthermore, as fully aquatic animals, ostracods are scarcely trapped in amber in contrast to water-bound insect larvae. The few cases known include those from Cenozoic ambers from early Miocene in Mexico and the Eocene of the Baltic region (e.g. Keyser and Friedrich 2017; Matzke-Karasz et al. 2019). Kachin amber containing the most diverse biota of all known Cretaceous ambers provides a unique window into mid-Cretaceous ecosystem (Yu et al. 2019). Over the past two decades, more than 500 families of invertebrates, vertebrates, protists, plants, and fungi have been reported, including scorpions, spiders, insects, frogs, a feather and a lizard (Ross 2019; Ross 2020). However, for Kachin amber, only three ostracod specimens were found, without soft parts, prior to the discovery of the material on which the current study is focused (Xing et al. 2018; Wang et al. 2020a). Wang et al. (2020b) first reported ostracods with soft parts (appendages and reproductive organs) in a single piece of mid-Cretaceous Kachin amber (approximately 100 million years old) and erected a new species and genus, *Myanmarcypris hui* Wang et al., 2020 and gave only brief consideration to two additional species in the same assemblage. In the present study we provide a full taxonomic, taphonomic and palaeoenvironmental appraisal of the exceptionally preserved ostracods in this amber piece, adopting a palaeobiological approach to compare them with living relatives from the same Paracypridinae lineage, and the Loxoconchidae, respectively.

2. Materials and methods

The amber piece used for this study is from an amber mine near Noije Bum Village, Tanai Town, Hukawng Valley in Kachin Province, northern Myanmar (approx. latitude 26°13'47"N, 96°36'15"E). Grimaldi et al. (2002) and Ross et al. (2010) provided a general introduction to the amber deposit and its geological settings. The age of the studied amber was considered to be late Albian–early Cenomanian according to an ammonite trapped in the amber (Yu et al. 2019), which is also supported by U-Pb zircon dating of the volcanoclastic matrix with a maximum age of 98.79 ± 0.62 Ma (earliest Cenomanian) (Shi et al. 2012).

The elliptical amber piece (Suppl. material 1: Fig. S1; length 18 mm, width 14 mm, height 4 mm; volume approx. 0.78 cm^3) is permanently curated in the Lingpoge Amber Museum (Building No. 59, No. 2338 Duhui Road, Minhang District, Shanghai 201108, China) in compliance with the International Code of Zoological Nomenclature (Ride et al. 1999) and the instruction of International Palaeoentomological Society (Szwedo et al. 2020). This amber piece was acquired in 2016 and has been deposited in the Lingpoge Amber Museum (Shanghai) since January 2017, before the Myanmar military closed the Kachin amber mining in November 2017. The specimen is permanently housed in the Lingpoge Amber Museum in Shanghai (Building No. 59, No. 2338 Duhui Road, Minhang District, Shanghai 201108, China) which is a private museum (Director: Fangyuan Xia; Email: 138120076@qq.com). The fossils in the Lingpoge Amber Museum are held safely in trust for the benefit of researchers and educators throughout the world; the specimens reported in this study may be accessed by contacting, in the first instance, the corresponding author.

To further support unlimited access to the primary types of *Electrocypria burmitei* gen. et spec. nov. described in the present work, our tomographic data (virtual types) have been incorporated into the collection of the Chinese Academy of Sciences (NIGP175852) and cross referenced between the NIGP and the Lingpoge Amber Museum. Additionally, the data will be deposited in the Geobiodiversity Database (GBDB, http://www.geobiodiversity.com).

The studied ostracods were scanned at the micro-CT laboratory of Nanjing Institute of Geology and Palaeontology (NIGPAS), using a 3D X-ray microscope (3D-XRM), Zeiss Xradia 520 versa, to three-dimensionally reconstruct the ostracods. Wang et al. (2020b) provide more detailed information on tomographic methods. Volume data processing was performed using software VGStudio Max (version 3.0; Volume Graphics) and the open source volume exploration tool Drishti v2.6 (Limaye 2012).

For the analysis of morphological details, volume renderings from Drishti were used and the chaetotaxy was identified at the model itself by using a red-cyan 3D mode, so that the position of every detail could be identified in three dimensions (e.g., Suppl. material 2: Fig. S2). By using manipulation tools (rotate, zoom, clip, carve, etc) every desired view could be adjusted. Drawings were made by choosing an optimal view of each appendage, and using a screen shot as a basis for the drawing to then add all morphological details. This process is very similar to the drawing process from a light microscope with a camera lucida, where several focus levels are integrated in a final drawing.

3. Systematic palaeontology

Terminology for the appendages, segment numbering, and their chaetotaxy was adopted from Meisch (2000) and Maddocks (1992). Hierarchical taxonomic positions of non-marine taxa are based on the checklist by Meisch et al. (2019). The higher classification follows Smith et al. (2015).

The line drawings of appendages in this study can only reflect those anatomical details which are clearly observable in the available tomographies. A seta missing in a certain place where it would be expected in related modern species does not mean that it was not present in the amber-entrapped animal when it was still alive. Consequently, missing features such as setae cannot be used as a taxonomic feature in the following species descriptions – only the presence of a seta can. This shortcoming limits the possibilities of comparing the Myanmar amber ostracods to known species in related modern taxa. Drawings of the appendages may appear coarse and sometimes schematic compared to those of living ostracods, but since they are based on tomographic data of what is left of the appendages, this deficiency is inevitable.

Abbreviations

A1	first antenna (antennula);
A2	second antenna (antenna);
H	height;
HP	hemipenis;
L	length;
L5–L7	fifth to seventh limbs;
LV	left valve;
Md	mandibula;
Mxl	maxillula;
RV	right valve;
UR	uropodal ramus;
W	width.

Class Ostracoda Latreille, 1802
Order Podocopida Sars, 1866
Suborder Cypridocopina Jones, 1901
Superfamily Cypridoidea Baird, 1845
Family Candonidae Kaufmann, 1900
Subfamily Paracypridinae Sars, 1923
Tribe Renaudcypridini, McKenzie, 1980
Genus *Myanmarcypris* Wang et al., 2020

Myanmarcypris hui Wang et al., 2020

Figs 1–7; Suppl. material 3: Movie S1, Suppl. material 4: Movie S2, Suppl. material 5: Movie S3

Material. 31 specimens, 5 of which were analyzed using 3D X-ray microscopy: adult male, holotype (BA19005-1) – L = 600 μm, H = 356 μm, W ≈ 290 μm; paratypes: adult female, (BA19005-2) – L = 609 μm, H = 382 μm, W ≈ 300 μm; A-2 juvenile (BA19005-3) – L = 400 μm, H = 261 μm, W ≈ 175 μm; A-3 juvenile (BA19005-4) – L = 313 μm, H = 204 μm, W ≈ 161 μm; A-4 juvenile (BA19005-5) – L = 226 μm, H = 156 μm, W ≈ 120 μm; material not tomographed: BA19005-11–36 (Suppl. material 1: Fig. S1).

Emended description. Carapace (Figs 1, 2): Adults small, in lateral view subtriangular. Female with higher and more pointed dorsal peak than male. In dorsal view, anterior and posterior ends blunt, not pointed. Valves thick and strongly reticulate, with prominent transverse muri, except for the dorsal region, which is smooth. In adults, a conspicuous antero-ventral lateral node present on each of the valves (Figs 1E, J, 2A). Antero-dorsally with smooth

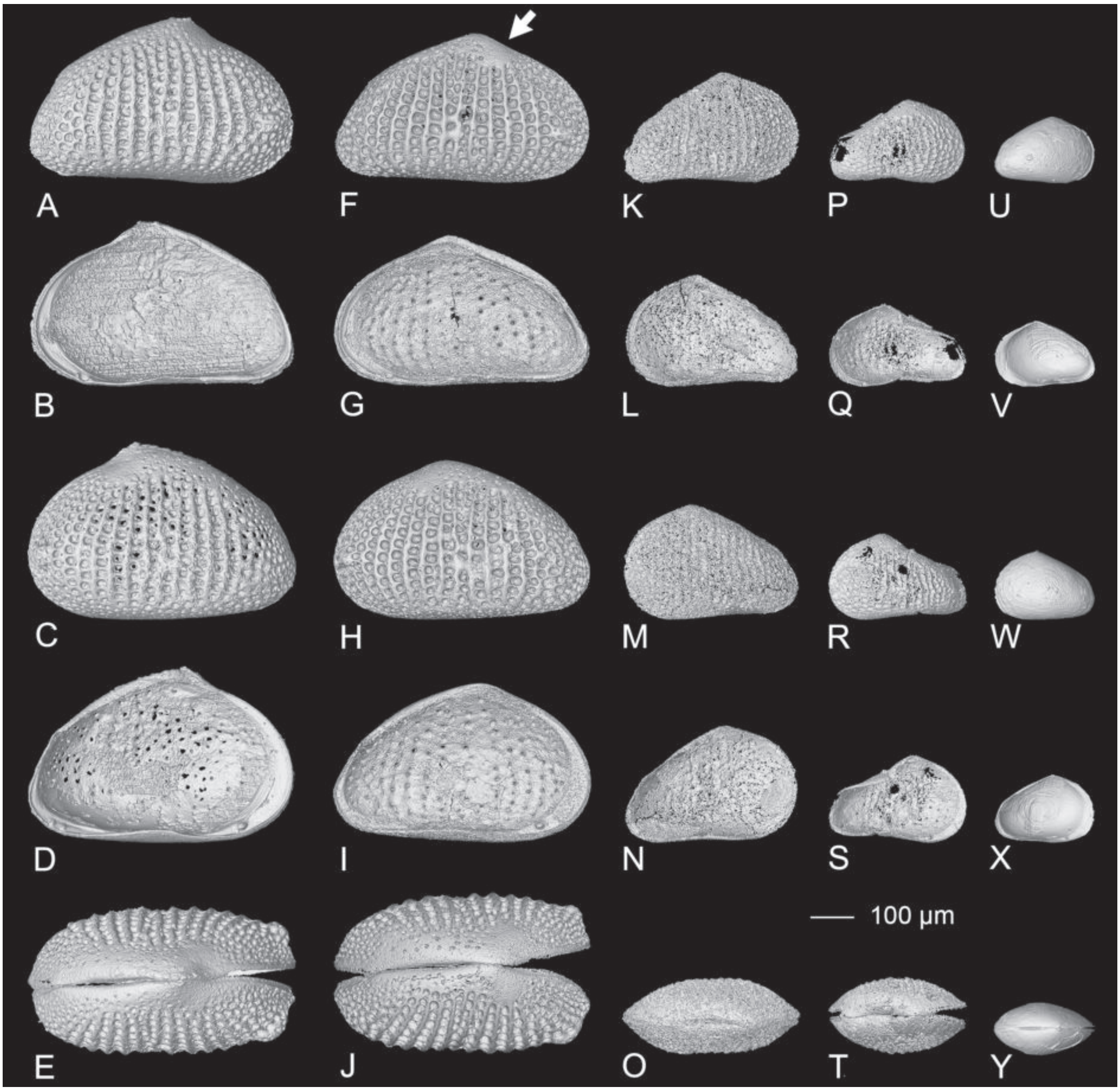

Figure 1. Microtomographic reconstruction of *Myanmarcypris hui*, surface rendering. **A–E.** Female, BA19005-2; **F–J.** Male, BA19005-1; **K–O.** Juvenile (A-2) BA19005-3; **P–T.** Juvenile (A-3), BA19005-4; **U–Y.** Juvenile (A-4), BA19005-5. First (uppermost) row: RV externally; second row: RV internally; third row: LV externally; fourth row: LV internally; fifth row: dorsal view of carapace, anterior to right. Arrow: smooth eye spot. Note: **D** and **E** are from Wang et al. (2020b).

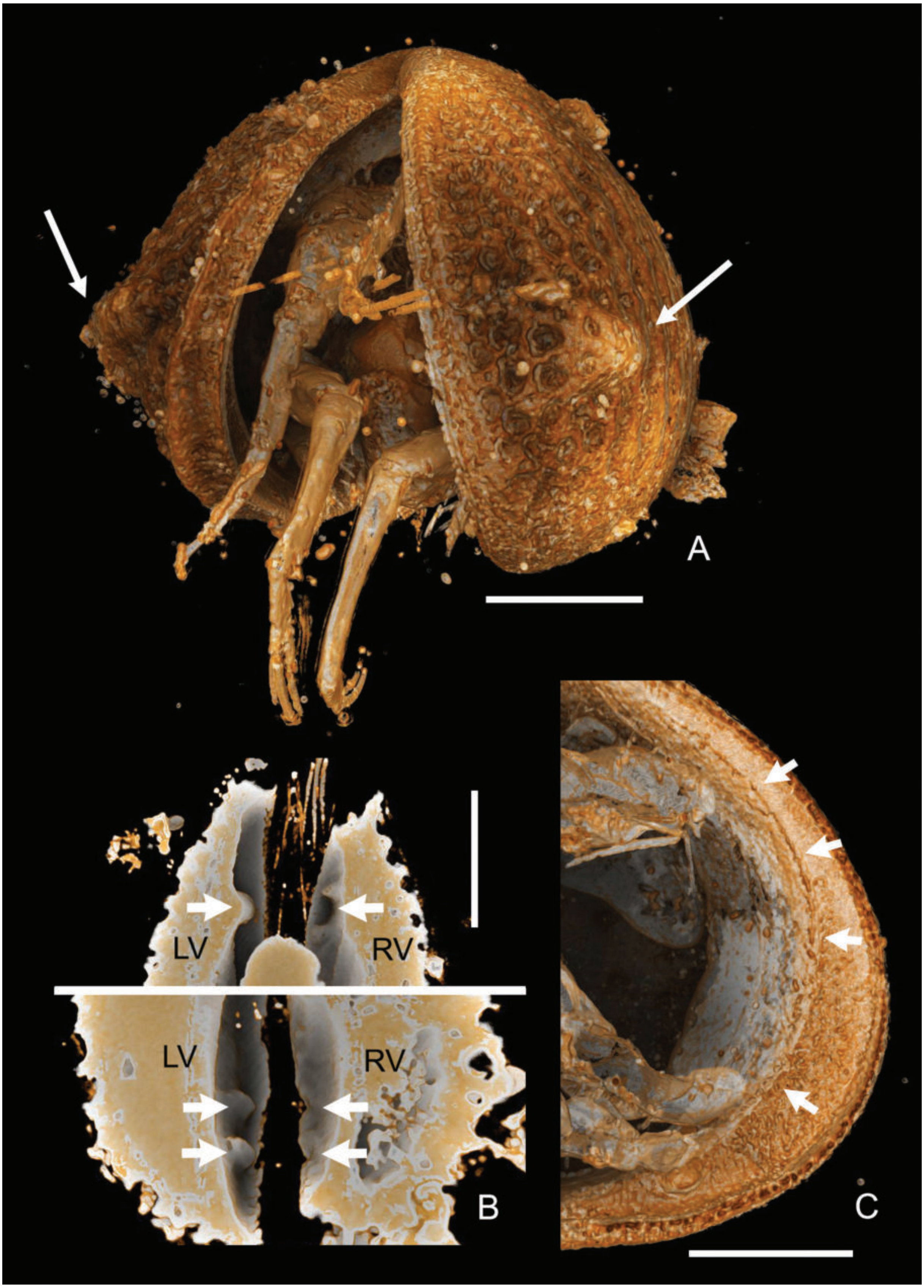

Figure 2. Microtomographic reconstruction of *Myanmarcypris hui* (volume rendering). **A.** Holotype, male, oblique anterior view with pairs of A1 and A2 reaching through gaping carapace. Arrows indicate pair of antero-lateral nodes on the ornamented carapace surface; **B.** Section of carapace of adult female paratype, dorsal view through ventral carapace gap. Upper part arrows showing single tooth in anterior LV and corresponding socket in RV. Lower part arrows showing pair of teeth and sockets in the posterior part of the valves. C, male holotype, anterior part of internal view with arrows pointing to inner list. Scale bars: 100 µm.

Figure 3. Microtomographic reconstruction of soft parts of male holotype of *Myanmarcypris hui* (BA19005-1), and female soft parts of *Myanmarcypris hui* (BA19005-2), surface renderings. **A–N.** With same scale, BA19005-1; **O–AC.** With same scale, BA19005-2; **A.** A1, right; **B.** A1, left; **C.** A2, right; **D.** A2, left; **E.** Md, right; **F.** Md, left; **G.** Mxl, right; **H.** L5, right; **I.** L5, left; **J.** L6, right; **K.** UR; **L.** Zenker organ, right; **M.** Zenker organ, left; **N.** Sperm duct; **O.** A1, right; **P.** A1, left; **Q.** A2, right; **R.** A2, left; **S.** Md, right; **T.** Md, left; **U.** Mxl, right; **V.** Mxl, left; **W.** L5, right; **X.** L5, left; **Y.** L6, right; **Z.** L6, left; **AA.** L7, right; **AB.** L7, left; **AC.** UR.

eye-spot (Fig. 1F). Normal pores distributed all over the valves except dorsal area. LV overlaps RV along dorsal and ventral margins. Hinge adont. Well-developed calcified inner lamella in adult carapaces, broader anteriorly than posteriorly, and anteriorly with inner list (Fig. 2C). Ventral margin of calcified inner lamella with conspicuous anterior tooth in LV and corresponding socket in RV, and two smaller posterior teeth in LV with corresponding sockets in RV, the latter much less developed than anterior socket (Fig. 2B). No central muscle scars preserved. Preserved juveniles show similar carapace ornamentation as adults except for A-4 stage, which is smooth (Fig. 1).

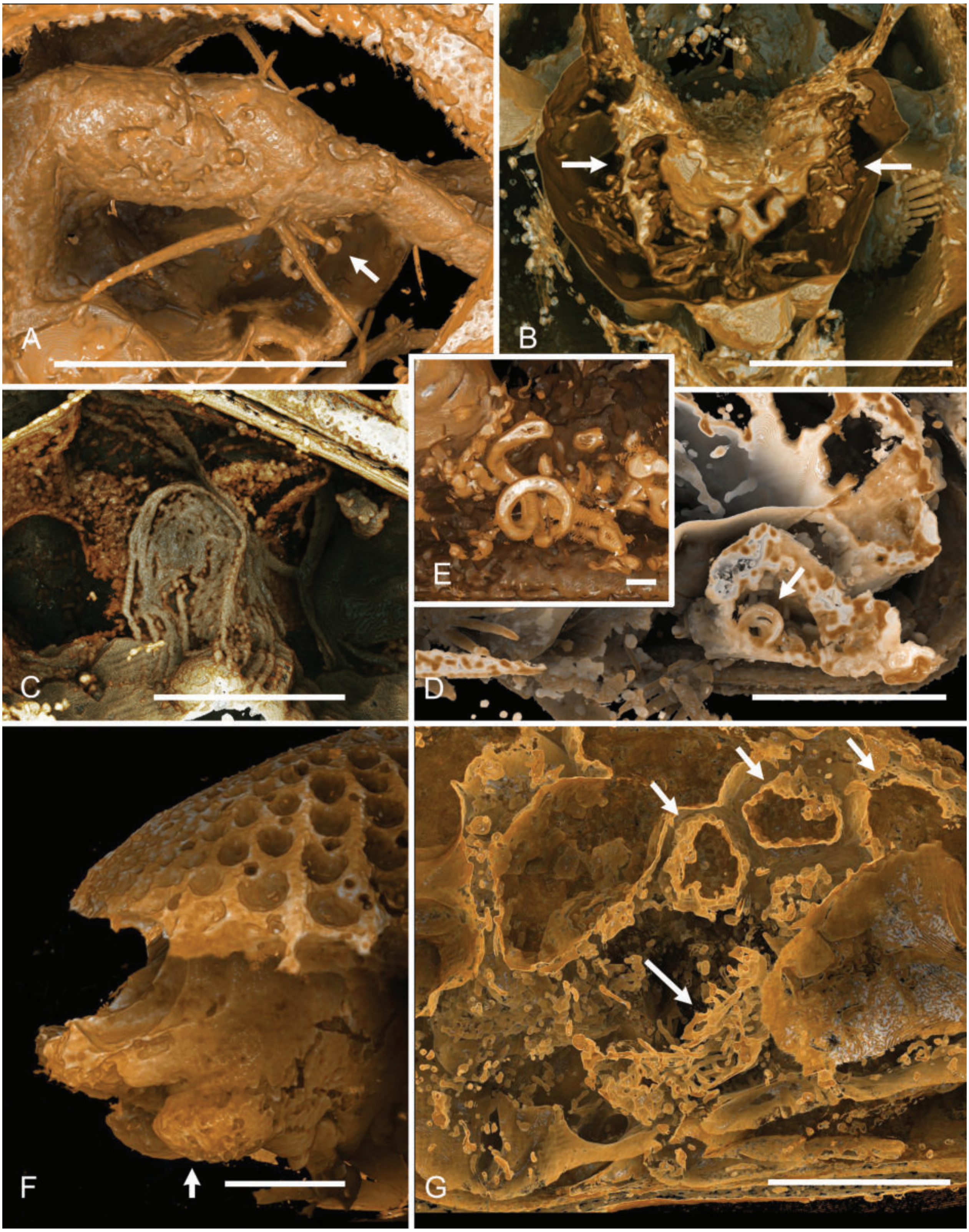

Figure 4. Microtomographic reconstruction of adult male (BA19005-1) and adult female (BA19005-2) *Myanmarcypris hui* (volume rendering). **A.** Male A1 with prominent Rome Organ (arrow); **B.** Male with pair of Zenker Organs in their body cavity (arrows); **C.** Loop of long sperm duct (vasa deferentia) in body cavity of male; **D.** Posterior body of male with hempenis, which partly exposes coiled internal sperm duct (arrow); **E.** Detail of preserved sperm duct in hemipenis; **F.** Posterior body of female, with female genital lobes exposed (arrow); **G.** Section of female posterior body with eggs (short arrows) and stored spermatozoa (long arrow). Scale bars: 100 µm (**A–D, F–G**); 10 µm (**E**).

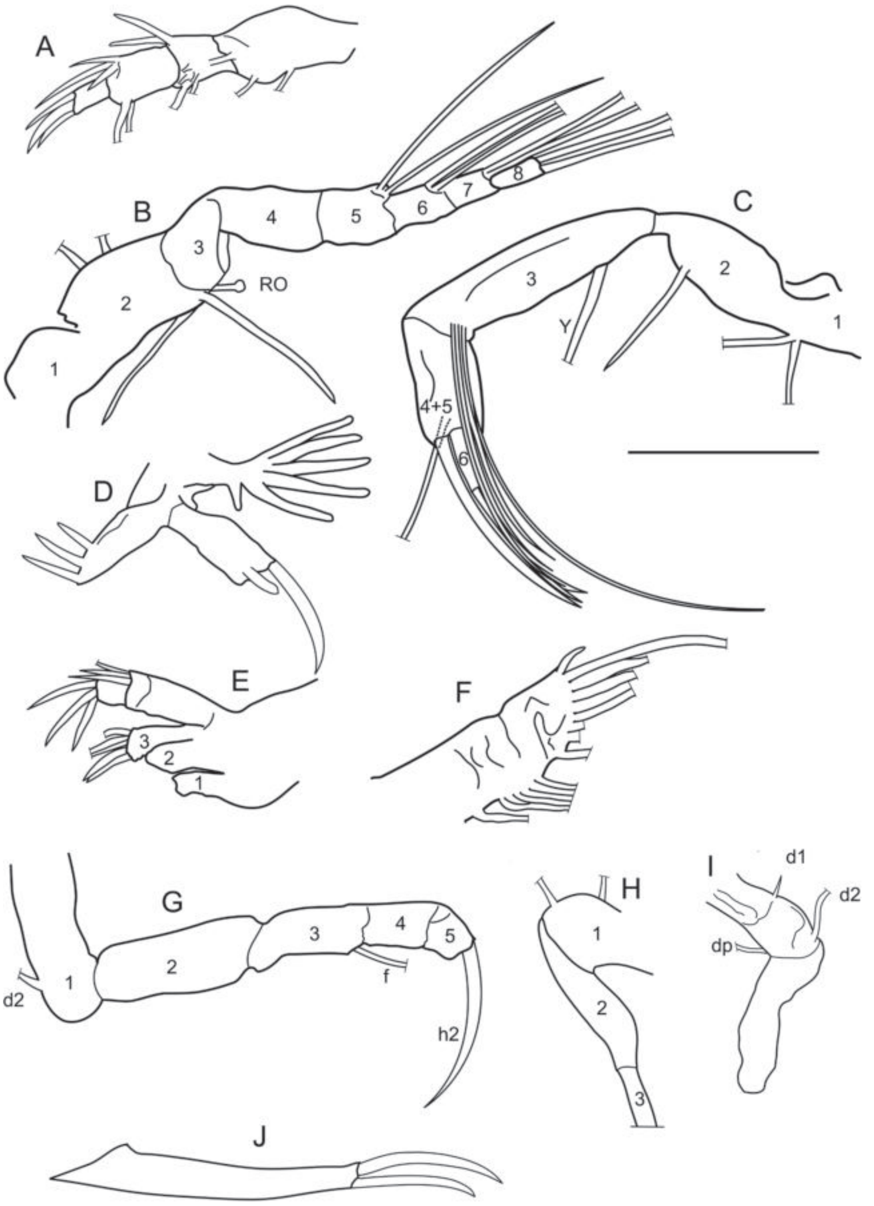

Figure 5. Drawings of appendages of *Myanmarcypris hui*, based on microtomography of adult male (BA19005-1) and adult female (BA19005-2). **A.** Right Md endopod (interior view); **B.** A1; **C.** A2; **D.** Male L5; **E.** Mxl palp and endites; **F.** Mxl branchial plate; **G.** L6; **H.** Female L7; **I.** Male L7; **J.** UR. Scale bar: 100 µm. RO = Rome Organ; Y = Aesthetasc Y.

Soft Body (Figs 3–6): A1 (Figs 3A, B, O, P, 4A, 5B) with eight segments. Segments 1 and 2 fused forming large base, with two setae of unknown length originating dorso-median and long setae situated ventro-distally on segment 2. Only a little more distal, ventro-basally on segment 3, prominent Rome Organ with inflated tip (Figs 4A, 5B). Segment 3 short and sub-triangular. Segment 4 longer than twice its width. Segments 5 to 8 not fused and rectangular, with decreasing widths. Presence of setae confirmed for segments as figured. Setae at least as long as figured, possibly longer.

A2 (Male) (Figs 3C, D, 5C) Segment 1 (coxa) small, with 2 setae ventrally. Segment 2 (basis) elongate and carrying long ventro-apical seta. Segment 3 (first endopodal segment) elongate, with aesthetasc Y (ventro-median) and four natatory setae ventro-apically on the interior side of the appendage. Natatory setae possibly not complete and maximum length not known. Segments 4 and 5 possibly fused, together around half the length of segment 3. Apically with at least one seta subapical-exteriorly and three claws. Segment 6 small with at least one claw apically. Preservation of female A2 not sufficient for detailed chaetotaxy (Fig. 3Q, R).

Md (Figs 3E, F, S, T, 5A) Masticatory process of coxa too poorly preserved to describe morphology. Palp consisting of 4 separate segments and straight (i.e., not bent ventrally). Branchial plate not observed. Segment 1 (basis) with two setae ventrally, one at medium-length of the segment, the other more distally. Third seta originating on interio-apical margin. Shape of this segment subrectangular with

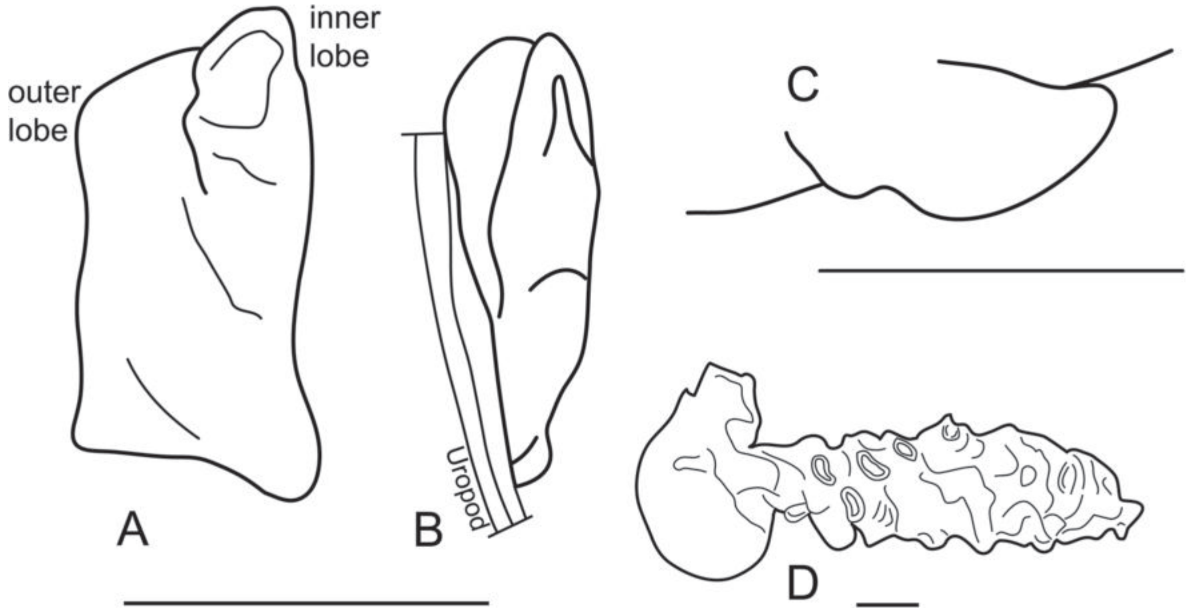

Figure 6. Drawings of appendages of *Myanmarcypris hui*, based on microtomography of adult male (BA19005-1) and adult female (BA19005-2). **A.** Hemipenis ventral view; **B.** Hemipenis, lateral view; **C.** Female genital lobe; **D.** Zenker Organ. Scale bars: 100 µm (**A–C**); 10 µm (**D**).

angulation on dorsal margin. Segment 2 square-shaped, with at least five setae apically (2 dorsally, 3 ventrally). Segment 3 rectangular with at least 5 setae confirmed 3 dorsally, 2 ventrally). Segment 4 much thinner than proximal segments, rectangular, distally with at least 1 claw and 2 setae.

Mxl (Figs 3G, U, V, 5E, F) Protopod with branchial plate with at least 15 marginal setae. Three masticatory lobes (endites 1–3) with distal claws/setae. Palp with two segments, both with at least 3 setae on their apical margins.

L5 Male (Figs 3H, I, 5D) no setae on protopod confirmed. Branchial plate with six marginal setae. Palp (endopod) a jointed clasping organ, carrying a long claw/finger-like process distally, and a shorter (sensory?) process more ventrally. Masticatory process with three or more setae. Female L5 badly preserved (Fig. 3W, X).

L6 (Figs 3J, Y, Z, 5G) Walking leg with 5 segments. Segment 1 with setae d1 and d2. Segment 2 elongate with no seta preserved. Segments 3 and 4 separate, not fused. Segment 3 with seta f distally, segment 4 with no seta g observed. Segment 5 with long claw h2.

L7 (Figs 3AA, AB, 5H, I) Distal parts of this appendage not preserved. Bending of this appendage dorsally suggests it being used as a typical cleaning leg. Segment 1 (basis) with setae d1, d2 and dp present. Segment 2 (first endopodal segment) long, with no seta preserved. Segment 3 preserved in one of the male's L7, however, only partially.

Ur ramus (Figs 3K, AC, 5J) Elongate, only slightly bent, with two relatively long terminal claws of similar length preserved (approx. half the length of the posterior edge of the ramus). Posterior and anterior setae not observed.

HP (Figs 4D, E, 6A, B) nearly rectangular in lateral view, with outer distal lobe wider and shorter than inner lobe. Several loops of sperm duct preserved in HP (Fig. 4E).

Female genital lobes (Fig. 4F) formed as spindle-shaped projections towards posterior and extending nearly to the posterior-most end of the soft body (i.e. basis of the UR). Inside the female BA19005-2, several eggs and stored spermatozoa are preserved (Fig. 4G).

Zenker Organs (Figs 3L, M, 4B, 6D) preserved in male BA19005-1 with five whorls of spines, one with the efferent part of the vas deferens attached. Vasa deferentia forming narrow U-shaped loops mid-laterally (Figs 3N, 4C).

Remarks. In the original description, it was stated that this species (and genus) belongs to the Candonidae because of the morphology of the Zenker Organ. Further, it was assigned to the Paracypridinae and tentatively to the tribe Renaudcypridini (Wang et al. 2020b) based on the presence of an internal antero-ventral tooth in LV and a corresponding socket in RV. This character has been defined as tribe-specific by Wouters (2001), while in the other tribes of the Paracypridinae the sockets are missing. As specified in the present analysis, the two postero-ventral teeth in LV of *M. hui* also possess corresponding sockets, albeit less pronounced than the anterior one. The other diagnostic features of the Renaudcypridini on L7 cannot be verified with the investigated specimens, namely the strong, spiny processes situated dorso-distally on each of the segments 3 and 4 and the arrow-shaped setules on the d2 seta. Nevertheless, we here assign this genus to the Renaudcypridini on the basis of the teeth/socket-characters of the valves, hoping that future findings of this species will offer more morphological characters to eventually verify, or falsify, this decision.

Although there is clearly some affinity with the genus *Renaudcypris* McKenzie, 1980, *Myanmarcypris* is easily distinguished by its dorsal hump, its strong and exceptional surface ornamentation and the striking antero-lateral nodes of the valves. Some living species of the cypridid subfamily Cypricercinae share carapace morphological characteristics with *M. hui*, notably the dorsal hump and the anterior tubercles. For example, *Strandesia martensi*

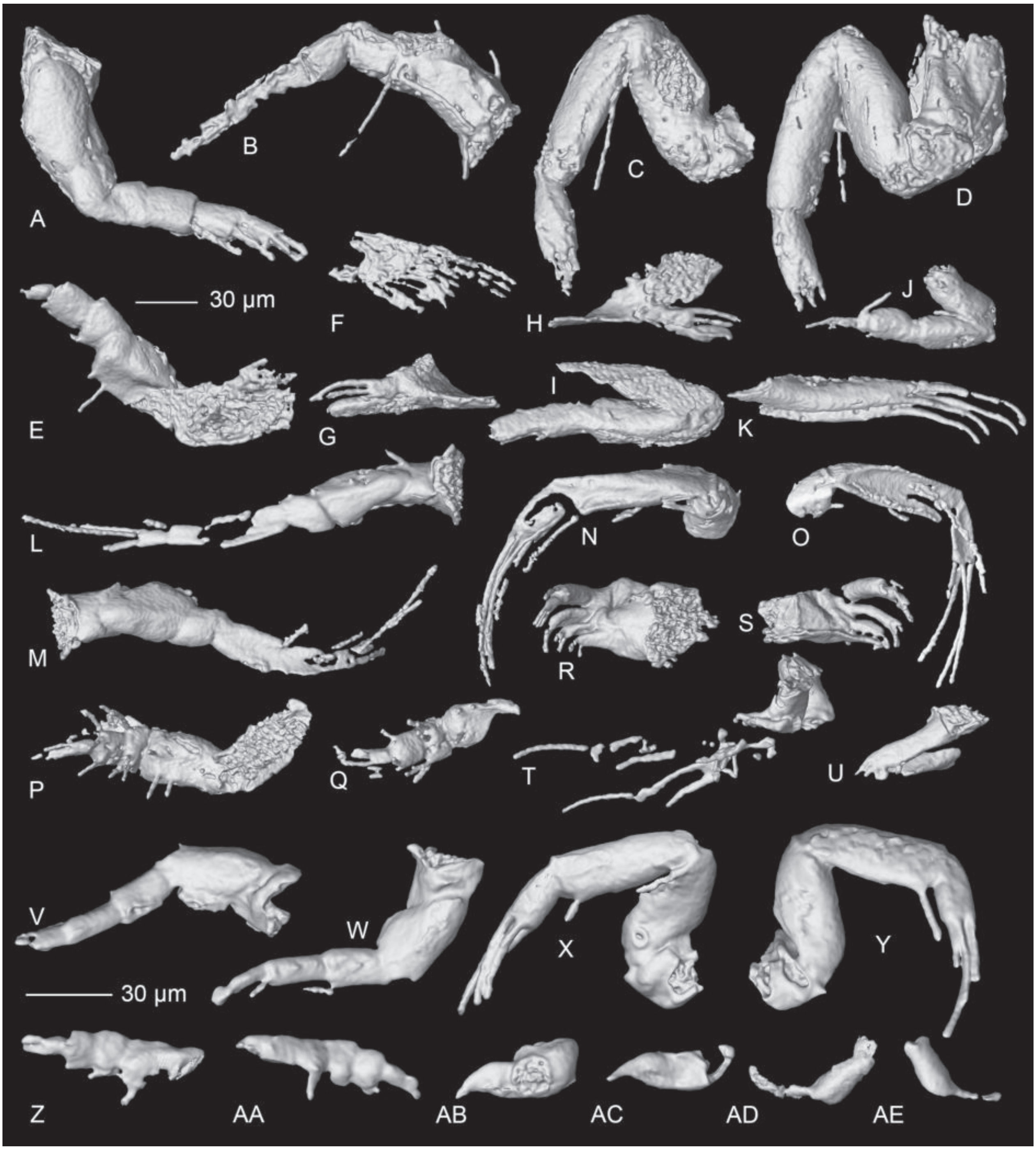

Figure 7. Microtomographic reconstruction of juvenile (A-2, A-3, A-4) soft parts of *Myanmarcypris hui* (BA19005-3, BA19005-4, BA19005-5), surface renderings. **A–U.** With same scale; **A–K.** Juvenile (A-2), BA19005-3; **L–U.** juvenile (A-3), BA19005-4; V-AE with same scale, juvenile (A-4), BA19005-5. **A.** A1, right; **B.** A1, left; **C.** A2, right; **D.** A2, left; **E.** Md, right; **F.** Mxl, left; **G.** L5, right; **H.** L5, left; **I.** L6, right; **J.** L7, right; **K.** UR; **L.** A1, right; **M.** A1, left; **N.** A2, right; **O.** A2, left; **P.** Md, right; **Q.** Md, left; **R.** Mxl, right; **S.** Mxl, left; **T.** L6; **U.** UR; **V.** A1, right; **W.** A1, left; **X.** A2, right; **Y.** A2, left; **Z.** Md, right; **AA.** Md, left; **AB.** L5, right; **AC.** L6, left; **AD.** L7, right; **AE.** L7, left.

Savatenalinton, 2015 from Thailand has a dorsal hump situated in front of mid-length, but in contrast to *M. hui* its RV overlaps the LV dorsally and it lacks internal ventral marginal teeth and sockets (Savatenalinton 2015). The genus *Sataracypris* Deb, 1983 from India also has a similar dorsal hump and has been tentatively assigned to the Cypricercinae pending redescription (Savatenalinton 2015). *Bradleytriebella tuberculata* (Hartmann, 1964) from Thailand has a prominent external tubercle close to the anterior margin of each valve, in a similar position to the node on each valve of *M. hui*, but it has no dorsal hump or internal ventral marginal teeth and sockets (Savatenalinton and Martens 2009a). Soft parts of *M. hui* are broadly similar to those of Cypricercinae, but the morphology of the caudal ramus attachment, which in Cypricercinae features a diagnostic Triebel's loop, remains unknown for *Myanmarcypris* and *Sataracypris*. For now, therefore, we consider the carapace similarities of *M. hui* with cypricercine species to be examples of homeomorphy rather than close phylogenetic affinity.

Several juvenile specimens were embedded in the same amber piece (Wang et al. 2020b), allowing for the presentation of an ontogenetic series from A-4 to A-2 (Fig. 1K–Y), including soft parts (Fig. 7, Suppl. material 3: Movie S1, Suppl. material 4: Movie S2, Suppl. material 5: Movie S3) (no A-1 specimen found). These juveniles lack the pair of antero-lateral nodes present in the adults' valves. The A-4 specimen even lacks the pronounced surface ornamentations of older stages (Fig. 1U).

Family Candonidae Kaufmann, 1900
Subfamily Paracypridinae Sars, 1923

Electrocypria gen. nov.

http://zoobank.org/9AC4D9B2-3D6C-422A-9319-EBA9E4430951

Type species. *Electrocypria burmitei* sp. nov.

Etymology. Name referring to 'electrum', the Latin term for amber + cypria, a common epithet in candonid ostracods.

Diagnosis. Small ostracods of the family Candonidae, with subrectangular (male) to trapezoidal (female) lateral carapace shape. Dorsal margin with greatest height at about 1/3rd of length, tapering down in straight line from there towards anterior and posterior ends. Anterior end curved broadly, posterior end with narrow curve, but not pointed. Calcified inner lamella not broad. Female higher than male. Fusiform in dorsal view with greatest width at mid-length. A1 with segments 3 to 8 separate (not fused). Natatory setae present on A2. L7 with segments 3 and 4 clearly separate, each without dorso-apical, marginal spiny processes (hooks). Terminal segment short (not longer than wide), carrying a robust and long claw h2 and a long reflexed seta h3. UR with anterior and posterior claws of the same length.

Remarks. The new genus is excluded from the Ilyocyprididae and Notodromadidae by its carapace morphology, and from the most Cyprididae subfamilies by its lack of a terminal pincer on the L7 (see, e.g., Horne et al. 2019). We are aware of some extant cypridid genera of the subfamily Cypridopsinae with non-pincer L7 (e.g., *Neocypridopsis* Klie, 1940; *Paranadopsis* Almeida et al., 2021; *Cyprettadopsis* Savatenalinton, 2020) or incomplete pincer structure (e.g., *Brasilodopsis* Almeida et al., 2021) but all of these share the cypridopsine character of a reduced UR, unlike *Electrocypria* which has a fully developed UR. There is also the genus *Batucypretta* (subfamily Batucyprettinae) with a much reduced UR and lacking the L7 pincer, considered by its describing authors (Victor and Fernando 1981) to be transitional to the Cypridopsinae. The cyprid genus *Zonocypretta* De Deckker, 1981 (subfamily Bradycypridinae) lacks the L7 pincer and has a fully-developed UR, but differs from *Electrocypria* by virtue of other features including marginal septa in the valves.

Within the three subfamilies of the Candonidae, *Electrocypria* is best allocated to the Paracypridinae, foremost because of the natatory setae observed in the female specimen. Such natatory setae are not present in the Candoninae. The third subfamily, Cyclocypridinae, can be excluded by the valve morphology and shape, as well as by the cyclocypridine L7 morphology with segments 3 and 4 being fused, and the terminal segment carrying a long reflexed seta h3 and two short h1 and h2 setae distally. The genus *Electrocypria* therefore belongs to the subfamily Paracypridinae, which is currently subdivided into three tribes, these being the marine Paracypridini and the marine to brackish Thalassocypridini and Renaudcypridini. Although the carapace morphology may point to the Thalassocypridini, *Electrocypria* cannot be allocated to this tribe because of its L7 morphology, with segments 3 and 4 not being fused, a short terminal segment and its two long h setae distally. In the Thalassocypridini, segments 3 and 4 of L7 are fused, the terminal segment is long and bears only a long reflexed seta, while the other two h setae are short. *Electrocypria* does not qualify as a Renaudcypridini because of the lack of a unique feature of this tribe: the strong, spiny processes situated dorso-distally on both segments 3 and 4 of L7. In *Electrocypria* the dorsal edges of these segments are clearly smooth. Also, Renaudcypridini possess a well-developed tooth in the antero-ventral area of the inner lamella in the LV, complemented by a defined socket on the inner lamella of the RV (Wouters 2001) – characters that could not be observed in *Electrocypria*. Species of the third tribe, Paracypridini, typically show wide calcified inner lamellae with narrow vestibula and broad fused zones with radial pore canals in their well-calcified carapaces. These characters are not present in *Electrocypria*. The genera of the Paracypridini are more diverse in their soft body features than those of the Thalassocypridini and Renaudcypridini, as shown in the detailed review of anatomical features in the Paracypridinae by Maddocks (1992). The anatomy of A1 with its varying degrees of segment fusion and the variable combination of L7 features in the different genera may serve as examples. However, none of these mosaic patterns of characteristics fits to those observed in the type species of *Electrocypria*. Due to the valve morphology, combined with the lack of congruence in important soft body features with any genus of the Paracypridini, we refrain from attributing *Electrocypria* to this tribe. Consequently, we cannot allocate the genus *Electrocypria* to any of the currently accepted three tribes of the Paracypridinae.

Electrocypria burmitei sp. nov.

http://zoobank.org/5BE413FE-3EC1-48ED-9C82-EF25C4776D2F

Figs 8–13; Suppl. material 6: Movie S4, Suppl. material 7: Movie S5

Etymology. Referring to 'burmite', which is one of the names of amber from Myanmar.

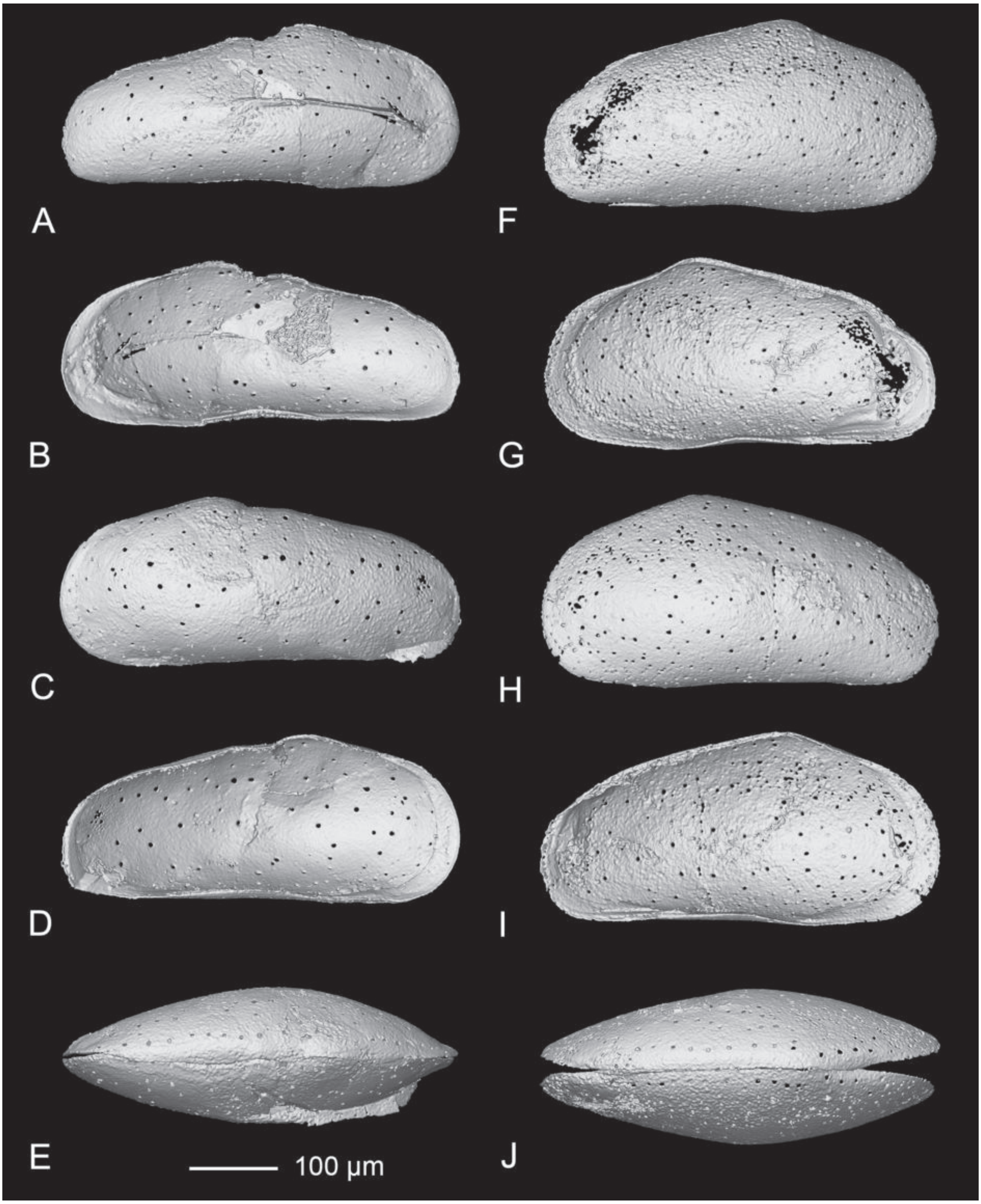

Figure 8. Microtomographic reconstruction of *Electrocypria burmitei* gen. et sp. nov., surface rendering. **A–E.** Male, BA19005-6; **F–J.** Female, BA19005-7. First (uppermost) row: RV externally; second row: RV internally; third row: LV externally; fourth row: LV internally; fifth row: dorsal view of carapace, anterior to right.

Material. Seven specimens enclosed in one amber piece (BA19005-6, 7, 37–41) (Fig. S1), two of which (male holo- and female paratype) were analyzed using 3D X-ray microscopy. The species description is based on the tomographic data.

Type locality and stratigraphy. Hukawng Valley, Kachin Province, northern Myanmar; upper Albian–lower Cenomanian.

Types. Holotype: BA19005-6 (male); Paratype: BA19005-7 (female).

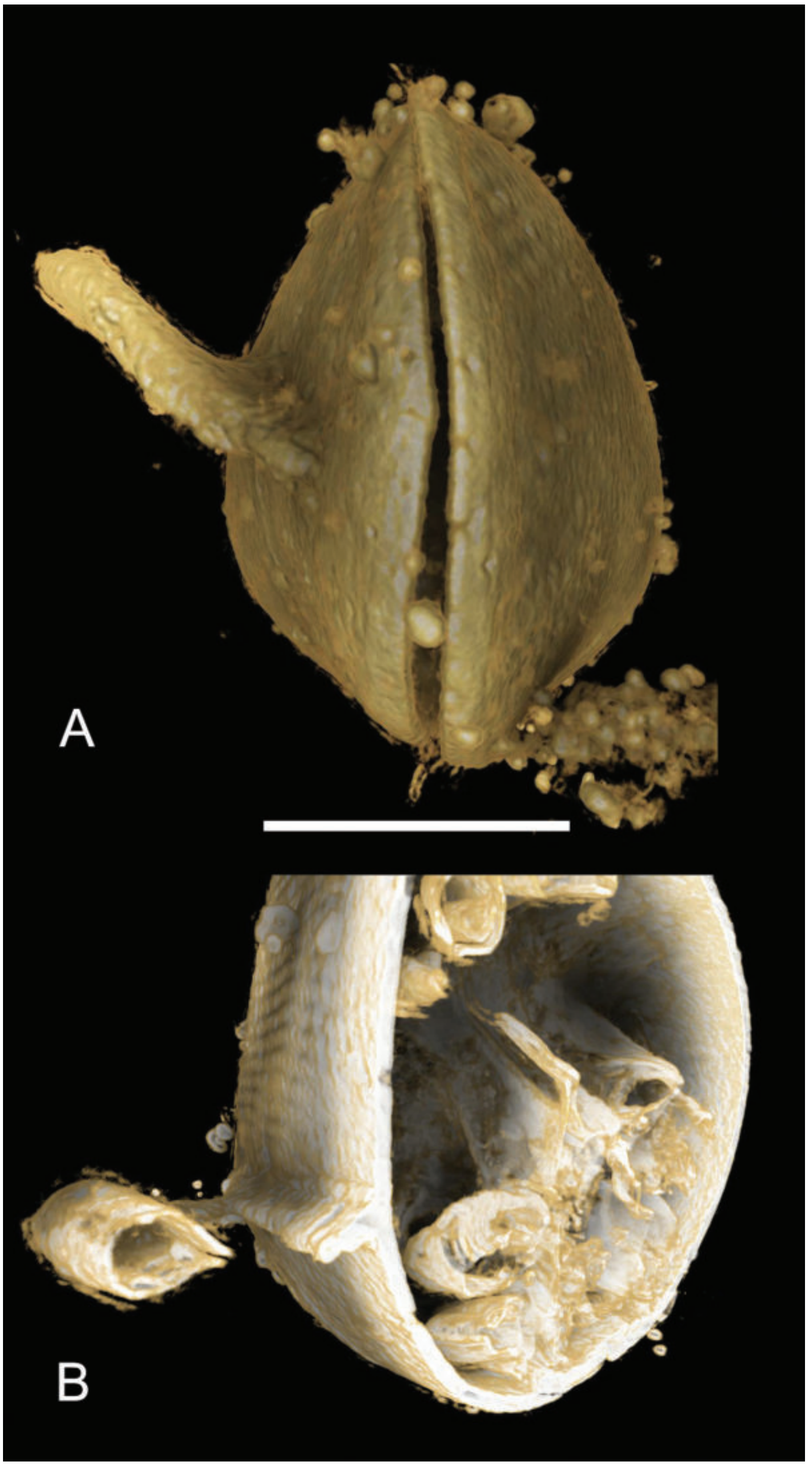

Figure 9. Microtomographic reconstruction of *Electrocypria burmitei* gen. et sp. nov., volume rendering. **A.** Male, BA19005-6, anterior view, with solidified body liquid extruding from breakage of RV; **B.** Cross section of same specimen, showing extrusion along the breakage in detail. Scale bar: 100 µm.

Repository. Lingpoge Amber Museum (Shanghai).

Dimensions. L = 470 µm, H = 200 µm, W ≈ 160 µm (male, holotype); L = 470 µm, H = 217 µm, W ≈ 145 µm (female, paratype).

Diagnosis. see diagnosis of the currently monospecific genus.

Description (The species description is based on the tomographic data, NIGP175852). Carapace (Figs 8, 9): LV overlaps RV along the dorsal and ventral margins. Dorsal margin with greatest height at about 1/3rd of length, tapering down in straight line and same angle to anterior and posterior ends. Hinge well-developed, straight, between highest point and posterior end. Both anterior and posterior margins nearly equicurvate, with the latter curved much narrower than the former, but lacking an acute angle or pointed tip. Fusiform in dorsal view with greatest width at mid-length. Ventral margin slightly concave at mid-length. Calcified inner lamella relatively

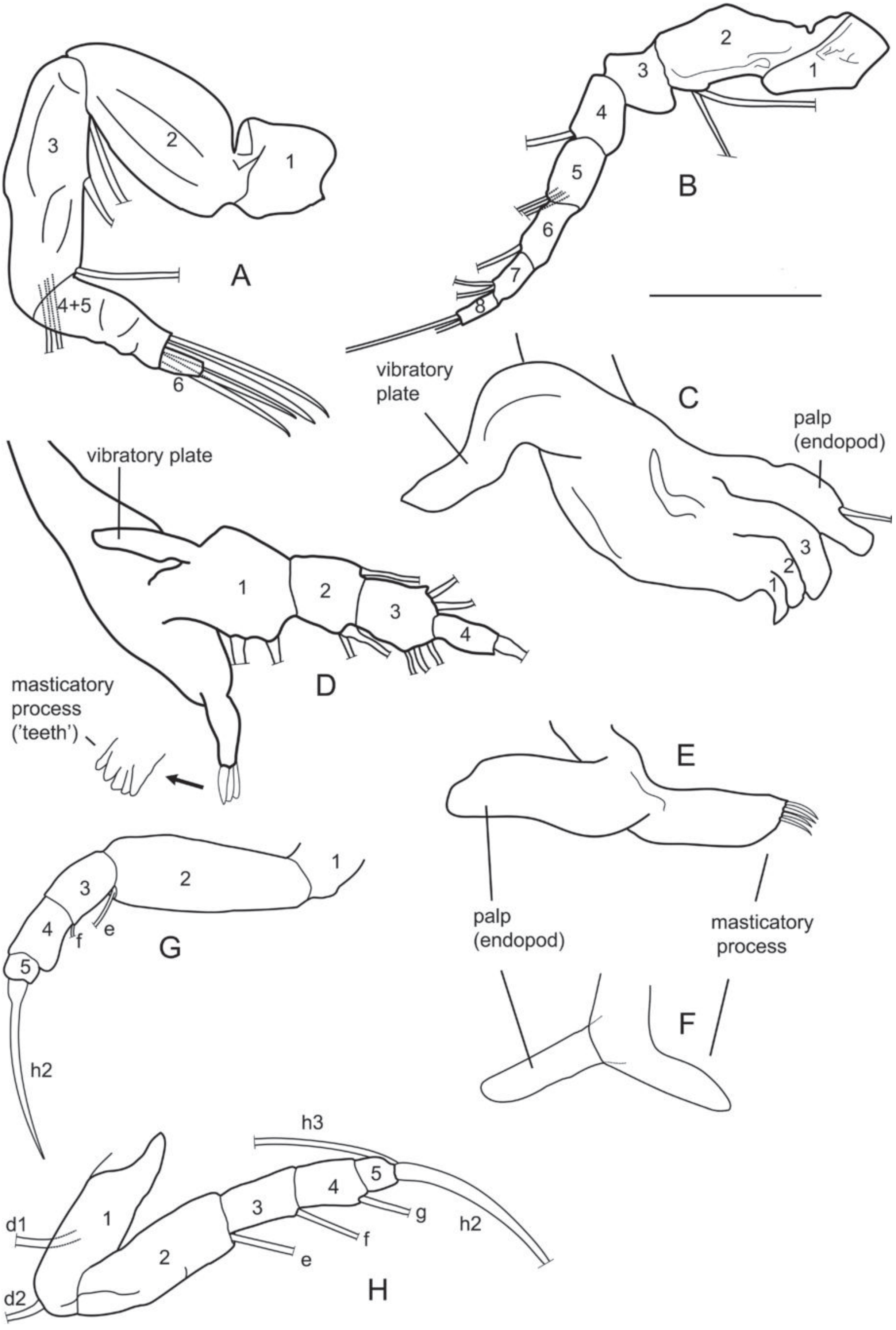

Figure 10. Drawings of appendages of *Electrocypria burmitei* gen. et sp. nov., based on data of adult male (BA19005-6) and adult female (BA19005-7). **A.** A2; **B.** A1; **C.** Mxl; **D.** Md; **E.** male L5; **F.** female L5; **G.** L6; **H.** L7. Scale bar: 50 µm.

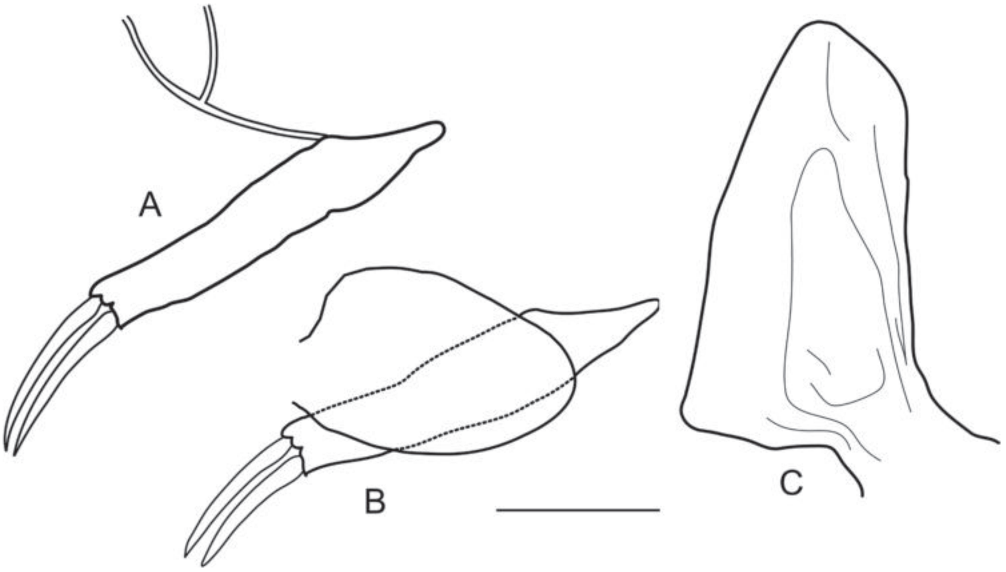

Figure 11. Drawings of appendages of *Electrocypria burmitei* gen. et sp. nov., based on microtomography of adult male (BA19005-6) and adult female (BA19005-7). **A.** UR with proximal attachment; **B.** UR with female genital lobe; **C.** Hemipenis, ventral view. Scale bar: 50 µm.

narrow at free margin, slightly broader at posterior end, and broadest at anterior end. Central muscular scars not visible. Normal pores scattered over smooth surface.

Soft Body (Figs 10–13): A1 (Figs 10B, 12A, B, N, O, 13A) with eight segments. Segments 1 and 2 fused forming large base, with two long setae originating ventro-distally on segment 2. Segment 3 short and asymmetric, sub-triangular, with ventral extension. Segment 4 connected to segment 3 with ventral inclination. Segments 4 to 8 all separate (not fused) and rectangular, with decreasing widths. Presence of setae confirmed for segments as figured. Setae on segment 8 at least as long as figured, possibly longer.

A2 (Figs 10A, 12 C, D, P, 13A) Segment 1 (coxa) subrectangular, segment 2 (basis) elongate and carrying long ventro-apical seta. Knee between segment 2 and 3. Segment 3 (first endopodal segment) very similar to segment 2 in shape and length, also carrying ventro-apical seta. Exopod not confirmed, but aesthetasc Y present. Natatory setae not observed in male, but at least 2 natatory setae present in one of the female's A2 (Fig. 12P); their exact point of origin at segment 3 is unclear. Segments 4 and 5 possibly fused, since clear segmental boundary could not be confirmed. Their length approximately half the length of segment 3. Apically with at least three claws (G1, G2, G3). Segment 6 small with at least one claw apically (GM or Gm).

Md (Figs 10D, 12E, F, Q, 13B) Masticatory process of coxa with teeth (total number uncertain). Palp consisting of 4 separate segments and remarkably straight (i.e., not bent ventrally towards mouth). Segment 1 (basis) with vibratory (branchial) plate on dorsal edge (no setae observed), and two thick setae ventrally, one at medium-length of the segment, the other more distally, but still at a considerable distance to segment 2. Shape of this segment obliquely trapezoidal due to angulation on dorsal margin. Segment 2 nearly square-shaped, with at least three setae apically (one dorsally, two ventrally). Segment 3 more elongate, with shoulders distally towards segment 4. On these shoulders, at least 5 setae confirmed (2 dorsally, 3 ventrally). Segment 4 much thinner than proximal segments, distally at least one thick seta or claw present.

Mxl (Fig. 10C) Protopod with branchial plate (no setae confirmed), three masticatory lobes (endites 1–3) and palp. Palp possibly two-segmented, as dorsal seta might indicate. Distal claws and/or setae not confirmed.

L5 Male (Figs 10E, 12G, H, 13C): no setae on protopod confirmed. Palp (endopod) truncated, possible finger-like process of this clasping organ not observed. Masticatory process with several distal setae. Female (Figs 10F, 12R): masticatory process and palp preserved with no detail.

L6 (Figs 10G, 12I, J, S) Walking leg. Segment 1 small, segment 2 elongate with seta e distally. Segments 3 and 4 separate, not fused. Segment 3 with seta f distally, segment 4 with no seta g observed. Segment 5 with long claw h2.

L7 (Figs 10H, 12K, L, T, U, 13D) Cleaning leg, directed dorsally. Segment 1 (basis) with setae d1 and d2 present. Segment 2 (first endopodal segment) long, with distal seta e. Segments 3 and 4 separate, not fused. Segment 3 with seta f, segment 4 with seta g distally. Segment 5 short, nearly quadrate; distally long claw h2 and long reversed seta h3 present.

Ur ramus (Figs 11A, B, 12M, V, 13E) Relatively stout and straight, with two relatively long terminal claws of similar length preserved (approx. half the length of the posterior edge of the ramus). Posterior and anterior setae not observed. UR attachment simply branched.

HP (Figs 11C, 13F) roughly triangular in lateral view, with no differentiation of lobes observed. Greatest length of HP nearly a quarter of carapace length.

Female genital lobes (Figs 11B, 13G) formed as spindle-shaped projections towards posterior and extending nearly to the posterior-most end of the soft body (i.e. basis of the UR).

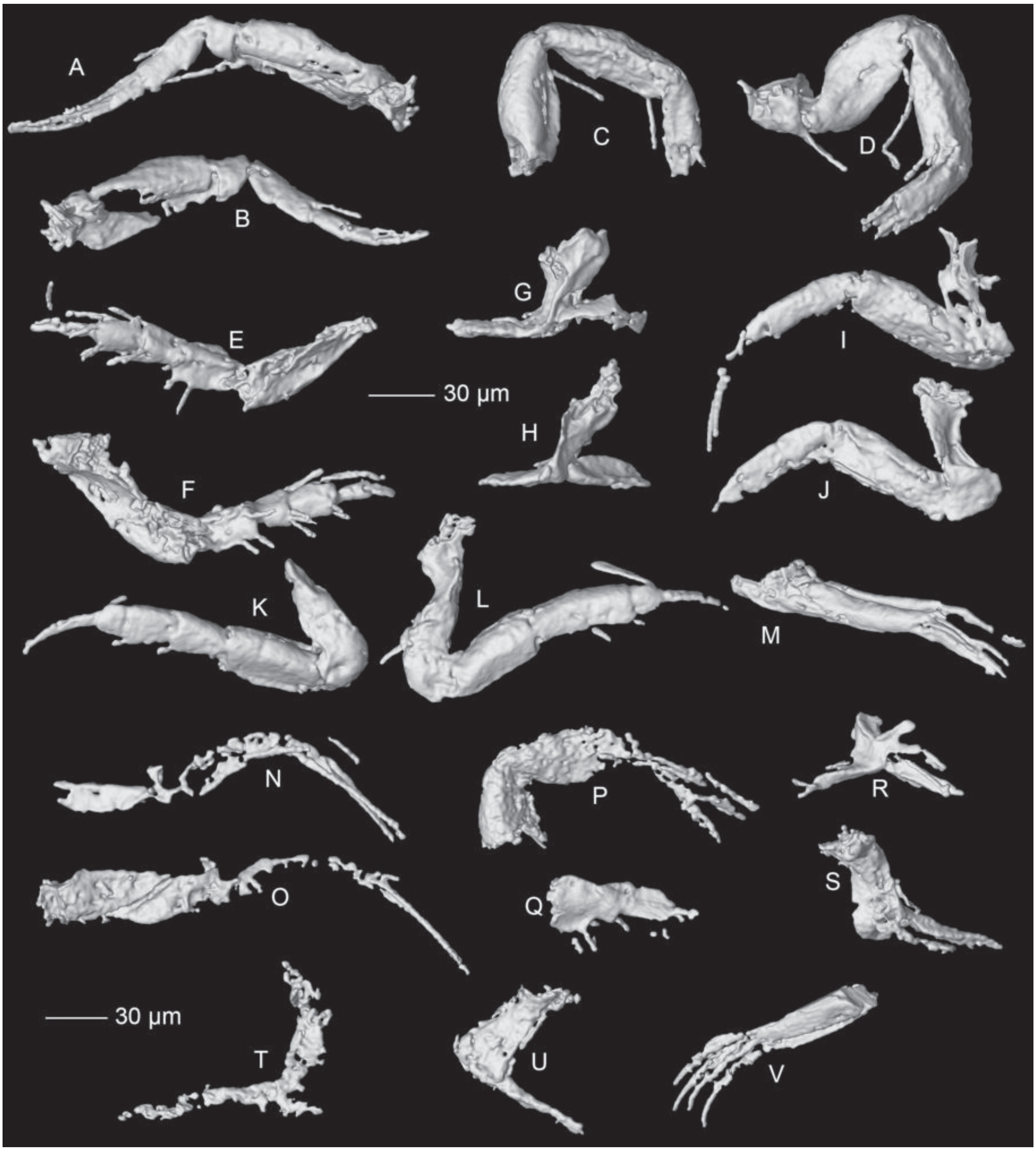

Figure 12. Microtomographic reconstruction of soft parts of male (BA19005-6) and female (BA19005-7) *Electrocypria burmitei* gen. et sp. nov., surface renderings. **A–M.** With same scale, male (BA19005-6); **N–V.** With same scale, female (BA19005-7). **A.** A1, right; **B.** A1, left; **C.** A2, right; **D.** A2, left; **E.** Md, right; **F.** Md, left; **G.** L5, left; **H.** L5, right; **I.** L6, right; **J.** L6, left; **K.** L7, right; **L.** L7, left; **M.** UR; **N.** A1, right; **O.** A1, left; **P.** A2, right; **Q.** Md, right; **R.** L5, left; **S.** L6, left; **T.** L7, right; **U.** L7, left; **V.** UR.

Remarks. *Electrocypria burmitei* gen. et sp. nov. possesses relatively long setae on A1, as well as at least 2 natatory setae on A2, however, the latter are only preserved partly, and possibly not at their full lengths. It is therefore impossible to evaluate the swimming capability of this species.

The straight appearance of the Md palp results from segment 2 being nearly square-shaped and not as wedge-shaped as is often the case in other Cypridoidea. None of the L5s is completely preserved in either specimen and it remains unclear how the male claspers look in *E. burmitei* gen. et sp. nov. While L6 is formed as a walking leg with a long distal claw and segments 3 and 4 not fused, L7 is formed as a 5-segmented cleaning leg with setae e, f and g present, as well as long terminal h2 and h3 setae/claws. The holotype shows a linear breakage in its LV, in parallel to the dorsal margin, as well as minor breaking marks in its RV. The external pressure of the resin seems to have squeezed body liquid out of the animal on the LV into the surrounding resin (Figs 8A, B, 9A, B).

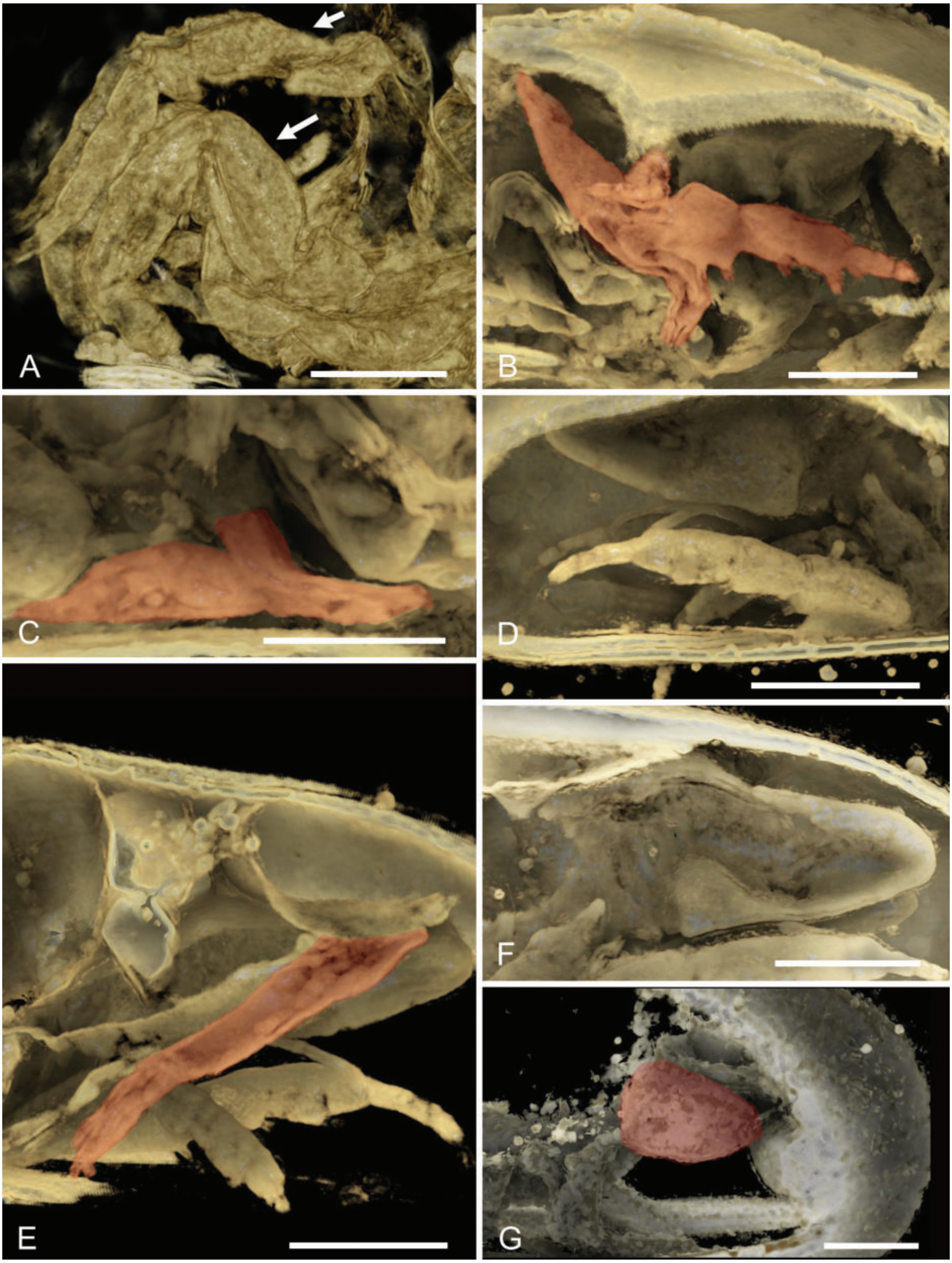

Figure 13. Microtomographic reconstruction of *Electrocypria burmitei* gen. et sp. nov., based on data of adult male (BA19005-6) and adult female (BA19005-7), volume rendering. **A.** A1 (short arrow) and A2 (long arrow); **B.** Right Md (highlighted); **C.** Male L5 (highlighted); **D.** Left L7; **E.** UR (highlighted); **F.** Right HP, interior view; **G.** Female genital lobe (highlighted). Scale bars: 50 µm.

Suborder Cytherocopina Baird, 1850
Superfamily Cytheroidea Baird, 1850
Family Loxoconchidae Sars, 1925

Genus *Sanyuania* Zhao & Han, 1980

Type species. *Sanyuania psaronius* Zhao & Han, 1980.

***Sanyuania* sp.**

Figs 14–16; Suppl. material 8: Movie S6

Material. Single male specimen; BA19005-8.

Dimensions. L = 245 µm, H = 116 µm, W ≈ 120 µm.

Description. Carapace (Figs 14A–E, 16A, C) small subtriangular shape in lateral view. Greatest height at ¼ of length. Anterior margin broadly rounded. Posterior margin narrowly rounded. Dorsal margin straight, moderately sloping down from the greatest height to the posterior margin. Ventral margin straight in middle part in both valves, with slightly concave regions in the very middle, forming distinct flaps as an area of valve overlap (LV>RV) (Fig. 16A). From posterior third, ventral margin ascending towards posterior end. Carapace in dorsal view elliptical, with posterior and anterior part compressed and central region strongly protruding. The valve's lateral surface punctate in the flat anterior and posterior marginal regions, while pitted (i.e., covered with wider and deeper depressions) in the central region and dorsally. Valves thick in cross section (Fig. 16C). Inflated central region with distinct sulcus mid-dorsally. Inner calcified lamella wide. Central muscular scar pattern, pore morphology and detailed hinge elements not preserved.

Soft parts almost all preserved, but with a low degree of detail.

A1 (Figs 14F, G, 15A, 16D) rod-shaped. Segmentation and setation not preserved.

A2 (Figs 14H, I, 15B, 16D) more robust than A1, number of segments unknown. With prominent knee between protopodite and endopodite, close to which the spinneret seta (exopodite) originates, the only preserved setation of both A2 in this specimen.

Between the right A2 and the internal side of RV, a roundish, disk-shaped body is preserved, which we tentatively interpret as the sac of the spinneret gland containing the secretion (Fig. 16D).

Md (Figs 14J, K, 15E, 16B, E) Masticatory process of coxa preserved, reaching into the oral opening, but teeth only weakly preserved. The palp's segmentation and setation not preserved. Vibratory plate not preserved.

Mxl (Figs 14L, M, 15C, 16B) Protopod with three masticatory lobes (endites 1–3) and two-segmented palp, without any claws/setae preserved; branchial plate preserved.

L5 (Figs 14N, O, 15F, 16F) Walking leg, elongate, with long endopodite consisting of indeterminate number of segments.

L6 (Figs 14P, Q, 15G, 16F) Presumed walking leg, protopodite elongate, endopod not well preserved.

L7 (Figs 14R, 15H) Walking leg, elongate protopodite and long endopodite, the latter with at least three segments.

HP (Figs 15D, 16F, G) almost triangular in shape, apically forming distinct tip, shaped like an arrowhead.

Remarks. We assign the studied specimen to the genus *Sanyuania* within the Loxoconchidae, mainly based on shape, ornamentation and morphology of its carapace. Preserved soft parts, although with little detail, and without genus-specific features being observable, at least do not oppose this assignment. The morphology of the preserved hemipenes is clearly in line with Hartmann's (1966: 758) description of hemipenes typical of Loxoconchinae as consisting of a voluminous capsule and a triangular, distally rounded top piece. A direct comparison of our specimens' hemipenis with that of *Sanyuania segersi* Savatenalinton & Martens, 2009a shows a high degree of similarity (Savatenalinton and Martens 2009a: fig. 5A) with its triangular (arrow-head-like) distal tip on a broad, rounded main body. Regarding the shape of the carapace, as well as the flattened anterior and posterior margins, our specimen is most similar to *S. cuneata* Zhao & Whatley, 1992. However, the surface ornamentation of the valves with broader pits centrally and smaller ones marginally, comes closer to that of *S. wangi* Zhao & Whatley, 1992. None of the known *Sanyuania* species, however, possess the mid-dorsal sulcus featured in our specimen. Clearly our data on this single specimen are too limited for more certainty; more specimens are needed for a full taxonomic assessment. We therefore present this specimen in open nomenclature here.

4. Discussion

4.1. Taphonomy

The potential for aquatic organisms to be trapped in amber is well-established from studies of modern tree resin in a swamp forest and supported by quite numerous fossil examples (Schmidt and Dilcher 2007). Previously reported invertebrates trapped in amber have included ostracods (e.g., Keyser and Weitschat 2005), although it should be noted that the example illustrated by Schmidt and Dilcher (2007: fig. 2J) is not an ostracod but perhaps a cladoceran branchiopod. In total, 39 ostracod specimens have been found in a single piece of amber of less than 1 cm^3 volume. All of our preserved ostracods have articulated valves, most of them preserved with soft parts, and they include juveniles as well as adults, all of which suggests optimal environmental conditions immediately prior to the ostracods becoming trapped in the tree resin. We interpret this to indicate in-situ preservation of the ostracod specimens after a rapid burial in the plant sap; such an assessment of the coenosis according to criteria used for ostracods preserved in sediments is legitimate and represents as close an approximation to a biocoenosis as is possible in

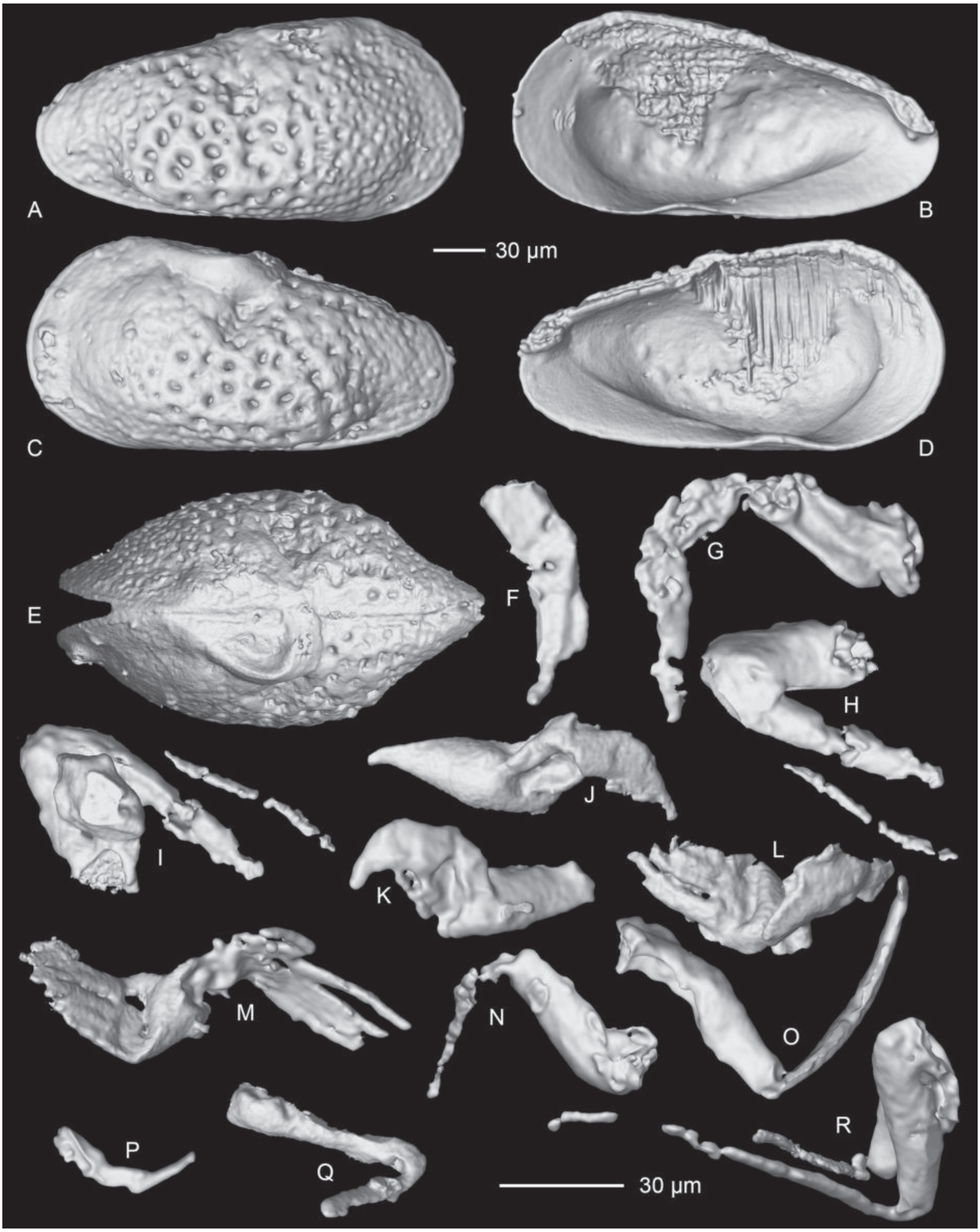

Figure 14. Microtomographic reconstruction of *Sanyuania* sp., based on microtomography of adult male (BA19005-8), surface rendering and soft parts of BA19005-8, surface renderings. **A–E.** With same scale, carapace; **F–R.** With same scale, soft parts. **A.** RV external; **B.** RV internal; **C.** LV external; **D.** LV internal; **E.** Dorsal view, anterior to left; **F.** A1, right; **G.** A1, left; **H.** A2, right; **I.** A2, left; **J.** Md, right; **K.** Md, lef; **L.** Mxl, right; **M.** Mxl, left; **N.** L5, right; **O.** L5, left; **P.** L6, right; **Q.** L6, left; **R.** L7, right.

Cretaceous material. With three ostracod species, partly represented by specimens of different ontogenetic stages and sexes, the preserved death assemblage resembles a low energy thanatocoenosis with minimal post-mortem disturbance (Boomer et al. 2003). Therefore the studied ostracod assemblage may be considered representative of the autochthonous ostracod population, allowing for an evaluation of the environmental conditions at the moment

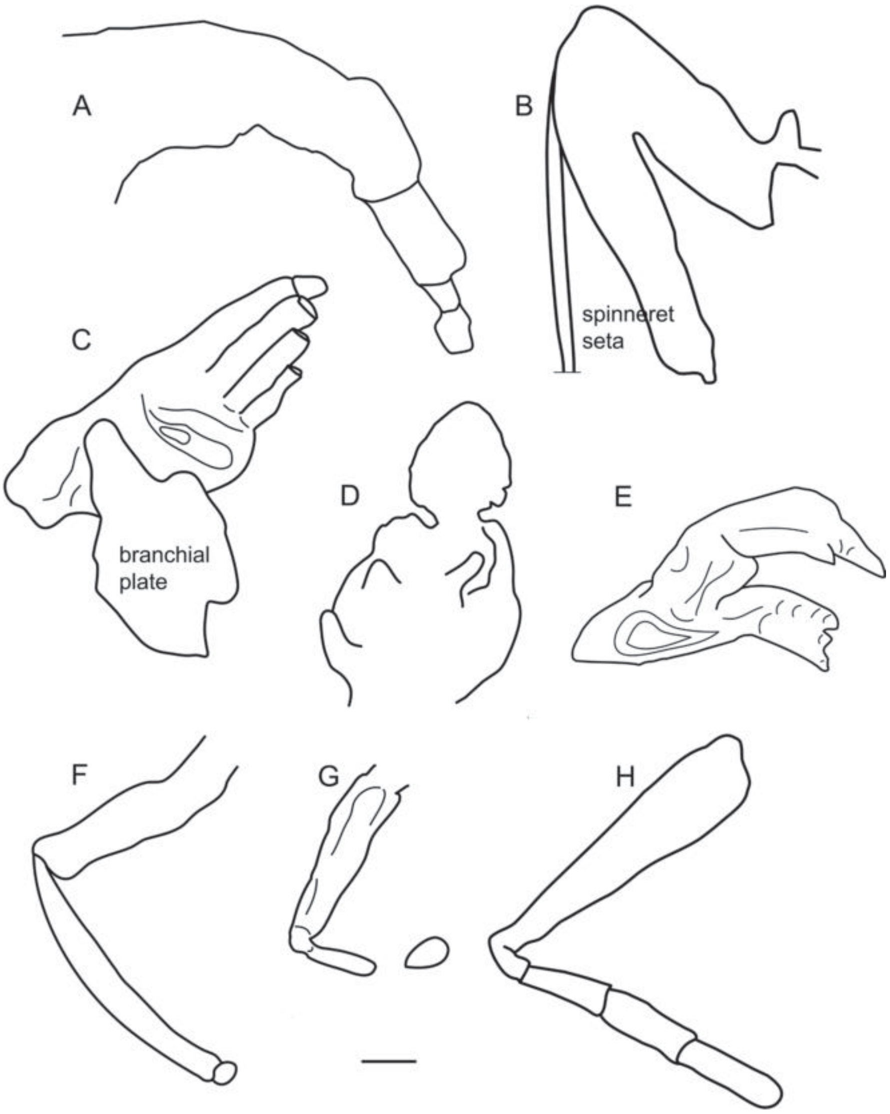

Figure 15. Drawings of appendages of *Sanyuania* sp., based on microtomography of adult male (BA19005-8). **A.** A1; **B.** A2; **C.** Mxl; **D.** HP; **E.** Md; **F.** L5; **G.** L6; **H.** L7. Scale bar: 10 µm.

of embedding (Boomer et al. 2003; Matzke-Karasz et al. 2019). Moreover, reproductive organs of male and female *M. hui*, including giant sperms stored in a female's seminal receptacles (Wang et al. 2020b), indicate recent reproductive activity involving sexual intercourse and support the scenario of a thanatocoenosis.

Cypridoidean ostracods use their antennules and antennae, as well as their walking legs and uropodal rami for swimming and walking, respectively. During active movement, these appendages can be seen protruding from the carapaces (Schreiber 1922; Hunt et al. 2007). Such protruding appendages could also be observed in some of the trapped specimens, suggesting that they were trying to walk or swim in the resin before its viscosity impeded any further movement.

We conclude that the studied ostracods were quickly surrounded by resin fallen into the water or extruded from plant parts immersed in the water. The resin was not yet marginally hardened, and quite instantly immobilized the ostracods as they became embedded in this viscous matrix while swimming, climbing on vegetation, or walking on the sediment surface. This conclusion is also consistent with one of the possibilities for embedding of aquatic organisms in resin: attaching to resin surface and struggling deeper (Schmidt and Dilcher 2007). The difference in pressure between the resin and internal body pressure becomes visible in the male *E. burmitei* gen. et sp. nov. (BA19005-6), where external pressure of the resin seems to have caused a linear breakage in the valve, through which body liquid was pressed out.

The above scenario resembles the taphonomic situation suggested for the ostracods from Mexican amber (Matzke-Karasz et al. 2019), while it differs from the entombment of the only three known ostracods preserved in Baltic amber, none of which seems to have been trapped in resin under water, but e.g. splashed (within a drop of water) or blown (dry) onto liquid tree resin (Keyser and Weitschat 2005; Keyser and Friedrich 2017).

Rare occurrences of marine organisms embedded in amber are usually interpreted as having formed in coastal forest settings by (e.g.) high tides, storm surges or wind and sea spray (Schmidt et al. 2018). In the case

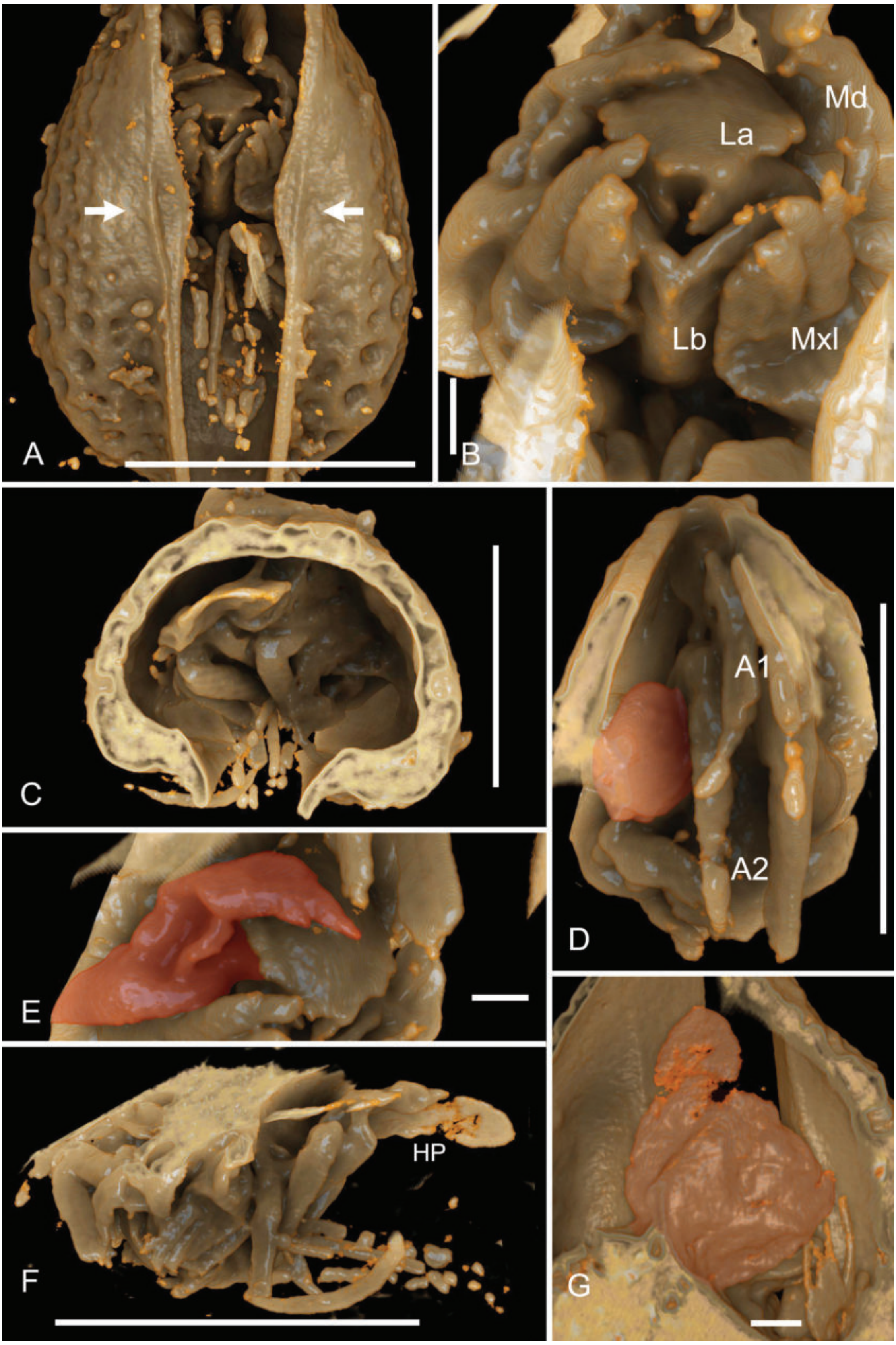

Figure 16. Microtomographic reconstruction of *Sanyuania* sp., based on data of adult male (BA19005-8), volume rendering. **A.** Oblique ventral view into gaping carapace with flaps for improved valve overlap (arrows); **B.** Mouth area from ventral, with labrum (la), labium (lb), mandible (Md) and maxillula (Mxl); **C.** Cross section in posterior region, with very thick and robust valves; **D.** Anterior body region with A1 and A2 and presumed sac of spinneret gland (highlighted); **E.** Mandible (highlighted); **F.** Soft body with L5, L6 and L7 and HP; **G.** HP in dorsal view (highlighted). Scale bars 100 µm (**A, C, D, F**); 10 µm (**B, E, G**).

of Burmese Cretaceous amber, in which freshwater organisms are common, marine fossils represented only by empty shells, such as an ammonite and gastropods (Yu et al. 2019) as well as a myodocopan ostracod (Xing et al. 2018), were probably subject to post-mortem transport before becoming embedded in resin. On the other hand, pholadid bivalves that apparently bored into the amber in which they were found are considered to be indicative of immediate proximity to fresh or estuarine waters (Smith and Ross 2017; Bolotov et al. 2021). The strong likelihood that our assemblage of 39 ostracods represents an in-situ thanatocoenosis is therefore of special importance for the palaeoenvironmental interpretation of Kachin amber (see next section).

4.2. Palaeoenvironment and distribution

Previous work has established the palaeoenvironmental context of the Kachin amber as a coastal forest (Yu et al. 2019). This kind of coastal amber forest could have both terrestrial and marine organism preserved in resin (e.g., Girard et al. 2008; Girard et al. 2009; Masure et al. 2013; Saint Martin et al. 2015). The assemblage of 39 ostracods in a single piece of amber provides valuable new insight into the aquatic palaeoenvironment associated with the forest. *Myanmarcypris hui* belongs to the Paracypridinae, tribe Renaudcypridini. This is the only fossil record of the Renaudcypridini, so that palaeoenvironmental assessments must rely on what is known about extant representatives of this tribe. It contains only two genera, *Hansacypris* Wouters, 1984, known to occur in oligo- and mesohaline as well as in fully marine environments (Wouters 2001), and *Renaudcypris* McKenzie, 1980, which seems to have a preference for lower salinities than *Hansacypris*. Of the four known *Renaudcypris* species, only one (*R. gorongae* McKenzie, 1980) was described from a marine environment (a beach of Gorong Island); however, it was sampled in a section that was under strong freshwater influence from a rivulet causing salinity fluctuations. *Renaudcypris wolffi* (Harding, 1962) was reported from (e.g.) the oligohaline lake Te-Nggano (Rennel Island/Solomon Islands) with subterranean channels connecting it with the sea, and from brackish and freshwater sites in Papua New Guinea (Wouters 1984); *R. natans* Hartmann, 1984 (from a pond without connection to the sea on Rangiroa Atoll, French Polynesia) and *R. luzonensis* Wouters, 1986 (from Lake Taal, Philippines) clearly both thrive in full freshwater.

Living species of *R. gorongae* were recorded from a 1:1 mix of coralline sands and algae (McKenzie 1980); for *R. luzonensis*, Wouters (1986) reported them living on the lake bottom and on algae, while *R. natans* was found on a coralline rock with a layer of organic detritus. Given these ecological data of extant *Renaudcypris*, we here suggest that *M. hui*, being closely related to *Renaudcypris*, may indicate a palaeoenvironment of fluctuating salinity from fully freshwater to brackish waters, accepting occasional marine influx. The presence of algae and organic detritus in the habitat is likely, as well as the possibility of occasional higher water energy (due to wave action, perhaps) and/or the presence of small predators, since the robust, ornamented shells of *M. hui* with their efficacious closure mechanism (3 teeth and corresponding sockets on the calcified inner lamellae) provide protection against both. Its longer natatory setae would allow this species to swim in the water column to cover short distances.

The autecology of *E. burmitei* gen. et sp. nov. cannot be inferred from its taxonomic relationships, because it is currently impossible to assign it to any of the existing three tribes within the Paracypridinae, and therefore an ecological approximation would remain doubtful. Unfortunately, the natatory setae of our two type specimens are only partly preserved, so that it is not even possible to evaluate the swimming ability of this species (although it was at least capable of swimming).

In contrast, Cytheroidea are always non-swimming, benthonic ostracods, crawling and burrowing on and in sediments or climbing on aquatic plants. A single specimen in our material could be ascribed to this superfamily, and here to the genus *Sanyuania*, of which six species have been described so far from China, Korea, Japan and Thailand. The geologically oldest of them, *S. psaronius* Zhao & Han, 1980 has a fossil record dating back to the Pliocene but has also living representatives, while the other species are all geologically younger, with *S. abei* (Choe, 1988) and *S. segersi* being known from living occurrences only. Our finding of a representative of a *Sanyuania* species pushes the roots of this genus c. 94 million years deeper in time. As to their habitat salinity preferences, the known species of this genus are very heterogeneous, inhabiting fully marine bottom mud (*S. abei*), ocean-connected and continental brackish water bodies (*S. psaronius*, *S. wangi*, *S. cuneata* and *S. sublaevis* Zhao & Whatley, 1992) as well as a fully freshwater river habitat (*S. segersi*) (Zhao and Han 1980; Choe 1988; Zhao and Whatley 1992; Tanaka 2006; Savatenalinton and Martens 2009a). Consequently, the assignment of our Cretaceous specimen to the genus *Sanyuania* as such cannot help in narrowing down its salinity preference, but in concert with *M. hui*, for which we showed a close relationship with the predominantly brackish to freshwater genus *Renaudcypris*, the likelihood of a brackish environment in the oligohaline/mesohaline range increases.

4.3. Outlook

Through its taxonomy and morphology, the ostracod fauna that was found in a single amber piece sheds a light on the environmental settings and the process of entombment in the liquid plant resin. The presence of reproductive organs and sperms are the basis of substantiated conclusions on the cypridoidean reproductive strategies at the time. Unfortunately, the poor soft part preservation in specimens of *E. burmitei* gen. et sp. nov. and *Sanyuania* sp. precluded some conclusions for the time being, but future amber-findings of these taxa will likely help in resolving (e.g.) the three following issues.

First, *E. burmitei* gen. et sp. nov. could not yet be assigned to one of the three existing tribes in Paracypridinae, but with only a few more taxonomically relevant characters at hand. In the future, it should be possible to either assign it to one of the existing tribes, or to expand the subfamily with the addition of a fourth tribe. Either case will help to consolidate an evolutionary tree of this rather enigmatic (due to rare findings of Renaudcypridini and Thalassocypridini) and ecologically diverse lineage.

Second, the genus *Sanyuania* could hold some key information on the family Loxoconchidae, but a few more specimens with good soft part preservation will be needed for unequivocal conclusions. *Sanyuania segersi*, a fully freshwater species from an inland river of Thailand, has been used by Savatenalinton and Martens (2009b) for a phylogenetic assessment of freshwater inhabiting lineages within the Loxoconchidae based on (soft part) morphological characters. This assessment could gain much more impact if soft parts of this ancient member of the genus could be analyzed in more detail in better-preserved specimens.

Third, Savatenalinton and Martens (2009b) found *S. segersi* to be morphologically close to *S. cuneata*, of which living representatives live under shallow-marine, mesohaline conditions (Tanaka 2006). Zhao and Whatley (1992) developed an evolutionary model of the genus suggesting a Holocene origin of *S. segersi*, branching off of Pleistocene representatives of *S. cuneata* or their ancestors, either inhabiting coastal or inland brackish water. New data on the soft parts of the *Sanyuania* species from Myanmar amber would considerably improve this tentative evolutionary model, shedding light on an Asian brackish-water ostracod genus of high interest with regard to regional Cenozoic faunal provinces (Tanaka 2006).

5. Conclusions

With rare exceptions, fossil ostracods are classified based on carapace alone – and must be, because normally it is only the calcified parts of the animal that are preserved. In very few cases ostracod soft parts were preserved and could provide unique taxonomic information through their morphological details (Matzke-Karasz and Smith 2020), which occasionally even call into question the taxonomy of extinct ostracods established on carapaces alone (Siveter et al. 2013). In our study, the preserved appendages and setae had a strong impact on the final taxonomic evaluation and we emphasize the value of fossil soft part preservation for key questions in ostracod evolution.

According to the taphonomy of the three studied ostracod species, we suggest that these ostracods were preserved in situ, having been quickly surrounded by resin and instantly immobilized when trapped in the amber. After considering the present-day affinities of the embedded ostracods, the palaeoenvironment is suggested to have been a vegetated lagoonal setting with mesohaline to oligohaline water salinities being dominant. The resin producing trees and other coastal vegetation, in combination with surface barriers, created relatively still microhabitats along the Cretaceous coasts of Myanmar, where podocopid ostracods could thrive swimming and walking on submerged vegetation and in the organic detritus on the bottom.

Author statement

Tomographic data have been processed by He Wang and Renate Matzke-Karasz. Resulting models have been analyzed by all authors. The manuscript has been written by all authors and all agree with the presented ideas.

Ethical statement

We acknowledge the controversial nature of the study of fossils in amber from Myanmar and the need for vigilance regarding ethical and legal issues in palaeontology (e.g., Haug et al. 2020). Our research is limited to material acquired prior to the 2017 resumption of armed conflict in the region, and we hope that it will contribute to raising awareness of the current conflict in Myanmar and the hard work of Burmese miners, to the benefit of disadvantaged communities (Peretti 2021).

Declaration of competing interest

The authors declare that they have no known competing financial interests or personal relationships that could have appeared to influence the work reported in this paper

Acknowledgements

We thank two anonymous reviewers and the editor-in-chief for their careful reading of our submission and their constructive suggestions for improvements. This work was supported by the Natural Science Foundation of Jiangsu Province (No. BK20210991) and the State Key Laboratory of Palaeobiology and Stratigraphy (Nanjing Institute of Geology and Palaeontology Chinese Academy of Sciences) (No. 20202104).

References

Almeida NMD, Higuti J, Ferreira VG, Martens K (2021) A new tribe, two new genera and three new species of Cypridopsinae (Crustacea, Ostracoda, Cyprididae) from Brazil. European Journal of Taxonomy 762(1): 1–48. https://doi.org/10.5852/ejt.2021.762.1451

Baird W (1838) The natural history of the British Entomostraca: part IV. Magazine of Zoology and Botany 2: 132–144.

Baird W (1845) Arrangement of the British Entomostraca, with a list of species, particularly noticing those which have as yet been discovered within the bounds of the club. Transactions of the Berwickshire Naturalist's Club 2(13): 145–158.

Baird W (1850) The natural history of the British Entomostraca. The Ray Society, London, [i–viii,] 364 pp. https://doi.org/10.5962/bhl.title.39641

Bolotov IN, Aksenova OV, Vikhrev IV, Konopleva ES, Chapunrina YE, Kondakov AV (2021) A new fossil piddock (Bivalvia: Pholadidae) may indicate estuarine to freshwater environments near Cretaceous amber-producing forests in Myanmar. Scientific Reports 11: e6646. https://doi.org/10.1038/s41598-021-86241-y

Boomer I, Horne DJ, Slipper IJ (2003) The use of ostracods in palaeoenvironmental studies, or what can you do with an ostracod shell? In: Park LE, Smith AJ (Eds) Bridging the gap: trends in the ostracode biological and geological sciences. The Palaeontological Society Papers 9: 153–179. https://doi.org/10.1017/S1089332600002199

Choe KL (1988) On ostracod biofacies and five new genera in Korean Seas. Developments in Palaeontology and Stratigraphy 11: 121–133. https://doi.org/10.1016/S0920-5446(08)70177-8

Deb M (1983) Brief descriptions of new species of Ostracoda: Crustacea from Maharashtra State (India). Records of the Zoological Survey of India 81: 135–166.

De Deckker P (1981) Taxonomic notes on some Australian ostracods with description of new species. Zoologica Scripta 10(1): 37–55. https://doi.org/10.1111/j.1463-6409.1981.tb00483.x

Girard V, Schmidt AR, Saint Martin S, Struwe S, Perrichot V, Saint Martin JP, Grosheny D, Breton G, Néraudeau D (2008) Evidence for marine microfossils form amber. Proceedings of the National Academy of Sciences of the United States of America 105: 17426–17429. https://doi.org/10.1073/pnas.0804980105

Girard V, Saint Martin S, Saint Martin J-P, Schmidt AR, Struwe S, Perrichot V, Breton G, Néraudeau D (2009) Exceptional preservation of marine diatoms in upper Albian amber. Geology 37: 83–86. https://doi.org/10.1130/G25009A.1

Grimaldi DA, Engel MS, Nascimbene PC (2002) Fossiliferous Cretaceous amber from Myanmar (Burma): Its rediscovery, biotic diversity, and paleontological significance. American Museum Novitates 3361: 1–72. https://doi.org/10.1206/0003-0082(2002)361%3C0001:FCAFMB%3E2.0.CO;2

Hartmann G (1964) Asiatische Ostracoden. Systematische und zoogeographische Untersuchungen. Internationale Revue der gesamten Hydrobiologie, Systematische Beihefte 3: 1–155.

Hartmann G (1966) Ostracoda (1. Lieferung). Dr. H.G. Bronns Klassen und Ordnungen des Tierreichs: Band 5 (Arthropoda), Abteilung I (Crustacea), Buch 2, Teil IV (Ostracoda): Lieferung 4. Geest and Portig, Leipzig.

Hartmann G (1984) Zur Kenntnis der Ostracoden der polynesischen Inseln Huahine (Gesellschaftsinseln) und Rangiroa (Tuamotu-Inseln). Mitteilungen aus dem hamburgischen zoologischen Museum und Institut 81: 117–169.

Haug JT, Azar D, Ross A, Szwedo J, Wang B, Arillo A, Baranov V, Bechteler J, Beutel R, Blagoderov V, Delclòs X, Dunlop J, Feldberg K, Feldmann R, Foth C, Fraaije RHB, Gehler A, Harms D, Hedenäs L, Hyžny M, Jagt JWM, Jagt-Yazykova EA, Jarzembowski E, Kerp H, Khine PK, Kirejtshuk AG, Klug C, Kopylov DS, Kotthoff U, Kriwet J, McKellar RC, Nel A, Neumann C, Nützel A, Peñalver E, Perrichot V, Pint A, Ragazzi E, Regalado L, Reich M, Rikkinen J, Sadowski E-M, Schmidt AR, Schneider H, Schram FR, Schweigert G, Selden P, Seyfullah LJ, Solórzano-Kraemer MM, Stilwell JD, van Bakel BWM, Vega FJ, Wang Y, Xing L, Haug C (2020) Comment on the letter of the Society of Vertebrate Paleontology (SVP) dated April 21, 2020 regarding "Fossils from conflict zones and reproducibility of fossil-based scientific data": Myanmar amber. PalZ 94: 413–429. https://doi.org/10.1007/s12542-020-00522-x

Horne DJ, Meisch C, Martens K (2019) Arthropoda: Ostracoda. In: Rogers DC, Thorp J (Eds) Thorp and Covich's Freshwater Invertebrates, Fourth Edition, Volume IV, Keys to Palaearctic Fauna, Ch. 16.3, Academic Press, London, 725–760. https://doi.org/10.1016/B978-0-12-385024-9.00019-8

Hunt G, Park LE, Labarbera M (2007) A novel crustacean swimming stroke: coordinated four-paddled locomotion in the cypridoidean ostracode *Cypridopsis vidua* (Müller). The Biological Bulletin 212: 67–73. https://doi.org/10.2307/25066581

Jones TR (1901) On some Carboniferous shale from Siberia. Geological Magazine Decade 4 (8): 433–436. https://doi.org/10.1017/S0016756800179749

Kaufmann A (1900) Cypriden und Darwinuliden der Schweiz. Revue Suisse de Zoologie. Annales de la Société Zoologique de Suisse 8: 209–423. https://doi.org/10.5962/bhl.part.10584

Keyser D, Friedrich F (2017) An exceptionally well preserved new species of ostracod (Crustacea) with soft parts in Baltic amber. Historical Biology 29: 53–62. https://doi.org/10.1080/08912963.2015.1123554

Keyser D, Weitschat W (2005) First record of ostracods (Crustacea) in Baltic amber. Hydrobiologia 538: 107–114. https://doi.org/10.1007/s10750-004-5941-5

Klie W (1940) Süßwasserostracoden aus Nordostbrasilien VI. Zoologischer Anzeiger 130: 59–73.

Latreille PA (1802) Histoire naturelle, générale et particulière des crustacés et des insectes. Ouvrage faisant suite à l'Histoire Naturelle générale et particulière, composée par Leclerc de Buffon, et rédigée par C. S. Sonnini, membre de plusieurs Sociétés savantes. Tome 3. F. Dufart, Paris, [xii + 13–467] 467 pp. https://doi.org/10.5962/bhl.title.15764

Limaye A (2012) Drishti: a volume exploration and presentation tool. In: Proceedings SPIE (International Society for Optics and Photonics) 8506, Developments in X-Ray Tomography VIII, 85060X. See https://github.com/nci/drishti/wiki. https://doi.org/10.1117/12.935640

Maddocks RF (1992) Anchialine Cyprididae (Ostracoda) from the Galapagos Islands, with a review of the subfamily Paracypridinae. Zoological Journal of the Linnean Society 104: 1–29. https://doi.org/10.1111/j.1096-3642.1992.tb00912.x

Masure E, Dejax J, De Ploëg G (2013) Blowin' in the wind… 100 Ma old multistaged dinoflagellate with sexual fusion trapped in amber: Marine–freshwater transition. Palaeogeography, Palaeoclimatology, Palaeoecology 388: 128–144. https://doi.org/10.1016/j.palaeo.2013.08.008

Matzke-Karasz R, Serrano-Sánchez ML, Pérez L, Keyser D, Pipík R, Vega FJ (2019) Abundant assemblage of Ostracoda (Crustacea) in Mexican Miocene amber sheds light on the evolution of the brackish-water tribe Thalassocypridini. Historical Biology 31: 65–101. https://doi.org/10.1080/08912963.2017.1340471

Matzke-Karasz R, Smith RJ (2020) A review of exceptional preservation in fossil ostracods (Ostracoda, Crustacea). Marine Micropaleontology: e101940. https://doi.org/10.1016/j.marmicro.2020.101940

McKenzie KG (1980) A new subfamily from Gorong, Seram, Moluccas, with the description of *Renaudcypris* new genus (Crustacea, Ostracoda). Bulletin du Muséum national d'Histoire naturelle de Paris série 4, 2(section A: 2): 507–515.

Meisch C (2000) Freshwater Ostracoda of Western and Central Europe. In: Schwoerbel J, Zwick P (Eds) Süßwasserfauna von Mitteleuropa 8/3. Spektrum Akademischer Verlag, Heidelberg, Berlin, 522 pp.

Meisch C, Smith RJ, Martens K (2019) Subjective global checklist of the extant non-marine Ostracoda (Crustacea). European Journal of Taxonomy 492: 1–135. https://doi.org/10.5852/ejt.2019.492

Peretti A (2021) An alternative perspective for acquisitions of amber from Myanmar including recommendations of the United Nations Human Rights Council. Journal of International Humanitarian Action 6: e12. https://doi.org/10.1186/s41018-021-00101-y

Ride WDL, Cogger HG, Dupuis C, Kraus O, Mineli A, Thompson FC, Tubbs PK (1999) International code of zoological nomenclature. International Commission on Zoological Nomenclature. The Natural History Museum, London, UK.

Rodriguez-Lazaro J, Ruiz-Muñoz F (2012) A general introduction to ostracods: morphology, distribution, fossil record and applications. In: Horne DJ, Holmes J, Rodriguez-Lazaro J, Viehberg F (Eds) Ostracoda as Proxies for Quaternary Climate Change: Developments in Quaternary Science (17). Elsevier Science, Amsterdam, 1–14. https://doi.org/10.1016/B978-0-444-53636-5.00001-9

Ross A, Mellish C, York P, Crighton B (2010) Chapter 12. Burmese amber. In: Penney D (Ed.) Biodiversity of fossils in amber from the major world deposits. Siri Scientific Press, Manchester, 208–235.

Ross AJ (2019) Burmese (Myanmar) amber checklist and bibliography 2018. Palaeoentomology 2: 22–84. https://doi.org/10.11646/palaeoentomology.2.1.5

Ross AJ (2020) Supplement to the Burmese (Myanmar) amber checklist and bibliography, 2019. Palaeoentomology 3: 103–118. https://doi.org/10.11646/palaeoentomology.3.1.14

Saint Martin S, Saint Martin J-P, Schmidt AR, Girard V, Néraudeau D, Perrichot V (2015) The intriguing marine diatom genus *Corethron* in Late Cretaceous amber from Vendée (France). Cretaceous Research 52: 64–72. https://doi.org/10.1016/j.cretres.2014.07.006

Sars GO (1866) Oversigt af Norges marine Ostracoder. Forhandlinger i Videnskabs-Selskabet i Christiania 1865: 1–130.

Sars GO (1923) An account of the Crustacea of Norway with short descriptions and figures of all the species, vol. 9: Ostracoda, Parts 3/4. Bergen Museum, Bergen, 33–72.

Sars GO (1925) An account of the Crustacea of Norway with short descriptions and figures of all the species, vol 9: Ostracoda, Parts 5/6. Bergen Museum, Bergen, 73–208.

Savatenalinton S (2015) On three new species of non-marine ostracods (Crustacea: Ostracoda) from Northeast Thailand. Zootaxa 3914: 275–300. https://doi.org/10.11646/zootaxa.3914.3.3

Savatenalinton S (2018) New genus of subfamily Cypridopsinae Kaufmann, 1933 (Crustacea: Ostracoda) from Thailand. European Journal of Taxonomy 487: 1–17. https://doi.org/10.5852/ejt.2018.487

Savatenalinton S (2020) A new cypridopsine genus (Crustacea, Ostracoda) from Thailand. European Journal of Taxonomy 631: 1–16. https://doi.org/10.5852/ejt.2020.631

Savatenalinton S, Martens K (2009a) On a freshwater species of the genus *Sanyuania* Zhao and Han, 1980 (Crustacea, Ostracoda, Loxoconchidae) from Thailand, with a discussion on morphological evolution of the freshwater Loxoconchidae. Journal of Natural History 43: 259–285. https://doi.org/10.1080/00222930802590885

Savatenalinton S, Martens K (2009b) Generic revision of Cypricercinae McKenzie, 1971 (Crustacea, Ostracoda), with the description of three new genera and one new species and a phylogenetic analysis of the subfamily. Hydrobiologia 632: 1–48. https://doi.org/10.1007/s10750-009-9826-5

Schmidt AR, Dilcher DL (2007) Aquatic organisms as amber inclusions and examples from a modern swamp forest Proceedings of the National Academy of Sciences of the United States of America 104: 16581–16585. https://doi.org/10.1073/pnas.0707949104

Schmidt AR, Grabow D, Beimforde C, Perrichot V, Rikkinen J, Saint Martin S, Thiel V, Seyfullah LJ (2018) Marine microorganisms as amber inclusions: insights from coastal forests of New Caledonia. Fossil Record 21: 213–221. https://doi.org/10.5194/fr-21-213-2018

Schreiber E (1922) Beiträge zur Kenntnis der Morphologie, Entwicklung und Lebensweise der Süßwasser-Ostracoden. Zoologische Jahrbücher, Abteilung fur Anatomie und Ontogenie der Tiere 43: 485–539.

Shi G, Grimaldi DA, Harlow GE,Wang J, Wang J,Wang M, Lei W, Li Q, Li X (2012) Age constraint on Burmese amber based on U-Pb dating of zircons. Cretaceous Research 37: 155–163. https://doi.org/10.1016/j.cretres.2012.03.014

Siveter DJ, Briggs DE, Siveter DJ, Sutton MD, Joomun SC (2013) A Silurian myodocope with preserved soft-parts: cautioning the interpretation of the shell-based ostracod record. Proceedings of the Royal Society B: Biological Sciences 280(1752): e20122664. https://doi.org/10.1098/rspb.2012.2664

Smith AJ, Horne DJ, Martens K, Schön I (2015) Class Ostracoda. In: Rogers DC, Damborenea C, Thorp J (Eds) Ecology and General Biology, Thorp and Covich's Freshwater Invertebrates, 4th edn., Vol. 5. Academic Press, London, New York, 757–780. https://doi.org/10.1016/B978-0-12-385026-3.00030-9

Szwedo J, Wang B, Soszyńska-Maj A, Azar D, Ross A (2020) International Palaeoentomological Society Statement. Palaeoentomology 003: 221–222. https://doi.org/10.11646/palaeoentomology.3.3.1

Tanaka G (2006) *Sanyuania cuneata* Zhao and Whatley, 1992 (Ostracoda, Cytheroidea, Cytherideidae) from Japan: morphology, distribution and environmental significance. Journal of Micropalaeontology 25: 187–188. https://doi.org/10.1144/jm.25.2.187

Victor R, Fernando CH (1981) A new freshwater ostracod (Crustacea, Ostracoda) from Batu Caves, West Malaysia, with the description of Batucyprettinae new subfamily. Canadian Journal of Zoology 59(3): 405–414. https://doi.org/10.1139/z81-059

Wang H, Schädel M, Sames B, Horne DJ (2020a) New record of podocopid ostracods from Burmese Cretaceous amber. PeerJ 8: e10134. https://doi.org/10.7717/peerj.10134

Wang H, Matzke-Karasz R, Horne DJ, Zhao XD, Cao MZ, Zhang HC, Wang B (2020b) Exceptional preservation of reproductive organs and giant sperm in Cretaceous ostracods. Proceedings of the Royal Society B 287: e20201661. https://doi.org/10.1098/rspb.2020.1661

Wouters K (1984) The Renaudcypridinae (Crustacea: Ostracoda) from Bogia area (Papua New Guinea). Indo-Malayan Zoology 2: 163–175.

Wouters K (1986) A new *Renaudcypris* (Crustacea: Ostracoda) from Lake Taal (Philippine Islands). Bulletin de l'Institut royal des Sciences naturelles de Belgique, Biologie 56: 125–129.

Wouters K (2001) On the genera *Dolerocypria* and *Hansacypris* (Crustacea, Ostracoda), with the description of three new species from Papua New Guinea. Bulletin de l'Institut royal des Sciences naturelles de Belgique, Biologie 71: 101–112.

Xing LD, Sames B, McKellar RC, Xi DP, Bai M, Wan XQ (2018) A gigantic marine ostracod (Crustacea: Myodocopa) trapped in mid-Cretaceous Burmese amber. Scientific Reports 8: e1365. https://doi.org/10.1038/s41598-018-19877-y

Yu TT, Kelly R, Mu L, Ross A, Kennedy J, Brolly P, Xia FY, Zhang HC, Wang B, Dicher, D (2019) An ammonite trapped in Burmese amber. Proceedings of the National Academy of Sciences of the United States of America 116: 11345–11350. https://doi.org/10.1073/pnas.1821292116

Zhao G, Han D (1980) Late Quaternary brackish-water ostracod faunas from the area to the west of Weishanhu Lake, Jiangsu and their significance. In: Wang P (Ed.) Papers on Marine Micropaleontology. Ocean Press, Beijing, 120–129.

Zhao G, Whatley R (1992) A Revision of the Genus *Sanyuania* Zhao and Han, 1980 (Ostracoda, Crustacea) with the Description of New Species from the Late Cainozoic of China. Journal of Micropalaeontology 11: 151–158. https://doi.org/10.1144/jm.11.2.151

Supplementary material 1

Figure S1

Authors: He Wang, Renate Matzke-Karasz, David J. Horne

Data type: Figure (pdf file)

Explanation note: Light-microscopical images of the Kachin amber piece with 39 embedded ostracods mapped with their collection numbers. Revised from Wang et al. (2020b).

Copyright notice: This dataset is made available under the Open Database License (http://opendatacommons.org/licenses/odbl/1.0). The Open Database License (ODbL) is a license agreement intended to allow users to freely share, modify, and use this Dataset while maintaining this same freedom for others, provided that the original source and author(s) are credited.

Link: https://doi.org/10.3897/fr.25.84604.suppl1

Supplementary material 2

Figure S2

Authors: He Wang, Renate Matzke-Karasz, David J. Horne

Data type: Figure (pdf file)

Explanation note: View inside the anterior part of the carapace of the adult male *Myanmarcypris hui* specimen (BA19005-1). Data visualization by volume rendering in Drishti in red-cyan. In this mode the investigation of appendages and chaetotaxy were carried out by using tools such as rotate, zoom, clip, and carve, and by modifying the two-dimensional transfer functions.

Copyright notice: This dataset is made available under the Open Database License (http://opendatacommons.org/licenses/odbl/1.0). The Open Database License (ODbL) is a license agreement intended to allow users to freely share, modify, and use this Dataset while maintaining this same freedom for others, provided that the original source and author(s) are credited.

Link: https://doi.org/10.3897/fr.25.84604.suppl2

Supplementary material 3

Movie S1

Authors: He Wang, Renate Matzke-Karasz, David J. Horne

Data type: Movie (mp4. file)

Explanation note: Movie S1. Micro-tomographic reconstruction of *Myanmarcypris hui* juvenile (A-2), BA19005-3. Color code: A1: orange; A2: yellow; Md: light green; Mxl: light blue; L5: blue; L6: purple; L7: red; UR: olive.

Copyright notice: This dataset is made available under the Open Database License (http://opendatacommons.org/licenses/odbl/1.0). The Open Database License (ODbL) is a license agreement intended to allow users to freely share, modify, and use this Dataset while maintaining this same freedom for others, provided that the original source and author(s) are credited.

Link: https://doi.org/10.3897/fr.25.84604.suppl3

Supplementary material 4

Movie S2

Authors: He Wang, Renate Matzke-Karasz, David J. Horne

Data type: Movie (mp4. file)

Explanation note: Movie S2. Micro-tomographic reconstruction of *Myanmarcypris hui* juvenile (A-3), BA19005-4. Color code: A1: orange; A2: yellow; Md: light green; Mxl: light blue; L6: purple; UR: olive.

Copyright notice: This dataset is made available under the Open Database License (http://opendatacommons.org/licenses/odbl/1.0). The Open Database License (ODbL) is a license agreement intended to allow users to freely share, modify, and use this Dataset while maintaining this same freedom for others, provided that the original source and author(s) are credited.

Link: https://doi.org/10.3897/fr.25.84604.suppl4

Supplementary material 5

Movie S3

Authors: He Wang, Renate Matzke-Karasz, David J. Horne

Data type: Movie (mp4. file)

Explanation note: Movie S3. Micro-tomographic reconstruction of *Myanmarcypris hui* juvenile (A-4), BA19005-5. Color code: A1: orange; A2: yellow; Md: light green; L5: blue; L6: purple.

Link: https://doi.org/10.3897/fr.25.84604.suppl5

Supplementary material 6

Movie S4

Authors: He Wang, Renate Matzke-Karasz, David J. Horne

Data type: Movie (mp4. file)

Explanation note: Movie S4. Micro-tomographic reconstruction of *Electrocypria burmitei* gen. et sp. nov., BA19005-6, male. Color code: A1: orange; A2: yellow; Md: light green; L5: blue; L6: purple; L7: red; UR: olive.

Link: https://doi.org/10.3897/fr.25.84604.suppl6

Supplementary material 7

Movie S5

Authors: He Wang, Renate Matzke-Karasz, David J. Horne

Data type: Movie (mp4. file)

Explanation note: Movie S5. Micro-tomographic reconstruction of *Electrocypria burmitei* gen. et sp. nov., BA19005-7, female. Color code: A1: orange; A2: yellow; Md: light green; Mxl: light blue; L5: blue; L6: purple; L7: red; UR: olive; female genital lobe: blue-green.

Link: https://doi.org/10.3897/fr.25.84604.suppl7

Supplementary material 8

Movie S6

Authors: He Wang, Renate Matzke-Karasz, David J. Horne

Data type: Movie (mp4. file)

Explanation note: Movie S6. Micro-tomographic reconstruction of *Sanyuania* sp., BA19005-8. Color code: A1: orange; A2: yellow; Md: light green; Mxl: light blue; L5: blue; L6: purple; L7: red; HP: pink; presumed part of spinneret gland: pistachio; mouth: gray-green.

Link: https://doi.org/10.3897/fr.25.84604.suppl8

Fossil Record 25 (1) 2022, 173–186 | DOI 10.3897/fr.25.80706

The last African metatherian

Vicente D. Crespo[1,2,3,4], Francisco J. Goin[1,2], Martin Pickford[5]

1 *CONICET (Consejo Nacional de Investigaciones Científicas y Técnicas), La Plata, Argentina*
2 *División Paleontología Vertebrados, Facultad de Ciencias Naturales y Museo, Universidad Nacional de La Plata, Paseo del Bosque s/n, B1900FWA, La Plata, Argentina*
3 *GIUV2016-303 Grup d'Investigació en Paleontologia de Vertebrats del Cenozoic (PVC-GIUV), Àrea de Paleontologia, Departament de Botànica i Geologia, Universitat de València, Dr. Moliner 50, 46100, Burjassot, Valencia, Spain*
4 *Departamento de Ciências da Terra, FCT-UNL Faculdade de Ciências E Tecnologia, GeoBioTec, Universidade Nova de Lisboa, 2829-516 Caparica, Portugal*
5 *Sorbonne Universites, CR2P, UMR 7207 du CNRS, Departement Histoire de la Terre, Museum National d'Histoire Naturelle et Universite Pierre et Marie Curie, Paris, France*

http://zoobank.org/F14B83B4-7D67-4C01-96B3-DA98C72261D4

Corresponding author: Vicente D. Crespo (vidacres@gmail.com)

Academic editor: Torsten Scheyer ♦ **Received** 17 January 2022 ♦ **Accepted** 11 May 2022 ♦ **Published** 3 June 2022

Abstract

Morotodon aenigmaticus **gen. et sp. nov.** (Mammalia, Metatheria, ?Herpetotheriidae) from the early or early-middle Miocene of equatorial Africa (Moroto II locality, Moroto District, northeastern Uganda) is characterized by a short anterior cingulum, a buccal shelf, a well-developed hypoconulid in a central position, and a trigonid and talonid with similar mesio-distal lengths. Its small size and morphology suggest mostly insectivorous-faunivorous feeding habits. The faunal association of Moroto II, as well as previous palaeoenvironmental analyses, suggest that *Morotodon* lived in open woodland and bushland areas surrounded by grasses. *Morotodon aenigmaticus* shows several features reminiscent of early herpetotheriids, such as *Golerdelphys stocki* (late Paleocene of North America), and *Amphiperatherium ambiguum* (Eocene of Europe); this suggests an origin for its lineage previous to the Oligocene. In summary, its affinities lie with Northern Hemisphere herpetotheriids, and, most probably, with European ones.

Key Words

Africa, Herpetotheriidae, Metatheria, Miocene, Moroto II, Uganda

Introduction

The record of extinct African metatherians is scarce and, up to now, restricted to the Paleogene of its northernmost portion (Fig. 1; Table 1); in addition, the identity nature of several putative African metatherians has been contested (Gheerbrant 1995; Gunnell 2010; see a review in Crespo and Goin 2021). Unambiguous metatherians include *Peratherium africanum* Simons & Bown, 1984, from the Early Oligocene (Rupelian) of Egypt, and *Kasserinotherium tunisiense* Crochet, 1986 from the early Eocene of Chambi, Tunisia. *P. africanum* was originally described from remains found at Fayum Quarry M in northern Egypt; subsequently, it was also recognized at similarly aged sediments at Taqah, Oman (Simons and Bown 1984; Crochet et al. 1992). Originally assigned to *Peratherium* (Herpetotheriidae), it was later referred to a new genus, *Qatranitherium* (Peradectidae; Crochet et al. 1992). More recently Hooker et al. (2008), while describing new material from Quarry M, argued in favour of the close affinity of this taxon with the European species *Peratherium lavergnense* Crochet, 1979; thus, the generic name *Peratherium* was retained.

The other undisputed African metatherian, *K. tunisiense*, is solely known from two upper molars, and was included by Crochet (1986) within the Peradectidae.

McKenna and Bell (1997) placed this genus as an enigmatic taxon in the Supercohort Theria, without arguing on their taxonomic decision. Gunnell (2010) stated that there is no compelling reason to believe it represents a marsupial. To us, there is no compelling reason to believe it is not a metatherian (see also Hooker et al. 2008; Crespo and Goin 2021). Several authors have previously noted similarities between *Kasserinotherium* and other Southern Hemisphere metatherians: Goin and Candela (2004) suggested affinities between *Kasserinotherium* and *Wirunodon chanku*, from the late Eocene Santa Rosa local fauna in Peru, while Beck (2013) noted similar dental features among *Kasserinotherium*, *Wirunodon*, and *Archaeonothos henkgodhelpi*, from the early Eocene Tingamarra fauna of Northern Queensland, Australia.

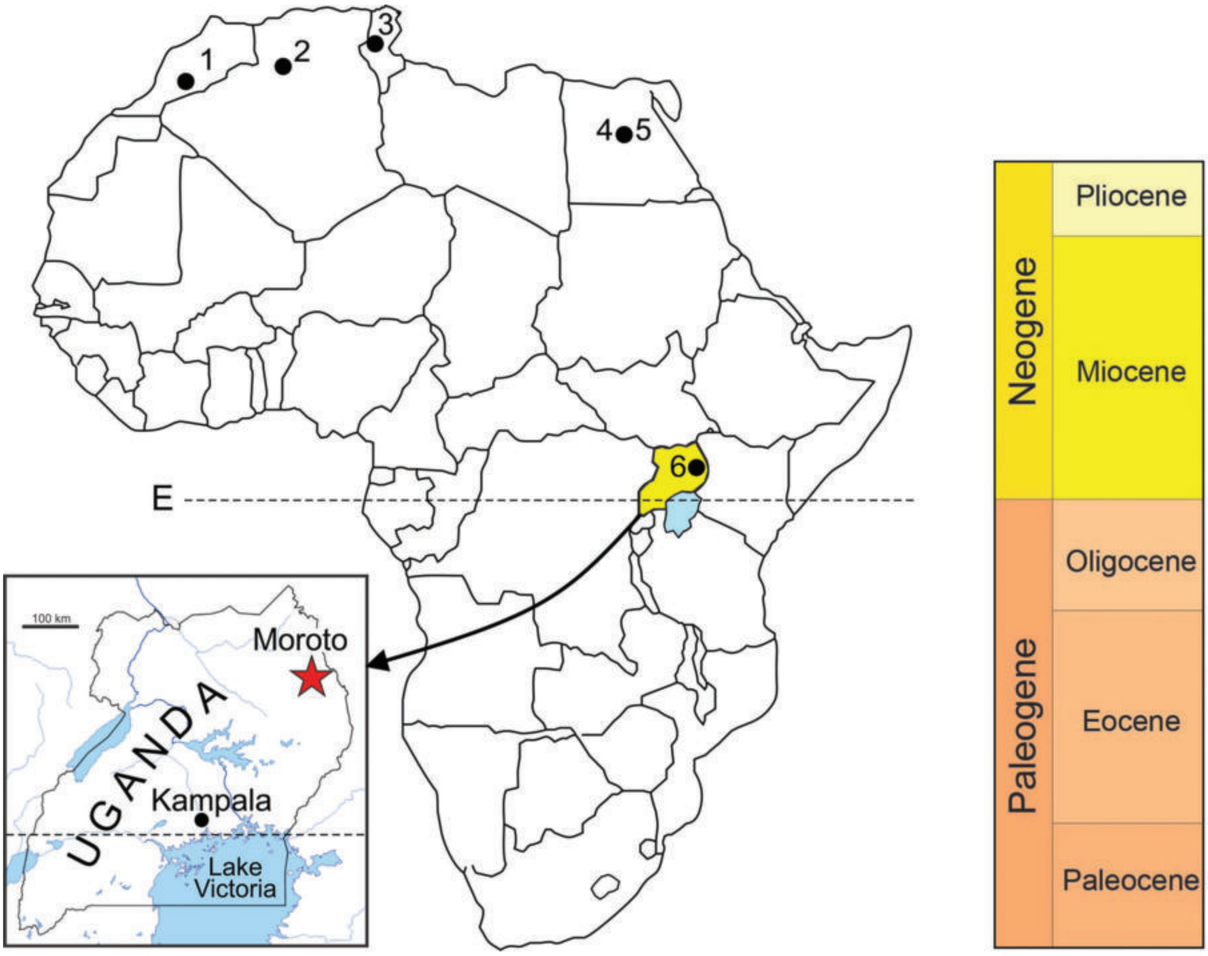

Figure 1. Map of Africa indicating the occurrences of extinct metatherians, or taxa previously regarded as Metatheria. Bottom left, map of Uganda indicating the Moroto II locality. Right, geologic time column indicating the age of each taxon. References: E, Equator; 1,?*Garatherium todrae*; 2, *Garatherium mahboubii*; 3, *Kasserinotherium tunisiense*; 4, *Ghamidtherium dimaiensis*; 5, *Peratherium africanum*; 6, *Morotodon aenigmaticus* gen. et sp. nov. See the text and Table 1 for more information on these taxa.

Other extinct African taxa referred to the Metatheria are more probably eutherians (see Table 1). *Garatherium mahboubii* Crochet, 1984 from the Early Eocene of El Kohol (Algeria) was described as a peradectid by Mahboubi et al. (1983) and Crochet (1984). Later, Gheerbrant (1995), describing a new species from the Paleocene of Morocco (?*Garatherium todrae* Gheerbrant, 1995), tentatively referred it to *Garatherium* and argued that both species actually represent adapisoriculid eutherians. Its referral to the Adapisoriculidae is currently maintained (De Bast et al. 2012; Crespo and Goin 2021).

Ghamidtherium dimaiensis Sánchez-Villagra, Seiffert, Martin, Simons, Gunnell, & Attia, 2007 was recovered from the Late Eocene of the Fayum Depression (Quarry L-41; Egypt). Sánchez-Villagra et al. (2007) described *Ghamidtherium* from a partial jaw with m2-3, and referred to this species as an isolated molar, probably an m1. They regarded it as a possible marsupial, noting the difficulty in distinguishing these materials from those of various chiropteran groups. Additional material (two upper molars) was also described as belonging to enigmatic mammals of uncertain affinities. To the authors (Sánchez-Villagra et al. 2007: 413), the upper molars could be "... either a marsupial with some bat-like dental features, or a bat with marsupial-like dental features". Later, other authors such as Gunnell (2010) and Simmons et al. (2016) argued that both *Ghamidtherium* as well as the still unnamed upper molars are more probably referrable to the Chiroptera (see also Crespo and Goin 2021).

Table 1. Cenozoic African metatherians (or putative metatherians) described up to now. The type localities of all these taxa are shown in the map of Fig. 1.

	Species	Family	Age and locality	Author	Observations
1	*?Garatherium todrae*	Adapisoriculidae (Eutheria)	Late Paleocene, Morocco	Gheerbrant et al. (1998)	See Seifert (2010), De Bast et al. (2012)
2	*Garatherium mahboubii*	Adapisoriculidae (Eutheria)	Early Eocene, Algeria	Mahboubi et al. (1983); Crochet (1984).	See Gheerbrant (1995); De Bast et al. (2012)
3	*Kasserinotherium tunisiense*	?Peradectidae (Metatheria)	Early Eocene, Tunisia	Crochet (1986)	See Goin and Candela (2004); Beck (2013)
4	*Ghamidtherium dimaiensis*	?Chiroptera, fam. indet. (Eutheria)	Late Eocene, Egypt	Sánchez-Villagra et al. (2007)	See Gunnell (2010); Simmons et al. (2016)
5	*Peratherium africanum*	Herpetotheriidae (Metatheria)	Early Oligocene, Egypt and Oman	Simons & Bown (1984)	See Hooker et al. (2008)
6	*Morotodon aenigmaticus* gen. et sp. nov.	Herpetotheriidae (Metatheria)	Early-middle Miocene, Uganda	This work	See Pickford and Mein (2006)

Here we describe a third taxon unambiguously referrable to the Metatheria, on the basis of a single, isolated lower molar. It has two unusual features: it comes from equatorial Africa (Uganda), and represents the youngest African metatherian so far known (early Neogene). The specimen was previously studied by Pickford and Mein (2006), together with all other small mammals from the type locality. These authors argued that the specimen belongs to a possible marsupial (Metatheria), discarding it as referrable to the Tenrecidae or Chrysochloridae (Eutheria) on the basis of the number of the cuspids in the talonid. They also noted (Pickford and Mein 2006: 364) that the specimen "...belongs to a hitherto undescribed insect-eating mammal but the material is too restricted for us to be able to determine its precise affinities." Later, Crespo and Goin (2021) mentioned the specimen and commented briefly on its metatherian nature and its possible herpetotheriid affinities. Here we provide a description of the new taxon, together with comparisons with both eutherian and metatherian lineages, and a discussion of its possible affinities, origins and biogeographical significance.

Institutional abbreviation

UM MOR II	Uganda Museum, Kampala, Moroto II locality.

Methods

The type specimen was obtained while screen-washing sediments at the Moroto II locality. Comparisons were made with original specimens, casts, photographic stereopairs, drawings, photographs, and SEM micrographs provided in the literature. Measurements were done with a microscope with measuring table to 0.01 mm resolution. Dental terminology is provided in Fig. 4. For some species, their respective m4 have not been found for the purpose of a correct comparison with the holotype of *Morotodon*: *Peradectes chesteri*, *P. californicus*, *Asiadidelphis* (= *Indodelphis*) *luoi*, *Thylacodon montanensis*, *Herpetotherium merriami*, *H. tabrumi*, *H. valens*, and *Peratherium cuvieri*.

Locality, geology and age

The series of fossil localities of Moroto II are located near Kogole Hill, north of Nakiloro Village, in Moroto District, northeastern Uganda (Fig. 1). These sites have been well known since the 1960s, and contain an abundant and diverse mammal assemblage. The first field trip to these sites was carried out by a team led by William (Bill) Bishop; later in the 1980s, and until nowadays, field trips (as the Uganda Palaeontology Expedition of 1985) have been carried out by a team led by one of us (M.P.). The fauna of Moroto II has been intensively studied, especially the hominoids, as well as many other mammalian groups (e.g., eulipotyphlans, bats, anthracotheriids and the metatherian here described; see Pickford et al. 2017; Pickford 2020 and references therein).

The area of the geological succession is in the vicinity of Kogole; it is underlain by basement complex gneisses (Mozambique Belt; Fleuty 1968) and has small outcrops of Neogene deposits comprising Miocene sediments infilling valleys cut into the Precambrian gneisses and schists (Bishop 1958, 1964; Bishop et al. 1969; Pickford and Tassy 1980; Musalizi et al. 2009). They are capped by basalt lava presumably from the Mount Moroto volcano (Horne 1953; Varne 1966, 1967; Fleuty 1968). The fluvial deposits that comprise the mammal-bearing levels are dominated by clays and silts, with less frequent grits and conglomerates (Pickford et al. 2017).

The age of Moroto II is controversial, with two different opinions in the literature: one, based on the geology, dates the locality as 21–20 Ma (early Miocene), around the transition between the Aquitanian and the Burdigalian; it is regarded as older than Napak (Uganda, Faunal Set I, ca 20.5–19.5 Ma; Gebo et al. 1997; Werdelin 2010) (or 19.2 after Van Couvering and Delson 2021). A second view is based on the chronological significance of the faunal assemblage, which suggests an early-middle Miocene age (16.5–15.5 Ma, or late Burdigalian; Ogg et al. 2016); the latter is regarded by us as the most likely age for the mammal-bearing levels of Moroto II.

Systematic palaeontology

Mammalia Linnaeus, 1758
Metatheria Huxley, 1880
?Herpetotheriidae Trouessart, 1879

***Morotodon* gen. nov.**

http://zoobank.org/68CAD3FD-63A1-411F-8F4F-8287DAEA716E

Type species. *Morotodon aenigmaticus* gen. et sp. nov.

***Morotodon aenigmaticus* gen. et sp. nov.**

http://zoobank.org/916A2124-80EE-4B16-A2FF-D7E4A48C529A

Etymology. "The mysterious tooth from Moroto". Moroto II is the fossil locality where this taxon was found; "-odon", from *odontos*, genitive of *odous*, ancient Greek for tooth; gender is masculine; *aenigmaticus*, from the Latin *aenigma* (mystery), refers to the unexpected finding of a metatherian near the Equator in the Neogene of Africa.

Holotype. UM MOR II, 48'04, a last lower left molar (m4; Figs 2, 3; Suppl. material 1 and Suppl. material 2).

Measurements. Total length, 1.63 mm (1 mm trigonid length, 0.63 talonid length); trigonid width, 0.93 mm; talonid width, 0.94 mm (from Pickford and Mein 2006).

Locality and age. Moroto II, north of Nakiloro Village, Moroto District, northeastern Uganda (Fig. 1). Late early Miocene, upper Burdigalian (16.5–15.5 Ma).

Diagnosis. ?Herpetotherid metatherian with lower molars having a short anterior cingulid, a buccal shelf, and a trigonid and talonid with subequal length and width; the m4 has a vertical, well-developed hypoconulid in a central position. The specific diagnosis extends to the genus by monotypy.

Description. Specimen UM MOR II, 48'04 is bi-rooted, both roots being subcircular in section; the anterior root is smaller than the posterior one. The anterior cingulid is short and relatively wide at its central portion. The trigonid is open. The main cusps of the trigonid are well-developed. The paraconid is mesio-lingually positioned. The protoconid is the largest cusp of the tooth, and is slightly anteriorly placed with respect to the metaconid. The paracristid and metacristid are notched. The talonid is bucco-lingually compressed in its anterior half; at its posterior face its width is almost the same as that of the trigonid. The entoconid is broken; apparently, it was bucco-lingually compressed; the pre-entocristid is straight and ends in at posterolingual edge of the metaconid. The hypoconulid is separated from the entoconid; it is well-developed and is centrally placed on the posterior edge of the tooth; it is a vertical cusp (i.e., it is not posteriorly oriented or dorso-ventrally compressed). The hypoconid is only moderately developed; it is also buccally salient, but does not exceed buccally the level of the protoconid. The oblique cristid joins the posterior wall of the trigonid at the labiolingual midpoint of the tooth, below the metacristid notch. There is a well-developed buccal

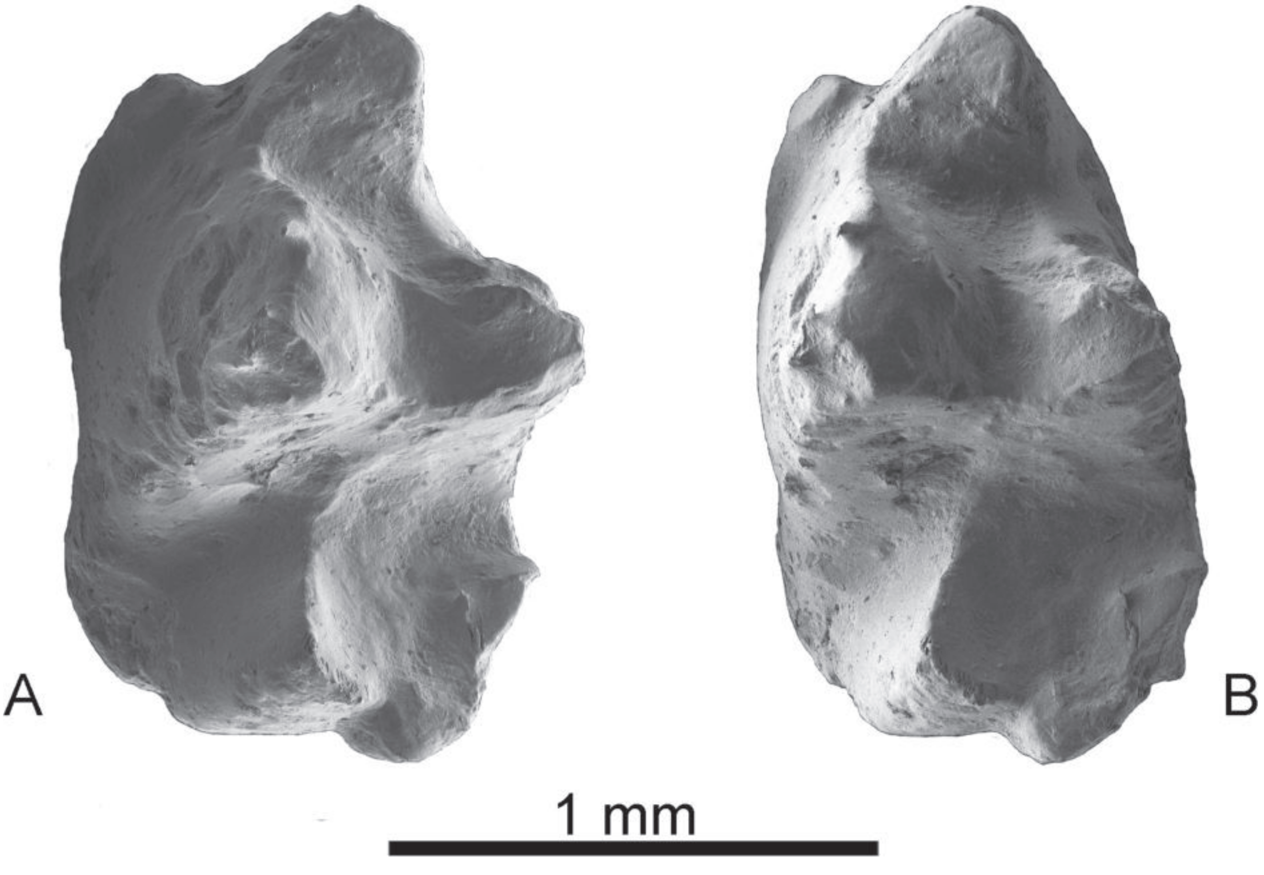

Figure 2. *Morotodon aenigmaticus* gen. et sp. nov. SEM images of specimen UM MOR II, 48'04 (an isolated left m4) in occluso-labial (**A**) and occlusal (**B**) views. Scale bar: 1 mm.

shelf, or cingulid, at the base of the crown, running from the base of the hypoconid to the posterobuccal edge of the protoconid. The tooth shows soil corrosion.

Comments. The specimen was originally described as a m1 or m2 (Pickford and Mein 2006). The reduced (laterally compressed) talonid at its anterior half, only moderately developed hypoconid, relatively central position of the hypoconulid, as well as the quite oblique orientation of the oblique cristid, allow us to reassign the specimen to an m4. This kind of reduction in the m4's talonid appears in several metatherians (e.g., *Peradectes russelli* Crochet, 1979 or *Amphiperatherium giselense* (Heller, 1936)).

Comparisons. Specimen UM MOR II, 48'04 is clearly not a deciduous tooth, due to the size and shape of its roots and the angle at which they would be inserted into the mandible. Several eutherian lineages have molar morphologies that are superficially similar to that of *Morotodon aenigmaticus*: afrosoricid "insectivores" (Afrotheria), bats (Chiroptera), some eulipothyplans (Laurasiatheria, Eulipotyphla), and adapisoriculids (Euarchonta). Early afrotherians include *Ocepeia*, from the late Paleocene of Morocco, which is strikingly different from *Morotodon*. *Ocepeia* has bunoid, almost inflated lower molars with low protoconid, paraconid close to the metaconid; enclosed, deep trigonid basin; the metacristid is not vertical but gently sloping; talonids are multicuspid (up to five cusps), with a reduced hypoconulid. Among the Afroinsectiphilia, macroscelidians can also be discarded: for instance, the middle-late Eocene *Nementchatherium* has very low cusps, the paraconid is close to the protoconid and the hypoconulid, if present, is almost indistinguishable. *Chambius*, from the early or early middle Eocene of Tunisia, has its lower molars rounded in profile, with an indistinguishable hypoconulid, indistinct paraconid, and the talonid narrower than the trigonid.

Afrosoricids such as tenrecs and golden moles (of which at least members of the former were contemporaneous with *Morotodon*), were already discarded on the basis of the number of talonid cusps, three in metatherians and a single, elongated one in tenrecs (Pickford and Mein 2006). Effectively, tenrecids such as *Promicrogale*, from the Miocene of Namibia (Pickford 2018) or *Nanogale* from the Eocene of Namibia (Pickford 2019), have quite different lower molars in which the talonid is much smaller than the trigonid and lacks a hypoconulid, the paraconid in m2-3 is low and close to the metaconid, and the protoconid is proportionally very large; the talonid basin is much lower than that of the trigonid. Chrysochlorids have highly derived molars, of which the lower ones lack the talonid, while the paraconid and metaconid are reduced and twinned.

Chiropterans can also be ruled out because of the morphology and position of the hypoconulid, which in *Morotodon* is more developed and more centrally placed at the distal edge of the tooth; additionally, chiropterans have a buccal shelf or cingulid which is mesiodistally complete, linking the anterior and posterior cingulids. *Morotodon* differs from the probable chiropteran *Ghamidtherium dimaiensis* Sánchez-Villagra, Seiffert, Martin, Simons, Gunnell, & Attia, 2007 in that the anterior cingulid is shorter and does not extend distally at the crown base; the metaconid is anteriorly positioned with respect of the protoconid; the entoconid is less developed; it lacks a posterior cingulid; the hypoconulid is larger, higher and less dorso-ventrally compressed, and it is not placed immediately distal to the entoconid but instead buccal to it; finally, the oblique cristid in *Morotodon* is less parallel to the dental axis.

Morotodon differs from the Eulipotyphla in the presence and morphology of the hypoconulid. In their lower molar morphology representatives of the Soricidae and Talpidae have some similarities with *Morotodon*. However, the anterior cingulid in soricids is better developed and may continue posteriorly towards the buccal surface of the crown, and in the talonids the hypoconulid is reduced (or, if not reduced, is placed very low regarding the entoconid) and located immediately posterior to the entoconid. Generalized erinaceids such as *Galerix* lack a hypoconulid, and, in the last molar, the paraconid is crest-like, and the oblique cristid is parallel to the dental axis. Among other more derived soricomorphs, the living *Solenodon*, for instance, has extremely reduced talonids and mesio-distally compressed trigonids.

Being more similar in overall morphology (but see below), a more detailed comparison of *Morotodon* with individual adapisoriculid taxa is worthwhile. *Morotodon* differs from *Afrodon gheerbranti* De Bast & Smith, 2017 in having a more lingual paraconid, more developed protoconid, presence of a buccal shelf (or cingulid), better developed hypoconid and entoconid, and a more centrally placed hypoconulid. It differs from *Afrodon chleuhi* Gheerbrant, 1988 in having a longer trigonid, a better developed protoconid, trigonid and talonid of similar width, and a less developed, more anteriorly placed hypoconulid. It differs from *Bustylus marandati* (Crochet and Sigé 1983) in having a narrower anterior cingulum, longer trigonid, more centrally placed metaconid, a developed buccal shelf, a larger entoconid, and an independent hypoconulid. It differs from the todralestid *Todralestes variabilis* Gheerbrant, 1991 in having a less reduced talonid, the presence of a buccal shelf, and a larger hypoconulid.

Comparisons with early Marsupialiformes. *Morotodon aenigmaticus* compares best with metatherian mammals, especially with Marsupialiformes (most metatherians except the early clade Deltatheridia). The best known early marsupialiform (i.e., non deltatheroid) metatherian is *Kokopellia juddi* Cifelli, 1993, from the medial Cretaceous of Utah in North America (see Cifelli and Muizon 1997 for a detailed description of the dentition of *Kokopellia*). Molars of *Kokopellia* represent the generalized condition for almost all Cenozoic metatherians. *Morotodon aenigmaticus* differs from *Kokopellia juddi* in that its m4 lacks a posterior cingulid, and a shorter talonid (clearly longer in *Kokopellia* in all lower molars), a less posteriorly placed metaconid, a smaller hypoconulid (in *Kokopellia* it is larger and closer to the entoconid), and a smaller and less anteriorly placed hypoconid. Both *Morotodon* and *Kokopellia* share a well-developed buccal shelf (or cingulid), and a similarly oriented oblique cristid, which ends anteriorly at a point below the metacristid notch.

Comparisons with Peradectidae. Most Cenozoic Holarctic metatherians belong either to the Peradectidae or to the Herpetotheriidae, so a detailed comparison with species of these two groups is needed in order to clarify the affinities of *Morotodon aenigmaticus*. Most representatives of both families are known from the Northern Hemisphere. In North America, peradectids and herpetotheriids are known from the Late Cretaceous to the Miocene, while in Eurasia they span the early Eocene to the Miocene (in Europe, peradectids are restricted to the Eocene). In Africa, peradectids had been known only for the early Eocene (*Kasserinotherium*), .while herpetotheriids are known for the early Oligocene (*Peratherium*). Our allocation of *Morotodon* to herpetotheriids expands the group to the Miocene.

Peradectes. *Morotodon aenigmaticus* differs from *Peradectes louisi* Crochet, 1979 in having a proportionally longer talonid, less difference in height between the trigonid and the talonid, and in that the hypoconid is more salient. Differs from *Peradectes californicus* (Stock, 1936) (m4 of this species is unknown) in that the metaconid is more anteriorly placed than the protoconid, and the talonid is proportionally narrower. Differs from *Peradectes chesteri* Gazin, 1952 (although the m4 of this species is unknown) in having a larger paraconid which is not as close to the metaconid, and a proportionally larger hypoconulid. Differs from *Peradectes coprexeches* Williamson & Taylor, 2011 in having a narrower trigonid, the oblique cristid is not subparallel to the preentocristid (in such a way that the talonid is anteriorly narrower), the hypoconulid is more developed and less paired to the entoconid; finally, a buccal cingulid is present. Differs from *Peradectes minor* Clemens, 2006 and *Peradectes mutigniensis* Crochet, 1979 in having a paracristid which is less transverse to the dental axis, the hypoconulid is farther from the entoconid, it lacks a posterior cingulid and has a buccal shelf or cingulid. Differs from *Peradectes pauli* (Gazin, 1956) in having a more salient hypoconid, while the oblique cristid is less parallel to the dental axis. Differs from *Peradectes protinnominatus* McKenna, 1960 in having a longer talonid, a larger hypoconulid which is farther from the entoconid, and in that the oblique cristid is less parallel to the dental axis. Differs from *Peradectes russelli* Crochet, 1979 in that the paraconid and metaconid are less close to each other, the entoconid is smaller, the hypoconulid is farther from the entoconid, and the oblique cristid is less parallel to the dental axis.

Mimoperadectes. Differs from *Mimoperadectes labrus* Bown & Rose, 1979 in having a less developed anterior cingulid, a shorter trigonid, a paraconid that is farther from the metaconid and the hypoconulid and the entoconid are more detached (for this reason, the talonid is wider posteriorly).

Nanodelphys. Differs from *Nanodelphys hunti* (Cope, 1873) in having a narrower trigonid and shorter talonid, a hypoconulid that is set farther from the entoconid, and the oblique cristid not being subparallel to the preentocristid.

Armintodelphys. Differs from *Armintodelphys dufraigni* Smith & Smith, 2013 in having a wider anterior cingulid, a less reduced paraconid, a slightly posteriorly placed paraconid (relative to the protoconid), a less straight oblique cristid, a hypoconulid that is farther from the entoconid, and in the presence of a buccal shelf. Differs from *Armintodelphys dawsoni* Krishtalka & Stucky, 1983 in having a more developed paraconid which is less mesio-distally compressed, and a narrower talonid. Differs from *Armintodelphys blacki* Krishtalka & Stucky, 1983 in having an anteriorly placed metaconid with respect to the protoconid, the anterior half of the oblique cristid not being parallel to the dental axis, a smaller hypoconulid that is farther from the entoconid, and a narrower talonid basin.

Comparisons with Herpetotheriidae. *Asiadidelphis.* *Morotodon aenigmaticus* differs from *Asiadidelphis zaissanense* Gabunia, Shevyreva, & Gabunia, 1990 (described in Ziegler et al. 2007; fig. 3.3) in having a wider anterior cingulid, oblique cristid less parallel to the dental axis, and a more buccally placed hypoconulid. Differs from *Asiadidelphis tjutkovae* Emry, Lucas, Szalay, & Tleuberdina, 1995 in its smaller size, a more centrally positioned hypoconulid on the posterior edge of the talonid, and a larger entoconid. Differs from *Asiadidelphis* (= *Indodelphis*) *luoi* (Bajpai, Kapur, Thewissen, Tiwari, & Das, 2005) in having a more developed anterior cingulid, a proportionally higher protoconid relative to the metaconid, a mesio-distally less compressed paraconid, a narrower talonid an oblique cristid that is less parallel to the dental axis.

Swaindelphys. Differs from *Swaindelphys encinensis* Williamson & Taylor, 2011 in having a shorter anterior cingulid, narrower trigonid and talonid, a less developed, lower hypoconulid, and, in occlusal view, a straight but not curved oblique cristid. Differs from *Swaindelphys cifelli* Johanson, 1996 in having a more developed anterior cingulid, in its hypoconulid which is farther from the entoconid, a smaller hypoconulid, and a talonid that is longer relative to the trigonid.

Thylacodon. Differs from *Thylacodon montanensis* Williamson, Brusatte, Carr, Weil, & Standhardt, 2012 in having (although the m4 was not preserved in the latter) a narrower entoconid, a hypoconulid that is farther from the entoconid, and in the absence of a posterior cingulid. Differs from *Thylacodon pusillus* (Archibald, 1982) in having a better developed anterior cingulid, smaller entoconid, and a hypoconulid that is not twinned to the entoconid.

Golerdelphys. Differs from *Golerdelphys stocki* Williamson & Lofgren, 2014 in lacking a posterior cingulid and in that the entoconid is proportionally smaller.

Copedelphys. Differs from *Copedelphys titanelix* (Matthew, 1903) in having a shorter and wider anterior cingulid, a proportionally smaller trigonid, a paraconid that is not mesio-distally compressed, an oblique cristid obliqua is not straight, a buccally more salient hypoconid, and in that the hypoconulid is less posteriorly projected. Differs from *Copedelphys stevensoni* (Cope, 1873) in having a shorter and wider anterior cingulid, a less antero-posteriorly compressed paraconid, an oblique cristid obliqua that is less parallel to the preentocristid, and in the presence of a buccal shelf (or cingulid).

Herpetotherium. Differs from *Herpetotherium youngi* (McGrew, 1937) in having a shorter anterior cingulid, an oblique cristid that meets the trigonid more lingually, a more developed hypoconulid that is not twinned to the entoconid, and a more salient hypocone. Differs from *Herpetotherium fugax* Cope, 1873 in having a shorter and wider anterior cingulid, a proportionally narrower trigonid, a paracristid that is less transversal to the dental axis, an oblique cristid that is not subparallel to the preentocristid, and a hypoconulid that is farther from the entoconid. Differs from *Herpetotherium comstocki* (Cope, 1884) in having a shorter anterior cingulid, an oblique cristid that is subparallel to the dental axis, a proportionally larger hypoconulid that is farther from the entoconid; in turn, this last cusp is proportionally smaller. Differs from *Herpetotherium edwardi* (Gazin, 1952) in having larger paraconid and hypoconulid, the latter smaller and farther from the entoconid, and an oblique cristid that is less parallel to the dental axis. Differs from *Herpetotherium marsupium* Troxell, 1923 in having a smaller entoconid, more buccal hypoconulid, and a straighter oblique cristid that is less parallel to the dental axis. Differs from *Herpetotherium merriami* (Stock & Furlong, 1922) in having (although the m4 was not preserved) a larger hypoconulid which is placed farther from the entoconid. Differs from *Herpetotherium tabrumi* Korth, 2018 in having (although the m4 is not present) a larger hypoconulid which is farther from the entoconid, a shorter preentocristid, and an oblique cristid that is less parallel to the dental axis. Differs from *Herpetotherium valens* (Lambe, 1908) in having (although the m4 was not preserved) a shorter and wider anterior cingulid, relatively narrower talonid, a paracristid that is less transversal to the dental axis, paraconid and metaconid clearly set apart from each other, a smaller entoconid and a proportionally larger hypoconulid that is farther from the entoconid.

***Peratherium* (Fig. 3).** Differs from *Peratherium africanum* in having a shorter and wider anterior cingulid, deeper oblique cristid which is less parallel to the dental axis, a slightly sloping and not vertical posterior wall of the trigonid (the metacristid), and a more buccally placed hypoconulid. Differs from *Peratherium bretouense* Crochet, 1979 in having a shorter anterior cingulid, a less developed entoconid, a less bucco-lingually compressed hypoconulid that is placed farther from the entoconid, and lack of a posterior cingulid. Differs from *Peratherium cayluxi* Filhol, 1877 in having a shorter anterior cingulid, a more buccally salient hypoconid, and a smaller entoconid. Differs from *Peratherium constans* (Teilhard de Chardin, 1927) in having a wider and shorter anterior cingulid, a more buccally salient hypoconid, a smaller hypoconulid that is placed farther from the entoconid. Differs from *Peratherium cuvieri* (Fischer, 1829) in having (although the m4 was not preserved in the latter) a proportionally larger hypoconulid which is more buccally placed, lack of a posterior cingulid, a smaller entoconid, and a longer talonid. Differs from *Peratherium elegans* (Aymard, 1846) in having a narrower anterior cingulid, a larger hypocone which is less rounded, a larger and more buccally placed hypoconulid of which the buccal slope does not form a continuum with the posthypocristid. Differs from *Peratherium lavergnense* Crochet, 1979 in that the hypoconid is more buccally salient, the hypoconulid is larger and not placed immediately posterior to the entoconid. Differs from *Peratherium matronense* Crochet, 1979 in having a shorter anterior cingulid, a more anteriorly placed metaconid regarding the protoconid, and a hypoconulid that is not immediately distal to the entoconid. Differs from *Peratherium monspeliense* Crochet, 1979 in having a shorter anterior cingulid, and in that the oblique cristid is less parallel to the dental axis. Differs from *Peratherium perrierense* Crochet, 1979 in having a shorter anterior cingulid, an oblique cristid that is less parallel to the dental axis, and a hypoconulid that is farther from the entoconid. Differs from *Peratherium sudrei* Crochet, 1979 in that the hypoconulid is closer to the entoconid, and the entoconid and the hypoconid are at the same level (while in *P. sudrei* the entoconid is more anteriorly placed).

***Amphiperatherium* (Fig. 3).** Differs from *Amphiperatherium brabatense* Crochet, 1979 in having a wider anterior cingulid, and a proportionally larger and more buccally placed hypoconulid. Differs from *Amphiperatherium minutum* (Aymard, 1846) in having a less reduced talonid and in that the hypoconid is more buccally salient. Differs from *Amphiperatherium goethei* Crochet, 1979 in having a shorter anterior cingulid, a paraconid that is less close to the metaconid (therefore, the trigonid is less mesiodistally compressed), and an anteriorly slightly narrower talonid. Differs from *Amphiperatherium lamandini* (Filhol, 1876) in having a more salient hypoconid, larger hypoconulid which is farther from the entoconid, and in lacking a posterior cingulid. Differs from *Amphiperatherium frequens* (Meyer, 1846) in having a less reduced talonid, a shorter anterior cingulid, presence of a buccal cingulid, and the hypoconulid that is farther from the entoconid. Differs from *Amphiperatherium maximum* Crochet, 1979 in its smaller size, shorter anterior cingulid, a mesio-distally less compressed paraconid, a larger hypoconulid that is placed farther from the entoconid, and a smaller entoconid. Differs from *Amphiperatherium bastbergense* Crochet, 1979 in having a shorter anterior cingulid, a mesio-distally less compressed paraconid, a smaller entoconid, a larger hypoconulid that is farther from the entoconid, and in the absence of a posterior cingulid. Differs from *Amphiperatherium fontense* Crochet, 1979 in having a smaller anterior cingulid, an anteriorly narrower talonid, a proportionally smaller entoconid, and a hypoconulid that is larger and placed farther from the entoconid. Differs from *Amphiperatherium ambiguum* (Filhol, 1877) in having a shorter anterior cingulid and the hypoconulid being farther from the entoconid.

Differs from *Amphiperatherium exile* (Gervais, 1848–52) in having a shorter anterior cingulid, a mesio-distally less compressed paraconid and an anteriorly narrower talonid. Differs from *Amphiperatherium bourdellense* Crochet, 1979 in having a narrower talonid and a more central position of the hypoconulid, which is placed farther from the entoconid. Differs from *Amphiperatherium giselense* (Heller, 1936) in having a mesio-distally less compressed paraconid, larger hypoconulid, anteriorly narrower talonid, and lack of a posterior cingulid.

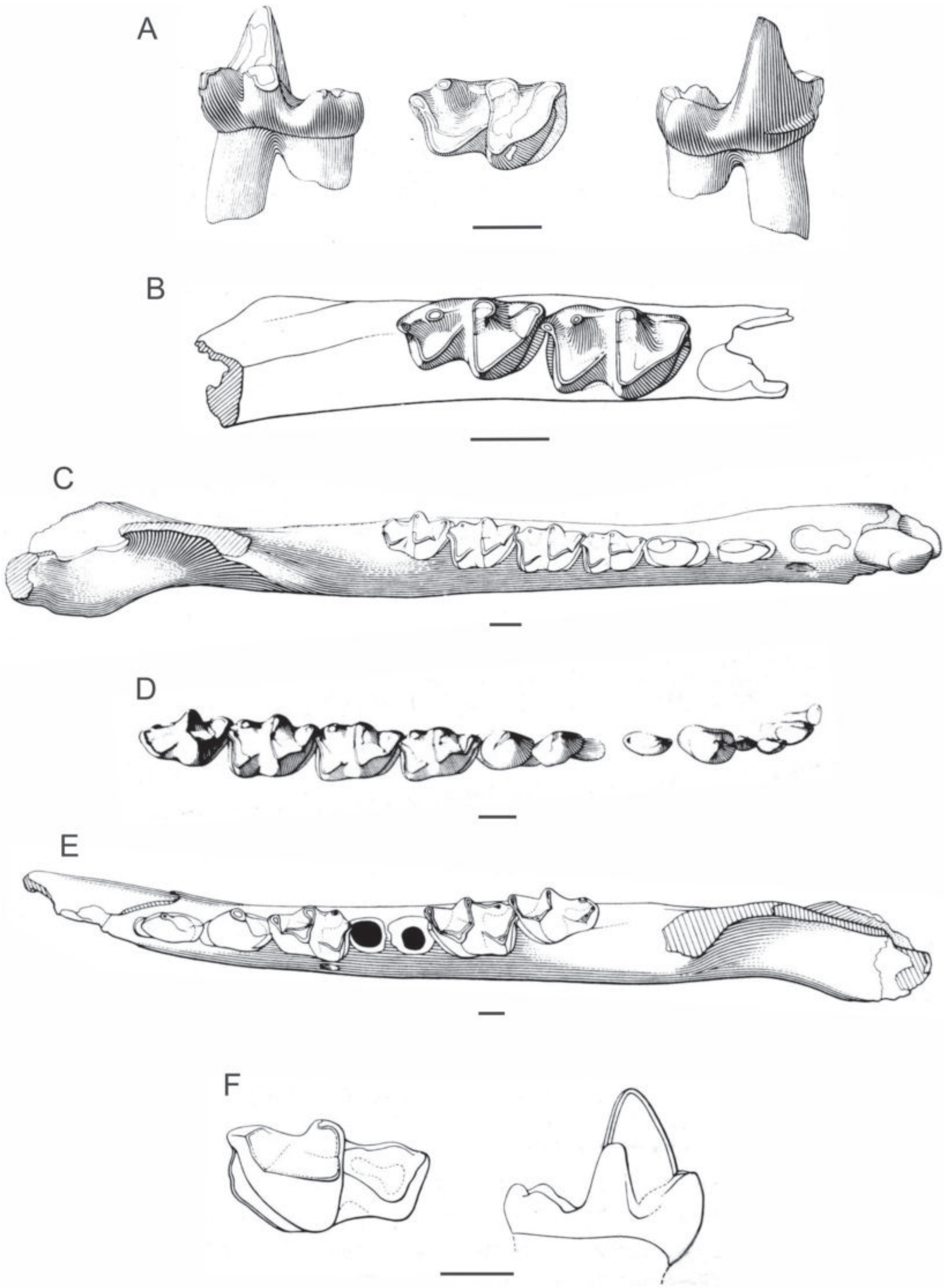

Figure 3. Lower molar series of various marsupial taxa belonging to Peradectidae (**A**) and Herpetotheriidae (**B–F**). **A.** *Peradectes russelli*, CB 1027 (CL), right m4 in lingual, occlusal, and labial views; **B.** *Amphiperatherium lamandini*, ECA 3104 (UM), fragment of right mandible with m3-4 in occlusal view; **C.** *Peratherium elegans* (type of *Peratherium agmardi* Filhol), QU 8216 (MNHN), right mandible with c and p1-m4 in occlusal view; **D.** *Peratherium perrierense* (holotype), PRR 2524, right mandible with i1-m4 in occlusal view; **E.** *Peratherium cayluxi*, QU 8217 (MNHN) (holotype), left mandible with p2-m1 and m3-4 in occlusal view; **F.** *Amphiperatherium ambiguum*, PLA 1042 (UM), left m4 in occlusal and lingual views. Figures after Crochet (1980). Scale bars: 1 mm.

***Rumiodon*.** Differs from *Rumiodon inti* Goin & Candela, 2004 in having a wider anterior cingulid, distinct hypoconulid that is larger and not twinned with the entoconid, and an oblique cristid that is less parallel to the dental axis.

Comparisons with other Cenozoic Holarctic metatherians. *Estelestes*. Differs from *Estelestes ensis* Novacek, Ferrusquía-Villafranca, Flynn, Wyss, & Norell, 1991 (early Eocene; referred by the authors to the "Didelphidae"), in that it lacks a postcingulid (in *Estelestes* the postcingulid extends anteriorly forming a buccal cingulid basal to the hypocone), the hypocone is more buccally salient, the hypoconulid is farther from the entoconid and less posteriorly tilted; finally, an oblique cristid is less parallel to the dental axis.

***Orhaniyeia*.** Differs from *Orhaniyeia nauta* Métais, Coster, Kappelman, Licht, Ocakoğlu, Taylor, & Beard, 2018 (middle Eocene of Turkey) in being much smaller, has less bunoid molars, the anterior cingulid is better developed, the paraconid is placed farther from the metaconid, the paracristid is less transverse to the dental axis, the talonid is shorter, the hypoconid is much more distally placed, an oblique cristid that is less parallel to the dental axis; finally, it lacks multiple cuspids on the pre-entocristid.

Comparisons with South American "opossum-like" metatherians. *Morotodon aenigmaticus* differs from the Protodidelphidae (early to middle Eocene) in being much smaller, has less bunoid molars, and smaller and narrower talonids. Differs from the Derorhynchidae (Paleogene of South America and Antarctica) in having a longer talonid, no posterior cingulid, smaller entoconid and larger hypoconulid. Differs from species of *Gaylordia* (early Eocene) in having a less developed anterior cingulid, longer talonid, less lingually placed paraconid; finally, an oblique cristid that is less parallel to the dental axis. Differs from species of *Marmosopsis* (early Eocene) in lacking a posterior cingulid and an oblique cristid that is less subparallel to the dental axis. Differs from species of *Minusculodelphis* (Eocene) in its larger size, better developed talonids and hypoconid, and in the persistence of the hypoconulid. Differs from species of *Monodelphopsis* (early Eocene) in having a narrower talonid, an oblique cristid that is less subparallel to the dental axis, and better developed entoconid and hypoconulid which are less closely set to each other. Differs from species of *Carolopaulacoutoia* (early Eocene) in its shorter talonid, less parallel oblique cristid to the dental axis, more salient hypoconid, and smaller and more centrally placed hypoconulid. Differs from species of *Itaiboraidelphys* (early Eocene) in having a poorly developed anterior cingulid, the paraconid is more distant from the metaconid, an oblique cristid that is less parallel to the dental axis, and the hypoconulid is more centrally placed. Differs from species of *Didelphopsis* (Paleocene-early Eocene) in having a shorter anterior cingulid, proportionally longer trigonid, the paraconid is placed farther from the metaconid, an oblique cristid that is less parallel to the dental axis, and the hypoconulid is larger and farther from the encotonid. Differs from *Pucadelphys andinus* Marshall & Muizon, 1988 (early Paleocene) in having a larger hypoconulid and an oblique cristid that is less parallel to the dental axis.

Discussion

Affinities of *Morotodon aenigmaticus* gen. et sp. nov.

With only two exceptions (the deltatheroidan *Gurbanodelta kara*, from the Paleocene of China, and the

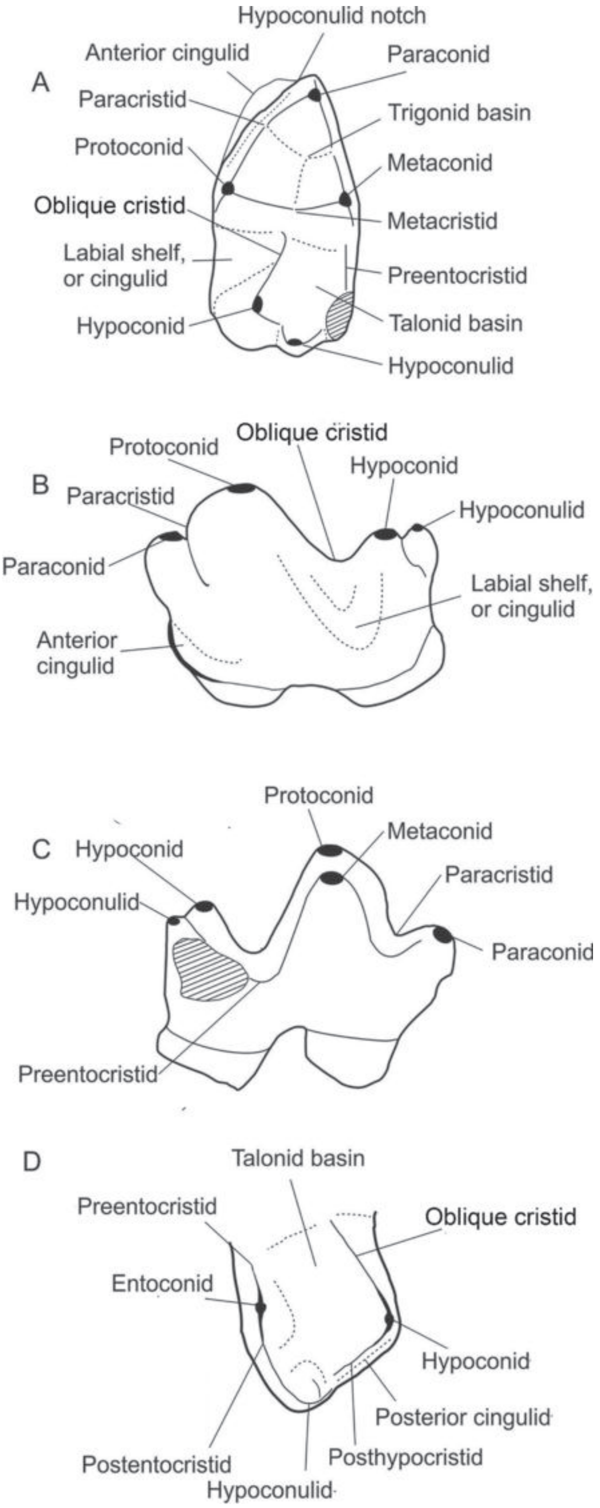

Figure 4. Schematic drawing of *Morotodon aenigmaticus* gen. et sp. nov. in occlusal (**A**), buccal (**B**), and lingual (**C**) views; talonid of the *Armintodelphys* (based on specimen IRSNB M2152 published by Smith and Smith (2013) (**D**).

anatoliadelphids, from the middle Eocene of Turkey), all other Cenozoic Afro-Eurasian metatherians (36 species) have been referred either to the Peradectidae (six species) or to the Herpetotheriidae (the remaining ones). It is obvious to us that *Morotodon aenigmaticus* is neither a deltatheroidan nor an anatoliadelphid. On the contrary, its molar pattern is much more similar to that of "opossum-like marsupials" such as herpetotheriid and peradectid marsupialiforms. Herpetotheriids differ from peradectids in several aspects of their respective molar structure. Regarding the lower ones, Crochet (1979, 1980) noted that the former (his "Didelphini") have hypoconulids and entoconids of unequal height (the entoconid is higher in m1-3, but not in m4). On the contrary, peradectids (his "Peradectini") have entoconids and hypoconulids of similar height in all lower molars, including the m4. Even though the entoconid is broken in the m4 of *Morotodon aenigmaticus*, it is clear that the hypoconulid was a larger cusp (see the lingual views of specimen UM MOR II 48'04 in Figs 2, 3). However, it is impossible to assign *Morotodon* to either family with certainty. Our observations on the relative height of both cuspids in the m4 of species of *Peradectes*, *Peratherium*, and *Amphiperatherium* indicate high variability in this feature. Among both herpetotheriid genera, all states can be observed: entoconid higher, hypoconulid higher, or both cusps being subequal. In Table 2 we have summarized our observations of several features of the m4 of *Morotodon aenigmaticus* and species of *Peradectes*, *Peratherium*, and *Amphiperatherium* figured in the literature. It can be seen that in most of the surveyed features there is variability enough among species, in such a way that it precludes any certain assignation of *Morotodon*. In general terms, however, as well as in at least one feature (see below and Table 2) we note that *Morotodon aenigmaticus* resembles species of Herpetotheriidae more closely than of any peradectid so far known.

Table 2. A comparison of dental features of the last lower molar in *Morotodon aenigmaticus* and in species of *Peradectes*, *Peratherium* and *Amphiperatherium*.

Features in m4	*Morotodon*	*Peradectes*	*Peratherium*	*Amphiperatherium*
1. Paracristid inclination	45°	45°, or less	45° or less	45°, less than 45°, more than 45°
2. Metaconid position relative to the protoconid	Slightly posterior	Posterior, or at the same level	Same level, or metaconid posterior	Same level, or metaconid posterior, or protoconid posterior
3. Hypoconulid position on the rear of the entoconid / proximity with the entoconid	Central	Almost central, or far lingual, or almost twinned to entoconid	Almost central, or far lingual, or almost twinned to entoconid	Almost central, or far lingual, or almost twinned to entoconid
4. Postcingulid (present /absent /variable)	Absent	Variable	Variable	Variable
5. Buccal cingulid (pres/abs/var)	Present	Variable	Variable	Variable
6. Relative heights, entoconid / hypoconulid	Hypoconulid higher	Hypoconulid higher, or equal	Hypoconulid higher, or equal, or entoconid higher	Hypoconulid higher, or equal, or entoconid higher
7. Width of the talonid at its anterior edge	Narrow	Less narrow, or wide	Narrow	Narrow, or less narrow
8. Mesiodistal compression of paraconid	Not compressed	Compressed, or not compressed	Compressed, or not compressed	Compressed, or not compressed
9. Entoconid position relative to hypoconid	Entoconid slightly anterior	Same level, or ent. Slightly anterior, or ent. Slightly posterior	Same level, or ent. slightly anterior	Same level, or ent. slightly anterior
10. Width of distal edge of the talonid	Wide	Wide, or reduced but wider than the anterior edge	Narrow, or almost as wide as the trigonid	Almost as wide as the trigonid, or narrow
11. Postentocristid linking entoconid with hypoconulid	Absent	Present	Absent	Absent
12. Metacristid slope (almost vertical, gently sloping)	Almost vertical	Almost vertical	Almost vertical	Almost vertical, one species gently sloping

Ladevéze et al. (2012) studied a large sample of dental materials (around 400 specimens) belonging to herpetotheriid metatherians from the earliest Eocene of Dormaal (Belgium). Previous reviews of the herpetotheriids from Dormaal led to the recognition of only two species: *Peratherium constans* Teilhard de Chardin, 1927 and *Amphiperatherium brabantense* Crochet, 1979. Ladevéze et al. (2012) concluded that, due to the dental variability shown by the dental materials, the two species are indistinguishable, therefore they referred both to *Peratherium constans*. Actually, they not only questioned the validity of the *Amphiperatherium* species but also the status of the genus *Amphiperatherium* itself. While we agree that several features used to distinguish the two genera are subtle, and subject to variability (see above), we prefer to maintain the validity of *Amphiperatherium* until a thorough review of all Northern Hemisphere (North American and Eurasian) herpetotheriids is made.

If molars in general are subject to some degree of variability, the case of m4 is more evident. Unlike several eutherians, metatherian molars invariably erupt successively, from front to back; the hypoconulid of the preceding molar serves as a guide for the alignment of the succeeding one. The hypoconulid of the former fits in the hypoconulid notch of the latter – a groove delimited lingually by the mesial end of the anterior cingulid, and buccally by the paraconid. In such a way, the succeeding molar erupts in precise alignment in the molar row. In mammals with mostly orthal jaw movements, such as those with insectivorous, faunivorous or carnivorous feeding habits, it is understandable that selective pressures strongly favour stable morphologies among these structures – any malocclusion could lead to the breaking of teeth. Not having a succeeding molar behind, the m4 in metatherians, and especially the talonid, is subject to a larger degree of variability (see, e.g., Martin 2005 on the various talonid morphologies in the m4 of the living didelphid *Lestodelphys halli*). The position of the hypoconulid at the distal edge of the talonid, for instance, tends to be located much more buccally with respect to the entoconid than in the preceding molars (m1-3; see, e.g., Hooker et al. 2008).

Table 2 shows a dozen features of the m4 structure, most of them dealing with the talonid. All these features were used to compare *Morotodon aenigmaticus* with several species of *Peradectes* (Peradectidae), and *Peratherium* and *Amphiperatherium* (Herpetotheriidae). Many of them are subject to some, or much, variability. When all features are considered, however, *Morotodon* fits better in the herpetotheriid than in the peradectid general pattern.

Following Ladéveze et al. (2012), Smith and Smith (2013) stated that the presence of a postentocristid (Fig. 4) in the lower molars was a diagnostic feature of the Peradectidae, while in herpetotheriids there is a notch between the entoconid and the hypoconulid. *Morotodon aenigmaticus* lacks a postentocristid, thus suggesting affinities to the Herpetotheriidae.

Among herpetotheriids, *Morotodon* is more similar to some species of *Peratherium*, such as *P. sudrei*, *P. perrierense*, *P. constans* and *P. cayluxi*, but differs in the position of the hypoconulid, the size of the hypoconid and the length of the anterior cingulid. More remarkable is the similarity with *Amphiperatherium goethei*; among other features, the two taxa share a proportionally similar size and position of the hypoconulid. Among North American metatherians, we note a general similarity with *Golerdelphys stocki*, even though the materials referred to this species have not preserved the m4. However, judging from its preserved molars, similar morphologies can be observed: short and wide anterior cingulid, not mesiodistally compressed paraconid, proportionally large and vertical hypoconulid, laterally compressed entoconid, and, probably, presence of a buccal shelf (or cingulid; see fig. 4E in Williamson and Lofgren 2014). Summarizing, we find that *Morotodon aenigmaticus* shares more features with herpetotheriids than with any other group of Marsupialiformes. Not being able to establish this assignment with complete certainty, we opt to refer the African taxon to the ?Herpetotheriidae.

Origin of *Morotodon aenigmaticus* gen. et sp. nov.

Most of the similarities between the m4 of *Morotodon* and that of several herpetotheriids are based on features which are generalized for the family: relatively large hypoconulid, non-reduced talonid, paraconid in a mesio-lingual location, not appressed to the metaconid. The already mentioned species of European genera that show these similarities are all from the Eocene except *P. cayluxi*, from the basal Oligocene (Crochet 1980). In turn, *Golerdelphys stocki* comes from the late Palaeocene Goler Formation in USA, North America (Williamson and Lofgren 2014). Summarizing, all metatherians showing similarities with *Morotodon aenigmaticus* come from Paleogene levels of the Northern Hemisphere. Its origin from some region of Eurasia, by the Eocene or Oligocene is, in consequence, the most probable hypothesis. Additional evidence supporting this hypothesis is the high abundance of Eocene metatherians in Europe (Crochet 1980) and previously recognized migrations between the two continents by several taxa: the occurrence of metatherians in the Eocene-Oligocene of northern Africa and Arabia (Gunnell 2010), the entrance into Africa of several lineages of rodents (zegdoumyids, anomaluroids and phiomyids), primates, and anthracotheres. Inversely, it should be noted the record of embrithopods and a probable proboscidean of African affinities in the Paleocene-Eocene of Europe and/or Asia (Sen 2013; and references therein).

The hypothesis of an Eurasian origin of *Morotodon* is reinforced by the tectonic, climatic and eustatic events that happened by the latest Paleocene and earliest Eocene, which may have facilitated these faunal exchanges. Evidence of a land bridge at northwestern Iran and southeastern Turkey is yielded by the Gercüs Formation; these floodplain/lacustrine/lagoonal/coastal plain sediments were deposited during the first phases of the collision between Africa and Eurasia (Haq et al. 1987; Zachos et al. 2001; Sengör et al. 2008; Sen 2013).

Palaeoecology

The sediments of the southern layers of Moroto II were deposited in a shallow valley, similar to the present day Karamoja Plain (Pickford and Mein 2006), in the Moroto region. The composition of these sediments indicates a depositional environment dominated by shallow rivers, but with more or less permanent bodies of water in dry seasons. This is evident from the high number of aquatic or amphibious taxa, including invertebrates (e.g., crabs) and vertebrates such as fishes, frogs, crocodiles, aquatic turtles or amphibious mammals (e.g., anthracotheres; see Pickford and Mein 2006).

The plentiful presence of the terrestrial snail *Nothapalinus*, suggests the presence of grassy areas (Pickford 1995). However, the record of anomalurid rodents, galagids, cercopithecids, hominoids and folivorous proboscideans also suggests the nearby presence of thicker vegetation. In summary, the evidence at hand suggests that during the basal middle Miocene the Moroto landscapes were dominated by open woodland and bushland (see Suppl. material 3).

Following the palaeoecological analysis of some herpetotheriid species made by Kurz (2005), we infer similar ecological patterns in *Morotodon aenigmaticus*. Its molar pattern matches that of other insectivorous "opossum-like" marsupialiforms; in addition, the relatively well-developed paracristid also suggests some faunivorous habits. Briefly, it can be inferred that it had an insectivorous-faunivorous diet and, probably, cursorial locomotion. Species of *Amphiperatherium* were scansorial and more insectivorous than those of *Peratherium* (see Kurz 2005). The terrestrial character of the representatives of this family is confirmed by a study of a complete skeleton referable to *Herpetotherium*, found in North America (Horovitz et al. 2008); it differs from peradectids in that the latter were more arboreal and insectivorous to frugivorous in their feeding habits (Kurz 2005; Rose et al. 2012). The suggested habits of *Morotodon* are consistent with the inferred palaeoenvironment of Moroto II.

Disclosure statement

No potential conflict of interest was reported by the authors.

Funding details

F.J.G. and V.D.C. thank Agencia (Foncyt, Mincyt; PICT 2019-03283) and CONICET (PIP KB2 - 11220200100150CO).

Acknowledgements

We thank the Uganda Museum, Kampala (Rose Mwanja, Sarah Musalizi, Christopher Sebuyungo) for access to fossil material in its care, and the Uganda National Council for Science and Technology for authorization to carry out research in the country. Pierre Mein measured the specimen from Moroto and made preliminary identifications. Hugo Salais (Metazoa Studio) for the 3D reconstruction, Agustín Ruella for a previous version of the 3D reconstruction, Marcela Tomeo for the realisation of Figs 1 and 3, and Juana Yañez for the reconstruction of the palaeoenvironment. Francisco Javier Ruiz-Sánchez of University of València provided the use of the electron microscopy. Maria Dolores Marin-Monfort for the taphonomical comments. We should thank Frank Sénégas for making the casts (Sorbonne University). The fossils were collected by the Uganda Palaeontology Expedition led by B. Senut and funded by the Ministry of Foreign Affairs, Commission des Fouilles. We thank the villagers of Rupa for participating in the screening of the sediments which yielded the holotype of *Morotodon aenigmaticus*. The support of the Consejo Nacional de Investigaciones Científicas y Técnicas (CONICET) toward this research for V. D. Crespo is hereby acknowledged. V.D.C. is the beneficiary of a grant (ZA21-044) for the requalification of the Spanish university system from the Ministry of Universities of the Government of Spain, financed by the European Union, Next Generation EU.

References

Beck RM (2013) A peculiar faunivorous metatherian from the early Eocene of Australia. Acta Palaeontologica Polonica 60: 123–130. https://doi.org/10.4202/app.2013.0011

Bishop WW (1958) Fossil apes and ivory. Bulletin of the Uganda Society 1958: 127–129.

Bishop WW (1964) More fossil Primates and other Miocene mammals from North-east Uganda. Nature 203: 1327–1331. https://doi.org/10.1038/2031327a0

Bishop WW, Miller JA, Fitch FW (1969) New potassium-argon age determinations relevant to the Miocene fossil mammal sequence in East Africa. American Journal of Science 267: 669–699. https://doi.org/10.2475/ajs.267.6.669

Cifelli RL, de Muizon C (1997) Dentition and jaw of *Kokopellia juddi*, a primitive marsupial or near-marsupial from the medial Cretaceous of Utah. Journal of Mammalian Evolution 4: 241–258. https://doi.org/10.1023/A:1027394430433

Crespo VD, Goin FJ (2021) Taxonomy and affinities of African Cenozoic metatherians. Spanish Journal of Palaeontology 36: 1–16. https://doi.org/10.7203/sjp.36.2.20974

Crochet J-Y (1979) Diversité systématique des Didelphidae (Marsupialia) européens tertiaires. Geobios 12: 365–378. https://doi.org/10.1016/S0016-6995(79)80117-5

Crochet J-Y (1980) Les Marsupiaux du Tertiaire d`Europe. Singer-Polignac, Paris.

Crochet J-Y (1984) *Garatherium mahboubii* nov. gen., nov. sp., marsupial de l'Éocène inférieur d'El Kohol (Sud-Oranais, Algérie). Annales de Paléontologie 70: 275–294.

Crochet J-Y (1986) *Kasserinotherium tunisiense* nov. gen., nov. sp., troisième marsupial découvert en Afrique (Eocène inférieur de Tunisie). Comptes Rendus de l'Académie des Sciences 302: 923–926.

Crochet J-Y, Thomas H, Sen S, Roger J, Gheerbrant E, Al-Sulaimani Z (1992) Découverte d'un Péradectidé (Marsupialia) dans l'Oligocène inférieur du Sultanat d'Oman: Nouvelles données sur la paléobiogéographie des Marsupiaux de la plaque arabo-africaine. Comptes Rendus de l'Académie des Sciences 314: 539–544.

De Bast E, Sigé B, Smith T (2012) Diversity of the adapisoriculid mammals from the early Palaeocene of Hainin, Belgium. Acta Palaeontologica Polonica 57: 35–53. https://doi.org/10.4202/app.2010.0115

Fleuty MJ (1968) Explanation of the Geology of Sheet 27 (Moroto). Reports of the Geological Survey of Uganda, 13.

Gebo DL, Maclatchy L, Kityo R, Deino A, Kingston J, Pilbeam D (1997) A hominoid genus from the Early Miocene of Uganda. Science 276: 401–404. https://doi.org/10.1126/science.276.5311.401

Gheerbrant E (1995) Les mammifères Paléocènes du Bassin D'Ouarzazate (Maroc). III. Adapisoriculidae et autres mammifères (Carnivora, ?Creodonta, Condylarthra, ?Ungulata et incertae sedis). Palaeontographica A 237: 39–132. https://doi.org/10.1127/pala/237/1995/39

Goin FJ, Candela AM (2004) New Paleogene marsupials from the Amazon Basin of eastern Peru. The Paleogene Mammalian Fauna of Santa Rosa, Amazonian Peru. Natural History Museum of Los Angeles County, Science Series 40: 15–60.

Gunnell G (2010) Marsupialia. In: Werdelin L, Sanders WJ (Eds) Cenozoic Mammals of Africa. University of California Press, Berkeley, Los Angeles, London, 77–79. https://doi.org/10.1525/california/9780520257214.003.0006

Haq BU, Hardenbol J, Vail PR (1987) Chronology of fluctuating sea levels since the Triassic. Science 235: 1156–1167. https://doi.org/10.1126/science.235.4793.1156

Hooker JJ, Sánchez-Villagra MR, Goin FJ, Simons EL, Attia Y, Seiffert ER (2008) The origin of Afro-Arabian "didelphimorph" marsupials. Palaeontology 51: 635–648. https://doi.org/10.1111/j.1475-4983.2008.00779.x

Horne RG (1953) The geology of the lower mountain slopes adjacent to Moroto Township. Unpublished Report of the Geological Survey of Uganda 1953: 1–47.

Horovitz I, Ladevèze S, Argot C, Macrini TE, Martin T, Hooker JJ, Kurz C, De Muizon C, Sánchez-Villagra M (2008) The anatomy of *Herpetotherium* cf. *fugax* Cope 1873, a metatherian from the Oligocene of North America. Palaeontographica A 284: 109–141. https://doi.org/10.1127/pala/284/2008/109

Kurz C (2005) Ecomorphology of opossum-like marsupials from the Tertiary of Europe and a comparison with selected taxa. Kaupia 14: 21–26.

Ladevèze S, Smith R, Smith T (2012) Reassessment of the Morphology and Taxonomic Status of the earliest Herpetotheriid Marsupials of Europe. Journal of Mammalian Evolution 19: 249–261. https://doi.org/10.1007/s10914-012-9195-0

Mahboubi M, Ameur R, Crochet J-Y, Jaeger J-J (1983) Première découverte d'un marsupial en Afrique. Comptes Rendus de l'Académie des Sciences 297: 691–694.

Martin GM (2005) Intraspecific variation in *Lestodelphys halli* (Marsupialia: Didelphimorphia). Journal of Mammalogy 86: 793–802. https://doi.org/10.1644/1545-1542(2005)086[0793:IVILHM]2.0.CO;2

Mckenna MC, Bell S (1997) Classification of Mammals above the Species Level. Columbia University Press, New York.

Musalizi S, Senut B, Pickford M, Musiime E (2009) Geological and palaeontological archives relating to Early Miocene localities of Uganda, 1957–1969. Geo-Pal Uganda 1: 2–96.

Ogg JG, Ogg GM, Gradstein FM (2016) A Concise Geologic Time Scale 2016. Cambridge University Press, New York. https://doi.org/10.1016/B978-0-444-59467-9.00005-4

Pickford M (1995) Fossil land snails of East Africa and their palaeoecological significance. Journal of African Earth Sciences 20: 167–226. https://doi.org/10.1016/0899-5362(95)94397-R

Pickford M (2018) Tenrecoid mandible from Elisabethfeld (Early Miocene) Namibia. Communications of the Geological Survey of Namibia 18: 87–92.

Pickford M (2019) Tiny Tenrecomorpha (Mammalia) from the Eocene of Black Crow, Namibia. Communications of the Geological Survey of Namibia 21: 15–25.

Pickford M (2020) Anthracotheriidae (Mammalia: Artiodactyla) from Moroto, basal middle Miocene, Uganda. Geo-Pal Uganda 14: 1–75.

Pickford M, Mein P (2006) Early Middle Miocene mammals from Moroto II, Uganda. Beiträge zur Paläontologie 30: 361–386.

Pickford M, Senut B, Gommery D, Musalizi S, Musiime E (2017) Revision of the Miocene Hominoidea from Moroto I and II, Uganda. Geo-Pal Uganda 10: 1–32.

Pickford M, Tassy P (1980) A new species of *Zygolophodon* (Mammalia, Proboscidea) from the Miocene hominoid localities of Meswa Bridge and Moroto (East Africa). Neues Jahrbuch für Geologie und Paläontologie 4: 235–251. https://doi.org/10.1127/njgpm/1980/1980/235

Rose KD, Chew AE, Dunn RH, Kraus MJ, Fricke HC, Zack SP (2012) Earliest Eocene mammalian fauna from the Paleocene-Eocene thermal maximum at Sand Creek Divide, southern Bighorn Basin, Wyoming. Papers on Palaeontology 36: 1–122.

Sánchez-Villagra MR, Seiffert ER, Martin T, Simons EL, Gunnell GF, Attia Y (2007) Enigmatic new mammals from the late Eocene of Egypt. Palaontologische Zeitschrift 81: 406–415. https://doi.org/10.1007/BF02990252

Seiffert ER (2010) The oldest and youngest records of afrosoricid placentals from the Fayum Depression of northern Egypt. Acta Palaeontologica Polonica 55: 599–617. https://doi.org/10.4202/app.2010.0023

Sen S (2013) Dispersal of African mammals in Eurasia during the Cenozoic: ways and whys. Geobios 46: 159–172. https://doi.org/10.1016/j.geobios.2012.10.012

Sengör AMC, Özeren MS, Keskin M, Sakinc M, Özbakir AD, Kayan I (2008) Eastern Turkish high plateau as a small Turkic-type orogen implications for post-collisional crust-forming processes. Earth Science Reviews 90: 1–48. https://doi.org/10.1016/j.earscirev.2008.05.002

Simmons NB, Seiffert ER, Gunnell GF (2016) A new family of large omnivorous bats (Mammalia, Chiroptera) from the Late Eocene of the Fayum Depression, Egypt, with comments on use of the name "Eochiroptera". American Museum Novitates 3857: 1–44. https://doi.org/10.1206/3857.1

Simons EL, Bown TM (1984) A new species of *Peratherium* (Didelphidae; Polyprotodonta): the first African marsupial. Journal of Mammalogy 65: 539–548. https://doi.org/10.2307/1380836

Smith T, Smith R (2013) A land micro-mammal fauna from the Early Eocene marine Egem deposits (NP12, Belgium) and the first occurrence of the peradectid marsupial *Armintodelphys* outside North America. Geologica Belgica 16(4): 302–310.

Van Couvering JA, Delson E (2020) African Land Mammal Ages. Journal of Vertebrate Paleontology 40(5): e1803340. https://doi.org/10.1080/02724634.2020.1803340

Varne R (1966) The petrology of Moroto Mountain, Eastern Uganda. Proceedings of Petrology Society 1629: 23.

Varne R (1967) The growth of the Moroto volcano, Eastern Uganda. Bulletin of Volcanology 31: 163–174. https://doi.org/10.1007/BF02597012

Werdelin L (2010) Chronology of Neogene Mammal Localities. In: Werdelin L, Sanders WJ (Eds) Cenozoic Mammals of Africa. University of California Press, Berkeley, Los Angeles, London, 27–43. https://doi.org/10.1525/california/9780520257214.003.0003

Williamson TE, Lofgren DL (2014) Late Paleocene (Tiffanian) metatherians from the Goler Formation, California. Journal of Vertebrate Paleontology 34: 477–482. https://doi.org/10.1080/02724634.2013.804413

Zachos J, Pagani M, Sloan L, Thomas E, Billups K (2001) Trends, rhythms, and aberrations in global climate 65 Ma to present. Science 292: 686–693. https://doi.org/10.1126/science.1059412

Supplementary material 1

3-D video of a digital reconstruction of *Morotodon aenigmaticus* gen. et sp. nov.

Authors: Vicente D. Crespo, Francisco J. Goin, Martin Pickford

Data type: 3-D video (avi file)

Explanation note: 3-D video of a digital reconstruction of *Morotodon aenigmaticus* gen. et sp. nov.

Link: https://doi.org/10.3897/fr.25.80706.suppl1

Supplementary material 2

Morotodon aenigmaticus gen. et sp. nov. Stereoscopic pairs and schematic drawing of specimen UM MOR II, 48’04

Authors: Vicente D. Crespo, Francisco J. Goin, Martin Pickford

Data type: Stereoscopic pairs and schematic drawing

Explanation note: A–E, *Morotodon aenigmaticus* gen. et sp. nov. Stereoscopic pairs and schematic drawing of specimen UM MOR II, 48’04 (an isolated left m4) in occlusal (A), labial (B), lingual (C), anterior (D), posterior (E), and basal views. Scale bar: 1 mm.

Link: https://doi.org/10.3897/fr.25.80706.suppl2

Supplementary material 3

Reconstruction of the palaeoenvironment of Moroto II

Authors: Vicente D. Crespo, Francisco J. Goin, Martin Pickford

Data type: Images

Explanation note: Reconstruction of the palaeoenvironment of Moroto II. Left to right: the anthracothere *Brachyodus* sp.; the primate *Afropithecus turkanensis* Leakey & Leakey, 1986 ; the deinothere *Deinotherium hobleyi* Andrews, 1911; the creodont *Hyainailouros sulzeri* Biedermann, 1863 and the metatherian *Morotodon aenigmaticus* gen. et sp. nov.

Link: https://doi.org/10.3897/fr.25.80706.suppl3

Fossil Record 25 (1) 2022, 187–212 | DOI 10.3897/fr.25.83034

Revision of 18 ichneumonid fossil species (Hymenoptera, Ichneumonidae) highlights the need for open nomenclature in palaeontology

Tamara Spasojevic[1,2], Gavin R. Broad[3], Seraina Klopfstein[1,2]

1 *Naturhistorisches Museum Basel, Augustinergasse 2, Basel, Switzerland*
2 *Institute of Ecology and Evolution, University of Bern, Baltzerstrasse 6, Bern, Switzerland*
3 *Natural History Museum, Cromwell Road, London SW7 6BD, UK*

http://zoobank.org/6402F8F1-5229-4153-823F-CAEA106F90A1

Corresponding author: Seraina Klopfstein (Seraina.klopfstein@bs.ch)

Academic editor: Christian Klug ♦ **Received** 3 March 2022 ♦ **Accepted** 11 May 2022 ♦ **Published** 7 June 2022

Abstract

The fossil record of Darwin wasps (Ichneumonidae) is extremely understudied relative to their enormous extant diversity, with only around 300 species described. Moreover, the taxonomic placement of many of the fossils is based on an outdated classification system. We here revise 18 ichneumonid fossils, all described before the most comprehensive revision of ichneumonid classification by Henry Townes. After a careful reinterpretation of character evidence, we leave the original placement of only five fossils, while expressing uncertainty about the placement of two of them, *Pimpla*? *seyrigi* Theobald and *Polysphincta*? *inundata* Brues, by following the principles of open nomenclature. In addition, we move *Parapimpla rhenana* Theobald, 1937 **stat. rev.** from Pimplinae to Ctenopelmatinae. We describe a new phygadeuontine genus to accommodate two fossils previously described in Pimplinae, *Armadilleon morticinus* (Brues) **gen. et comb. nov.** and *A. petrorum* (Brues) **gen. et comb. nov.** Finally, we change the genus and, almost always, the subfamily placement for ten fossils: *Hallocinetus*? *arvernus* (Piton) **comb. nov.**, *Dimophora*? *longicornis* (Theobald) **comb. nov.**, *Dimophora*? *wickhami* (Cockerell) **comb. nov.**, *Lycorina*? *indura* (Theobald) **comb. nov.**, *Acerataspis*? *revelata* (Brues) **comb. nov.**, *Hypsicera*? *solidata* (Brues) **comb. nov.**, *Orthocentrus*? *mortuaria* (Brues) **comb. nov.**, *Zagryphus tilloyi* (Theobald) **comb. nov.**, *Lithoserix antiquus* (Saussure) **comb. nov.** and *Monoblastus*? *senilis* (Brues) **comb. nov.** Our revision highlights the need for the re-interpretation of perhaps a majority of ichneumonid fossils and for widely adopting the open nomenclature framework. This framework allows uncertainty in fossil classification to be expressed in an intuitive and explicit manner, which contributes to alleviating misinterpretation of the palaeontological literature, for instance in phylogenetic dating studies.

Key Words

compression fossils, Darwin wasps, dating, Florissant Formation, fossil record, Palaeogene, taphonomy

Introduction

Darwin wasps constitute the largest family of parasitoid wasps, with currently more than 25,000 species described and many more awaiting discovery. They attack immature stages of holometabolan insects and spiders and, by controlling their populations, fulfill a crucial role in nearly all terrestrial ecosystems. Their fossil record dates back to the late Jurassic, although the first unequivocal representatives of extant subfamilies are from the late Palaeocene, so after the K-Pg boundary (Kopylov 2009). The first molecular dating study of Ichneumonidae (Spasojevic et al. 2021) recovered a Jurassic origin of crown group ichneumonids, a result that implies ghost ranges of at least 45 million years for the extant subfamilies. However, the associations of the Mesozoic ichneumonid fossils, which have been classified in extinct subfamilies, currently remain uncertain, as they show many similarities with some extant subfamilies

(Kopylov 2010; McKellar et al. 2013). In any case, the fossil record of ichneumonids appears very patchy. Also later periods, such as the Palaeocene and the early Eocene, are represented by only very few described ichneumonid fossils. A pronounced incompleteness of the fossil record and thus long ghost ranges are common in insects (Rasnitsyn 2000; Ronquist et al. 2012), which only fossilize under rather rare conditions. However, there is an additional explanation for the poverty of the Darwin wasp fossil record: it is drastically understudied, with around 300 described fossil species in contrast to the 25,000 extant species (Yu et al. 2016; PaleoBioDB 2020). Ichneumonid fossils simply have not attracted much attention by palaeoentomologists (Khalaim 2008; Kopylov 2010; Kopylov et al. 2010, 2018; Antropov et al. 2014; Spasojevic et al. 2018a, 2018b; Klopfstein 2021; Meier et al. 2022; Viertler et al. 2022), and extensive undescribed material of this family is present in numerous fossil collections at museums worldwide.

Even among the described fossil ichneumonids, much work remains to be done. Of the 302 known fossils, more than half were described before Henry Townes published his seminal genus-level treatments of the family (Townes 1969a, 1969b, 1970, 1971) in which he profoundly revised the genus and subfamily classification; any work from before that date thus reflects an outdated taxonomy. Unfortunately, the great majority of ichneumonid fossils have not been revised since their original description (Yu et al. 2016). Their current taxonomic placement is thus not reliable, which greatly diminishes their use for informing molecular dating studies and distorts our understanding of the evolutionary history of the group. For example, a recent review of the ten described ichneumonid species from the Green River Formation overturned the placement of four of them, while noting considerable uncertainty in the placement of the remaining ones (Spasojevic et al. 2018b).

We here make a modest contribution to improving the interpretation of the ichneumonid fossil record by redescribing and carefully illustrating 18 ichneumonid fossil species that have been described between 1910 and 1940 (Saussure 1852; Brues 1910; Cockerell 1919; Théobald 1937; Piton 1940). These fossils are from the Palaeocene Menat Formation (one species), the Late Eocene Florissant shales (12 species), the Early Oligocene Kleinkembs locality (three species), and the Late Oligocene locality in Aix-en-Provence (three species). For the majority of the revised fossils, we suggest new genus and often subfamily placement. We describe a new genus, *Armadilleon* gen. nov., for two species with remarkable sculpture. Moreover, we apply open nomenclature to express placement uncertainty and discuss its usefulness in communication with scientists outside the palaeontological community.

Materials and methods

Information about fossil ichneumonids was first obtained through the EDNA fossil insect database (Mitchell 2013: https://fossilinsectdatabase.co.uk), with stratum names and current age estimates taken from the Paleobiology Database accessed through Fossil works (http://fossilworks.org). We mostly chose fossils described in one of the subfamilies of the informal but monophyletic Pimpliformes group of subfamilies (Gauld 1985; Klopfstein et al. in press; Wahl 1986), but also from some other ichneumonid subfamilies. Those fossils were originally chosen for inferring the absolute age of Pimpliformes in a total-evidence dating analysis (Spasojevic et al. 2021), which revealed that a redescription and/or revision of most of them is necessary. Most fossil types could not be sent to us by mail because of restrictions by the institutions, in which cases we either visited the corresponding museums to study the type specimens or obtained high-resolution photographs. The redescribed fossils are from the Palaeontology collection at the Muséum National d'Histoire Naturelle in Paris, France (**MNHN.F**: Menat, Aix-en-Provence), the Museum of Comparative Zoology in Harvard, USA (**MCZ**: Florissant Formation), the University of Colorado Museum of Natural History in Boulder, USA (**UCM**: Florissant Formation), and the Natural History Museum in Basel, Switzerland (**NMBA**: Kleinkembs).

For the redescriptions, we followed the morphological nomenclature in Broad et al. (2018), except for wing venation characters, which follow Spasojevic et al. (2018b) (Fig. 1). If a character is visible only in the holotype or paratype, this is indicated with a #h or #p, respectively, or by the specimen numbers in the case of several paratypes or non-type specimens. Metasomal tergites and sternites are numbered and abbreviated as T1, T2, etc. and S1, S2, etc., respectively. Measurements were taken in ImageJ (Abramoff et al. 2004). Unless stated otherwise, measurements reflect the length-to-width ratio of the structure mentioned, such as pterostigma, hind femur, or T2. Ovipositor length was measured as the entire visible length of the ovipositor, and it is also expressed in relation to the length of the hind tibia or, if the hind tibia was not preserved or incomplete, to the length of the metasoma. If more than one specimen was used for measurements, the value of the holotype follows in brackets after the recorded range.

Our interpretations of the characters visible in the fossils are represented both in the descriptive text and in the form of a drawing created by overlaying high-resolution photographs of holotypes and sometimes also paratypes in Adobe Photoshop CC v. 14.2. Thicker lines are used to indicate outlines of body structures, thinner lines show characters inside these outlines, and uncertain interpretations (mostly where lines were extrapolated between clearly visible portions) are represented as dotted lines. Conspicuous sculpture of the cuticle, which in some cases was preserved in great detail, is shown in grey.

To express uncertainty in the taxonomic placement of the fossils, we made use of the open nomenclature framework (Matthews 1973; Sigovini et al. 2016), a system that has been proposed to complement the International Code of Zoological Nomenclature (Ride et al. 1999; Ferraris and Eschmeyer 2000). Following this framework, we put

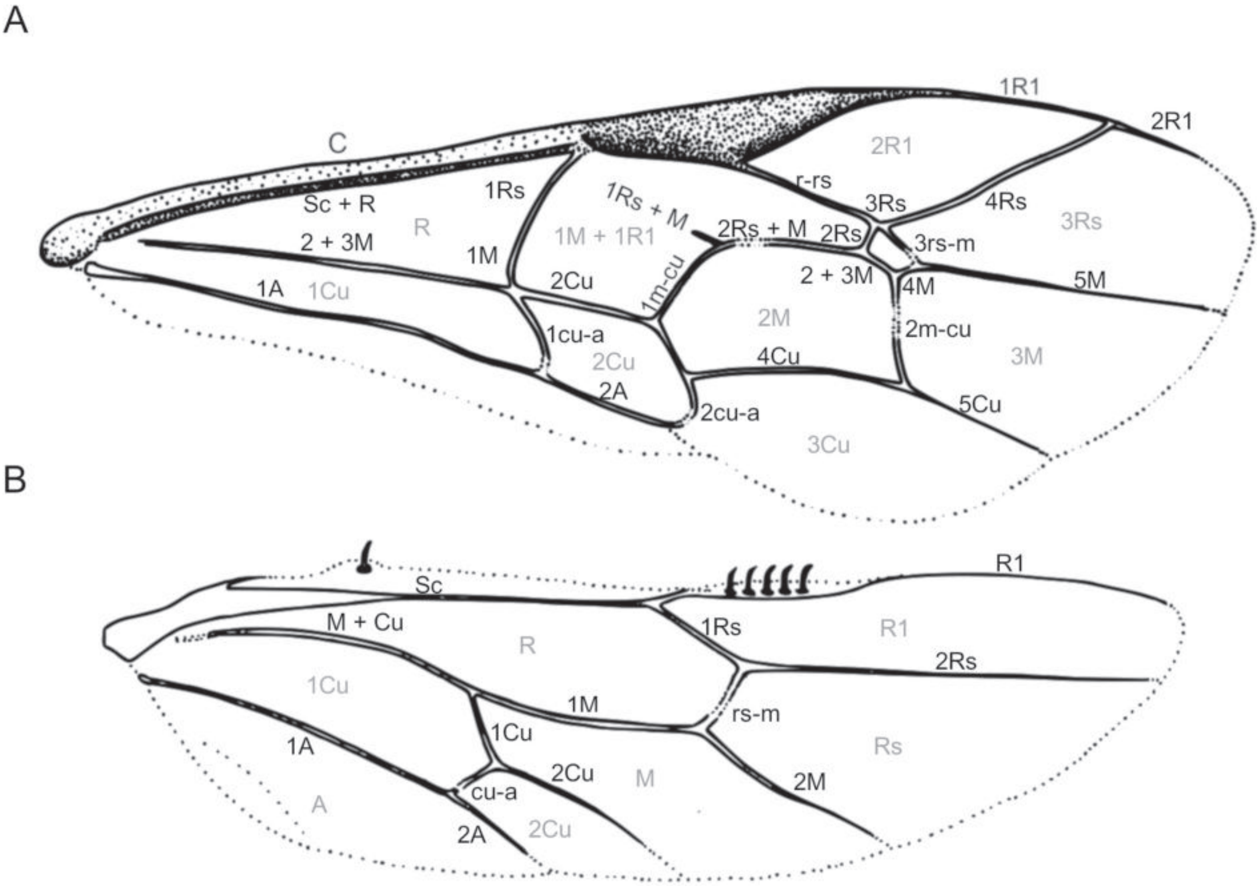

Figure 1. Wing venation nomenclature in ichneumonids. **A.** Fore wing; **B.** Hind wing. The nomenclature follows Spasojevic et al. (2018b). Figure modified after Spasojevic et al. (2018b) and Klopfstein and Spasojevic (2019). Names of wing veins are given in black and of wing cells in grey.

a question mark behind an uncertain generic or subfamily placement (Spasojevic et al. 2018b; Viertler et al. 2022) and, in one case where the subfamily placement could not be established, we labelled the subfamily placement of the fossil as incertae subfamiliae.

Results

We here redescribe 18 fossil species described before 1941. The classification of most species had to be revised, with eleven out of 18 now placed in a different subfamily and twelve in a different genus (Table 1). Considerable uncertainty remains, especially for the less well-preserved fossils. For all but one species, placement in the family Ichneumonidae is unambiguous given the fore wing venation, especially the combined discocubital cell and complete 2m-cu, and the long, multi-segmented antennae. We thus only discuss the evidence for family placement if these characters are not clearly visible. The exception is *Lycorina*? *indura* (Theobald, 1937) comb. nov., for which wing venation is not preserved and family placement is thus ambiguous (for further details, see under that species). The fossil taxa are sorted alphabetically by subfamily and genus in which we have placed them, which in some cases deviates strongly from their original placement.

Acaenitinae? Förster, 1869

Hallocinetus? Viktorov, 1962

Hallocinetus? *arvernus* (Piton, 1940) comb. nov.

Fig. 2

**Phaenolobus arvernus* Piton, 1940

Material. ***Holotype*** (part only, MNHN.F.A57301) examined at MNHN.F.

Stratum. Menat Formation, Puy-de-Dôme, France. Late Palaeocene (Thanetian), 58.7–55.8 Ma.

Description. Sex unknown. Holotype in lateral view, rather poorly preserved, with head, outline of mesosoma and partial metasoma, partial fore wing and outline of hind legs. Body length ~10 mm.

Dark brown including wing venation, legs and posterior part of metasoma lighter brown or reddish.

Head rather large and high, compound eye about 0.7–0.8× head height in lateral view. Antennae incomplete, scape rather short. ***Mesosoma*** rather short, without any details preserved. ***Fore wing*** 7.2 mm; areolet obliquely quadrate and strongly petiolate, 2 + 3M longer than 4M; 1cu-a meeting M + Cu nearly opposite of 1M & 1Rs; 3Cu a bit longer than 2cu-a; cell 2R1 3.2× longer than wide; 2m-cu without bullae in posterior half, potentially with

Table 1. List of fossils treated and summary of taxonomic changes. Eleven subfamily and 12 generic classifications have changed (*Xylonomus* is variously treated as a subgenus or junior synonym of *Xorides* and is thus not included in this count).

New placement				Original placement		Provenance	
Subfamily	**Genus**	**Species**	**Author**	**Subfamily**	**Genus**	**Formation**	**Epoch**
Acaenitinae	*Hallocinetus?*	*arvernus*	(Piton, 1940)	Acaenitinae	*Phaenolobus*	Menat	Late Palaeocene
Cremastinae	*Dimophora?*	*longicornis*	(Theobald, 1937)	Campopleginae	*Nemeritis*	Aix-en-Provence	Late Oligocene
Cremastinae	*Dimophora?*	*wickhami*	(Cockerell, 1919)	Pimplinae	*Theronia*	Florissant	Late Eocene
Metopiinae	*Acerataspis?*	*revelata*	(Brues, 1910)	Pimplinae	*Pimpla*	Florissant	Late Eocene
Metopiinae	*Hypsicera?*	*solidata*	(Brues, 1910)	Orthocentrinae	*Camaratops*	Florissant	Late Eocene
Orthocentrinae	*Orthocentrus*	*defossus*	Brues, 1910	Orthocentrinae	*Orthocentrus*	Florissant	Late Eocene
Orthocentrinae	*Orthocentrus?*	*mortuaria*	(Brues, 1910)	Pimplinae	*Polysphincta*	Florissant	Late Eocene
Phygadeuontinae	*Armadilleon*	*morticinus*	(Brues, 1910)	Pimplinae	*Pimpla*	Florissant	Late Eocene
Phygadeuontinae	*Armadilleon*	*petrorum*	(Brues, 1910)	Pimplinae	*Polysphincta*	Florissant	Late Eocene
Pimplinae	*Lithoserix*	*antiquus*	(Saussure, 1852)	Pimplinae	*Pimpla*	Aix-en-Provence	Late Oligocene
Pimplinae	*Lithoserix*	*williamsi*	Brown, 1986	Pimplinae	*Lithoserix*	Florissant	Late Eocene
Pimplinae?	*Pimpla?*	*seyrigi*	Theobald, 1937	Pimplinae	*Pimpla*	Kleinkembs	Early Oligocene
Pimplinae	*Polysphincta?*	*inundata*	Brues, 1910	Pimplinae	*Polysphincta*	Florissant	Late Eocene
Lycorininae?	*Lycorina?*	*indura*	(Theobald,1937)	Pimplinae	*Pimpla*	Kleinkembs	Early Oligocene
Tryphoninae	*Monoblastus?*	*senilis*	(Brues, 1910)	Pimplinae	*Pimpla*	Florissant	Late Eocene
Tryphoninae	*Zagryphus*	*tilloyi*	(Theobald, 1937)	Diplazontinae	*Promethes*	Aix-en-Provence	Late Oligocene
Xoridinae	*Xorides*	*sejugatus*	(Brues, 1910)	Xoridinae	*Xylonomus*	Florissant	Late Eocene
Ctenopelmatinae	*Parapimpla*	*rhenana*	Theobald,1937	Pimplinae	*Parapimpla*	Kleinkembs	Early Oligocene

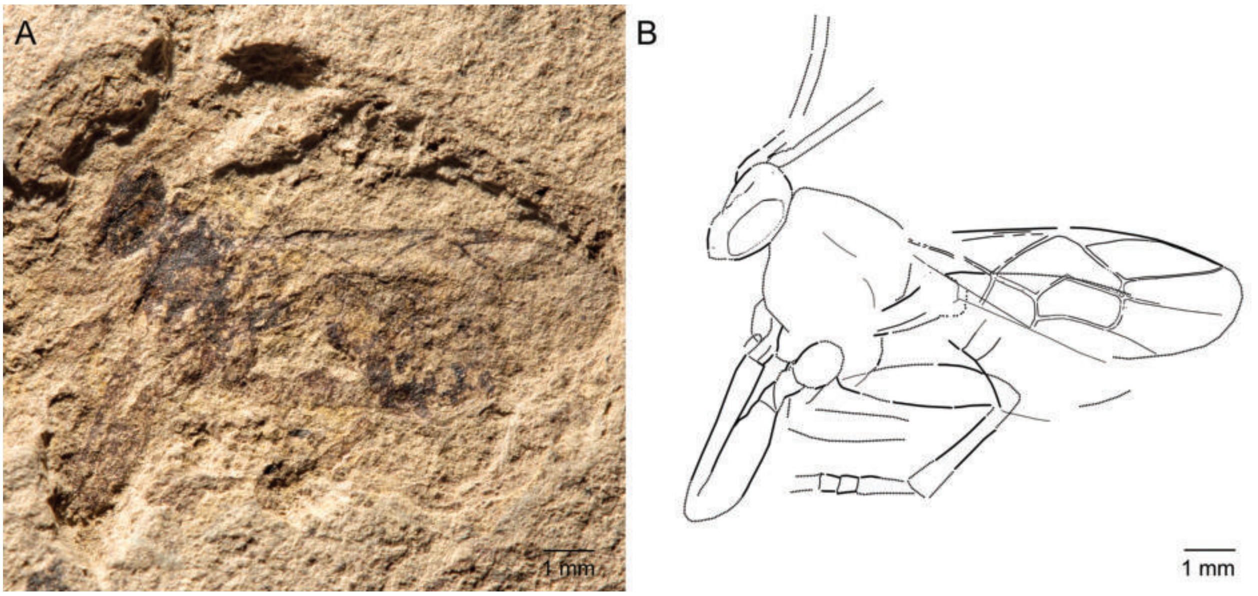

Figure 2. *Hallocinetus*? *arvernus* (Piton, 1940) comb. nov. **A.** Photograph of the holotype obtained from MNHN.F; **B.** Our interpretative drawing of the fossil. Thicker lines indicate outlines of body structures, thinner lines show characters inside these outlines, and dotted lines represent uncertain interpretations.

one or two bullae in anterior half. ***Hind legs*** rather stout; femur 3.5×, tibia 5.2× longer than wide; hind tarsi with first segment much longer than second and third, which are about as long as wide. ***Metasoma*** with T1 elongate, probably with a dorso-lateral carina; sternites rather well sclerotized; tip not well preserved.

Interpretation. This is a rather poorly preserved fossil, from which not many characters can be discerned. Comparing the holotype and its high-resolution photograph with the drawing in the original description (p. 228, fig. 94, Piton 1940), we found that the latter shows a considerable amount of artistic freedom. The antennae are drawn as very short and apically expanded, while they are incomplete and parallel-sided in the fossil. The head shows a beak-like structure not discernible clearly in the fossil and unknown in extant representatives of the subfamily, and the small eyes appear around 0.5× as long as the head length in profile, compared to 0.7–0.8× in the fossil. The areolet is depicted as being open, while we found it to be closed and strongly petiolate in the fossil. The tarsi of the fore and hind legs appear complete with claws present in the drawing, while at most the first tarsal segments are visible in the fossil. The femora of all legs are much thinner in the drawing than in the fossil, and the drawing of the posterior half of the fore wing, which largely overlaps the metasoma, contains veins not found in any ichneumonid wasp. Piton also drew the elongate-triangular hypopygium typical for the subfamily

Acaenitinae; we are more cautious, noting that the apical part of the metasoma is too poorly preserved to draw conclusions about the shape of the hypopygium. Additional characters that could help subfamily placement, such as the shape of T1 and position of its spiracle, the propodeal carination and length of the ovipositor are indiscernible. The general habitus of the fossil, especially the shape of the metasoma in profile and stout legs, does resemble Acaenitinae, but in a rather vague fashion. Other characters are somewhat at odds with this placement, although not completely so. For instance, most Acaenitinae have 2m-cu with two bullae, one in the anterior and one in the posterior half, which would disagree with the fossil; however, some genera in former Acaenitini, such as *Hieroceryx* Tosquinet, 1896 and *Prosacron* Townes, 1971, have both bullae in the anterior half and separated by a very short tubular part of the vein. Moreover, *Phaenolobus* and *Phorotrophus* Saussure, 1892 can in fact have a single bulla, in the former located in the dorsal half of 2m-cu. However, all former Acaenitini have an open areolet, while a closed and petiolate areolet occurs only in the former tribe Coleocentrini, which has turned out paraphyletic with respect to the former Acaenitini (Wahl and Gauld 1998; Quicke et al. 2009; Klopfstein et al. 2019; Spasojevic et al. 2021). The characters for generic placement within the former Coleocentrini, such as the shape of the clypeus, size and shape of the hypopygium and modifications on tarsal claws (Townes 1971) are not visible in the fossil. Since we also have no character evidence for placing the fossil in a different subfamily, we tentatively place it in *Hallocinetus* Viktorov, 1962, to which it superficially resembles in the shape of the anterior margin of the mesoscutum and stout and large hind legs. However, we acknowledge the uncertainty in its placement by placing a question mark after the genus and subfamily names.

Cremastinae Förster, 1869
Dimophora? Förster, 1869

Dimophora? *longicornis* (Theobald, 1937), comb. nov.

Fig. 3

**Nemeritis longicornis* Theobald,1937

Material. ***Holotype*** (part only, MNHN.F.B24398) examined at MNHN.F.

Stratum. Aix-en-Provence, Bouche-du-Rhône, France. Late Oligocene (Chattian), 28.4–23.0 Ma.

Description. Female. Lateral aspect of head, most of both antennae, mesosoma, both fore wings, part of fore and hind legs, and metasoma including ovipositor with sheaths preserved. Body length ~5.3 mm.

Mostly black in colour, with some reddish colouration on metasoma and dark brown to orange-brown legs, wing veins brown.

Head rather short, with eyes not clearly outlined but might be rather prominent. ***Antennae*** with scape and pedicel short, with at least 24 flagellomeres, but tips broken. ***Mesosoma*** not well preserved; mesoscutum conspicuously elongate, notauli probably present, as is epicnemial carina and probably posterior transverse carina of mesosternum; propodeum evenly rounded, carination unclear given bad preservation. ***Fore wings*** 3.1 mm, well preserved; pterostigma broad triangular (3.1×) with light base; areolet closed, quadrate and a bit oblique; cell 2R1 (radial cell) short (2.5×), ending rather distant from tip of the wing; 2m-cu quite short, forming inner angle greater than 90° with 4Cu, with a single broad bulla; 1cu-a meeting M + Cu opposite of 1M & 1Rs; 3Cu shorter than 2cu-a; vein 1M & 1RS a bit bowed; r-rs shorter than 2Cu. ***Legs*** partially preserved; fore coxa, trochanters, base of femur preserved, dark

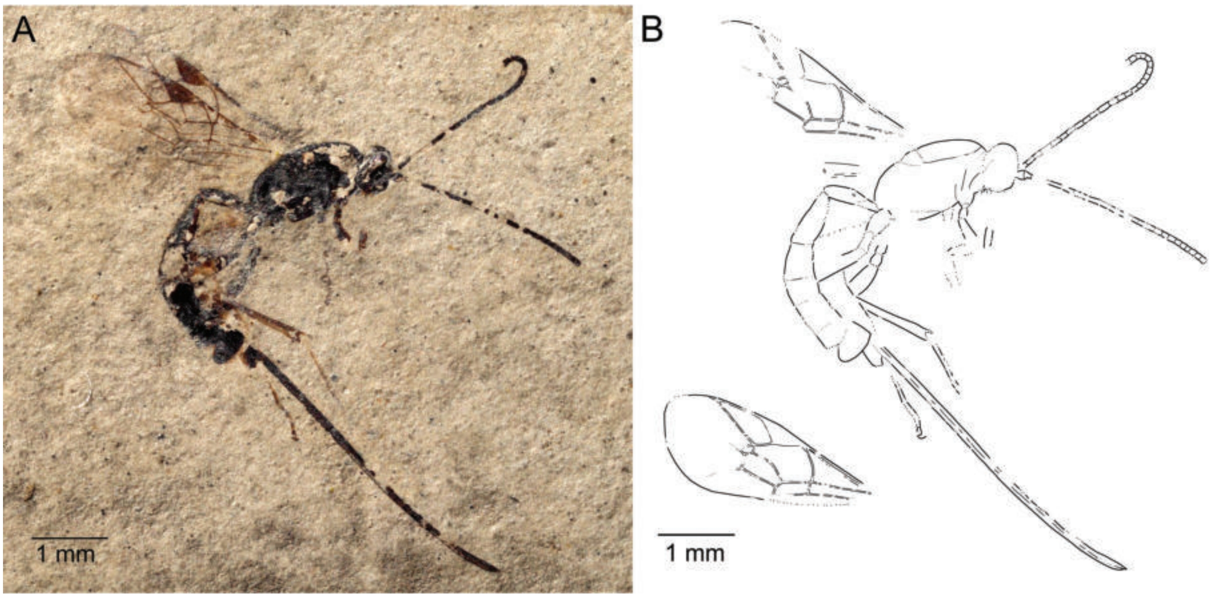

Figure 3. *Dimophora*? *longicornis* (Theobald, 1937) comb. nov. **A.** Photograph obtained from MNHN.F; **B.** Our interpretative drawing of the fossil. Thicker lines indicate outlines of body structures, thinner lines show characters inside these outlines, and dotted lines represent uncertain interpretations.

brown; mid leg weakly indicated; hind legs both partially preserved, including elongate hind coxa; hind femur apparently toothless, dimensions unclear, dark brown or orange (the latter colouration might come from overlaying sternites instead); hind tibia very long and slender (10×), brown on anterior, orange on posterior half, potentially showing a deep emargination at apex indicative of spurs present in membranous area separate from tarsus (unique character for Cremastinae, but interpretation in fossil not unequivocal); tarsi elongate, one partial claw might show pecten, but interpretation rather uncertain. ***Metasoma*** compressed from T3 or T4, mostly black, with reddish colouration on laterotergite 2 and partly on T3 and T4; T1 petiole-shaped, narrow and long (4.7×), probably with glymma, spiracle slightly behind middle; T2 as long as T1, laterotergite might be indicated by red colouration; T3 and following shorter, T7 quite long, not distinctly shorter than T6. Ovipositor preserved with sheaths, very long, 4.4 mm, about 3.3× as long as hind tibia, a bit bowed downwards towards tip.

Interpretation. The reason that we have covered this species, which was originally described in the genus *Nemeritis* (Campopleginae), is a remark by Theobald in the original description (Theobald 1937) that this species could be identical with *Pimpla renevieri* Meunier, 1903, which was later repeated by Menier et al. (2004) when he compiled a list of fossil ichneumonids. Based on this list, Yu and Horstmann (Yu et al. 2012, 2016) catalogued *N. longicornis* as a synonym of *P. renevieri*. We could not cover the latter species because the type could not be located. But we studied the former and concluded that several characters support a placement in the subfamily Cremastinae: the narrow T1 in the shape of a petiole, compressed metasoma, fore wing with a short and wide pterostigma and cell 2R1, 3Cu shorter than 2cu-a, hind tibia very long and slender, ovipositor much longer than metasoma. The first set of characters are also present in Campopleginae, but the broad pterostigma and, to a lesser extent, very long ovipositor point to Cremastinae. Given the large and only slightly oblique areolet, the fossil might belong to the genus *Dimophora*, but crucial characters for generic placement such as the thyridiae are unfortunately not visible. The affinity of the fossil with *Dimophora* was also supported in the recent total-evidence dating analysis (see supplementary file S12 in Spasojevic et al. 2021), which however included only limited sampling of Cremastinae and Campopleginae. We therefore remove it from synonymy with *P. renevieri* and tentatively place it in the genus *Dimophora*.

Cremastinae Förster, 1869
Dimophora? Förster, 1869

Dimophora? *wickhami* (Cockerell, 1919), comb. nov.
Fig. 4

**Theronia wickhami* Cockerell, 1919

Material. Photograph examined of the holotype (part, PALE-3915 and counterpart, #UCM8604), obtained from the MCZ and UCM, respectively.

Stratum. Wilson Ranch, Florissant shales, Colorado, USA. Late Eocene (Chadronian), 37.2–33.9 My.

Description. Female. Rather well-preserved fossil. Part with dorsal and posterior aspect of head, antennae almost complete, mesosoma including propodeum and details of propodeal carination, weak impressions of fore wings with only few veins visible, incomplete hind legs, and dorsal aspect of metasoma with ovipositor and ovipositor sheaths. Counterpart with ventral aspect of head with antennae showing flagellomeres, mesosoma, weakly but almost completely preserved impressions of fore wings, partial mid and almost complete hind legs, and ventral aspect of metasoma with ovipositor sheaths. Body length 8.5 mm.

Dark brown on head, mesosoma and first metasomal segment, lower part of face possibly lighter coloured (but could be artefactual), antennae lighter brown, wing venation very light, legs and metasoma from T2 or T3 orange.

Head with parallel-sided inner eye margins; mandibles with two teeth; clypeal sulcus weakly developed; occipital carina strong and probably complete and evenly rounded dorsally. ***Antennae*** 5.4 mm, with scape a bit longer than wide and pedicel short; with about 31 flagellomeres, these transverse except for most basal ones. ***Mesosoma*** showing deep median sternal groove, probably complete epicnemial and complete posterior transverse carina of mesosternum. Metapleuron with submetapleural carinae shown as two longitudinal lines; propodeum with complete propodeal carination. ***Fore wing*** 5.9 mm, with large and slightly oblique areolet, vein 2m-cu meeting M close to its outer corner (4M very short), number of bullae unclear; 1cu-a meeting M + Cu opposite of 1M and inclivous; 3Cu about as long as 2cu-a; cell 2R1 2.6× longer than wide. ***Legs*** rather slender; hind femur 3.6×, hind tibia 6.2× longer than wide, without ventral tooth. ***Metasoma*** slender, apical segments compressed; T1 petiolate, narrow at base and expanded from about mid-length; S1 reaching to about 0.65 of length of T1, probably with laterotergites parallel and not meeting ventrally at midline; T2 about 2.2× longer than basally wide, with narrow laterotergite visible; following tergites transverse; hypopygium inconspicuous. Ovipositor 1.5 mm, around 1.7× as long as hind tibia, straight, enclosed by sheaths.

Interpretation. The petiolate T1 excludes the subfamily Pimplinae and thus the genus *Theronia*, and the compressed metasoma and complete posterior transverse carina of mesosternum carina point to either Campopleginae or Cremastinae. The clypeus separated from the lower face by a groove and the rather stout fore wing cell 1M+1R1 point to the latter. Within Cremastinae, the large areolet is reminiscent of *Dimophora*, even though it is slightly oblique. A recent revision of the Australian members of the genus (Klopfstein 2016) expanded the generic definition to also include larger representatives, with fore wing lengths of up to 7.1 mm found. As the areolet does not entirely match extant *Dimophora* and characters excluding some other genera in the subfamily are not visible, we tentatively place the fossil in this genus. It can be distinguished from all extant representatives of the genus

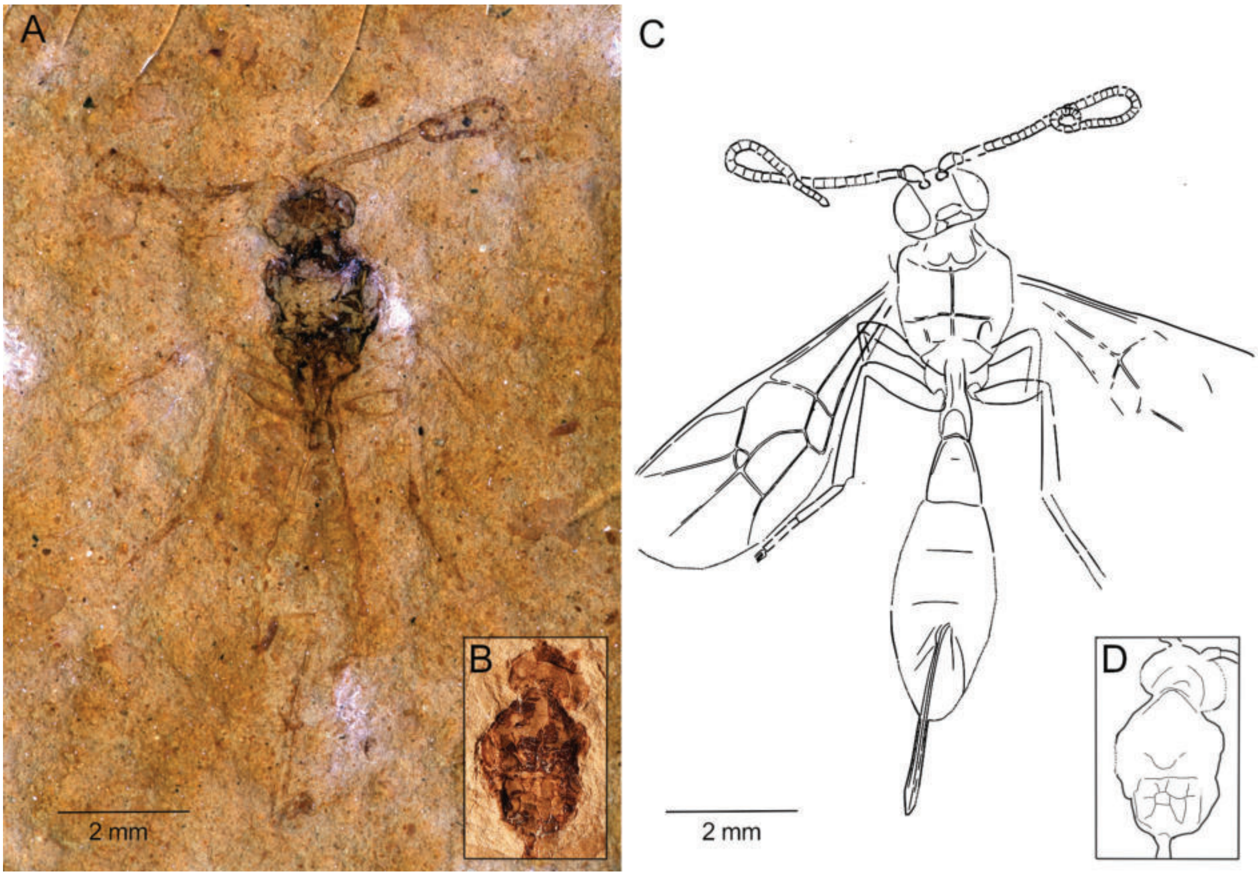

Figure 4. *Dimophora*? *wickhami* (Cockerell, 1919) comb. nov. **A.** Photograph of the counterpart of the holotype obtained from the UCM; **B.** Photograph of the propodeum from the part of the holotype obtained from the MCZ; **C.** Our interpretative drawing of the counterpart; **D.** our interpretative drawing of the propodeum of the part. Thicker lines indicate outlines of body structures, thinner lines show characters inside these outlines, and dotted lines represent uncertain interpretations.

by fore wing vein 2m-cu originating close to the distal end of the areolet, from *D. antiqua* (Brues 1910; also from the Florissant shales) by the larger areolet and less stout fore wing, from *D. fumipennis* (Theobald 1937; Oligocene of Aix-en-Provence) by the hyaline wings and longer ovipositor, and from the here revised *D.*? *longicornis* by the much shorter ovipositor, more slender pterostigma and different coloration.

Metopiinae Förster, 1869
Acerataspis? (Uchida, 1934)

Acerataspis? *revelata* (Brues, 1910), comb. nov.

Fig. 5

**Pimpla revelata* Brues, 1910

Material. Photographs examined of the holotype (#PALE-2158, referred to as #h) and of another specimen (#PALE-2159), which Brues (1910) placed tentatively in the same species, but expressing doubts; obtained from the MCZ.

Stratum. Teller County, Florissant shales, Colorado, USA. Late Eocene (Chadronian), 37.2–33.9 Ma.

Description. Sex unknown in holotype, second specimen is a female; we support the notion that the two specimens belong to the same species and base our description on both of them. Holotype showing ventral aspect; specimen #PALE-2159 in lateral (head and mesosoma) and dorsolateral (metasoma) aspect. Holotype with part of head, base of antennae, mesosoma, fore and most of hind wings, partial hind leg and segments on to partial five of metasoma. Specimen #PALE-2159 with head, almost complete antennae, mesosoma, fore wings, hind legs including tarsi and complete metasoma. Body length 9 mm (#PALE-2159).

Fragments of dark colouration on most of body including T1, T2–T5 with orange or reddish colouration and lighter hind margins.

Head with face apparently protruding (#PALE-2159), eyes smaller than usual in ichneumonids. ***Antennae*** with scape short and ovoid (#h), with more than 30 mostly transverse flagellomeres (#PALE-2159). ***Mesosoma*** rather short, with rather high and short pronotum with strong epomia; mesopleuron with strong but probably interrupted epicnemial carina curving anteriorly at mid height of pronotum (#PALE-2159), complete ventrally and dipping into medial sternal groove (#h); at least mesosternum, mesopleuron and metapleuron covered in strong and very dense punctures (#h). Propodeum with pleural carina complete (#PALE-2159), remaining carination unclear but probably with some portion of apical transverse

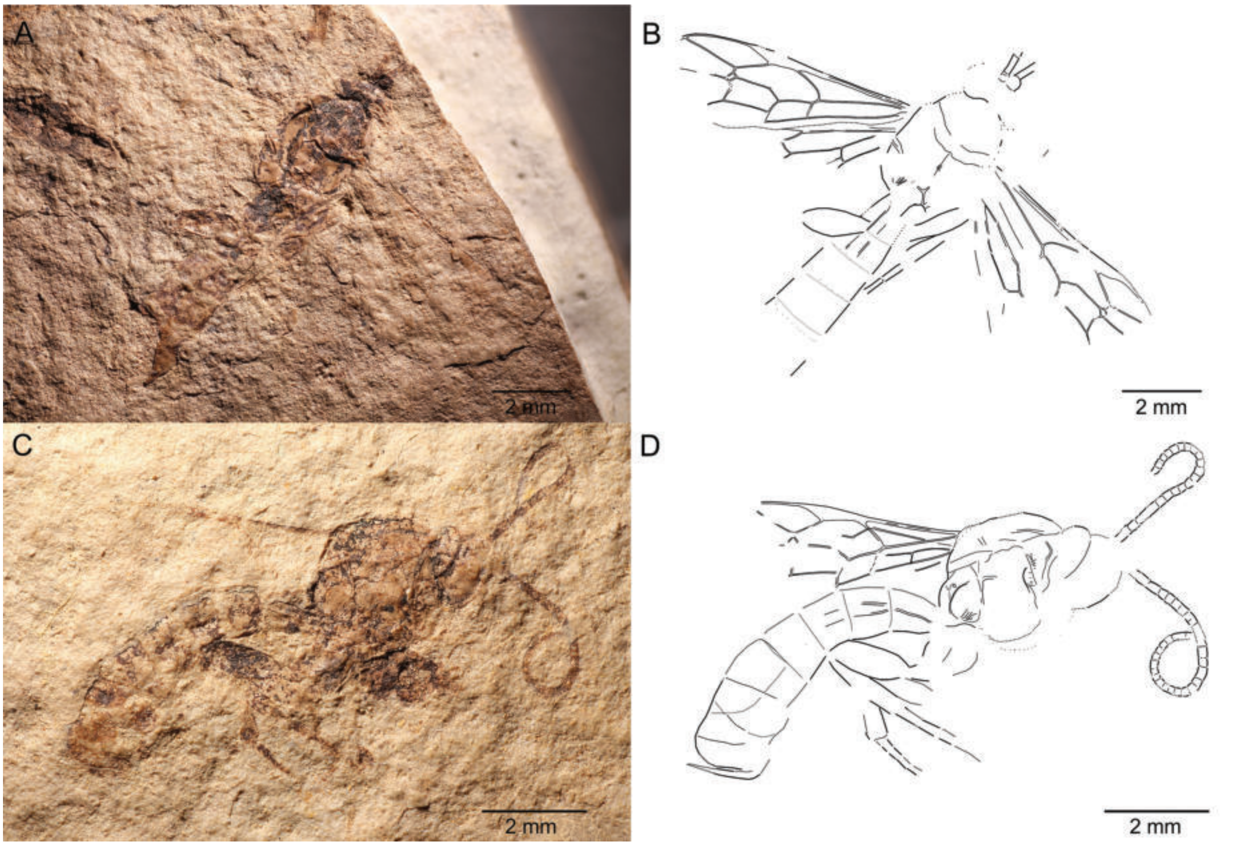

Figure 5. *Acerataspis*? *revelata* (Brues, 1910), comb. nov. **A.** Photograph of the holotype obtained from the MCZ; **B.** Our interpretative drawing of the holotype; **C.** Photograph of the paratype obtained from the MCZ; **D.** Our interpretative drawing of the paratype. Thicker lines indicate outlines of body structures, thinner lines show characters inside these outlines, and dotted lines represent uncertain interpretations.

and lateral longitudinal carina present (#PALE-2159); metapleuron rather high, with several diagonal carinulae starting at lower hind corner of metapleuron (visible in both specimens, in #h on both sides from ventral). ***Fore wing*** 6.4 mm (#PALE-2159 5.0 mm), with areolet oblique-quadrate and strongly petiolate; pterostigma 4.5× longer than wide; cell 2R1 of average proportions (3×); vein 2m-cu with strong curve and one wide bulla anteriorly; 1cu-a meeting M + Cu far distally of 1M; 3Cu a bit longer than 2cu-a; 1M distinctly curved at base. ***Hind wing*** with cell 1Cu rather narrow and with subparallel sides; vein 1Rs a bit longer than rs-m; 1Cu about 1.5 times longer than cu-a. ***Hind legs*** with femur short and thick (#p 2.7×); hind tibia (#p 4.5×) with strong spines on outer side, mostly lightly coloured with dark base and apex (#PALE-2159). ***Metasoma*** rather short and stout; T1–T3 with two subparallel dorsal carinae; last tergites and last sternite enlarged; short ovipositor indicated, probably not much longer than metasoma height at apex (#PALE-2159).

Interpretation. Brues (1910) interpreted the holotype as showing a dorsal aspect, which probably led him to miss some crucial characters. The stout body, protruding face, short flagellomeres, and carinae on T1–T3 place these fossils in the subfamily Metopiinae. The extant genus *Acerataspis* seems a good match in terms of tergite carination, carinulae low on metapleuron and closed areolet, but the latter is much larger in the extant species and the antenna much more elongate; we thus place it in this genus with a question mark.

Metopiinae Förster, 1869
Hypsicera? Latereille, 1829

Hypsicera? *solidata* (Brues, 1910), comb. nov.

Fig. 6

**Camerotops solidatus* Brues, 1910

Material. Photographs of the holotype (part only, #PALE-2239) obtained from the MCZ.

Stratum. Teller County, Florissant shales, Colorado, USA. Late Eocene (Chadronian), 37.2–33.9 Ma.

Description. Female. ***Holotype*** in ventro-lateral view, with nearly complete antennae, outline of head, details of mesosoma, one fore wing, partial fore and mid and nearly complete hind legs, and metasoma with ovipositor sheaths. Body length 6.1 mm.

Black or dark brown on head, mesosoma and T1, dark brown on antennae, red on hind legs and T2 until end of metasoma, orange on fore and mid legs; wing venation very light.

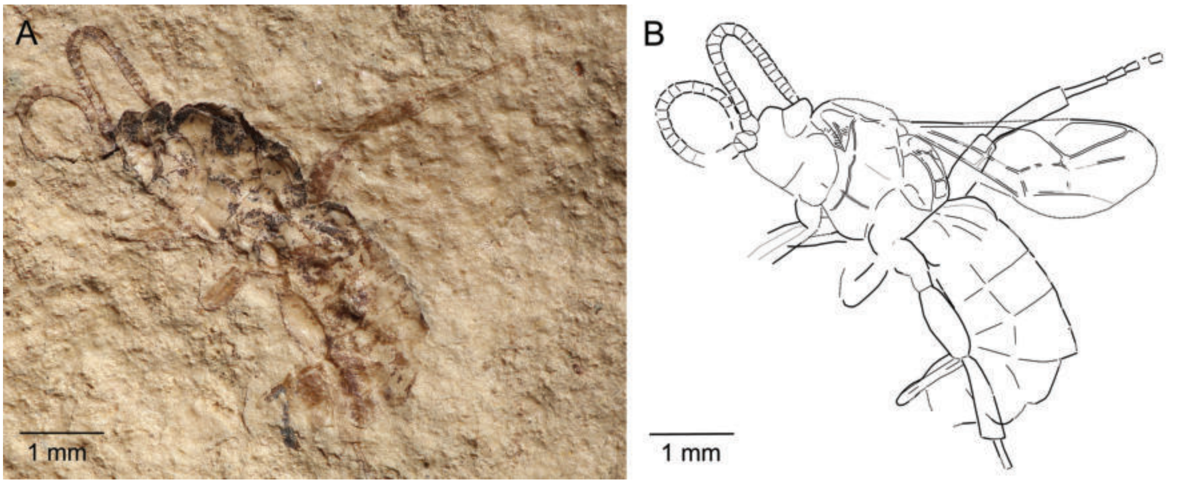

Figure 6. *Hypsicera*? *solidata* (Brues, 1910) comb. nov. **A.** Photograph of the holotype obtained from the MCZ; **B.** Our interpretative drawing of the fossil. Thicker lines indicate outlines of body structures, thinner lines show characters inside these outlines, and dotted lines represent uncertain interpretations.

Head with face bulging, eye rather small (if interpreted correctly). ***Antennae*** stout, with about 23 flagellomeres; scape about 1.1× as long as wide; first flagellar segments subquadrate, following transverse. ***Mesosoma*** short and compact; pronotum with long epomia and parallel wrinkles; mesopleuron with epicnemial carina strong and reaching at least to half the height of the pronotum, probably more; with deep mesosternal scrobe and possibly indication of sternaulus (which could be an artefact), and with very closely spaced, parallel wrinkles on most of its surface. Metapleuron large, higher than wide; propodeum rather short, with pleural, lateral longitudinal, and a low-sitting posterior and probably also anterior transverse carina complete, delimiting areas; median longitudinal carina unclear. ***Fore wing*** 3.0 mm, with areolet probably open; 1cu-a meeting 2Cu at same position as 1M; cell 2R1 short (2.1×). ***Legs*** very stout, hind femur 2.5× and hind tibia 3.7× as long as wide. ***Metasoma*** short, with both strongly sclerotized tergites and at least partial sternites; T1 about 1.6× longer than wide, expanding towards apex, with distinct longitudinal lines which probably represent the median dorsal and dorsolateral carinae; T2 and following transverse; T6 and T7 of about same length as previous ones. ***Ovipositor*** short, around 1 mm long, and around as long as hind tibia, internal portion longer than sheaths.

Interpretation. The bulging face, long malar space, short flagellar segments and thickened legs indicate either Metopiinae or the *Orthocentrus* genus-group of Orthocentrinae. Brues (Brues 1910) placed the specimen in the latter, but the short scape and the presence of a clear epomia and costula clearly point to the former. Brues also stated that the “abdomen flaked off in the specimen” and did not make a decision about the sex; we note that the ovipositor sheaths are clearly visible, even though its base is crossed by a hind leg. Within Metopiinae, the placement is more difficult, but *Hypsicera* and *Exochus* Gravenhorst, 1829 seem a good match given the similarity of the propodeal carination, bow in 1M of the fore wing and long T7. If we interpreted the head correctly, the small eyes and the bulging of the face closer to the antennal sockets correspond more to *Hypsicera*. However, the longer and stouter ovipositor sheaths indicate *Exochus*, while the fore wing venation is typical for *Exochus* and only rarely seen in *Hypsicera*. Thus, even though we place the fossil in *Hypsicera*, this placement should be seen as preliminary with *Exochus* as a valid alternative.

Orthocentrinae Förster, 1869

Orthocentrus Gravenhorst, 1829

**Orthocentrus defossus* Brues, 1910

Fig. 7

Material. Photographs of the holotype (part only, #2238) obtained from the MCZ.

Stratum. Teller County, Florissant shales, Colorado, USA. Late Eocene (Chadronian), 37.2–33.9 Ma.

Description. Probably female. Holotype in ventro-lateral view with metasoma bent under the body, with nearly complete antennae, head, mesosoma, both fore and one hind wing and nearly complete hind legs. Overlapping metasoma, legs and fore wing make interpretation partially difficult. Hairs on wings and hind legs very well preserved. Body length 8.2 mm.

Black or dark brown on head, mesosoma and T1; dark brown on antennae, base of hind coxa, hind femur and outer side of hind tibia, red on remainder of hind legs and T2 until end of metasoma; wing venation dark brown to orange.

Head with face bulging, eye rather small, malar space very long and with a deep groove. ***Antennae*** stout, with at least 20 flagellomeres, scape elongate, 1.8× as long as wide. ***Mesosoma*** short and stout; pronotum with a short lower part of epomia and parallel wrinkles posteriorly, which are mirrored on mesopleuron; epicnemial carina might be present ventrally (or this is the impression of a fore coxa). Metapleuron rather high, with what seems like

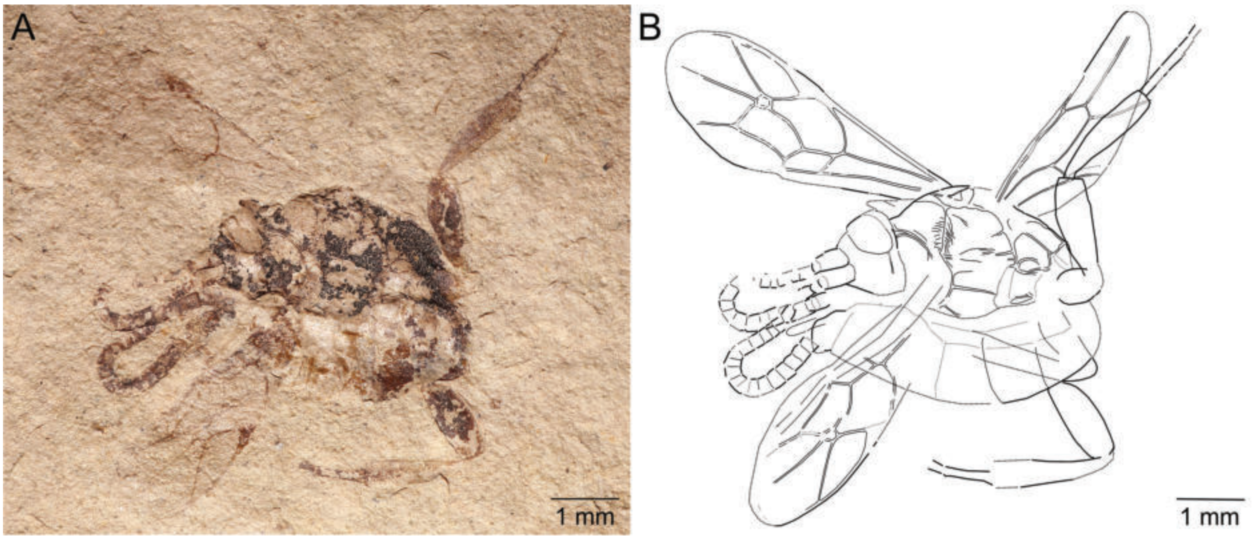

Figure 7. *Orthocentrus defossus* (Brues, 1910) **A.** Photograph of the holotype obtained from the MCZ; **B.** Our interpretative drawing of the fossil. Thicker lines indicate outlines of body structures, thinner lines show characters inside these outlines, and dotted lines represent uncertain interpretations

strong juxacoxal carina visible on both sides; propodeum with pleural and a low apical transvers carina visible, remainder unclear. ***Wings*** evenly hairy, fore wing 4.5 mm, with areolet rather large and pentagonal, receiving 2m-cu close to its outer corner, 4M thus very short; 1cu-a meeting 2Cu distinctly after 1M; 3Cu a little shorter than 2cu-a; cell 2R short and stout (2.6×). Hind wing with 1Cu almost 4× longer than 1cu-a, 2Cu rather weak, 1Rs somewhat longer than rs-m. Hind ***legs*** rather stout, femur 2.5× and tibia 4.5× longer than wide. ***Metasoma*** poorly preserved, but last segments seemingly compressed and tergites transversal. ***Ovipositor*** sheaths about as long as height of tip of metasoma.

Interpretation. We agree with the original placement of this species. Despite the difficulties in interpreting the ventral part of the mesosoma and the metasoma, the characters visible on the head and wings allow confidence in placing this species in the *Orthocentrus* genus-group of Orthocentrinae. Character evidence for this placement are the bulging face, long malar space, and shortened antennae with an elongate scape. Within the group, only *Orthocentrus* contains species with such a large, pentagonal areolet, and the malar groove and 1cu-a meeting 2Cu distinctly after 1M are a further good match with this genus.

Orthocentrinae Förster, 1869
Orthocentrus? Gravenhorst, 1829

Orthocentrus? *mortuaria* Brues, 1910, comb. nov.

Fig. 8

**Polysphincta mortuaria* Brues, 1910

Material. Photographs of the holotype (part, #PALE-2134) obtained from the MCZ.

Stratum. Teller County, Florissant shales, Colorado, USA. Late Eocene (Chadronian), 37.2–33.9 Ma.

Description. Female. *Holotype* in lateral view, with head and a few segments of antennae, mesosoma, fore

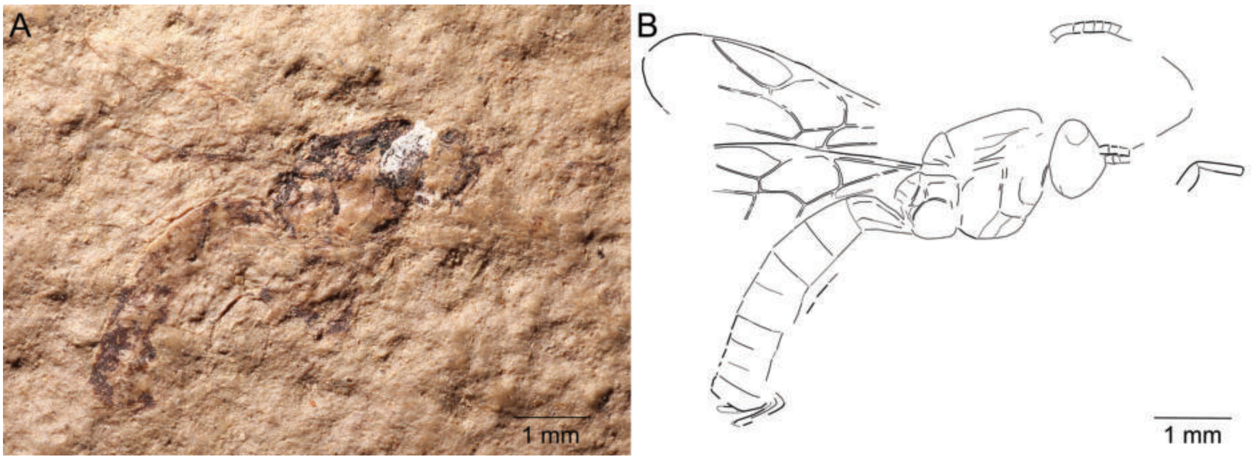

Figure 8. *Orthocentrus*? *mortuaria* (Brues, 1910) comb. nov. **A.** Photograph of the holotype obtained from the MCZ; **B.** Our interpretative drawing of the fossil. Thicker lines indicate outlines of body structures, thinner lines show characters inside these outlines, and dotted lines represent uncertain interpretations.

wings, and metasoma with ovipositor, all rather poorly preserved; legs and hind wings missing. Body length 6.3 mm.

Head light brown, mesosoma black with light brown portions, metasoma mostly light brown on T1–T3, remainder dark brown (the light brown colouration could actually be a preservation artefact: it shows different sculpture and its texture is repeated on the rock outside the body).

Head with face bulging below antennal sockets, with eye very small, with very long malar space. ***Antennae*** more than 3.9 mm, incompletely preserved. ***Mesosoma*** rather short, poorly preserved, unclear if with epicnemial carina. Propodeum with pleural carina and lateral longitudinal carina, maybe also with posterior transverse carina. ***Fore wing*** 4.1 mm, rather short and stout, with areolet open and vein 2Rs longer than 3M; vein 1cu-a strongly inclivous meeting M + Cu clearly distally of 1M; cell 2R1 only 2.9× longer than wide. ***Metasoma*** compressed from about fourth segment; T1 short and tapering towards base, with latero-median carinae converging on basal half, parallel on apical half; T2 and following tergites transverse. Ovipositor 0.5 mm.

Interpretation. The bulging face with small eyes and long malar space are only found in Metopiinae and Orthocentrinae, and wing venation and ovipositor shape point to the latter. Given the size, 1cu-a meeting M + Cu clearly distally of 1M, and possible presence of the lateral portion of the epicnemial carina, *Orthocentrus* is the best guess, but the poor preservation of the fossil precludes a certain placement.

Phygadeuontinae Förster, 1869 (*sensu* Santos (2017)

Armadilleon gen. nov.

http://zoobank.org/63B3D98F-89CF-4CAE-B2EE-3AE254F5649E

Type species. *Armadilleon morticinus* (Brues 1910).

Etymology. This genus is named after the heavily armoured armadillo due to its unique, heavy sculpture.

Diagnosis. The placement within the subfamily Phygadeountinae is evident from the strong and long sternaulus, which posteriorly ends above the mid-height of the hind coxa, the probably pentagonal areolet, T1 in the shape of a petiole, and the ovipositor clearly protruding from the metasomal apex and without a dorsal subapical notch. In strong and wavy structure on the mesosoma, *Armadilleon* resembles several described phygadeuontine genera, such as *Astomaspis* Föster, 1869 and *Bentyra* Cameron, 1905 from the subtribe Chiroticina, *Diaglyptidea* Viereck, 1913 and *Acrolyta* Förster, 1869 from Acrolytina, and *Brachypimpla*, Strobl 1902 from the subtribe Mastrina; it also resembles some undescribed tropical phygadeuontines with similar sculpture (Mabel Alvarado pers. comm.). In the fore wing venation, propodeal carination, clypeus shape in the profile and shape of the ovipositor, *Armadilleon* is very similar to *Brachypimpla*, but it differs from it in the more extensive longitudinal striate sculpture on the mesosoma that is additionally present on the mesoscutum, anterior half of the propodeum and gena, absent notauli and lack of ramulus in the fore wing, stouter legs, and the flatter T1 in the profile. In addition, *Armadilleon* has longer metasoma as the posterior tergites are exposed, while they are retracted below each other in *Brachypimpla*. However, our interpretation of the metasoma should be regarded with caution, as the tergites might have been pushed out and distributed evenly during the preservation process.

Description. ***Head*** above and possibly on front with conspicuous, nubby sculpture. ***Mesosoma*** with mesoscutum with strong and dense punctures, which fuse into parallel carinae towards the posterior end; mesopleuron and propodeum nearly completely covered with strong striae forming wavy patterns; sternaulus on mesopleuron strong, reaching almost to its end. Propodeum with strong carinae enclosing area petiolaris, areal lateralis, area basalis, and at least first and second lateral areas. ***Fore wing*** areolet pentagonal. ***Metasoma*** with T1 broad at apex and strongly tapering towards the narrow base, humped around middle and thus forming a petiole and postpetiole. ***Ovipositor*** clearly protruding from metasoma by about the length of the hind tibia, without a dorsal notch.

Circumscription. *Armadilleon* includes *A. morticinus* and *A. petrorum*, both from the Oligocene Florissant formation.

Armadilleon morticinus (Brues, 1910), comb. nov.

Fig. 9

**Pimpla morticina* Brues, 1910

Material. Photographs examined of the holotype (#PALE-2156) and paratype (#PALE-2157) females (parts only), obtained from the MCZ.

Stratum. Teller County, Florissant shales, Colorado, USA. Late Eocene (Chadronian), 37.2–33.9 Ma.

Description. ***Holotype*** and ***paratype*** (both females) very well preserved, including carination and sculpture of mesosoma, with fore wings, partial hind wings, some almost complete legs and ovipositor including sheaths. Both holotype and paratype with remains of dark colouration on most body parts, but overall, colouration not well preserved; metasoma possibly orange or red from T2 (#p, somewhat uncertain). Body length 10.4 mm (#p 10.1 mm).

Head short, only partly preserved, one lateral ocellus and strong sculpture on frons visible (#h). ***Antennae*** rather stout, scape about 1.6 times longer than wide, pedicel short, about 24 flagellomeres, basal ones subquadrate, becoming quadrate and transverse towards apex (#h). ***Mesosoma*** strongly sculptured; pronotum about 0.7× as long as high, with longitudinal rugae and with epomia strong, angled forward above; mesoscutum with strong punctures, in posterior half increasingly arranged in longitudinal lines; notauli absent; scutellum and postscutellum slightly convex; mesopleuron with very strong

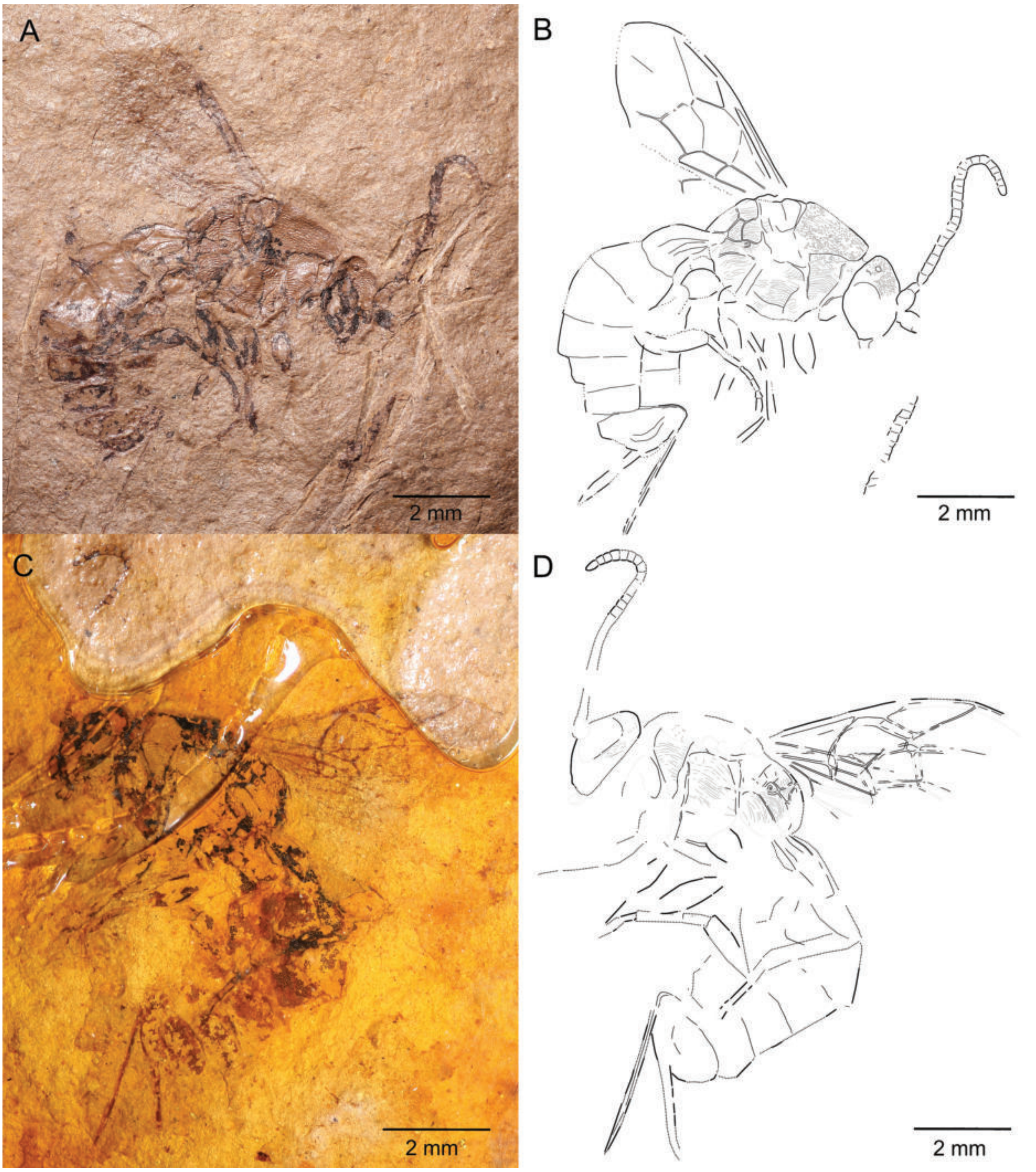

Figure 9. *Armadilleon morticinus* (Brues, 1910) comb. nov. **A.** Photograph of the holotype obtained from the MCZ; **B.** Our interpretative drawing of the holotype; **C.** Photograph of the paratype obtained from the MCZ; **D.** Our interpretative drawing of the paratype. Thicker black lines indicate outlines of body structures, thinner lines show characters inside these outlines, and dotted lines represent uncertain interpretations. Grey lines and circles show conspicuous sculpture of the cuticle.

and conspicuous longitudinal carinae forming wave-like patterns; sternaulus strong and reaching posterior end in sinusoid curve; epicnemial carina long and curving towards front end of mesopleuron at around mid-height of pronotum. Propodeum with all three lateral, three pleural and petiolar areas enclosed by carinae, basal area and areola fused (or basal area very short); pleural carina complete; propodeal spiracle slightly elliptic; propodeum covered by strong rugae forming wavy patterns, unpunctured. ***Fore wing*** 5.2 mm (#p 5.3 mm), venation only partially preserved, brown or dark brown; areolet probably closed and pentagonal (cf. #p); 1cu-a meeting M + Cu opposite of 1M; 3Cu a bit longer than 2cu-a; hind wing reconstruction difficult. ***Legs*** rather stout, hind leg with

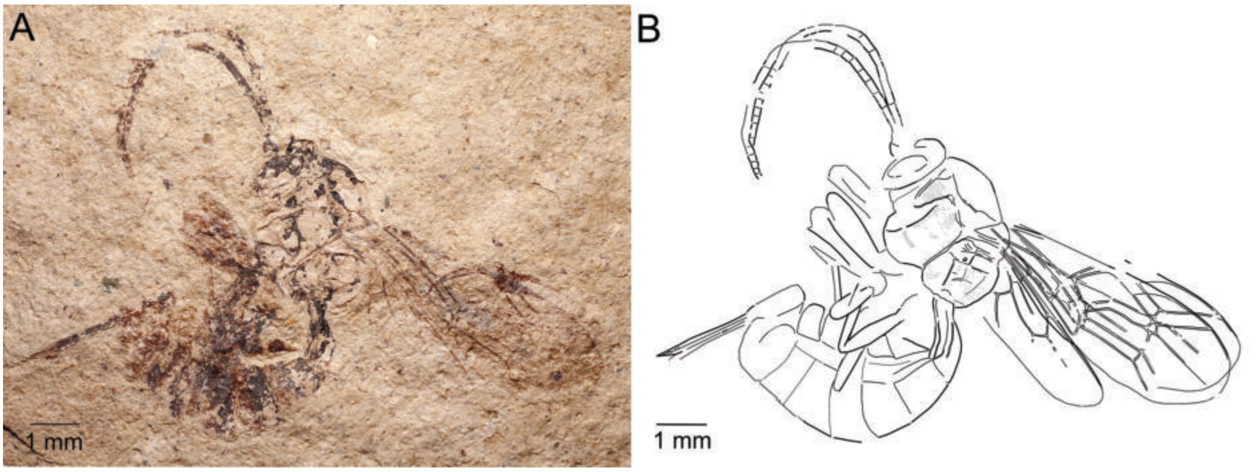

Figure 10. *Armadilleon petrorum* (Brues, 1910) comb. nov. **A.** Photograph of the holotype obtained from the MCZ; **B.** Our interpretative drawing of the fossil. Thicker black lines indicate outlines of body structures, thinner lines show characters inside these outlines, and dotted lines represent uncertain interpretations. Grey lines and circles show conspicuous sculpture of the cuticle.

femur less than 3× longer than wide. ***Metasoma*** dorsoventrally depressed or with apical segments somewhat compressed; T1 broad posteriorly, but strongly narrowed towards base, forming petiole, 1.6× as long as apically wide; latero-median and dorso-lateral carinae present on entire length; T2 and following transverse; T7 not much shorter than T6. ***Ovipositor*** 2.8 mm (#p 3.2 mm); ovipositor sheaths about 1.6 mm (#p 1.7 mm), as long as hind tibia; ovipositor straight, parallel-sided, without dorsal subapical notch, with weak nodus and potentially some ridges apically on lower valve (#p).

Interpretation. For subfamily placement and genus diagnosis, see description of the genus above. For distinguishing features from the other species in the genus, *A. petrorum*, see under that species.

Armadilleon petrorum (Brues, 1910), comb. nov.

Fig. 10

**Polysphincta petrorum* Brues, 1910

Material. Photographs of the holotype (part, #PALE-2136) obtained from the MCZ.

Stratum. Teller County, Florissant shales, Colorado, USA. Late Eocene (Chadronian), 37.2–33.9 Ma.

Description. Female. ***Holotype*** in lateral view with nearly complete antennae, partial head, mesosoma detailing sculpture, both fore and hind wings, at least parts of all legs, and metasoma with ovipositor with sheaths. Body length 9.2 mm.

Mostly black, antennae and wing venation dark brown, T2 and following with broad, reddish apical bands, legs orange to dark brown.

Head very short, eyes of normal dimensions. ***Antennae*** 6.6 mm, with at least 24 (probably about 32) flagellomeres, basal segments elongate, apical segments transverse. ***Mesosoma*** with strong sculpture; pronotum with epomia strong and with numerous longitudinal wrinkles especially along hind margin which continue on mesopleuron; epicnemial carina complete to about mid-height of pronotum; sternaulus long and strong, with transverse carinulae; sculpture of mesopleuron dominated by longitudinal carinulae on much of its surface. Metanotum rather short and high, with some carinulae visible on lower part. Propodeum with pleural carina, indications of lateral and lateromedian longitudinal carinae, anterior transverse and at least lateral portions of posterior transverse carinae, with rugulo-punctate sculpture between the carinae. ***Wings*** evenly and densely hairy; fore wing 5.8 mm, with pentagonal areolet; 2m-cu probably with a single bulla; 1cu-a meeting M + Cu opposite of 1M; cell 2R1 3.0× longer than wide. Hind wing with 1Rs longer than rs-m and 1Cu longer than Cu-a; M + Cu probably strongly curved in apical half. ***Legs*** somewhat hard to tease apart, but of rather average dimensions; hind femur 4.5× longer than wide. ***Metasom*a** seems somewhat compressed towards apex; T1 clearly elongate and petiolate, with strong lateral and dorsolateral carinae, remaining tergites transverse; sternites rather strongly sclerotized; hypopygium short and inconspicuous. Ovipositor 2.2 mm, 0.4× as long as metasoma, straight and parallel-sided, its ventral valve with indications of oblique ridges close to apex, without dorsal subapical notch.

Interpretation. The conspicuous sculpture visible on the propleuron, mesoscutum, mesopleuron and propodeum, together with the subfamily characteristics (strong sternaulus, petiolate T1 and pentagonal areolet), firmly place this species in the new genus *Armadilleon*. Additional similar features between the current and the type species of the genus, *A. morticinus*, include the short head, carination of propodeum, and ovipositor length and shape. The two species differ by the shape of the antennae, which are much stouter in *A. morticinus*, the different colouration of the metasomal tergites, and fore wing vein 1cu-a meeting M + Cu somewhat distally of 1M in the type species and opposite of 1M in *A. petrorum*.

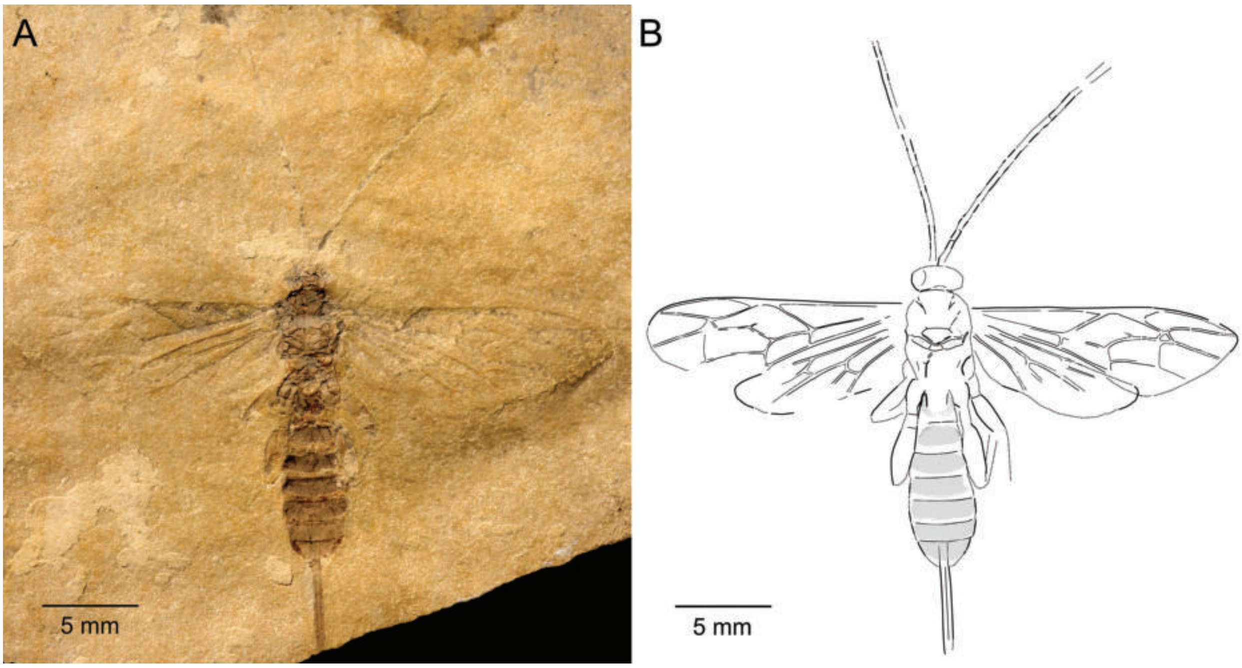

Figure 11. *Lithoserix antiquus* (Saussure, 1852) comb. nov. **A.** Photograph of the holotype obtained from MNHN.F; **B.** Our interpretative drawing of the fossil. Thicker lines indicate outlines of body structures, thinner lines show characters inside these outlines, dotted lines represent uncertain interpretations and grey surface indicates sculpture of the cuticle. Grey areas show conspicuous sculpture of the cuticle.

Pimplinae Wesmael, 1845
Lithoserix Brown, 1986

Lithoserix antiquus (Saussure, 1852), comb. nov.

Fig. 11

**Pimpla antiqua* Saussure, 1852
(*Pimpla antiquus* Saussure according to Theobald, 1937)

Material. Specimen databased as ‘holotype’ (part and counterpart, Am 21 / #MNHN.F.B24391-1 and Am 21 2 / #MNHN.F.B24391-2) examined (but see notes under Interpretation) at MNHN.F, from where its photographs were also obtained.

Stratum. Aix-en-Provence, Bouche-du-Rhône, France. Late Oligocene (Chattian), 28.4–23.0 Ma.

Description. Female. Part showing dorsal view with almost complete antennae, partial head, mesosoma with both fore and hind wings, partial mid and hind legs, and metasoma including detailed sculpture and ovipositor sheaths except tip. Counterpart with negative impression of wings, ventral aspect of mesosoma, while metasoma shows a mix of a ventral aspect and what we interpreted as the inner sides of the tergites, where the sternites were weakly sclerotized, ovipositor sheaths complete. Body length 15.2 mm.

Brown, wing veins dark brown where colour is preserved, legs and hind margins of tergites orange.

Head only partially preserved, rather short; ***Antennae*** at least 13.7 mm, segment boundaries not discernible. ***Mesosoma*** preservation patchy; notauli present on about basal third; scutellum rather short, might be bounded by carinae; axilliary trough with transverse wrinkles; metanotum short. Propodeum with pleural carina and at least lateral longitudinal carinae complete, anterior transverse carinae probably present, remainder unclear. ***Fore wing*** 13.9 mm, with areolet almost triangular with outer vein longer than inner vein, 4Rs a little bowed at base and apex; 1cu-a meeting M + Cu opposite of 1M, 3Cu about as long as 2cu-a; ramulus longer than twice the width of the surrounding veins; cell 2R1 4.6× longer than wide. Hind wing with 1Rs longer than rs-m and 1Cu clearly shorter than cu-a. ***Legs*** rather stout, hind femur 3.5× longer than wide. ***Metasoma*** with T1 quadrate, only slightly narrowed towards base, with dorsal longitudinal carinae distinct on basal half and far away from each other, with parallel carinulae and some punctures along outer margins and towards lateromedian transverse impressions in posterior half; T2–T7 transverse, with a band along hind margin smooth, remainder strongly and densely punctate; T2 with oblique grooves cutting off anterolateral corners, maybe with thyridiae sunken. Ovipositor 4.7 mm, 0.5× as long as metasoma, straight and parallel sided, rather robust.

Interpretation. The specimen covered here was described by Theobald (1937), who stated that it was close but not identical to the holotype described by Saussure (1852), and that he could not find the latter. The drawing in the original description (plate 23, fig. 5 in Saussure 1852) indeed shows a different outline of the rock where the fossil is placed in, and Theobald mentions several differences especially in the wing venation. However, there are multiple lines of evidence that the present specimen might indeed represent the holotype, most of all the remarkable similarity of the positioning of the body of the specimen, including the exact angle between the antennae and positions of the legs. We thus suspect that this is indeed the holotype of *P. antiqua*, and that either Saussure took the artistic liberty to draw a more generous outline of the rock, or it was trimmed to a smaller size later on.

The species was transferred to Braconidae by Aubert (1967) without any comment, and thus listed as "Species incertae sedis", in the world catalogue (Yu et al. 2012). It clearly belongs to the family Ichneumonidae, given the venation in fore and hind wings, and to the subfamily Pimplinae given the triangular areolet, hind wing 1Cu shorter than cu-a, quadrate T1, long ovipositor, and sculpture of the metasoma. The carinae on the propodeum, long ramulus and broad smooth bands apically on the tergites preclude a placement in the genus *Pimpla* as it is defined today (Gauld et al. 2002). However, in all the afore-mentioned characters, it is very similar to the only species placed in the Eocene genus *Lithoserix* Brown, *L. williamsi* (Brown 1986) from the Florissant formation. We thus transfer it to this genus; see there for details on the differences to other genera. *Lithoserix antiquus* can be distinguished from *L. williamsi* by the much shorter ovipositor, shorter mesoscutum and the dorsal carinae on T1 extending to less than the mid-length of the tergite.

Pimplinae Wesmael, 1845
Lithoserix Brown, 1986

**Lithoserix williamsi* Brown, 1986

Fig. 12

Material. Photograph examined of the holotype (part, #UCM31179), obtained from the UCM.

Stratum. Old Scudder Pit, Florissant shales, Colorado, USA. Late Eocene (Chadronian), 37.2–33.9 My.

Description. Female. Part showing dorsal view including partially preserved antennae, partial head, mesosoma preservation rather patchy, with right fore wing partial and complete left fore and hind wings, partial mid and hind legs, and metasoma including ovipositor sheaths and ovipositor except tip. Body length 22 mm.

Brown, wing veins dark brown where colour is preserved, femora and posterior half of tergites darker brown, posterior half of tergites possibly darker than anterior.

Head, with complete occipital carina straight to evenly rounded or slightly dipped medially. ***Antennae*** at least 14 mm long, first few segments probably short, only slightly longer than wide. ***Mesosoma*** with notauli strongly impressed, converging and extending past half of mesoscutum; scutellum borders unclear, might be displaced posteriorly and visible as small triangular structure or

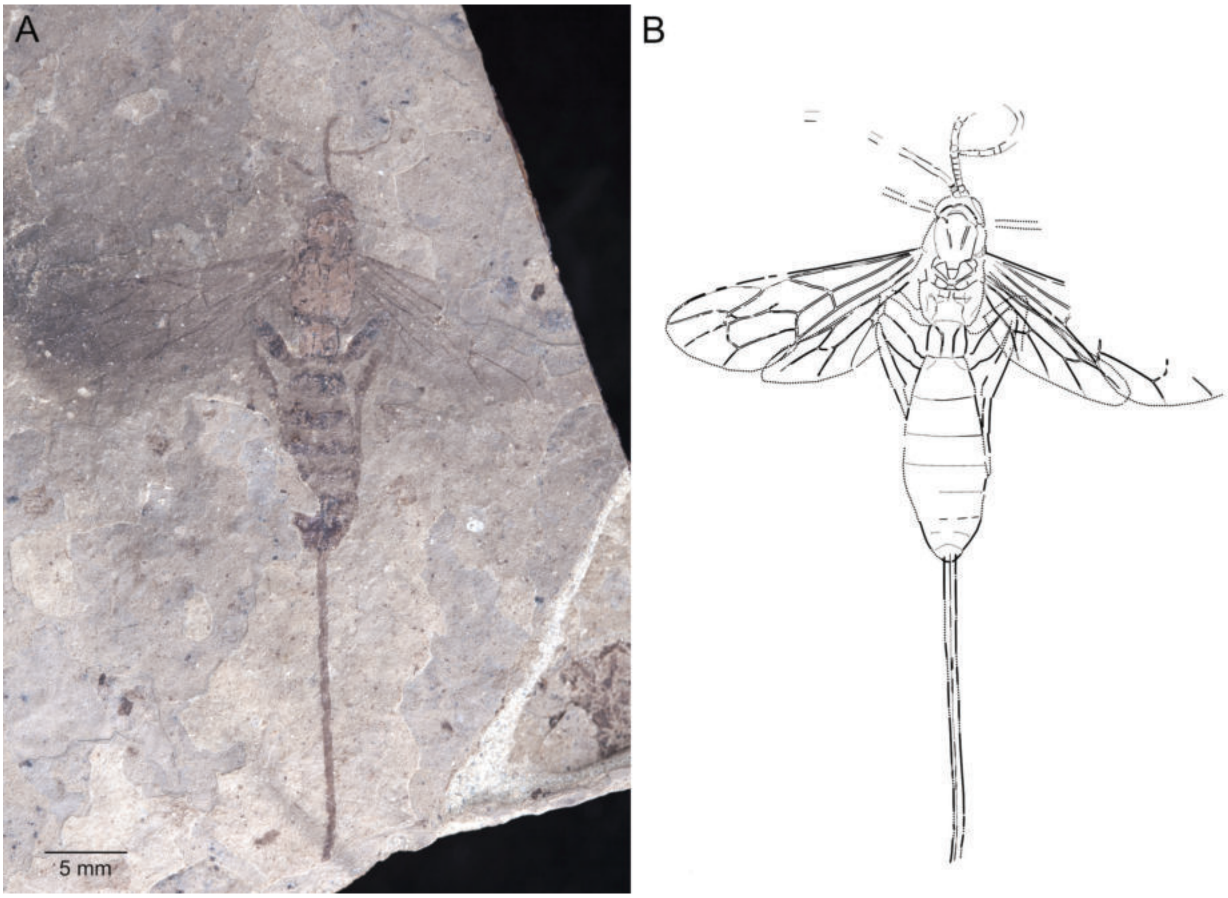

Figure 12. *Lithoserix williamsi* (Brown, 1986) comb. nov. **A.** Photograph of the holotype obtained from the UCM; **B.** Our interpretative drawing of the fossil. Thicker lines indicate outlines of body structures, thinner lines show characters inside these outlines, and dotted lines represent uncertain interpretations.

larger and broken around middle; metanotum visible, of regular size. Propodeum with carinae difficult to interpret, but at least with complete lateral longitudinal carinae, anterior portion of median longitudinal carinae, anterior transverse carina and some indication of pleural carinae; spiracle small and oval. ***Fore wing*** 16.5 mm, with areolet almost triangular, 2 + 3M longer than 4M; 4Rs clearly bowed at base; 1cu-a meeting M + Cu opposite of 1M, 3Cu slightly longer than 2cu-a; ramulus longer than twice the width of the surrounding veins; cell 2R1 4.3× longer than wide. Hind wing with 1Rs longer than rs-m and 1Cu clearly shorter than cu-a. ***Legs*** rather stout, hind femur around 3.4× longer than wide. ***Metasoma*** with T1 quadrate, only slightly narrowed towards base, with dorsal longitudinal carinae parallel to each other and almost reaching or reaching posterior margin of tergite; T2 subquadrate with oblique grooves cutting off anterolateral corners; T3–T7 transverse. ***Ovipositor*** at least 19 mm long, at least 3.5× as long as hind tibia, straight and parallel sided, rather robust.

Interpretation. Described originally in the symphytan family Siricidae, this taxon was moved to the tribe Ephialtini in Pimplinae more recently (Kasparyan and Rasnitsyn 1992). It clearly belongs to Ichneumonidae based on the wing venation. A quadrate areolet and 2m-cu evenly curved outwards, with two bullae, quadrate T1 with lateromedian longitudinal carinae and long ovipositor, clearly support the placement of the genus in Pimplinae. Tribal placement is in fact not unequivocal, as some Delomeristini genera also show as much resemblance to *Lithoserix* as the ephialtine *Dolichomitus* Smith, 1877 mentioned by Kasparyan and Rasnitsyn (1992). The presence of a transverse carina in the anterior part of the propodeum is unusual for Pimplinae and can be seen only in *Xanthopimpla* Saussure, 1892 (Pimplini) some Theroniini and, in a very reduced form, in *Delomerista* Förster, 1869 (Delomeristini), In fact, the presence of rather extensive carination on the propodeum is rather reminiscent of Delomeristini, although this is probably the plesiomorphic state in the subfamily (Kopylov et al. 2018). To distinguish between Delomeristini and Ephialtini, the tarsal claws would need to be examined, which are not preserved in either of the two specimens currently attributed to the genus. In any case, the long ramulus and short flagellar segments are unique for *Lithoserix*, which we suggest to keep without tribal assignment in Pimplinae.

Pimplinae? Wesmael, 1845
Pimpla? Fabricius, 1804

Pimpla? *seyrigi* Theobald, 1937

Fig. 13

**Pimpla seyrigi* Theobald,1937

Material. ***Holotype*** (part F1322/1 and counterpart F1322/2) examined at the NMBA.

Stratum. Kleinkembs, Pays de Bade, Haut-Rhin, France. Early Oligocene (Rupelian), 33.9–28.4 Ma.

Description. Sex unknown. Dorsal aspect of head (part), fairly complete antennae, mesosoma, almost complete fore wings and one nearly complete and one partial hind wing, partial hind legs, and metasoma present. Body length ~9.3 mm.

Mainly black, dark brown on wing veins, antennae and most of tergites, those with light end margins, legs lighter brown.

Head seemingly elongate with long gena, rather than representing front view, given that antennae insert at the anterior edge. ***Antenna*** almost as long as body, 1.25× longer than fore wing, with more than 34 flagellomeres, evenly tapered from middle to apex. ***Mesosoma*** not well preserved, with no details discernible. ***Fore wing*** 6.6 mm; areolet closed, somewhat petiolate anteriorly and almost triangular, with vein 2m-cu meeting 3M almost at outer corner; 2m-cu bowed outwards, probably with two bullae; 1cu-a meeting M + Cu clearly distally of 1M, 3Cu clearly longer than 2cu-a; cell 2R1 2.5× longer than wide. ***Hind wing*** with cell R conspicuously narrow, vein 1Rs a bit longer than rs-m; cell 1Cu broad with vein M + Cu bowed; 1Cu only about half as long as cu-a. ***Legs*** not well preserved; hind legs rather elongate; hind tibia 6.4× as long as wide. ***Metasoma*** with T1 parallel-sided, 1.7× longer than broad; T2 and following tergites transverse; each tergite except for T1 with a light band apically which from T4 becomes narrower medially until it is cut into two lateral spots. ***Ovipositor*** not discernible.

Interpretation. The taxonomic affinity of this fossil is very difficult to discern. The elongate, tapering antennae and shape of the metasoma point to Ctenopelmatinae, but some Pimplinae cannot be ruled out. In addition, the wide quadrate areolet and outwards curved 2m-cu are rarely seen in Ctenopelmatinae, but they are quite common in Pimplinae. Given the poor preservation of the mesosoma, many important characters cannot be observed. As we cannot decide on the subfamily placement, removing the fossil from Pimplinae and labelling it as incertae subfamiliae would require description of a new genus based on the insufficient character evidence. We thus take a conservative approach, leaving the fossil within the genus *Pimpla*, but emphasizing the uncertainty in this placement by adding a question mark behind both the genus and subfamily name.

Pimplinae Wesmael, 1845
Polysphincta Gravenhorst, 1829

Polysphincta? *inundata* Brues, 1910

Fig. 14

**Polysphincta inundata* Brues, 1910

Material. Photographs of the holotype (part only, #PALE-2135) obtained from the MCZ.

Stratum. Teller County, Florissant shales, Colorado, USA. Late Eocene (Chadronian), 37.2–33.9 Ma.

Description. Female. ***Holotype*** in lateroventral view, with one nearly complete and one partial antenna,

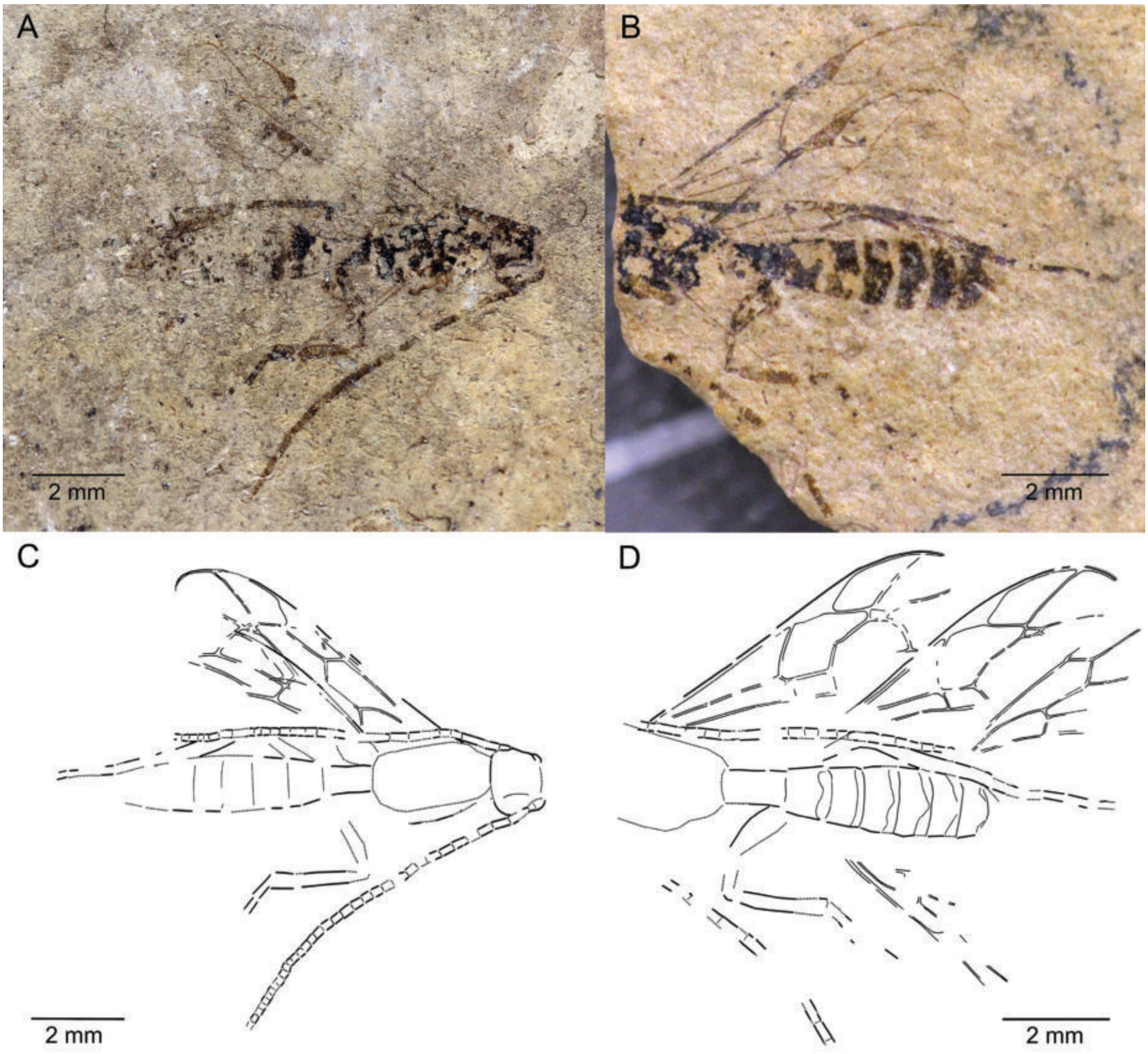

Figure 13. *Pimpla*? *seyrigi* (Theobald, 1937), comb. nov. **A.** Photograph of the part and **B.** Counterpart of the holotype of taken at the NMBA; **C, D.** Corresponding interpretative drawings. In the drawings, thicker lines indicate outlines of body structures, thinner lines show characters inside these outlines, and dotted lines represent uncertain interpretations.

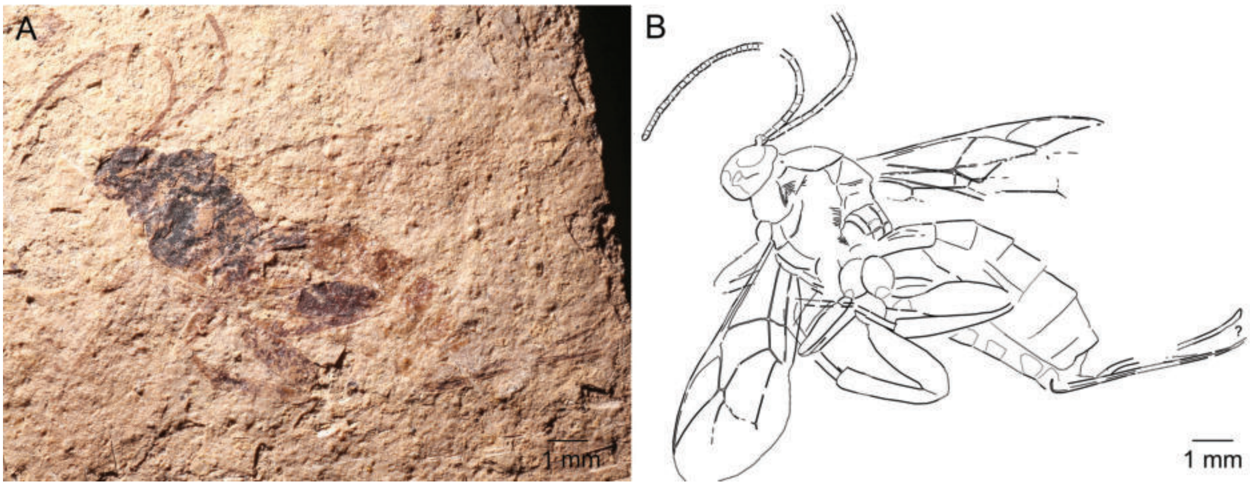

Figure 14. *Polysphincta*? *inundata* (Brues, 1910) comb. nov. **A.** Photograph of the holotype obtained from the MCZ; **B.** Our interpretative drawing of the fossil. Thicker lines indicate outlines of body structures, thinner lines show characters inside these outlines, and dotted lines represent uncertain interpretations.

head, mesosoma showing some carinae and sculpture, nearly complete fore wings and one partial hind wing, hind legs strongly and mid and fore legs weakly outlined, metasoma complete with ovipositor with sheaths. Body length 10.1 mm.

Black or dark brown on head, mesosoma and T1, antennae and remaining metasoma orange, hind legs dark brown at least on femur and apex of hind tibia, other legs probably orange.

Head rather short, poorly preserved but outline of eyes partially indicated. ***Antennae*** 7.1 mm, with more than 39 (probably around 43) flagellomeres, basal segments longer than wide, from about mid length transverse, scape short. ***Mesosoma*** rather stout, with epomia present on pronotum; mesopleuron with epicnemial carina curved forward around mid-height of pronotum, with fine longitudinal carinulae at least in front of mesepimeron. Propodeum with pleural, lateral and lateromedian longitudinal carinae seemingly complete, with indication of low posterior transverse carina and maybe also part of anterior transverse carina. ***Fore wing*** 6.8 mm; areolet open, vein 2 + 3M twice as long as 2Rs; 1cu-a meeting 2Cu at the same position as 1M; cell 2R1 rather long, 3.6 × as long as wide. Hind wing with vein 1Rs much longer than rs-m; 1Cu about as long as cu-a (but a bit difficult to see). ***Legs*** rather stout; hind femur 3.0× and hind tibia 7× as long as wide. ***Metasoma*** mostly dorsoventrally depressed and somewhat compressed towards apex, with T1 a bit elongate and nearly parallel sided, with what are probably latero-median and dorso-lateral carinae; T2 and following tergites transverse. ***Ovipositor*** 3.8 mm, 1.6× as long as hind tibia, upcurved at apex, seemingly tapering from about middle to apex; ovipositor sheaths parallel-sided.

Interpretation. Members of the *Polysphincta* group of genera are koinobiont ectoparasitoids of spiders and have a unique ovipositor, which is expanded at the base and again around mid-length, from where it evenly tapers into a narrow point. The state of the ovipositor in *P. inundata* seems consistent with this description, but this is somewhat unclear, despite the in general very good preservation of this fossil. Alternatively, if our interpretation of the ovipositor is wrong and there is not a median swelling, it would point to *Clistopyga* Gravenhorst, 1829, a sister genus of the polysphinctines. The fact that we cannot see any paired swellings, impressions or raised areas on tergites, which are typical for many but not all polysphinctines, speaks also more for *Clistopyga*. However, the propodeal carination never occurs in *Clistopyga*, and although it is reduced in most extant members of the polysphinctines, with at most longitudinal carinae present, the posterior transverse carina occurs in some genera, e.g., *Sinarachna* Townes, 1960, *Acrodactyla* Haliday, 1838 and *Zatypota* Förster, 1869. These genera, however, have shorter ovipositors without the upcurved tip. Because we cannot find a convincing alternative placement for the fossil, we leave it in the current genus but express uncertainty in its placement.

Lycorininae? Cushman & Rohwer, 1920
Lycorina? Holmgren, 1859

Lycorina? *indura* (Theobald, 1937), comb. nov.

Fig. 15

**Pimpla indura* Theobald, 1937

Material. ***Holotype*** (part #1323/1 and counterpart #1323/2) examined at the NMBA.

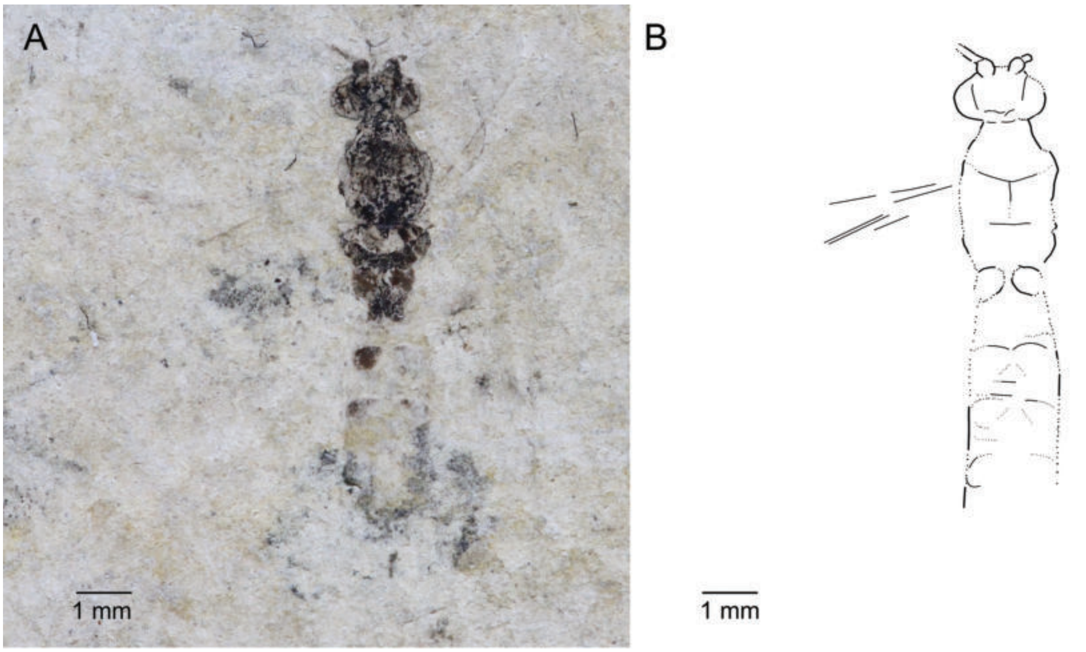

Figure 15. *Lycorina*? *indura* (Brues, 1910) comb. nov. **A.** Photograph of the holotype obtained from NMBA; **B.** Our interpretative drawing of the fossil. Thicker lines indicate outlines of body structures, thinner lines show characters inside these outlines, and dotted lines represent uncertain interpretations.

Stratum. Kleinkembs, Pays de Bade, Haut-Rhin, France. Early Oligocene (Rupelian), 33.9–28.4 Ma.

Description. Sex unclear. Ventral aspect (see 'Interpretation' below) of head, base of antenna, mesosoma, base of fore wing, and T1–T4 of metasoma partly preserved. Body length ~9 mm.

Mostly dark brown in colour, with some light colouration on mesosoma and with metasoma mostly light-coloured, with base of T1 and paired dark markings on top of rounded swellings on T2 to T4.

Head rather short, with prominent eyes and clypeus and mandibles indicated. ***Antennae*** with scape and pedicel short, flagellar segments not discernible. ***Mesosoma*** not well preserved, with epicnemial carina complete at least ventrally; apparent constriction after mesoscutum probably due to lighter colouration on mesepimeron. Propodeum quite short. ***Wings*** very poorly preserved, but counterpart showing base of one fore wing with C, Sc + R, M + Cu on the left side in their normal position and Sc + R and M + Cu on the right side folded over, with 1cu-a meeting M + Cu opposite of 1M. ***Legs*** not preserved, but reddish-brown hind coxae visible in front of T1. ***Metasoma*** with broad T1, 0.8× as long as broad; T2 0.8×, T3 0.7× as long as wide; T2–T4 with paired, rounded swellings which bear traces coarse punctuation; diagonal grooves obvious on T2 and indicated on T1 and T3, transverse impressions unclear; remainder of metasoma not preserved.

Interpretation. The interpretation of this fossil was difficult given the poor preservation. Some of the interpretation hinges upon the question of whether it shows its ventral or dorsal aspect. Theobald (Theobald 1937) concluded that he was looking at a dorsal aspect, that the mesosoma was "clearly segmented", and that he saw the three ocelli. However, we believe that the transverse line across the thorax represents the epicnemial carina, followed by the longitudinal mesosternal scrobe. Additional evidence for a ventral view is what we interpret as the two hind coxae lying in front of T1. Instead of very much enlarged ocelli, we think that the three light parts on the head represent the clypeus and mandibles. This interpretation is also in better agreement with the position of the antennae, which would be very low on the head if we were looking at a dorsal aspect. The metasoma is still interpreted as showing the tergites, but from inside; the sternites are usually so weakly sclerotized in ichneumonids that they are missing in fossils.

Overall, this fossil is badly preserved, with only the base of one fore wing visible and most of the mesosoma squashed so that no carination is discernible. The lack of complete fore wing venation makes even the family association seem uncertain; however, all the visible features correspond very well to ichneumonids, especially when comparing ventral view to other ichneumonid fossils (e.g., see the holotype of *Acerataspis*? *revelata* Brues). Several unusual features are very clearly visible, especially the diagonal grooves on T2 and paired dark swellings with strong punctation on T2 and T3. There are only a few ichneumonids with such strong diagonal grooves on the tergites: the tribe Glyptini in the subfamily Banchinae, some genera in Pimplinae, and the members of the subfamily Lycorininae. Only in the pimpline genus *Xanthopimpla* and in some *Lycorina* do the diagonal groves come together with a light colouration of the metasoma and two basal swellings, which are then often black-marked as in the fossil. In *Xanthopimpla*, however, the grooves are closer to the anterior margin; if dark markings are present on T2, they are usually part of the medial swollen area and thus lie behind the diagonal groves, which does not seem to be the case in this fossil. Furthermore, *Xanthopimpla* species have a yellow or orange mesosoma, although there is a recently described *Xanthopimpla* species from the Fur Formation with a dark mesoscutum (Klopfstein 2021). The subfamily Lycorininae matches much more closely with the same arrangement of carinae and markings found in extant species, the mesosoma often dark and the rather short scapus. This subfamily comprises only the genus *Lycorina*, which shows the basal part of the median longitudinal carinae on the propodeum, even though this state is somewhat equivocal in the fossil. We thus transfer the species to *Lycorina* in the subfamily Lycorininae but mark it with a question mark given the poor preservation.

Tryphoninae Shuckard, 1840
Monoblastus? Hartig, 1837

Monoblastus? *senilis* (Brues, 1910), comb. nov.

Fig. 16

**Pimpla senilis* Brues, 1910

Material. Photographs of the holotype (part only, #PALE-2160) obtained from the MCZ.

Stratum. Teller County, Florissant shales, Colorado, USA. Late Eocene (Chadronian), 37.2–33.9 Ma.

Description. Female. *Holotype* in lateral to ventro-lateral view, with head, base and tip and some intermediate segments of antennae, mesosoma, fore and nearly complete hind wings, hind legs, metasoma and ovipositor with sheaths. Body length 8.0 mm.

Colouration unclear, as with irregular dark and lighter patches on head, mesosoma and metasoma which are probably a preservation artefact but with what looks more real orange colouration on parts of pronotum, last sternites and legs. Hind tibia with apex darkened. Tergites of metasoma with apical third to half of lighter colour.

Head with rather long gena, thus almost globular in shape. ***Antennae*** 6.2 mm, with more than 30 (probably about 45) flagellomeres, tapering strongly on last third of its length, with basal segments longer than wide and apical segments transverse. ***Mesosoma*** stout; pronotum probably with strong epomia; mesoscutum rather short, maybe with notauli, with short carinulae on outer side; mesosternum with deep medial sternal groove with

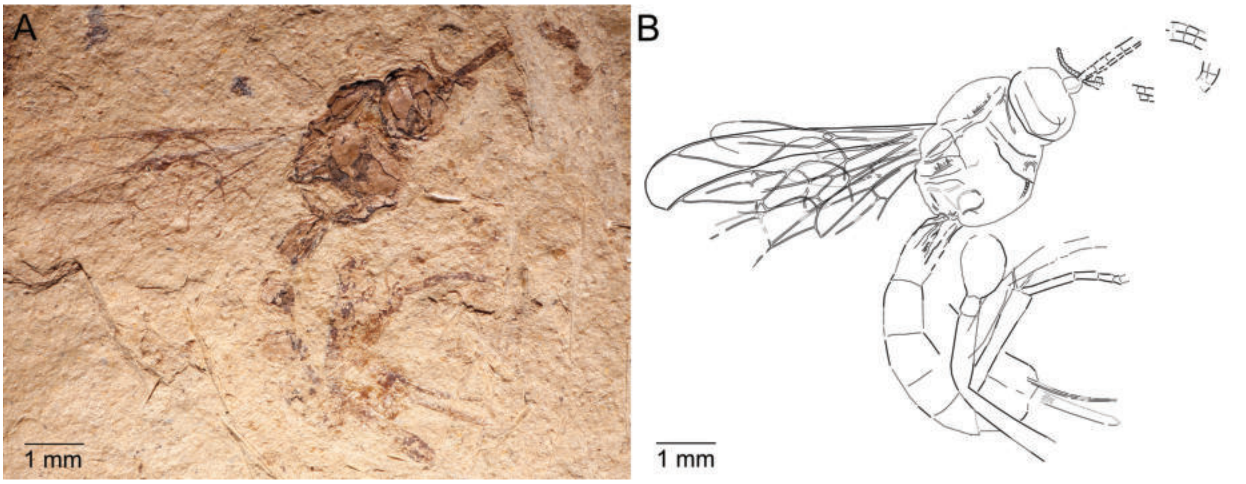

Figure 16. *Monoblastus*? *senilis* (Brues, 1910) comb. nov. **A.** Photograph of the holotype obtained from the MCZ; **B.** Our interpretative drawing of the fossil. Thicker lines indicate outlines of body structures, thinner lines show characters inside these outlines, and dotted lines represent uncertain interpretations.

transverse carinulae; epicnemial carina curved and reaching up to about mid-height of mesopleuron. Propodeum short, not well preserved, with pleural and submetapleural and probably additional carination present. ***Fore wing*** 5.35 mm, with areolet quadrate and slightly oblique, receiving 2m-cu a bit apical of its centre, 4M thus shorter than 3M; 1cu-a meeting 2Cu distinctly after 1M; 3Cu a little longer than 2cu-a; vein 1m-cu & 2Rs+M conspicuously bowed; cell 2R about 3.5 as long as wide. ***Hind wing*** with 1Cu a bit longer than 1cu-a and 1Rs about 1.6× longer than rs-m. ***Legs*** of normal dimensions, hind femur 3.6× longer than wide, hind tibia with two slender spurs. ***Metasoma*** with T1 clearly longer than wide, with strong lateral and laterodorsal carinae and probably deep glymma, with dorsal longitudinal carinae at least present on basal half and with some longitudinal carinulae; T2 a bit longer than wide, following tergites subquadrate, all with what look like rather deep punctures; hypopygium rather prominent, triangular. ***Ovipositor*** about 1.5 mm, 1.3× as long as hind tibia, parallel sided and down-curved; ovipositor sheaths evenly hairy and somewhat expanded around middle.

Interpretation. The deep glymma, bowed vein 1m-cu & 2Rs+M in the fore wing, and shape of the metasoma suggest membership in Tryphoninae, where the down-curved ovipositor and possibly medially expanded sheaths point to genera such as *Thymaris* Förster, 1869 or *Neliopisthus* Thomson, 1883 in the tribe Oedemopsini. In addition, *Monoblastus* from Tryphonini also has a down-curved tip of the ovipositor and sheaths which are weakly medially expanded. As the extant *Thymaris* have a more slender first tergite and *Neliopisthus* more strongly expanded ovipositor sheaths than what we see in the fossil, we place the fossil in *Monoblastus*, to which the fossil also closely resembles in the wing venation. However, we add a question mark behind the genus name as the laterally extended epicnemial carina and longitudinal sculpture on T1 correspond better to *Thymaris*.

Tryphoninae Shuckard, 1840
Zagryphus Cushman, 1919

Zagryphus tilloyi (Theobald, 1937), comb. nov.

Fig. 17

**Promethes tilloyi* Theobald, 1937

Material. ***Holotype*** (part only, #Am_8 / MNHN.F.B24392) examined at MNHN.F. Photograph obtained from MNHN.F.

Stratum. Aix-en-Provence, Bouche-du-Rhône, France. Late Oligocene (Chattian), 28.4–23.0 Ma.

Description. Female. ***Holotype*** in lateral to ventrolateral view with nearly complete antennae, head, mesosoma with details indistinct; fore wings darkened and on top of each other, venation in part difficult to discern, one hind wing; at least parts of all legs, and metasoma with ovipositor with sheaths. Body length 6.1 mm.

Dark brown, antennae reddish at base and with white bands around mid-length; with reddish colouration on head and mesosoma, wings strongly tinted, brown; legs dark brown; metasoma dark, but possibly with irregular lighter markings on T2, ovipositor orange, its sheaths dark brown.

Head quite round, with large eyes, with a nose-like protrusion where clypeus would be. ***Antennae*** 4.5 mm, with at least 28 (probably around 32) flagellomeres, basal ones elongate, those apically of white band quadrate to transverse. ***Mesosoma*** not well preserved, with mesosternal scrobe, indication of epicnemial carina and notauli reaching at least over first third of mesoscutum. Metapleuron as long as wide, with submetapleural carina complete; propodeum with pleural carina, lateral longitudinal and maybe other carinae complete, meeting point of lateral longitudinal and posterior transverse carina might be thickened (cf. propodeal apophyses). ***Fore wing*** 3.6 mm, rather stout; areolet open, 2Rs rather short; 1cu-a meeting M + Cu opposite of 1M; 1M & 1Rs bowed inwards; 3Cu more than 3× longer than 2cu-a, strongly inclivous; cell 2R1 2.9× lon-

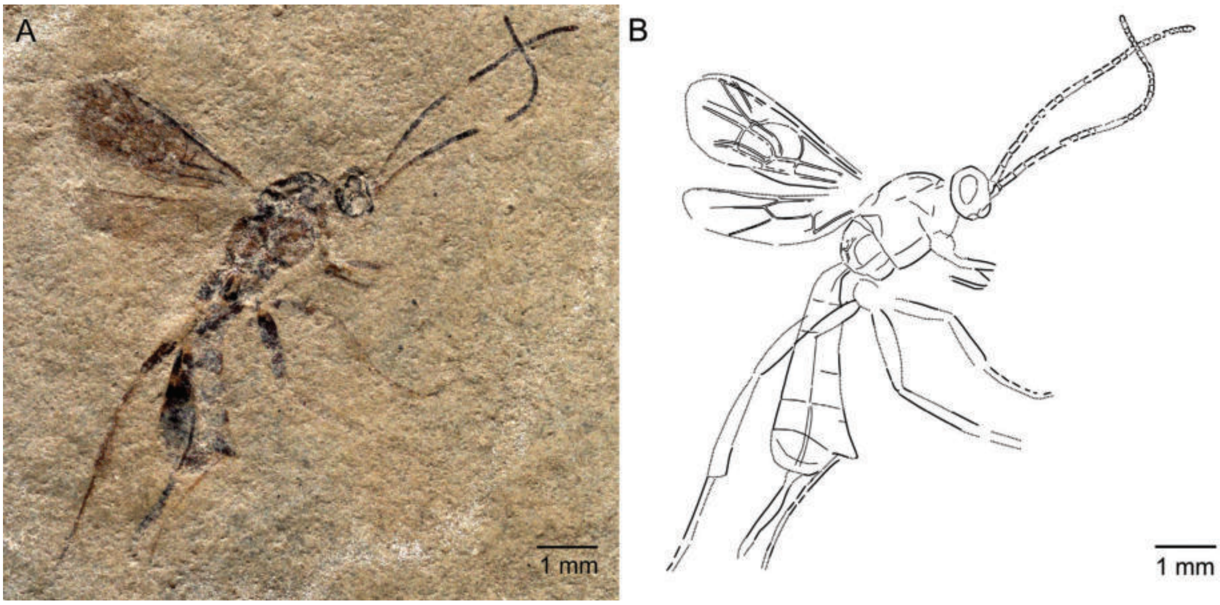

Figure 17. *Zagryphus tilloyi* (Theobald, 1937) comb. nov. **A.** Photograph of the holotype obtained from MNHN.F; **B.** Our interpretative drawing of the fossil. Thicker lines indicate outlines of body structures, thinner lines show characters inside these outlines, and dotted lines represent uncertain interpretations.

ger than wide. ***Hind wing*** with 1Rs about as long as rs-m and 1Cu much longer than cu-a. ***Legs*** slender, hind femur 4.4×, hind tibia 7× longer than wide, dark dorsally light ventrally. ***Metasoma*** compressed from T4 or T5; T1 not well preserved, but slightly elongate and tapering towards base, following tergites transverse; sternites quite well sclerotized; hypopygium triangular in lateral view. Ovipositor 1.9 mm, about 1.3× as long as hind tibia, curved downwards; ovipositor sheaths widened around mid-length.

Interpretation. Even though many characters are not clearly visible, the medially expanded ovipositor sheaths firmly place this fossil in the Tryphoninae tribe Oedemopsini. Indeed, the specimen shows a remarkable similarity to the extant *Zagryphus nasutus* (Cresson, 1868): the nose-like expansion of the clypeus, inclivous 3Cu in the fore wing and short cu-a in the hind wing, triangular but not strongly elongate hypopygium, and down-curved ovipositor with medially expanded sheaths support a placement in this genus. Even the colouration is a good match, including the white band on the antenna and orange base, a pattern often observed in *Zagryphus* and related genera. *Zagryphus tilloyi* can be distinguished from the other members of the genus by its smaller size (at least 4.8 mm in extant species) and more strongly tinted wings.

Xoridinae Shuckard, 1840
Xorides Latreille, 1809

Xorides sejugatus (Brues, 1910)
Fig. 18

**Xylonomus sejugatus* Brues, 1910

Material. Photographs of the holotype (#PALE-2211) and of two paratypes (#PALE-2212 and #PALE-2213), obtained from the MCZ.

Stratum. Teller County, Florissant shales, Colorado, USA. Late Eocene (Chadronian), 37.2–33.9 Ma.

Description. Female. *Holotype*, paratypes with sex unknown. Holotype in lateral aspect showing head, few basal segments of antennae, rather well-preserved mesosoma, almost complete fore and hind wings, nearly complete legs, metasoma and ovipositor with partial sheaths. Paratypes less well preserved, #2212 showing lateral aspect of partial mesosoma, base of wings, T1–T5 and most of hind legs; #2213 with lateroventral aspect of head, partly discernible antennae, outlined but not well-preserved meso- and basal metasoma, wings and partial legs. Body length 17.25 mm.

Black or dark brown on head and mesosoma and hind coxae, brown wing veins and metasoma, legs lighter brown except for darkened hind femur. Ovipositor dark brown.

Head rather short and high, with long cheek, in #2213 with what looks like two chisel-shaped mandibles. ***Antennae*** incomplete, but rather slender and at least 1.3× as long as fore wing. ***Mesosoma*** cylindric, not very elongate, pronotum with epomia strong and reaching mesoscutum; mesoscutum with long notauli, mesopleuron with epicnemial carina reaching pronotum at about mid-height. Propodeum strongly areolated, with lateromedian and lateral longitudinal and pleural carinae, posterior transverse and at least partial anterior transverse carina. ***Fore wing*** 11 mm, with areolet open, vein 2Rs almost obliterate; 1cu-a meeting 2Cu slightly distally from 1M; cell 2R1 strongly elongate, 4.2× as long as wide. ***Hind wing*** with 1Cu a little longer than cu-a and 1Rs a little shorter than rs-m. ***Legs*** partly preserved, hind femur 3.0×, and hind tibia 5.8× as long as wide. ***Metasoma*** depressed, slightly enlarged apically; T1 about 2.3× as long as wide, slightly expanding apically, with strong ventrolateral, dorsolateral and median dorsal carinae, and with distinct diagonal groves laterally which form

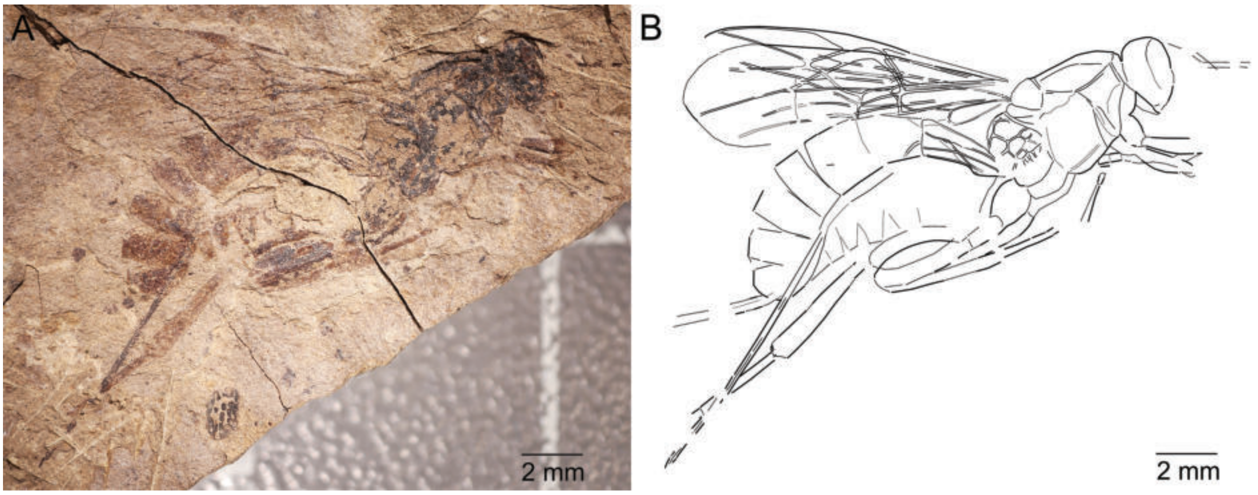

Figure 18. *Xorides sejugatus* (Brues, 1910) comb. nov. **A.** Photograph of the holotype obtained from the MCZ; **B.** Our interpretative drawing of the fossil (below). Thicker lines indicate outlines of body structures, thinner lines show characters inside these outlines, and dotted lines represent uncertain interpretations.

part of a constriction around middle of tergite; T2 approximately quadrate, with oblique basal grooves cutting off basolateral corners; T3 a bit wider than long; T4–T6 transverse; T7 slightly longer than T6; S2–S5 visible as brown patches. ***Ovipositor*** 9.6 mm, 2.2× as long as hind tibia, rather narrow.

Interpretation. Several characters firmly place this fossil in *Xorides*, including the chisel-like mandibles, long epomia that seems to connect with the dorsal margin of the pronotum, fore wing venation including an open areolet with very short 3rs-m, grooves anteriorly on T2, and lateral diagonal impressions on T1. The only character not usually observed in recent species of the genus are the thickened hind femora.

Ctenopelmatinae Förster, 1869
Parapimpla Theobald, 1937

Parapimpla rhenana Theobald, 1937, stat. rev.

Fig. 19

Material. ***Holotype*** (part F1321/1 and counterpart F1321/2) examined at the NMBA.

Stratum. Kleinkembs, Pays de Bade, Haut-Rhin, France. Early Oligocene (Rupelian), 33.9–28.4 Ma.

Description. Sex unclear. Dorsal aspect of head, base and some fragments of antennae, dorsolateral view on mesosoma, partial fore wings (one of which is folded longitudinally), partial hind wing and legs, and first five

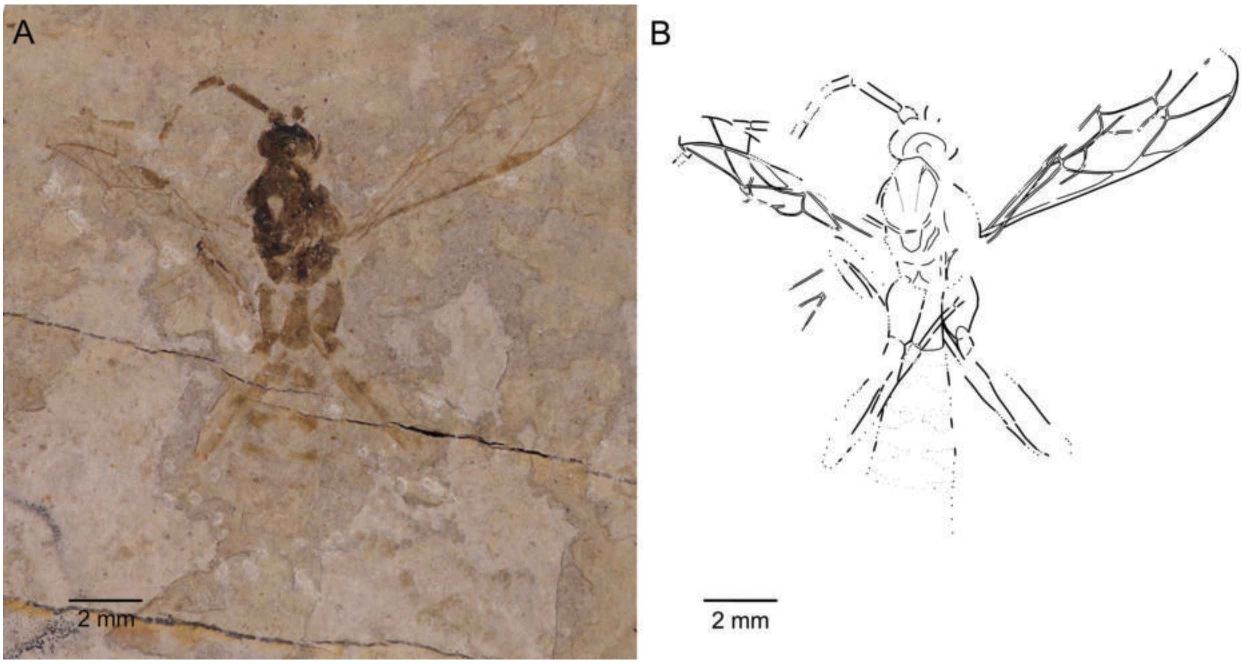

Figure 19. *Parapimpla rhenana* Theobald, 1937 stat. rev. **A.** Photograph of the holotype taken at NMBA; **B.** Our interpretative drawing of the fossil. Thicker lines indicate outlines of body structures, thinner lines show characters inside these outlines, and dotted lines represent uncertain interpretations.

tergites visible. Body length unclear as tip of metasoma is missing, but probably a bit more than 10 mm.

Dark brown on head and mesosoma, orange-brown legs, wing veins, T1, and basal spots on T2–T5, remainder very light brown or yellow.

Head short, with short gena, occipital carina well developed and evenly rounded above. ***Antenna*** only partly preserved, scape and pedicel of average dimensions; first flagellomere 6× as long as wide, the few other visible fragments showing rather elongate flagellomeres. ***Mesosoma*** partly crushed, with lighter parts and of normal dimensions; mesoscutum rather long, front margin truncated and prominent, with an indication of a long, converging notaulus, with a light mark in middle; propodeum with pleural, lateral longitudinal and at least partial lateromedian longitudinal carinae, transverse carinae probably present but a bit unclear. ***Fore wings*** well preserved, 8.3 mm, but left fore wing longitudinally folded on itself; pterostigma 4.6× as long as wide, brown with a light base; areolet large and quadrate, almost rhombic, with veins r-rs and 4Rs meeting at its anterior end in ~110° angle; 2m-cu very short and probably with a single bulla anteriorly; cell 2R1 very long (3.5×); 1M somewhat curved just before it meets M + Cu. ***Hind wing*** only partially preserved, cell R nearly complete; 1Rs almost 3× longer than rs-m. ***Hind legs*** partly preserved, elongate, femur more than 4.5×; tibia 9.5× longer than wide. ***Metasoma*** only partly preserved; T1 narrow anteriorly and evenly tapering posteriorly, almost twice as long as wide at apex, without distinct division into petiole and postpetiole; T2 subquadrate; T3 and T4 transverse, each with light colouration and brown paired marks near base.

Interpretation. This fossil has a very elongate and narrow T1, which does not occur in Pimplinae. The poor preservation, especially of the wing venation and tip of the metasoma, makes a clear attribution of this genus to any of the extant subfamilies challenging. If the shape of T1 is as preserved, then Ctenopelmatinae would be a good match, as they also often have similar wing venation. Similar T1 also occurs in some Banchinae, Cremastinae and Campopleginae. However, we can rule out Banchinae based on the presence of longitudinal carinae on the propodeum, and Cremastinae and Campopleginae can be discounted based on the wing venation. Thus, we move this monotypic genus to Ctenopelmatinae.

Discussion

We here revised 18 fossil ichneumonid species from the Palaeogene, all described before the major reclassification of ichneumonids by Henry Townes. We concluded that the original subfamily placement of 12 of them are unreliable and for 11 of them, we demonstrated a wrong subfamily placement and moved them mostly to extant genera in the better fitting subfamilies. As the main reasons for the initially erroneous taxonomic placement, we identified the shortcomings of the initial classification systems for ichneumonids, inaccurate interpretation of preserved characters and undue reliance on homoplastic characters.

Artefacts of the pre-Townes classification in the ichneumonid fossil record

The most common genus of ichneumonids in the fossil record is *Pimpla* with 22 described species, all from the Palaeogene. We here revised six of those species, none of which turned out to belong to *Pimpla* with certainty. *Pimpla* is a type genus of one of the five ichneumonid subfamilies recognized in the first half of the 20th century (Cryptinae, Ichneumoninae, Ophioninae, Pimplinae, Tryphoninae), each of which was split into several different subfamilies in the comprehensive taxonomic work of Henry Townes (Townes 1969a, 1969b, 1970, 1971). Therefore, many ichneumonid fossils were probably named based on superficial resemblance to the type genera of the five subfamilies. Moreover, these genera used to be very broadly defined and often included subgenera that today have genus status. Finally, the subfamily association of some ichneumonid genera and even tribes has changed multiple times, even after Townes' seminal work (Quicke et al. 2009; Santos 2017; Bennett et al. 2019; Klopfstein et al. 2019). There are already indications that these artefacts of the pre-Townes classifications, as well as homoplasy (see below), also impact fossils placed in *Tryphon* (Bennett 2015; Spasojevic et al. 2018b), and we expect that the case is similar in fossils placed in the genera *Ichneumon* and *Cryptus*, which are all very common in the fossils record. This stresses the importance of the revision of more than 140 ichneumonid fossils described before Townes' work. As in the *Pimpla* species treated here, we can expect that only very few fossil species will retain their original placement after a thorough revision incorporating recent taxonomic and phylogenetic insights (Quicke et al. 2009; Broad et al. 2018; Klopfstein et al. 2019).

High prevalence of homoplasy in ichneumonids

Homoplasy has been pointed out as one of the major problems in classifying extant (Gauld and Mound 1982) and, even more so, fossils ichneumonids (Spasojevic et al. 2018b). Our findings strongly support those observations, especially in the case of the revised *Pimpla* fossils, where we had sufficient character evidence for moving three of them to a different genus in a different subfamily: *P. morticiina* to the newly described genus *Armadilleon* in Phygadeuontinae, *P. revelata* to *Acerataspis* in Metopiinae, and *P. senilis* to *Monoblastus* in Tryphoninae. All three fossils do resemble *Pimpla* in the relatively stout body, broad and short T1, and fore wing with a closed areolet, but these are all highly homoplastic characters and thus not informative for classification. Therefore, it is important to avoid homoplastic and fast-evolving characters for identifying fossil taxa, acknowledging all possible placements of a fossil and express the uncertainty in the chosen placement.

Difficulties in character interpretation in ichneumonid fossils

Many crucial autapomorphies of different subfamilies and genera were not preserved in the revised fossils and this greatly impairs their original as well as revised placements. For instance, the association of *Hallocinetus*? *arvernus* with Acaenitinae could neither be confirmed nor refuted due to the poorly preserved apical part of the metasoma. However, the identification of a closed areolet in the holotype, which was overlooked by the original author (Piton 1940) renders the original generic placement untenable. The placement of two fossils in *Dimophora*, both of which were formerly placed in different subfamilies, was uncertain because the presence of the thyridium was unclear. In Pimplinae, many genera can be confirmed or ruled out by the state of their tarsal claws, which are very rarely preserved in fossils (but see Spasojevic et al. 2018b). As a result, for more than half of the fossils, we could not establish a firm generic placement. As missing data is inevitable when studying fossilized organisms, the correct interpretation of those characters that are preserved is even more crucial for their taxonomic placement.

The wrong interpretation of the aspect in which the fossil is preserved, such as dorsal versus ventral, contributed to erroneous placements of *Lycorina*? *indura* and *Acerataspis*? *revelata*. Indeed, because of the weakly sclerotized sternites in Ichneumonoidea, the metasoma of a fossil might appear to show a dorsal view, as certain aspects of the more strongly sclerotized tergites often show prominently even in ventral view (Spasojevic et al. 2018b). This can lead to darkened parts of sternites being mistaken for colour patterns on tergites, and careful interpretation is needed to avoid such pitfalls (Kopylov 2009). For a correct interpretation of the orientation of the body of a fossil, it is thus crucial to combine clues from all body parts, with the often strongly sclerotized mesosternal scrobe often acting as an important guide in Ichneumonoidea fossils.

Aside from the aspect of a fossil, several other characters were wrongly interpreted in the fossils studied here. For instance, head parts were mistaken for ocelli in *Lycorina*? *indura*, T1 was interpreted as pimpline-like (short and stout) instead of petiolate in *Dimophora*? *wickhami*, while the areolet was interpreted as open instead of closed and petiolate in *Hallocinetus*? *arvernus*. To better understand the preservation state of a fossil, it is important to study taphonomic processes which cause deformation of the preserved structures (Martínez-Delclòs et al. 2004). Although there are many studies concerning the taphonomy of insects in rock deposits (e.g., Henning et al. 2012; Smith 2012; Wang et al. 2013; Cunningham et al. 2014; Greenwalt et al. 2014; Karr and Clapham 2015; Osés et al. 2016), none addressed ichneumonids specifically. Therefore, the interpretation of the aspect in which an animal is preserved and of specific body parts, such as the propodeum and its carination and the sternites of the metasoma, remains difficult. Deposits where several dozen ichneumonids have been preserved in various aspects, such as the Fur Formation in Denmark (Klopfstein 2021), Messel Pit in Germany (Spasojevic et al. 2018a), Green River and Kishenehn Formations in the USA (Spasojevic et al. 2018b, personal observations), can provide invaluable information on the taphonomy of ichneumonids. Furthermore, experiments with extant species can provide important insights into how the body of a particular taxon reacts to decay and pressure under different environmental conditions (Martínez-Delclòs et al. 2004; Briggs and McMahon 2016; Gäb et al. 2020; Slater et al. 2020), but such experiments still have to be performed on this group.

Implications of erroneous fossils placement

With the spread of phylogenetic dating studies, which rely on fossils to estimate the absolute divergence times of organisms, the correct interpretation of fossil classification became crucial to a broader scientific community. In particular, erroneous fossil placement affects the node dating approach, where the age of a fossil is directly used to calibrate the age of the node in the phylogeny of extant taxa that it is associated with (Parham et al. 2012). Several simulations and empirical studies support this notion, where wrong calibrations lead to wrong age estimates (Warnock et al. 2011; Parham et al. 2012). This mostly happens because molecular phylogeneticists often rely on the original placement of a fossil without reevaluating it or because they misinterpret the affiliation of the fossil with stem versus crown lineages and vice versa. The alternative approach, total-evidence dating (Pyron 2011; Ronquist et al. 2012), has the advantage of not a priori assuming the taxonomic position of a fossil, but instead it infers it by employing morphological data from both extant and fossil taxa. It has already been shown that the total-evidence analysis combined with RoguePlots, a graphical visualisation of placement probabilities of fossils in Bayesian phylogenetic inference (Klopfstein and Spasojevic 2019), can be a helpful tool for assessing placement of fossils. Although the total-evidence approach is immune to erroneous fossil placements, it is not immune to wrong character interpretations that lead to biased morphological data. Therefore, it is crucial that palaeontologists express uncertainty in both character interpretation and taxonomic placement of newly described fossils. The latter is easily done by applying open taxonomic nomenclature, such as adding a question mark behind an uncertain subfamily or genus placement.

Conclusions

Contributions to the fossil record of Darwin wasps, either through descriptions of new taxa or revisions of the described species, are needed for understanding the past diversity and evolutionary history of this group. We here contributed to this topic by revising 18 fossil species from the Palaeogene, all described before the taxonomic work of Henry Townes. The placement of all but three fossils was unreliable, resulting in a new generic and, almost always, a new subfamily placement for most of the fossils. Underlying reasons for the initial erroneous taxonomic placement of the revised fossils are mostly due to the shortcomings of the initial classification systems for ichneumonids, erroneous interpretation of character evidence and reliance on homoplastic characters for placement of the fossils. Our revision highlights the need for further reinterpretation of the ichneumonid fossil record and for widely adopting the open taxonomic nomenclature, which will greatly allow for more adequate integration of fossils in phylogenetic dating studies.

Acknowledgements

We are extremely grateful to the curators and collection managers Talia Karim (UCM), Olivier Béthoux (MNHN.F), and Walter Etter (NMBA) who provided access to the type material studied here. Also, we thank David Zelagin (UCM), Gaëlle Doitteau (MNHN.F) and Ricardo Pérez-de la Fuente (MCZ) for taking photographs of the fossil types and their institutions for allowing us to reproduce their images. Mabel Alvarado (Lima), Bernardo Santos (MNHN.F), and Andrew Bennett (Ottawa) shared invaluable taxonomic insights with us that improved the classification of the fossils. Lastly, but not least, we thank Brandon Claridge for providing valuable comments on the manuscript and fossil placement during the review process, and the editor Christian Klug. This study was supported by the Swiss National Science Foundation (grant 310030_192544 to SK).

References

Abramoff MD, Magalhães PJ, Ram SJ (2004) Image processing with ImageJ. Biophotonics International 11: 36–42.

Antropov AV, Belokobylskij SA, Compton SG, Dlussky GM, Khalaim AI, Kolyada VA, Kozlov MA, Perfilieva KS, Rasnitsyn AP (2014) The wasps, bees and ants (Insecta: Vespida=Hymenoptera) from the Insect Limestone (Late Eocene) of the Isle of Wight, UK. Earth and Environmental Science Transactions of the Royal Society of Edinburgh 104: 335–446. https://doi.org/10.1017/S1755691014000103

Bennett AMR (2015) Revision of the world genera of Tryphoninae (Hymenoptera: Ichneumonidae). American Entomological Institute, Gainesville, FL, 387 pp.

Bennett AMR, Cardinal S, Gauld ID, Wahl DB (2019) Phylogeny of the subfamilies of Ichneumonidae (Hymenoptera). Journal of Hymenoptera Research 71: 1–156. https://doi.org/10.3897/jhr.71.32375

Briggs DEG, McMahon S (2016) The role of experiments in investigating the taphonomy of exceptional preservation. Palaeontology 59: 1–11. https://doi.org/10.1111/pala.12219

Broad GR, Shaw MR, Fitton MG (2018) The ichneumonid wasps of Britain and Ireland (Hymenoptera: Ichneumonidae): their classification and biology. Handbooks for the Identification of British Insects 7(12): 1–418.

Brues CT (1910) The parasitic Hymenoptera of the Tertiary of Florissant, Colorado. Bulletin of the Museum of Comparative Zoology at Harvard College 54: 1–125.

Cockerell TDA (1919) Some fossil parasitic Hymenoptera. American Journal of Science 47: 376–380. https://doi.org/10.2475/ajs.s4-47.281.376

Cunningham JA, Donoghue PCJ, Bengtson S (2014) Distinguishing Biology from Geology in Soft-Tissue Preservation. The Paleontological Society Papers 20: 275–288. https://doi.org/10.1017/S1089332600002898

Ferraris Jr CJ, Eschmeyer WN (2000) International Code of Zoological Nomenclature: Fourth Edition. Copeia 2000: 907–908. https://doi.org/10.1643/0045-8511(2000)000[0907:BR]2.0.CO;2

Gäb F, Ballhaus C, Stinnesbeck E, Kral AG, Janssen K, Bierbaum G (2020) Experimental taphonomy of fish - role of elevated pressure, salinity and pH. Scientific Reports 10: e7839. https://doi.org/10.1038/s41598-020-64651-8

Gauld ID, Mound LA (1982) Homoplasy and the delineation of holophyletic genera in some insect groups. Systematic Entomology 7: 73–86. https://doi.org/10.1111/j.1365-3113.1982.tb00127.x

Goulet H, Huber JT (1993) Hymenoptera of the world: An identification guide to families. Agriculture Canada, Ottawa, 668 pp.

Greenwalt DE, Rose TR, Siljestrom SM, Goreva YS, Constenius KN, Wingerath JG (2014) Taphonomy of the Fossil Insects of the Middle Eocene Kishenehn Formation. Acta Palaeontologica Polonica 60: 931–947. https://doi.org/10.4202/app.00071.2014

Henning JT, Smith DM, Nufio CR, Meyer HW (2012) Depositional setting and fossil insect preservation: a study of the late Eocene Florissant Formation, Colorado. PALAIOS 27: 481–488. https://doi.org/10.2110/palo.2011.p11-084r

Karr JA, Clapham ME (2015) Taphonomic biases in the insect fossil record: shifts in articulation over geologic time. Paleobiology 41: 16–32. https://doi.org/10.1017/pab.2014.3

Khalaim AI (2008) Fossil Ichneumon wasps (hymenoptera: Ichneumonidae) from Biamo (Russia), Oligocene. Alavesia 2: 101–112.

Klopfstein S (2021) High diversity of pimpline parasitoid wasps (Hymenoptera, Ichneumonidae, Pimplinae) from the lowermost Eocene Fur Formation. bioRxiv: 2021.11.18.468631. https://doi.org/10.1101/2021.11.18.468631

Klopfstein S, Spasojevic T (2019) Illustrating phylogenetic placement of fossils using RoguePlots: An example from ichneumonid parasitoid wasps (Hymenoptera, Ichneumonidae) and an extensive morphological matrix. PLoS ONE: 425090. [preprint, 51 pp.] https://doi.org/10.1101/425090

Klopfstein S, Langille B, Spasojevic T, Broad GR, Cooper SJB, Austin AD, Niehuis O (2019) Hybrid capture data unravel a rapid radiation of pimpliform parasitoid wasps (Hymenoptera: Ichneumonidae: Pimpliformes). Systematic Entomology 44: 361–383. https://doi.org/10.1111/syen.12333

Kopylov DS (2009) A new subfamily of ichneumonids from the Lower Cretaceous of Transbaikalia and Mongolia (Insecta: Hymenoptera: Ichneumonidae). Paleontological Journal 43: 83–93. https://doi.org/10.1134/S0031030109010092

Kopylov DS (2010) A new subfamily of ichneumon wasps (Insecta: Hymenoptera: Ichneumonidae) from the Upper Cretaceous of the Russian Far East. Paleontological Journal 44: 422–433. https://doi.org/10.1134/S003103011004009X

Kopylov DS, Brothers DJ, Rasnitsyn AP (2010) Two New Labenopimpline Ichneumonids (Hymenoptera: Ichneumonidae) from the Upper Cretaceous of Southern Africa. African Invertebrates 51: 423–430. https://doi.org/10.5733/afin.051.0211

Kopylov DS, Spasojevic T, Klopfstein S (2018) New ichneumonids (Hymenoptera, Ichneumonidae) from the Eocene Tadushi Formation, Russian Far East. Zootaxa 4442: 319–330. https://doi.org/10.11646/zootaxa.4442.2.8

Martínez-Delclòs X, Briggs DEG, Peñalver E (2004) Taphonomy of insects in carbonates and amber. Palaeogeography, Palaeoclimatology, Palaeoecology 203: 19–64. https://doi.org/10.1016/S0031-0182(03)00643-6

Matthews S (1973) Notes on Open Nomenclature and on Synonymy Lists. Paleontology 16: 713–719.

McKellar RC, Kopylov DS, Engel MS (2013) Ichneumonidae (Insecta: Hymenoptera) in Canadian Late Cretaceous amber. Fossil Record 16: 217–227. https://doi.org/10.5194/fr-16-217-2013

Meier N, Wacker A, Klopfstein S (2022) New fossil wasp species from the earliest Eocene Fur Formation has its closest relatives in late Eocene ambers (Hymenoptera, Ichneumonidae, Pherhombinae). Bulletin of the Society of Systematic Biologists 1(1): e8427. https://doi.org/10.18061/bssb.v1i1.8427

Osés GL, Petri S, Becker-Kerber B, Romero GR, Rizzutto M de A, Rodrigues F, Galante D, Silva TF da, Curado JF, Rangel EC, Ribeiro RP, Pacheco MLAF (2016) Deciphering the preservation of fossil insects: a case study from the Crato Member, Early Cretaceous of Brazil. PeerJ 4: e2756. https://doi.org/10.7717/peerj.2756

PaleoBioDB (2020) The Paleobiology Database. The Paleobiology Database. https://paleobiodb.org [July 31, 2020]

Parham JF, Donoghue PCJ, Bell CJ, Calway TD, Head JJ, Holroyd PA, Inoue JG, Irmis RB, Joyce WG, Ksepka DT, Patané JSL, Smith ND, Tarver JE, van Tuinen M, Yang Z, Angielczyk KD, Greenwood JM, Hipsley CA, Jacobs L, Makovicky PJ, Müller J, Smith KT, Theodor JM, Warnock RCM, Benton MJ (2012) Best Practices for Justifying Fossil Calibrations. Systematic Biology 61: 346–359. https://doi.org/10.1093/sysbio/syr107

Piton LEA (1940) Paléontologie du gisement éocène de Menat (Puy-de-Dôme): flore et faune. Imprimeries P. Vallier, Clermont-Ferrand, 303 pp.

Pyron RA (2011) Divergence Time Estimation Using Fossils as Terminal Taxa and the Origins of Lissamphibia. Systematic Biology 60: 466–481. https://doi.org/10.1093/sysbio/syr047

Quicke DLJ, Laurenne NM, Fitton MG, Broad GR (2009) A thousand and one wasps: a 28S rDNA and morphological phylogeny of the Ichneumonidae (Insecta: Hymenoptera) with an investigation into alignment parameter space and elision. Journal of Natural History 43: 1305–1421. https://doi.org/10.1080/00222930902807783

Rasnitsyn AP (2000) Testing cladograms by fossil record: the ghost range test. Contributions to Zoology 69: 251–258. https://doi.org/10.1163/18759866-06904003

Ride WDL, Ride WDL, International Commission on Zoological Nomenclature, International Union of Biological Sciences [Eds] (1999) International code of zoological nomenclature. 4th ed. International Trust for Zoological Nomenclature, London, 306 pp.

Ronquist F, Klopfstein S, Vilhelmsen L, Schulmeister S, Murray DL, Rasnitsyn AP (2012) A Total-Evidence Approach to Dating with Fossils, Applied to the Early Radiation of the Hymenoptera. Systematic Biology 61: 973–999. https://doi.org/10.1093/sysbio/sys058

Santos BF (2017) Phylogeny and reclassification of Cryptini (Hymenoptera, Ichneumonidae, Cryptinae), with implications for ichneumonid higher-level classification. Systematic Entomology 42: 650–676. https://doi.org/10.1111/syen.12238

Saussure H de (1852) Note sur un nouvel insecte Hyménoptère fossil. Revue et Magasin de Géologie: 579–581.

Sigovini M, Keppel E, Tagliapietra D (2016) Open Nomenclature in the biodiversity era. Methods in Ecology and Evolution 7: 1217–1225. https://doi.org/10.1111/2041-210X.12594

Slater TS, McNamara ME, Orr PJ, Foley TB, Ito S, Wakamatsu K (2020) Taphonomic experiments resolve controls on the preservation of melanosomes and keratinous tissues in feathers. Palaeontology 63: 103–115. https://doi.org/10.1111/pala.12445

Smith DM (2012) Exceptional preservation of insects in lacustrine environments. PALAIOS 27: 346–353. https://doi.org/10.2110/palo.2011.p11-107r

Spasojevic T, Wedmann S, Klopfstein S (2018a) Seven remarkable new fossil species of parasitoid wasps (Hymenoptera, Ichneumonidae) from the Eocene Messel Pit. PLoS ONE 13: e0197477. https://doi.org/10.1371/journal.pone.0197477

Spasojevic T, Broad GR, Bennett AMR, Klopfstein S (2018b) Ichneumonid parasitoid wasps from the Early Eocene Green River Formation: five new species and a revision of the known fauna (Hymenoptera, Ichneumonidae). Paläontologische Zeitschrift 92: 35–63. https://doi.org/10.1007/s12542-017-0365-5

Spasojevic T, Broad GR, Sääksjärvi IE, Schwarz M, Ito M, Korenko S, Klopfstein S (2021) Mind the Outgroup and Bare Branches in Total-Evidence Dating: a Case Study of Pimpliform Darwin Wasps (Hymenoptera, Ichneumonidae). Systematic Biology 70: 322–339. https://doi.org/10.1093/sysbio/syaa079

Théobald N (1937) Les insectes fossiles des terrains oligocènes de France. Imprimerie Georges Thomas, Nancy, 473 pp.

Townes HK (1969a) The genera of Ichneumonidae, Part 1. Memoirs of the American Entomological Institute 11: 1–300. https://doi.org/10.1007/BF02027741

Townes HK (1969b) The genera of Ichneumonidae, Part 2. Memoirs of the American Entomological Institute: 1–543. https://doi.org/10.1007/BF02027741

Townes HK (1970) The genera of Ichneumonidae, Part 3. Memoirs of the American Entomological Institute: 1–310.

Townes HK (1971) The genera of Ichneumonidae, Part 4. Memoirs of the American Entomological Institute: 1–372.

Viertler A, Klopfstein S, Jouault C, Spasojevic T (2022) Darwin wasps (Hymenoptera, Ichneumonidae) in Lower Eocene amber from the Paris basin. Journal of Hymenoptera Research 89: 19–45. https://doi.org/10.3897/jhr.89.80163

Wahl D, Gauld I (1998) The cladistics and higher classification of the Pimpliformes (Hymenoptera: Ichneumonidae). Systematic Entomology 23: 265–298. https://doi.org/10.1046/j.1365-3113.1998.00057.x

Wang B, Zhang H, Jarzembowski EA, Fang Y, Zheng D (2013) Taphonomic variability of fossil insects: a biostratinomic study of Palaeontinidae and Tettigarctidae (Insecta: Hemiptera) from the Jurassic Daohugou lagerstätte. PALAIOS 28: 233–242. https://doi.org/10.2110/palo.2012.p12-045r

Warnock RCM, Yang Z, Donoghue PCJ (2011) Exploring uncertainty in the calibration of the molecular clock. Biology Letters 8(1): 156–159. https://doi.org/10.1098/rsbl.2011.0710

Yu DSK, van Achterberg C, Horstmann K (2012) Taxapad 2012, Ichneumonoidea 2011. Ottawa, Ontario, Canada. http://www.taxapad.com

Yu DSK, van Achterberg C, Horstmann K (2016) Taxapad 2016, Ichneumonoidea 2015. Nepean, Ontario, Canada. http://www.taxapad.com

Fossil Record 25 (1) 2022, 213–230 | DOI 10.3897/fr.25.82362

Extending the diversity of the bryoflora in Kachin amber (Myanmar), with the description of *Radula patrickmuelleri*, sp. nov. and *R. tanaiensis*, sp. nov. (Jungermanniopsida, Porellales, Radulaceae)

Kathrin Feldberg[1], Alfons Schäfer-Verwimp[2], Ya Li[3], Matt A. M. Renner[4]

1 *Department of Geobiology, University of Göttingen, Goldschmidtstraße 3, 37077 Göttingen, Germany*
2 *Mittlere Letten 11, 88634 Herdwangen-Schönach, Germany*
3 *Nanjing Institute of Geology and Palaeontology, Chinese Academy of Sciences, Nanjing 210008, China*
4 *Wildland Consultants, 99 Sala Street, Whakarewarewa, Rotorua, New Zealand*

http://zoobank.org/45048AF3-36F0-4E93-AB96-07BE0F9258D9

Corresponding author: Kathrin Feldberg (kathrin.feldberg@uni-goettingen.de)

Academic editor: Florian Witzmann ♦ **Received** 16 February 2022 ♦ **Accepted** 10 May 2022 ♦ **Published** 16 June 2022

Abstract

The most prolific source of exquisitely preserved bryophyte fossils is amber, which often contains inclusions in a three-dimensional and life-like state of preservation. In recent years, many fossil species have been described from 16 worldwide deposits ranging in age from the Miocene to the Cretaceous. One of the oldest is mid-Cretaceous Kachin amber from Myanmar. It includes the moss genera *Vetiplanaxis* and *Calymperites* as well as the leafy liverwort genera *Frullania*, *Gackstroemia*, *Protofrullania*, and *Radula*. All liverwort fossils belong to the mainly epiphytic Porellales, a group which was probably strongly influenced by the rise of angiosperms and underwent significant lineage turnover in the Cretaceous. Hence, Kachin amber provides important information on the evolution of leafy liverworts during a period characterized by fundamental changes in terrestrial ecosystems. Here, we describe two new species of the mainly epiphytic leafy liverwort genus *Radula* (Radulaceae), *R. patrickmuelleri* **sp. nov.** and *R. tanaiensis* **sp. nov.**, and emend the description of *Frullania kachinensis* (Frullaniaceae). *Radula* is now represented by four species and one fossil only described to genus level, which indicates a high diversity already in the mid-Cretaceous. Furthermore, we describe additional fossil specimens of Frullaniaceae, including the third fertile specimen of *Frullania baerlocheri*, one sterile fossil of *F. cretacea*, and 12 sterile fossils of *Protofrullania cornigera*. The new fossil evidence necessitates an emendation of a recently published determination key for Cretaceous Jungermanniidae.

Key Words

Amber fossils, Cretaceous, epiphytes, leafy liverworts

Introduction

The description of bryophyte fossils from worldwide amber deposits underwent much progress in recent years with the number of species as well as the number of deposits increasing steadily (e.g., Bouju et al. 2021; Feldberg et al. 2021a, 2021b; Wang et al. 2021). Most of these fossils derive from Cenozoic deposits and have been found in middle Miocene Zhangpu amber from China (Wang et al. 2021), early Miocene Chiapas amber from Mexico (e.g., Estrada-Ruiz and Riquelme 2017; Feldberg et al. 2021a), early Miocene Dominican amber (e.g., Frahm and Newton 2005; Feldberg et al. 2021a), early Miocene Shewa amber from Ethiopia (Bouju et al. 2021), Miocene Cape York amber from Australia (Hand et al. 2010), Paleogene Bitterfeld amber from Germany (e.g., Frahm 2010; Feldberg et al. 2021a), late Eocene Baltic amber (e.g., Frahm 2010; Feldberg et al. 2021a), late Eocene Rovno amber from Ukraine (e.g., Ignatov et al. 2019; Feldberg et al. 2021a), late middle Eocene Anglesea amber from

Australia (Stilwell et al. 2020), middle Eocene Sakhalin amber from Russia (Ignatov and Perkovsky 2013), early Eocene Cambay amber from India (e.g., Heinrichs et al. 2016a), and Paleocene-Eocene amber from the Chickaloon Formation in Alaska (Grimaldi et al. 2018). The oldest sources are Late Cretaceous Taimyr amber from Russia (e.g., Ignatov et al. 2016), Late Cretaceous Kuji amber from Japan (e.g., Katagiri et al. 2013; Katagiri and Shinden 2020), mid-Cretaceous Alaskan amber (Heinrichs et al. 2011), and mid-Cretaceous Kachin amber from northern Myanmar (e.g., Hedenäs et al. 2014; Heinrichs et al. 2014; Feldberg et al. 2021a, 2021b; Li et al. 2021b, 2022b). The latter includes the moss genera *Vetiplanaxis* with four species and *Calymperites* with one (Bell and York 2007; Hedenäs et al. 2014; Heinrichs et al. 2014) as well as a very diverse flora of porellalean leafy liverworts which has recently been revised by Feldberg et al. (2021b) and regularly yields new and interesting fossil species (e.g., Li et al. 2020, 2021b, 2022b).

Amber fossils provide important information on the evolution of leafy liverworts (Jungermanniidae) which are otherwise comparatively rare in the fossil record (e.g., Heinrichs et al. 2018; Tomescu et al. 2018). In contrast, thalloid liverworts (Pelliidae, Metzgeriidae, Marchantiopsida) and mosses (Bryophyta) are found more frequently in sedimentary rocks since the Middle Devonian and the Carboniferous, respectively (Tomescu et al. 2018; Ignatov and Maslova 2021). The often excellent and three-dimensional preservation state in amber allows utilization of many amber inclusions as minimum age constraints in divergence time estimates based on molecular phylogenies of extant species (e.g., Feldberg et al. 2014, 2021a; Laenen et al. 2014; Bechteler et al. 2017). Subsequent diversification analyses of Jungermanniidae indicate that the order Porellales, which mainly comprises epiphytes and epiphylls, underwent a lineage turnover beginning in the Cretaceous when flowering plants were on the rise (Feldberg et al. 2014). The Angiosperm Terrestrial Revolution (e.g., Magallón et al. 2019; Benton et al. 2022) caused fundamental changes in terrestrial ecosystems and has likely influenced the evolution of epiphytic lineages. Furthermore, Cretaceous Porellales often show distinct morphological differences to modern taxa which is another indicator of significant changes within this taxon during this period (Feldberg et al. 2021a, 2021b).

The most striking differences can be found in Frullaniaceae, by far the most diverse taxon included in amber. The family includes one extant genus, the mainly epiphytic *Frullania*, which is morphologically well defined but has a very complex subgeneric taxonomy with 576 accepted species in several subgenera whose circumscription is often unclear (e.g., Hentschel et al. 2009b, 2015; Heinrichs et al. 2010; von Konrat et al. 2013; Söderström et al. 2016; Carter et al. 2017). Extant *Frullania* has a subcosmopolitan distribution with a center of diversity in humid tropical regions, but also occurs in temperate as well as arctic and alpine areas (Schuster 1992; Hentschel et al. 2009b). The family also includes the extinct *Protofrullania cornigera* Heinrichs from Kachin amber (Heinrichs et al. 2017a; Feldberg et al. 2021b) and probably the extinct *Kaolakia borealis* Heinrichs et al. from Alaskan amber (Heinrichs et al. 2011) as well as *Pseudofrullania hamatosetacea* (Grolle) Heinrichs et al. from Bitterfeld amber (Heinrichs et al. 2018).

Despite having an extant center of diversity in the tropics, Cenozoic *Frullania* fossils are rarely reported from tropical regions. To date, only one inclusion of *Frullania* has been found in Dominican amber, which otherwise contains a very diverse leafy liverwort flora (Heinrichs and Schmidt 2010; Feldberg et al. 2021a), and two species have recently been described from Ethiopian Shewa amber, namely *F. shewanensis* Feldberg et al. and *F. palaeoafricana* Feldberg et al. (Bouju et al. 2021). In contrast, the genus is highly diverse in Cenozoic European ambers (Feldberg et al. 2021a). Fifteen species of *Frullania* have been described, with *F. grabenhorstii* Heinrichs et al. and *F. mammilligera* Grolle occurring only in Bitterfeld amber (Grolle 2003; Feldberg et al. 2018), *F. acutata* Casp. only in Baltic amber (Caspary 1887), and *F. ekaterinae* Mamontov et al., *F. riclefgrollei* Mamontov et al., *F. rovnoi* Mamontov et al., *F. schmalhausenii* Mamontov et al., *F. vanae* Mamontov et al., and *F. zerovii* Mamontov et al. only in Rovno amber (Mamontov et al. 2015, 2017, 2018, 2019, 2020). *Frullania baltica* Grolle, *F. casparyi* Grolle, *F. schumannii* (Casp.) Grolle, and *F. truncata* Casp. occur in Bitterfeld as well as Baltic amber (Caspary 1887; Grolle 1981, 1985; Grolle and Meister 2004), *F. pycnoclada* Grolle occurs in Baltic and Rovno amber (Grolle and Meister 2004; Mamontov et al. 2020), and *F. varians* Casp. occurs in Bitterfeld, Baltic, and possibly also Rovno amber (Caspary 1887; Grolle and Meister 2004; Konstantinova et al. 2012; Mamontov et al. 2020). While some of these species show some unique characters, which make an assignment to extant subgenera or sections difficult, many are very similar to the extant diversity and could be employed in divergence times estimates, given extended DNA datasets of extant species which can solve the remaining taxonomic problems (Mamontov et al. 2020; Feldberg et al. 2021a).

The oldest unequivocal Frullaniaceae fossils have been described from Kachin amber and these tend to differ strongly from the extant diversity (Feldberg et al. 2021a, 2021b). The most common leafy liverwort inclusion found in this deposit is *Protofrullania cornigera* (Heinrichs et al. 2017a; Feldberg et al. 2021b), which differs from *Frullania* by its elongated ovate to strap-shaped underleaves which carry rhizoid bundles at their apical regions, a character unknown in *Frullania* where the undivided or bifurcated underleaves carry rhizoid bundles near their base or near the middle. But *Protofrullania* is not the only Frullaniaceae with morphological characters unknown or rare in extant representatives, also the mid-Cretaceous species assignable to *Frullania* show unique or rare characters and character combinations. One example is *F. cretacea* Hentschel et al. (Hentschel et al. 2009a; Heinrichs et al. 2012) with its long ciliate underleaves, and another is *F. kachinensis* Y.Li et al. (Li et al. 2021b), which has bifurcated underleaves with serrate lobes and rhizoid bundles inserted just below the sinus. The remaining fossil species *F. baerlocheri* Heinrichs et al. and *F. partita* Y.Li et al. might look more similar to the extant diversity, but do not fit any extant lineage within the genus due to the unusual combination of characters (Feldberg et al. 2021b; Li et al. 2021a).

Another diverse genus found in Kachin amber is *Radula*, which comprises ca. 200 extant species in seven subgenera (e.g., Devos et al. 2011; Söderström et al. 2016), most of which are epiphytes or epiphylls. *Radula* has a subcosmopolitan distribution with a center of diversity in tropical to warm temperate regions. In recent years several molecular phylogenetic studies greatly extended the knowledge of this taxonomically challenging genus (Devos et al. 2011; Renner et al. 2013a, 2013b; Renner 2014, 2015; Patiño et al. 2017). However, species delimitation based on morphological characters alone can be difficult because of the high degree of morphological homoplasy and sometimes subtle differences among relatively unrelated taxa (e.g., Renner et al. 2013a, 2014, 2015). This especially applies to fossil material which is often fragmentary and sterile.

Radula has a comparatively extensive fossil record with nine species known from different amber deposits (Grolle 1987; Heinrichs et al. 2016b, 2018; Kaasalainen et al. 2017; Stilwell et al. 2020; Feldberg et al. 2021a, 2021b). Most appear very similar to the extant diversity, though this might be misleading. The youngest fossils are *R. intecta* M.A.M.Renner et al. (Kaasalainen et al. 2017) and *R. steerei* Grolle (Grolle 1987) from Miocene Dominican amber, which are sterile and cannot be assigned to a subgenus with confidence. *Radula intecta* may belong to subg. *Volutoradula* and *R. steerei* has been compared to the extant Japanese endemic *R. fauriana* Steph. (Grolle 1987), which is listed as *incertae sedis* in Söderström et al. (2016) but was included in subgen. *Radula* sect. *Faurianae* by Yamada (1979). Three fossil species have been found in Cenozoic ambers of Europe. *Radula baltica* Heinrichs et al. is known only from the holotype in Eocene Baltic amber, while *R. sphaerocarpoides* Grolle and *R. oblongifolia* Casp. are common fossils in Baltic as well as Bitterfeld amber (Caspary 1887; Grolle 1980; Grolle and Meister 2004; Heinrichs et al. 2016b). The latter species is autoicous and is often preserved with androecia, gynoecia, and sporophyte, while the former two are only known in sterile condition and might represent several biological entities given their morphological heterogeneity (Heinrichs et al. 2016b). Furthermore, two fossil specimens have been reported from late middle Eocene amber of Anglesea, Victoria, Australia (Stilwell et al. 2020) but have not been formally described. The oldest previously described species are *R. cretacea* Bechteler et al., which is preserved with apparently unfertilized gynoecia, and the likely distantly related and sterile *R. heinrichsii* Feldberg et al. from Kachin amber (Bechteler et al. 2017; Feldberg et al. 2021b; Wang et al. in press). *Radula cretacea* is probably a member of subg. *Odontoradula* and may even represent one of the several crown group lineages, given the shared possession of characters displayed by extant species of *Radula* subg. *Odontoradula* sect. *Acutifoliae* (Bechteler et al. 2017). The relationship of *R. heinrichsii* is more obscure, because its microphyllous (amentulose) branches have no exact equivalent among extant species, though their presence along with the longitudinal lobule stem insertion suggests the species belongs to subg. *Amentuloradula* (Feldberg et al. 2021b).

Here we describe two further fossil species of this diverse genus from Kachin amber as *R. patrickmuelleri* sp. nov. and *R. tanaiensis* sp. nov. and provide an updated determination key for Cretaceous Jungermanniidae. Furthermore, we obtained several new specimens of previously described fossil species which we list and evaluate. These include several sterile specimens of *Protofrullania cornigera*, one sterile specimen each of *Frullania cretacea* and *F. kachinensis*, the third fertile specimen of *F. baerlocheri* with gynoecium, as well as a fossil showing strong similarities to *Radula cretacea*. Furthermore, two additional specimens of the moss *Calymperites burmensis* Heinrichs et al. are illustrated. Most specimens are in good accordance with the type material, others require diagnoses and descriptions to be emended.

Material and methods

All fossils derive from Kachin amber of northern Myanmar which was mined from outcrops about 20 km southwest of the village of Tanai located on the Ledo Road ca. 105 km north of Myitkyina in Kachin State, northern Myanmar (Cruickshank and Ko 2003; Grimaldi and Ross 2017). Several lines of evidence point to a mid-Cretaceous age of Kachin amber (Grimaldi et al. 2002; Grimaldi and Ross 2017). Biostratigraphic studies by Cruickshank and Ko (2003) suggested an age of ca. 100 Ma (late Albian) of the amber-bearing deposit, and Shi et al. (2012) assigned a minimum age of 98 Ma (earliest Cenomanian) based on recent U-Pb dating of zircons. These age estimates have recently been confirmed by the discovery of an ammonite shell of the genus *Puzosia*, a late Albian–late Cenomanian index fossil, enclosed in a piece of Kachin amber (Yu et al. 2019).

The specimens of *Protofrullania cornigera* (BuB 3811, 3812, 4333–4338, 4394, 4408, 4409, 4413), *Frullania cretacea* (BuB4411), and *Calymperites burmensis* (BuB 4339, 4398) are housed in the Patrick Müller Amber Collection (Amber Research Group, c/o Geological-Palaeontological Institute and Museum (CeNak) of the University of Hamburg). *Frullania baerlocheri* GZG.BST.22039 (BuB4220), *F. kachinensis* GZG.BST.22040 (BuB4431), *Radula patrickmuelleri* GZG.BST.22041 (BuB4395), *R. tanaiensis* GZG.BST.22042 (BuB4329), and *Radula* sp. GZG.BST.22043 (BuB4420) are housed in the Geoscience Centre (GZG) at the University of Göttingen, Germany (all formerly Patrick Müller Amber Collection). *Frullania kachinensis* PB22711a (holotype) is housed in the Nanjing Institute of Geology and Palaeontology, Chinese Academy of Sciences.

Relating to the recent conflicts in Myanmar (e.g., Sokol 2019), we declare that all Kachin amber pieces mentioned in this study have been collected before the year 2017 and that we follow the recommendations by Haug et al. (2020). The specimens from the American Museum of Natural History were provided to the museum prior to 2010 (refer to Hentschel et al. 2009a and Heinrichs et al. 2012). The fossils deposited in the Nanjing Institute of Geology and Palaeontology and the Zhejiang Museum of Natural History were collected in compliance with the laws of Myanmar and China, including Myanmar's import and export regulations of jewelry, and China's fossil law. Specimens deposited in the remaining collections were legally purchased from an authorized trader from Myanmar in 2016.

Frullania kachinensis (PB22711a, holotype) was examined under a ZEISS Axio ZoomV16 microscope equipped with a high-resolution digital camera (Axiocam 512 colour). All images were digitally stacked photomicrographic composites from ca. 50 individual focal planes using the software package ZEN 2.3 pro. All other specimens were prepared for study according to procedures described by Sadowski et al. (2021). Photographic documentation of the specimens was carried out under Zeiss AxioScope A1 compound microscopes equipped with Cannon Eos 70D and Cannon Eos 5D digital cameras. All images are digitally stacked photomicrographic composites from up to 76 individual focal planes using the software package HeliconFocus version 7.6.1. Pro.

Results

Systematic paleontology

Newly described specimens of new as well as known species are indicated in bold print.

Phylum BRYOPHYTA
Class BRYOPSIDA
Subclass DICRANIDAE
Order DICRANALES
Family *incertae sedis*
Genus *Calymperites*

Calymperites burmensis Heinrichs, Schäf.-Verw., Hedenäs, Ignatov & A.R.Schmidt

Suppl. material 1: Fig. S1

Calymperites burmensis Heinrichs, Schäf.-Verw., Hedenäs, Ignatov & A.R.Schmidt; in Cretaceous Research 51: 261, figs 1, 2. 2014.

Holotype. AMNH Bu ASJH-2, Amber collection of the Division of Invertebrate Zoology of the American Museum of Natural History, New York, USA.

Additional specimens investigated. BuB4339, BuB4398, Patrick Müller Amber Collection.

Locality and horizon. Amber mines southwest of the village of Tanai ca. 105 km north of Myitkyina in Kachin State, northern Myanmar, fossil enclosed in upper Albian–lower Cenomanian Kachin amber.

Remarks. To date, this acrocarpous moss was only known from one specimen (Suppl. material 1: Fig. S1A; Heinrichs et al. 2014). As far as the disintegrated state of the new fossils allows to ascertain, they are in good accordance with the type. In both specimens the leaves are erect-spreading and slightly crisped, their bases are oblong-ovate and sheathing the stem before they taper into lanceolate upper regions, and the costa is single and excurrent on intact leaves (Suppl. material 1: Fig. S1B–D). The apices are acute to awned in BuB4398 (Suppl. material 1: Fig. S1B), while they are mostly broken in BuB4339 (Suppl. material 1: Fig. S1C, D). It is not visible if the leaves are serrulate, or if large hyaline cells are present near the apex. Furthermore, the leaf cells are not clearly visible for the largest part, but they appear to be small and quadrate on upper parts of the lamina (Suppl. material 1: Fig. S1D) and more elongated on lower parts (Suppl. material 1: Fig. S1B).

Phylum MARCHANTIOPHYTA
Class JUNGERMANNIOPSIDA
Subclass JUNGERMANNIIDAE
Order PORELLALES
Family FRULLANIACEAE
Genus *Frullania*

Frullania baerlocheri Heinrichs, M.E.Reiner, K.Feldberg, von Konrat, Hentschel, Váňa & A.R.Schmidt

Suppl. material 1: Fig. S2A–E

Frullania baerlocheri Heinrichs, M.E.Reiner, K.Feldberg, von Konrat, Hentschel, Váňa & A.R.Schmidt; in Review of Palaeobotany and Palynology 169: 26, plate IV, figs 2, 3. 2012.

= *Frullania pinnata* Heinrichs, K.Feldberg, Schäf.-Verw. & M.Krings; in Cretaceous Research 78: 57, figs 1–3. 2017.—Holotype: GZG. BST.21963, Geoscience Centre (GZG) at the University of Göttingen, Germany; *syn. fide* Li et al., 2021a.

Holotype. AMNH Bu-FB 1 g, Amber collection of the Division of Invertebrate Zoology of the American Museum of Natural History, New York, USA.

Additional specimens investigated. SNSB-BSPG 2021 XII 1 (Müller BuB1874; syninclusion *Protofrullania cornigera*), Bavarian State Collection for Palaeontology and Geology, Munich, Germany; GZG.BST.22015 (Müller BuB3538), **GZG.BST.22039 (Müller BuB4220; with gynoecia),** Geoscience Centre (GZG) at the University of Göttingen, Germany; PB22712, PB23288 (with gynoecia), Nanjing Institute of Geology and Palaeontology, Chinese Academy of Sciences; BuB3681, BuB3682, Patrick Müller Amber Collection; ZMNH155044a (syninclusion *Radula heinrichsii*), ZMNH155047b, c (syninclusion *Frullania kachinensis*), Zhejiang Museum of Natural History, China.

Locality and horizon. Amber mines southwest of the village of Tanai ca. 105 km north of Myitkyina in Kachin State, northern Myanmar, fossil enclosed in upper Albian–lower Cenomanian Kachin amber.

Remarks. The new fossil specimen is in good accordance with the type as well as subsequently described material and represents the third fertile specimen (Suppl. material 1: Fig. S2A–E; compare descriptions in Heinrichs et al. 2012, 2017b; Feldberg et al. 2021b; Li et al. 2021a). Two unfertilized gynoecia are situated on short side branches similar to specimen PB23288 (Li et al. 2021a), but they are less far developed and most characters are obscured (Suppl. material 1: Fig. S2A, C). A subinvolucral lateral leaf with an explanate lobule is well visible (Suppl. material 1: Fig. S2D, indicated by black arrow), whereas the bracteoles and bracts are concealed for the largest part. The typical acute lobe tip can be seen on one bract (Suppl. material 1: Fig. S2E, indicated by white arrow).

Frullania cretacea Hentschel, A.R.Schmidt & Heinrichs

Suppl. material 1: Fig. S2F, G

Frullania cretacea Hentschel, A.R.Schmidt & Heinrichs; in Cryptogamie, Bryologie 30: 326, figs 1–10. 2009.

Holotype. AMNH B-011, Amber collection of the Division of Invertebrate Zoology of the American Museum of Natural History, New York, USA.

Additional specimens investigated. AMNH Bu-FB 1 a–f (AMNH Bu-FB 1 b with gynoecium), AMNH Bu-FB 51, Amber collection of the Division of Invertebrate Zoology of the American Museum of Natural History, New York, USA; GZG.BST.22016, (Müller BuB3533), GZG.BST.22017 (Müller BuB1190), Geoscience Centre (GZG) at the University of Göttingen, Germany; PB23687 Nanjing Institute of Geology and Palaeontology, Chinese Academy of Sciences; BuB1772, BuB3530, **BuB4411,** Patrick Müller Amber Collection; F3157/BU/CJW, Jörg Wunderlich Amber Collection.

Locality and horizon. Amber mines southwest of the village of Tanai ca. 105 km north of Myitkyina in Kachin State, northern Myanmar, fossil enclosed in upper Albian–lower Cenomanian Kachin amber.

Remarks. This small specimen is in good accordance with the type and previously described material (Suppl. material 1: Fig. S2F, G; compare descriptions in Hentschel et al. 2009a; Heinrichs et al. 2012; Feldberg et al. 2021b). The typical rectangular to ovate underleaves with two long apical cilia (Suppl. material 1: Fig. S2G) and the lobules, which are inserted parallel to the stem to slightly oblique, are well visible.

Frullania kachinensis Y.Li, Y.-D.Wang & K.Feldberg

Figs 1, 2

Frullania kachinensis Y.Li, Y.-D.Wang & K.Feldberg; in Geological Journal 56: 5048, figs 1–3. 2021.

Holotype. PB22711a, Nanjing Institute of Geology and Palaeontology, Chinese Academy of Sciences.

Paratypes. PB22711c, d, Nanjing Institute of Geology and Palaeontology, Chinese Academy of Sciences; ZMNH155047a, d, e, ZMNH155048c, Zhejiang Museum of Natural History, China.

Additional specimens investigated. GZG.BST.22040 (Müller BuB4431), Geoscience Centre (GZG) at the University of Göttingen, Germany.

Locality and horizon. Amber mines southwest of the village of Tanai ca. 105 km north of Myitkyina in Kachin State, northern Myanmar, fossil enclosed in upper Albian–lower Cenomanian Kachin amber.

Emended diagnosis. Sterile shoots irregularly branched. Foliation incubous; lateral leaves complicate-trilobed, dorsal lobe ovate to elliptic with rounded apex and mamillose cells, ventral lobule *Frullania*-type, cylindrical, helmet-shaped to campanulate, with toothed margins, stylus narrow lanceolate to linear. Underleaves distant to contiguous, elliptic to elongate ovate, bilobed 0.3–0.8 × their length; lobes lanceolate, entire-margined to strongly toothed or ciliate, sinus more or less V-shaped. Rhizoids in bundles, inserted just below sinus.

Emended description. Gametophyte fragments 2.89–4.91 mm long, reddish to yellowish brown (Figs 1A, B, 2A), main shoots 0.46–1.00 mm wide, irregularly branched; branches 0.64–1.67 mm long and 0.28–0.92 mm wide. Stem reddish brown to dark brown, 37–65 µm in diameter. Lateral leaves incubous, (sub)horizontally spreading, alternate, imbricate to contiguous, complicate-trilobed. Dorsal lobe slightly concave to nearly flat (Figs 1A–D, 2A–C), ovate to elliptic, on main shoots 290–550 µm long × 200–380 µm wide, length:width ratio 1.2–1.5:1; entire-margined, gradually narrowed towards apex or apex broadly rounded; dorsally extending 0.5–1.2 × the stem width beyond the farther edge of the stem. Lobe cells hexagonal, marginal cells (sub)isodiametric, 15–25 µm in diameter, medial cells slightly elongate, 16–36 µm long × 12–25 µm wide, up to 1.5 × as long as wide (Figs 1C–E, 2B, C); cell walls thin to moderately thickened, with small triangular trigones, no intermediate thickenings seen; one large mamilla per cell, ca. 5 µm high and 7.5–10 µm in diameter (Figs 1E, 2C), or leaf cells smooth. Ocelli not seen, but occasionally dorsal lobes with conspicuous large and elongated cells in the middle. Ventral lobule *Frullania*-type (Figs 1A–D, 2), cylindrical, helmet-shaped to campanulate, inflated, broadest part near opening, 110–220 µm long × 80–210 µm wide, length–width ratio 0.8–2.2:1, inserted in ca. 30–90 µm distance to stem, either nearly parallel to stem or obliquely positioned with upper part oriented towards stem and sometimes overlapping stem; opening not constricted, slightly emarginated, with short, acute tip on outer margin, dorsal and ventral margins angular, with one acute tooth in the middle (Figs 1B–D, 2C, D), tooth up to 10 µm (one cell) long, possibly bearing slime papillae at tip [seen on one tooth in GZG.BST.22040]; lobule cells isodiametric, hexagonal, 11–24 µm in diameter, smooth to mamillose. Stylus narrow, lanceolate to linear, 30–40 µm long, base 2–3 cells wide with uniseriate apex of 1–3 cells. Underleaves distant to contiguous, 180–310 µm long × 50–150 µm wide,

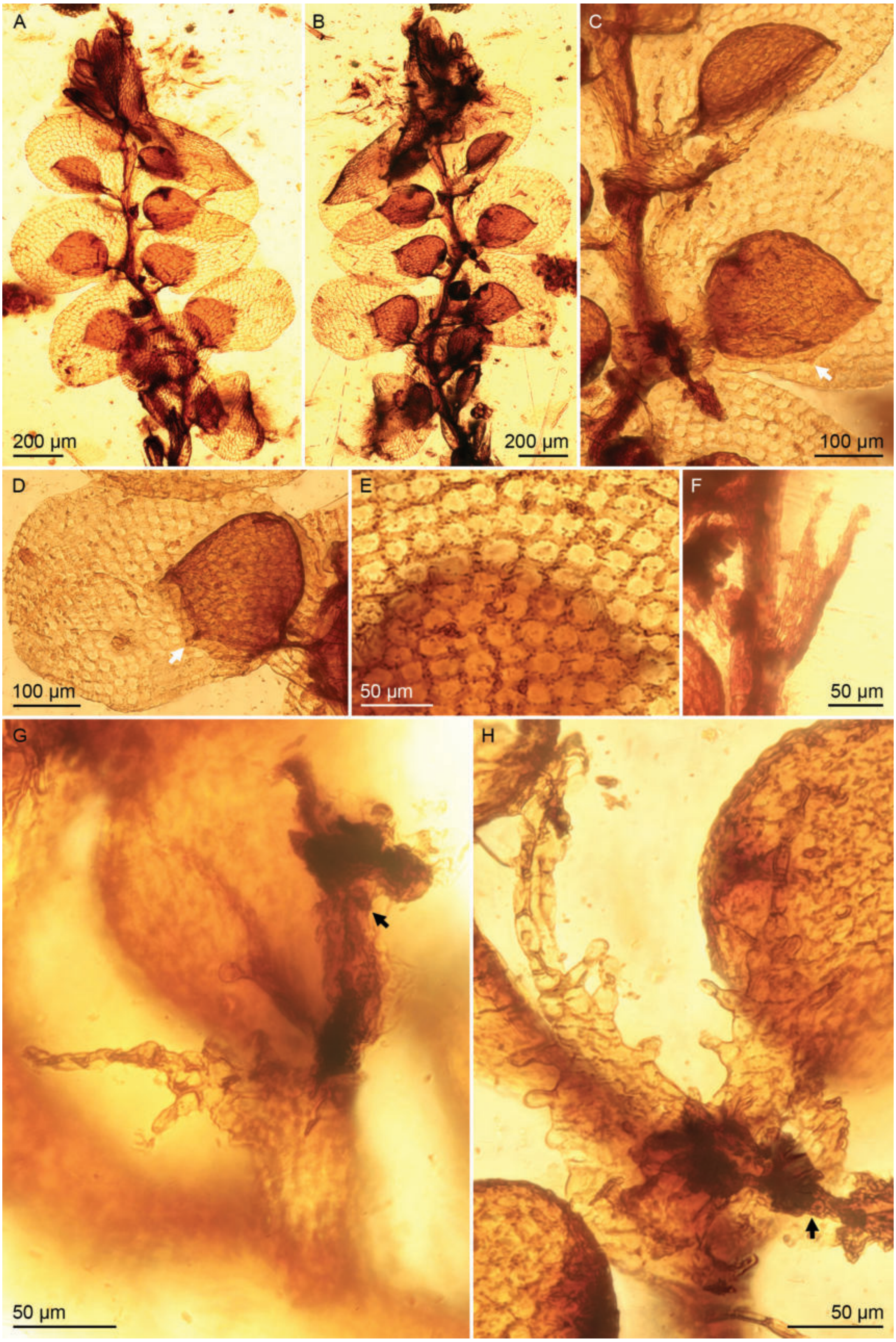

Figure 1. *Frullania kachinensis* Y.Li et al., GZG.BST.22040 (Müller BuB4431). **A.** Gametophyte fragment, dorsal; **B.** Gametophyte fragment, ventral; **C.** *Frullania*-type lobules (marginal tooth indicated by white arrow) and ciliate underleaves, ventral; **D.** Dorsal lobe and ventral lobule (marginal teeth indicated by white arrow); **E.** Lobe cells with large central mamillae, dorsal; **F.** Small underleaf on lower part of stem, lateral; **G, H.** Underleaves with ciliate to toothed lobes and rhizoid bundles (indicated by black arrows) inserted just below the vertexes of the sinus.

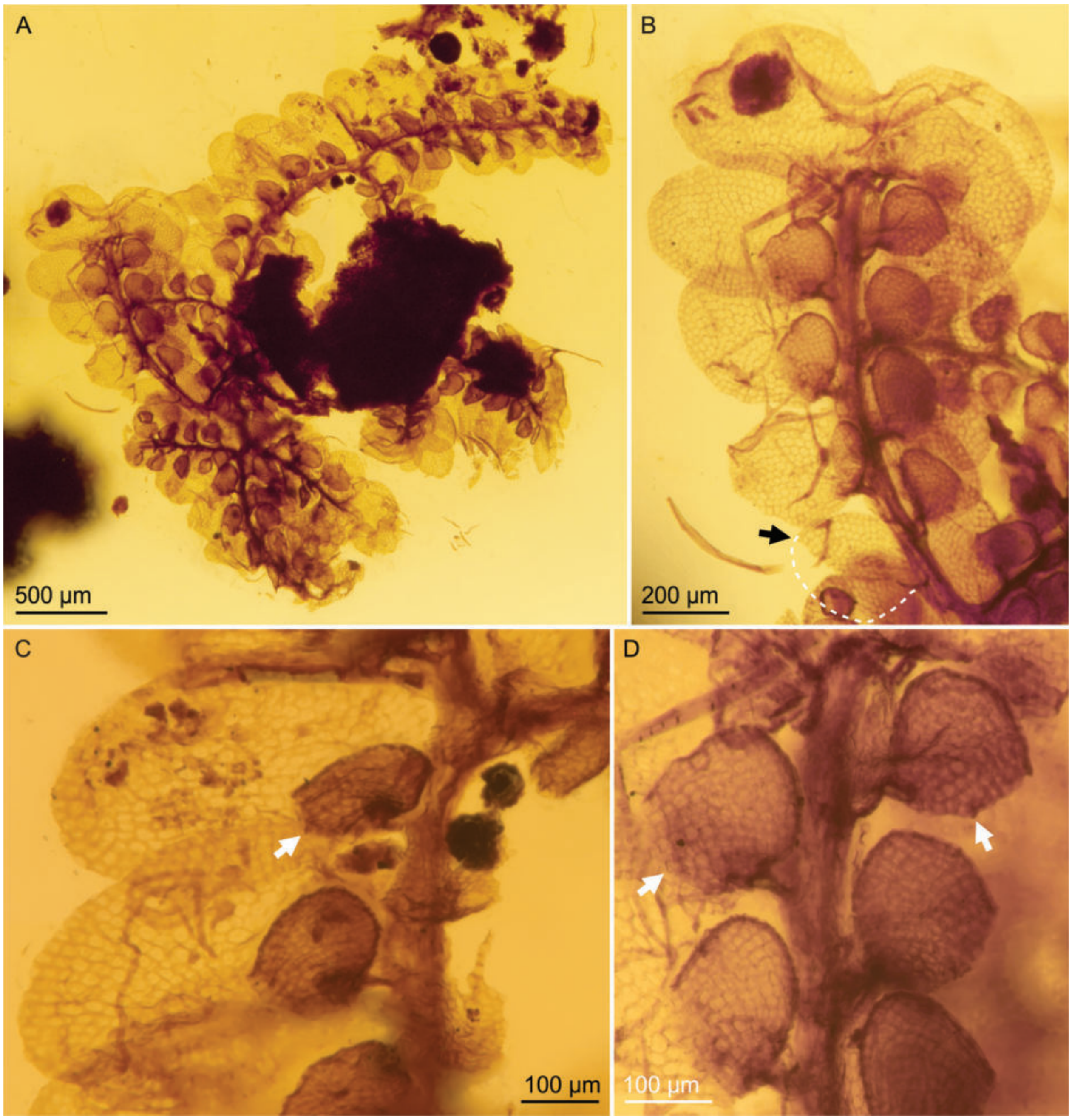

Figure 2. *Frullania kachinensis* Y.Li et al., PB22711a, holotype. **A.** Gametophyte fragment, ventral; **B.** Detail of main shoot, ventral (the black arrow and the dashed line indicate a broken leaf which was described as apiculate in Li et al. 2021a); **C, D.** Leaf lobules with toothed margins (teeth indicated by white arrows) and underleaves, ventral.

length:width ratio 2.1–3.6:1, elliptic to elongate ovate, bilobed 0.3–0.8 × their length (Figs 1F–H, 2C, D), underleaf lobes lanceolate, (2)4–5(8) cells wide at base [not well visible on GZG.BST.22040], gradually narrowing into a single cell wide filament, apically terminated by a slime papilla; lobes entire or weakly to strongly toothed or ciliate, with up to six 10–55 µm long teeth or cilia consisting of 1–3 uniseriate, quadrate to rectangular cells; teeth and cilia becoming successively smaller towards lobe tip; margins of lower lamina generally entire, occasionally crenulate due to protruding cells or with short teeth (Fig. 2C, D); underleaf sinus more or less V-shaped with an acute to obtuse vertex. Rhizoids in bundles (Fig. 1G, H), inserted just below sinus of underleaves, bundles up to 160 µm long and 20–30 µm wide at base; rhizoids ca. 10 µm in diameter. Sterile.

Remarks. The new fossil of *F. kachinensis* (Fig. 1) is in rather good accordance with the type (Fig. 2), but some characters are more conspicuous. Most notable are the rhizoid bundles inserted directly below the underleaf sinus as well as the strongly toothed to ciliate underleaf lobes (Fig. 1G, H) and the toothed lobule margins (Fig. 1B–D, indicated by white arrows). A reinvestigation of the holotype also revealed toothed lobule margins (Fig. 2C, D, indicated by white arrows) and the absence of acute lobe apices (Fig. 2B, indicated by black arrow and dashed line). All lobes are gradually narrowed towards the apex or have a broadly rounded apex. The presence of rhizoids in the type material could not be ascertained.

Genus *Protofrullania*

Protofrullania cornigera Heinrichs

Suppl. material 1: Figs S3–S5

Protofrullania cornigera Heinrichs; in Cretaceous Research 74: 225, figs 1, 2. 2017.

Holotype. GZG.BST.21956, Geoscience Centre (GZG) at the University of Göttingen, Germany.

Additional specimens investigated. SNSB-BSPG 2021 XII 1 (Müller BuB1874; syninclusion *Frullania baerlocheri*), SNSB-BSPG 2021 XII 2 (Müller BuB1893; with juvenile gynoecium), SNSB-BSPG 2021 XII 3 (Müller BuB1897), Bavarian State Collection for Palaeontology and Geology, Munich, Germany; GZG.BST.22018 (Müller BuB1999; with perianth), GZG.BST.22019 (Müller BuB3534; with oval underleaves), GZG.BST.22020 (Müller BuB3535; with gynoecium), GZG.BST.22021 (Müller BuB3537; with androecia and oval underleaves), GZG.BST.22022 (Müller BuB3677; with oval underleaves), Geoscience Centre (GZG) at the University of Göttingen, Germany; PB22707, PB22711b (syninclusion *Frullania kachinensis*), PB23289, Nanjing Institute of Geology and Palaeontology, Chinese Academy of Sciences; BuB3521, BuB3536, BuB3675, BuB3679 (with oval underleaves), **BuB3811, BuB3812, BuB4333–4338, BuB4394 (with oval underleaves), BUB4408a, b, BUB4409, BUB4413 (with oval underleaves),** Patrick Müller Amber Collection; F3251/BU/CJW, Jörg Wunderlich Amber Collection.

Locality and horizon. Amber mines southwest of the village of Tanai ca. 105 km north of Myitkyina in Kachin State, northern Myanmar, fossil enclosed in upper Albian–lower Cenomanian Kachin amber.

Remarks. All specimens are in good accordance with the type and previously described material (Suppl. material 1: Figs S3–S5; compare descriptions in Heinrichs et al. 2017a; Feldberg et al. 2021b) and show the characteristic helmet-shaped to campanulate *Frullania*-type lobules which are often large in relation to the lobes (Suppl. material 1: Figs S3D, S4F, S5B, D, F). As in previously investigated material, the form of the underleaves is very heterogenous (Feldberg et al. 2021b). Most are elongate rectangular to strap-shaped and taper progressively towards the apex (Suppl. material 1: Figs S3D, S4B, S5B). Below the apex they are usually somewhat increasing with the uppermost sector being obtriangular or irregularly rounded and often carrying rhizoid bundles and marginal teeth or cilia. Some underleaves on main shoots and occasionally also on primary branches are ovate to obovate to rectangular with the widest part in the middle and often less prominent cilia (Suppl. material 1: Figs S4F, S5F). One specimen (BuB4334) has a very distinct flagelliform branch (Suppl. material 1: Fig. S3E).

Family RADULACEAE
Genus *Radula*

Radula patrickmuelleri K.Feldberg, Schäf.-Verw. & M.A.M.Renner, sp. nov.

http://zoobank.org/2CC0D59C-44E5-4B9B-B81A-5D40606F24DF

Figs 3, 4A–E

Holotype. GZG.BST.22041 (Müller BuB4395), Geoscience Centre (GZG) at the University of Göttingen, Germany.

Etymology. The specific epithet honors the amber collector Patrick Müller (Zweibrücken, Germany) who generously supports our research by providing numerous amber fossils for study.

Locality and horizon. Amber mines southwest of the village of Tanai ca. 105 km north of Myitkyina in Kachin State, northern Myanmar, fossil enclosed in upper Albian–lower Cenomanian Kachin amber.

Diagnosis. Gametophyte with zig-zagged stems and complicate bilobed lateral leaves; dorsal lobe oblong-elliptic with broadly rounded to obtuse apex; ventral lobule small, *Lejeunea*-type, longitudinally inserted, rounded rectangular to ovate with subacute to rounded apex, inner margin not ampliate, not exceeding stem; irregularly shaped gemmae produced on lobe margins.

Description. Unbranched gametophyte fragment ca. 4.84 mm long, yellowish to reddish brown (Fig. 3A–D); main shoot 1.68–2.28 mm wide with leaves. Stem dark reddish brown, distinctly zig-zagged, ca. 60 µm wide [numbers of cell rows not clearly visible, possibly 4–5]; surface cells elongated, 2–3 × as long as wide; ventral and dorsal leaf-free strips ca. 2 cells wide. One rhizoid bundle visible on the lobule of a basal leaf (Fig. 3E), bundle 7.5–10 µm wide, rhizoids up to 130 µm long. Foliation incubous, lateral leaves alternate, complicate bilobed, divided into large dorsal lobe and smaller ventral *Lejeunea*-type lobule enclosing the ventral leaf surface and forming a sharp postical keel (Fig. 3D–F). Dorsal lobes imbricate, oblong-elliptic, longer than wide, nearly flat, spreading to more erect on upper part of shoot, but not obliquely patent (Fig. 3A–D); margin entire to slightly crenulate due to gemmae production; postical margin slightly emarginated at end of keel, then regularly arched towards apex, apex broadly rounded to obtuse, antical margin regularly arched and nearly parallel to postical margin in the lobe middle, abruptly curved near stem and forming an angle of ca. 90° to the inner margin, inner margin not ampliate, extending onto the dorsal stem surface up to 0.5–1 × the stem width; lobe 550–600 µm long × 340–420 µm wide, length:width ratio 1.3–1.7:1, length exterior to keel 410–510 µm, length of stem insertion ca. 170–190 µm [not clearly visible on most leaves]. Cells of lobe margin quadrate to rectangular, 10–20 µm long × 15–25 µm wide, long axis parallel with leaf margin; medial cells hexagonal, mostly isodiametric to occasionally weakly elongated, 20–35 µm long × 20–30 µm wide; basal cells of the same size or slightly larger than medial cells, 20–40 µm long × 20–35 µm wide (Fig. 4A, B); cell walls thin, with small, triangular trigones possibly present at cell

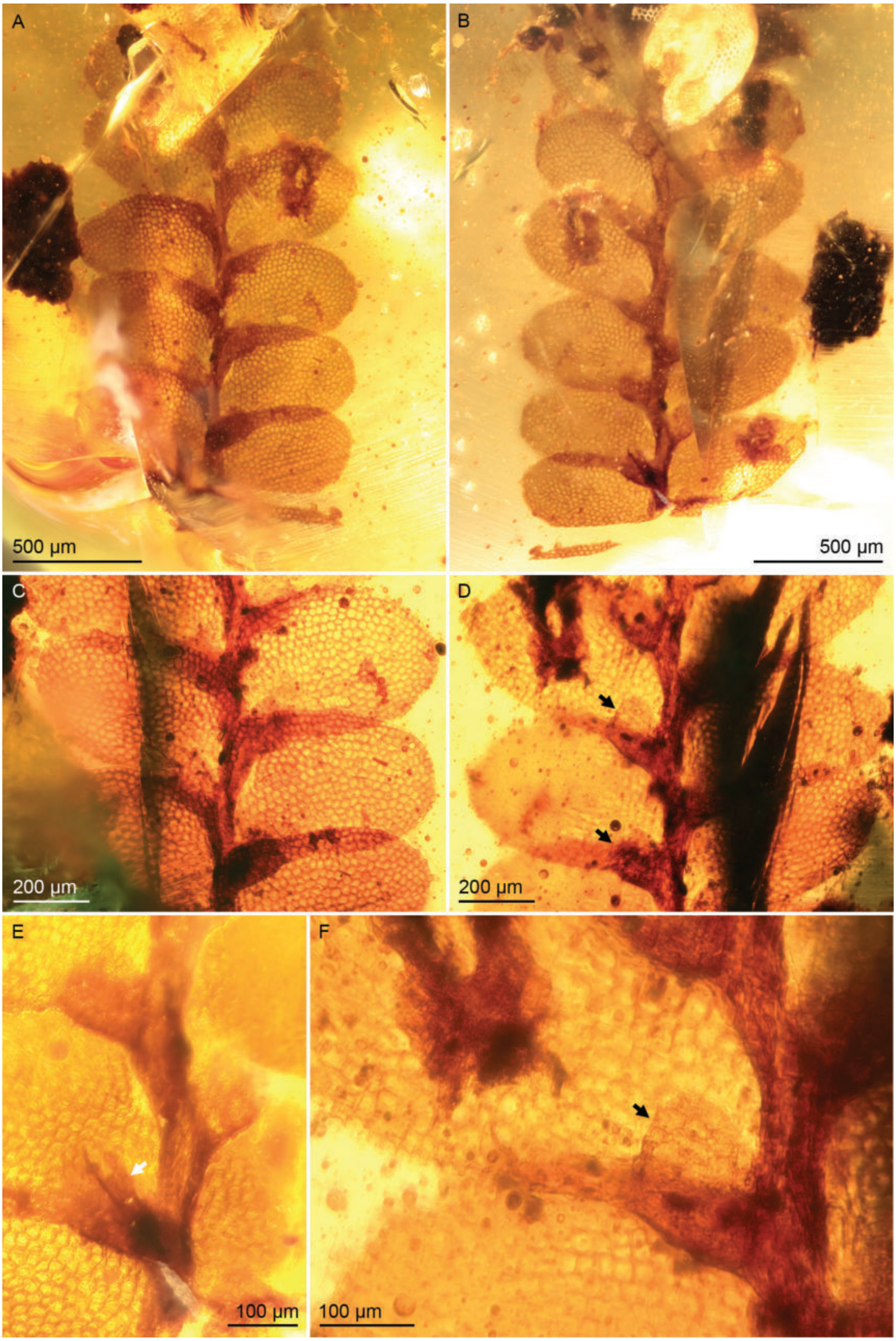

Figure 3. *Radula patrickmuelleri* sp. nov., GZG.BST.22041 (Müller BuB4395), holotype. **A.** Gametophyte fragment, dorsal; **B.** Gametophyte fragment, ventral; **C.** Insertion of leaf lobes, dorsal; **D.** Leaves with large lobes and small lobules (indicated by black arrows), ventral; **E.** Lobules, ventral (rhizoid bundle on the lobule surface indicated by white arrow); **F.** Longitudinally inserted leaf lobule, ventral (lobule indicated by black arrow).

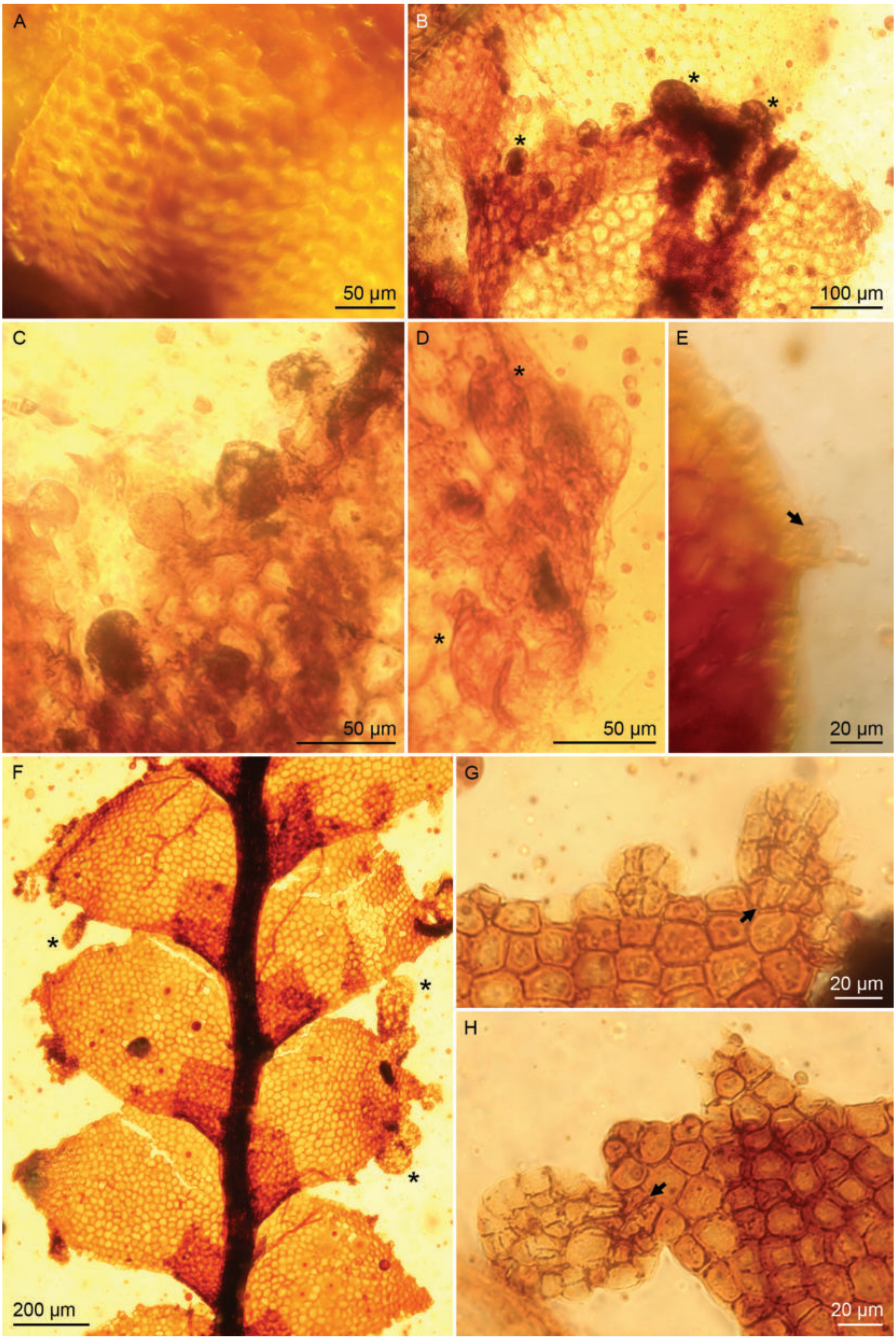

Figure 4. *Radula patrickmuelleri* sp. nov. and *R. cretacea*. **A–E.** *R. patrickmuelleri*, GZG.BST.22041 (Müller BuB4395), holotype; **A.** Lobe cells, dorsal; **B.** Antical leaf margin with gemmae, dorsal; **C.** Detail of gemmae (smaller spherical bodies possibly represent air bubbles and debris); **D.** Lobe apex with large gemmae, dorsal; **E.** Lobe margin with gemmae in the initial stage of development, dorsal (initial periclinal cell division visible and indicated by black arrow); **F–H.** *R. cretacea*, PB22484, holotype; **F.** Gametophyte with large gemmae on the lobe margins, ventral; **G, H.** Gemmae in different stages of development (initial anticlinal cell division visible and indicated by black arrow). The asterisks indicate selected gemmae in different stages of development.

angles; free exterior wall of marginal cells unthickened. Ventral lobules small in relation to lobe (< 0.2 ×), rounded rectangular to ovate, insertion longitudinal, exterior margin curved, antical margin slightly curved or nearly straight, interior margin not ampliate, barely extending onto the stem surface (Fig. 3D–F), apex subacute to broadly rounded; keel emerging at an angle of ca. 45° from the stem, slightly convex; lobule ca. 150 µm long × ca. 150 µm wide, length:width ratio 0.9–1.1:1, keel length 140–160 µm, length of stem insertion 90–140 µm. Underleaves lacking. Asexual reproduction by gemmae produced from cells of leaf margin (Fig. 4B–E, indicated by asterisks), gemmae possibly unistratose, subdiscoid to obcordate to irregularly thalloid as size increases, 20–110 µm long × 25–70 µm wide, first cell division seemingly periclinal (Fig. 4C, E); stalk cell of gemmae rectangular. Sterile.

Remarks. This fossil consists of a short, sterile gametophyte fragment but shows all relevant characters to delimitate it from other *Radula* fossils from Kachin amber (Figs 3, 4A–E). The small, rounded rectangular to ovate lobules allow to differentiate it from *R. heinrichsii* as well as *R. tanaiensis* which have much larger lobules (Fig. 5A, B), and the apically rounded lobes with nearly parallel margins distinguish it from *R. cretacea* (Fig. 4F).

***Radula tanaiensis* K.Feldberg, Schäf.-Verw. & M.A.M.Renner, sp. nov.**

http://zoobank.org/3442B8BB-79AD-44C6-8BCB-A2EAC0259B6F
Fig. 5A–E

Holotype. GZG.BST.22042 (Müller BuB4329), Geoscience Centre (GZG) at the University of Göttingen, Germany.

Etymology. The specific epithet refers to the village of Tanai, where Kachin amber is mined.

Locality and horizon. Amber mines southwest of the village of Tanai ca. 105 km north of Myitkyina in Kachin State, northern Myanmar, fossil enclosed in upper Albian–lower Cenomanian Kachin amber.

Diagnosis. Gametophyte irregularly branched, branches similar to main shoot, *Radula*-type. Lateral leaves complicate bilobed; dorsal lobe oval to ovate with rounded apex, deeply emarginated at end of keel; free exterior wall of marginal cells distinctly thickened; ventral lobules *Lejeunea*-type, up to 0.4 × as big as dorsal lobes, ovate to rounded trapezoid, insertion longitudinal, antical free margin often reaching antical margin of lobe.

Description. Branched gametophyte fragment ca. 4 mm long [tip of main shoot broken off], yellowish to reddish brown (Fig. 5A–C); main shoot up to 2.12 mm wide with leaves. Branching irregular, *Radula*-type (Fig. 5A, C); three intact branches with reduced leaves near their base, becoming main shoot-like, 2.6–2.72 mm long and 1.2–2.1 mm wide with leaves. Stem dark reddish brown, straight to slightly zig-zagged, on main shoot ca. 70–90 µm wide [strongly decomposed], on branches ca. 60 µm wide; surface cells not visible; ventral and dorsal leaf-free strips not visible. Rhizoids not seen. Foliation incubous, lateral leaves alternate, complicate bilobed, divided into large dorsal lobe and smaller ventral *Lejeunea*-type lobule enclosing the ventral leaf surface and forming a sharp postical keel (Fig. 5B). Dorsal lobes imbricate, oval to ovate, insertion longitudinal, flat, spreading, not obliquely patent, riding onto dorsal stem surface; margin entire, postical margin deeply curved along inner half, first nearly straight then evenly curved towards apex along outer half, lobe apex broadly rounded, exterior antical margin evenly curved, interior margin curved and slightly ampliate, overlapping the stem up to 1 × the stem width beyond the father edge of the stem; lobes on main shoot 600–610 µm long × 440–510 µm wide, length:width ratio 1.2–1.4:1, length exterior to keel 390–400 µm, length of stem insertion not clearly visible; lobes on branches 390–520 µm long × 300–360 µm wide, length exterior to keel 180–320 µm, length of stem insertion not visible. Marginal lobe cells quadrate to rectangular, 10–20 µm long × 15–25 µm wide, long axis either perpendicular or parallel with leaf margin (Fig. 5E); medial cells (sub)isodiametric to slightly elongated, 15–30 µm long × 12.5–25 µm wide (Fig. 5D); basal cells not visible; cell surfaces appearing smooth, but possible ornamentation visible in some parts (Fig. 5D) [cells generally indistinct]; cell walls moderately thickened, with small triangular to subnodulose trigones, free exterior wall of marginal cells distinctly thickened (Fig. 5E). Ventral lobules ovate to rounded trapezoid, up to 0.4 × as big as lobe, free antical margin often reaching antical margin of lobe (Fig. 5B), insertion longitudinal, free exterior and antical margins nearly straight to curved, apex narrowly rounded to rounded, interior margin ampliate, ventrally extending up to 1 × the stem width beyond the farther edge of stem; keel emerging at an angle of ca. 45° from the stem, lobe deeply emarginated at end of keel; lobules on main stem 290–310 µm long × 340–370 µm wide, length:width ratio ca. 0.9:1, keel length 210–230 µm, length of stem insertion not visible; on branches 270–330 µm long × 300–340 µm wide, length:width ratio 0.8–1:1. Underleaves lacking. No asexual reproduction. Sterile.

Remarks. The new fossil material consists of a short shoot fragment with the apex broken off and three main shoot-like *Radula*-type branches. It is not very well preserved, and many branches and leaves are broken (Fig. 5A–E). The lobules are generally very large in relation to the lobes (Fig. 5A, B) and differentiate this fossil clearly from *R. patrickmuelleri* as well as the much smaller *R. cretacea* whose lobules are less than 0.2 × the lobe size (Figs 3, 4F). Superficially the new species looks similar to *R. heinrichsii* (Fig. 5F, G; compare descriptions in Feldberg et al. 2021b), but the lobules of *R. tanaiensis* are up to 0.4 × the lobe size and their antical margin often reaches the antical margin of the lobe (Fig. 5B), while the lobules of *R. heinrichsii* remain smaller and are more rounded (Fig. 5F). The lobe cells are somewhat indistinct, but it is clearly visible that the outer walls of the marginal cells are distinctly thickened (Fig. 5E) whereas those of *R. heinrichsii* are thinner (Fig. 5G).

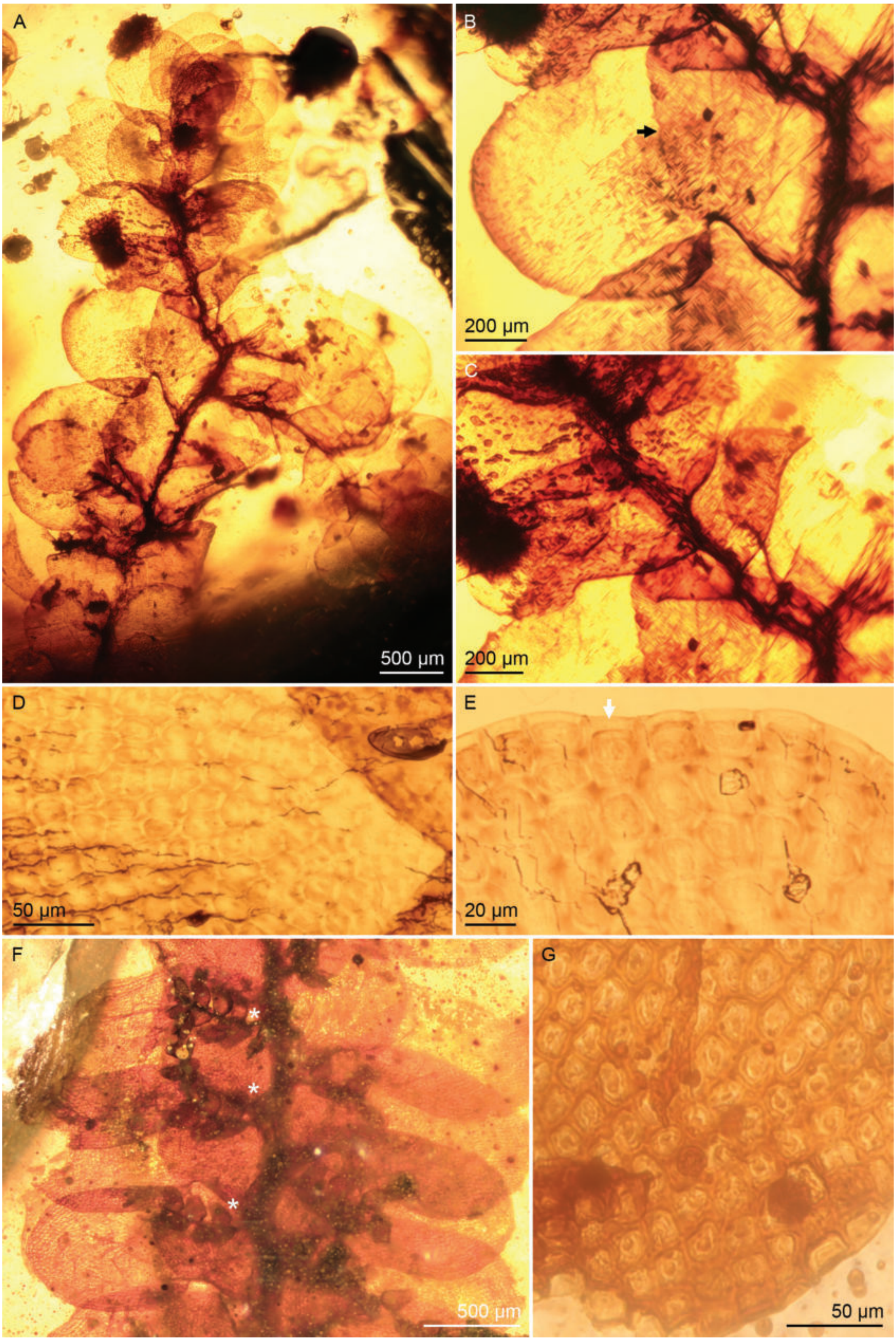

Figure 5. *Radula tanaiensis* sp. nov. and *R. heinrichsii* Feldberg et al. **A–E.** *R. tanaiensis*, GZG.BST.22042 (Müller BuB4329), holotype; **A.** Gametophyte, ventral; **B.** Lobe and lobule, ventral (lobule indicated by black arrow); **C.** Lower part of *Radula*-type branch; **D.** Medial lobe cells; **E.** Marginal lobe cells with thickened free exterior walls (indicated by white arrow); **F, G.** *R. heinrichsii*, GZG.BST.22023 (Müller BuB3683), holotype; **F.** Gametophyte with microphyllous (amentulose) branches (indicated by asterisks), ventral; **G.** Lobe cells with central mamillae.

Radula sp.

Suppl. material 1: Fig. S6

Locality and horizon. Amber mines southwest of the village of Tanai ca. 105 km north of Myitkyina in Kachin State, northern Myanmar, fossil enclosed in upper Albian–lower Cenomanian Kachin amber.

Specimen investigated. GZG.BST.22043 (Müller BuB4420), Geoscience Centre (GZG) at the University of Göttingen, Germany.

Remarks. The new fossil GZG.BST.22043 is not very well preserved, and the identification is difficult. It strongly resembles *R. cretacea* (Fig. 4F–H) in having smooth lobe cells (Suppl. material 1: Fig. S6E, F), quadrate to trapeziform lobules (Suppl. material 1: Fig. S6C, D, indicated by arrows), which are very small in relation to the lobes, and globose gemmae on the lobe margins (Suppl. material 1: Fig. S6F). However, the new fossil has obliquely patent leaves on the upper part of the shoot, whereas the posture of the lower leaves is not as dorsoventrally erect and more similar to *R. cretacea* (Figs 5F, Suppl. material 1: S6A–D). It also differs in having slightly narrower leaf lobes with a longer acuminate apex (Suppl. material 1: Fig. S6), though the obliqueness of the lobes makes this difficult to assess.

Key to leafy liverworts from Cretaceous ambers

1 Leaves with *Frullania*-type lobule, enclosing the dorsal leaf surface and having a postical opening (Figs 1, 2) 2
– Leaves with *Lejeunea*-type lobule, enclosing the ventral leaf surface and having an antical opening (Figs 3–5) ....8 (*Radula*)
2 Lobules with a long cilium on the outer margin .... *Gackstroemia cretacea* Heinrichs et al.
– Lobules occasionally toothed, but never with cilium on outer margin 3
3 Two lobules per leaf, underleaves apparently lacking .... *Kaolakia borealis*
– One lobule per leaf, underleaves usually present 4
4 Underleaves generally longer than the lobules, strap-shaped to long ovate, with two apical and 0–4 lateral teeth or cilia; rhizoids inserted on apical part of underleaf (Suppl. material 1: Figs S3–S5) .... *Protofrullania cornigera*
– Underleaves of a different shape, shorter than lobules and rectangular to ovate with apical cilia and lateral teeth, elliptic to ovate and bifurcated, or undivided with entire margins (‘holostipous’) .... 5 (*Frullania*)
5 Underleaves undivided and entire (‘holostipous’), ovate to suborbicular to reniform (Suppl. material 1: Fig. S2A–E)...... .... *F. baerlocheri*
– Underleaves with apical cilia and lateral teeth, or bifurcated with entire or serrate margins 6
6 Lobe apex acute to acuminate; lobules small in relation to lobes; underleaves bifurcated, entire .... *F. partita*
– Lobe apex rounded; underleaves with two apical cilia and few lateral teeth, or underleaf lobes toothed to strongly serrate 7
7 Underleaves elliptic, bifurcated up to 0.5–0.8 × their length, lobes weakly to strongly serrate (Figs 1, 2)...... *F. kachinensis*
– Underleaves rectangular to elongate triangular or ovate, with two slender apical cilia and often few additional lateral teeth (Suppl. material 1: Fig. S2F, G) .... *F. cretacea*
8 Plants small, ≤ 1.2 mm wide; lobe apex acute; small lobules quadrate to trapeziform (Fig. 4F–H) .... *R. cretacea*
– Plants larger, ≥ 1.3 mm wide; lobe apex rounded 9
9 Leaf lobules small in relation to the lobes (< 0.2 ×), inner margins not ampliate, not overlapping the stem (Figs 3, 4A–E) .... *R. patrickmuelleri* sp. nov.
– Leaf lobules larger in relation to the lobes (> 0.2 ×), inner margins ampliate, overlapping stem 10
10 Leaf lobules ovate to rounded trapezoid, very large in relation to lobes (0.3–0.4 ×), apices rounded to narrowly rounded, free margins curved to nearly straight; microphyllous branches unknown (Fig. 5A–E) .... *R. tanaiensis* sp. nov.
– Leaf lobules orbicular to obovate, ca. 0.2–0.3 × as big as lobes, apices broadly rounded, free margins strongly curved; microphyllous (amentulose) branches present (Fig. 5F, G) .... *R. heinrichsii*

Discussion

The new fossil material described in this publication includes some well-preserved sterile specimens of *Frullania cretacea* (Suppl. material 1: Fig. S2F, G), which is represented by 15 fossils in total, and *Protofrullania cornigera* (Suppl. material 1: Figs S3–S5), which is now represented by altogether 30 fossils. The latter is by far the most common species found in Kachin amber and the only species for which androecia as well as gynoecia are known (Feldberg et al. 2021b). *Frullania baerlocheri* (Suppl. material 1: Fig. S2A–E) is now represented by 12 fossils, including three fertile specimens with gynoecia, while *F. kachinensis* (Figs 1, 2) is known from eight sterile fossils, and *F. partita* from only two specimens (Li et al. 2020, 2022a). Several of these species occur together in individual amber pieces, namely *F. baerlocheri* and *P. cornigera* (SNSB-BSPG 2021 XII 1; described in Feldberg et al. 2021b), *F. kachinensis* and *P. cornigera* (PB22711; described in Li et al. 2021b), *F. kachinensis* and *F. baerlocheri* (ZMNH155047; described in Li et al. 2021a), and *F. baerlocheri* and *Radula heinrichsii* (ZMNH155044; described in Wang et al. in press). This indicates that these species grew very close to each other, obviously even on the same tree.

The new material allowed us to emend the diagnosis and description of *F. kachinensis.* Like many fossil species from Cretaceous ambers, *F. kachinensis* shows some characters that are unusual or even unknown in extant Frullaniaceae, e.g., rhizoid bundles inserted directly below the underleaf sinus (Fig. 1G, H). Extant *Frullania* has rhizoid bundles inserted at the base of underleaves or towards the middle (e.g., Hattori 1975, 1983; Schuster 1992), and the unusual insertion point aligns *F. kachinensis* with *Protofrullania cornigera*. The form of the underleaves, however, is completely different. While *P. cornigera* mostly has strap-shaped underleaves with a wider apical area armed with two to four cilia and carrying the rhizoid bundle (Suppl. material 1: Figs S3–S5), *F. kachinensis* has elliptic to elongate ovate underleaves which are bifid to ca. 0.3–0.8 × their length into two lanceolate lobes and are more consistent with typical underleaves of extant *Frullania* in this aspect (Figs 1F–H, 2C, D). However, another difference to extant species is the strong armature of the underleaf lobes which can be weakly to strongly toothed or ciliate and resemble the bracteoles of extant species more than vegetative underleaves (Figs 1G, H, 2C). Some extant *Frullania* species from different subgenera, e.g., *F. monocera* (Hook.f. & Taylor) Gottsche, Lindenb. & Nees of subgen. *Acutilobae*, *F. blepharozia* Spruce of subgen. *Chonanthelia*, *F. curvistipula* Steph. of subgen. *Diastaloba* I, and *F. amamiensis* Kamim. of subgen. *Frullania*, also have toothed vegetative underleaf lobes, but these teeth are mostly shorter and situated on the outer side of the triangular lobes (Yuzawa 1991, 2001). Another example would be *F. papulosa* Steph., which has lanceolate, pilose underleaf lobes with two spinose teeth at the lower margins.

Radula tanaiensis, *R. patrickmuelleri*, and the additional fossil GZG.BST.22043 can be confidently assigned to the genus. The presence of complicate bilobed lateral leaves with a large dorsal lobe and a small *Lejeunea*-type lobule, the absence of underleaves, as well as the presence of rhizoids on the lobules in the case of *R. patrickmuelleri* allow a definite assignment to *Radula*. The new species are morphologically well differentiated from the other two fossil species from Kachin amber, while the classification of *R.* sp. is ambiguous.

Radula tanaiensis can be clearly differentiated from *R. cretacea*, *R. heinrichsii*, and *R. patrickmuelleri* by the very large lobules on what are probably primary shoots. Lobules are up to 0.4 × as big as the lobes and their free antical margin often reaches the antical margin of the lobe (Fig. 5A, B). Lobules in *R. cretacea* are less than 0.2 × as big as the lobes and also the acute triangular-ovate lobes separate it from the new species (Fig. 4F). *Radula patrickmuelleri* has similarly small lobules and the lobes are less wide and have nearly parallel postical and antical margins in their middle parts (Fig. 3). *Radula heinrichsii* is the most similar species, but the lobules are only 0.2–0.3 × as big as the lobes, obovate to nearly orbicular instead of ovate to rounded trapezoid, and have more broadly rounded apices (Fig. 5A, B, F). The lobes of *R. heinrichsii* are more elongated, and the free exterior cell walls of the marginal lobe cells are not as distinctly thickened as in *R. tanaiensis* (Fig. 5E, G). Contrary to *R. heinrichsii*, the cell walls of *R. tanaiensis* also appear smooth for the largest part (Fig. 5D, E), but the cells are often indistinct, and some might have rounded mamillae in their center. Furthermore, microphyllous axes (Fig. 5F) have not been seen in the new species. It has three intact branches with a few small and somewhat reduced basal leaves which soon become main shoot-like and some broken remnants of branches whose character is not discernible (Fig. 5A, C).

Radula patrickmuelleri has roughly the same shoot size as *R. heinrichsii* and *R. tanaiensis* but can be clearly separated by the size and shape of the small lobules which are less than 0.2 × as big as the lobes, the absence of microphyllous branches, and the gemmae formation (Figs 3, 4). *Radula cretacea* resembles *R. patrickmuelleri* at first glance, because it also has small lobules as well as irregular gemmae on the lobe margins (Fig. 4F–H). The form of the lobules and the longitudinal insertion might be similar, but those of *R. cretacea* are quadrate to trapeziform, have slightly curved exterior and antical margins which are somewhat irregular due to bulging marginal cells, and an obtuse to slightly attenuate apex with a papilla in a shallow notch (Fig. 4F). In contrast, the lobules of *R. patrickmuelleri* are rounded rectangular to ovate, have more strongly curved exterior and antical margins which do not show any bulging marginal cells, and subacute to broadly rounded apices (Fig. 3D–F). Notches with papillae have not been seen. The most conspicuous differences are the size of the plants and the form of the dorsal lobes. *Radula cretacea* is much smaller and has triangular-ovate leaf lobes (Fig. 4F) while *R. patrickmuelleri* is larger and has oblong-elliptic lobes (Fig. 3A–D). The antical and postical margins of the lobes also show a different curvature. The antical lobe margin of *R. cretacea* is more strongly arched than the postical margin, whereas *R. patrickmuelleri* has nearly parallel medial postical and antical margins. Furthermore, *R. cretacea* has acute to slightly acuminate lobe apices, whereas *R. patrickmuelleri* has broadly rounded lobe apices. Another differentiating character are the gemmae. While the first cell division in the gemmae of *R. cretacea* seems to be mainly anticlinal (Fig. 4G, H), all clearly visible first divisions in *R. patrickmuelleri* are periclinal (Fig. 4B–E).

The presence of four species in Kachin amber and recent divergence time estimates indicate a high diversity of *Radula* already in the Cretaceous (Bechteler et al. 2017; Patiño et al. 2017; Feldberg et al. 2021a, 2021b). *Radula cretacea* and *R. heinrichsii* show close morphological affinities to the extant subgenera *Odontoradula* and *Amentuloradula*, respectively (Bechteler et al. 2017; Feldberg et al. 2021b). The assignment of the two new species, however, is more difficult due to the scarcity of the fossil material. Based on the available evidence, it is not possible to assign *R. patrickmuelleri* and *R. tanaiensis* to any subgenus with confidence, and because of the high degree of morphological homoplasy in extant *Radula*, a comparison with extant lineages is premature. The gemmae formation in *R. patrickmuelleri* is perhaps consistent with an epiphyllous lineage in extant subg.

Metaradula, where the first cell division is always periclinal. However, the species also shares some similarities with the extant *R. pugioniformis* M.A.M.Renner of subg. *Odontoradula* but differs in having larger leaf lobe cells with thin walls and distinct trigones, as well as gemmae (Renner et al. 2013b). A more accurate assignment of the new species might be possible when more fossil material is discovered. Both the age of each *Radula* subgenus, and the relatively long stem lineages leave open the possibility that fossils belong to extinct lineages that diverged from the various stem lineages. Bechteler et al. (2017) evaluated how misleading an assignment solely based on morphological similarity may be, and assigned *R. cretacea* to different nodes in the molecular phylogeny of *Radula.* An assignment of *R. cretacea* to the stem of subgenus *Odontoradula* proved to be most likely and resulted in an estimated mean age of 176.3 Ma for the genus.

Conclusions

DNA-based divergence time estimates provide evidence for a species turnover within Jungermanniidae during the Angiosperm Terrestrial Revolution, and fossils in Kachin amber offer unique insights into the evolution and diversification of leafy liverworts during this time span (Feldberg et al. 2014; Laenen et al. 2014; Benton et al. 2022). They are essential as age constraints in divergence time estimations, because only very few Mesozoic fossils from the rock record show enough details to allow a reliable assignment to extant lineages (Heinrichs et al. 2018; Tomescu et al. 2018; Feldberg et al. 2021a, 2021b).

Unfortunately, neither *Radula patrickmuelleri* nor *R. tanaiensis* can contribute to age constraints beyond what is already gleaned from other fossils, which is an absolute minimum age for the lineage stem node of *Radula*, though they provide more evidence of a high species diversity of *Radula* already in the mid-Cretaceous. The newly detected fossil of *Frullania kachinensis* allowed emendation of the species diagnosis and description for some important characters but can likewise not provide new age constraints, because some unusual characters make it impossible to assign it to any group within the crown group of *Frullania*. The rhizoid insertion resembles *Protofrullania cornigera* more than any extant *Frullania* and it might thus be more closely related to this genus.

Our results suggest that new fossil liverwort material should preferably be described based on as many specimens as possible, as every specimen is incomplete. Not only does fossil material often consist of sparse and damaged fragments which do not show all relevant characters, leafy liverworts often show significant morphological homoplasy between lineages as well as some morphological plasticity within a species, with characters varying in expression between individuals or even between different parts on the same plant, e.g., the main shoot and branches. This high variability may obscure species boundaries in extant leafy liverworts and is even more obstructive in the description of extinct species.

Author contribution (CRediT)

K.F. designed research. K.F. and Y.L. prepared and documented the specimens. K.F., A.S.-V., Y. L., and M.A.M.R. analyzed the data and wrote the paper. All authors commented on the manuscript.

Competing interests

The authors have no competing interests to declare.

Acknowledgements

We would like to thank Patrick Müller (Zweibrücken) and Jörg Wunderlich (Hirschberg an der Bergstraße) for providing specimens for study. We are grateful to Alexander R. Schmidt (Göttingen) for commenting on an earlier version of the manuscript as well as to Grzegorz J. Wolski, an anonymous reviewer, and the editor Florian Witzmann for constructive comments that improved the manuscript. Financial support from the German Research Foundation (DFG, project 428174246 to K.F.) and the National Natural Science Foundation of China (grant number 41790454 to Y.L.) is gratefully acknowledged.

References

Bechteler J, Schmidt AR, Renner MAM, Wang B, Pérez-Escobar OA, Schäfer-Verwimp A, Feldberg K, Heinrichs J (2017) A Burmese amber fossil of *Radula* (Porellales, Jungermanniopsida) provides insights into the Cretaceous evolution of epiphytic lineages of leafy liverworts. Fossil Record 20: 201–213. https://doi.org/10.5194/fr-20-201-2017

Bell NE, York PV (2007) *Vetiplanaxis pyrrhobryoides*, a new fossil moss genus and species from Middle Cretaceous Burmese amber. The Bryologist 110: 514–520. https://doi.org/10.1639/0007-2745(2007)110[514:VPANFM]2.0.CO;2

Benton MJ, Wilf P, Sauquet H (2022) The Angiosperm Terrestrial Revolution and the origins of modern biodiversity. New Phytologist 233: 2017–2035. https://doi.org/10.1111/nph.17822

Bouju V, Feldberg K, Kaasalainen U, Schäfer-Verwimp A, Hedenäs L, Buck WR, Wang B, Perrichot V, Schmidt AR (2021) Miocene Ethiopian amber: A new source of fossil cryptogams. Journal of Systematics and Evolution. https://doi.org/10.1111/jse.12796

Carter BE, Larraín J, Manukjanová A, Shaw B, Shaw AJ, Heinrichs J, de Lange P, Suleiman M, Thouvenot L, von Konrat M (2017) Species delimitation and biogeography of a southern hemisphere liverwort clade, *Frullania* subgenus *Microfrullania* (Frullaniaceae, Marchantiophyta). Molecular Phylogenetics and Evolution 107: 16–26. https://doi.org/10.1016/j.ympev.2016.10.002

Caspary R (1887) Einige neue Pflanzenreste aus dem samländischen Bernstein. Schriften der Physikalisch-Ökonomischen Gesellschaft zu Königsberg (Abhandlungen) 27: 1–8 [209], Tafel I [1886].

Cruickshank RD, Ko K (2003) Geology of an amber locality in the Hukawng Valley, Northern Myanmar. Journal of Asian Earth Sciences 21: 441–445. https://doi.org/10.1016/S1367-9120(02)00044-5

Devos N, Renner MAM, Gradstein SR, Shaw J, Vanderpoorten A (2011) Molecular data challenge traditional subgeneric divisions in the leafy liverwort *Radula*. Taxon 60: 1623–1632. https://doi.org/10.1002/tax.606007

Estrada-Ruiz E, Riquelme F (2017) First fossil record of *Hypnodontopsis* (Bryopsida: Rhachitheciaceae) from the Americas. Ameghiniana 54: 124–131. https://doi.org/10.5710/AMGH.22.09.2016.3019

Feldberg K, Schneider H, Stadler T, Schäfer-Verwimp A, Schmidt AR, Heinrichs J (2014) Epiphytic leafy liverworts diversified in angiosperm-dominated forests. Scientific Reports 4: e5974. https://doi.org/10.1038/srep05974

Feldberg K, Müller AS, Schäfer-Verwimp A, von Konrat M, Schmidt AR, Heinrichs J (2018) *Frullania grabenhorstii* sp. nov., a fossil liverwort (Jungermanniopsida: Frullaniaceae) with perianth from Bitterfeld amber. Bryophyte Diversity and Evolution 40: 91–103. https://doi.org/10.11646/bde.40.2.7

Feldberg K, Gradstein SR, Gröhn C, Heinrichs J, von Konrat M, Mamontov YS, Renner MAM, Roth M, Schäfer-Verwimp A, Sukkharak P, Schmidt AR (2021a) Checklist of fossil liverworts suitable for calibrating phylogenetic reconstructions. Bryophyte Diversity and Evolution 43: 14–71. https://doi.org/10.11646/bde.43.1.6

Feldberg K, Schäfer-Verwimp A, Renner MAM, von Konrat M, Bechteler J, Müller P, Wang Y-D, Schneider H, Schmidt AR (2021b) Liverworts from Cretaceous amber. Cretaceous Research 128: 104987. https://doi.org/10.1016/j.cretres.2021.104987

Frahm J-P (2010) Die Laubmoosflora des Baltischen Bernsteinwaldes. Weissdorn-Verlag, Jena, 101 pp.

Frahm J-P, Newton AE (2005) A new contribution to the moss flora of Dominican amber. The Bryologist 108: 526–536. https://doi.org/10.1639/0007-2745(2005)108[0526:ANCTTM]2.0.CO;2

Grimaldi DA, Ross AJ (2017) Extraordinary Lagerstätten in Amber, with particular reference to the Cretaceous of Burma. In: Fraser NC, Sues H-D (Eds) Terrestrial Conservation Lagerstätten: Windows into the Evolution of Life on Land. Dunedin Academic Press, Edinburgh, 287–342.

Grimaldi DA, Engel MS, Nascimbene PC (2002) Fossiliferous Cretaceous amber from Myanmar (Burma): its rediscovery, biotic diversity, and paleontological significance. American Museum Novitates 3361: 1–71. https://doi.org/10.1206/0003-0082(2002)361%3C0001:FCAFMB%3E2.0.CO;2

Grimaldi DA, Sunderlin D, Aaroe GA, Dempsky MR, Parker NE, Tillery GQ, White JG, Barden P, Nascimbene PC, Williams CJ (2018) Biological inclusions in amber from the Paleogene Chickaloon Formation of Alaska. American Museum Novitates 3908: 1–37. https://doi.org/10.1206/3908.1

Grolle R (1980) Lebermoose im Bernstein 2. Feddes Repertorium 91: 401–407. https://doi.org/10.1002/fedr.19800910704

Grolle R (1981) Was ist *Lejeunea schumannii* Caspary aus dem baltischen Bernstein? Occasional Papers of the Farlow Herbarium of Cryptogamic Botany 16: 101–110. https://doi.org/10.5962/p.317795

Grolle R (1985) Monograph of *Frullania* in Baltic amber. Prace Muzeum Ziemi 37: 87–100 [plates I–VI].

Grolle R (1987) *Radula steerei* sp. nov.—A further hepatic in Dominican amber. Memoirs of the New York Botanical Garden 45: 259–263.

Grolle R (2003) *Frullania mammilligera* sp. nov., a new Eocene species of Hepaticae found in Bitterfeld Amber of central Germany. Courier Forschungsinstitut Senckenberg 241: 155–161.

Grolle R, Meister K (2004) The Liverworts in Baltic and Bitterfeld Amber. Weissdorn-Verlag, Jena, 91 pp.

Hand S, Archer M, Bickel D, Creaser P, Dettmann M, Godthelp H, Jones A, Norris B, Wicks D (2010) Australian Cape York amber. In: Penney D (Ed.) Biodiversity of Fossils in Amber from the Major World Deposits. Siri Scientific Press, Manchester, 69–79.

Hattori S (1975) Notes on the Asiatic species of the genus *Frullania*, Hepaticae. VIII. Bulletin of the National Science Museum, Tokyo, Series B (Botany) 1: 141–163.

Hattori S (1983) A revision of the Australasian species of the genus *Frullania*, Hepaticae. III. Journal of the Hattori Botanical Laboratory 54: 133–182.

Haug JT, Azar D, Ross A, Szwedo J, Wang B, Arillo A, Baranov V, Bechteler J, Beutel R, Blagoderov V, Delclòs X, Dunlop J, Feldberg K, Feldmann R, Foth C, Fraaije RHB, Gehler A, Harms D, Hedenäs L, Hyžný M, Jagt JWM, Jagt-Yazykova EA, Jarzembowski E, Kerp H, Khine PK, Kirejtshuk AG, Klug C, Kopylov DS, Kotthoff U, Kriwet J, McKellar RC, Nel A, Neumann C, Nützel A, Peñalver E, Perrichot V, Pint A, Ragazzi E, Regalado L, Reich M, Rikkinen J, Sadowski E-M, Schmidt AR, Schneider H, Schram FR, Schweigert G, Selden P, Seyfullah LJ, Solórzano-Kraemer MM, Stilwell JD, van Bakel BWM, Vega FJ, Wang Y, Xing L, Haug C (2020) Comment on the letter of the Society of Vertebrate Paleontology (SVP) dated April 21, 2020 regarding “Fossils from conflict zones and reproducibility of fossil-based scientific data”: Myanmar amber. Paläontologische Zeitschrift 94: 431–437. https://doi.org/10.1007/s12542-020-00524-9

Hedenäs L, Heinrichs J, Schmidt AR (2014) Bryophytes of the Burmese amber forest: Amending and expanding the circumscription of the Cretaceous moss genus *Vetiplanaxis.* Review of Palaeobotany and Palynology 209: 1–10. https://doi.org/10.1016/j.revpalbo.2014.05.008

Heinrichs J, Schmidt AR (2010) An inclusion of *Frullania* subgen. *Diastaloba* s. l. (Frullaniaceae, Porellales) in Dominican amber. Tropical Bryology 31: 91–94. https://doi.org/10.11646/bde.31.1.15

Heinrichs J, Hentschel J, Bombosch A, Fiebig A, Reise J, Edelmann M, Kreier H-P, Schäfer-Verwimp A, Caspari S, Schmidt AR, Zhu R-L, von Konrat M, Shaw B, Shaw AJ (2010) One species or at least eight? Delimitation and distribution of *Frullania tamarisci* (L.) Dumort. s. l. (Jungermanniopsida, Porellales) inferred from nuclear and chloroplast DNA markers. Molecular Phylogenetics and Evolution 56: 1105–1114. https://doi.org/10.1016/j.ympev.2010.05.004

Heinrichs J, Reiner-Drehwald ME, Feldberg K, Grimaldi DA, Nascimbene PC, von Konrat M, Schmidt AR (2011) *Kaolakia borealis* nov. gen. et sp. (Porellales, Jungermanniopsida): A leafy liverwort from the Cretaceous of Alaska. Review of Palaeobotany and Palynology 165: 235–240. https://doi.org/10.1016/j.revpalbo.2011.04.002

Heinrichs J, Reiner-Drehwald ME, Feldberg K, von Konrat M, Hentschel J, Váňa J, Grimaldi DA, Nascimbene PC, Schmidt AR (2012) The leafy liverwort *Frullania* (Jungermanniopsida) in the Cretaceous amber forest of Myanmar. Review of Palaeobotany and Palynology 169: 21–28. https://doi.org/10.1016/j.revpalbo.2011.10.002

Heinrichs J, Schäfer-Verwimp A, Hedenäs L, Ignatov MS, Schmidt AR (2014) An acrocarpous moss in Cretaceous amber from Myanmar. Cretaceous Research 51: 260–265. https://doi.org/10.1016/j.cretres.2014.06.010

Heinrichs J, Scheben A, Bechteler J, Lee GE, Schäfer-Verwimp A, Hedenäs L, Singh H, Pócs T, Nascimbene PC, Peralta DF, Renner M, Schmidt AR (2016a) Crown group Lejeuneaceae and pleurocarpous mosses in early Eocene (Ypresian) Indian amber. PloS ONE 11: e0156301. https://doi.org/10.1371/journal.pone.0156301

Heinrichs J, Schmidt AR, Schäfer-Verwimp A, Bauerschmidt L, Neumann C, Gröhn C, Krings M, Renner MAM (2016b) Revision of the leafy liverwort genus *Radula* (Porellales, Jungermanniopsida) in Baltic and Bitterfeld amber. Review of Palaeobotany and Palynology 235: 157–164. https://doi.org/10.1016/j.revpalbo.2016.09.004

Heinrichs J, Feldberg K, Bechteler J, Müller P, Renner MAM, Váňa J, Schäfer-Verwimp A, Schmidt AR (2017a) A fossil genus of the Frullaniaceae (Porellales, Jungermanniopsida) from the mid-Cretaceous of Myanmar. Cretaceous Research 74: 223–226. https://doi.org/10.1016/j.cretres.2017.02.023

Heinrichs J, Feldberg K, Müller P, Schäfer-Verwimp A, von Konrat M, Ilsemann B, Krings M (2017b) *Frullania pinnata* spec. nov. (Frullaniaceae, Porellales), a new leafy liverwort in mid-Cretaceous Burmese amber from Myanmar. Cretaceous Research 78: 56–60. https://doi.org/10.1016/j.cretres.2017.05.030

Heinrichs J, Feldberg K, Bechteler J, Regalado L, Renner MAM, Schäfer-Verwimp A, Gröhn C, Müller P, Schneider H, Krings M (2018) A comprehensive assessment of the fossil record of liverworts in amber. In: Krings M, Harper CJ, Cúneo NR, Rothwell GW (Eds) Transformative Paleobotany. Papers to Commemorate the Life and Legacy of Thomas N. Taylor. Elsevier/Academic Press, London, 213–252. https://doi.org/10.1016/B978-0-12-813012-4.00012-7

Hentschel J, Schmidt AR, Heinrichs J (2009a) *Frullania cretacea* sp. nov. (Porellales, Jungermanniopsida), a leafy liverwort preserved in Cretaceous amber from Myanmar. Cryptogamie, Bryologie 30: 323–328.

Hentschel J, von Konrat MJ, Pócs T, Schäfer-Verwimp A, Shaw AJ, Schneider H, Heinrichs J (2009b) Molecular insights into the phylogeny and subgeneric classification of *Frullania* Raddi (Frullaniaceae, Porellales). Molecular Phylogenetics and Evolution 52: 142–156. https://doi.org/10.1016/j.ympev.2008.12.021

Hentschel J, von Konrat M, Söderström L, Hagborg A, Larraín J, Sukkharak P, Uribe J, Zhang L (2015) Notes on Early Land Plants Today. 72. Infrageneric classification and new combinations, new names, new synonyms in *Frullania* (Marchantiophyta). Phytotaxa 220: 127–142. https://doi.org/10.11646/phytotaxa.220.2.3

Ignatov MS, Maslova EV (2021) Fossil Mosses: What do they tell us about moss evolution? Bryophyte Diversity and Evolution 43: 72–97. https://doi.org/10.11646/bde.43.1.7

Ignatov MS, Perkovsky EE (2013) Mosses from Sakhalinian amber (Russian Far East). Arctoa 22: 79–82. https://doi.org/10.15298/arctoa.22.11

Ignatov MS, Heinrichs J, Schäfer-Verwimp A, Perkovsky EE (2016) The first record of a bryophyte in Upper Cretaceous amber from Taimyr, northern Siberia: *Taimyrobryum martynoviorum* gen. et sp. nov. (Bryopsida). Cretaceous Research 65: 25–31. https://doi.org/10.1016/j.cretres.2016.04.005

Ignatov MS, Lamkowski P, Ignatova EA, Kulikovskiy MS, Mamontov YS, Vasilenko DV (2019) Mosses from Rovno amber (Ukraine). 5. New findings and comparison of mosses from Rovno and Baltic amber. Paleontological Journal 53: 1084–1094. https://doi.org/10.1134/S0031030119100071

Kaasalainen U, Heinrichs J, Renner MAM, Hedenäs L, Schäfer-Verwimp A, Lee GE, Ignatov MS, Rikkinen J, Schmidt AR (2017) A Caribbean epiphyte community preserved in Miocene Dominican amber. Earth and Environmental Science Transactions of the Royal Society of Edinburgh 107: 321–331. https://doi.org/10.1017/S175569101700010X

Katagiri T, Shinden H (2020) Discovery of a simple thalloid liverwort *Metzgeriites kujiensis* (Metzgeriaceae), a new species from Late Cretaceous Japanese amber. Hattoria 11: 13–21. https://doi.org/10.18968/hattoria.11.0_13

Katagiri T, Mukai M, Yamaguchi T (2013) A new fossil moss *Muscites kujiensis* (Bryopsida) preserved in the Late Cretaceous amber from Japan. The Bryologist 116: 296–301. https://doi.org/10.1639/0007-2745-116.3.296

Konstantinova NA, Ignatov MS, Perkovsky EE (2012) Hepatics from Rovno amber (Ukraine). Arctoa 21: 265–271. https://doi.org/10.15298/arctoa.21.25

Laenen B, Shaw B, Schneider H, Goffinet B, Paradis E, Désamoré A, Heinrichs J, Villarreal JC, Gradstein SR, McDaniel SF, Long DG, Forrest LL, Hollingsworth ML, Crandall-Stotler B, Davis EC, Engel J, von Konrat M, Cooper ED, Patiño J, Cox CJ, Vanderpoorten A, Shaw AJ (2014) Extant diversity of bryophytes emerged from successive post-Mesozoic diversification bursts. Nature Communications 5: e5134. https://doi.org/10.1038/ncomms6134

Li Y, Wang Y-D, Schneider H, Wu P-C (2020) *Frullania partita* sp. nov. (Frullaniaceae, Porellales), a new leafy liverwort from the mid-Cretaceous of Myanmar. Cretaceous Research 108: 104341. https://doi.org/10.1016/j.cretres.2019.104341

Li Y, Li L-Q, Feldberg K, Wu P-C, Schneider H, Schmidt AR, Wang Y-D (2021a) Re-appraisal of two fossil Frullaniaceae species (Marchantiophyta, Porellales) from the mid-Cretaceous Burmese amber. Cretaceous Research 124: 104803. https://doi.org/10.1016/j.cretres.2021.104803

Li Y, Wang Y-D, Feldberg K, Wang Q, Yang X-J (2021b) A new leafy liverwort of *Frullania* (Frullaniaceae, Porellales) from the mid-Cretaceous Kachin amber, Myanmar. Geological Journal 56: 5046–5057. https://doi.org/10.1002/gj.4222

Li Y, Li Y-D, Wang Y-D, Schneider H, Shi G-L (2022a) Re-appraisal of lacewing mimicry of liverworts from the mid-Cretaceous Kachin amber, Myanmar with a description of *Selaginella cretacea* sp. nov. (Selaginellales, Selaginellaceae). Cretaceous Research 133: 105143. https://doi.org/10.1016/j.cretres.2022.105143

Li Y, Wang Y-D, Feldberg K, Wang S, Shi C, Cui Y-M, Zhang X-Q (2022b) New insights into the moss genus *Vetiplanaxis* with a description of *V. obtusus* sp. nov. from the mid-Cretaceous Kachin amber, Myanmar. Review of Palaeobotany and Palynology 301: 104659. https://doi.org/10.1016/j.revpalbo.2022.104659

Magallón S, Sánchez-Reyes LL, Gómez-Acevedo SL (2019) Thirty clues to the exceptional diversification of flowering plants. Annals of Botany 123: 491–503. https://doi.org/10.1093/aob/mcy182

Mamontov YS, Heinrichs J, Schäfer-Verwimp A, Ignatov MS, Perkovsky EE (2015) Hepatics from Rovno amber (Ukraine), 4. *Frullania riclefgrollei*, sp. nov. Review of Palaeobotany and Palynology 223: 31–36. https://doi.org/10.1016/j.revpalbo.2015.08.007

Mamontov YS, Hentschel J, Konstantinova NA, Perkovsky EE, Ignatov MS (2017) Hepatics from Rovno amber (Ukraine), 6. *Frullania rovnoi*, sp. nov. Journal of Bryology 39: 336–341. https://doi.org/10.1080/03736687.2017.1343220

Mamontov YS, Ignatov MS, Perkovsky EE (2018) Hepatics from Rovno amber (Ukraine), 7. *Frullania zerovii*, sp. nov. Nova Hedwigia 106: 103–113. https://doi.org/10.1127/nova_hedwigia/2017/0446

Mamontov YS, Ignatov MS, Perkovsky EE (2019) Liverworts from Rovno amber (Ukraine). 8. *Frullania ekaterinae* sp. nov. and *F. schmalhausenii* sp. nov. Paleontological Journal 53: 1095–1103. https://doi.org/10.1134/S0031030119100113

Mamontov YS, Atwood JJ, Perkovsky EE, Ignatov MS (2020) Hepatics from Rovno amber (Ukraine): *Frullania pycnoclada* and a new species, *F. vanae.* The Bryologist 123: 421–430. https://doi.org/10.1639/0007-2745-123.3.421

Patiño J, Wang J, Renner MAM, Gradstein SR, Laenen B, Devos N, Shaw AJ, Vanderpoorten A (2017) Range size heritability and diversification patterns in the liverwort genus *Radula.* Molecular Phylogenetics and Evolution 106: 73–85. https://doi.org/10.1016/j.ympev.2016.09.020

Renner MAM (2014) *Radula* subg. *Radula* in Australasia and the Pacific (Jungermanniopsida). Telopea 17: 107–167. https://doi.org/10.7751/telopea20147553

Renner MAM (2015) Lobule shape evolution in *Radula* (Jungermanniopsida): one rate fits all? Botanical Journal of the Linnean Society 178: 222–242. https://doi.org/10.1111/boj.12279

Renner MAM, Devos N, Brown EA, von Konrat MJ (2013a) Three modes of heterochrony explain lobule diversity in *Radula* subgenus *Cladoradula* (Porellales: Jungermanniopsida), a small lineage of early land plants today. Botanical Journal of the Linnean Society 173: 153–175. https://doi.org/10.1111/boj.12087

Renner MAM, Devos N, Patiño J, Brown EA, Orme A, Elgey M, Wilson TC, Gray LJ, von Konrat MJ (2013b) Integrative taxonomy resolves the cryptic and pseudo-cryptic *Radula buccinifera* complex (Porellales, Jungermanniopsida), including two reinstated and five new species. PhytoKeys 27: 1–113. https://doi.org/10.3897/phytokeys.27.5523

Sadowski E-M, Schmidt AR, Seyfullah LJ, Solórzano-Kraemer MM, Neumann C, Perrichot V, Hamann C, Milke R, Nascimbene PC (2021) Conservation, preparation and imaging of diverse ambers and their inclusions. Earth-Science Reviews 220: 103653. https://doi.org/10.1016/j.earscirev.2021.103653

Schuster RM (1992) The Hepaticae and Anthocerotae of North America. V. Columbia University Press, New York, 854 pp.

Shi G, Grimaldi DA, Harlow GE, Wang J, Wang J, Yang M, Lei W, Li Q, Li X (2012) Age constraint on Burmese amber based on U–Pb dating of zircons. Cretaceous Research 37: 155–163. https://doi.org/10.1016/j.cretres.2012.03.014

Söderström L, Hagborg A, von Konrat M, Bartholomew-Began S, Bell D, Briscoe L, Brown E, Cargill DC, Costa DP, Crandall-Stotler BJ, Cooper ED, Dauphin G, Engel JJ, Feldberg K, Glenny D, Gradstein SR, He X, Heinrichs J, Hentschel J, Ilkiu-Borges AL, Katagiri T, Konstantinova NA, Larraín J, Long DG, Nebel M, Pócs T, Puche F, Reiner-Drehwald E, Renner MAM, Sass-Gyarmati A, Schäfer-Verwimp A, Moragues JGS, Stotler RE, Sukkharak P, Thiers BM, Uribe J, Váňa J, Villarreal JC, Wigginton M, Zhang L, Zhu R-L (2016) World checklist of hornworts and liverworts. PhytoKeys 59: 1–828. https://doi.org/10.3897/phytokeys.59.6261

Sokol J (2019) Troubled treasure. Science 364: 722–729. https://doi.org/10.1126/science.364.6442.722

Stilwell JD, Langendam A, Mays C, Sutherland LJM, Arillo A, Bickel DJ, De Silva WT, Pentland AH, Roghi G, Price GD, Cantrill DJ, Quinney A, Peñalver E (2020) Amber from the Triassic to Paleogene of Australia and New Zealand as exceptional preservation of poorly known terrestrial ecosystems. Scientific Reports 10: e5703. https://doi.org/10.1038/s41598-020-62252-z

Tomescu AMF, Bomfleur B, Bippus AC, Savoretti A (2018) Why are bryophytes so rare in the fossil record? A spotlight on taphonomy and fossil preservation. In: Krings M, Harper CJ, Cúneo NR, Rothwell GW (Eds) Transformative Paleobotany. Papers to Commemorate the Life and Legacy of Thomas N. Taylor. Elsevier/Academic Press, London, 375–416. https://doi.org/10.1016/B978-0-12-813012-4.00016-4

von Konrat M, de Lange P, Larraín J, Hentschel J, Carter B, Shaw J, Shaw B (2013) A small world: Uncovering hidden diversity in *Frullania* – a new species from Aotearoa-New Zealand. Polish Botanical Journal 58: 437–447. https://doi.org/10.2478/pbj-2013-0056

Wang B, Shi G, Xu C, Spicer RA, Perrichot V, Schmidt AR, Feldberg K, Heinrichs J, Chény C, Pang H, Liu X, Gao T, Wang Z, Ślipiński A, Solórzano-Kraemer MM, Heads SW, Thomas MJ, Sadowski E-M, Szwedo J, Azar D, Nel A, Liu Y, Chen J, Zhang Q, Zhang Q, Luo C, Yu T, Zheng D, Zhang H, Engel MS (2021) The mid-Miocene Zhangpu biota reveals an outstandingly rich rainforest biome in East Asia. Science Advances 7: eabg0625. https://doi.org/10.1126/sciadv.abg0625

Wang Q, Li Y, Feldberg K, Wang Y-D, Yang X-J (in press) *Radula heinrichsii* (Radulaceae, Porellales), a leafy liverwort from the mid-Cretaceous of Myanmar. Palaeoworld. https://doi.org/10.1016/j.palwor.2022.01.006

Yamada K (1979) A revision of Asian taxa of *Radula*, Hepaticae. Journal of the Hattori Botanical Laboratory 45: 201–322.

Yu T, Thomson U, Mu L, Ross A, Kennedy J, Broly P, Xia F, Zhang H, Wang B, Dilcher D (2019) An ammonite trapped in Burmese amber. Proceedings of the National Academy of Sciences USA 116: 11345–11350. https://doi.org/10.1073/pnas.1821292116

Yuzawa Y (1991) A monograph of subgen. *Chonanthelia* of gen. *Frullania* (Hepaticae) of the world. Journal of the Hattori Botanical Laboratory 70: 181–291. https://doi.org/10.18968/jhbl.70.0_181

Yuzawa Y (2001) Species of the genus *Frullania* (family Frullaniaceae, Hepaticae) in Japan. II. Natural Environmental Science Research 14: 1–47. [in Japanese]

Supplementary material 1

Figures S1–S6

Authors: Kathrin Feldberg, Alfons Schäfer-Verwimp, Ya Li, Matt A. M. Renner

Data type: Images (PDF file).

Explanation note: Extending the diversity of the bryoflora in Kachin amber.

Link: https://doi.org/10.3897/fr.25.82362.suppl1